108
4-14-81
BNL 51304
R3486
(1)
Dr. 2518
MASTER

Proceedings of the Second International Symposium on the Production and Neutralization of Negative Hydrogen Ions and Beams

1980

Brookhaven National Laboratory
Upton, New York

DISTRIBUTION OF THIS DOCUMENT IS UNLIMITED

DISCLAIMER

This report was prepared as an account of work sponsored by an agency of the United States Government. Neither the United States Government nor any agency Thereof, nor any of their employees, makes any warranty, express or implied, or assumes any legal liability or responsibility for the accuracy, completeness, or usefulness of any information, apparatus, product, or process disclosed, or represents that its use would not infringe privately owned rights. Reference herein to any specific commercial product, process, or service by trade name, trademark, manufacturer, or otherwise does not necessarily constitute or imply its endorsement, recommendation, or favoring by the United States Government or any agency thereof. The views and opinions of authors expressed herein do not necessarily state or reflect those of the United States Government or any agency thereof.

DISCLAIMER

Portions of this document may be illegible in electronic image products. Images are produced from the best available original document.

BNL 51304
UC-34a
(Physics-Atomic and Molecular
TIC-4500)

CONF-801068--

Proceedings of the Second International Symposium on the Production and Neutralization of Negative Hydrogen Ions and Beams

October 6-10, 1980

TH. SLUYTERS, *Editor*

DISCLAIMER

This book was prepared as an account of work sponsored by an agency of the United States Government. Neither the United States Government nor any agency thereof, nor any of their employees, makes any warranty, express or implied, or assumes any legal liability or responsibility for the accuracy, completeness, or usefulness of any information, apparatus, product, or process disclosed, or represents that its use would not infringe privately owned rights. Reference herein to any specific commercial product, process, or service by trade name, trademark, manufacturer, or otherwise, does not necessarily constitute or imply its endorsement, recommendation, or favoring by the United States Government or any agency thereof. The views and opinions of authors expressed herein do not necessarily state or reflect those of the United States Government or any agency thereof.

Sponsored by:
U.S. Department of Energy
Accelerator Department of Brookhaven National Laboratory,
Upton, New York, 11973
Contract No. De-AC02-76CH00016

DISTRIBUTION OF THIS DOCUMENT IS UNLIMITED

DISCLAIMER

This report was prepared as an account of work sponsored by an agency of the United States Government. Neither the United States Government nor any agency thereof, nor any of their employees, nor any of their contractors, subcontractors, or their employees, makes any warranty, express or implied, or assumes any legal liability or responsibility for the accuracy, completeness, or usefulness of any information, apparatus, product, or process disclosed, or represents that its use would not infringe privately owned rights. Reference herein to any specific commercial product, process, or service by trade name, trademark, manufacturer, or otherwise, does not necessarily constitute or imply its endorsement, recommendation, or favoring by the United States Government or any agency, contractor or subcontractor thereof. The views and opinions of authors expressed herein do not necessarily state or reflect those of the United States Government or any agency, contractor or subcontractor thereof.

Printed in the United States of America
Available from
National Technical Information Service
U.S. Department of Commerce
5285 Port Royal Road
Springfield, VA 22161
Price: Printed Copy $21.00; Microfiche $3.50

Foreword

The Second International Symposium on the Production and Neutralization of Negative Hydrogen Ions and Beams reflects the progress made during the last three years. Principle emphasis was placed upon the development of high current DC negative ion sources and related atomic physics, for their application in future fusion experiments.

At the symposium, attended by 59 delegates from 7 countries, 48 papers were presented during 8 sessions, devoted to: fundamental processes (3 sessions), negative ion source concepts (3 sessions), neutralizers (1 session) and beam systems (1 session). Transcripts of the discussions follow the text of each paper. In addition to the regular sessions, two panel sessions were arranged to emphasize the general state-of-the-art, to consider future experiments and problems, and to discuss divergent points of view. The transcripts of these panel sessions, as well as the concluding remarks, are included in these Proceedings. We are indebted to the moderators of the panels who aided in the editing of the panel sessions.

In the planning and functioning of this symposium we had to rely on many people. We are grateful to the Brookhaven Neutral Beam Development Group for their indispensable contribution to the organization of the scientific and social events. And special appreciation goes to Lillian Kouchinsky who handled the numerous administrative details and to our Proceedings secretary Carmen Falkenbach.

TH. J.M. SLUYTERS, *Chairman*
December, 1980 Organizing/Program Committee

THIS PAGE

WAS INTENTIONALLY

LEFT BLANK

Local Organizing Committee

J.A. ALESSI
A. HERSHCOVITCH
R.A. LARSON
V. KOWARIK
R. MCKENZIE-WILSON
K. PRELEC *(Co-Chairman)*
TH. SLUYTERS *(Chairman)*

Program Committee

R.W. EHLERS	Lawrence Berkeley Laboratory
E.B. HOOPER, JR.	Lawrence Livermore Laboratory
K. PRELEC *(Co-Chairman)*	Brookhaven National Laboratory
TH. SLUYTERS *(Chairman)*	Brookhaven National Laboratory
S. STATEN	U.S. Department of Energy

Symposium Secretary

MRS. LILLIAN KOUCHINSKY

Proceedings Secretary

MRS. CARMEN FALKENBACH

THIS PAGE

WAS INTENTIONALLY

LEFT BLANK

Table of Contents

SESSION I - FUNDAMENTAL PROCESSES 1
J.N. Bardsley, Chairman

Hydrogen Negative Ions and Collisions of Atomic Particles..... 1
D.H. Crandall and F.W. Meyer

The Production and Destruction of H^- and D^- Ions in Hydrogen and Deuterium Plasmas..... 10
J.N. Bardsley

Formation of H^- and D^- Ions by Particle Backscattering from Alkali/Transition Metal Complexes..... 15
J.R. Hiskes and P.J. Schneider

Positive and Negative Ionization by Scattering from Surfaces..... 23
J. Los, E.A. Overbosch and J. van Wunnik

Production of Negative Ions under Non-Equilibrium Conditions..... 33
W.F. Bailey and A. Garscadden

SESSION II - FUNDAMENTAL PROCESSES 2
D.H. Crandall, Chairman

D^- Production by Charge Transfer in Metal Vapors..... 42
A.S. Schlachter

Theoretical Investigations of the Collisions Dynamics in H^- Formation and Destruction..... 51
R.E. Olson

Angular Scattering in Electron Capture and Loss D^- Beam Formation Processes..... 58
M.J. Coggiola, R.V. Hodges, D.L. Huestis and J.R. Peterson

H^- Formation from a Surface Conversion Type Ion Source..... 65
K.N. Leung and K.W. Ehlers

Relaxation of H_2 Vibrational Motion by Wall Collisions..... 74
A.M. Karo, T.M. Deboni and J.R. Hiskes

Limiting Secondary Plasma Effects in Cesium Cells or Jets Used in the Double Charge Exchange Method for D^- Beam Production..... 81
J.M. Dolique

SESSION III - FUNDAMENTAL PROCESSES 3
J.R. Hiskes, Chairman

Measurement of H^- and D^- Density in Plasma by Photodetachment..... 90
G.W. Hamilton, M. Bacal, A.M. Bruneteau, H.J. Doucet and M. Nachman

H^- and D^- Production in Plasma..... 95
M. Bacal, A.M. Bruneteau, H.J. Doucet, W.G. Graham and G.W. Hamilton

H^- Production in H^+ and H^o Collisions with Alkaline Earth Metal Vapors..... 106
M. Mayo, J. Stone, T.J. Morgan, I. Alvarez, C. Cisneros

Emission of Negative Hydrogen Ions from Metal Hydrides Bombarded with Cesium Ions..... 111
M. Seidl, A.N. Pargellis, J. Greer

Low Work Function Surface for Improving the Yield of Negative Hydrogen Ions..... 119
F.N. Huffman and P.E. Oettinger

Properties of Alkali Metals Absorbed onto Metal Surfaces..... 126
W.G. Graham

SESSION IV - SURFACE CONVERSION SOURCES I
K.W. Ehlers, Chairman

Some Effects of Surface-Plasma Mechanism for Production of Negative Ions..... 137
V.G. Dudnikov

Progress in the Development of High Current, Steady State H^-/D^- Sources at BNL..... 145
K. Prelec

Regular and Asymmetric Negative Ion Sources with Grooved Cathodes..... 153
J. Alessi and Th. Sluyters

Mark V Magnetron with H.C.D. Plasma Injection..... 160
A. Hershcovitch and K. Prelec

Extraction and Transport of H^-, D^- Beams from Magnetron Sources..... 166
Th. Sluyters and J. Alessi

H^- Ion Source Research at Los Alamos..... 171
P. Allison, H.V. Smith, Jr., J.D. Sherman

A Rotating Penning Surface-Plasma Source for DC H^- Beams..... 178
H.V. Smith, Jr., P. Allison, J.D. Sherman

H^- Beam Formation from a Penning Surface-Plasma Source Using Circular Emission-Extractor Electrodes..... 184
J.D. Sherman, P. Allison, H.V. Smith, Jr.

Operation of the Fermi H^- Magnetron Source..... 189
C.W. Schmidt

SESSION V - SURFACE-CONVERSION SOURCES 2
K. Prelec, Chairman

An Overview of the LBL/LLNL Negative-Ion Based Neutral Beam Program..... 194
R.V. Pyle

Characteristics of a Self-Extraction Negative Ion Source..... 198
K.W. Ehlers and K.N. Leung

Transport of Low Energy Positive and Negative Ion Beam by Permanent Magnets..... 207
K.N. Leung, K.W. Ehlers and E.B. Hooper, Jr.

Proposed Electrode Design for Direct Extraction of Negative Ion Beams..... 213
A.J.T. Holmes, T.S. Green and M. Inman

Modified Calutron Negative Ion Source Operation and Future Plans..... 217
W.K. Dagenhart, W.L. Stirling, H.H. Haselton, G.G. Kelley, J. Kim, C.C. Tsai, J.H. Whealton

Characteristics of a Modified Duopigatron Negative Ion Source..... 225
C.C. Tsai, R.R. Feezell, H.H. Haselton, D.E. Schechter, W.L. Stirling, J.H. Whealton

A Conceptual D^- Source Exploiting Negative Surface Ionization of Deuterons..... 233
H.J. Hopman, P.J. van Bommel, P. Massman, E.H.A. Granneman

Development of Negative Ion Sources at the IPP Nagoya University..... 240
T. Kuroda, H. Okamura, O. Kaneko and Y. Oka

SESSION VI - DOUBLE CHARGE EXCHANGE SOURCES
R. Geller, Chairman

Prospects for Negative Ion Systems Based on Charge Exchange..... 247
E.B. Hooper, Jr., and P. Poulsen

Production of D^- Ions by Double Charge Exchange of D^+ on Cesium..... 255
M. Delauny, J.L. Foucher, R. Geller, C. Jacquot, P. Ludwig, F. Mazhari, E. Ricard, J.C. Rocco, P. Sermet, F. Zadworny

Negative Ion Production by Charge Exchange of Hydrogen Clusters With A Cesium Vapor Target - Status Report..... 263
O.F. Hagena, P.R.W. Henkes, R. Klingelhöfer, B. Krevet, H.O. Moser

Cesium Supersonic Jet for D^- Production by Double Electron Capture..... 270
M. Bacal, J.M. Buzzi, H.J. Doucet, G. Labaune, H. Lamain, J.P. Stephan, M. Delaunay, C. Jacquot, P. Ludwig, S. Verney

SESSION VII - NEUTRALIZERS
J. Fink, Chairman

The Stripping of 30-200 keV H^- Ions..... 285
L.W. Anderson, C.J. Anderson, R.J. Girnius and A.M. Howald

Plasma Neutralizers for H^- or D^- Beams..... 291
K.H. Berkner, R.V. Pyle, S.E. Savas and K.R. Stalder

A Simple, Efficient Neutralizer for D^- Ions..... 298
J. Fink and K. Prelec

Laser Neutralization of Negative Ion Beams for Fusion..... 304
M.W. McGeoch

SESSION VIII - NEUTRAL BEAM SYSTEMS
H.S. Staten, Chairman

U.S. Negative Ion Neutral Beam Development Program..... 315
H.S. Staten, G.M. Haas, F.E. Coffman

Merits of D^- Based Neutral Beam Injectors for Tokamaks..... 321
L.D. Stewart, A.H. Boozer, H.P. Eubank, R.J. Goldston, D.L. Jassby, D.R. Mikkelsen, D.E. Post, B. Prichard, J.A. Schmidt, C.E. Singer

Negative Deuterium Ions for Tandem Mirror Next Step and Tandem Mirror Reactors..... 330
G. W. Hamilton

Negative Ions as a Source of Low Energy Neutral Beams..... 339
J. Fink

A D^- Ion Accelerator Immersed in a Magnetic Field..... 350
J.L. Foucher, R. Geller, C. Jacquot, J.C. Rocco, P. Sermet, J.B. Berström, H.G. Gustavson, Hellblöm, R. Pauli

Large-Aperture D^- Accelerators..... 355
O.A. Anderson

PANEL SESSION - FUNDAMENTAL PROCESS IN SOURCES
(A.S. Schlachter, Moderator)..... 365

PANEL SESSION - SOURCES OF NEGATIVE IONS
(K. Prelec, Moderator)..... 373

CONCLUDING REMARKS (K.W. Ehlers)..... 385

LIST OF ATTENDEES, INDEX OF AUTHORS..... 389

FUNDAMENTAL PROCESSES

SURFACE CONVERSION SOURCES

DOUBLE CHARGE EXCHANGE SOURCES

NEUTRALIZERS

NEUTRAL BEAM SYSTEMS

PANEL SESSIONS

CONCLUDING REMARKS

LIST OF ATTENDEES—LIST OF AUTHORS

FUNDAMENTAL PROCESSES

HYDROGEN NEGATIVE IONS AND COLLISIONS OF ATOMIC PARTICLES*

D. H. Crandall and F. W. Meyer
Oak Ridge National Laboratory
Oak Ridge, Tennessee

Abstract

This paper will be an overview presenting some of the basic atomic collisions processes (gas phase) which are fundamental to production and destruction of H^- (D^-). More detailed discussions of the most important processes will be left to other papers at this Symposium, and primarily new results since the 1977 Symposium will be discussed. Recent results provide insight into mechanisms responsible for the high H^- (D^-) ion fractions in hydrogen gas discharges, and the ion-atom collision processes important for "double capture" negative ion sources are better understood than in 1977.

I. Introduction

This paper is a sequel to the paper given at the 1977 Symposium[1] and will concentrate on the new results since that time. Those processes for creation and destruction of H^- or D^- which had been well studied in 1977 left a mystery as to how there could be a large fraction of negative ions in an ion source, since known creation collisions all had cross sections around 10^{-18} cm^2 or lower while several destruction mechanisms had cross sections exceeding 10^{-14} cm^2. Various unstudied collision processes were discussed in Ref. 1, and additional ones were suggested at the 1977 Symposium. Various insights have been provided in the interim, principally that vibrationally excited H_2 will have a large rate for production of H^- through dissociative attachment, but the picture is certainly not complete. Nevertheless, the new basic collisions results are exciting for ion source development not only because they provide understanding of what has been observed in discharges but also because they may provide suggestions for improving H^- production in discharges.

Cross sections for conversion of H^+ to H^- by double capture are also better known than they were in 1977. This issue is perhaps of less urgency than direct ion source production since the information was reasonably complete in 1977.[2] However, the improved collisions data do allow a more reliable assessment of the technique of "double capture" for production of H^- (D^-).

The needs for atomic collisions studies relevant to fusion were recently outlined at a meeting called by the IAEA,[3] and the listed needs include needs for ion source development. The atomic collisions needs for modeling and understanding divertor performance in plasma fusion are not yet well defined, but it is clear that there is considerable overlap of the basic collisions processes operative in ion sources and divertors. This additional area of fusion interest can thus provide further justification for some of the collisions studies discussed here.

II. Electron Collisions

Cross Sections Known in 1977

A number of cross sections of interest were well characterized in the previous paper.[1] Though there were no direct measurements, it was pointed out that three-body recombination for H^- was unlikely in ion sources since for electrons as the third body, a density, n_e, greater than 10^{+18} cm^{-3} would be required for three-body attachment to be comparable to radiative attachment (10^{-22} cm^2), and a three-body recombination with any atom or molecule as the third body would require a density, n_{atom}, about 10^{+16} cm^{-3} to be competitive with radiative recombination. Examples of further specific, well-characterized processes in 1977 are electron detachment, $e^- + H^- \rightarrow H + 2e^-$ (destruction of H^-) with peak cross section near 10 eV of 4×10^{-15} cm^2 (Ref. 4) and dissociative recombination, $e^- + H_2^+ \rightarrow H^* + H^-$ (formation of H^-) with a cross section of 5×10^{-18} cm^2 at 0.3 eV.[5]

Dissociative attachment, $e + H_2 \rightarrow H_2^- \rightarrow H^- + H$, was discussed at some length at the 1977 Symposium in part because it provided a dramatic isotope effect. The resonance state of H_2^- at 3.75 eV above the H_2 ground state can either autodetach (no H^- formed) or dissociate to form H^-. Since dissociation is faster for H_2^- than D_2^-, while detachment is constant, the measured cross sections at 3.75 eV[6] are 0.9×10^{-24} cm^2 for D^- formation from D_2 and 1.7×10^{-21} cm^2 for H^- formation from H_2 — an isotope effect of over three orders of magnitude. While such an isotope effect raised the question of D^- production relative to H^- production in ion sources, the cross sections were so small that no one was alarmed. However, it is this process that has provided greatest interest since 1977.

Dissociative Attachment with Vibrational and Rotational Excitation

In 1978 Allan and Wong[7] showed that dissociative attachment increased four to five orders of magnitude if the $H_2(D_2)$ were heated to 1400 K with accompanying vibrational excitation up to v = 4 and rotational levels up to j = 7. Wadehra and Bardsley[8] explained these results primarily in terms of vibrational excitation. Bardsley will discuss these results in more detail, but they are pointed out here as critical to the understanding of H^- (D^-) production in discharges.

*Research sponsored by the Office of Fusion Energy, U.S. Department of Energy, under contract W-7405-eng-26 with Union Carbide Corporation.

These results were missed by previous investigators. In 1967 Chen and Peacher[9] predicted a strong dependence of dissociative attachment on rotational excitation, and Spence and Schulz[10] subsequently investigated the cross section at 3.75 eV searching for the predicted effect. Figure 1 shows their result that indicated no rotational excitation effect. However, Fig. 2 shows part of the work by Allan and Wong which clearly demonstrates the strong dependence of dissociative attachment on temperature. The results of Spence and Schulz are probably not wrong, but they looked only at electron impact energy of 3.75 eV and hence saw only H^- from the ground vibrational state of H_2. The small increase they might have expected in their signal due to rotational heating of ground vibrational state could easily be offset by depletion of the ground vibrational state. The predictions of Chen and Peacher about rotational excitation probably are too high as suggested by the data of Spence and Schulz. When Allan and Wong did the same experiment but with variable energy electrons, an important result emerged. When part of the required 3.75 eV is present as internal vibrational excitation of the initial molecule, the integrated effective cross section (1-5 eV) increased dramatically.

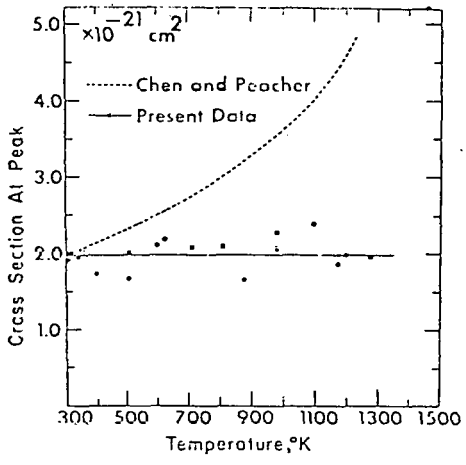

Fig. 1. Temperature dependence of the cross section for H^- formation in H_2 at 3.75 eV electron energy (Spence and Schulz, Ref. 10).

There is also good news for ion source production of H^- (D^-) on the issue of the isotope effect. When $e + H_2$ (vib) $\rightarrow H_2^-$ (vib), dissociation of the negative molecule begins to dominate over autodetachment because of more rapid dissociation when vibrational energy is already present. Thus for D^- from D_2 (vib), the increase in cross section is even greater than for H_2 and presumably for sufficiently high vibrational level the H^-/H_2 (vib) and D^-/D_2 (vib) will be equal and autodetachment will be negligible. Thus the effect of vibrational excitation helps to explain not only the high content of negative ions in discharges but also the lack of isotope effect — both recently confirmed in improved measurements by Bacal and Hamilton[11] in their low-pressure plasma.

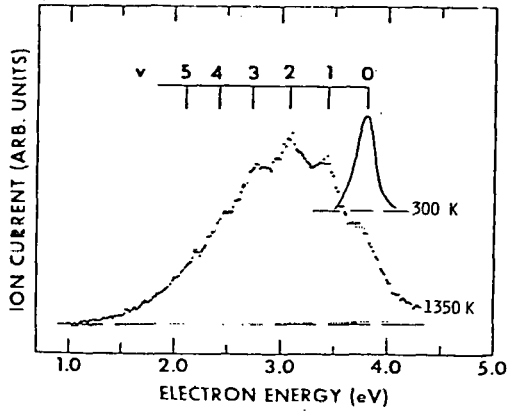

Fig. 2. D^- formation in D_2 as a function of electron energy at 1350 K (Allan and Wong, Ref. 7). The inset at 300 K has been added to indicate approximate results at room temperature.

These basic collision studies have provided us with clues to production of negative ions in discharges and could even suggest ways to tune the discharge for higher ion production. However, a number of unanswered questions remain. It is of some interest to ask how general the vibrational excitation mechanism is. For N_2 molecules, recent experimental work[12] shows that for electron dissociative attachment the vibrational heating of the N_2 only increases N^- production by about a factor of four rather than the four orders of magnitude in the H_2 case; thus the vibrational heating effects are not universal. In contrast, recent studies by Beterov et al.[13] (Fig. 3) invoke vibrational excitation to explain an observed increase of negative ion production on surfaces. The negative ion being produced in this case is SF_6^-, but the authors show that irradiation of the surface with a CO_2 laser greatly enhances negative ion production, and apparently they believe this to be associated with vibrational excitation of adsorbed surface molecules. These two examples are removed from the immediate question of H^- (D^-) production but illustrate the broad interest in vibrational excitation.

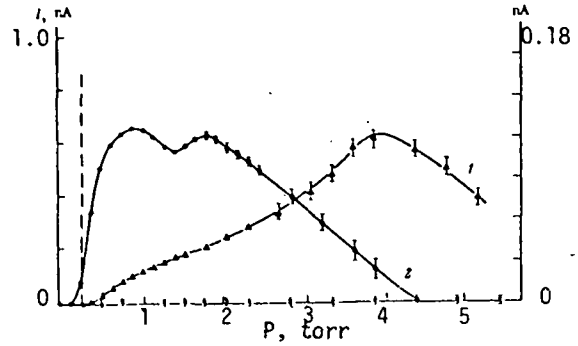

Fig. 3. Negative-ion current produced by SF_6 contact with hot thoriated tungsten. Curve 1 and scale at right are the normal results while Curve 2 and scale at left show enhancement of negative-ion current when the surface is irradiated with CO_2 laser — 10.6 μ (Beterov et al., Ref. 13).

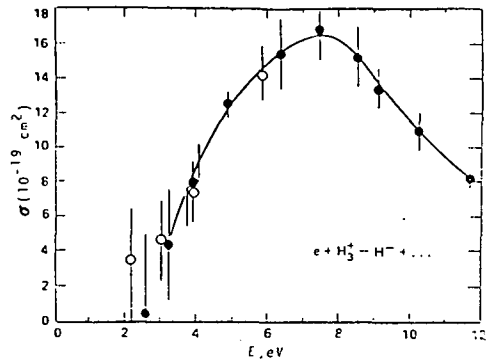

Fig. 4. Direct production of H^- from dissociative recombination. Open points are at reduced source pressure to enhance vibrational excitation of H_3^+ (Peart et al., Ref. 18).

There are specific unanswered questions about the hydrogen discharge production of H^- as well. Hiskes[14] recently reviewed the H^- production in light of the vibrational excitation discoveries. For this mechanism to provide the observed H^-, a significant fraction of H_2 molecules in the discharge needs to be highly excited vibrationally, $v \geq 6$. The question as to where such vibrationally excited molecules would come from has a number of possible answers.

Dissociative Recombination of H_3^+

Low energy discharges (like the one studied at Ecole Polytechnique[15,11]) often contain high fractions of H_3^+. This is at least in part due to the fast reaction of $H_2^+ + H_2 \rightarrow H_3^+ + H$ which rises rapidly as energy decreases and is above 10^{-15} cm^2 at energies below 1.2 eV.[16,17] At any rate the presence of H_3^+ in large quantity leads to speculation that the higher than anticipated H^- fractions may involve reactions of H_3^+. The most obvious speculation is that dissociative recombination, $e^- + H_3^+ \rightarrow H^- + H_2^+$, could directly produce H^-. In response to such speculation the cross section was measured by Peart, Forrest, and Dolder.[18] Figure 4 shows their result and demonstrates that the H^- production cross section does not exceed 1.8×10^{-18} cm^2 and is thus an unlikely candidate for the source of H^- in plasma. They use the statement of Kulander and Guest[19] that H^- production from ground state H_3^+ would have a threshold near 5.8 eV to infer that their H_3^+ is vibrationally excited. In addition, Peart et al. reduced ion source pressure to attempt to heat their H_3^+ vibrationally and found little enhancement of the cross section. (It is noted that Vogler[20] infers that the H_3^+ from such an ion source is likely to be vibrationally excited independent of the source pressure.)

While H_3^+ apparently does not directly produce H^-, it might produce the vibrationally excited H_2 needed for dissociative attachment to be effective in H^- production.[21-24] A number of measurements of dissociative recombination, $e^- + H_3^+ \rightarrow H_2 + H$ (Fig. 5), demonstrate that this reaction is fast. Statements that the H_2 produced is vibrationally excited are somewhat speculative but Kulander and Guest,[19] theoretically studying the likely states of H_3, suggest that the dissociation will favor vibrational excitation, and the experimental work of Vogler[20] on the angle and energy distributions of dissociating H_3 also suggests high vibrational energy in the system.

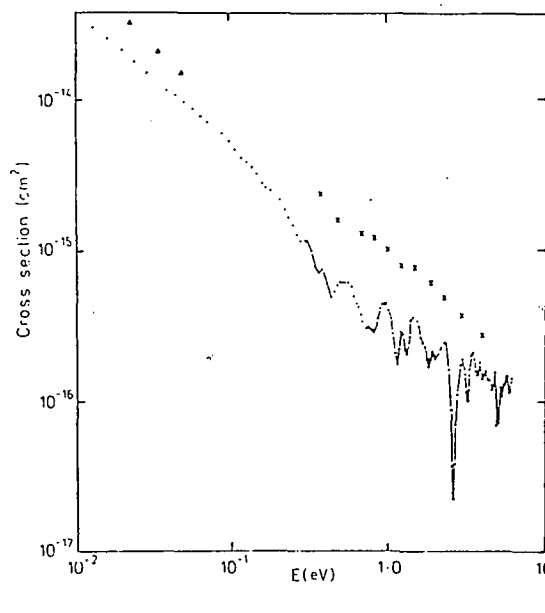

Fig. 5. Total dissociative recombination of H_3^+. Data are: Δ - Leu et al., Ref. 21; x - Peart and Dolder, Ref. 22; · - Auerbach et al., Ref. 23.

Long-Lived States of H_2^-, D_2^-, H_3^-

The question of the possible existence of long-lived (excited) states of H_2^- appears to be still unresolved, as far as theoretical calculations are concerned,[25,26] although promising candidates such as the $^4\Sigma_g^-(1\sigma_g)(1\pi_u)^2$ state and others have been suggested. Experimental results, however, have indicated the existence of both diatomic and even triatomic negative hydrogen (and deuterium) molecular ions that appear to be stable against electron emission with lifetimes exceeding 10^{-5} s.[27-29] Figure 6 shows the production efficiencies of H^-, D^-, HD^-, D_2^-, D_2H^-, and D_3^- in a hollow cathode duoplasmatron ion source (arc voltage 500 V, arc current 60-100 mA) found by Aberth et al.[27] as a function of H_2/D_2 source pressure ratio. Although the relative abundances in ion sources of these molecular negative hydrogen ions compared to $H^-(D^-)$ are quite low (typically 10^{-6}-10^{-8} at 1 Torr source pressure), insight into their modes of formation and destruction would promote an understanding of the reaction processes occurring in hydrogen plasma sources which produce $H^-(D^-)$.

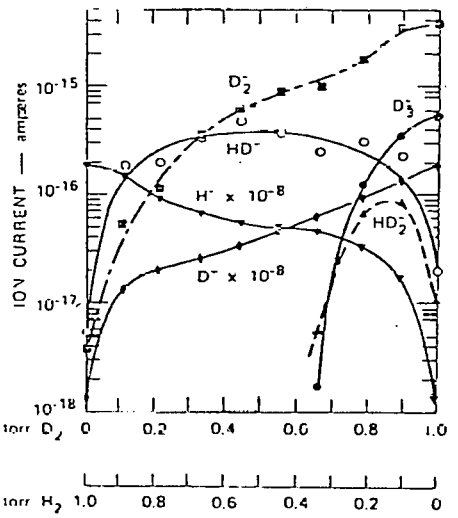

Fig. 6. Observed negative ion currents from a duoplasmatron source with mixture of H_2 and D_2 gas (Aberth et al., Ref. 27).

III. Ion-Atom Collisions

Vibrationally Excited H_2

There are at least two known reactions worth mentioning in the context of producing vibrationally excited H_2. One, that is also a collisional destruction of H^-, is associative detachment, $H^- + H_2 \rightarrow H_2 + e$. This reaction proceeds via the autodetaching $^2\Sigma_u$ state of H_2^-. Measurement in a flowing afterglow by Fehsenfeld et al.[30] gave a room temperature reaction rate of 1.8×10^{-9} cm^3/s implying a cross section near 10^{-14} cm^2.

Catherinot et al.[31] preformed an experiment to monitor excited states of H (n = 3, 4, 5) in a low pressure hydrogen discharge. Their observations are of general interest, but two results are noted here. One is that significant amounts of electronically excited H_2 ($c^3\Pi_u$ and $a^3\Sigma_g^+$) were present in the plasma. The other is that they determine average cross sections in their discharge for excitation transfer H (n = 3, 4, or 5) + H_2 → H (n = 1 or 2) + H_2 (vibrationally excited). For their mixture of initial H_2 states, they obtain about 1.5×10^{-14} cm^2 for the excitation transfer cross sections which quench excited H but may produce vibrationally excited H_2.

There may be invoked a number of such mechanisms for producing vibrationally excited H_2, but dissociative recombination, $e^- + H_3^+$, still must rank as a primary candidate.

Ion-Atom Destruction of H^-

As was previously known,[1,32] mutual neutralization $H^- + H^+ \rightarrow 2H^0$ (Fig. 7); $H^- + H_2^+ \rightarrow$ neutral products (even faster than $H^- + H^+$); and presumably $H^- + H_3^+ \rightarrow$ neutrals, are dominant reactions for destroying H^-, or D^- for D reactants.

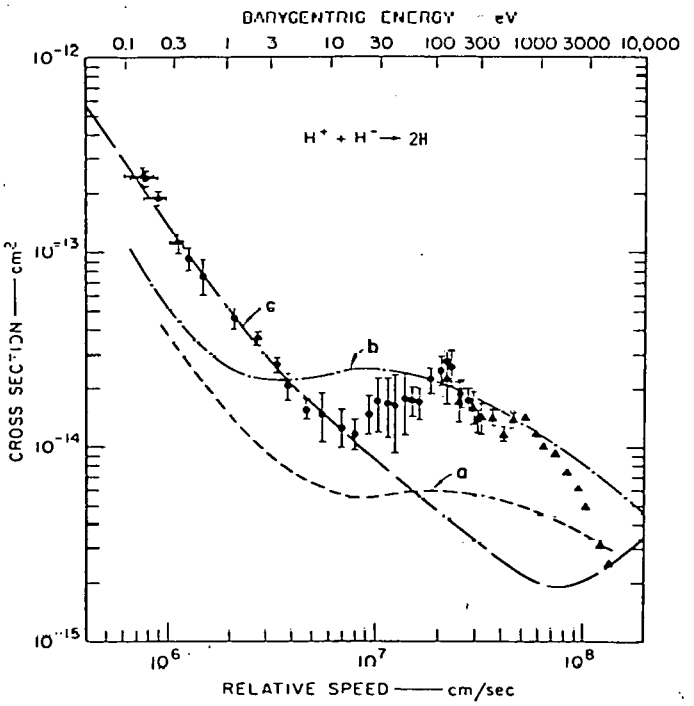

Fig. 7. Cross section for mutual neutralization. Data are: ▼ - Moseley et al., Ref. 33; ▲- Rundel et al., Ref. 34. Theoretical curves are: a - Bates and Lewis, Ref. 35; b - Dalgarno et al., Ref. 36; c - Olson et al., Ref. 37. See also Peart et al., Ref. 38. Figure from Ref. 32.

A related reaction which is fast enough to draw interest is associative ionization $H^- + H^+ \rightarrow H_2^+ + e^-$ shown in Fig. 8 (Ref. 39). The E^{-1} behavior is familiar by now; it usually signifies high rates at low energy and generally occurs when a negative and positive particle react. The associative ionization probably proceeds through an autoionizing state of H_2 (Ref. 40) and probably results in vibrationally excited H_2^+.

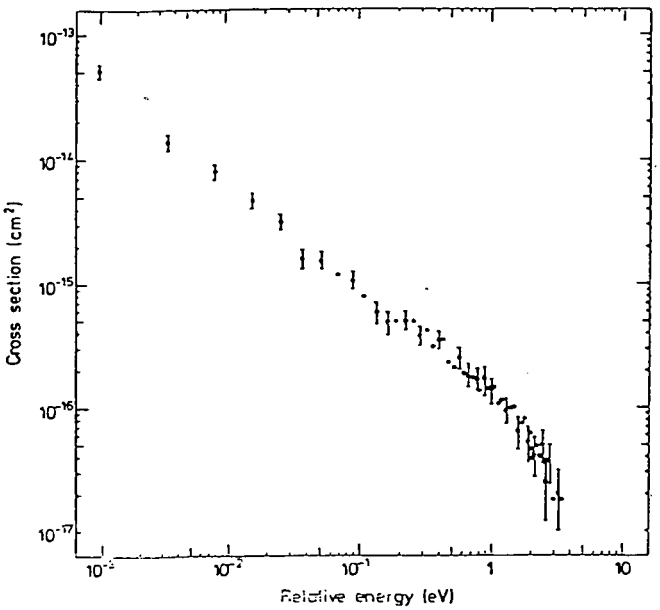

Fig. 8. Cross section for associative ionization; $H^+ + H^- \rightarrow H_2^+ + e$ (Poulaert et al., Ref. 39).

A recent review[41] and an extensive new paper[42] on negative ion detachment, or stripping, cross sections will direct the interested reader to many results for electron loss or neutralization in $H^-(D^-)$ collisions with atoms and molecules. Other papers at this Symposium will treat negative ion detachment with a view toward employment of this process in neutralization of fast $H^o(D^o)$ beams. Single electron loss resulting in $H^o(D^o)$ has generally large cross sections, typically above 10^{-16} cm^2 from a few eV to near 1 MeV energies. Between 30 and 200 keV, these cross sections are typically 1-2 x 10^{-15} cm^2. With respect to neutralization of $H^-(D^-)$ the limit in fractions neutralized at beam injection energies is determined primarily by the ratio of single electron loss to double electron loss. Cross sections for stripping both electrons are usually one order of magnitude smaller than single loss cross sections at beam injection energies which crudely suggests that neutralization with gas targets could be as high as 70%.

Electron loss from H^- in alkali vapors has been of particular interest at low energies (0.1-2 keV) because of interest in production of H^- beams by passage of H^+ through these vapors. Recent time of flight, as well as differential,[43] cross section measurements on $H^- + Na \rightarrow H^o$ below 1 keV indicate that electron loss occurs by combined autodetachment of the quasi-molecule and charge transfer in proportions roughly 3 to 2. This suggests that in theoretical calculations of electron loss, the interaction of the $(alk\ H)^-$ and $(alk\ H)^o$ potential curves at small internuclear separations (2-4 a_o), where (auto)detachment occurs, may be just as important to the total loss as the interaction at larger separations (10-20 a_o) where the charge transfer occurs.[44]

In the above energy range, experimental electron loss cross sections for H^- + Cs are available[46-48] and are included on Fig. 9. Curve 1 on Fig. 9 is the calculated electron loss by Olson and Liu[44] which contains the long-range coupling. This theoretical result falls below the experimental total loss cross section suggesting that addition of a short-range (auto)detachment component may be appropriate to this case. Qualitatively, the (auto)detachment contribution to the loss cross section should be approximately πR_c^2 with $R_c \simeq 4\ a_o$.[48] If such a contribution is added to the calculated cross section,[44] reasonable agreement with the experiment is obtained.

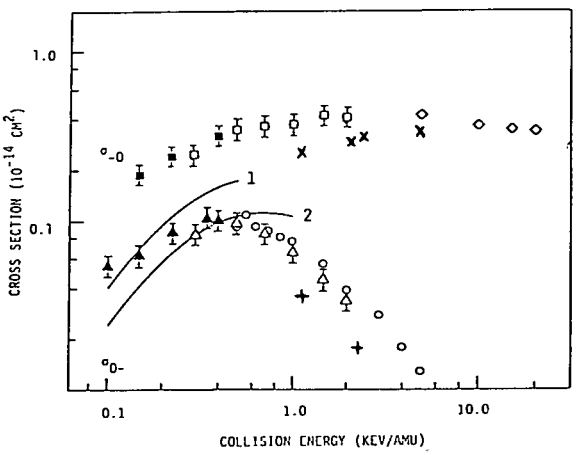

Fig. 9. Electron capture and loss cross sections for hydrogen and deuterium projectiles on Cs. Data are: symbols with error bars (open - hydrogen and closed - deuterium) — Meyer, Ref. 46; o - Nagata, Ref. 50; ◇ - Leslie et al., Ref. 48; + and x - Schlachter et al., Ref. 45. Theoretical curves: 1 - σ_{-o} by Olson and Liu, Ref. 44; 2 - σ_{o-} by Olson, Ref. 47.

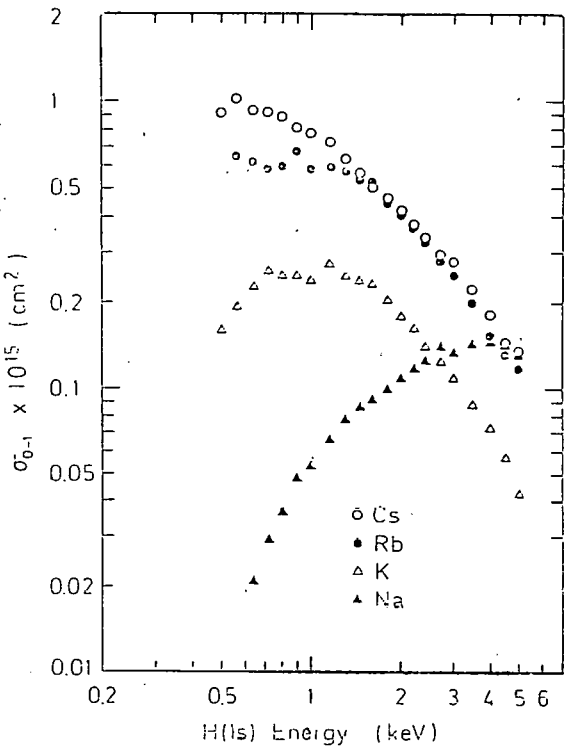

Fig. 10. Cross sections for H^- formation from H^0 + alkalis (Nagata, Ref. 50).

Production of H^- in Ion-Atom Collision

Considerable new data on production of H^- in alkali and alkali earths have been produced since 1977. Refs. 44-51 are samples of the most recent results. Fig. 9 shows some of the cross sections for Cs and Fig. 10 from Nagata[50] shows measured cross sections for production of H^- from collisions of H^0 with a number of alkalis. Several other papers at this Symposium will discuss these results and their application to H^- beam production. Fig. 11 illustrates the progress in this area since 1977. The original figure is from Schlachter's 1977 paper[2] but has been changed by removal of results now discounted by the original authors and by addition of recent results by Meyer.[46] Finally, Fig. 11 shows a reasonably consistent and reliable picture for the equilibrium fraction for H^- in a thick target of Cs.

Of some general interest to the subject of $H^-(D^-)$ formation are recent results for low energy collisions of H, D + Ar, Kr, and Xe by Aberle, Grosser, and Krüger.[52] Figure 12 shows their measurements of ion pair formation H(D) + Xe → $H^-(D^-)$ + Xe^+ just above threshold (10-100 eV). A remarkable oscillation of the cross section is obvious and is interpreted by the authors with reference to Fig. 13. The oscillation in cross section is interpreted as due to interaction of the colliding system between molecular curves which have two crossings and which separate to the ion pair observed or to a state of H(D) excitation plus the original rare gas atoms. The isotope effect is an artifact of the energy scale and disappears on a constant velocity scale. In fact, if plotted on a scale proportional to (velocity)$^{-1}$ corresponding to collision time, the oscillations are very regular as has been observed for other scattering events in which such molecular potential curves are appropriate.

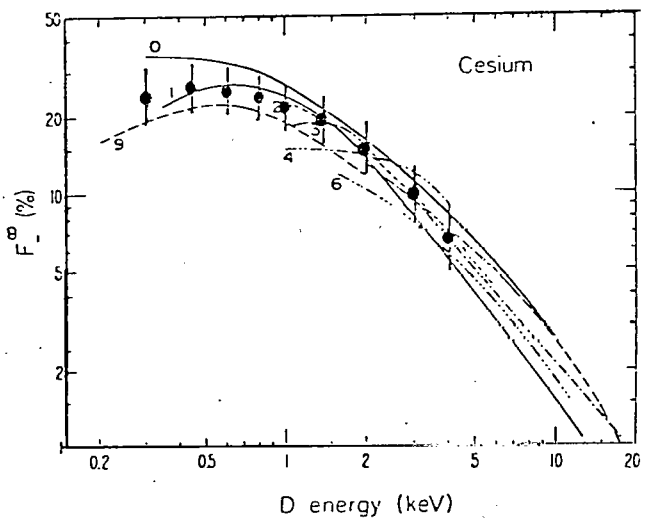

Fig. 11. Equilibrium fraction of D^- for deuterium projectiles in Cs (see text).

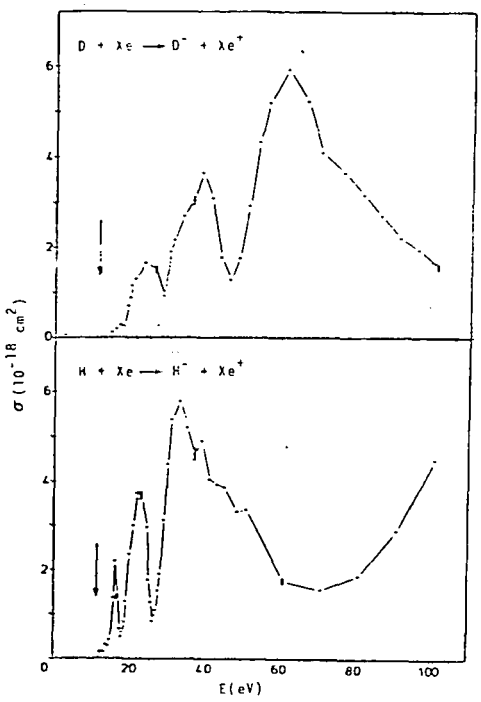

Fig. 12. Formation of $H^-(D^-)$ in Xe (Aberle et al., Ref. 52).

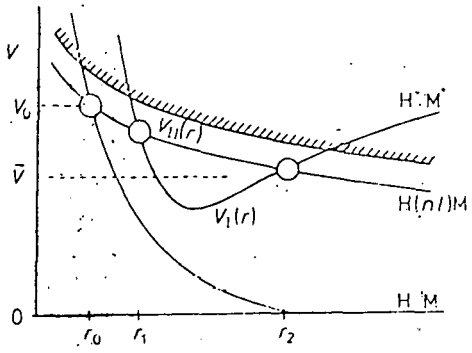

Fig. 13. Schematic potential curves leading to oscillation of cross section for ion pair formation seen in Fig. 12 (Aberle et al., Ref. 52).

Photodetachment of H^-

Photodetachment of H^- received some attention at the 1977 Symposium, and the cross section was given in Ref. 1. The reason for significant interest is that very high neutralization efficiencies are conceivable in a very clean environment employing laser photodetachment.[53] The huge resonances in photodetachment cross section near 10 eV (1200 Å)[54,55] photon energy may even be accessible with new lasers, but the broad maximum in photodetachment in the easily accessible 6000-10 000 Å range is still the obvious choice for a photodetachment neutralizer.

IV. Summary

The atomic collisions data needed to understand double capture production of H^- in beams and for neutralization of H^- beams are reasonably complete. A small portion of these data have been shown here, and more will be presented in other papers. On the other hand, the atomic collisions data for understanding of gas discharge production of H^- seem much less complete in spite of stimulating recent work. To the extent that collisions data can help suggest ways to optimize discharge production of $H^-(D^-)$ and because of parallel application, for example for plasma divertors, it seems highly desirable to extend these data. The roles of vibrational, rotational, and even electronic excitation of molecules and the understanding of molecular negative ions seem quite pertinent to the $H^-(D^-)$ production. The role of H_3^+ and H_3 molecules in formation of H^- is not well characterized and is important because of large cross sections and high density of H_3^+ in low temperature discharges.

References

1. D. H. Crandall and C. F. Barnett, Proc. of the Symp. on the Production and Neutralization of Negative Hydrogen Ions and Beams, 1977, K. Prelec, Editor (Brookhaven National Laboratory, 1977), pp. 3-10.

2. A. S. Schlachter, Proc. of the Symp. on the Production and Neutralization of Negative Hydrogen Ions and Beams, 1977, K. Prelec, Editor (Brookhaven National Laboratory, 1977), pp. 11-23.

3. Second Technical Meeting on Atomic and Molecular Data for Fusion, Report of the Committee and A & M Data Needs, Fontenay-aux-Roses, France, May 1980 (to be published in Physica Scripta).

4. D. S. Walton, B. Peart, and K. T. Dolder, J. Phys. B 4, 1343 (1971).

5. B. Peart and K. T. Dolder, J. Phys. B 8, 1570 (1975).

6. G. J. Schulz and R. K. Asundi, Phys. Rev. 158, 25 (1967).

7. M. Allan and S. F. Wong, Phys. Rev. Lett. 41, 1791 (1978).

8. J. M. Wadehra and J. N. Bardsley, Phys. Rev. Lett. 41, 1795 (1978).

9. J.C.Y. Chen and J. L. Peacher, Phys. Rev. 163, 103 (1967).

10. D. Spence and G. J. Schulz, J. Chem. Phys. 54, 5424 (1971).

11. M. Bacal and G. W. Hamilton, Phys. Rev. Lett. 42, 1538 (1979).

12. A. Huetz, F. Gresteau, R. I. Hall, and J. Mazeau, J. Chem. Phys. 72, 5297 (1980).

13. I. M. Beterov, N. V. Fateev, and V. P. Chebotaev, Sov. Tech. Phys. Lett. 5, 500 (1979).

14. J. R. Hiskes, Lawrence Livermore Laboratory Report UCRL-82889 (1979). Also see J. Phys. (Paris) Colloq. Vol. C7, Part II, 179 (1979).

15. M. Bacal, E. Nicolopoulou, and H. J. Doucet, Proc. of the Symp. on the Production and Neutralization of Negative Hydrogen Ions and Beams, 1977, K. Prelec, Editor (Brookhaven National Laboratory, 1977), pp. 26-34.

16. R. H. Neynaber and S. M. Trujillo, Phys. Rev. 167, 63 (1968).

17. A. B. Lees and P. K. Rol, J. Chem. Phys. 61, 444 (1974).

18. B. Peart, R. A. Forrest, and K. T. Dolder, J. Phys. B 12, 3441 (1979).

19. K. C. Kulander and M. F. Guest, J. Phys. B 12, L501 (1979).

20. M. Vogler, Phys. Rev. A 19, 1 (1979).

21. M. T. Leu, M. A. Biondi, and R. Johnsen, Phys. Rev. A 8, 413 (1973).

22. B. Peart and K. T. Dolder, J. Phys. B 7, 1948 (1974).

23. D. Auerbach, R. Cacak, R. Caudano, T. D. Gaily, C. J. Keyser, J. Wm. McGowan, J.B.A. Mitchell, and S.F.J. Wilk, J. Phys. B 10, 3797 (1977).

24. D. Mathur, S. U. Khan, and J. B. Hasted, J. Phys. B 11, 3615 (1978).

25. J. N. Bardsley, "Molecular Resonance Phenomena," Electron Molecule and Photon-Molecule Collisions, T. Rescigno, V. McKoy, and B. Schneider, Editors (Plenum Press, New York, 1979), p. 275.

26. H. S. Taylor and J. K. Williams, J. Chem. Phys. 42, 4063 (1965).

27. W. Aberth, R. Schnitzer, and M. Anbar, Phys. Rev. Lett. 34, 1600 (1975).

28. R. Schnitzer and M. Anbar, J. Chem. Phys. 65, 1117 (1976).

29. R. Schnitzer, R. W. Odom, and M. Anbar, J. Chem. Phys. 68, 1489 (1978).

30. F. C. Fehsenfeld, C. J. Howard, and E. E. Ferguson, J. Chem. Phys. 58, 5841 (1973).

31. A. Catherinot, B. Dubreuil, and M. Gand, Phys. Rev. A 18, 1097 (1978).

32. J. T. Moseley, R. E. Olson, and J. R. Peterson, Case Studies in Atomic Physics V, (North-Holland Publishing Company, Amsterdam, Oxford, and New York, 1975), p. 35.

33. J. T. Moseley, W. Aberth, and J. R. Peterson, Phys. Rev. Lett. 24, 435 (1970).

34. R. D. Rundel, R. L. Aitken, and M.F.A. Harrison, J. Phys. B 2, 954 (1969).

35. D. R. Bates and J. T. Lewis, Proc. Phys. Soc. (London) A 68, 173 (1955).

36. A. Dalgarno, G. A. Victor, and P. Blanchard, Air Force Cambridge Research Laboratory Report 71-0342.

37. R. E. Olson, J. R. Peterson, and J. T. Moseley, J. Chem. Phys. 53, 3391 (1970).

38. B. Peart, R. Grey, and K. T. Dolder, J. Phys. B 9, L369 (1976).

39. G. Poulaert, F. Brouillard, W. Claeys, P. Defrance, J. Wm. McGowan, and G. Van Wassenhoue, J. Phys. B 11, L671 (1978).

40. G. Poulaert, F. Brouillard, W. Claeys, P. Defrance, and J. Wm. McGowan, Proc. XIth Int. Conf. on Physics of Electronic and Atomic Collisions, (Kyoto, Japan, 1979), p. 876.

41. J. S. Risley, Electronic and Atomic Collisions, Invited Papers and Progress Reports of the XIth Int. Conf. on Physics of Electronic and Atomic Collisions, N. Oda and K. Takayanagi, Editors (North-Holland Publishing Company, Amsterdam, Oxford, and New York, 1980), pp. 619-633.

42. C. J. Anderson, R. J. Girnius, A. M. Howald, and L. W. Anderson, Phys. Rev. A 22, 822 (1980).

43. V. A. Esaulov and V. N. Tuan, Proc. XIth Int. Conf. on Physics of Electronic and Atomic Collisions, (Kyoto, Japan, 1979), p. 615; private communication (1980).

44. R. E. Olson and B. Liu, J. Chem. Phys. 73 (scheduled for October 1980).

45. A. S. Schlachter, R. K. Stadler, and J. W. Stearns, Proc. XIth Int. Conf. on Physics of Electronic and Atomic Collisions, (Kyoto, Japan, 1979), p. 526. Also Lawrence Berkeley Laboratory Report LBL-10255 (1980) and accepted for publication in Phys. Rev. A.

46. F. W. Meyer, J. Phys. B 13 (scheduled for October 1980).

47. R. E. Olson, Phys. Lett. 77A, 143 (1980).

48. T. E. Leslie, K. P. Sarver, and L. W. Anderson, Phys. Rev. A 4, 408 (1971).

49. A. M. Karo, M. A. Gardner, and J. R. Hiskes, J. Chem. Phys. 68, 1942 (1980).

50. T. Nagata, J. Phys. Soc. Jpn. 48 (scheduled for No. 6, October 1980).

51. T. J. Morgan, J. Stone, M. Mayo, and J. Kurose, Phys. Rev. A 20, 54 (1979).

52. W. Aberle, J. Grosser, and W. Krüger, J. Phys. B 13, 2083 (1980).

53. J. H. Fink and G. W. Hamilton, Proc. of the Symp. on the Production and Neutralization of Negative Hydrogen Ions and Beams, 1977, K. Prelec, Editor (Brookhaven National Laboratory, 1977), p. 185.

54. H. C. Bryant, D. B. Dieterle, J. Donahue, H. Sarifian, H. Tootoonchi, D. M. Wolfe, P.A.M. Gram, and M. A. Yates-Williams, Phys. Rev. Lett. 38, 228 (1977).

55. H. C. Bryant, Electronic and Atomic Collisions, Invited Papers and Progress Reports of the XIth Int. Conf. on Physics of Electronic and Atomic Collisions, N. Oda and K. Takayanagi, Editors (North-Holland Publishing Company, Amsterdam, Oxford, and New York, 1980), p. 145.

DISCUSSION

HOOPER Just a quick comment on your statement about the possibility of making H_2 vibrationally excited by collisions between H^- and H_3. Of course you need H^- present to do that or you would not get it into the H_2 vibrational state. However, if the cross-sections work out right, there is a potential for an effective instability. A very small amount of H^- could cause it to run away and end up with a substantial amount in a final state, whereas if the cross-sections were wrong it could go the other way and you would always have just a very low level of the H^-. If someone is serious about looking at that process I think very careful measurements of the cross-section would be essential in order to determine whether it is an important effect or not.

CRANDALL It is not really desirable to have the H^- go away that way, is it?

THE PRODUCTION AND DESTRUCTION OF H^- AND D^- IONS IN HYDROGEN OR DEUTERIUM PLASMAS*

J. N. Bardsley
Physics Department, University of Pittsburgh
Pittsburgh, Pennsylvania

Abstract

This paper reviews the status of calculations of the cross sections for processes which may lead to the production or destruction of H^- (or D^-) in hydrogen plasmas. Particular attention is given to the collisions involving vibrationally excited H_2 molecules.

I. Introduction

Recent experiments by Bacal and coworkers[1] have shown that in hydrogen plasmas, at pressures between 10^{-3} Torr and 10^{-2} Torr and positive-ion densities around 10^{10} cm^{-3}, over 10% of the negative charge can reside on H^- ions. Such large negative ion fractions were initially very surprising in view of the very small cross sections for H^- production in reactions involving ground state species. The non-linear dependence of the H^- density upon the total ion density suggests that the H^- is formed through collisions of two charged particles, or of one charged particle with an excited neutral atom or molecule. These results can perhaps be understood in terms of electron collisions with vibrationally excited H_2 molecules. The experimental and theoretical work pertaining to dissociative attachment to excited molecules, and vibrational excitation in e-H_2 collisions will be discussed in section II. Other processes involving electron-impact dissociation of hydrogen molecules will be reviewed briefly in section III.

Dissociative attachment can be regarded as a resonant scattering process, in that it involves the formation and decay of a compound negative ion state

$$e + H_2 \rightarrow H_2^- \rightarrow H + H^- \qquad (1)$$

It is still unclear as to what extent the reverse process of electron detachment can be described by a similar theory. It seems clear that at low energies (below 0.75 eV) associative detachment

$$H + H^- \rightarrow H_2^- \rightarrow H_2 + e \qquad (2)$$

will lead predominantly to molecules in high vibrational levels. At higher energies the detached electron will emerge with relatively little kinetic energy and the dominant process should be

$$H + H^- \rightarrow H_2^- \rightarrow H + H + e \qquad (3)$$

The application of resonant scattering theories to the processes (2) and (3) will be described in section IV, in which we survey the detachment processes that are important in hydrogen plasmas. Electron detachment in collisions of H^- with other atoms will be reviewed by other speakers at this symposium.

II. Dissociative Attachment to Vibrationally Excited H_2 and D_2

It has long been suspected that the cross section for dissociative attachment in low-energy electron-molecule collisions might be sensitive to the initial vibrational state of the molecule. Henderson et al.[5] demonstrated that this effect could be seen in O_2 simply by heating the oxygen gas to around 2000°K. Their results were interpreted in terms of resonant scattering theory by O'Malley[6]. A similar effect was expected in H_2 and Chen and Peacher[7] also predicted a significant dependence of the attachment cross section upon the rotational state, due to centrifugal stretching in the molecule. However Spence and Schulz[8] saw no clear increase in the attachment cross section when they heated hydrogen gas to 1300 K. However their experiment was performed at a fixed electron energy.

In 1978 Allan and Wong[9] performed a more comprehensive study of the temperature dependence of attachment in H_2 and D_2. The threshold for attachment to ground state H_2 molecules is at 3.72 eV. However as the temperature of the gas was raised from 300 K to 1600 K attachment was observed with electrons of much lower energy. Since theory suggests that the cross section for each vibrational or rotational state peaks close to threshold Allan and Wong were able to deduce the threshold values of the attachment cross section for several vibrational and rotational levels. A theoretical study was performed[11], independently, using a resonant scattering model with resonance parameters chosen to fit the previously obtained experimental data on collisions with ground state H_2 and D_2 molecules. This study provided more complete information on the cross sections and confirmed that the threshold cross section rises by a factor of more than 10^4 as the vibrational quantum number is increased from 0 to 4 in H_2. The increase is even larger in D_2 and the large isotope effect seen for low values of v disappears for high v. Thus attachment to high vibrational levels of H_2 and D_2, producing H^- or D^-, is very efficient, as shown by the attachment rates calculated by Wadehra[12].

The cross section for dissociative attachment can qualitatively be written as a product of a capture cross section $\sigma_{cap}(\varepsilon)$, which describes the formation of the H_2^- ion, and a survival factor $S(\varepsilon)$, which gives the probability that the molecular ion will dissociate without the emission of the extra electron. Near threshold the process occurs predominantly through the lower $^2\Sigma_u$ state of H_2^-, which becomes stable against electron emission for $R > R_{SI}$ (equal to 2.9 a_o). The initial capture of the electron can be regarded within the Born-Oppenheimer picture

to occur instantaneously with little change in the position or momentum of the nuclei. An incident electron of given energy ε can therefore be accepted only near the point where the difference between the potential curves for H_2 and H_2^- is equal to ε. Low energy electrons can be captured near the stabilization point R_{su} and the survival factor is then large. On the other hand if the electrons are captured at smaller R the competition from autodetachment is severe and the survival factor becomes very small. Hence the magnitude of the dissociative capture rate is determined mainly by the probability that the nuclei are close to the stabilization point R_{su}. This is small for ground state molecules, since R_{su} is well outside the range of the zero-point motion. Only relatively fast electrons can be captured and these soon become detached from the H_2^- molecule. For highly excited vibrational states the nuclear motion extends past R_{su}. The capture of very slow electrons is then possible and very little further stretching of the molecule is required for stabilization of the negative ion. In general the slower motion of the nuclei in D_2, as compared with H_2, leads to increased competition from autodetachment and thus to smaller values for $S(\varepsilon)$ and $\sigma_{DA}(\varepsilon)$. However for low energy collisions with highly excited molecules $S(\varepsilon)$ is close to 1 and this effect is small.

Given that vibrational excitation of H_2 can result in a large increase in the attachment rate, one must study the processes leading to vibrational excitation and de-excitation. Experimental[13-15] and theoretical[11,16] data on electron-impact excitation suggest that the cross sections for inelastic collisions in which $\Delta v = 1$ are large ($\sim 10^{-16}$ cm^2) whereas those for $\Delta v > 1$ are considerably smaller. Bailey and Garscadden have examined the extent to which the molecules can be excited to high vibrational levels through electron excitation of the v = 1 levels followed by vibrational energy transfer e.g.

$$e + H_2(v = 0) \rightarrow H_2(v = 1) + e \qquad (4a)$$

$$H_2(v = 1) + H_2(v = 1) \rightarrow H_2(v = 2) + H_2(v = 0) \qquad (4b)$$

An interesting alternative scheme, suggested by W. Kunkel, has been examined by Hiskes[17]. Electrons with energy greater than $\sim$ 12 eV can produce electronic excitation in the H_2 or D_2 molecules, e.g. to the B $^1\Sigma_u^+$ of C $^1\Pi_u$ states. These states will decay radiatively with the electrons returning to the ground electronic state. However the probability that the nuclei will return to the ground vibrational level is very small. For example, for the B $^1\Sigma_u^+$ state, only 8% of radiative decays lead to the level with v = 0, and the remaining 92% is distributed almost equally between the fourteen excited vibrational levels. For incident electron energies around 100 eV, the effective cross section for the production of H_2 states with $v \geq 5$ is $\sim 3 \times 10^{-17}$ cm^2.

The greatest uncertainty in this scheme for H^- production is in the effect of wall collisions upon the vibrational excitation of the H_2 molecules. Theoretical or experimental study of these effects would be valuable.

III. Further Dissociative Processes Leading to Negative Ions

An alternative two-step process that might explain the volume production of H^- ions involves attachment to the metastable C $^3\Pi_u$ state of H_2.

$$e + H_2(X\ ^1\Sigma_g) \rightarrow H_2(C^3\Pi_u) + e \qquad (5a)$$

$$e + H_2(C\ ^3\Pi_u) \rightarrow H + H^- \qquad (5b)$$

Bottcher and Buckley[18] estimate the cross section for the second step (5b) to be $\sim 10^{-18}$ cm^2. For electron densities of $\sim 10^{10}$ cm^{-3} the probability that a metastable molecule will capture an electron would then be only $\sim 10^{-4}$. Unless this estimate of the cross section is much too small, it seems unlikely that this process is important in the H^- sources.

The cross section for ion-pair production in e-H_2 collisions,

$$e + H_2 \rightarrow H^+ + H^- + e \qquad (6)$$

is of order 10^{-20} at energies between 15 and 25 eV[19,20]. Although the cross section rises with increasing energy it is unlikely that it will exceed $\sim 10^{-19}$ at any energy.

H^- ions can also be produced in the dissociative recombination reactions

$$e + H_2^+ \rightarrow H^+ + H^- \qquad (7a)$$

$$e + H_3^+ \rightarrow H_2^+ + H^- \qquad (7b)$$

Experiments[21,22] show that the cross section for process (7a) decreases from 5×10^{-18} cm^2 at 0.4 eV to 1×10^{-18} cm^2 at 4 eV, whereas that for process (7b) peaks at $\sim$ 8 eV and never exceeds 2×10^{-18} cm^2.

For a complete understanding of hydrogen plasmas we need more information about many other processes such as

$$e + H_2 \rightarrow H + H + e \qquad (8)$$

$$e + H_2^+ \rightarrow H + H^* \qquad (9)$$

Although experimental data is available on many of the important reactions, the experiments are often difficult and sometimes involve gases with the molecules in many different initial states. Experimental and theoretical methods are being developed slowly and during the next few years we should obtain much more detailed information about reactions with molecules in specific initial states, both for the ground state and

long-lived excited states.

IV. Electron Detachment From H^- in Hydrogen Plasmas

Low energy collisions between H^- ions and H atoms can also be interpreted in terms of the formation of autodetaching states of H_2^-. In collisions involving H^- and H in their ground states, two electronic states of H_2^- can be formed. The ground, $^2\Sigma_u$, state is unstable against electron emission for $R \lesssim 2.9\ a_o$, whereas the first excited, $^2\Sigma_g$, state is unstable for $R \lesssim 5.3\ a_o$. The potential curve for the latter state is repulsive except for the long-range polarization interaction.

When the energy of relative motion is less than 0.75 eV, the only allowed process is associative detachment

$$H + H^- \rightarrow H_2(v) + e \qquad (10)$$

Using resonant scattering theory Browne and Dalgarno were able to show that the thermal rate for detachment should be close to 2×10^{-9} $cm^3\ s^{-1}$ for temperatures below 10 K, rising to $\sim 5 \times 10^{-9}$ $cm^3\ s^{-1}$ at 3×10^4 K. This result is consistent with the value of 1.8×10^{-9} $cm^3\ s^{-1}$, measured at room temperature by Fehsenfeld et al.[24]

Autodetachment from the two H_2^- states is so rapid that most of the electrons will be emitted while the nuclear separation is close to the points, R_{sg} and R_{su}, at which the H_2 and H_2^- curves cross. Following the Born-Oppenheimer principal, the electrons will emerge with very little kinetic energy, and most of the H_2 molecules that are formed will be in high vibrational and rotational levels[25]. Reattachment of electrons to these molecules will then be likely unless this internal energy is removed rapidly.

These arguments also suggest that at energies between 1 eV and 10^3 eV the total cross section for electron detachment should be close to

$$\sigma \approx \frac{1}{2}\pi(R_{sg}^2 + R_{su}^2) = 1.6 \times 10^{-15}\ cm^2 \qquad (11)$$

The measurement of absolute cross sections for this reaction is not easy, because of the difficulty of determining the density of H atoms, but the experiments[26,27] suggest that the cross section has a broad peak with a maximum value of 16 $Å^2$ at a relative energy near 250 eV. For higher energy, Born approximation calculations have been made by Bell et al[28].

Risley and Geballe[29,30] observed the cross section for electron production in $H^- + H_2$ collisions to rise from 7 $Å^2$ at a laboratory energy of 250 eV, peaking at 13 $Å^2$ near 4 keV. Almost identical cross sections were obtained for $H^- + H_2$ and $D^- + H_2$ collisions when compared at the same energy of relative motion.

As was shown in the preceding paper by Crandall and Meyer, the mutual neutralization process

$$H^+ + H^- \rightarrow H(1s) + H(n\ell) \qquad (12)$$

has a large cross section which decreases monotonically for relative energies below 10 eV. It is believed that in this energy range one of the atoms is left in a state with n = 3. Between 10 eV and 100 eV, the cross section rises from 1.0×10^{-14} cm^2 to $\sim 2.5 \times 10^{-14}$ cm^2. It then decreases again at higher energies. The existence of this peak has been attributed to the formation of states with n = 2.

For electron impact detachment from H^- both theory[31] and experiment[32] predict cross sections that peak near 15 eV with a maximum value of $\sim 4 \times 10^{-15}$ cm^2. However the structure that is seen in the experimental data near 17 eV is still a matter of theoretical debate. The cross section for double-detachment by electron impact peaks at 5×10^{-17} cm^2 around 50 eV.

V. Concluding Remarks

We have seen that the rates for some important reactions involving molecules are very sensitive to the amount of internal excitation energy contained in the molecules. One then must perform more detailed measurements or calculations which are time-consuming and expensive. Furthermore one needs to understand the many process that affect the internal energy content of the molecules. Thus it is important to the academic community to learn the extent to which molecular processes are important in H^- ion sources, so that the necessary experiments or calculations can be identified and planned.

References

1. E. Nicolopoulou, M. Bacal and H. J. Doucet, J. Phys. (Paris) 38, 1399 (1979).

2. M. Bacal, E. Nicolopoulou and H. J. Doucet, Proc. of the Symp. on the Production and Neutralization of Negative Hydrogen Ions and Beams, K. Pralec, Ed, (Brookhaven National Laboratory, 1977) pp. 26-34.

3. M. Bacal and G. W. Hamilton, Phys. Rev. Lett. 42, 1538 (1979).

4. M. Bacal, A. M. Bruneteau, W. G. Graham, G. W. Hamilton and M. Nachman, to be published (1980).

5. W. R. Henderson, W. L. Fite and R. T. Brackmann, Phys. Rev. 183, 157 (1969).

6. T. F. O'Malley, Phys. Rev. 155, 59 (1967).

7. J.C.Y. Chen and J. L. Peacher, Phys. Rev. 163, 103 (1967).

8. D. Spence and G. J. Schulz, J. Chem. Phys. 54, 5424 (1971).

9. M. Allen and S. F. Wong, Phys. Rev. Lett. 41, 1791 (1978).

10. J. M. Wadehra and J. N. Bardsley, Phys. Rev. Lett. 41. 1795 (1978).

11. J. N. Bardsley and J. M. Wadehra, Phys. Rev. A 20, 1398 (1979).

12. J. M. Wadehra, Appl. Phys. Lett. 35, 917 (1979).

13. H. Ehrhardt, L. Langhans, F. Linder and H. S. Taylor, Phys. Rev. 173, 222 (1968).

14. F. Linder and H. Schmidt, Z. Naturf. 26a, 1603 (1971).

15. R. W. Crompton, D. K. Gibson and A. I. McIntosh, Aust. J. Phys. 22, 715 (1969).

16. A. Klonover and V. Kaldor, J. Phys. B 12, 323, 3796 (1979).

17. J. R. Hiskes, J. Appl. Phys. 51, 4592 (1980).

18. C. Bottcher and B. D. Buckley, J. Phys. B 12, L497 (1979).

19. G. J. Schulz, Phys. Rev. 113, 816 (1959).

20. D. Rapp, T. E. Sharp and D. D. Briglia, Phys. Rev. Lett. 14, 533 (1965).

21. B. Peart and K. Dolder, J. Phys. B 8. 1570 (1975).

22. B. Peart, R. A. Forrest and K. Dolder, J. Phys. B 12, 3441 (1979).

23. J. C. Browne and A. Dalgarno, J. Phys. B 2, 885 (1969).

24. F. C. Fehsenfeld, C. J. Howard and E. E. Ferguson, J. Chem. Phys. 58, 5841 (1973).

25. R. J. Bieniek and A. Dalgarno, Astrophys. J. 228, 635 (1979).

26. D. G. Hummer, R. F. Stebbings, W. L. Fite and L. M. Branscomb, Phys. Rev. 119, 668 (1960).

27. V. Esaulov, J. Phys. B, in press (1980).

28. K. L. Bell, A. E. Kingston and P. J. Madden, J. Phys. B 11, 3357 (1976).

29. J. S. Risley and R. Geballe, Phys. Rev. A 9, 2485 (1974).

30. J. S. Risley, Phys. Rev. A 10, 731 (1974).

31. F.H.M. Faisal and A. K. Bhatia, Phys. Rev. A 5, 2144 (1972).

32. B. Peart, D. S. Walton and K. T. Dolder, J. Phys. 3, 1346 (1970).

33. B. Peart, D. S. Walton and K. T. Dolder, J. Phys. B 4, 88 (1971).

*Research sponsored by the National Science Foundation through grant PHY-79-00957 and by the Office of Naval Research under contract N001-48-OC-023.

DISCUSSION

HISKES Is it possible to extend these V-V' excitation cross-sections down to near threshold like 0.5 or 0.8 volt?

BARDSLEY It is possible to do that. Our calculations of vibrational excitation were based on a resonance scattering model whose validity becomes more in question at low energies, but we can at least insure that our theory has the right threshold behavior. However, there have been calculations by Cloniver and Caldor which should be more reliable and maybe that is the better way to go. Unfortunately they give their results only to a discrete set of points and not very many in the low energy region. But, I would suggest that the Cloniver and Caldor method would be the method that I would prefer, but if they can not get it, then we could. But our calculations are semi-empirical; they involve the supposition of a resonant state with properties that we get from experimental fitting to experimental data.

BACAL I want to know if it is possible to calculate the branching ratio for producing H_2 vibrationally excited molecules from dissociative recombination of H_3^+?

BARDSLEY As far as I know there are two people that are working on H_3^+ recombination and trying to do such calculations; one is Michels at United Technologies the other is Kulander at LLL. However, I should point out that as far as I know, no one has reliably calculated or measured branching ratios for $e\text{-}H_2^+$ recombination. So, if calculations are produced, then one should retain a healthy skepticism when they come out, but I think that is a very useful calculation to try.

CRANDALL In 1977 we discussed the possibility of actual electronic excitation of molecules, particularly H_2^+ in the plasma and whether or not that could have any effect. I think that there is some recent observations that neutral H_2 excited states do exist in some quantity in low temperature discharges. Do you have any thoughts about that? Has anybody done any work on real electronic excitation in the plasma and what its effect might be?

BARDSLEY Calculations are beginning to be done. In the last few years, there has been one published calculation of electronic excitation in H_2 and people are systematically developing the computer programs necessary for doing this routinely. I think it will be a matter of two years before these programs are ready. Certainly vibrational excitation of H_2^+ by electron impact is something that can be done now. Excitation of the triplet state of H_2 has been done. Electronic excitation of H_2^+ to the repulsive state, I am sure should be fairly easy. But for anything more than that, things might be a little tough to do. Now I am thinking of calculations near threshold at which the Born approximation is not valid. For calculations of higher energy, where you can use the Born approximation, there have been calculations, and I think, say from 50 or 100 volts up, we are in a better situation. But for calculations near threshold we are just starting to get some results.

CRANDALL If an electron collides with an excited H_2 is that a likely way to make a negative ion?

BARDSLEY No.

CRANDALL Compared by vibrational excitation you just described?

BARDSLEY No.

BACAL Would you comment on the production of vibrationally excited molecules via excitation of molecules by fast electrons going to single states and decay by emission of the photon? There was some recent work on that.

BARDSLEY I would not comment on that, except to thank you for reminding me that I left this out. John Hiskes has been recently looking at the excitation of vibrational motion in H_2 by two step processing which should first of all excite H_2 to an excited electronic state which then decays radiatively down to the ground state and I am sure John would be able to tell everyone about his results. The reference to that would be in the written paper.

HISKES Recently we calculated the excitation cross-section from the ground state of the molecule to some higher vibrational state and the cross-sections appear to be in the range of 10^{-18} to 10^{-17} cm^2. It looks like this may be an interesting part for interpretation of the experiment at École Polytechnique. But I would not say anymore about that at this time.

GRAHAM At the higher plasma densities the neutralization process becomes very important in these plasmas and Crandall pointed out that experimentally it seems difficult to measure neutralization with H_3^+. Can the theorists help us with that problem?

BARDSLEY Use the same as for H_2^+. I could spend 6 or 8 months and ask Phil Stone for the money to do it but I am not sure that the theorists give you in a short time a better answer than saying that H_3^+ is a little bit more complicated than H_2^+. It should be slightly easier to absorb the nuclear motion so the cross-section maybe slightly bigger. But the cross-section for neutralization to small atoms and small molecules do not change very much. If you want an upper limit then you can use Olson's absorbing sphere model; maybe Olson would have a better answer to this question than I just did.

OLSON We get 10^{-6} for the reaction rate at thermal energy. We can not do much better than that theoretically. We just spent two years on it and we are still out by a factor of two.

CRANDALL Just a comment about that sort of behavior. If you have a minus and a plus reacting, the cross-section always goes up as you go down in energy. You can argue the fine points, but in terms of the total cross-section you can get an idea of what its behavior is. I think the most interesting question about that cross-section might be whether or not you get final vibrational excitation.

BARDSLEY That is right.

JACQUOT Have you any measurements on the mutual neutralization cross-sections $Cs^+ + H^-$?

BARDSLEY Yes, I am sure there are, Ron?

OLSON I think we calculated those in '76. They flatten out at about 10^{-14} and then they go up (as 1/E) towards lower energies; but I think the number you want is about 10^{-14}. I think Yanev also calculated that in '79 and their numbers are about the same: 10^{-14} for the cross-section at reasonable energies, being 100 eV to 1 keV. It goes fast, it goes into excited states of the cesium.

JACQUOT Can you repeat the reference?

OLSON There is one, Olson et al, '76 Phys. Rev. A and Janev et al., Phys. Rev. A, 1979 or that vintage.

FORMATION OF H^- AND D^- IONS BY PARTICLE BACKSCATTERING FROM ALKALI/TRANSITION METAL COMPLEXES*

J. R. Hiskes
Lawrence Livermore National Laboratory, University of California
Livermore, California 94550

P. J. Schneider†
Lawrence Berkeley Laboratory, University of California
Berkeley, California 94720

Abstract

The data for negative ion reflection yields is analyzed using a backscattering model for the secondary emission coefficient. The enhancement of the secondary emission coefficient is discussed in terms of reflection, formation, and survival probabilities. The yield of negative ions from alkali/transition metal surfaces by low energy atoms emitted from the ion-source discharge is calculated. Volume production of negative ions generated by plasma-surface interactions in a low-work-function-surface bucket-discharge is discussed.

I. Introduction

The central theme of this paper is the generation of negative ions by hydrogen particles reflecting from surfaces. The early observations of negative ions produced by hydrogen molecular ions incident on nickel surfaces have been reviewed by Massey.[1] New evidence is accumulating for surface-ion production in ion-source discharges,[2,3] evidence which is supported by a growing body of surface backscattering data.[4,5,6] On the astrophysical scale, the negative ion composition of planetary and lunar ionospheres is thought to be sustained by continuous particle bombardment and reflection from the planetary surfaces.[7,8] The presence of negative ions in cometary atmospheres may also have their origin in particle backscattering processes.[9] It would seem that the full scope of these different phenomena is still only lightly perceived, and reflection yields may provide a new paradigm for a variety of diverse and novel phenomena.

We shall be concerned with the formation of H^- and D^- as caused by hydrogen and deuterium particles backscattering from alkali metals and alkali/transition metal complexes. The main thrust of this presentation is directed towards the explication and enhancement of negative ion yields from ion source plasma-surface interactions. The range of incident particle energies of interest here extends from the threshold incident energy, E_{TH}, given by the difference of the surface work function and the negative ion affinity,[10] $E_{TH} = \phi - A$, upwards to incident energies of order one keV. The experimental data on reflection yields is used in conjunction with a theoretical model for the negative-ion-secondary-emission-coefficient, NISEC, which is used both for the interpretation of the data and as a basis for extrapolating the negative ion yields down to incident energies near the threshold region. In this paper the terms reflection and backscattering are used interchangeably.

II. NISEC

Our model for NISEC is taken to be the product of the reflected particle velocity distribution, the reflected angular distribution, the formation probability for negative ions in the near-surface region, and the survival probability of negative ions as they move to great distances away from the surface.[11-13] The functional form for the formation and survival probabilities assumes the underlying granular structure of the crystal surface can be replaced with a uniform charge distribution, in analogy with the jellium surface model,[14] and that these probabilities can be taken to be functions only of the perpendicular (normal) component of the backscattered particle velocity, $v_\perp = v \cos\theta$. The NISEC for a particle with incident energy E_i is then

$$\mathrm{NISEC}(E_i) = 2 \iint f_i(v) \cos\theta \left[1 - e^{-\frac{\alpha}{v\cos\theta}}\right] e^{-\frac{\beta}{v\cos\theta}} \, dv \, d(\cos\theta) \, . \qquad (1)$$

This expression is integrated over $\cos\theta$ to yield a single integral over the backscattered velocity,

$$\mathrm{NISEC}(E_i) = 2 \int f_i(v) \, g(\alpha, \beta, v) dv \, . \qquad (2)$$

The reflected particle velocity distributions, $f_i(v)$, are generated using the Marlowe Monte Carlo reflection code developed at Oak Ridge by the Solid State Physics Group.[15,16]

The experimental data is analyzed by inserting experimental NISEC values on the left

*Work performed under the auspices of the U.S. Department of Energy by the Lawrence Livermore National Laboratory under contract number W-7405-ENG-48.

†Present Address: Max Planck Institute for Plasma Physics, Garching, Federal Republic of Germany

hand side of Eq. (2) for several different values of incident energy, E_i, and adjusting the α, β to obtain a least-squares fit to the data. The semi-emperical values for α, β found in this way then determine the formation and survival probabilities, $1 - \exp - \alpha/v \cos\theta$, and $\exp-\beta/v \cos\theta$, respectively, that enter into the integrand of Eq. (1).

In Figure one is shown the NISEC data[6] for protons incident upon the alkalies Li, Na, K, Rb, and Cs plotted as a function of incident proton energy. The lower case letters superimposed on the data indicate the least squares fits of Eq. (1) to the experimental data for the respective alkalies. In Figure two is shown a similar set of data but for incident deuterium.

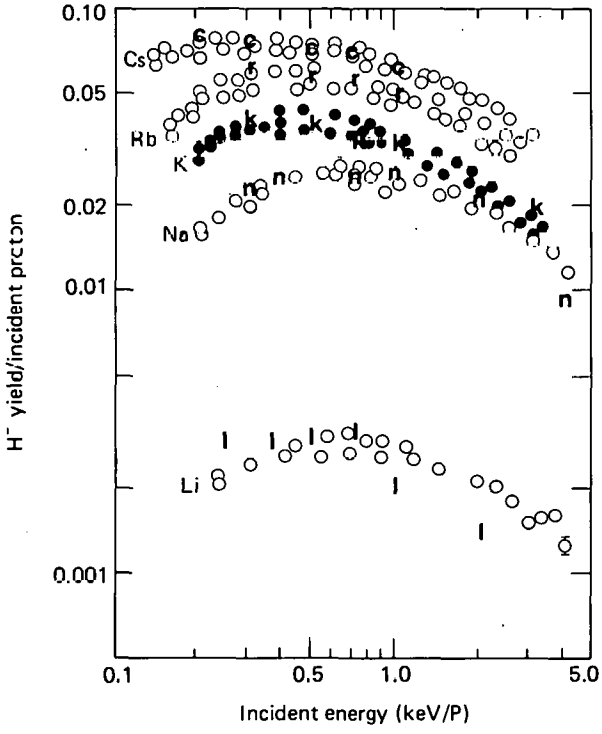

Fig. 1. NISEC vs incident proton energy.

Figure three summarizes the formation and survival probabilities plotted here as a function of the hydrogen perpendicular energy; the α, β that enter into these probabilities are taken from the least squares fits of the first two figures. The formation probabilities approach unity at low energy and decrease monotonically toward higher energies, while the survival probabilities increase toward higher energies. Note that at any particular energy the survival probability varies in an inverse way with work function, i.e., these probabilities increase from lithium through cesium. (The lithium curve has been suppressed but would lie immediately below the sodium curve.) The dashed lines are the survival probabilities for potassium and cesium calculated using a resonant electron transfer model and reported at the previous Symposium in this series.[17] The

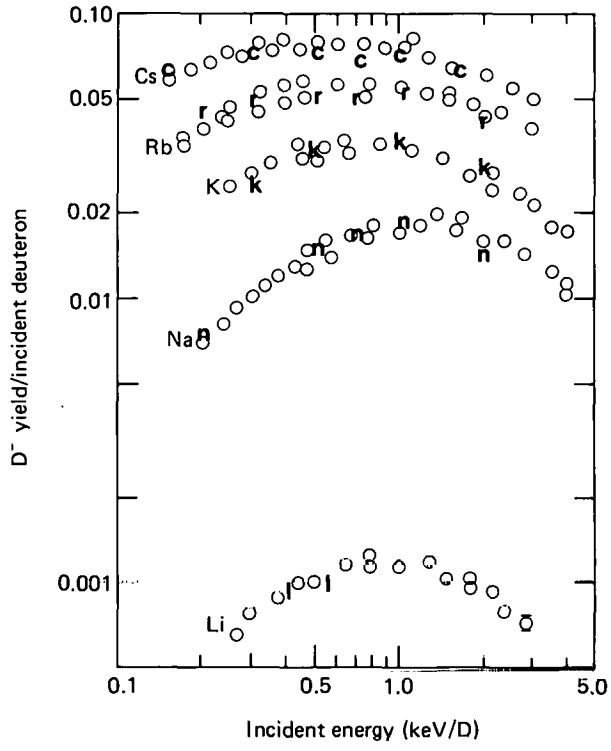

Fig. 2. NISEC vs incident deuteron energy.

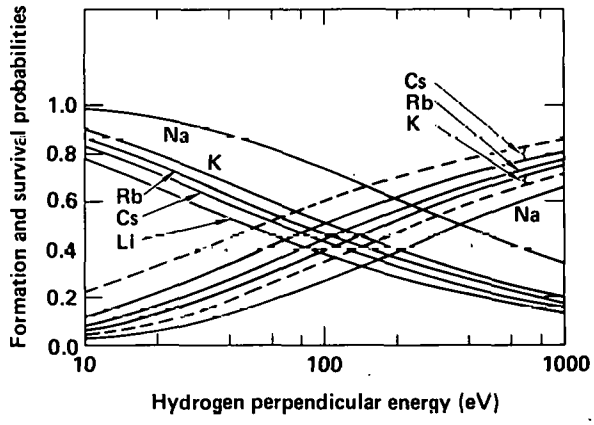

Fig. 3. Formation and survival probabilities for the alkalies.

agreement between the calculated and semi-emperical values is not precise but is sufficiently close to suggest that no essential effects have been neglected. Figure one, two, and three are taken from reference 13.

III. NISEC Enchancement

Although the alkali targets provide relatively large yields, these yields can be enhanced by reflection from alkali/transition metal complexes for which the adsorbate alkali is a partial monolayer coating chosen to give a

minimum surface work function, and the substrate chosen to give high particle reflectivity. We shall consider the NISEC to be approximated by three factors: particle reflection, formation, and survival probabilities.

The enhancement of the particle reflection coefficent for normally incident deuterium particles is discussed in reference 11. In this paper it is shown that for low-Z substrates the reflection coefficient is an increasing of function of atomic number Z up to some intermediate value, and remains roughly constant for higher Z values. For 300 eV incident deuterium the reflection coefficient varies only slightly for elements with atomic number greater than that of cesium. For lower energy 50 eV deuterium, the coefficient increases rapidly with Z, reaching an approximately asymptotic value for a nickel substrate. For nickel or higher Z substrates, the optimum substrate material can be selected independently of particle reflection considerations.

The underlying surface phenomena affecting the magnitude of the formation probability are still only partly understood. In reference 13 we present evidence to the effect that the density of occupied electronic states near the Fermi level of the surface is a relevant parameter. We have already noted that a general feature of the formation probability is to increase towards unity as the perpendicular energy component of the backscattered particles is decreased.

The survival probability at low energies is especially susceptible to enhancement by working with partial-monolayer alkali/transition metal complexes. The electric dipole layer that is formed between the adsorbate layer and the substrate inhibits the tunneling loss of the electron from the outwardly moving negative ion to the metal substrate; if the adsorbate layer is non-conducting, the survival probability that results can remain near unity for energies as low as a few electron volts.[17]

In figure four is shown the NISEC versus incident ion energy for protons incident on Cs/Cu and deuterons incident on Cs/Ni together with the deuterium-cesium data of figure two. The deuterium least-squares fits are indicated by slanted crosses, the hydrogen fits by vertical crosses. In the case of the composite layers the cesium coverage was varied to give the optimum negative ion yield shown here. Inspection of the figure shows a considerable increase in NISEC for the composite surfaces compared with cesium. Note in particular that the yield for Cs/Ni is increasing at the lower energies. Our projection using Eq. (1) shows this NISEC reaching a maximum for energies below 100 eV.

In figure five is a comparison of the survival probabilities derived from the least-squares fits of figure four. A substantial improvement in survival probability occurs at lower energies for the composite systems, but still short of the limiting theoretical expectation for a non-conducting adsorbate.

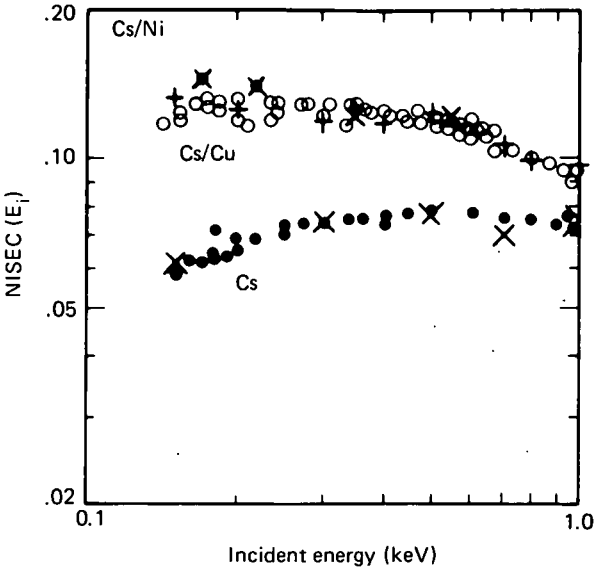

Fig. 4.

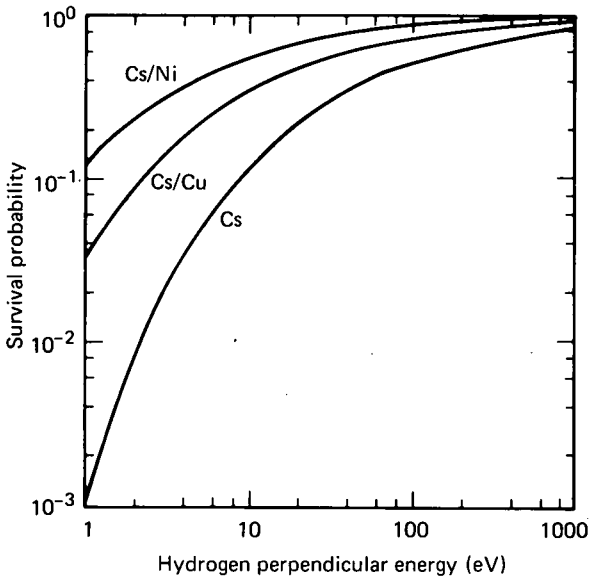

Fig. 5.

The survival probability can presumably be enhanced further by increasing the strength of the adsorbate/substrate electric dipole layer while maintaining a low minimum work function, ϕ_m. The strength of this layer is related to the change in work function, $\Delta\phi$, that is equal to the difference of the minimum composite work function, ϕ_m, and the clean substrate work function, ϕ_s. A semi-emperical relation for $\Delta\phi$ for alkali/transition metal complexes has been given by Swanson and Strayer,[18]

$$\Delta\phi = k_1(k_2 I_a - \phi_s) \quad .$$

Here k_1 and k_2 are emperically determined constants, and I_a is the ionization potential of the isolated adsorbate atom. For a particular adsorbate, e.g., cesium, $\Delta\phi$ has its largest (negative) magnitude for substrate materials with the largest work function. In Table I are listed the optimum cesium/transition metal complexes in the order of decreasing $|\Delta\phi|$ for both polycrystalline and monocrystalline substrates. The ϕ_s values are taken from the paper of Michaelson.[19] The ϕ_s and $\Delta\phi$ are in units of electron volts.

Table I

Polycrystalline				Monocrystalline		
	ϕ_s	$\lvert\Delta\phi\rvert$		Crystal Face	ϕ_s	$\lvert\Delta\phi\rvert$
Cs/Pt	5.65	4.21	Cs/Ir	111	5.76	4.33
Cs/Ir	5.27	3.79		100	5.67	4.23
				110	5.42	3.96
Cs/Ni	5.15	3.66	Cs/Re	1011	5.75	4.32
Cs/Pd	5.12	3.63	Cs/Pt	111	5.7	4.26
Cs/Au	5.1	3.61	Cs/Pd	111	5.6	4.15
Cs/Co	5.0	3.50	Cs/Au	100	5.47	4.01
Cs/Rh	4.98	3.48	Cs/Ni	111	5.35	3.88
				100	5.22	3.74
Cs/Re	4.96	3.46		110	5.04	3.54
Cs/Te	4.95	3.44	Cs/W	110	5.25	3.77
				100	4.63	3.10
Cs/Os	4.83	3.31		111	4.47	2.92
Cs/Ru	4.71	3.18	Cs/Mo	110	4.95	3.44
Cs/Cu	4.65	3.12		111	4.55	3.01
Cs/Mo	4.6	3.06		100	4.53	2.99
Cs/W	4.55	3.01	Cs/Cu	111	4.94	3.43

The polycrystalline values for ϕ_s listed here must be used with caution since these values can vary as much as 0.3 eV depending on how the substrate material is prepared. Selenium exhibits the largest known work function, 5.9 eV, but is not a transition element and is not listed here because its cesium adsorbtion properties are unknown.

In the table we have referred only to cesium adsorbates because cesium will provide the lowest values for ϕ_m. If we were selecting the adsorbate/substrate combination on the basis of $\Delta\phi$ alone, other alkali adsorbates would be interpolated among the entries.

Inspection of the table suggests that a significant increase in the survival probability over that of polycrystalline Cs/Ni may be possible, particularly for certain monocrystalline substrate crystals of Ir, Re, and Pt.

Finally, several workers have confirmed a low work function, $\phi_m = 1.1$ eV, and a large $|\Delta\phi| = 4.1$ eV for a Cs/O/W complex.[18,20,21] By further saturating with oxygen a maximum $|\Delta\phi| = 6.4$ eV can be achieved, but at the cost of increasing ϕ_m to 1.4 eV. However, the presence of oxygen in the O/W substrate is expected to reduce its reflectivity; whether or not the improved values for ϕ_m, $\Delta\phi$ can offset this reduced reflectivity in the overall NISEC is uncertain.

IV. The Fast Atom Flux

Given the prospect of relatively large survival probabilities in the low energy, 1 - 10 eV range, we consider next the backscattering yield of negative ions due to energetic atoms emanating from the discharge plasma. Negative ion production by few electron-volt atoms incident on a cesium-coated surface has been reported by Graham.[22] A low energy peak in the distribution of negative ions is reported at this Symposium in the paper by Leung and Ehlers. Some plasma and wall reactions that produce energetic atoms with energies above one electron volt are

$$e + H_2 \longrightarrow H(m\ell) + H(n\ell) + e \qquad (a)$$

$$e + H_2 \longrightarrow H(n\ell) + H^+ + 2e, \qquad (b)$$

$$H_2^+ + H_2 \longrightarrow H_3^+ + H, \qquad (c)$$

$$H_2^+ + e(\text{wall}) \longrightarrow H + H \qquad (d)$$

$$H_3^+ + e(\text{wall}) \longrightarrow H_2 + H, \qquad (e)$$

$$H_3^+ + e(\text{wall}) \longrightarrow 3H \qquad (f)$$

$$H_3^+ + H^- \longrightarrow H_2 + 2H, \qquad (g)$$

$$H_3^+ + H \longrightarrow 4H \qquad (h)$$

$$H_2^+ + H^- \longrightarrow 3H. \qquad (i)$$

The corresponding deuterium reaction rates would be quite similar to the hydrogen rates since these reactions are essentially all electronic processes.

Another source of very energetic atoms arises from the slowing down of positive ions initially accelerated through the cathode or convertor sheath and then successively reflected off the discharge walls. The particle current density of these neutrals may be of the same order-of-magnitude as the positive ion current density striking the cathode,[10,23,24] with an energy distribution extending downward from the incident positive atomic energy. The negative ions resulting from this atomic flux are not considered in this section.

Process (a) for $n = m = \ell = 1$ proceeds through the first excited $b\,{}^3\Sigma_u^+$ electronic state of the molecule[25] yielding atoms with kinetic energies of 2 - 4 eV and peaked near 2.7 eV. For $n = m = 2$ process (a) yields[26] excited atoms with kinetic energies of approximately 3.8 eV. Excitation for n = 1, m, leading to energetic atoms in the 1 - 12 eV

range have also been identified.[27] Reaction (b) proceeds mainly through the H_2^+ first excited $^2\Sigma_u^+$ state yielding an equal-energy proton-atom pair with the energy distribution of either particle peaked near 8 eV.[28,29] Process (c) yields an atom whose energy distribution is dependent upon the initial vibrational level of the ions on the right and left. The final vibrational distribution of H_3^+ is uncertain, but the atom energies will range from zero up to 3.25 eV. The corresponding H_2 channels in reactions (d) and (f), and reaction (e) have already been discussed as a means for producing vibrationally excited molecules in a discharge.[30]

In figure six is shown the fast atom energy distributions obtained for processes (a) and (b). The 2.7 distribution has been calculated using an $H_2(v = 0)$ ground state vibrational function[31] and a delta-function final state. The curves labeled 50 eV and 75 eV are measured proton distributions obtained by energetic electron collisions via process (b). Momentum and energy conservation imply similar distributions for the atomic fragments. The backscattered distribution of H^- ions obtained from the fast atom flux will be distorted from the incident distribution due to energy transfers to the crystal lattice and to the energy dependence of the survival probability. For 10 eV hydrogen particles incident on nickel or tungsten Marlowe shows the backscattered distributions peaked near 9 eV. Also shown in the figure for comparison is the backscattered distribution of H^- ions obtained using Eq. (1) for 200 eV hydrogen ions incident on cesium.

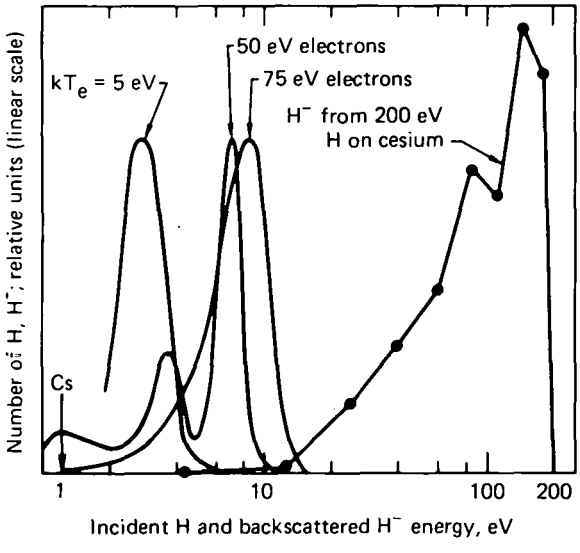

Fig. 6.

The rate of growth of the atom density in the discharge due to reaction (a) is given by

$$\frac{dn_H}{dt} = 2n_o n_e \langle\sigma v\rangle - \frac{n_H}{b}\frac{V}{L} \quad , \qquad (4)$$

where n_o and n_e are the gas and electron densities, V/L the atom collision rate with the walls, and b the number of atom wall bounces prior to H^- formation or sticking.

The fast atoms are formed in an isotropic distribution, and those with glancing collisions will have small survival probabilities. We can underestimate the yield by considering only the fraction incident within a 90° cone centered on the normal, i.e., one-eighth of the total distribution, and take the mean perpendicular energy to be one-half the incident energy for purposes of estimating the survival probability. Using the equilibrium atom density obtained from Eq. (4), we calculate the negative ion current density equal to the product of the NISEC, N, and the atomic flux onto the active connector electrode to be

$$j_- = \frac{N}{4} n_o n_e \langle\sigma v\rangle bL \quad . \qquad (5)$$

To estimate the current density we shall choose the following parameters appropriate to a high-power discharge[3]:

$kT_e = 5$ eV

$n_o = 8 \times 10^{13}$ molecules cm^{-3}

$n_e = 1 \times 10^{12}$ electrons cm^{-3}

$L = 10$ cm

$f_1 = .2$

$f_2 = .4$

$f_3 = .4$

$\overline{\sigma v}(a) = 0.5 \times 10^{-8}$

$\overline{\sigma v}(b) = 0.18 \times 10^{-8}$

$\overline{\sigma v}(c) = 0.2 \times 10^{-9}$

$b \leq 3$ such that $Nb \leq 1$

Using these parameters and Eq. (5) or its equivalent for reactions (b) and (c) we have calculated the negative ion current densities emitted from the convertor electrode for different surfaces and listed these current densities in Table II. The NISEC's have been evaluated using reflected fractions 0.55 and 0.9 for Cs and Ni, respectively,[32] and survival probabilities taken from figure four. Included is the limiting case for a survival probability near unity and NISEC = .9. For reaction (c) we have used the same NISEC's as for reaction (b). The table entries are listed in units of mA cm^{-2}.

Reaction	Cs	Cs/Ni	NISEC = .9
(a)	.75	70	160
(b)	.09	.6	1.3
(c)	.8	13.	13.

Inspection of the table shows that interesting current densities may be obtained via reaction (a). For any particular reaction it is evident that the negative ion yield will

be very sensitive to the condition of the surface coverage.

Reactions (d), (e), and (f) may provide a flux of energetic atoms larger than the equivalent ion flux onto the convertor cathode, depending on the relative area of the discharge chamber and the convertor cathode.

V. Volume Production of H^-, D^- Ions Via a Plasma Surface Cascade

In this section we shall consider the volume production of negative ions in a discharge that is confined by a magnetic bucket system with walls coated to provide a low work function, large $|\Delta\phi|$ surface. The electric potential between the plasma and wall is presumed to be a minimum to allow negative ions formed by wall reflection to join the plasma via bucket collisions and ion-ion coulomb-collisional energy deposition. The plasma is presumed to be sufficiently dense that negative ion collision rates are dominated by ion-ion collisions:

$$D^- + D^+ \longrightarrow 2D \quad , \qquad (i)$$

$$D^- + D_2^+ \longrightarrow 3D \quad , \qquad (ii)$$

$$D^- + D_3^+ \longrightarrow 4D \quad . \qquad (iii)$$

Reactions (ii) and (iii) proceed through the D_2 triplet channels, and for lack of detailed information we shall assume these couplings occur in the ratio of 3 to 1 compared with the singlet channels. Interaction potentials for reactions (i) and (ii) are available,[33,34] and (ii) will be taken as the prototype for (iii).

The first step in reaction (ii) may proceed via either of the two triplet states

$$D^- + D_2^+ \longrightarrow D_2(a^3\textstyle\sum_g^+,\ c^3\Pi_u) + D(1s) \quad , \qquad (iv)$$

and will release about 4.8 eV, 3.2 eV of which appears as D(1s) kinetic energy. The triplets formed will ultimately decay to the $D_2(b^3\textstyle\sum_u^+)$ repulsive state in times of order 10^{-8} to 10^{-5} seconds, releasing two D(1s) atoms with kinetic energies ranging up to about 3.5 eV.

If f_1, f_2, f_3 are the respective species fractions of the positive ions, $\overline{\sigma v}\,(+,-)$ is the reaction rate taken equal for each of the above reactions, the rate of growth of the atom density in the discharge is given by

$$\frac{dn_D}{dt} = n_-\left[2 + \frac{1}{4}\,f_2 + f_3\right] n_+\ \overline{\sigma v}(+,-) - \frac{n_D}{b}\,\frac{V}{L} \quad , \qquad (v)$$

where V/L is the collision rate of the atoms with the walls and b is the number of times an atom will collide with the wall before sticking to the wall or being converted to a negative ion. If G is the fraction of wall area activated for negative ion formation, N the NISEC for fast atom collisions, and $\overline{\sigma v}$ the electron collisional detachment rate, the rate of growth of the negative ion density in the discharge by negative ions returning from the wall becomes

$$\frac{dn_-}{dt} = GN\,\frac{V}{L}\,n_D - n_-\left[n_+\ \overline{\sigma v}(+,-) + n_e\ \overline{\sigma v}\right] \quad . \qquad (vi)$$

The rate Eqs. (v) and (vi) are coupled through n_-, n_D. It is easily shown that the growth of the negative ion density given by (vi) will increase exponentially provided that

$$\left[GNb\left(2 + \frac{1}{4}\,f_2 + f_3\right) - 1\right]$$

$$n_+\ \overline{\sigma v}(+,-) - n_e\ \overline{\sigma v} > 1 \quad . \qquad (vii)$$

If $kT_e \leq 3$ eV and $n_e \leq n_+$, then $n_+\ \overline{\sigma v}(+,-) \geq n_e\ \overline{\sigma v}$. In the case where the equalities hold the exponentiation conditions are the most stringent and the term in the brackets must be greater than unity. Taking as an example $f_1 = .1$, $f_2 = .4$, $f_3 = .5$, and noting that $Nb \leq$ unity, exponentiation occurs for $G > .77$ provided Nb is unity. If kT_e is less than 3 eV or n_e is less than n_+, these conditions are relaxed.

In circumstances where the exponentiation condition is met, fast atoms produced in ion-ion collisions strike the active walls and return as negative ions which in turn generate a new and larger generation of fast atoms, etc. This cascading processes will continue until the negative ion density approaches the positive ion density, at which point the cascade is interrupted by a changing plasma potential.

VI. Acknowledgments

The authors have benefited from conversations with K. W. Ehlers and K. N. Leung concerning operation of the convertor-cathode bucket-source. We also wish to acknowledge many valuable conversations with F. Burrell, C. F. Chan, and W. Cooper concerning the fast atom flux and the electron energy distribution in an ion source discharge. We are also indebted to W. G. Graham for informative discussions on surface work functions.

References

1. H.S.W. Massey, Negative Ions, Cambridge Press (1950).

2. Proc. Symp. Production and Neutralization of Negative Hydrogen Ions and Beams, Brookhaven, 1977, K. Prelec, Editor, September, 1977.

3. K.W. Ehlers and K.N. Leung, Rev. Sci. Instr. 51(6), 721 (1980).

4. H. Verbeek, W. Eckstein, and R.S. Bhattacharya, Surface Sci. 95, 380 (1980).

5. W. Eckstein, H. Verbeek, and R.S. Bhattachorya, Surface Sci. 98, (1980)

6. P.J. Schneider, K.H. Berkner, W.G. Graham, R.V. Pyle, and J.W. Stearns, Phys. Rev. B, (1980). To be published.

7. A. Wekhof, Moon and Planets 22, 185 (1980).

8. A. Wekhof, Astrophys. and Space Sci., (1980). To be published.

9. A. Wekhof, Moon and Planets, (1980). To be published.

10. J.R. Hiskes, A.M. Karo, and M.A. Gardner, J. Appl. Phys. 47, 3888 (1976).

11. J.R. Hiskes and P.J. Schneider, Int. Conf., Univ. of Bath, April (1980). To be published by the Inst. of Phys., London 1980.

12. J.R. Hiskes and P.J. Schneider, J. of Nucl. Materials (1980). To be published.

13. J.R. Hiskes and P.J. Schneider, Phys. Rev. B (1980). To be published.

14. S.C. Ying, J.R. Smith, and W. Kohn, Phys. Rev. B 11, 1483 (1975).

15. M.T. Robinson and I.M. Torrens, Phys. Rev. B 9, 5008 (1974).

16. O.S. Oen and M.T. Robinson, Nucl. Instr. and Methods 132, 647 (1976).

17. J.R. Hiskes and A.M. Karo, Proc. of Brookhaven Symp., 1977, K. Prelec, Editor, p. 42.

18. L.W. Swanson and R.W. Strayer, J. Chem. Phys. 48, 2421 (1968).

19. H.B. Michaelson, J. Appl. Phys. 48, 4729 (1977).

20. B. Gunther and F.N. Huffman, IEEE Int. Conf. Plasma Sci., Madison, 1980, Conf. Record-Abstract 4E4.

21. J.L. Desplat and C.A. Papageorgopolous, Surf. Sci. 92, 97 (1980).

22. W.G. Graham, Phys. Ltrs. 73A, 186 (1979).

23. V.G. Dudnikov and G.I. Fiksel, J. de Physique, Tome 40, Colloque C-7, Suppl. 7, Vol. I, C7-479, July (1979).

24. Y.I. Belchenko and V.G. Dudnikov, J. de Physique, Tome 40, Colloque C-7, Suppl. 7, Vol. I, C7-501, July (1979).

25. S.J.B. Corrigan, J. Chem. Phys. 43, 4381 (1965).

26. M. Misakian and J.C. Zorn, Phys. Rev. A 6, 2180 (1972).

27. A. Crowe and J.W. McConkey, Phys. Rev. Ltrs. 31, 192 (1973).

28. G.H. Dunn and L.J. Kieffer, Phys. Rev. 132, 2109 (1963).

29. R.J. Van Brunt and L.J. Kieffer, Phys. Rev. A 2, 1293 (1970).

30. M. Bacal, A.M. Bruneteau, W.G. Graham, G.W. Hamilton, and M. Nachman, J. Appl. Phys. (1980). To be published.

31. L. Wolniewicz, J. Chem. Phys. 45, 515 (1966).

32. J.R. Hiskes, J. de Physique, Tome 40, Colloque C-7, Suppl. 7, Vol. II, C7-479, July (1979).

33. J.T. Moseley, R.E. Olson, and J.R. Peterson, Case Studies In Atomic Phys. 5, 1 (1975).

34. K.C. Kulander and M.F. Guest, J. Phys. B 12, L501 (1979).

DISCUSSION

HAGENA One of the problems of surface experiments is always the proper control of the surface conditions in particular for effects where the surface conditions are strongly dependent on the properties one is interested in. So I wonder how sensitive would be, for example, your estimates of the negative ion yield for actual negative ion source conditions. For example the reflectivity. You compared it with a sponge but if you have enough water then you can not absorb any more water into a sponge and that may happen with the surface too. Similarly with the cesium coverage there seems to be a practical problem to properly control it. Do you have any estimates of what the best combination would be or is it not so dependent on the exact surface properties?

HISKES The best combination is the one that Pete Schneider has found so far, cesium on nickel. There are other possibilities and I showed you that table of 10 or so possibilities. I would hate to pick out which is the best of those 10. But, your point is well taken. The details of the surface are going to strongly influence what happens in these sources. In particular if you want to take advantage of the low energy spectrum that is extremely sensitive to the surface work functions and the condition of the surface. Whether or not one can achieve that in practice is a matter of speculation at this point.

EHLERS I am wondering if your last proposed mechanism for volume production, or should I say apparent volume production, is a possible contender for an explanation of the low energy negative ion seen in the magnetron as well as in the PIG source?

HISKES I think it is a possible contender, but until we have a demonstration that the NISEC or the work function at the surface is sufficient to give us a good survival probability, then it is just a speculation. Somebody has to demonstrate that we can get a surface which gives you a large NISEC for a few volt atoms. Bill Graham has observed negative ions produced by few volt atoms on cesium surface but I do not think he measured the NISEC. Is that correct?

GRAHAM Yes.

EHLERS Could I ask Martha Bacal if she has ever put any cesium in any of her experiments?

BACAL Not in Palaiseau, but in Berkeley we did this last year. We did not see any pleasant effect really. And I think Olson gave me some reasons why that should not be a pleasant effect by putting cesium into the plasma.

HISKES I would hope that she does not put cesium in the plasma until we understand the plasma without the cesium.

CRANDALL I am just trying to see if I understand your scenario. It sounded like you would like a nice low temperature discharge and that in fact a vibrational excitation of molecules would be beneficial.

HISKES No, there is no vibrational excitation.

CRANDALL You do not have to have it, but would it help you?

HISKES Not in the diagram I have shown here, this is just ion-ion neutralization. If you have vibrational excitation, the vibrational excitation produces negative ions by colliding with electrons and that gives you a term which is proportional to the neutral gas density times the electron density. It does not give you a term which is proportional to $n^=$. So those kinds of terms would not lead to exponential growth.

CRANDALL But those reactions you did show have to have a certain energy distribution to the neutrals...

HISKES That is right.

CRANDALL ...which is sensitive to the vibrational excitation in the molecules.

HISKES You are right. I am sorry, yes. That is a good point. These reactions here are somewhat sensitive to vibration. Not as sensitive as the others that I showed you, but there is some sensitivity here. The really important question is what is the relative coupling to the triplet and the single channels?

SCHLACHTER The figure you showed has the converter electrode in contact with a plasma and so presumably, your surface is hydrogen loaded. Does that help the possibility of desorbing hydrogen atoms from the surface that are already there?

HISKES Well, of course, it helps. The question is what is the magnitude of that effect? In the case of protons striking the surface, we did some estimates a year ago, that showed that the desorption by protons striking the surface was not competitive with the backscattered yield.

PETERSON I gather that one of the reasons that the triplets are important is because they give you a repulsive curve?

HISKES Yes, the lowest electronic state in a triplet spectrum is a repulsive state, so if you fall into these higher states, you are eventually going to get down with three atoms.

PETERSON I think that among those reactions, if you require energetic atoms for the production of D^-, then probably the second reaction is the most favorable. I think that the theory is a lot more likely to lead you to internally excited molecules.

HISKES Vibrationally excited molecules?

PETERSON Yes.

HISKES Even if they end up with a good bit of vibration the question is where do they end up on this curve? We prefer to have them make the transition on this side, so then they come apart and they will give you energetic atoms, but if they make the transition on the other part of the curve, you may be below the threshold for negative ion production. So, I think I agree with you, if you have high vibrational excitation the wave function tends to be peaked up on this side so it is more likely you will come down here and that will be a disadvantage.

POSITIVE AND NEGATIVE IONIZATION BY SCATTERING FROM SURFACES

J. Los, E.A. Overbosch and J. van Wunnik

FOM-Institute for Atomic and Molecular Physics,
Kruislaan 407, 1098 SJ Amsterdam, The Netherlands

Abstract

Results are reported on the determination of the shift ΔE and the bandwidth Γ of both the valence and the affinity level of Na interacting with a sodiated W(110) surface. The results on the valence band are obtained with a sodium coverage of about $1 \cdot 10^{14}$ atoms $cm^{-2}s^{-1}$. At a distance of $10\ a_o$ from the surface $\Delta E \simeq 0.7$ eV and $\Gamma \simeq 0.6$ eV. The formation of Na^- is obtained with a coverage of $5 \cdot 10^{14}$ atoms $cm^{-2}s^{-1}$. In this case $\Delta E \simeq -0.6$ eV and $\Gamma \simeq 0.2$ eV.

H^- and D^- formation is studied by scattering H^+ respectively D^+ from a cesiated W(110) surface at a coverage of $5 \cdot 10^{14}$ atoms $cm^{-2}s^{-1}$. The width and broadening are in agreement with the theoretical estimates. Maximum efficiency for the formation of negative hydrogen is about 40%. This is obtained at a normal velocity of $2 \cdot 10^6$ cm s^{-1} which corresponds with an energy of 2.5 eV for H and of 5 eV for D.

I. Introduction

Since the days of Langmuir and Taylor[1] it has been recognized that surface ionization by high workfunction metals is a very effective means to ionize the alkali metals and the alkaline-earth elements, and also many compounds of these elements. On the other hand from incandescent low workfunction surfaces negative ions can be emitted, especially the halide anions which have the highest electron affinities. Positive emission from surfaces is described by the well-known Saha-Langmuir equation (see for example references[2] and[3], and references cited therein). Saha-Langmuir gives for the ionziation coefficient β_+, which is defined as the positive ionic fraction emitted from a surface,

$$\beta_+ = \frac{n_+}{n_+ + n_o} = \frac{1}{1 + \frac{g_o}{g_+} \exp(-\frac{\phi - I}{kT})} \qquad (1)$$

where g_i is the statistical weight of the relevant state, ϕ the workfunction of the metal and I the ionization potential of the emitted atom. A similar relation can be derived for the emission of negative ions with an electron affinity S,

$$\beta_- = \frac{n_-}{n_- + n_o} = \frac{1}{1 + \frac{g_o}{g_-} \exp(-\frac{S - \phi}{kT})} \qquad (2)$$

These relations are valid under (quasi) equilibrium conditions. For thermal incident atomic beams the sticking factor commonly is close to unity, and the Saha-Langmuir equation can be applied with good results.

The Saha-Langmuir equation for the emission of negative ions does not give much hope to design a negative hydrogen ion source on the basis of thermal emission. The electron affinity of hydrogen being 0.75 eV, a surface with an equal workfunction would be required to attain an ionization coefficient of 1/3. Materials which have a workfunction which comes close to this value only can be used in sealed vacuum tubes, and certainly will deteriorate very rapidly in environments which are prevalent in practical applications. Many experiments, however, indicate that much higher ionization coefficients can be attained if the particles are emitted with higher velocities, corresponding to energies in the eV range. Evidence for that is obtained from SIMS, sputtering and also from beam experiments in the eV range. This holds for positive as well as for negative surface ionization. One of the first investigations which have been performed in order to get some quantitative information on the ionization coefficient as a function of the normal velocity of the emitted particle is of Hurkmans et al.[4]. These authors measured the ionization coefficient of sodium emitted from a W(110) surface under thermal conditions, and compared the results with the ionization coefficient of scattered sodium atoms from the same surface in the incident energy range of 2 - 10 eV. The thermal measurement gave a value for $\beta = 0.44$, while the results from the scattering experiment yielded a value of $\beta \simeq 0.6$ at an incident energy of 2 eV which rapidly increased with increasing energy. At about 5 eV the ionization coefficient reached a plateau which was equal to unity within experimental error.

The work reported upon in this paper is concerned with the investigation of surface ionization of hyperthermal atoms which are reflected from a surface under well defined conditions. In section II we will shortly resume the theoretical perturbation approach which has been applied to describe the measurements. In section III experiments on the positive and negative ionization of sodium atoms which are scattered from a partially sodium covered W(110) surface are discussed. In the last section we report the first results on the formation of H^- and D^- obtained by scattering positive ion beams from a cesiated W(110) surface.

II. Theoretical

1. Atom-metal interaction

Two different approaches are in common use to describe the atom-metal interaction. In the first one, originally proposed by Gurney[5] the atom-metal interaction is considered as a perturbation of the pure atomic and metal states. The second one, the local density functional (LDF) approximation using

the jellium model has been applied to calculate the chemisorption of single atoms on a metal substrate and to describe the workfunction change induced by alkali adsorption (see for example references[6] and[7]). Both methods essentially lead to the same results. When an alkali atom approaches a metal surface the atom-metal interaction leads to a gradual shift and broadening of the valence level of the atom, resulting in the binding of the atom to the surface. We will follow the first method, the perturbation approach, as this theory is better suited to describe the ionization probability of scattered particles.

The hypothesis of Gurney[5] has been worked out by Gadzuk[6] and has been presented in a lucid article on the theory of atom-metal interactions. When an alkali atom approaches a metal surface the valence electron will interact with both the image charges of the ion core and of the electron itself. Classically this leads to a shift of the valence level which is approximately equal to 1/4z when the distance of the atom to the surface equals z. First order quantal perturbation theory gives for large distances the same result. So

$$\Delta E_{+} \simeq \frac{1}{4z} \qquad (3)$$

When a negative ion interacts with a metal surface, the affinity level is also shifted. As in this case the perturbation is caused only by the image charge of the affinity electron, the shift has opposite sign

$$\Delta E_{-} \simeq -\frac{1}{4z} \qquad (4)$$

In this model the alkali is treated as a perturbed atom which is separated from the metal by a potential barrier. In other words the atom-metal system is treated as the combination of two virtual states, the virtual atomic state the wave function of which extends into the metal and the virtual metal state the wave function of which by barrier penetration extends into the ion core. The electron resonates between these two virtual states, the transition frequency being determined by the tunneling time through the barrier. As the tunneling time through a barrier depends exponentially on the product of the height and the width of the barrier, the transition frequency will exponentially decrease as a function of the distance to the surface, the height being no function of z. This model is valid provided the bandwidth of the perturbed state is small with respect to the width of the conduction band. As at the equilibrium distance of the adsorbed state the bandwidth is of the order of 1 eV, this condition is satisfied for most systems.

The electron transitions between virtual atomic and metal states have been calculated by Gadzuk applying rearrangement theory. The transition matrix element between the initial state $|\chi_i\rangle$ and the final state $|\chi_f\rangle$ is given by

$$T_{i,f} = \langle\chi_f| \; (1 - \Pi_i) \; H'_i \; |\chi_i\rangle \qquad (5)$$

where Π_i is an operator which projects onto the initial state and H' is the perturbation on the electron in the initial state. Applying Fermi's Golden Rule the transition frequency is obtained

$$w = \sum_{\text{deg}} \frac{2\pi}{\hbar} \rho_K \; |T_{i,f}|^2 \qquad (6)$$

where the summation is over all degenerate states on the energy shell. The bandwidth is given by

$$\Gamma \simeq \hbar w \qquad (7)$$

Calculations of level width and level shift as a function of the atom-metal separation have been presented by several authors[6,7,8].

In these early studies the spin of the electron, however, has been neglected. In more recent work based upon the Anderson[9] theory of metallic impurities in alloys, the simultaneous occupation of atomic states by electrons of opposite spin has been included (see references[10,11,12]). This approach gives the possibility to treat positive and negative surface ionization in a unified way.

In figure 1 we show an energy level diagram for the interaction between an alkali atom and a metal, borrowed from the work of Gadzuk[6,11]. The diagram shows the gradual shifting and broadening of the valence level of the atom upon approaching the metal surface. At the position z of the atom the shifted level is above the Fermi-level of the metal, but the band partially extends below the Fermi-level. At zero degree Kelvin the charge on the valence state of the ad-atom is given by the fractional part of the band which extends below the Fermi-level.

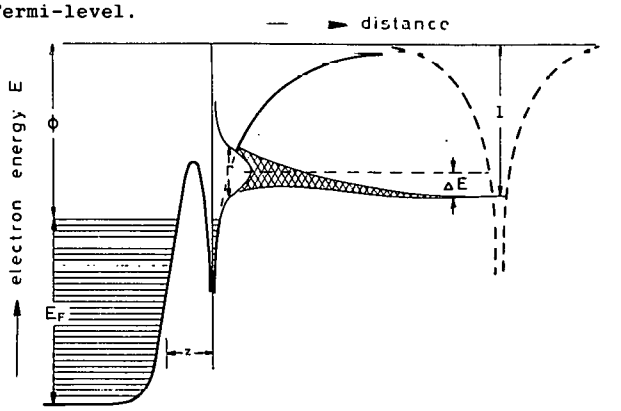

Fig. 1. Energy level diagram relevant to the alkali atom-metal interaction. ΔE is the shift, Γ the width of the valence level at distance z from the surface.

In figure 2 we give an example of the calculated transition frequencies between the affinity level of a hydrogen or deuterium atom and several metals. The calculations have been performed by Rasser et al.[13]. It is obvious that there is a large difference, about a factor of ten, between the transition frequency for the valence electron and the affinity electron. This difference is due to the difference in the range of the two potentials involved. All curves exhibit an approximately exponential behaviour as a function of the distance to the surface.

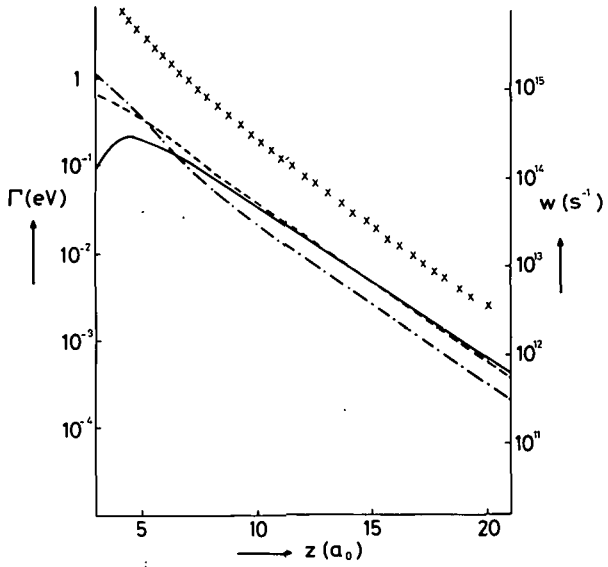

Fig. 2. The transition frequency w and the level width Γ for the affinity level of hydrogen interaction with a metal surface. H-Cs ———, H-Na ---, H-W -.-.-. Also shown is the perturbed valence level H-W xxxx.

2. The rate equation

The calculation of the ionization probability of an atom which is reflected from a metal surface is done in a semi-classical way. We follow here the treatment of Overbosch et al.[14]. The atom is assumed to follow the classical path, which is approximated by straight line trajectories. The scattering is assumed to be specular and the collision is considered to be a binary one between the projectile atom and a lattice atom. Let $P_n(t)$ denote the probability that the valence level of the atom is occupied at time t, then the time variation of $P_n(t)$ is given by

$$\frac{dP_n}{dt} = w_n(1 - P_n) - w_i P_n \tag{8}$$

where w_n and w_i represent the neutralization and ionization rates respectively. The sum of $w_n + w_i$ equals w, the transition frequency. Under stationary conditions P_{ns} is given by

$$P_{ns} = \frac{w_n}{w_n + w_i} = \frac{w_n}{w} \tag{9}$$

If we assume a Lorentzian shape for the broadened level, the density of states is given by

$$\rho_+ = \frac{1}{\pi} \frac{\Gamma/2}{(E + I - \Delta E)^2 + (\Gamma/2)^2} \tag{10}$$

At zero degree Kelvin the stationary state occupation then is obtained by integrating the density of states from $-V_o$, the energy of the bottom of the conduction band, till $-\phi$ the energy of the Fermi-level.

$$P_{ns} = \int_{-V_o}^{-\phi} dE \, \frac{1}{\pi} \frac{\Gamma/2}{(E + I - \Delta E)^2 + (\Gamma/2)^2} \simeq$$

$$\simeq \frac{1}{2} + \frac{1}{\pi} \arctan\left(\frac{I - \Delta E - \phi}{\Gamma/2}\right) \tag{11}$$

We thus obtain for the neutralization and ionization rates

$$w_n = \left\{\frac{1}{2} + \frac{1}{\pi} \arctan\left(\frac{I - \Delta E - \phi}{\Gamma/2}\right)\right\} w = n_+ w$$

$$w_i = \left\{+\frac{1}{2} - \frac{1}{\pi} \arctan\left(\frac{I - \Delta E - \phi}{\Gamma/2}\right)\right\} w = (1 - n_+) w \tag{12}$$

In these formulae $\Delta E \simeq 1/4z$, and w depends exponentially on z.

The formal solution of the rate equation (eq. 8) with the boundary condition $P_n(-\infty) = 1$ is given by

$$P_n(+\infty) = \exp\left(-\int_{-\infty}^{+\infty} dt\, w\right) + \int_{-\infty}^{+\infty} dt\, w_n(t) \exp\left(-\int_t^{\infty} dt w\right) \tag{13}$$

By substituting the expressions for the transition rates (eqs. 6 and 12) and transforming time to distance by applying the straight line approximation

$$z = \begin{cases} z_o - v_{z,in} t & \text{for } t < 0, \text{ inward path} \\ z_o + v_{z,out} t & \text{for } t > 0, \text{ outward path} \end{cases} \tag{14}$$

we obtain an expression for the neutral fraction after scattering which easily can be integrated numerically. Overbosch et al.[14], however, found an interesting approximation to the integral of eq. 13, making use of the approximate exponential dependence of the transition rate and of the high values of w in the case of the interaction between a sodium atom and a partially covered tungsten surface. If the transition rate at the distance of closest approach z_o is of the order of 10^{15} per sec, then the first term of eq. 13 and the inward path of the second term can be neglected for incident energies of the sodium atoms in the 100 eV range. The neutral fraction after scattering is then given by

$$P_n(+\infty) = \int_{z_o}^{+\infty} \frac{dz}{v_z} w_n(z) \exp\left(-\int_z^{\infty} dz' \frac{w(z')}{v_z}\right)$$

Substituting eq. 12 and w(z),

$$w(z) = w_o \exp(-az)$$

we obtain

$$P_n(+\infty) = \int_{z_o}^{\infty} dz\, n_+(z) \frac{w(z)}{v_z} \exp\left(-\frac{w(z)}{a v_z}\right)$$

The integrant now is peaked very sharply around

$$\frac{w(z^*)}{a v_z} = 1$$

Replacing now the rapidly varying part of the integrant by $\delta(z - z^*)$ we obtain as a good approximation

$$P_n(+\infty) = n_+(z^*) \equiv \frac{1}{2} + \frac{1}{\pi} \arctan\left(\frac{I - \Delta E(z^*) - \phi}{\Gamma/2}\right)$$

$$w(z^*) = a v_z \tag{15}$$

This approximation which has been called the "freezing approximation" emphasizes that the ionization

coefficient is determined by the charge distribution of the valence level at a distance z^* from the surface. This charge distribution actually is frozen out along the outgoing trajectory. It is clear that the validity of the freezing approximation depends on whether the dimensionless quantity $w(z)/av_z$ has a range which extends sufficiently above unity, the value at the freezing distance. This certainly is the case for the Na - W(110) interaction. For the H^- - W(110) + Cs interaction, however, the rate equation should be integrated over the entire outgoing trajectory. We summarized here the solution of the rate equation for positive ionization, for negative surface ionization the result is analogous.

III. The Na - W(110) Interaction

1. Experimental

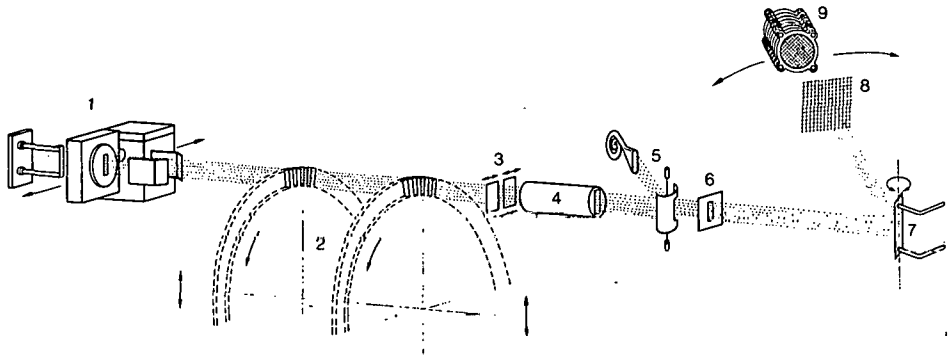

Fig. 3. The Apparatus
1. charge exchange source
2. slotted disc velocity selector
3,6. collimation apertures
4. vacuum channel
5. monitor
7. tungsten single crystal ribbon
8. detector grid
9. electron multiplier detector.

The experimental setup is shown in fig. 3. A fast sodium atom beam, with an energy which can be varied in the interval of 25 - 400 eV, is generated by means of a charge exchange source. This beam is collimated by two apertures which are in line with the tungsten target. A typical flux of the primary beam is 10^7 atoms $cm^{-2}s^{-1}$. The charge exchange source also emits a beam of thermal atoms with a flux of about 10^{12} atoms $cm^{-2}s^{-1}$. The two merged beams can be separated by the slotted disc velocity selector. The slits of the discs are in one plane with the axis of rotation so that the selector acts as a cut-off filter. At a rotation frequency of 20 Hz the thermal beam is completely suppressed while the fast beam is transmitted for 30%. The flux of the thermal beam can be determined by the hot wire rhenium monitor.

The two merged beams impinge on the (110) surface of a single crystal tungsten ribbon with dimensions 0.2×2 cm^2. The angle of incidence usually is 60 deg from the normal. The tungsten ribbon can be cleaned by oxygen treatment and ohmic heating. The thermal atoms impinging on the target have a sticking coefficient of one, the fast atoms are scattered from the surface under partial simultaneous ionization[16]. The ions are detected directly by the electron multiplier which is set in the specular direction. Neutral fast atoms are detected by suppressing the ions by a retardation voltage on the grid, and surface ionization of the atoms on the same grid. The tungsten target together with the electron multiplier detector are in a high vacuum chamber. Typical pressures under operation conditions are a few times 10^{-10} Torr.

The workfunction of the (110) plane of the tungsten ribbon decreases with the adsorption of sodium atoms. The behaviour of the workfunction as a function of the degree of coverage has been measured by Medvedev et al.[17]. The clean surface has a workfunction of 5.25 eV. At a coverage of $5 \cdot 10^{14}$ atoms cm^{-2} the minimum is reached at a value of 1.9 eV, after which the workfunction increases again with increasing coverage. At low coverages the decrease is linear with the coverage with a slope $(d\phi/dn)_{n=0} = 1.35$ eV/10^{14} atoms cm^{-2}. The workfunction at several coverages has been measured in situ by fotoemission, applying the Fowler method[18]. These measurements give a slope

$$\left(\frac{d\phi}{dn}\right)_{n=0} = 1.06 \text{ eV}/10^{14} \text{ atoms cm}^{-2}.$$

The measuring procedure is as follows. After proper cleaning of the tungsten ribbon both beams, the thermal and the eV beam, are switched on by opening a beam flag. The velocity selector is lowered below the beam line. As a function of time the ion yield is counted, or alternatively the neutral yield. In a separate run the flux of the thermal beam is determined.

2. The valence level

Figure 4 shows a typical result of the behaviour of the ion and neutral fractions of the scattered sodium atoms as a function of coverage. The ion flux which has been normalized to 0.97 at zero coverage according to the theoretically calculated value[14], rapidly decreases as a function of coverage. The neutral flux which has been normalized at a surface coverage of $1.6 \cdot 10^{14}$ atom cm^{-2}, such that the sum of the ion and neutral fluxes is unity, rapidly increases with surface coverage. If we assume that the surface coverage only results in a lowering of the workfunction, in other words a shift of the Fermi level, eq. 15, which gives the probability that the scattered sodium atom leaves

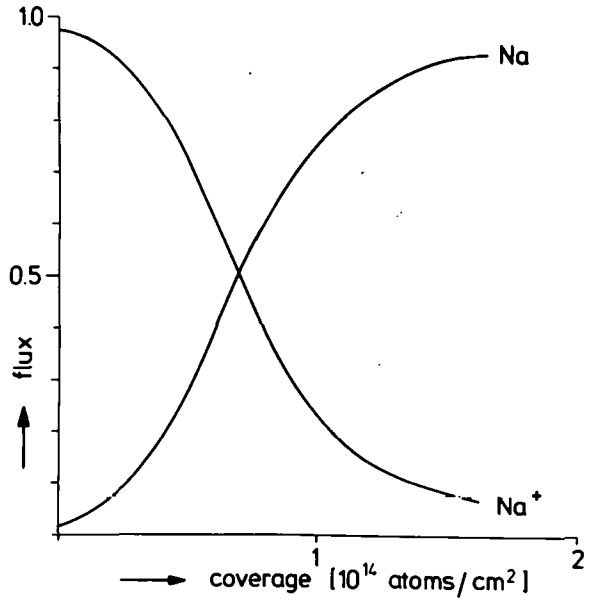

Fig. 4. The normalized ion and neutral fluxes of a 100 eV sodium beam, incident at 60 deg. from the normal, as a function of the coverage of the surface with sodium atoms.

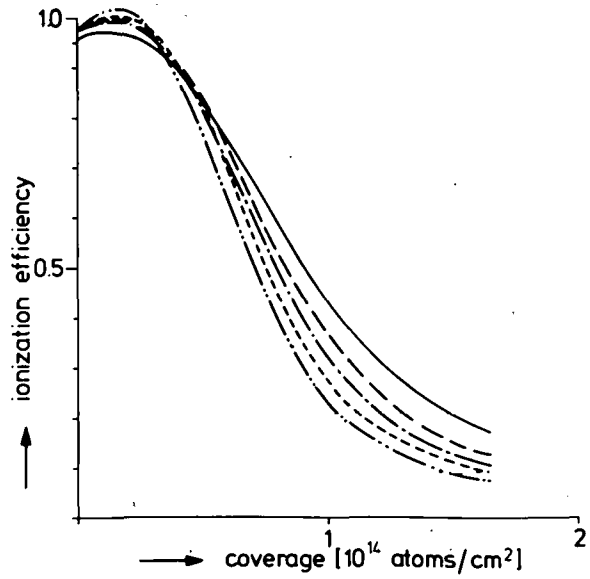

Fig. 5. Ionization efficiency of sodium atoms scattered from the surface as a function of coverage, and at several initial energies. 25 eV (-..-), 50 eV (-----), 100 eV (-.-.-), 200 eV (— — —) and 400 eV (———). The angle of incidence is 60 deg from the normal.

the surface in the neutral state, can be written as

$$P_n(+\infty) = n_+(z^*,\Theta) = \frac{1}{2} + \frac{1}{\pi} \arctan \frac{I - \Delta E(z^*) - \phi(\Theta)}{\Gamma/2} \qquad (16)$$

where $\phi(\Theta)$ is the workfunction which is a function of the coverage Θ. When $P_n(+\infty) = \frac{1}{2}$ the argument of the arctan is zero. This happens at a coverage of $7 \cdot 10^{13}$ atoms cm^{-2}, corresponding with a decrease in workfunction of 0.74 eV. As $(I - \phi)$ for the clean surface equals 0.06 eV, the level shift at the freezing distance z^* equals $\Delta E = 0.68$ eV. From this the freezing distance is determined, $z^* = 10\ a_o$. In an analogous way the bandwidth at the freezing distance is determined from the coverage difference between $P_n(+\infty)$ equals $\frac{1}{4}$ respectively $\frac{3}{4}$. In figure 4 this is $5 \cdot 10^{13}$ atoms cm^{-2} corresponding with a workfunction difference of 0.53 eV, so $\Gamma = 0.53$ eV. In fact differentiation of both the ion curve and the neutral curve give the shape, the width and the shift of the valence level, at the freezing distance.

Figure 5 gives a set of experiments performed at different energies of the fast sodium beam. From figure 5 we conclude that both the levelshift and the levelwidth increase with increasing velocity. This is to be expected from the freezing approximation, as the freezing distance decreases with increasing velocity.

A comparison with theoretical calculations[14] is given in fig. 6. We observe a reasonable agreement between theory and experiment for the level shift, although the experimentally obtained dependence on v_z is somewhat steeper than the theoretically predicted one. For the levelwidth, however, the experimentally determined values are a factor of 4 till 2 larger than the theoretical predictions. This certainly will be due partially to the symplifying assumption that the only effect of surface coverage is a lowering of the work function.

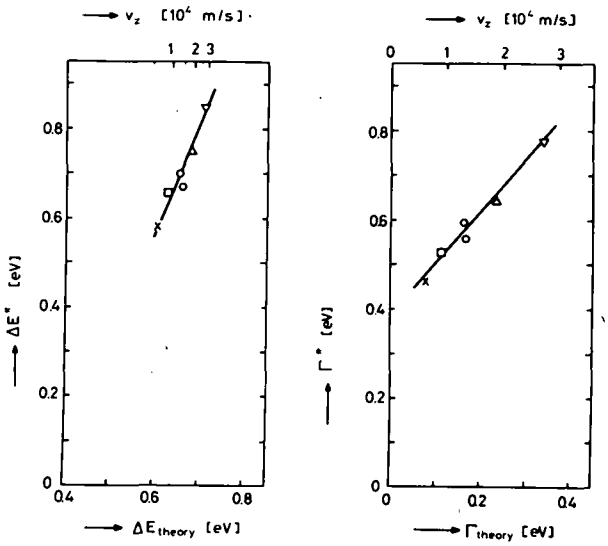

Fig. 6. Comparison between measured and theoretical values for the levelshift ΔE and the levelwidth Γ. v_z is the normal component of the final velocity. The energies of the incident Na atoms are 25 eV (X), 50 eV (□), 100 eV (Δ) and 400 eV (∇).

On the other hand the assumption of the scattering behaviour, e.g. specular reflection and binary collisions, is also too simple. Recent experiments did show that there is a non-negligible low energy tail in the energy distribution of potassium ions scattered from a clean tungsten surface. This definitely leads to a substantial broadening of the apparent width. For a more detailed discussion we

refer the reader to the forthcoming publication[19].

3. The affinity level

At large coverages, in the range of $2 \cdot 10^{14}$ till $25 \cdot 10^{14}$ atoms cm^{-2}, the scattering of a 100 eV sodium beam leads to the emission of negatively charged particles. This is shown in figure 7.

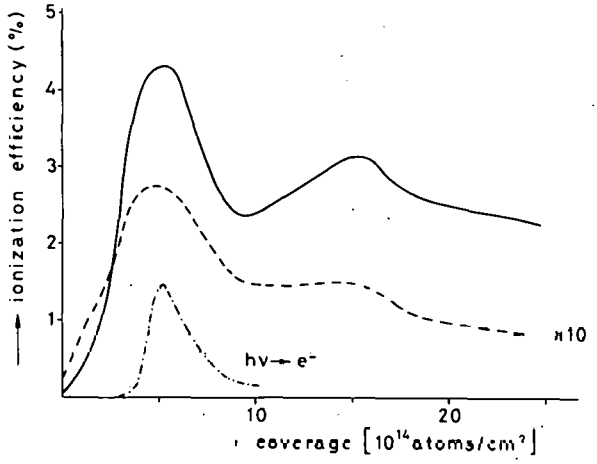

Fig. 7. Total negative yield of a 100 eV sodium beam, incident at an angle of 60 deg from the normal, as a function of the coverage of the surface with sodium atoms. The result of a retardation measurement (-----) and the photoemission current for photons with $h\nu = 1.95$ eV (-.-.-) are also shown.

The negative signal is 4.2% of the primary beam intensity at maximum. Assuming binary collisions the energy of the specularly scattered particles is about 25 eV. In order to verify that the negative signal is due to scattered Na^- ions the negative signal also has been measured with a retardation voltage of -20 V on the grid. In this way most of the Na^- scattered ions are suppressed, but surely all eventually emitted secondary electrons. As the curve has the same functional dependence on the coverage we feel confident that the negative yield is solely due to scattered Na^- ions. In order to verify the calibration of the coverage scale the photoemission current for a fixed wavelength corresponding to $h\nu = 1.9$ eV has been measured. The current peaks at a coverage of $5 \cdot 10^{14}$ atoms cm^{-2} which corresponds with the minimum in the workfunction.

In order to extract more quantitative information from the measurement, we refer again to the freezing approximation, discussed in section II.2. For the affinity level the freezing approximation yields for the occupation probability $P_{i,-}(+\infty)$

$$P_{i,-} \simeq \frac{1}{2} + \frac{1}{\pi} \arctan \left(\frac{S + \Delta E(z^*) - \phi(\Theta)}{\Gamma/2} \right) \qquad (17)$$

As $P_{i,-}$ is small the argument of the arctan function should be large. This allows an expansion in terms of the inverse of the argument. Retaining only the first term in the expansion we obtain a relation between the workfunction and $P_{i,-}^{-1}$ which depends parametrically on $\Delta E(z^*)$ and $\Gamma(z^*)$.

$$\phi(\Theta) - (S + \Delta E(z^*)) = \frac{\Gamma(z^*)}{2\pi P_{i,-}} \qquad (18)$$

By trial and error the best values for the shift and the width are obtained. This is shown in fig. 8. The workfunction has been taken from the work of Medvedev et al.[17].

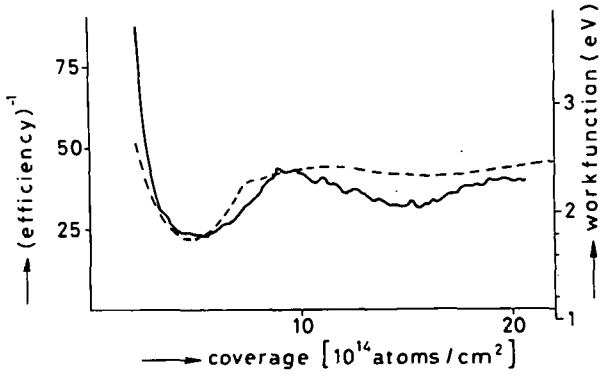

Fig. 8. Determination of the shift and the width of the affinity level of sodium interacting with a sodium covered W(110) surface. The inverse of the negative ion yield (———) and the workfunction (- - -) are matched.

A best fit is obtained for $\Delta E(z^*) \sim 0.6$ eV and $\Gamma(z^*) \simeq 0.19$ eV. According to the image potential model the freezing distance is 11.3 a_o. These values are quite reasonable compared to the values obtained for the valence level. For further discussion we again refer the reader to a forthcoming paper[20].

IV. Affinity level of hydrogen

1. Experimental

There are already numerous experiments on the emission of H^- and D^- from clean and cesiated surfaces by backscattering and sputtering. For these studies we refer the reader to a few reviews on this subject and to references cited therein[21,22,23]. Apart from discussing many experimental investigations these papers also review several theoretical models.

To our knowledge the overwhelming part of the experiments carried out thus far worked with normal incident beams in the low and medium keV energy range. The present experiment is designed in such a way as to study the double charge transfer under reflection conditions. That is to say the incident energy and the angle of incidence are chosen in such a way as to ensure that the particle and energy reflection coefficients are unity, or at any rate very close to unity. From a fundamental

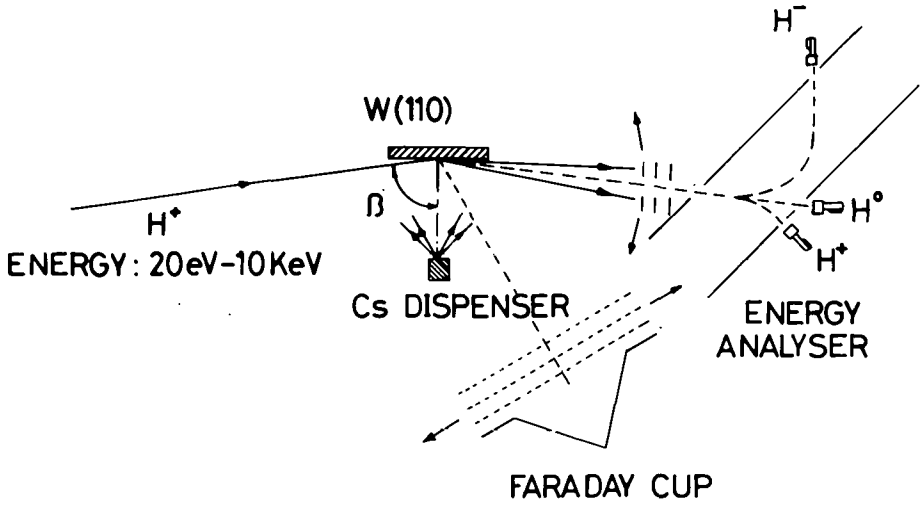

Fig. 9.

The apparatus for studying $H^+ \rightarrow H^-$ conversion at surfaces. Both the Faraday cup for total charge transfer measurements and the analyser and detector for differential measurements are shown.

point of view this has the advantage that the surface ionization process can be studied under well-defined conditions. On the other hand from a practical viewpoint the deterioration of the surface under the impact of the incident proton beam will be the least.

The target, a tungsten single crystal ribbon with dimensions 0.2×2 cm^2 is mounted in the center of a high vacuum chamber. The chamber is kept at a pressure of a few times 10^{-10} Torr. The crystal is rotatable around its own axis which coincides with the rotation axis of a detection system. This detection system consists of a parallel plate energy analyser and three channeltron open particle multipliers for detecting simultaneously H^-, H and H^+ or the same species of deuterium. Total efficiency measurements are carried through by measuring the total negative ion current with a large Faraday cup which is placed under specular direction. The incident ion beam is measured with a Faraday cup in the beam line by lowering the target and replacing it by a slit of the same dimensions. This slit is rigidly connected with the target so that the angle of incidence of the primary beam is the same in both positions of the target holder. The positive ion beam line consists of a small gas-discharge ion source and a five cylinder electrostatic lense system which allows to vary the energy of the incident particles from 20 eV till 10 keV. A cesium dispenser which is placed opposite to the target gives the possibility to cesiate the surface. As the target can be heated ohmically the possibility for static as well as dynamic coverage of the surface is open. Thus far we only experimented with a fixed coverage of cesium at room temperature. Workfunction determinations can be carried through by photoemission measurements.

2. Results and discussion

In this section we will discuss measurements on the total efficiency of the double charge transfer from the cesiated tungsten surface to the hydrogen ion. These measurements are performed for hydrogen and deuterium in an energy range 150 eV - 2000 eV. The angle of incidence has been varied from 75 deg to 85 deg from the normal. These results will be published shortly[24]. Preliminary to the determination of the total efficiency for H^- formation, there have been carried out measurements on the energy reflection coefficient in order to check whether this coefficient under the present conditions of grazing incidence is equal to unity. The measurements have been performed with a half monolayer cesium coverage and at incident proton energies of 1000 and 2000 eV. The energy analysis has been done at the specular scattering angle. Typical values for the energy loss and the full width half maximum of the energy distributions are 4% of the nominal energy at an angle of incidence of 85 deg and 8% at 75 deg. The angular distribution of the scattered particles showed to be almost specular. The FWHM of the angular distribution varied from 5 deg at 85 deg angle of incidence to 20 deg at 75 deg. This confirms that up till an angle of incidence of 75 deg reflection from the surface prevails above backscattering from deeper lying surface layers.

In fig. 10 we show the deuterium results. At various incident energies the efficiency I_{D^-}/I_{D^+} has been determined as a function of the angle of incidence, defined from the normal. The half monolayer cesium has been defined as the coverage which gives the maximum efficiency. This appears to be independent of incident energy and angle. A typical experimental run takes about 30 minutes; the surface, however, remains in the same condition for a much longer period, indicating that under the prevailent conditions the sputtering and contamination of the surface is of no importance.

In fig. 11 we display the results as a function of the normal velocity component. It is observed that up till 400 eV the data are falling on a uniform curve as is predicted by the theory. The maximum efficiency lies around 40% at a normal velocity of about $2 \cdot 10^8$ cm s^{-1}. The behaviour of the uniform curve can be explained with the aid of fig. 2, which gives the transition frequencies as a function of the distance to the surface. At normal velocities lower than $2 \cdot 10^6$ cm s^{-1} the freezing approximating still retains its validity.

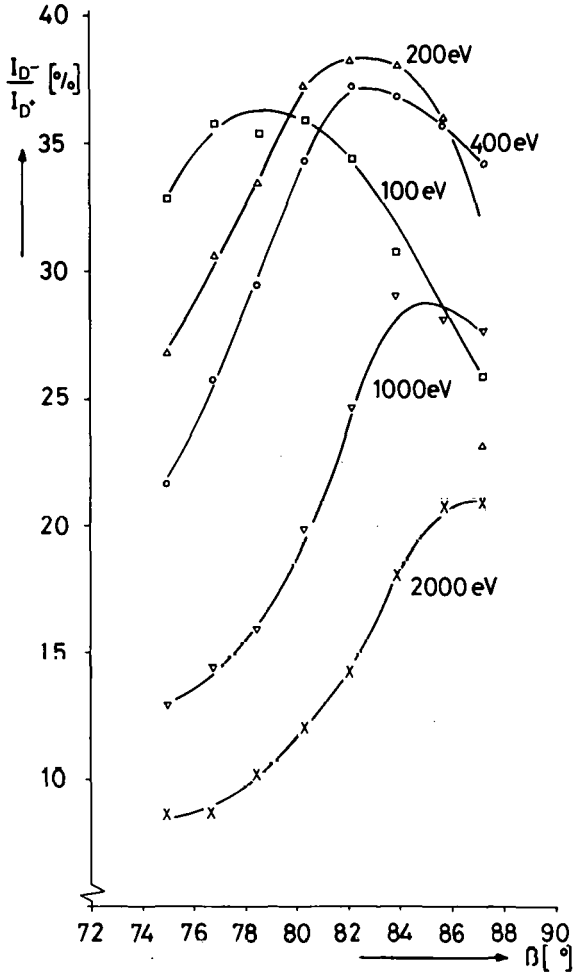

Fig. 10. The total efficiency I_{D^-}/I_{D^+} for the formation of D^- as a function of the angle of incidence at several incident energies.

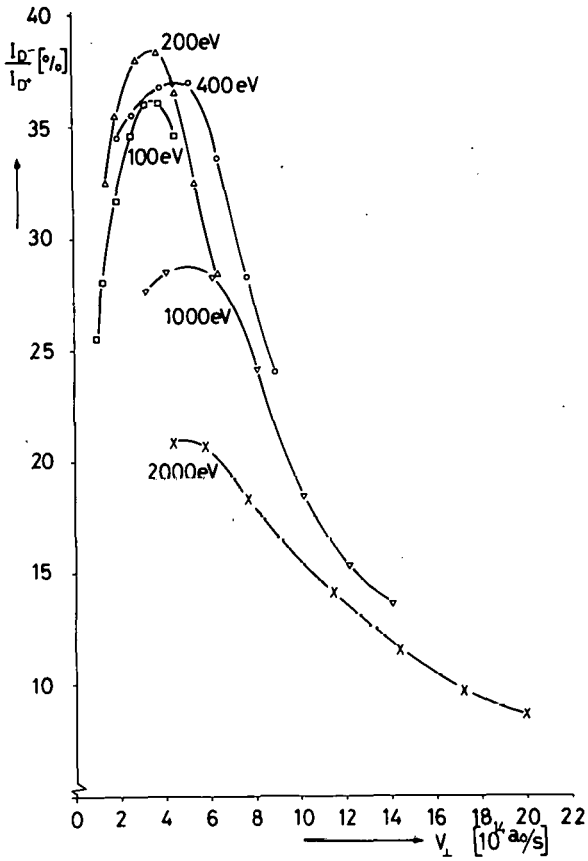

Fig. 11. The total efficiency I_{D^-}/I_{D^+} as a function of the normal velocity component at several incident energies.

Then the efficiency increases with increasing velocity. At the maximum, however, the freezing distance has come close to 5 a_o, where the transition frequency is maximal. Increasing the normal velocity leads then to a decreasing efficiency. The relatively low value of the transition frequency is caused by the small range of the potential and the small value of the conduction band of a cesiated metal surface.

Above 400 eV the absolute values of the efficiency are decreasing. We infer that this is due to relaxation effects in the formation of the image surface charge distribution. Further theoretical work, however, has to be done. Theoretical calculations based on the calculations of Rasser et al.[13] indicate a maximum efficiency of 50% at a normal velocity of about $2.5 \cdot 10^6$ cm s^{-1}. The theoretical curve shows, however, a much more gradual downward slope at higher velocities than the experiments indicate. This probably indicates that the H^- wave function in reality has a shorter range than assumed by Rasser. At last it should be mentioned that the results on hydrogen are the same as for deuterium if scaled on a $v_\perp$ scale.

Conclusions

Resonant charge transfer as a result of atom-metal interaction is a process which is reasonably well understood by now. Recent experiments indicate the promising prospects for using negative surface ionization of hydrogen as a tool for making D^- beam lines for injection in fusion plasmas.

Acknowledgements

This work is part of the research program of the Stichting voor Fundamenteel Onderzoek der Materie (Foundation for Fundamental Research on Matter) and was made possible by financial support from the Nederlandse Organisatie voor Zuiver-Wetenschappelijk Onderzoek (Netherlands Organization for the Advancement of Pure Research).

Literature References

1. J. Taylor and I. Langmuir, Phys.Rev. 44, 423 (1933).
2. M. Kaminsky, Atomic and Ionic Impact Phenomena on Metal Surfaces (Springer-Verlag, Berlin 1965).

3. E.Y. Zandberg and N.I. Ionov, Surface Ionization (IPST, Jerusalem, 1971).
4. A. Hurkmans, E.G. Overbosch, K. Kodera and J. Los, Nucl.Instr.and Meth. 132, 453 (1976).
5. R.W. Gurney, Phys.Rev. 47, 479 (1935).
6. J.W. Gadzuk, Surface Sci. 6, 133 (1967).
7. M. Remy, J.Chem.Phys. 53, 2487 (1970).
8. R.K. Janev, J.Phys.B 7, 1506 (1974).
9. P.W. Anderson, Phys.Rev. 124, 41 (1961).
10. D.M. Newns, Phys.Rev. 178, 1123 (1969).
11. J.W. Gadzuk, J.K. Hartman and T.N. Rhodin, Phys.Rev. B4, 241 (1971).
12. B. Rasser and M. Remy, Surface Sci. 93, 223 (1980).
13. B. Rasser, J. van Wunnik and J. Los, to be published.
14. E.G. Overbosch, B. Rasser, A.D. Tenner and J. Los, Surface Sci. 93, 310 (1980).
15. J.A. Aten and J. Los, J.Phys.E: Sci.Instr. 8, 408 (1975).
16. A. Hurkmans, E.G. Overbosch and J. Los, Surface Sci. 62, 621 (1977).
17. E.V. Klimenko and V.K. Medvedev, Sov.Phys.--Solid State 10, 1562 (1969).
V.K. Medvedev, A.G. Naumovets and A.G. Fedorus, Sov.Phys.-Solid State 12, 301 (1970).
18. M. Cardona and L. Ley, in: Photoemission in Solids, Ed. M. Cardona (Springer-Verlag 1978).
19. E.G. Overbosch and J. Los, submitted for publication.
20. E.G. Overbosch and J. Los, to be published.
21. J.R. Hiskes, "Formation of Hydrogen Negative Ions by Surface and Volume Processes with Application to Negative Ion Sources", Invited Paper XIVth Int.Conf.on Phenom.in Ion.Gases, Grenoble (1979), UCRL-82889.
22. W. Eckstein and H. Verbeek, "Data on Light Ion Reflection", Max Planck Institut für Plasmaphysik, Garching, IPP 9/32 (1979).
23. K. Wieseman, "H^- Ions in Plasmas", Laboratoire de Physique des Milieux Ionisés, Ecole Polytechnique, PMI 972 (1979).
24. J. van Wunnik, B. Rasser and J. Los, to be published.

DISCUSSION

HISKES In your last slide, what was the perpendicular energy at the lowest data point on the 200 V curve?

LOS That is la_o or 0.5×10^6 cm/sec.

HISKES That is about one volt.

LOS Yes. For deuterium it is about one volt.

HISKES What can you say about your experience of putting cesium on the tungsten 110? Is it easy to get the minimum work function coverage or is it a difficult problem?

LOS It is quite easy. You turn on a few times the dispenser (the dispenser is a very nice thing) which is heated up very quickly and cooled down very quickly. Then you draw these curves of H^- yield as a function of time and after knowing how much time you need for maximum yield, you put on the dispenser on that point and calibrate afterwards whether you were at the right point or not.

HISKES So in an ion source application it is not necessarily difficult to maintain that kind of a surface condition?

LOS I do not know. I forgot to mention that these experiments are done at room temperature where you could say that the sticking coefficient is unity and that the cesium is not yet desorbed. In plasma sources, I think, you should aim at a dynamic equilibrium between incoming cesium and outgoing cesium. I do not think it is difficult but it will take a lot of experimenting to find out what cesium vapor pressure you have to maintain in that neighborhood, in your specific conditions.

PETERSON In order to explain the decrease of the efficiency at higher energies it is possible that the atoms, as they go to the surface, become excited and thus are not in their ground state anymore. So the probability of catching the electron on their way out, becomes smaller than you would predict theoretically.

LOS I do not think so because there is nothing more efficient than a resonant process. So the H^- certainly will be formed in the lower state. Subsequently, when H^- is removed, you might excite it because your surface is not completely a flat potential, but is emulated by the next and the super next neighbor and there you might have an excitation, but then I would assume that a destruction is much more likely. In other words when you are going out as an H^- and you are going out in a grazing angle of incidence, the next neighbor might destroy the H^-.

PETERSON But I was saying that if the atom is not in its ground state, that the excited passes through the lattice.

LOS Why. I would say, when you are coming in (neutralized or not) at closest distance of approach, definitely Auger processes will take care that the H will be in the ground state.

HAGENA The ratio which you plot, is that the ratio of the negative current compared to the incident positive current?

LOS That is right. It is the total conversion.

HAGENA Are all the measurements done in ultra high vacuum conditions? Because that is very critical, I guess.

LOS Yes.

FORRESTER Many years ago I made some positive cesium ion sources in which cesium was diffused through a porous tungsten matrix with the pores small compared to the diffusion length of the cesium. It just occurs to me in connection with this surface kind of work, that one might much better control the cesium on the surface through such a porous matrix without much external cesium

to worry about. It is just a comment that might be useful.

LOS May I comment on this. Those porous plugs are still in use to make either normal cesium or cesium ions. But for a fundamental investigation it was necessary that we have a well defined surface. Therefore we started with a 100 surface and we took care that there was half a monolayer. Only in that way you can look to what are really the fundamental processes and if it follows theoretical predictions.

GELLER I am just puzzled to see that the overall efficiency of your system is the same than in the double charge exchange. You get 30% at 100 eV. Well, now I wonder, if you do not have just double charge exchange. If this is right, why to have this system?

LOS Let me at first comment on the first part. Van Wunnik, who has been doing this experiment and is still doing this experiment, was puzzled as well by that same efficiency and I think he asked you too, isn't it? And, of course, I was approached by him, being the professor, who should know everything. I thought about it and I think they have nothing to do with each other, they are fundamental physical processes. Now the second part of your question. When you do it in a charge transfer cell or in a vapor jet, you need in the first place a lot of cesium, which you have to recycle, I do not know how many kilograms. Secondly you have it in the vapor phase, that means you are deteriorating your plasma very much when you are directing it a little bit wrong. In our approach we have a cesium layer which is put on with a minimum amount of effort and which stays there for hours. How it goes with intense beams that is Hopman's task to look after.

PRODUCTION OF NEGATIVE IONS UNDER NON-EQUILIBRIUM CONDITIONS

W. F. Bailey
Air Force Institute of Technology
Wright-Patterson AFB, Ohio

and

A. Garscadden

Air Force Wright Aeronautical Laboratories
Wright-Patterson AFB, Ohio

Abstract

The results of experimental and theoretical studies have shown that the dissociative attachment cross-sections for electron impact of molecular hydrogen are very strong functions of the initial vibrational state of the molecule. The existence of this comprehensive set of cross-sections, which establish the vibrational level and rotational level dependencies of dissociative attachment from the ground electronic state, permits the evaluation of the effect of non-equilibrium level populations on the production rate of H^- in discharges.

In this work a self-consistent analysis of the effects of vibrational excitation on the electron energy distribution and on the dissociation attachment rates was performed for typical conditions in hydrogen discharges. The electron kinetics and excitation rates, obtained by numerically solving the electron Boltzmann transport equation, were coupled to the first order time derivative population equations for the vibrational levels. The dissociative attachment rate was calculated as a function of E/N, (where E is the applied electric field and N is the total gas density), gas temperature and fractional ionization. Under conditions of high vibrational excitation there is a significant increase in the energy deposited into dissociative attachment as compared to that for a gas at a low vibrational temperature. Calculations have been made which show that the cooling of the gas to $200^{\circ}K$, coupled with efficient vibrational pumping, results in the total rate of negative ion formation exceeding that from the ground state by over three orders of magnitude. The possibilities of achieving these conditions are considered.

Introduction

Measurements[1,2] of H^- and D^- concentrations in plasmas indicate that non-linear mechanisms involving intermediate excited states are required to explain the observed large magnitude and functional dependencies. Hiskes[3] has reviewed negative ion production in a hydrogen plasma and discussed three H^- production processes with large reaction rates. These processes, which involve excited hydrogen molecules or ions produced by intermediate mechanisms, are the following:

(a) Dissociative attachment of electrons from vibrationally excited states of hydrogen molecules:

$$e + H_2 \rightarrow (V) \rightarrow H_2^- \ (^2\Sigma_u^+) \rightarrow H(1S) + H^-$$

(b) Dissociative attachment of electrons from electronically excited long-lived states of hydrogen molecules:

$$e + H_2 \ (^3\pi_u) \rightarrow H_2^- \ (^2\pi_u) \rightarrow H(2p) + H^-$$

and

(c) Dissociative recombination of H_3^+ :

$$e + H_3^+ \rightarrow H_3^* \rightarrow H_2^+ + H^-$$

Hiskes concluded that, while the possibility of significant negative ion production via dissociative recombination of H_3^+ with electrons cannot be excluded, dissociative attachment of electrons from highly excited vibrational states of hydrogen molecules appeared to be the most important channel.

We have performed a theoretical investigation of the dissociative attachment from vibrationally excited molecules for a broad range of electric discharge conditions. In addition, because the non-equilibrium gas excitation achieved by electric discharge could be influenced by high velocity flows and gas dynamic cooling, we have considered hybrid negative ion sources utilizing both electric discharge techniques and high velocity flow.

High velocity flows frequently create rapid changes in such flow variables as temperature, specific energy and density. The internal energy modes of the gas molecules do not always equilibrate rapidly or simultaneously with such changes in the external flow environment. In various flow situations, non-equilibrium of rotational, vibrational, electronic modes and chemical populations can be observed.[4] If the positive ion or negative ion formation rates are coupled to the populations of these modes, then non-equilibrium of the ionization or attachment is also anticipated. The approach to equilibrium of the various modes is governed by first order time derivative kinetic equations which, when coupled

together, are called the Master Equation for the system. Examination of these equations reveals a time scale or relaxation time for the equilibration of the mode under consideration. Some modes have very short relaxation times. The rotational mode requires only a few collisions in order to equilibrate. In contrast, the vibrational mode may require many collisions to equilibrate, and this longer relaxation time can lead to population inversion in the other states that are coupled to long-lived vibrational states. Even longer times are required for ionization and chemical equilibrium. Thus, in a manner analogous to non-equilibrium populations of coupled excited states in lasers, an enhanced population can be obtained in the ionization or attachment products, if these processes are closely coupled to the vibrational populations.

Electron and Heavy Particle Kinetics

The primary dissociative attachment reaction considered in this analysis is

$$e + H_2\ (V = i) \rightarrow H_2\ (^2\Sigma_u^+) \rightarrow H(1S) + H^-,\ i = 0\text{-}10$$

This reaction will, in general, be non-linear in electron density since it involves intermediate excited states. To analyze this reaction sequence, it is necessary to obtain solutions for the electron impact dissociative attachment rate, and to determine the population density of each of the vibrationally excited states. The attachment rate and population densities are not independent because the electron impact processes which lead to dissociative attachment and reduce the excited state density, also provide an efficient method of generating the excited vibrational state population. Thus, in order to analyze properly the dissociative attachment reaction, a self-consistent solution of the electron and heavy particle kinetics is required. In this section we discuss the relevant processes that were included in the analysis and outline the method of solution. Briefly, the electron kinetics are analyzed by calculating the electron energy distribution which is obtained through a solution of the collisional Boltzmann equation. The vibrational kinetics are analyzed by calculating the vibrational distribution through a solution of the Master Equation.

Figure 1, from Kolos and Roothaan,[5] presents the potential energy curves for H_2 and illustrates the states under consideration. The solid lines indicate the electronic states for H_2; the dashed curves, the states of the negative molecular ion. The electron impact excitation processes considered are summarized in Table I. Vibrational excitation from the ground state to levels V=1→5, as well as all intermediate transitions such as V=1→2, 1→3, 2→3, 2→4, are included.

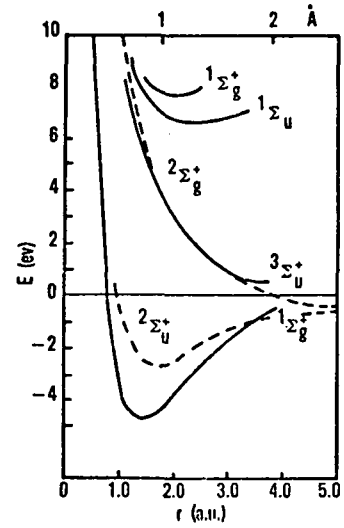

Figure 1. Potential Energy Curves for Several Electronic States of Hydrogen. (after Kolos and Roothaan)

H_2 CROSS SECTIONS	
PROCESS	**REFERENCE**
MOMENTUM TRANSFER	CROMPTON, R. W. ET AL, AUSTRALIAN J. PHYS. 22, 715 (1969).
ROTATION R(0-2) R(1-3)	GIBSON, D. K., AUSTRALIAN J. PHYS., 23, 683 (1970).
VIBRATION V(0-1)	FOR .52 < E < 2.6 EV, CROMPTON, GIBSON, & MCINTOSH, AUSTRALIAN J. PHYS., 22, 715, (1969). FOR E < 2.6 EV, KIEFFER, JILA INFORMATION CENTER REPORT 13, (1973).
V(0-2) V(0-3)	EHRHARDT, H., ET AL, PHYS. REV., 173, 222 (1968).
V(0-4) V(0-5)	PRIVATE COMMUNICATION WITH J. N. BARDSLEY & J. M. WADEHRA, 1979.
DISSOCIATIVE ATTACHMENT V0-V4	WADEHRA, J. M. & BARDSLEY, J. N., PHYS. REV. LETT., 41, 1795, (1978).
V5-V9	EXTRAPOLATED FROM POINTS RECEIVED VIA PRIVATE COMMUNICATION WITH J. N. BARDSLEY, & J. M. WADEHRA, 1979.
ELECTRONIC E1 E2	ENGELHARDT AND PHELPS, PHYS. REV., 131, 2215 (1963).
DISSOCIATION	CORRIGAN, S. J. B., CHEM. PHYS., 43, 4381 (1965).
IONIZATION	RAPP, D., AND ENGLANDER-GOLDEN, P., J. CHEM. PHYS., 43, 1464 (1965).

Table I. Electron Impact Excitation Processes

The dissociative attachment cross sections are the impetus and the key to this investigation. Allan and Wong[6] experimentally found that the threshold cross-section in the 3.75 eV resonance region increases by more than tenfold for each increase in vibrational quantum number, V=0 to 3, and by a three-fold increase from rotational level J=0 to J=7. Calculations by Bardsley and Wadehra[7] using resonant scattering theory have resulted in a comprehensive set of cross-sections (Fig 2) which establish the V-level and the J-level dependence of dissociative attachment from the ground electronic state $^1\Sigma_g^+$ of molecular hydrogen through the

$$(1\sigma_g)^2 \quad (1\sigma_u)^2\Sigma_u^+ \text{ and}$$

$$(1\sigma_g X 1\sigma_u)^2 \ ^2\Sigma_g^+ \text{ resonances.}$$

We have utilized these theoretical values. This data set includes dissociative attachment from vibrational states V=0→9 in H_2 and V=0→13 for D_2. Throughout this analysis, we conservatively assume that J=0 in each of the vibrational states. The electron impact cross sections for the additional processes were obtained from Kieffer's compilation.[8] These include the processes of momentum transfer, rotational and electronic excitation, ionization and dissociation. The consistency of this set of cross sections was checked by comparing the calculated values of drift velocity and Townsend ionization coefficient with the experimental compilation of Dutton.[9] These comparisons reveal good agreement.

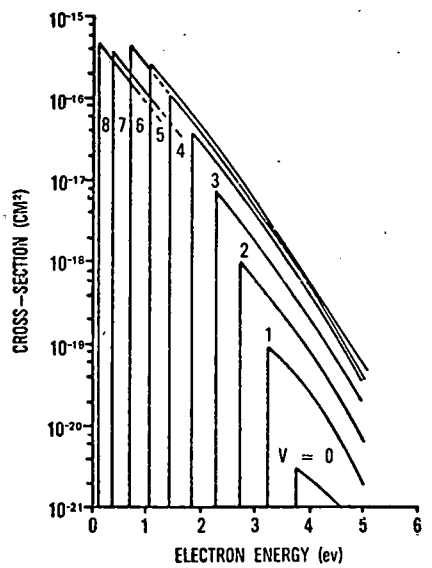

Figure 2. Vibrational State Cross Sections for Dissociative Attachment in H_2. (after Bardsley and Wadehra[7])

It is worth examining the magnitude and vibrational level scaling of the dissociative attachment (DA) cross sections of Bardsley and Wadehra[7] presented in Figure 2. Comparing the value from initial vibrational state V=0 to that from V=6, a five order of magnitude increase in the cross-sections is noted. In addition, the excitation threshold is reduced as the state of vibrational excitation increases. Consequently, one would anticipate a significant increase in the dissociative attachment rate as the vibrational excitation is increased.

Equally important are collision processes involving the heavy particle collisions: atom-molecule and molecule-molecule. The primary energy transfer mechanisms resulting from the collisional interaction of heavy particles are Vibration-Translation exchange (V-T) and Vibration-Vibration exchange (V-V).

A V-T exchange is characterized by a collision of a molecule with another molecule/atom in which the molecule gains or loses vibrational energy from/to the translational mode. A V-V exchange may occur when two molecules collide. In this exchange, one molecule gains vibrational energy, the other loses vibrational energy, and any energy mismatch is compensated by the translational mode.

Formally, each state population will be governed by an equation:

$$\frac{dN_V}{dt} = \sum_{I,J,K} \tilde{R}^{K,I}_{J,V} N_J N_K - \sum_{I,J,K} \tilde{R}^{I,K}_{V,J} N_V N_I$$

where N_V is the concentration of molecules in state V, and the $\tilde{R}$'s represent generalized rate coefficients for the population or depopulation of state V. This set of equations is commonly referred to as the Master Equation. We proceed by writing these rate equations for the instantaneous population of the V-th vibrational state, N_V.

$$\dot{N}_V = n_e \sum_K \left(-R_{VK} N_V + R_{KV} N_K\right) - N_V d_V +$$

$$r_V A^2 + N_{V+1}\left(VT_{V+1,V} + \sum_{K=0}^{V^*-1} VV^{K,K+1}_{V+1,V} N_K\right)$$

$$-N_V\left(VT_{V,V-1} + VTB_{V,V+1} + \sum_{K=0}^{V^*-1} VV^{K,K+1}_{V,V-1} N_K + \right.$$

$$\left. \sum_{K=1}^{V^*} VV^{V,V+1}_{K,K-1} N_K\right) + N_{V-1}\left(VTB_{V-1,V} + \sum_{K=1}^{V^*} VV^{V-1,V}_{K,K-1} N_K\right)$$

Here the first term accounts for electron impact collisions and the last five terms account for heavy particle collisions with

$d_V(sec^{-1})$ = dissociation rate out of level V

$N_V(cm^{-3})$ = vibrational population of level V

$r_V(cm^3\ sec^{-1})$ = recombination rate into level V

$A(cm^{-3})$ = atom number density

$n_e(cm^{-3})$ = electron number density

V* ≡ last bound vibrational state

$R_{VK}(cm^3 sec^{-1})$ = electron excitation rate from vibrational state V to K

$VV^{K,K+1}_{V+1,V}\ (cm\ sec^{-1}) = Z\ P^{K,K+1}_{V+1,V}$ = V-V transfer rate for V+1→V and K→K+1

$VT_{V+1,V}(sec^{-1}) = ZMP_{V+1,V}$ = V-T transfer rate for V+1→V

$VTB_{V,V+1}(sec^{-1}) = ZMP_{V,V+1}$ = V-T transfer rate for V→V+1

Z is the gas kinetic collision frequency and M is the total gas density.

We have utilized the V-V and V-T rate coefficients from the theory of Schwartz, Slawsky and Hertzfeld[10] as modified by Keck and Carrier[11] These results were fitted to the theoretical calculations of Billing [12] and the experimental data of Ducing.[13] These heavy particle rate coefficients were supplemented by the electron impact rates for vibrational excitation and dissociative attachment and the Master Equation was integrated. Since the temporal evolution is governed by the transition probabilities, V-V and V-T, which range over many orders of magnitude, the resulting time constants for the coupled set of equations differ substantially in magnitude. Consequently, we have utilized the multi-step implicit stiffly stable scheme proposed by Gear.[14]

Thus, the time evolution of the populations of the H_2 vibrational levels N_V can be calculated. The rate of excitation, R_{IJ}, of the vibrational state J from vibrational state I and the rate of dissociative attachment are calculated self-consistently with the existing excited state densities by solving the collisional Boltzmann equation for the electron energy distribution function. The electron distribution function, differing substantially from a Maxwellian, is then recalculated to account for changes in the molecular vibrational populations which, in turn modify the electron distribution and, consequently, the vibrational excitation and dissociative attachment rates. The calculation is carried on until a steady state solution for the electron energy distribution and the vibrational populations is found. Superelastic vibrational collisions, derived from the excitation cross sections by the principle of detailed balance, have been included.

Results of Calculations

Using the cross-section data and a numerical solution of the Boltzmann equation in the "P1 approximation,"[15], the electron energy distribution function was calculated for a wide range of values of the ratio $(\frac{E}{N})$. The values of $(\frac{E}{N})$ between 5 and 40 Townsend (1 Td ≡ 10^{-17} volts cm^2) correspond to electron energies in the range 0.5 - 3 eV. These mean energies are typical of those encountered in self-sustained and electron-beam sustained discharges. Having the electron energy distribution function, it is then possible to determine the fractional energy transfer by the electrons into the various rotational, vibrational and ionization channels as functions of E/N, as shown in Figure 3 for the assumed condition of zero vibrational (all molecules in the ground vibrational state) and rotational temperatures. Note that over most of the E/N range, the input energy is channeled mainly into vibrational excitation, dissociation, and electronic excitation. The dissociative attachment process from the ground vibration state absorbs a very minor fraction of the discharge energy. Vibrational excitation is the dominant energy loss in the E/N range of 10 - 50 Townsends. The dominant excitation channel is V=0 to V=1.

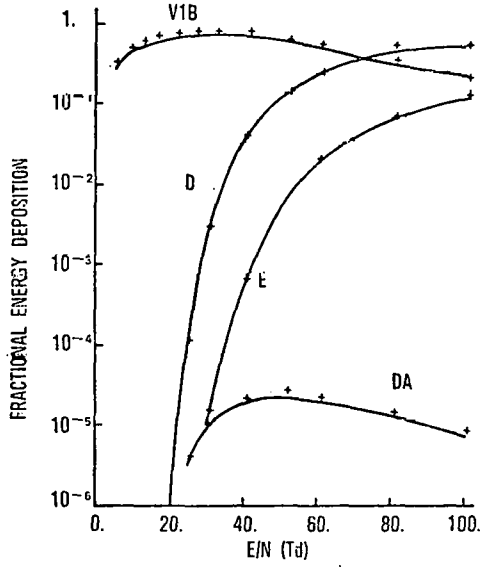

Figure 3. Fractional Energy Deposition into Hydrogen at Zero Vibrational and Rotational Temperatures.

(In Figure 3, VIB represents the fraction of energy into all vibrational levels,

D the fraction into dissociation,

E the fraction into electronic excitation,

DA the fraction into dissociative attachment.)

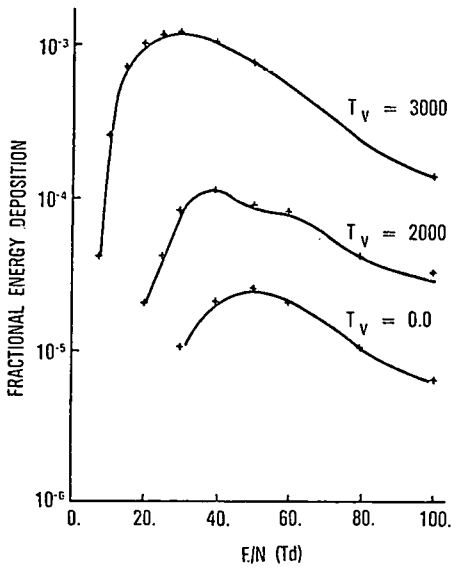

Figure 4. Influence of Vibrational Excitation in Hydrogen on the Fractional Energy Deposition into Dissociative Attachment.

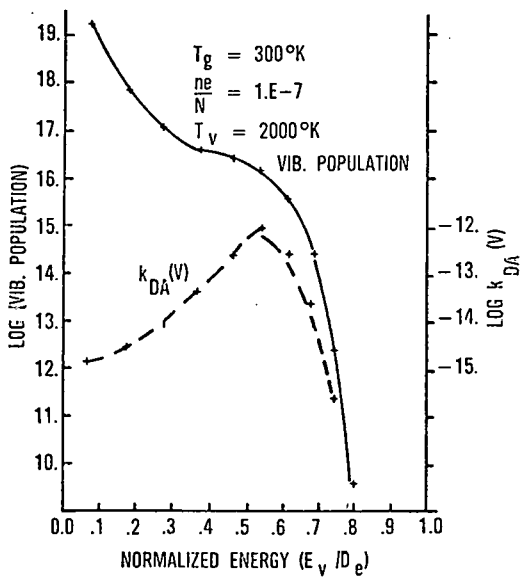

Figure 5. Self-Consistent Vibrational Distribution Function and Rates of Dissociative Attachment in Hydrogen.

To examine the influence of vibrational excitation on the fraction of energy deposited into dissociative attachment, the problem was initially uncoupled and a Boltzmann distribution in the vibrational states was assumed. The fractional energy deposition was calculated as a function of E/N for a realistic range of vibrational temperatures. The results are shown in Figure 4. As anticipated, there is a significant increase (X50) in the fraction of energy deposited into dissociative attachment for the higher vibrational temperatures. In addition, the location of the maximum of the dissociative attachment rate shifts to lower energies, reflecting the lower threshold for dissociative attachment from excited vibrational states.

These results encouraged us to obtain self-consistent solutions for the excited state populations, the electron energy distribution, and the rate of dissociative attachment. We coupled the electron kinetics and the excitation rates to the vibrational kinetics of the Master Equation and parameterized the non-equilibrium dissociative attachment process in hydrogen over a range of fractional ionization from 10^{-8} to 10^{-6} and E/N from 20 to 60 Townsend. Typical results are presented in Figure 5, for an E/N = 40 Townsend, fractional ionization of 10^{-7}, and a translational temperature of 300°K. The resulting vibrational distribution is presented in a semi-log plot as a function of the normalized vibrational energy. A Boltzmann distribution, characterized by a temperature T_V, would appear in this format as a straight line with slope of $(kT_V)^{-1}$. In this example, the vibrational temperature associated with the first two levels "$T_{V(1)}$" is approximately 2000°K. However, the actual vibrational distribution exhibits a significant departure from this straight line behavior. This departure can be understood by considering the relative magnitude of the V-V and V-T exchange rates. At low vibrational quantum numbers the Master Equation is dominated by V-V exchanges. In this regime, the vibrational distribution is given analytically by the Treanor distribution.[16]

$$N_V = N_0 \exp\left\{ -\frac{V(E_1-E_0)}{kT_{V(1)}} + \frac{V(E_1-E_0) - (E_V-E_0)}{kT} \right\}$$

Beyond the minimum of the Treanor distribution, the distribution departs from the Treanor form and a "resonance" or "plateau" region is established. In this region, resonant V-V exchanges dominate the distribution which is well approximated by $N_V V$=constant. In a third region, at high vibrational quantum numbers, a Boltzmann distribution at the gas temperature is obtained, reflecting the dominance of the V-T process.

Returning to Figure 5, note that the population in vibrational states V=5, 6, 7 exceeds the Boltzmann (at T_V = 2000°K) values by two orders of magnitude. This enhanced non-equilibrium population, encountered under conditions of strong vibrational excitation and low translational temperature, is caused by V-V exchanges. In a V-V collision, a quantum of vibrational energy is exchanged by the vibrational modes of the collision partners. Such exchanges are not typically an exact resonant energy transfer, due to the energy mismatch resulting from the anharmonic nature of the vibrational states. This energy defect must be compensated in a simultaneous exchange with the translational and rotational modes. As a result, at low translational temperatures, vibrational exchanges between states m and n (with m>n) have a greater probability of producing V-V transitions to states m + 1 and n - 1 compared to transitions to states m - 1 and n + 1. This biasing of the flux of vibrational quanta, termed anharmonic pumping, occurs because the former transition results in a net surplus of energy which is readily fed into the translational mode. The latter transition, in contrast, requires that energy be supplied from the translational mode; but, at low temperatures, relatively little energy is available.

Thus, anharmonic pumping, which leads to an enhancement in the population of the high lying vibrational states, produces a substantial increase in the rate constants for dissociative attachment, $k_{DA}(V)$, where

$$k_{DA}(V) = \frac{N_V}{N} \langle \sigma_V(v)\, v \rangle$$

These rate constants, also shown on Figure 5, exhibit a maximum for $(E_V/D_0) = 0.5$. This corresponds to the vibrational level V=5. The contribution of this level alone to dissociative attachment exceeds that of the ground state by almost three orders of magnitude.

Having established how the vibrational kinetics couple into the dissociative attachment coefficient, we examine the dependence of this coefficient on the fractional ionization. This establishes the dependence of the coefficient on the strength of the vibrational excitation. Using the numerical solution of the Boltzmann equation for the electrons and the coupled vibrational kinetics solutions, the dissociative attachment rate was calculated for fractional ionization ranging from 10^{-9} to 10^{-6} at gas temperatures of 100°, 200°, and 300°K. The results for an E/N = 40 Townsend are presented in Figure 6. Consider first the results at 300°K. At this temperature, the effective dissociative attachment rate per electron exhibits a linear dependence on fractional ionization. Thus, the net rate of dissociative attachment is quadratic in electron density. This is to be expected from a chained reaction consisting of an electron impact excitation and subsequent electron impact dissociative attachment. Contrast this result with the calculated value for the dissociative attachment rate when only the ground state is considered. For this case, the coefficient is independent of fractional ionization and is orders of magnitude lower.

Next, consider the influence of variations in the gas temperature on the calculated dissociative attachment coefficient by again referring to Figure 6. The reduction of the gas temperature from 300°K to 200°K enhances the anharmonic pumping which results in an increased vibrational population in the "plateau" region and an extension of this region to higher vibrational quantum number. As a result, a significant increase in k_{DA} is obtained. However, a further reduction in the temperature to 100°K produces only a small additional increase. This saturation of the enhancement reflects the leveling off of the dissociative attachment cross sections for vibrational levels V>6 and the increased influence of dissociative attachment losses on the vibrational distribution.

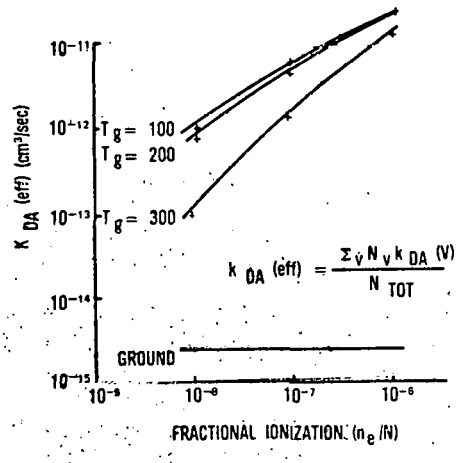

Figure 6. Non-Equilibrium Enhancement of Dissociative Attachment in Hydrogen Versus Translational Temperature (T_g) and Fractional Ionization.

Conclusions

As a result of this analysis, we conclude that under appropriate discharge conditions, the rate of production of negative ions in a hydrogen plasma can be significantly enhanced. For a high pressure discharge operating at an E/N of 40 Townsend and a gas temperature of 200°K, the effective rate constant is increased over three orders of magnitude. Since the negative ion production is dominated by contributions from high lying vibrational states whose populations are determined by non-equilibrium pumping, it is important to determine self-consistently the state of vibrational excitation when analyzing the H_2 discharge. Even in a discharge at low pressure, if the wall deactivation of the vibrational levels is not 100% effective, one may anticipate increased dissociative attachment

due to a finite vibrational temperature at the E/N values required for a self-sustained discharge (Figure 4).

Currently a similar calculation is underway for D_2 plasmas. While this analysis is incomplete at this time, some comments can be made. D_2 is similar to H_2 from both an electron kinetic and vibrational kinetic standpoint. Three important differences exist: the vibrational energy level spacing, the anharmonicity, and the vibrational dissociative attachment cross sections. H_2 has a first vibrational energy level spacing of approximately 0.5 eV, while that of D_2 is 0.35. H_2 is more anharmonic than D_2, with both D_2 and H_2 having essentially the same dissociation energy. These facts yield the net result that D_2 has 22 bound vibrational levels, whereas H_2 has 15. The D_2 cross sections, calculated by Bardsley and Wadehra[7] are presented in Figure 7. These cross sections should be compared with those for H_2 in Figure 2. Note that the ground state cross sections for H_2 exceed those for D_2 by a factor of 500, while the cross sections become comparable for higher vibrational states of similar energies. Using available cross sections for D_2, we obtained the fractional energy deposition into deuterium at zero vibrational and rotational temperatures shown in Figure 8. Given these data and accounting for the scaling of the V-V and V-T rates from H_2 to D_2, we predict that the dissociative attachment rate of D_2 will be similar to that of H_2 under similar excitation conditions.

Having established that the rate of production of negative ions in a hydrogen or deuterium plasma can be optimized and enhanced by suitable choice of discharge parameters and gas conditioning, we briefly consider candidate systems for accomplishing this goal. The non-equilibrium conditions required are obtained by operating the device at optimum E/N for vibrational excitation and a low translational temperature. By requiring that the fractional ionization can be made independent of E/N, we are led to consider two possible discharge arrangements: (1) a single discharge maintained by auxiliary ionization, (2) a tandem discharge in which a pre-excited plasma is flowed into a drift region. In order to enhance the anharmonic pumping, it is desirable to operate the single discharge at pressures high enough to ensure that V-V effects dominate the vibrational kinetics. The low translational temperature for this arrangement can be maintained with cryogenic cooling of the gas or by using convective cooling. The first stage of the tandem discharges may take place in a high pressure chamber with a slot nozzle expansion yielding the desired low translational temperature in the second discharge (drift) region. In the second discharge region, operating at a reduced pressure, we can incorporate an extraction field in addition to the drift field. Alternative configurations include a discharge in a supersonic stream under pulser sustainer excitation or use of an external electron beam to provide high fractional ionization and a sustainer field to give efficient vibrational excitation and dissociative attachment.

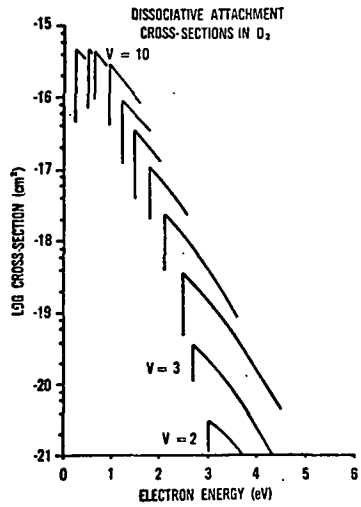

Figure 7. Vibrational State Cross Sections for Dissociative Attachment in D_2 (after Bardsley and Wadehra[7])

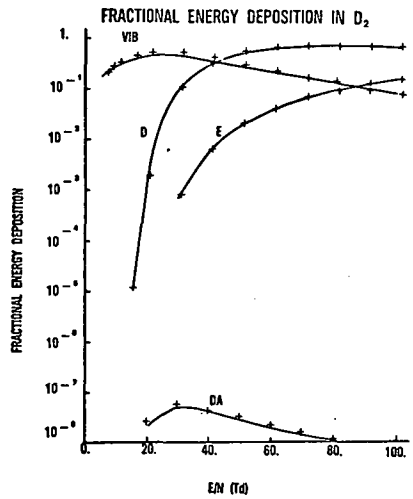

Figure 8. Fractional Energy Deposition into Deuterium

The first set of schemes is the preferred approach. Although the vibrational excitation is high over a wide range of E/N values, there is a distinct advantage to operating at low E/N. This avoids significant direct electron impact dissociation of the hydrogen and the subsequent rapid vibrational-translational energy transfer from the atomic hydrogen collisions with the vibrationally excited molecular hydrogen.

In summary, we have shown that numerical solutions of the Boltzmann transport equation coupled to a vibrational kinetics Master Equation can be used to calculate atomic hydrogen negative ion production under non-equilibrium electrical discharge conditions. The calculations indicate that production will be significantly enhanced by vibrationally exciting the molecular hydrogen and maintaining low translational temperatures by environmental control or by gas dynamic expansion. Studies to calculate the achievable negative densities for some of the proposed configurations are in progress.

References

1. Bacal, M., and Hamilton, G.W., "H^- and D^- Production in Plasmas," Phys. Rev. Letters, Vol. 42, 1538, (1979).

2. Bacal, M., Hamilton, G.W., Bruneteau, A.M., Daucet, H.J., and Taillet, J., Rev. Sci. Inst. 50, 719 (1979).

3. Hiskes, J.R., Bacal, M., and Hamilton, G.W., Lawrence Livermore Laboratory Report UCID-18031, (January 1979).

4. Rich, J.W., and Treanor, G.W., "Vibrational and Relaxation in Gas-Dynamic Flows," Annual Reviews of Fluid Mechanics, Vol. 2, pp. 355-396, (1970).

5. Kolos, W., and Roothaan, C.C.J., "Accurate Electronic Wave Functions for the H_2 Molecule," Rev. Mod. Phys., Vol. 32, pp. 219-232, (1960).

6. Allan, M., and Wong, S.F., "Effect of Vibrational and Rotational Excitation on Dissociative Attachment in Hydrogen," Phys. Rev. Letter, Vol. 41, 1791-1794, (1978).

7. Bardsley, J.N., and Wadehra, J.M., "Dissociative Attachment and Vibrational Excitation in Low Energy Collisions of Electrons with H_2 and D_2," Phys. Rev. Vol. A20, 1398, (1979).

8. Kieffer, L.J., "A Compilation of Electron Collision Cross Section Data for Modeling Gas Discharge Lasers." J.I.L.A. Information Center Report 13, September (1973).

9. Dutton, J., "A Survey of Electron Swarm Data" J. Phys. Chem. Ref. Data, 4, 577 (1975).

10. Schwartz, R. N., Slawsky, Z.I., and Herzfeld, K.F., "Calculation of Vibrational Relaxation Times in Gases." Journal of Chemical Physics, Vol. 20. 1591 (1952).

11. Keck, J.C., and Carrier, G. "Diffusion Theory of Non-Equilibrium Dissociation and Recombination." Journal of Chemical Physics, Vol. 43. 2284 (1965).

12. Billing, G.D. and Fisher, E.R., "VV and VT Rate Coefficients in H_2 by a Quantum-Classical Model" Wayne State University Report (1975).

13. Audiberty, J.J., Joffrin, C., and Ducing, J., "Vibrational Relaxation of H_2 in the Range 500-40°K," Chem. Phys. Letter, Vol. 25, pp. 158-163, (1974).

14. Gear, C.W., "The Automatic Integration of Stiff Ordinary Differential Equations" Communications in ACM, Vol. 14. 176 (1971).

15. Bailey, W.F., "Collisions Induced Dissociation of Diatomic Molecules," Air Force Aero Propulsion Laboratory Report AFAPL-TR-78-105, (1978).

16. Treanor, C.E., Rich, J.W., and Rehm, R.G., "Vibrational Relaxation of Anharmonic Oscillators with Exchange-Dominated Collisions," J. Chem. Phys., Vol. 48, pp. 1708-1807, (1968).

DISCUSSION

HISKES In your third region, where the population distribution is falling off very sharply, is that due mainly to the VV rates or the VT rates?

BAILEY The third region, the Boltzmann region, is driven by the large magnitude of the VT rates, not the VV. If the VV continued to control the distribution the plateau would extend.

HAMILTON And the VT rate increases just because the vibrational spacing goes smaller?

BAILEY Yes, and that indeed is the contribution that Keck and Carrier made. They were taking into account the change in the collision process from an adiabatic collision to a highly impulsive collision as the energy level spacing gets smaller. Another thing that I would like to point out is that when you are scaling these rates with respect to vibrational quantum number and with respect to temperature, you must be careful that these things increase very rapidly and you do not want them exceeding gas kinetic by 10 or 20 orders of magnitude. There has to be some reality. So we have truncated these rates at the gas kinetic collision frequency for both the VV and VT.

EHLERS What was this consideration that gave you an isotope effect?

BAILEY I think there would be essentially no isotope effect. What I have here is, I have over laid the cross-sections for deuterium over that of hydrogen and if we would look only at the ground state cross-sections as a function of vibrational level, we find that at similar energies the cross-sections have similar magnitudes. If we were to compare hydrogen and deuterium, we would find out that the main differences lie in the energy level spacing of the first level, the anharmonisity and also the dissociative attachment cross-sections. However, if we account for the vibrational level scaling and adjust our VT in the VV rates scaling according to the mass, what we will find out is that under similar excitation conditions the rate of dissociative attachment from D_2 is essentially equal to that in H_2.

GRAHAM As I understand it, if you run a hydrogen/deuterium mixture then that plateau region changes, is that correct? Then this might be an interesting way to test that these mechanisms are going on.

BAILEY I am not sure I understand your question. Are you talking about the influence of deuterium on the vibrational energy distribution?

GRAHAM Right, if you have instead of H_2 or D_2, you had HD molecules, then this plateau region tends to be somewhat more exaggerated, away from the Boltzmann. Is that correct?

BAILEY I am not familiar with this. I have not looked at that myself. I have looked at the deuterium and hydrogen, but never at HD and it is quite difficult to get a handle on the relative magnitude of the rates. And that is going to be the critical thing, the ratio of the VV exchanges to the VT in determining how far out this plateau extends. The actual functional dependance of the plateau should not be altered significantly. Does that answer your question?

GRAHAM Yes.

McGEOCH Have you considered the VT relaxation with H atoms rather than H_2 molecules.

BAILEY Yes we have. We have worried about it and that was our concern for tailoring the E/N. If we look at that fractional energy deposition curve that I showed you earlier, we will see that a fairly significant fraction of the discharge energy is going into dissociation. As you pointed out, the dissociation products, the atomic hydrogen turns out to be a very efficient quencher of the vibrational state. As a result when we are running the discharge we would like to operate in a regime where we are not generating that many atomic species. So, it is a concern.

D^- PRODUCTION BY CHARGE TRANSFER IN METAL VAPORS*

A. S. Schlachter

Lawrence Berkeley Laboratory
University of California
Berkeley, California 94720

Abstract

Fast D^- ions can be produced from D^+ by multiple charge-transfer collisions in a metal-vapor target. Experimental cross sections and thick-target D^- yields are presented and discussed. The high D^- yield experimentally observed from charge transfer in cesium vapor is consistent with recent low-energy cross-section calculations and measurements.

I. Introduction

Many studies are underway to find methods for producing fast D^- beams which, when neutralized, can be used for heating confined plasmas for fusion. Some of these studies[1] make use of multiple charge transfer of relatively low energy deuterium beams (keV energies) in metal-vapor targets to produce D^- ions which are subsequently accelerated and neutralized to produce high-energy D^0 beams. The atomic physics of D^- formation by charge transfer in metal vapors is the topic of this review. Experimental results for cross sections and D^- yield in thick targets are comprehensively presented, along with some commentary, and certain targets, particularly cesium vapor, are discussed in more detail, including a comparison of experimental and theoretical results.

Considerable progress has been made in understanding D^- formation in metal vapors since this topic was last reviewed[2] in 1977. Although there are still discrepancies between various measurements, consistent cross sections and yields, and more favorable agreement of experimental and theoretical results, have replaced the major discrepancies noted in 1977.

The earliest report of a large D^- yield by charge transfer in a metal vapor was by Drake and Krotkov,[3] who remarked in 1966 that as much as 25% of 1-keV D^+ could be converted to D^- in a thick cesium-vapor target. Grüebler et al.[4] and Schlachter et al.[5] reported more comprehensive results in 1969. We have recently[6] reported comprehensive measurements of D^- formation in cesium, sodium, and rubidium vapors.

There are two related quantities pertaining to thick-target yields: the equilibrium yield (F_i^∞) and the conversion efficiency (η_i^{opt}). Their relationship is discussed in detail in Ref. 6. The fraction of the total beam leaving a target in charge state i is $F_i(\pi)$, where π is the line density or target thickness. If $I_i(\pi)$ is the intensity of the component in charge state i leaving a target of line-density π:

$$F_i(\pi) = \frac{I_i(\pi)}{\sum I_j(\pi)}. \tag{1}$$

Thus,

$$F_i(\pi) = 1. \tag{2}$$

The equilibrium fraction in charge state i is:

$$F_i^\infty = \lim_{\pi\to\infty} F_i(\pi). \tag{3}$$

The conversion efficiency is:

$$\eta_i(\pi) = \frac{I_i(\pi)}{I_0} \tag{4}$$

where I_0 is the intensity of the beam incident on the target. Due to scattering losses in the target,

$$\lim_{\pi\to\infty} \eta_i(\pi) = 0. \tag{5}$$

For a given geometry, there is some optimum value of π such that $\eta_i(\pi)$ exhibits a maximum, which we call η_i^{opt}. The value of η_i^{opt} is dependent on target geometry.

II. Experimental Considerations

Typical apparatus for measuring thick-target yields or cross sections in a metal vapor generally requires a fast ion or atom beam, a suitable target, and means of detecting the ions and atoms leaving the target. Although these elements are common to both types of measurements, target and detector design considerations are quite different for the two measurements. For equilibrium-yield measurements one assumes that nearly all particles have undergone several scattering and charge-changing collisions. It is important to collimate the beam leaving the target so as to have equal collection effficiency for ions and atoms. For cross-section measurements, where only a small fraction of the incident particles undergo even one charge-changing collision, it is essential that negligibly few scattering

collisions take place which result in loss of particles before reaching the detectors. Scattering collisions include both elastic and inelastic processes. This requirement generally necessitates collimation of the beam incident on the target. Limited angular acceptance sets a lower energy limit for cross-section measurements for a given geometry; this limit can be determined by varying the target exit aperture.

A difficult part of yield or cross-section measurements is measurement of the flux of neutral atoms. Many authors[7] employ a secondary-electron-emission detector for this purpose. Calibration of the detector can be difficult since it requires a known flux of neutral atoms at the appropriate energy. To overcome this difficulty, some experiments invoke previous measurements[8] which show a constant ratio between secondary-electron emission due to incident D^+ as compared to D^0. Whether this assumption is justified or not, a further complication arises as the emitting surface becomes contaminated with the target material, which changes the secondary-electron-emission coefficient[9] during the course of an experiment. Another approach is to use a pyroelectric detector.[6,10] Since this type of detector is not sensitive to the charge state of the beam being detected, it can be calibrated with an ion beam.

Measurement of target thickness is required for cross-section measurements, i.e., target density and path length must be determined. Methods commonly used to determine target density are (1) inferred from temperature by use of known vapor-pressure data,[6,11] (2) surface-ionization gauge,[5,12] and (3) absorption of resonance radiation.[13]

III. Cross-Section Results

Reported cross-section results for D^+, D^0, and D^- in metal vapors are shown in Figs. 1-7. The labels in the figures are identified in a key.[14-43]

Cross sections for charge transfer in cesium vapor are shown in Figs. 1 and 2. The three experimental results[6,33,34] for σ_{-0} in cesium vapor are in fair agreement with each other for energies greater than 2 keV. Also shown is a theoretical calculation of σ_{-0} by Olson and Liu,[40] who conclude that electron transfer is the dominant electron-loss mechanism at low energies, with only a small contribution from molecular ionization. At high energies, however, they point out that direct impact ionization is the dominant mechanism of electron loss. Experiment and theory do not agree well at very low energies.

There have been several recent measurements[6,34,38] of σ_{0-} in cesium vapor, which are in fair agreement with each other. There have also been several recent calculations[29,31,39] of σ_{0-}. The experimental results for σ_{0-} fall between the various theoretical calculations.

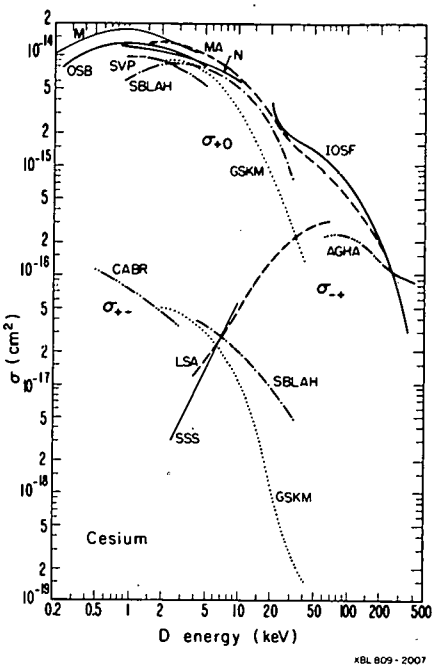

Fig. 1. Cross sections for D ions and atoms in cesium vapor.

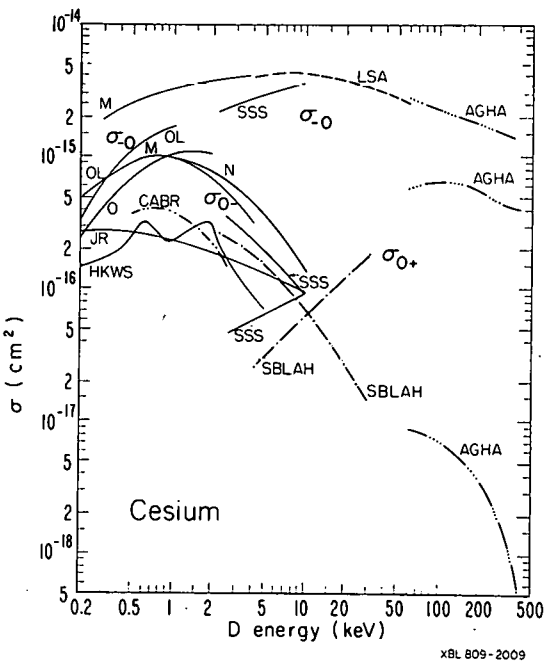

Fig. 2. Cross sections for D ions and atoms in cesium vapor.

Key to Figures

ADP76 Agafanov, D'yachkov, and Pavlii (1976)[14]
ADP80 Agafanov, D'yachkov, and Pavlii (1980)[15]
AGHA Anderson, Girnius, Howald, and Anderson (1977-1980)[16]
AHA Anderson, Howald, and Anderson (1979)[17]
BBPS Berkner, Bornstein, Pyle, and Stearns (1972)[18]
BCKP Berkner, Cooper, Kaplan, and Pyle (1969)[19]
BCW Bohlen, Clausnitzer, and Wilsch (1968)[20]
BLPSS Berkner, Leung, Pyle, Schlachter, and Stearns (1977)[21]
BSA Baragiola, Salvatelli, and Alonso (1973)[22]
CABR Cisneros, Alvarez, Barnett, and Ray (1976)[23]
D D'yachkov (1969)[24]
DR Dimov and Roslyakov (1974)[25]
DZP D'yachkov, Zinenko, and Pavlii (1968-1971)[26]
FM Futch and Moses (1966, 1967)[27]
GAS Girnius, Anderson, and Staab (1977)[28]
GSKM Gruebler, Schmelzbach, Konig, and Marmier (1969, 1970)[4]
HKWS Hiskes, Karo, Willman, and Stevens (1978)[29]
IOSF Il'in, Oparin, Solov'ev and Fedorenki (1965-1971)[30]
JR Janev and Radulovic (1978)[31]
KK Khirnyi and Kochemasova (1970)[32]
LSA Leslie, Sarver, and Anderson (1971)[33]
M Meyer (1980)[34]
MA Meyer and Anderson (1975-1977)[35]
ME Morgan and Ericksen (1978)[36]
MSMK Morgan, Stone, Mayo and Kurose (1979)[37]
N Nagata (1979-1980)[38]
O Olson (1980)[39]
OL Olson and Liu (1980)[40]
OMG O'Hare, McCullough, and Gilbody (1975)[41]
OSB Olson, Shipsey, and Browne (1976)[42]
SBLAH Schlachter, Bjorkholm, Loyd, Anderson, and Haeberli (1969)[5]
SSS Schlachter, Stalder and Stearns (1980)[6]
SVP Spiess, Valance, and Pradel (1972)[43]

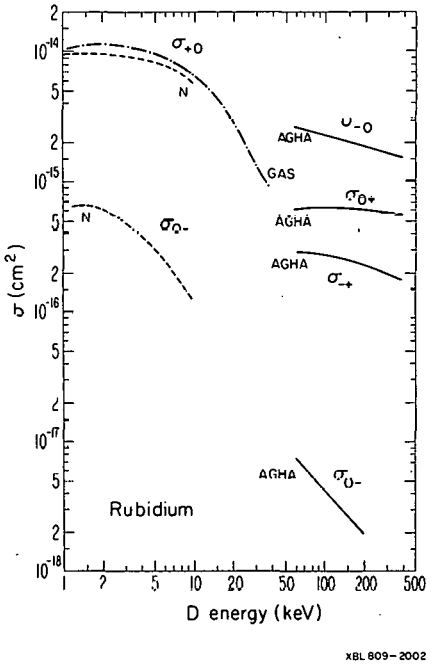

Fig. 3. Cross sections for D ions and atoms in rubidium vapor.

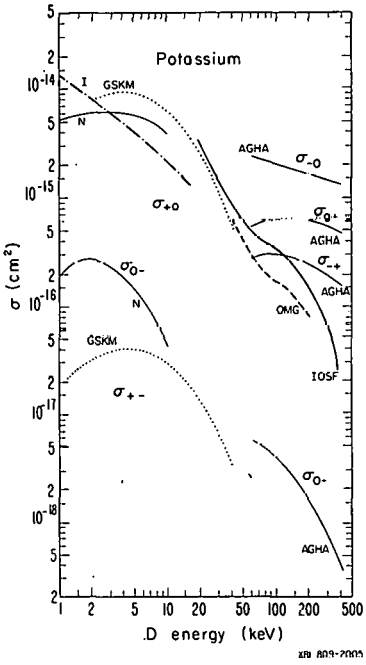

Fig. 4. Cross sections for D ions and atoms in potassium vapor.

IV. Thick-Target Yields

Thick target yields of D^- in alkali and alkaline-earth vapors are shown in Figs. 8-14. These figures include both the equilibrium yield, F_-^∞, and the optimum conversion efficiency, η_-^{opt}. Although η_-^{opt} should always be smaller than F_-^∞, there are some deviations observed in Na and Cs vapors, indicating experimental errors. Some discrepancies between results by different experimenters are probably due to the difficulty of measuring the flux of low-energy atoms leaving the target. Another possibility is failure to achieve sufficient target thickness for equilibrium, which could result from loss of signal due to beam attenuation, or to unwillingness to increase target thickness to avoid excessive loss of target material.

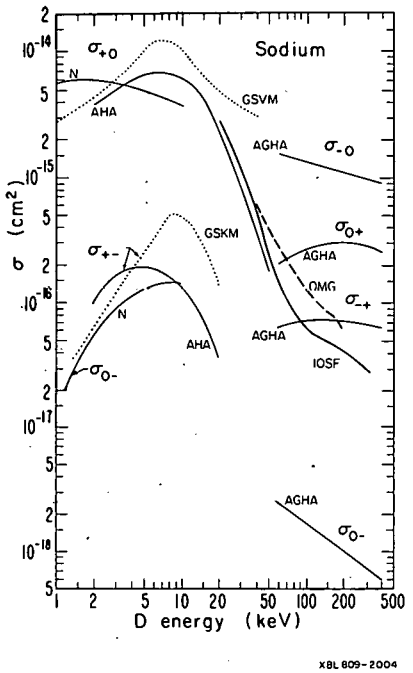

Fig. 5. Cross sections for D ions and atoms in sodium vapor.

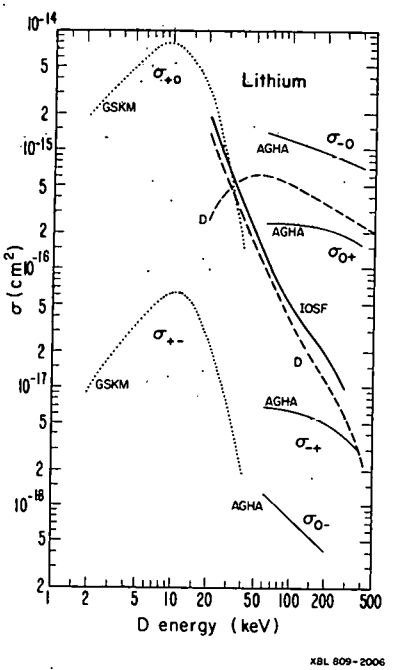

Fig. 6. Cross sections for D ions and atoms in lithium vapor.

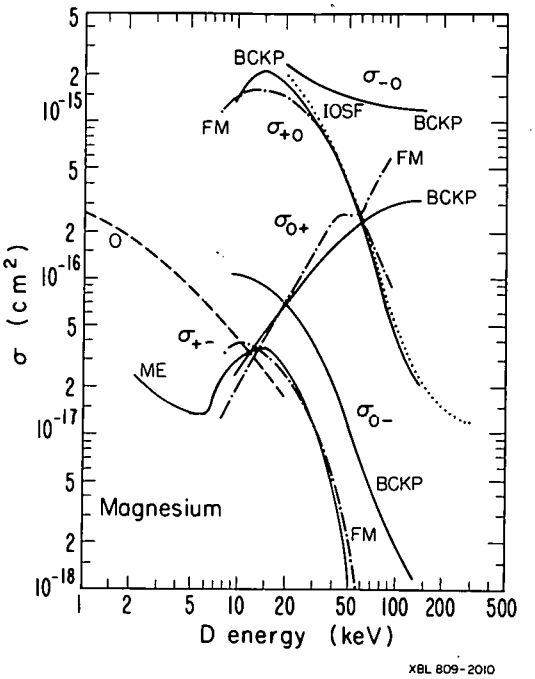

Fig. 7. Cross sections for D ions and atoms in magnesium vapor.

The possibility that differences in various experimental results might be accounted for by physical effects has been discussed elsewhere.[6] We considered three possible effects: target excitation, beam excitation, and target polymerization. We concluded that, although tantalizing, none of these effects could account for observed discrepancies in thick-target yield measurements. Any of these topics could potentially be a fruitful area for further investigation.

The thick-target yield for D^- in magnesium vapor (Fig. 13) is compared with that for beam transmitted through solid magnesium;[18] the yield from the solid is higher than the yield from the vapor. Further measurements of the negative-ion yield from passage through solids or from collision with large clusters of target atoms would be desirable.

D^- formation in the heavy alkaline earths is shown in Fig. 14. The F_-^∞ yield as a function of decreasing energy was observed in Sr vapor,[21] and later in Ca and Ba vapors,[37] to increase after a plateau. Olson and Liu[44] have recently calculated that the cross section σ_{-0} for H^- in Ca vapor will be extremely small at energies below 500 eV. If the cross section σ_{0-} is not correspondingly small at low energies, a large negative ion yield would be predicted. We are presently beginning such measurements.

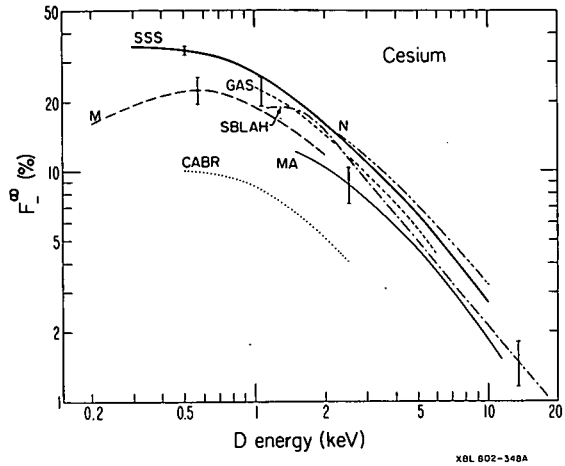

Fig. 8. Equilibrium yield (F_-^∞) for D in cesium vapor.

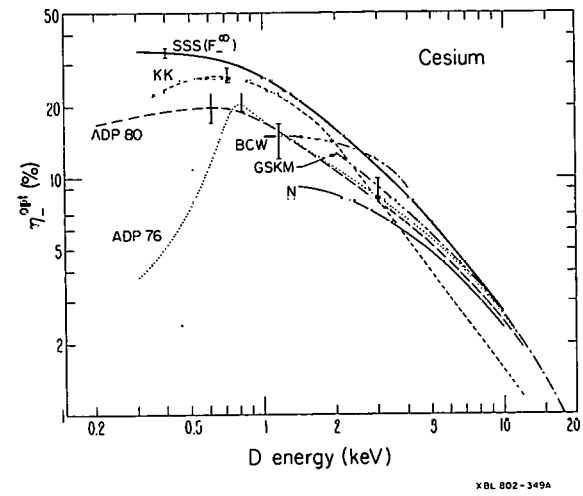

Fig. 9. Optimum conversion efficiency (η_-^{opt}) for D in sodium vapor.

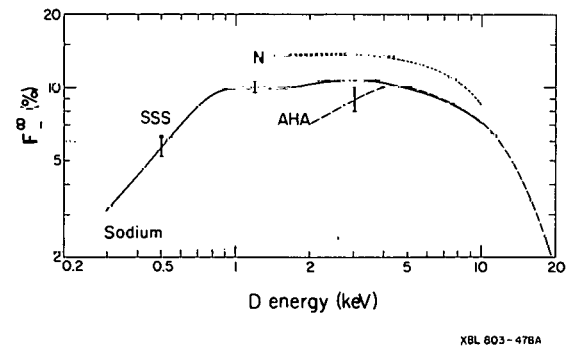

Fig. 10. Equilibrium yield (F_-^∞) for D in sodium vapor.

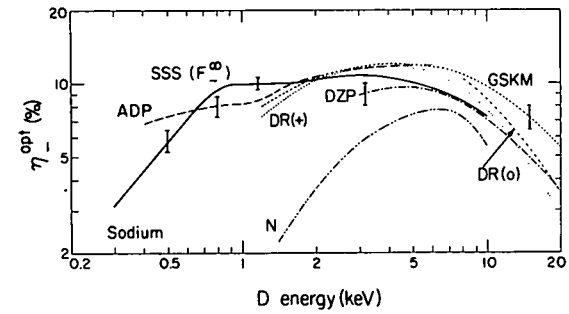

Fig. 11. Optimum conversion efficiency (η_-^{opt}) for D in sodium vapor.

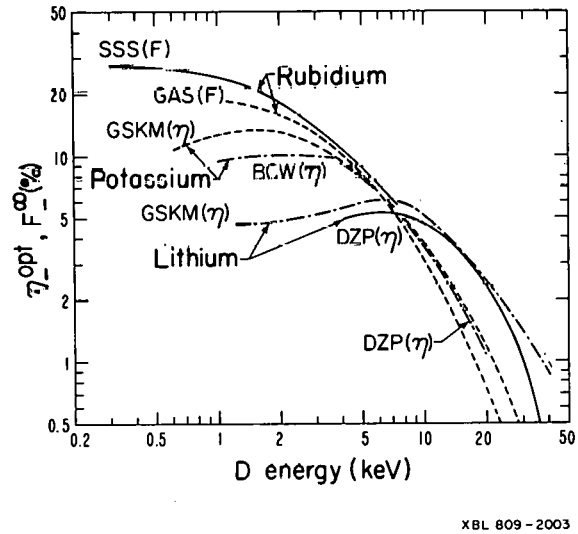

Fig. 12. Equilibrium yield (F_-^∞) and optimum conversion efficiency (η_-^{opt}) for D in rubidium, potassium, and lithium vapors.

We have made a few measurements using D_2^+ and D_3^+ as projectiles incident on cesium and sodium vapor targets, to check whether D_2^+ or D_3^+ might give a greater D^- yield per deuteron at thinner targets than at equilibrium. We discovered no enhancement. F_-^∞ per deuteron is the same for D^+, D^-, D_2^+, and D_3^+ projectiles at the same energy per deuteron. The target thickness required to dissociate D_2^+ or D_3^+ and to reach charge-state equilibrium was an order of magnitude greater than for D^+ or D^- incident, for both cesium and sodium vapor targets.

Equilibrium charge-state fractions can be compared with cross sections, especially for D^- formation at low energies, for which the small D^+ fraction can be neglected. In this case

$$F_-^\infty = \frac{\sigma_{0-}}{\sigma_{0-} + \sigma_{-0}} \quad (6)$$

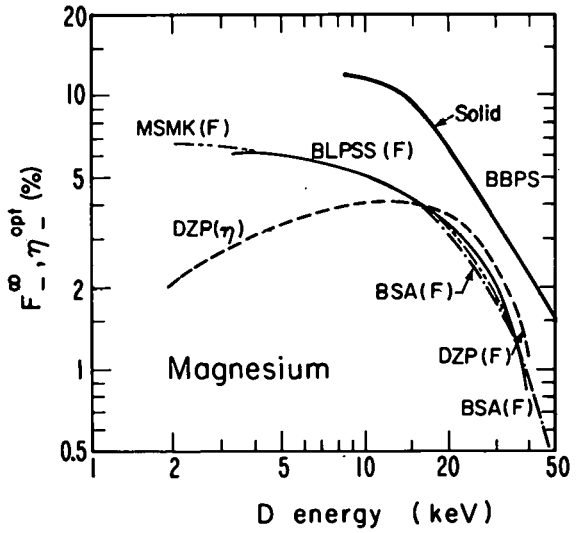

XBL 809-2008

Fig. 13. Equilibrium yield (F_-^∞) and optimum conversion efficiency (η_-^{opt}) for D in magnesium vapor. The curve labeled "solid" is the D^- fraction emerging from a solid magnesium target.

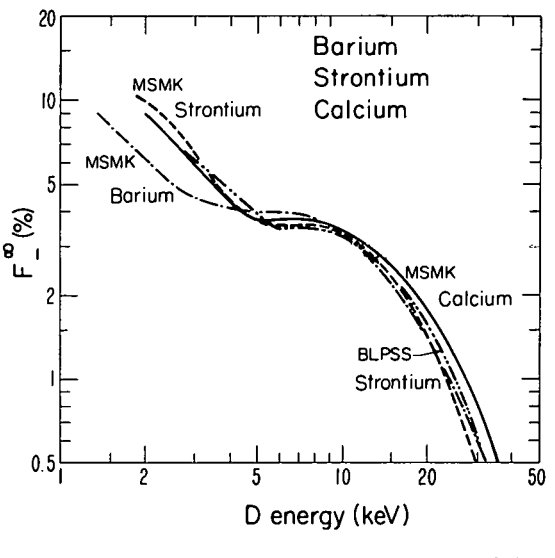

XBL 809-2012

Fig. 14. Equilibrium yield (F_-^∞) for D in barium, strontium, and calcium vapors.

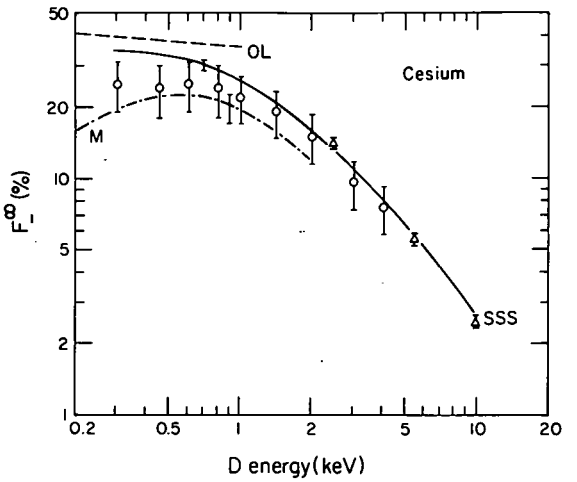

XBL 803-468A

Fig. 15. Equilibrium yield (F_-^∞) for D in cesium vapor measured directly compared with F_-^∞ deduced from calculated and measured cross sections.

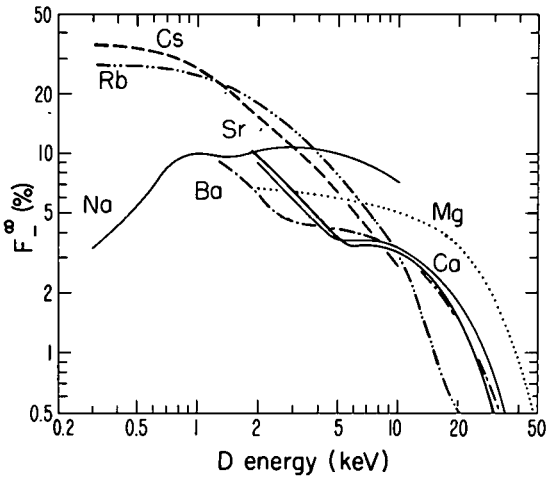

XBL 809-2011

Fig. 16. Equilibrium yield (F_-^∞) for D in various vapor targets.

For cesium vapor we show (Fig. 15) F_-^∞ measured directly,[6,34] deduced from measured cross sections,[6,34] and deduced from calculated cross sections.[39,40] The agreement is fairly good. The large D^- yield observed in cesium vapor at low energies is thus essentially consistent with recently measured and calculated cross sections.

V. Conclusion

Recent cross-section measurements and calculations for D^- formation in cesium vapor are consistent with large experimentally observed D^- yields at low energies. Areas where further research is desirable, especially for high-power D^- beam systems, include target excitation, target polymerization, the interaction of a D^- beam with an ionized target, differential cross sections and measurements of scattering, and collisions of molecular ions.

A summary of F_-^∞ for D in various vapor targets is shown in Fig. 16.

References

* This work was supported by the Fusion Energy Division of the U. S. Department of Energy under contract W-7405-ENG-48.

1. E. B. Hooper, Jr., P. Poulsen, and P. A. Pincosy, submitted to J. Appl. Phys.

2. A. S. Schlachter, in Proceedings of the Symposium on the Production and Neutralization of Negative Hydrogen Ions and Beams, BNL 50727, edited by K. Prelec (Brookhaven National Laboratory, 1978), pp. 11-23.

3. C. W. Drake and R. Krotkov, Phys, Rev. Lett. 16, 848 (1966).

4. W. Gruebler, P. A. Schmelzbach, V. Konig, and P. Marmier, Phys. Lett. A 29, 440 (1969); Helv. Phys. Acta 43, 254 (1970).

5. A. S. Schlachter, P. J. Bjorkholm, D. H. Loyd, L. W. Anderson, and W. Haeberli, Phys. Rev. 177, 184 (1969).

6. A. S. Schlachter, K. R. Stalder, and J. W. Stearns, Phys. Rev. A. (in press); and unpublished.

7. J. A. Ray, C. F. Barnett, and B. Van Zyl, J. Appl. Phys. 50, 6516 (1979); D. H. Crandall and J. A. Ray, Rev. Sci. Instrum. 41, 1282 (1970).

8. P. M. Stier, C. F. Barnett, and G. E. Evans, Phys. Rev. 96, 973 (1954).

9. J. B. Taylor and I. Langmuir, Phys. Rev.44, 423 (1933).

10. K. H. Berkner, B. R. Myers, and R. V. Pyle, Rev. Sci. Instrum. 39, 1204 (1968); M. W. Geis, K. A. Smith, and R. D. Rundel, J. Phys. E. 8, 1011 (1975).

11. R. R. Hultgren, P. D. Desai, D. T. Hawkins, M. Gleiser, K. K. Kelley and D. D. Wagman, Selected Values of the Thermodynamic Properties of the Elements, (American Society of Metals, Metals park, Ohio, 1973).

12. J. B. Taylor and I. Langmuir, Phys. Rev. 51, 753 (1937).

13. P. Pradel, F. Roussel, and G. Spiess, Rev. Sci. Instrum. 45, 45 (1974); P. Pradel, F. Roussel, A. S. Schlachter, G. Speiss, and A. Valance, Phys. Rev A 10, 797 (1974).

14. Y. A. Agafonov, B. A. D'yachkov, and M. A. Pavlii, Pisma Zh. Tekh. Fiz. 2, 757 (1976) [Sov. Tech. Phys. Lett. 2, 296 (1976)].

15. Y. A. Agafonov, B. A. D'yachkov, and M. A. Pavlii, to be published in Sov. Phys. - Tech Phys.

16. C. J. Anderson, R. J. Girnius, A. M. Howald, and L. W. Anderson, Phys. Rev. A 22, 822 (1980); R. J. Girnius, C. J. Anderson, and L. W. Anderson, Phys. Rev. A 16, 2225 (1977).

17. C. J. Anderson, A. M. Howald, and L. W. Anderson, Nucl. Instrum. and Methods 165, 583 (1979).

18. K. H. Berkner, I. Bornstein, R. V. Pyle, and J. W. Stearns, Phys. Rev. A 6, 278 (1972).

19. K. H. Berkner, W. S. Cooper, III, S. N. Kaplan, and R. V. Pyle, Phys. Rev. 182, 103 (1969).

20. H. Bohlen, G. Clausnitzer, and H. Wilsch, Z. Phys. 208, 159 (1968).

21. K. H. Berkner, D. Leung, R. V. Pyle, A. S. Schlachter, and J. W. Stearns, Nucl. Instrum. and Methods 143, 157 (1977); Phys. Lett. 64A, 217 (1977).

22. R. A. Baragiola, E. R. Salvatelli and E. Alonso, Nucl. Instrum. and Methods 110, 507 (1973).

23. C. Cisneros, I. Alvarez, C. F. Barnett, and J. A. Ray, Phys. Rev. A 14, 76 (1976).

24. B. A. D'yachkov, At. Energ. 27, 220 (1969) [Sov. At. Energ. 27, 958 (1969)].

25. G. I. Dimov and G. V. Koslyakov, Prib. Tekh. Eksp. 3, 31 (1974) [Instrum. Exp. Tech. 17, 658 (1974)].

26. B. A. D'yachkov and V. I. Zinenko, At. Energ. 24, 18 (1966) [Sov. At. Energ. 24, 16 (1968)]; R. A. D'yachkov, V. I. Zinenko, and M. A. Pavlii, Zh. Tekh. Fiz. 41, 2353 (1971) [Sov. Phys. - Tech. Phys. 16, 1868 (1972)].

27. K. G. Moses and A. H. Futch, Jr., Bull. Am. Phys. Soc. 11, 344 (1966) and private communication; A. H. Futch and K. G. Moses, Proc. V. Intl. Conf. on Phys. of Electronic and Atomic Collisions, Leningrad, 1967, I.

P. Flaks and E. S. Solovyov, Editors (Nauka, Leningrad, 1967), p. 12. These cross sections were renormalized (multiplied by 0.81) as suggested by K. H. Berkner, R. V. Pyle, and J. W. Stearns, Phys. Rev. 178, 248 (1969).

28. R. J. Girnius, L. W. Anderson, and E. Staab, Nucl. Instrum. and Methods 143, 505 (1977).

29. J. R. Hiskes, A. M. Karo, P. A. Willman, and W. J. Stevens, Phys. Lett. 68A, 221 (1978).

30. R. N. Il'in,. V. A. Oparin, E. S. Solv'ev and N. V. Fedorenko, Zh. Eksp. Teor. Fiz. Pis'ma Red. 2, 310 (1965) [JETP Lett. 2, 197 (1965)];Zh. Tekh, Fiz. 36, 1241 (1966) [Sov. Phys. - Tech. Phys. 11, 921 (1967)]; R. N. Il'in, V. A. Oparin, I. T. Serenkov, E. S. Solov'ev and N. V. Fedorenko, Proc. VII Intl. Conf. on Phys. of Electronic and Atomic Collisions, Amsterdam, 1971, L. M. Branscomb et al, Editors (North-Holland Publishing Co., Amsterdam, 1971), v. 2, p. 793.

31. R. K. Janev and Z. M. Radulovic, Phys. Rev. A 17, 889 (1978).

32. Yu. M. Khirnyi, and L. N. Kochemasova, Prib. Tekh. Eksp. 3, 56 (1970) [Instrum. Exp. Tech. 3, 693 (1970)].

33. T. E. Leslie, K. P. Sarver, and L. W. Anderson, Phys. Rev. A 4, 408 (1971). These results as plotted have been renormalized (multipled by 2.0) to take into account more recent measurements of σ_{+0}.

34. F. W. Meyer, J. Phys. B. (in press).

35. F. W. Meyer, and L. W. Anderson, Phys. Rev. A 11, 589 (1975); Phys. Lett. 54A, 333 (1975); F. W. Meyer, C. J. Anderson, and L. W. Anderson, Phys. Rev. A 15, 455 (1977).

36. I. J. Morgan and F. Ericksen, Phys. Lett. 66A, 198 (1978).

37. T. J. Morgan, J. Stone, M. Mayo, and J. Kurose, Phys. Rev. A. 20, 54 (1979).

38. T. Nagata in Proc. XI Int. Conf. on Phys. of Electronic and Atomic Collisions, edited by K. Takayanagi and N. Oda (Kyoto, Japan, 1979). pp. 512-513; J. Phys. Soc. Japan 46, 919 (1979); to be published in J. Phys. Soc. Japan 48 2068 (1980); and private communication.

39. R. E. Olson, Phys. Lett. 77A, 143 (1980).

40. R. E. Olson and B. Liu, to be published in J. Chem. Phys.

41. B. G. O'Hare, R. W. McCullough, and H. B. Gilbody, J. Phys. B. 8, 2968 (1975).

42. R. E. Olson, E. J. Shipsey, and J. C. Browne, Phys. Rev. A 13, 180 (1976). The results for σ_{0-} and σ_{-0} in this reference have been replaced by those of Refs. 39 and 40.

43. G. Spiess, A. Valance, and P. Pradel, Phys. Rev. A 6, 746 (1972).

44. R. E. Olson and B. Liu, Chem. Phys. Lett. (to be published).

DISCUSSION

HAGENA What is the true value of F^- for deuterium in cesium? Is it 25% or 35%?

SCHLACHTER I really can not do better than to show you these slides.

HAGENA In your experimental data you have a very nice small error bar.

SCHLACHTER Let me show you this slide where I do show the error bars. I can only say that I obtained this result with this kind of an uncertainty. These other results have these uncertainties and these magnitudes. There is a discrepancy and I do not have any way of resolving that at the present time. If you need to know more accurately than that, it will have to wait further measurements. I do not think that this particular discrepancy is going to be resolved.

HAGENA The second question I had in mind was whether the discrepancies may reflect that F^- may be sensitive to the angle of your detector. It may be that there are different values depending on what kind of angular losses or scattering losses you encounter? And a final question: are there any data available for incident neutral molecular beams?

SCHLACHTER In answer to your first question as to whether there could be differences in angle. I think the answer is no because I explored this very carefully by changing the size of the exit aperture of the target and I believe Fred Meyer did likewise. So we both explored this; we both looked as to whether there could be an effect due to excitation of the target. We both varied the intensity of the beam and we looked as to whether there could be an effect due to excitation of the projectiles. In other words that somehow nℓ was not the relevant parameter but that there was some short lived state; for example, that would mean a given choice of line density depended on the target length. The answer there is no also. So, I think that finally we just have a discrepancy and it is not due to anything that I can think of.

Now in answer to your question on incident lecular ions...

GENA Neutrals.

HLACHTER I think I can answer that in the llowing way. We have made measurements with $_2^+$ and D_3^+. That is not with neutrals but with he molecular ions incident on both cesium and sodium. What we have observed is that there are pparently two reaction channels. Let us take he case of D_2^+ incident. In one channel you ake D_2^0 and then you need a tremendously thick target to dissociate it: 10^{16} atoms/cm^2. There s another channel where you make two D^0 and then they reach equilibrium at 10^{14} atoms/cm^2 just as f you had incident D^+ or D^-. So, if you had D_2^0 incident I think you would need 10^{16} atoms/cm^2 in order to dissociate that, but then the result is hat you get the same yield per incident deuteron t the same velocity per deuteron, however a much igher target thickness is required because of the difficulty of dissociating the incident D_2^0.

MEYER I have one comment relative to the equilibrium yield measurements of Cisneros and Alvarez. You implied that my measurements essentially replaced their measurements while in fact there are two separate measurements; mine were done with an optimized geometry. But getting back to the comment on Cisneros and Alvarez. Their yields are artificially low because of a problem in there data analysis. If one properly analyzes their data they, in fact, come out somewhere close to the curve labeled M. So that there is no discrepancy there.

I have a question relating to your neutral particle detection. Have you ever considered the possibility of power reflection from your neutral detector as a function of cesium coverage? Because it is known that power reflection for example is a fairly strong function of surface composition, which would not show up in a calibration curve which was obtained with your target essentially cold.

SCHLACHTER I was going to show you a curve, you have already seen, where we have calibrated the detector as a function of energy. What it shows is that our detector is very linear with energy even down to the lowest energies, which would indicate that without the cesium coverage we are not suffering an energy reflection loss. We have also calibrated the detector at thick targets. This is more difficult to do because you are modulating the smaller fraction of the beam and we have found that the response of the detector is independent of the coverage of cesium upon it. Furthermore, we have used detectors that are silver plated and detectors that are nickel plated and they all behaved the same way. Then finally we made measurements with a solid state detector which we used as an ionization chamber of current amplifier and that behaved the same way also. So, I am actually quite convinced that our detector is independent of alkali metal coverage and I know that you have been concerned about the same problem when it is known that secondary emissions are sensitive functions of the alkali metal coverage.

MEYER Yes, we have verified that the calibration of the secondary emission detector is independent of cesium coverage. I just asked the question in light of some earlier slides that had been shown this morning regarding particle reflection coefficients. Even though it may not have been shown, power reflection coefficients are quite large at low energies.

SCHLACHTER We actually tried to do some calculations based upon some computer calculations. We found that down to a few hundred eV the energy reflection was not too bad. It is at lower energies that it becomes really significant.

PETERSON Would it be possible to analyze your curves which show the metastable population, to determine the deactivation cross section of the metastable?

SCHLACHTER We did that. Those measurements were not recent measurements on the metastables, but were rather measurements from Saclay of vintage 1974. We did do least square fits of charge state component differential equations and we did obtain a cross section for collisional deexcitation of the 2S. It was big, I don't know, 10^{-15} or a couple of times 10^{-15} cm^2.

THEORETICAL INVESTIGATIONS OF THE COLLISION DYNAMICS IN H^- FORMATION AND DESTRUCTION

R. E. Olson
Molecular Physics Laboratory, SRI International
Menlo Park, California 94025

Abstract

A short review will be presented on some of the recent theoretical investigations on heavy particle collision problems related to conversion of beams of H^+ to H^- via sequential capture of two electrons from metal vapor targets. Primarily, the investigations are on alkali metal vapor targets; however, recent calculations indicate there may be several advantages to using heavy alkaline earth vapor targets for ion sources based on low energy collisions, $E \leq 500$ eV/amu. Mention will also be given to the effects of using laser excited alkali atom targets and to collisional processes which dominate the angular scattering of the hydrogen beams.

Introduction

One method of H^- (or D^-) ion source design which is sometimes termed "double electron capture" is based on sequential capture of two electrons from metal vapor targets by intense beams starting as H^+. Such a method originates with H^+ ion sources which are well developed and offers the advantage of long duration operation without excessive heat loading. Results using this method are encouraging, with Hooper and colleagues[1] at LBL recently demonstrating the generation of a 10 msec, 2.2 A beam of D^- at 12 keV using a Na target.

The application of H^- beams for fueling and heating magnetically confined fusion plasmas are well documented[2] and will not be reviewed here. Likewise, we should note that Schlachter[3] has presented an excellent review of the status of experimental efforts on the basic collision problems related to ion sources based on "double electron capture". We will concentrate on the theoretical aspects of the collision processes.

In our review of recent theoretical efforts, we will primarily concentrate on alkali metal target systems because of the interest in these systems. However, we will also discuss alkaline earth systems because theoretical calculations indicate they offer several advantages over alkalis for low energy operation.

The basic collision processes which we will consider are the electron capture reactions

$$H^+ + A \rightarrow H^o + A^+ \qquad (1)$$

and

$$H^o + A \rightarrow H^- + A^+ \qquad (2)$$

and the electron loss reaction

$$H^- + A \begin{cases} \rightarrow H^o + A^- & (3a) \\ \rightarrow H^o + A + e^- & (3b) \end{cases}$$

The total cross section for the above reactions will be denoted by σ_{+o}, σ_{o-}, and σ_{-o}, respectively. We should note that the total cross sections calculated for hydrogen systems are very nearly equal to those for the deuterium systems if compared at the same relative velocity or energy/amu.

The important parameter needed for ion source design is the efficiency of H^- formation. Under multiple collision conditions if σ_{+o} is large and there are negligible reaction paths to reform H^+ from H^o or H^-, the H^- yield is given in terms of the cross sections as

$$Y = \frac{\sigma_{o-}}{\sigma_{o-} + \sigma_{-o}} \qquad (4)$$

In the next several sections, we will discuss the collision dynamics and the trends in the cross sections for reactions (1)-(3) for alkali and alkaline earth targets along with predicted behavior in the thick target yields, Eq. (4).

H^+ + Alkali Atoms

For "double-charge transfer" ion sources based on alkali vapor targets (Alk), the initiating step is the neutralization of the incident H^+ beam

$$H^+ + Alk \rightarrow H^o + Alk^+ . \qquad (5)$$

At low keV/amu energies, the σ_{+o} cross section is large,[3] $\sim 10^{-14}$ cm^2, due to the near degeneracy in potential energies between the reactants and the products in the $H^*(n=2) + Alk^+$ state (see Fig. 1). Excited H(2p) which is formed rapdily radiates to its ground state with the emission of Lyman-α radiation, while the H(2s) is collisionally mixed to the radiating H(2p) state via

subsequent collisions with the Alk. These latter cross sections are calculated[4] to be $\geq 10^{-14}$ cm^2.

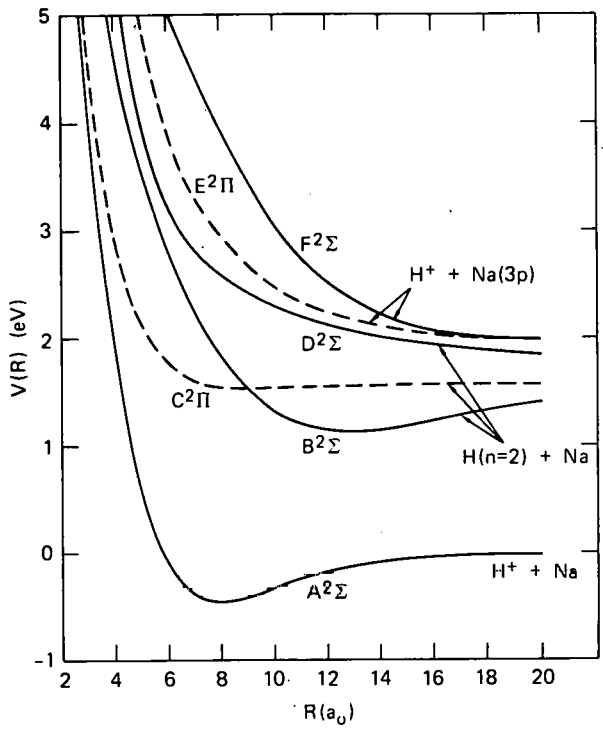

Fig. 1 Interaction energies for NaH^+ from Ref. 5

A question which is frequently asked is whether there would be a significant improvement in the cross sections if the alkali was optically pumped to its resonance state. Referring to NaH^+ interaction energies given in Fig. 1, we can see such a procedure will decrease the ΔE for the neutralization reaction and will lead to increased σ_{+o} cross sections at low energies, $\leq$ 500 eV, when compared to the ground state. For the heavier alkalis, and in particular Cs, the ΔE actually increases for the pumped versus the ground state alkali, so we would predict no significant improvement in the cross sections.[5] For moderate to high operation, E $\geq$ 5 keV/amu, optically pumping an alkali will have a detrimental effect because then impact ionization

$$H^+ + Alk^* \rightarrow H^+ + Alk^+ + e^- , \qquad (6)$$

will dominate over electron capture, reaction (5), giving rise to decreased negative ion yields for a given target gas density.

H^o + Alkali Atoms

The negative ion formation reaction

$$H^o + Alk \rightarrow H^- + Alk^+ \qquad (7)$$

is determined by a curve crossing at large internuclear separations, R $\approx$ 7-10 a$_o$, between the covalent potential originating with the reactants and the ion-pair coulomb potential from the products of Reaction (7) (see Fig. 2). Recent calculations of σ_{o-} for H+Cs reactions are given in Refs. 6 and 7. It is important to note that 75% of the collisions in (7) lead to non-reaction because the $a^3\Sigma$ channel of the reactants is not coupled to the $^1\Sigma$ state of the ion-pair products. This latter consideration severely restricts the maximum σ_{o-} cross section for Reaction (7) to $\sim 10^{-15}$ cm^2.

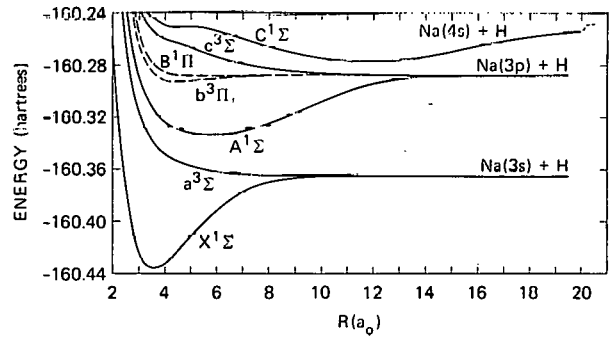

Fig. 2 Interaction energies for NaH from Ref. 8.

The $a^3\Sigma$ state of the alkali hydrides also has another detrimental effect on H^- yields realized in "double charge transfer" ion sources. This is, because the $a^3\Sigma$ state is highly repulsive, it gives rise to considerable large angle elastic scattering for the reaction

$$H^o + Alk \rightarrow H^o + Alk . \qquad (8)$$

As an illustration, elastic cross sections are given in Fig. 3 for Na targets; the heavier alkalis will have larger scattering cross sections. To indicate the extent of the large angle elastic scattering, in Figs. 4 and 5 are shown the percentage of elastic cross section outside a given angle under single collision conditions. Even at 500 eV, over 10% of the elastic cross section of 5×10^{-15} cm^2 is found outside 1°. This process certainly has an unacceptable effect on H^- yields and must be considered in ion source modeling efforts and in low energy σ_{o-} cross section measurements.

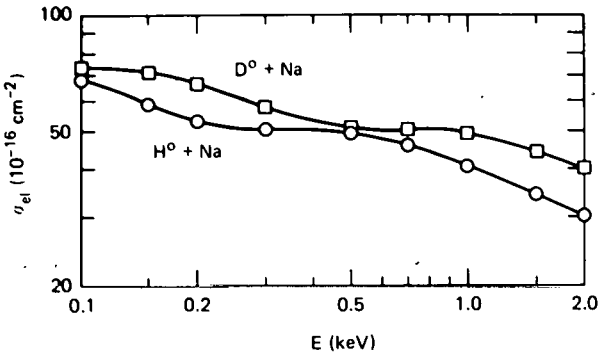

Fig. 3 Total elastic scattering cross sections for H^o + Na and D^o + Na calculated using the interaction energies of Ref. 8.

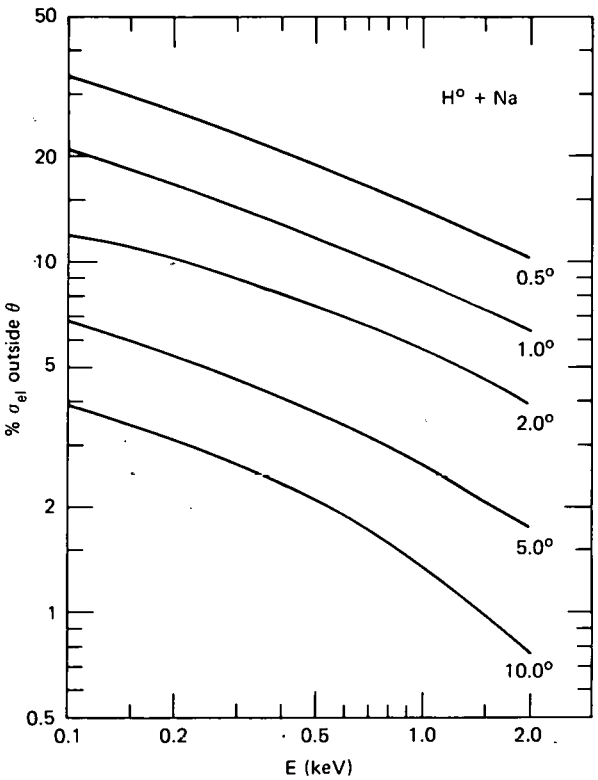

Fig. 4 Percent of the total elastic cross sections found outside various angles for the H^o + Na collision system.

In our theoretical studies, we could not find another $H^{+,o,-}$ + Alk reaction which lead to as much large angle scattering as seen in Reaction (8). Thus, Reaction (8) appears to be the rate-determining step in the angular divergence of the hydrogen beam.

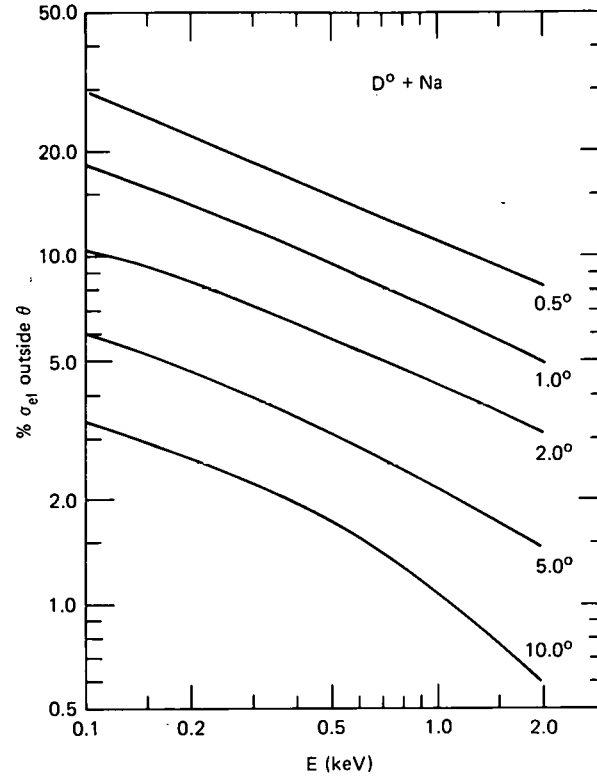

Fig. 5 Percent of the total elastic cross section found outside various angles for the D^o + Na collision system.

H^- + Alkali Atoms

The electron loss cross section σ_{-o} for the reaction

$$H^- + Alk \begin{cases} \rightarrow H^o + Alk^- & (9a) \\ \rightarrow H^o + Alk + e^- & (9b) \end{cases}$$

is especially interesting since two channels are available for reaction, electron capture (9a) and impact ionization (9b). At high energies, $E \geq 1$ keV/amu, the ionization process will dominate the electron loss collisions.

However, at low energies, $E \leq 0.5$ keV/amu, electron capture is a major process.[8] This is best illustrated by referring to the potential energy curves for NaH^-, Fig. 6. Because the alkalis support a bound and stable negative ion state with ionization energies of ~ 0.5 eV, there is a strong mixing between the H^- + Alk and H^o + Alk^- states that induces the electron capture process at large separations, $R \approx 15\ a_o$. Recent σ_{-o} calculations[8] for the alkalis at

E < 500 eV/amu indicate the electron capture component (9a) is ~ 80% of the overall electron loss process.

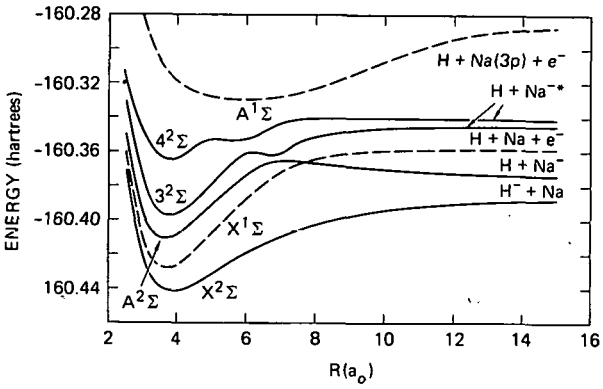

Fig. 6 Interaction energies for NaH$^-$, solid lines, and for NaH, dashed lines, taken from Ref. 8.

H$^+$ + Alkaline Earth Atoms

The H$^+$ neutralization process in alkaline earths (AE) proceeds in a different manner than for the alkalis. For the heavier alkaline earths (masses ≥ Mg), electron capture produces ground state H^o and excited AE ions:

$$H^+ + AE \rightarrow H^o + AE^{+*} . \qquad (10)$$

The potential energy curves[9] for MgH$^+$ can be used as an illustrative example, Fig. 7.

Because it is necessary to both transfer one of the valence shell electrons to the H$^+$ and excite the remaining valence electron, the coupling matrix elements for electron transfer are considerably reduced over those for the alkalis. This leads to smaller cross sections,[3] $\sigma_{+o} \sim 10^{-15}$ cm^2, for the initial neutralization step. However, the cross sections are not so small to prohibit the use of alkaline earths in "double-charge transfer" ion sources.

H^o + Alkaline Earth Atoms

The heavier alkaline earths are predicted to possess larger σ_{o-} cross sections at low energies than realized for the alkalis. This is because in the reaction

$$H^o + AE \rightarrow H^- + AE^+ , \qquad (11)$$

both the reactant and product states can give rise to only one molecular symmetry and spin, $^2\Sigma$. Hence, all collisions of the type (11) can give

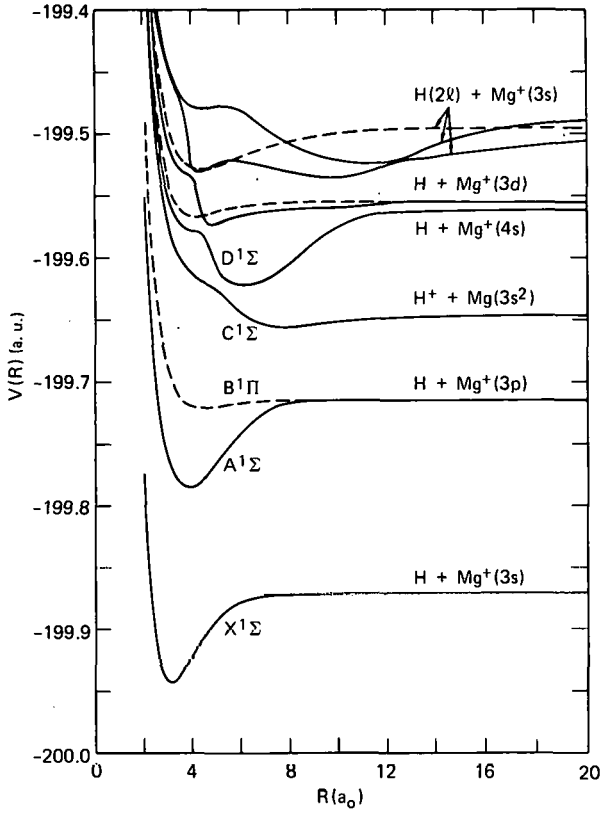

Fig. 7 Interaction energies for MgH$^+$ from Ref. 9

rise to H$^-$, unlike in the alkali systems where only 25% possess the necessary $^1\Sigma$ characteristic.

The potential wells of the X$^2\Sigma$ of the heavier alkaline earth-hydrides are primarily composed of the ion-pair configuration and are deeply bound,[10] Fig. 8. Hence, they should compete favorably with the alkalis for H$^-$ production. Furthermore, the elastic angular scattering will be reduced over the alkalis since there are no highly repulsive potentials in the entrance channel.

H$^-$ + Alkaline Earth Atoms

An interesting aspect of the alkaline earths is that they do not possess a bound and stable negative ion state due to their closed shell configuration. Hence, the electron detachment process can only proceed via the ionization channel

$$H^- + AE \rightarrow H + AE + e^- \qquad (12)$$

Crucial to the prediction of σ_{-o} at low energies, E ≤ 500 eV/amu, is the determination whether or not the potential energy curve for the negative ion reactants of (12) crosses or merges

with the neutral state continuum. If this occurs, as it does in the H^- + rare gas systems,[11] the σ_{-o} cross sections will be large down to very low energies and the H^- yield given by (4) will not surpass that of the alkalis.

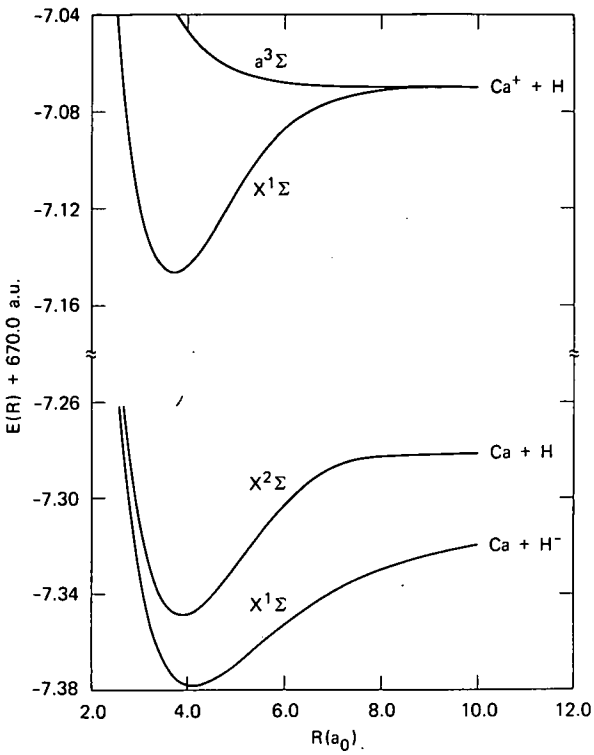

Fig. 8 Interaction energies for the CaH^+, CaH^o and CaH^- from Ref. 10.

However, potential energy calculations[10] indicate that no such crossing exists, Fig. 8. Hence, our prediction is that σ_{-o} for the heavier alkaline earth systems will be very small at $E \leq 500$ eV/amu. At higher energies, a molecular approach is not applicable and σ_{-o} is simply determined by the size of the target atom. Because σ_{o-} should remain large at low energies, we predict the heavier alkaline earths, and in particular Sr or Ba, will surpass the 35% maximum yield realized using Cs. Unfortunately, there are not experiments to test these predictions. However, the trends of the high energy equilibrium H^- yield measurements of Morgan and colleagues[12] indicate there is a possibility for improved H^- yields.

Concluding Remarks

Recent theoretical calculations indicate that:

a) There is no advantage to optically pump the alkalis for ion sources based on "double charge transfer".
b) The H^o + Alk elastic scattering process is primarily responsible for beam loss due to angular scattering.
c) The low energy, $E \leq 500$ eV/amu, electron loss reaction for H^- + Alk is dominated by electron capture to H^o + Alk^-.
d) For $E \leq 500$ eV/amu, the σ_{o-} cross section for H^o + AE should remain large and the σ_{-o} cross section for H^- + AE should be small. Thus, we predict that Sr or Ba targets will surpass the maximum H^- yields realized using Cs.

Acknowledgment

Work supported by the MFE division of the U. S. Department of Energy.

References

1. E.B. Hooper, Jr., T. Pousen, and P.A. Pincosy, J. Appl. Phys. (to be submitted).
2. J.R. Hiskes, J. de Physique 7, 179 (1979).
3. A.S. Schlachter, Proceedings of the Symposium on the Production and Neutralization of Negative Hydrogen Ions and Beams, BNL 50727, (1978), pp. 11-23.
4. R.E. Olson, E.J. Shipsey, and J.C. Browne, Phys. Rev. A 13, 180 (1976).
5. R.E. Olson, R.P. Saxon, and B. Liu, J. Phys. B 13, 297 (1980).
6. J.R. Hiskes, A.M. Karo, P.W. Willmann, and W.J. Stevens, Phys. Lett. 68A, 221 (1978).
7. R.E. Olson, Phys. Lett. 77A, 143 (1980).
8. R.E. Olson and B. Liu, J. Chem. Phys. (Oct. 1980 issue).
9. R.E. Olson and B. Liu, Phys. Rev. A 20, 1366 (1979).
10. R.E. Olson and B. Liu, Chem. Phys. Lett. (submitted).
11. R.E. Olson and B. Liu, Phys. Rev. A 17, 1568 (1978).
12. T.J. Morgan, J. Stone, M. Mayo, and J. Kurose, Phys. Rev. A 20, 54 (1979).

DISCUSSION

FORRESTER Since the double charge exchange is a two step process for, say hydrogen in cesium, is there a density effect? Is there a prospect at all of having the density of cesium for the same total thickness so great that you will actually catch some of the hydrogen not only in the 3S state but in the 2S state or in the 2P state as well?

OLSON You mean before the next collision? That cross section for going from the 2S to the 2P is in the order of 10^{-14} or a little bit larger. Now you are asking what would be the cross section for the (o-) coming out of the metastable state. Those have been measured and they are in the order of 10^{-16}. They are even smaller than coming out of the ground state. That is because your primary interaction is the initial state with this attractive Coulomb potential.

FORRESTER I have a brief comment. The prospect of beams in the region of 400 eV or so is being treated as a very improbable kind of thing. I would just like to say that we have now an 8 cm by 8 cm source operating at 400 eV with about 20 A.

OLSON The use of it will depend on the beam optics.

JACQUOT Are there excitation processes, which give a better conversion efficiency of negative ions?

OLSON Let me pull out this (o-) curve. When you are doing the calculations for the excited state of cesium for example, you will find that at energies below 1 kV the cross section for coming out into the ion-pair state forming the H^-, is up a factor of 3 or 4 above that coming out of the ground state. I am sure it is true because it just has a smaller energy gap to surmount, at higher energies it won't help you a bit. Nothing is known about the H^- on the excited states of the sodium. But as far as I can tell is that, although the (o-) cross section is going to be larger, the (o-) cross section is going up just as much and you have nothing gained. Then if you go to higher energies you are just going to ionize the target. So, I don't predict, except making things more complicated, you won't come out ahead.

EHLERS It sort of makes me wonder; both you and Fred have pointed it out, that although you get a real nice high cross section at the 3, 4, 500 eV region you also get very sizeable portions of your beam spread out 3, 4, 5° and that seems to be what kills our use of that.

OLSON That is a consideration.

MEYER Have you, in calculating your electron loss from the alkalis, have you put in any couplings between the incoming channel and outgoing channels aside from the long range coupling?

OLSON We have got the one where it crosses in the continuum.

MEYER In your incoming channel, for example, you have dynamical coupling to the neutral potential curves around...

OLSON No. I am sure at those energies it is not important. I mean, you have got an energy gap of 0.4 eV.

MEYER The reason I am wondering is, because there has been some recent measurements by Esaulov, who finds that the contribution to the charge transfer is only about 40% as opposed to 80%.

CRANDALL If you remember what Fred Schlachter showed, when you divide by too small a number you get too high a yield. I think that is good from the prospective of somebody who always was taught to distrust theory.

OLSON Let me answer your question. I put error bars of 40% on the cross sections. So you see you can put an awful big error bar on that equilibrium yield.

CRANDALL Look at this for a minute and let's see if I understand the problem. We consider this coupling. You get almost everything going out to the upper curve. The question being raised is that if there is something not quite right about that and some of it stays down on the lower curve, do you then get detachment? Whether it goes on the upper curve or not, you still get detachment, if you get into some distance like that. So, he thinks that this is in addition to your cross section.

OLSON Let me answer that. Esaulov's data was at 300 eV. I stated that electron capture is 80 to 90% of the electron loss. Now, if you look at Esaulov's data and you integrate it to get your total cross section one would hope that you come to a nice maximum and go down again. If you look at Esaulov's data for the electron loss, they indeed do. But for the electron capture even down to the lowest angle in which they measured, something like .06°, that quantity is still going up. If you translate this back to our calculations, all we are saying is that they have sampled the region for impact parameters inside ten atomic units because they are not looking right into the beam at very very small angles. You get almost no net deflection. I would say if they had a total cross section for that (-0) that they are going to be out by a factor of 3. If they could get down to smaller angles, it will be OK.

MEYER Maybe I misunderstand the measurement. I thought they used the time of flight where they had a relatively wide open detector for the relative ratio. They also did differential...

OLSON Yes they have a time of flight but they only get down to .06°.

MEYER Yes, essentially 0^{o} but there may be some experimental difficulties.

OLSON I am consistant with integrating their equations and these results are consistant with those.

ANGULAR SCATTERING IN ELECTRON CAPTURE AND LOSS D^- BEAM FORMATION PROCESSES

M. J. Coggiola, R. V. Hodges, D. L. Huestis
and J. R. Peterson
Molecular Physics Laboratory, SRI International
Menlo Park, California 94025

Abstract

The development of high energy (>150 keV) neutral beams for heating and fueling magnetic fusion devices depends on the ability to produce well-collimated negative ion beams. The double capture charge-exchange technique is a known, scalable method. In order to maximize the overall efficiency of the process and to achieve the desired beam characteristics, it is necessary to examine the optical qualities of the beams as well as the total efficiency of beam production. A combined modeling and experimental study of the angular scattering effects in negative ion formation and loss processes has therefore been undertaken.

Introduction

A program has recently been initiated to enable the modeling of D^- beam formation by the "double capture" method, including the attendant angular scattering which can have a strong effect on the optical quality and usefulness of the beam. In addition to the development and use of the model, the effort includes experimental measurements of angular differential and total cross sections required for the model's data base. This approach uses either experimental or theoretical input data for single collision cross sections, and allows predictions of optimum beam energy and target thickness to maximize the optical properties as well as the total yield of the beam for any target species.

In the following sections, we will outline the mathematical model used to describe the double charge exchange negative ion production process, and discuss the available experimental and theoretical input data and the preliminary results of the modeling. The second section of this report will describe the experimental apparatus used for cross section measurements. Finally, some preliminary experimental data will be presented and discussed.

Modeling of D^- Production

A computer model has been developed to calculate the angular distributions of the various charge species in a double charge exchange D^- source as a function of target thickness. The computations are carried out on the PDP 11/40 computer, and the graphical results are displayed on and copied from a video terminal. The model uses Legendre series expansions in the manner of multiple scattering theory.[1] We presently ignore excited states, assuming that the metal vapor target atoms are in the ground state, and that the excited D^0 states produced in (+o) collisions are rapidly quenched by radiation, stray electric fields or collisions before another angle-changing collision occurs. For each charge state $i = +, o, -$, the angular distribution $C_i(\theta,x)$ at a given thickness (line density) x (cm^{-2}) is expressed as

$$C_i(\theta,x) = \frac{1}{4\pi} \sum_n (2n+1) b_n^i(x) P_n(\cos\theta). \qquad (1)$$

The nine elastic and inelastic angular differential cross sections $\sigma_{ij}(\theta)$, are similarly expanded as

$$\sigma_{ij}(\theta) = S_{ij} \cdot \frac{1}{4\pi} \sum_n (2n+1) f_n^{ij} P_n(\cos\theta), \qquad (2)$$

where the total cross sections are

$$S_{ij} = 2\pi \int_o^\pi \sigma_{ij}(\theta) \sin\theta d\theta. \qquad (3)$$

In solving the multiple collision case, the use of the Legendre expansion is particularly useful because it separates the partial waves of the distribution so that in a charge-changing collision each partial wave n from the initial distribution scatters into the same n in the next. Thus, after part of a beam of + ions, whose angular distribution $C_+(\theta,x)$ has expansion coefficients b_n^+, undergoes one charge transfer collision of cross section σ_{+o}, with expansion coefficients f_n^{+o}, the angular distribution of the resulting neutrals is characterized by coefficients $b_n^o = b_n^+ f_n^{+o}$. Multiple scattering is thus rather easily treated by an iterative procedure.

The evolution of the angular distributions as the beams pass through the target is represented by the rate equations for the expansion coefficients

$$\frac{db_n^i}{dx}(x) = S_{ii}(1-f_n^{ii})b_n^i(x) + \sum_{k\neq i}^{m} [S_{ki}f_n^{ki}b_n^k(x) - S_{ik}b_n^i(x)] , \qquad (4)$$

where the first term represents elastic scattering and the terms inside the brackets represent charge-changing collisions into and out of the i^{th} charge state.

This is a linear, first-order, homogeneous system of differential equations with constant coefficients which can be represented formally by

$$\frac{d}{dx}\vec{b}_n(x) = -\vec{b}_n(x)\hat{D}_n \qquad (5)$$

where $\vec{b}_n$ is the row vector (b_n^+, b_n^o, b_n^-), and $\hat{D}_n$ is a "decay" matrix with elements

$$D_n^{ii} = S_{ii}(1-f_n^{ii}) + \sum_{k\neq i} S_{ki}, \quad D_n^{ij} = -S_{ij}f_n^{ij}.$$

We solve this system of differential equations as an eigenvalue problem. Hooper and Willman[2] followed a similar approach for the angular scattering due only to the charge-changing collisions between the o and - states neglecting elastic scattering. In that two-state problem, the matrix equations are solvable explicitly.

In order to expand the cross sections in a Legendre series we first expand their angles by 10 so that 18^o maps into 180^o. This expansion reduces the number of terms n required for a fit. We then approximate the cross sections by a least-squares fit to an approximately Gaussian expansion

$$\sigma_{ij}(\theta) \simeq \sum_k A_{ij}^k \exp[-\alpha_{ij}^k(1-\cos\theta)] . \qquad (6)$$

A satisfactory fit is generally found using only five terms (k = 1-5) with α_{ij}^k covering a wide dynamic range, e.g.,:8,32,124,512,1024. Fig. 1 shows such a fit to the $\sigma_{o-}(\theta)$ data of Cisneros et al.[3] for $D + Cs \rightarrow D^- + Cs^+$ at 500 eV.

Although there has been considerable experimental work on negative ion production from H^+ and D^+ beams in metal vapors, almost all of it has considered only the total charge fraction yields as functions of energy and target thickness, with almost no data being available on angular distributions. Most work has been done on Cs, but even here only $\sigma_{o-}(\theta)$ has been measured for 500 eV ≤ E ≤ 2500 eV by Cisneros et al.[3] and

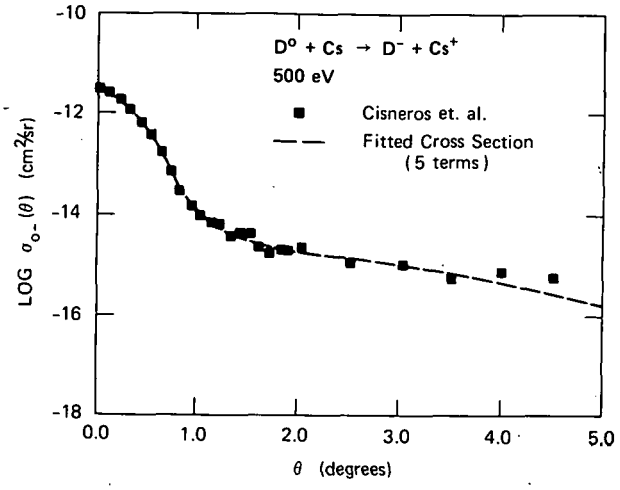

Fig. 1 Least squares fit (---) of a 5 term expansion of Eq. (6) to the σ_{o-} data (■) of Cisneros et al. (Ref. 3).

the relative values of σ_{oo} have been determined by Pradel, Maddarsi and Valance[4] at 30 eV < E < 528 eV. In order to test our model, we considered 500 eV D^+ + Cs, using the Cisneros data for σ_{o-} and the relative σ_{oo} of Pradel et al. for all elastic cross sections, arbitrarily scaled to yield total S_{ii} that were considered reasonable. The absolute values of σ_{+-} reported by Cisneros et al. display a dependence on x even at their lowest pressures, thus their quoted $S_{+-} = 1 \times 10^{-16}$ cm^2 is probably too high. We used their σ_{+-} angular dependence but set $S_{+-} = 2 \times 10^{-17}$, which is near the value of 1.4×10^{-17} cm^2 derived by Hooper et al.[5] Other angular distributions were estimated, and the magnitudes of the σ_{ij} were chosen to yield the total cross sections S_{ij} given in Table 1. Figure 2 shows the fitted angular scattering cross sections used to test the model.

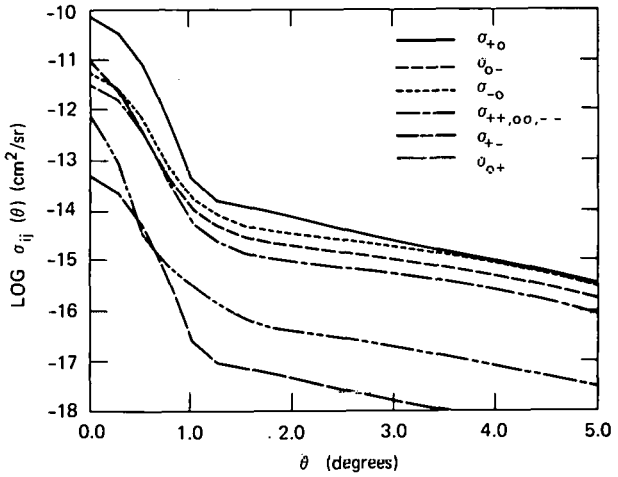

Fig. 2 Computer generated fits to σ_{ij} differential cross sections used in the modeling studies.

Table I Summary of total cross section values used for model testing. All cross sections are for $D^{+,o,-}$ + Cs at 500 eV collision energy.

S_{ij}	MI[a]	HWS[b]	Meyer[c]	MII[d]
+o	7.5(-15)[e]	1.1(-14)	1.5(-14)	1.6(-14)
o+	4.7(-18)	1.4(-17)		4.7(-18)
o-	3.5(-16)	4.5(-16)	8.5(-16)	4.5(-16)
-o	6(-16)	8.8(-16)	4.2(-15)	8.8(-16)
+-	2(-17)	1.4(-17)		1.5(-17)
-+	0			0
++	5(-16)			2.5(-15)
oo	5(-16)			2.5(-15)
--	5(-16)			5(-15)

[a]MI values were used to generate all model results shown in this report.
[b]HWS: Hooper et al., Ref. 5.
[c]Meyer: Ref. 6.
[d]MII values for elastic scattering and +o are thought to be more realistic.
[e]7.5(-15) = 7.5×10^{-15} cm^2.

The total fractional yields computed from the model (integrated over all θ) versus energy are shown in Fig. 3. They are similar but not identical to those of Schlachter, Stalder, and Stearns[7] because the S_{ij} are not quite the same. (The elastic S_{ii} do not enter here.) An example of the relative angular intensities of D^o and D^- is shown in Fig. 4 for a line density $x = 1 \times 10^{14}$ cm^{-2}. At this x, the D^o and D^- fractions are about 0.5 and 0.1, respectively, and the D^- angular distribution is still broader than D^o, reflecting the two step process. As x increases, the increased shuttling between the o and - charge states equalizes the angular distributions as the intensities approach their equilibrium value. The distributions continue to broaden, due to both elastic and charge-transfer scattering. For this first trial case, the elastic σ_{ii} were all set equal and $S_{ii} = 5 \times 10^{-16}$ cm^2. The angular distributions (from Pradel et al.[4]) are probably reasonable for σ_{oo} but, judging from recent calculations on D + Na by Olson,[8] S_{oo} should be about 10x larger. Our measurements will soon provide realistic values for these cross sections. Probably all S_{ii} are too small in our example, and thus the angular effects in this illustrative example are unrealistically small. Plots similar to Fig. 4 are easily obtained for any x.

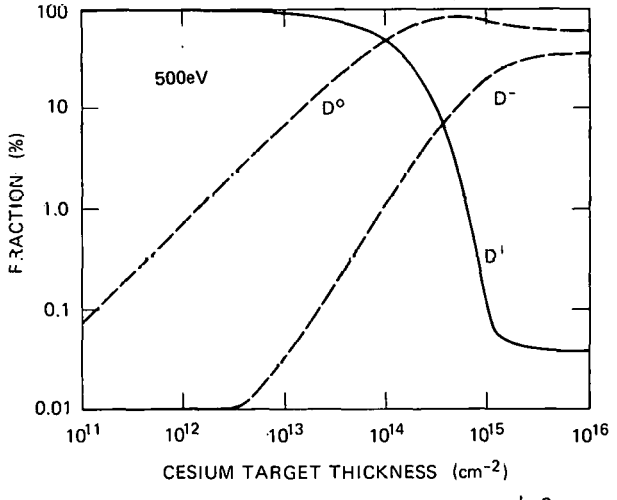

Fig. 3 Calculated fractional yields of $D^{+,o,-}$ as a function of Cs target thickness.

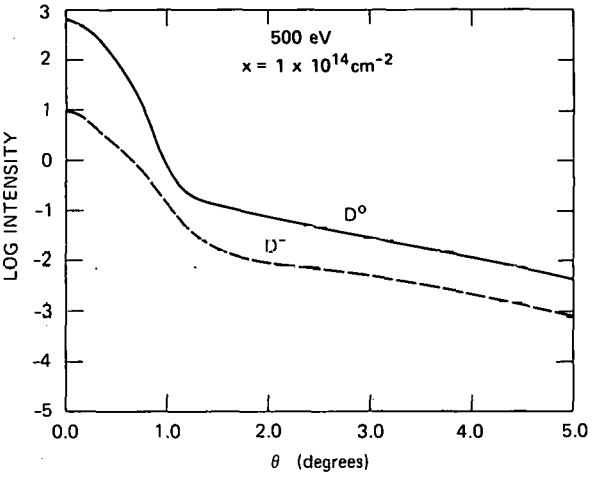

Fig. 4 Model generated angular distributions of the relative intensities of D^o and D^- for a Cs line density of 1×10^{14} cm^{-2}.

Figure 5 shows plots of the integrated o and - fractions of the beam as a function of beam angle for $x = 2 \times 10^{15}$ cm^{-2}, where the charge fractions are close to their equilibrium values. This graph only extends to $\theta = 1^o$ to show the small angle yields. The 50%, 90%, and 100% values of the total yield at this x are also drawn in by the computer. Their intersections with the angular integrated yield curves show that the 50% angle for D^- is $\theta^-_{0.5} = 0.57^o$, and for D^o, $\theta^o_{0.5} = 0.43^o$. Similarly, $\theta^-_{0.9} = 1.8^o$ and $\theta^o_{0.9} = 1.0^o$. A more realistic choice of cross sections given in column 4 of Table I yields $\theta_{0.5} \approx 3^o$ for both charge states at $x = 2 \times 10^{15}$ cm^{-2}. As x increases so that many collisions occur, the angular spreads tend to increase as $x^{\frac{1}{2}}$, as pointed out by Hooper et al.[9] A plot of the 50% and 90% angles is shown in Fig. 6, along with the values of Cisneros,[3] Hooper,[9] and Agafonov.[10] The model's approach to an $x^{\frac{1}{2}}$ behavior at large x is apparent. At midvalues of x, a flattening occurs representing the two-step (+o,o-) convolved cross section, and then at lower x ($< 10^{15}$ cm^{-2}) the angle decreases toward the single step (+-) scattering result which is given by value of the Cisneros points at $x = 3 \times 10^{13}$ cm^{-2}. Their "thin target"

value should be plotted at $x \leq 10^{13}$ cm^{-2} because of the density dependence effects mentioned above.

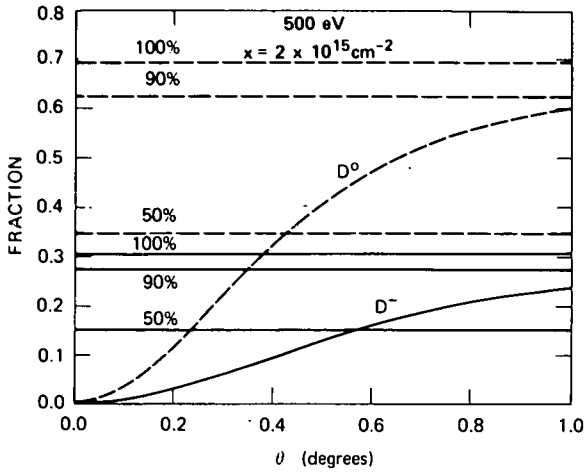

Fig. 5 Fractions of D^o and D^- within a beam whose angular width is θ, calculated for $x = 2 \times 10^{15}$ cm^{-2}.

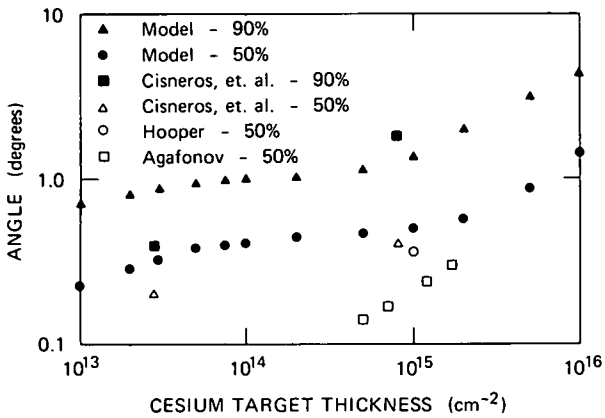

Fig. 6 50% (•) and 90% (▲) angles for D^- production as a function of Cs target thickness. Experimental values: (■,△) Ref. 3, (○) Ref. 9, (□) Ref. 10.

The $\theta_{\frac{1}{2}}$ results of Agafonov et al.[10] are lower than the other results perhaps because of the way they subtracted out the angular spread of the incident beam. Preliminary measurements of the σ_{o-} angular distribution in our lab (see below) agree well with the results of Cisneros et al., which are used in the model. However, we have not yet deconvoluted the incident beam profile, so it is possible that our σ_{o-} is too broad. This cross section introduces the most angular scattering at $10^{13} < x < 10^{15}$ cm^{-2}.

The model provides a powerful tool for examining the relative importance of different processes in the overall performance of double-capture D^- beam sources. It provides an insight and detail that is difficult to obtain from fractional yield measurements alone. Its future use is critically dependent on the required input data that must be provided by experiment or theory. On the other hand, for modeling purposes the differential cross sections can be represented as smooth functions of angle, and the S_{ij} are generally smooth functions of energy, therefore the number of energies required for the input data is reasonably limited.

Experimental

Supplementing the modeling effort is a companion experimental program to supply input data required by the model. As mentioned above, the differential scattering cross sections for most of the elastic and inelastic (charge-changing) collisions are presently unknown, despite their importance in determining an optimal negative ion source design. Furthermore, only a few total cross sections have been measured at energies below 0.5 keV/amu. Thus, our experimental program is designed to measure both total and differential scattering cross sections of $D^{+,o,-}$ in metal vapor targets at low collision energies.

A brief description of the apparatus will be given below, including its unique features and capabilities. In the final section, some preliminary cross section results will be presented.

The scattering apparatus is of straightforward design, and consists of three separately pumped vacuum regions: (1) ion source, (2) charge-exchange neutralization cell, (3) metal vapor target cell and differential detectors. For producing D^+ or D^o incident beams, a dc discharge type ion source is employed. In either case, positive ions are directly extracted from a discharge formed in pure D_2. The ion beam is accelerated, focussed, and magnetically mass analyzed to yield a pure D^+ beam. For D^- experiments, a duoplasmatron type ion source is used.

The second vacuum region contains a 10 cm long neutralization cell located just downstream from a 1 mm diameter collimating aperture. To produce a ground state D^o atom beam, a suitable gas such as Ar is admitted to the neutralizing cell, and residual ions are removed at the exit. The neutralization cell can also be filled with alkali metal vapor, thus allowing for the production of D(2S) atoms.

The scattering (target) cell itself is located in the final chamber immediately downstream from a second 1 mm diameter aperture. The two 1 mm apertures, located 35 cm apart, produce an angular collimation at the target of $\sim 0.15^o$.

The all stainless-steel target cell has a central well which serves as both the Cs reservoir and the scattering region. The entire cell is uniformly heated by tantalum wire heating elements which run the full vertical length of the unit. Additional elements are provided to heat the interchangeable entrance and exit apertures separately. These apertures, separated by 2.5 cm, consist of a 1.25 mm diameter circular entrance aperture and a 1.5 x 10 mm exit slit. This arrangement allows in-plane scattering out to $\pm 10^{\circ}$ to be observed. Two thermocouples are inserted into deep wells in the body of the cell, one accurately monitors the temperature, while the other is used with a set-point controller to regulate the temperature to $\pm 0.1^{\circ}$C. The entire assembly is mounted on a tilting mechanism which allows the cell to be moved into and out of the incident beam path. A cam system is used to locate the cell with a positional accuracy of ± 0.1 mm, thus ensuring reproducible alignment of the cell apertures with the fixed collimating apertures. No measurable change in the transmitted beam intensity occurs when the evacuated oven is moved into the beam path. This target in-out system simplifies accurate total attenuation cross section measurements and also allows background corrections to be made easily in differential experiments.

For total attenuation measurements, a large aperture ($\pm 8^{\circ}$ acceptance angle) Faraday cup is used to determine the beam flux. For neutral beams, detection is via secondary electron emission. Since a total attenuation method is used, no absolute detection sensitivities need be known to obtain total cross sections. Angular scattering distributions are observed using a detector which rotates about the center of the target cell. It consists of a 1 mm diameter defining aperture followed by a set of deflector plates for charge separation, and finally three separate, shielded detectors. Two channeltron electron multipliers and a suppressed Faraday cup are used as detectors, depending on the type of measurement being made. The overall angular resolution of the detector system is calculated to be $\sim 0.2^{\circ}$.

The measurement of absolute total cross sections requires a knowledge of the true target thickness, $x = \int n(\ell) d\ell$. Rather than determining this parameter by relying on the usual temperature-vapor pressure curves and the measured cell length, we have made use of previously measured absolute charge-exchange cross sections for $He^+ + Cs$.[11] It is a simple matter to measure the attenuation of a He^+ beam at a fixed cell temperature and thereby to determine the effective target thickness at that temperature. This calibration procedure is typically carried out at several He^+ beam energies between 0.3 and 1.5 keV for each cell temperature used. In general, we find that the value of x thus determined is within $\pm$ 5% of the value one would calculate from the measured cell temperature and length.

Initially, we have focused attention on measurements of both the total and differential cross sections for $D^+ + Cs \rightarrow D^o + Cs^+$. A number of previous measurements have been made of the total cross section for this process at energies above 0.5 keV/amu. Therefore, this system can serve to check the overall performance and calibration of the apparatus.

Figure 7 shows the results of our S_{+o} determinations made using the attenuation technique over a range of collision energies from 0.1 to 2 keV/amu. The cross sections at each energy were measured for several different Cs target densities and averaged together to yield the data shown. The error bars represent the statistical variation in the results as determined from the separate measurements. Day-to-day variations in the measured cross sections were always less than these error limits.

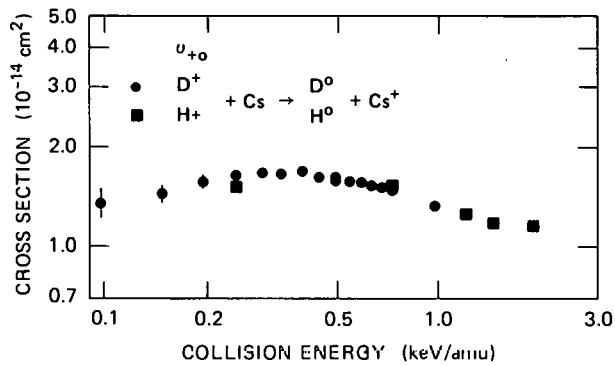

Fig. 7 Experimental total (+o) cross sections for D^+(•) and H^+(■) charge-exchange in Cs ($x = 1.1 \times 10^{13}$ cm^{-2}) as a function of collision energy.

The cross sections appear to have a broad maximum around 0.4 keV/amu, with a 10-25% decrease at lower and higher energies. This general behavior has been observed previously for this system, both experimentally and theoretically. The present data agree very well in magnitude with the results of Meyer and co-workers[6,12] where they overlap in energy, and with the calculated total cross sections of Sidis and Kubach.[13]

Preliminary results are shown in Figure 8 of σ_{+o} measurements made for 1.0 and 1.5 keV D^+ on Cs ($x = 6.5 \times 10^{12}$ cm^{-2}). No corrections have been made to the data either for the finite angular width of the incident beam or the detector

resolution. Clearly, the angular distribution of product D^o atoms at these energies is very sharply forward peaked, falling more than three orders of magnitude within 1° of the beam center. As might be expected, wide angle scattering becomes somewhat more pronounced as the collision energy is decreased.

Experiments are currently underway to measure the differential elastic scattering cross sections for $D^{+,o,-}$ in Cs at these energies where large angular effects will be most important. Additional measurements will also be made of the differential and total cross sections for several of the other major electron capture and loss processes occuring in the D-Cs system.

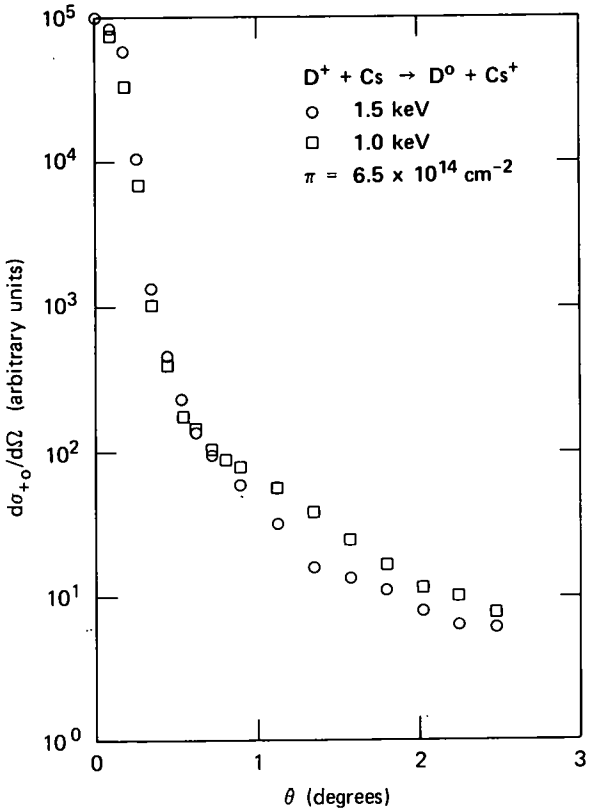

Fig. 8 Measured differential cross sections for $D^+ + Cs \rightarrow D^o + Cs^+$ at 1.0 keV (●) and 1.1 keV (■) collision energy.

Summary

A computer model has been developed to describe the effects of angular scattering in the formation of D^- from D^+ by the two-step charge-exchange process. The model has been successfully tested in the $D^+ + Cs$ system using a combination of measured and estimated differential scattering cross sections. We have also initiated an experimental program with the goal of measuring many of the presently unknown cross sections required as input for the model. As the range of input data is extended both by experiments and in some cases accurate theoretical calculations, the model will increasingly be used to predict optimum conditions for negative ion production. Although initial work has been confined to Cs, other promising target species will be examined in the future.

Acknowledgments

This work was supported by the MFE division of the U.S. Department of Energy. The computer used in this work was purchased under NSF grant PHY76-144361.

References

1. N.F. Mott and H.S.W. Massey, "Theory of Atomic Collisions," Oxford University Press (1965), p. 470.

2. E.B. Hooper, Jr. and P.A. Willmann, J. Appl. Phys. 48, 1041 (1977).

3. C. Cisneros, I. Alvarez, C.F. Barnett and J.A. Ray, Phys. Rev. A 14, 76 (1976).

4. P. Pradel, M. El Maddarsi, and A. Valance, Chem. Phys. Lett. 71, 55 (1980); and private communication.

5. E.B. Hooper, Jr., P.A. Willmann, and A.S. Schlachter, LLL Report UCID-17726 (1978).

6. F.W. Meyer, J. Phys. B, to be published.

7. A.S. Schlachter, K.R. Stalder, and J.W. Stearns, Phys. Rev. A, to be published.

8. R.E. Olson, private communication (see preceding paper in proceedings of this conference.

9. E.B. Hooper, Jr., P. Poulsen, T.A. Pincosy, O.A. Anderson, and T.J.Duffy, LBL Report in preparation, 1980.

10. Yu.A. Agafonov, B.A. Dyachkov, and M.A. Pavlii, to be published in Sov. Phys.-Tech. Phys.

11. J.R. Peterson and D.C. Lorents, Phys. Rev. 182, 152 (1969).

12. F.W. Meyer, C.J. Anderson, and L.W. Anderson, Phys. Rev. A 15, 455 (1977).

13. V. Sidis and C. Kubach, J. Phys. B 11, 2687 (1978).

DISCUSSION

LOS Most of the calculations have been carried out at 500 eV, I suppose at primary energy. Is it a function of energy, you think?

PETERSON Yes, definitely.

LOS Is energy x angular distribution constant?

PETERSON Certainly at the lower energies. In general, I think it would tend to be constant. What we will be able to do is, I think, use that characteristic to help interpolate between experimental data from energy to energy.

SCHLACHTER If I understood the curves correctly for relatively thick targets, you showed calculated angular distributions as neutrals and negatives approaching one another because of the targets recycling?

PETERSON That is correct.

SCHLACHTER Then I do not see how that supported your contention in your opening statement that it was your opinion that differences in thick target yield were due to angular effects.

PETERSON I think that a lot of the problems were because they were losing the charged states. Maybe I am wrong, but I think those fractional yields will be lowered if they are lost in the scattering.

SCHLACHTER I do not think I understood that.

PETERSON If they are scattered out of the detector as you increase the target thickness because of angular scattering, the effective yield will go down.

SCHLACHTER Not if they are scattered in equal amounts. Not if the tri-state distributions have the same angular distribution. Then I do not think it should affect the yield.

PETERSON As they approach that point, you will notice that the neutrals are scattered less; then at equilibrium values they should be equal. So, if you only do it by measuring neutrals and negatives, totally at that point, then that is right, then I do not know the answer.

HAGENA Would you like to comment on this angular spreading for the final goal of producing high energy negative beams? If I understood your first answer correctly then there would be a certain amount of perpendicular momentum given to the negative ions during the scattering loss and so this perpendicular momentum would be less troublesome the higher the final energy.

PETERSON As you generate the negative ion beams at low energy and accelerate them to high energy, the angular spread will certainly be reduced. The goal of this research is to find the optimum conditions for producing the negative ion beams. For instance it may not occur at the equilibrium value.

HAGENA As of now, one can not make a general statement that high angular spreading is always bad.

PETERSON That depends upon the needs of the user. That is true. If for instance the angular spread in the positive ion sources is larger than in the charge transfer cell, then it is of little importance.

H^- ION FORMATION FROM A SURFACE CONVERSION TYPE ION SOURCE*

K. N. Leung and K. W. Ehlers

Lawrence Berkeley Laboratory
University of California
Berkeley, California 94720

Abstract

Volume-produced H^- ions have been extracted from a multi-cusp ion source by using a standard extraction system. In addition, a molybdenum converter is installed in the source to generate surface-produced H^- ions. The H^- ion yield is measured by a mass spectrometer. Without cesium, the production of H^- ions by the surface process is very small compared with those generated by volume production. However, the presence of cesium can greatly enhance the surface production yield. The energy spectrum shows that the surface-generated H^- ions contain two distinct groups when cesium is added to the discharge. The energy of one group is essentially that of the sheath potential and appear to be produced by a desorption process. The second group of H^- ions have slightly higher energies and appear to be formed by a reflection process. Different types of converter materials have also been tested.

Introduction

In order to heat plasmas in future fusion reactors, the required neutral beam energy will be greater than 150 keV. The high neutralization efficiency (>60%) of H^- or D^- ions makes them favorable to form neutral beams with energies in excess of 150 keV.[1] There are different approaches for the production of negative ions.[2,3] H^- ions can be extracted directly from a hydrogen discharge plasma. Low-energy positive hydrogen or deuterium ions can be converted into negative ions by double charge exchange in a sodium or cesium cell. There are also H^- ion sources that are based on surface interactions.

It has been reported that there is a substantial quantity of H^- ions in a hydrogen discharge plasma.[4] The purpose of this experiment is to compare the amount of H^- ions extracted directly from a multi-cusp source with that generated by plasma surface interactions, principally via desorption or reflection. In order to optimize the surface production yield of H^- ions, different converter materials have been studied under the same gas pressure, cesium coverage, discharge current and converter voltage.

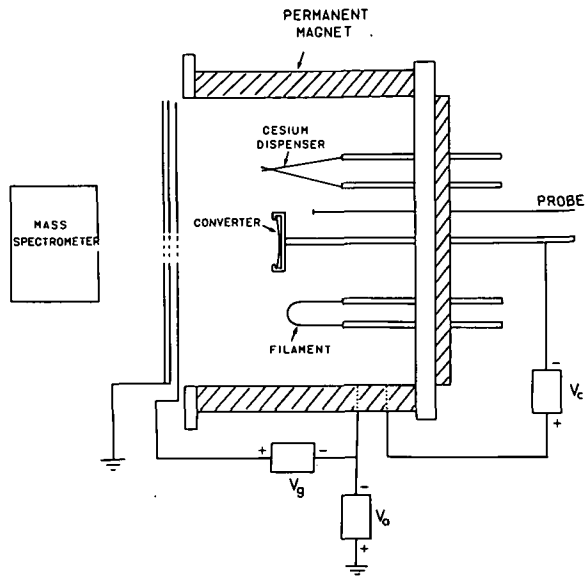

Fig. 1 Schematic diagram of the multi-cusp negative ion source.

Experimental Setup

A schematic diagram of the experimental arrangement is shown in Fig. 1. The device is a cylindrical multi-cusp ion source[5] (20 cm diam by 14 cm long) with the open end enclosed by a three-grid extraction system. The chamber is surrounded externally by 10 columns of samarium-cobalt magnet ($B_{max} \approx 4$ kG) to form a line-cusp configuration for primary electrons and plasma confinement.[6] A steady state hydrogen plasma is produced by primary ionizing electrons emitted from two 0.05 cm diameter tungsten filaments which are biased at -60 V with respect to the source chamber wall (anode). No actual source pressure has been measured. But in normal operation, the pressure indicated by a gauge located downstream after the mass spectrometer was 2×10^{-4} Torr. The H^- ions in the hydrogen plasma is extracted by means of a standard Berkeley accel-decel electrode system with the first (plasma) grid masked down to an extraction area of 0.2 x 2 cm^2. This plasma grid is biased positively at a potential V_g with respect to the anode which in turn is

aintained at a negative potential V_a elative to ground. The center and the utermost grid are both grounded electrically o extract and accelerate the H^- ions. A ompact magnetic-deflection mass spectro-eter[7] is installed just outside the extractor to detect the H^- ions.

In order to generate surface-produced H^- ions, a moveable, concave molybdenum converter (3 cm high by 5 cm long) is inserted into the plasma through a high-voltage insulator mounted on the end flange. By biasing the converter negatively V_c with respect to the anode, positive ions from the plasma are accelerated across the sheath and strike the converter surface. Any H^- ions formed at the surface will then be accelerated back across the sheath by the same potential. They pass through the plasma and the extraction slot and are focused geometrically at the entrance aperture of the mass spectrometer.

It has been shown that cesium coverage can reduce the work function of a metal surface and consequently enhance the yield of H^- ions.[8,9] In this source, cesium was deposited on the converter surface by evaporating the metal directly into the plasma from two 10 cm long S.A.E.S. getter dispensers.

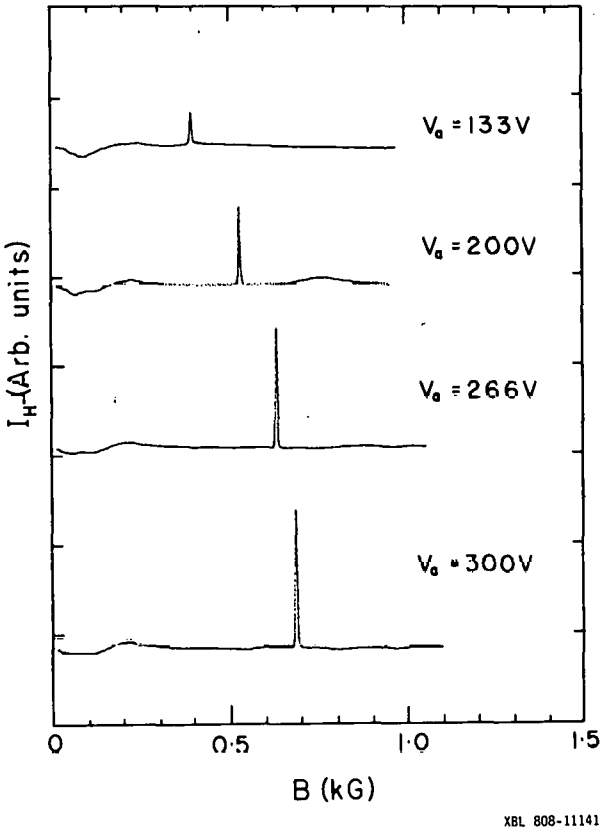

Fig. 2. The H^- ion spectrometer signal as a function of extraction voltage V_a at constant discharge power.

The amount of cesium introduced can be easily controlled by adjusting the heater current of the dispenser strips.

Experimental Results

The source was first operated without cesium with a discharge voltage of 60 V and a discharge current of 3.5 A. Langmuir probe characteristics indicated that the plasma density was 6 x 10^{10} cm^{-3} and the electron temperature was 1.5 eV when the plasma grid bias voltage V_g = 0.

When an acceleration potential V_a was applied to the source anode, a beam of H^- ions together with a large quantity of electrons were extracted from the source. The mass spectrometer output signal shows a sharp H^- ion peak as illustrated in Fig. 2. The height of this H^- ion peak increases as the bias voltage V_a increased until the extraction becomes emission limited. These H^- ions are not formed on the converter surface because the spectrometer signal remained unaltered even when the converter was removed from the source.

The following measurement also proves that the H^- ions are not coming directly from the source anode. The energy level diagram of Fig. 3 shows the relation between the energy of a H^- ion and the potential of the source plasma V_p. If the H^- ion is generated in the plasma by a volume process, then its energy $E = eV_a - eV_p$ when it arrives at the detector. However, if the H^- ion is generated by a desorption or a reflection process at the anode surface, then its energy E will range from a minimum of eV_a to a maximum of $eV_a + eV_p$. In this multi-cusp source, the plasma potential V_p can be varied by adjusting the plasma grid bias voltage V_g. Figure 4 indicates that when V_g is increased from 0 to +36 V, the plasma potential V_p increases by approximately 36 volts. At the

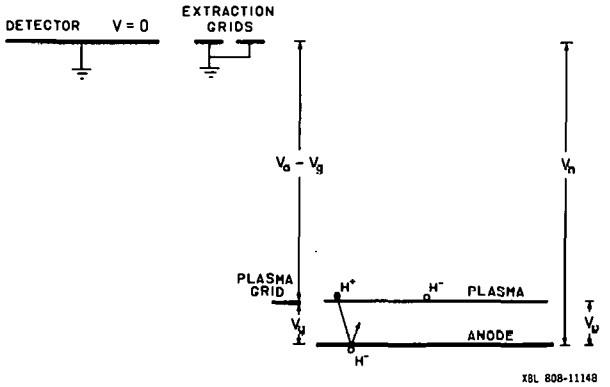

Fig. 3 Potential energy of the H^- ion produced in the plasma or at the anode surface.

same time the spectrometer signals in Fig. 5 show that the H^- ion peak shifts to the low energy side by the same amount. This result demonstrates that the H^- ions observed in Fig. 2 are indeed produced in the bulk of the plasma.

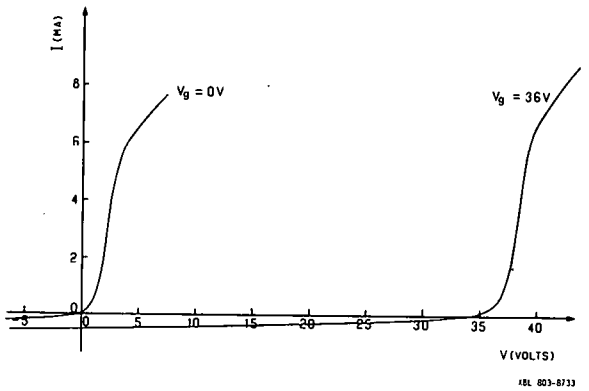

Fig. 4. Langmuir probe characteristics obtained with two different plasma grid voltages.

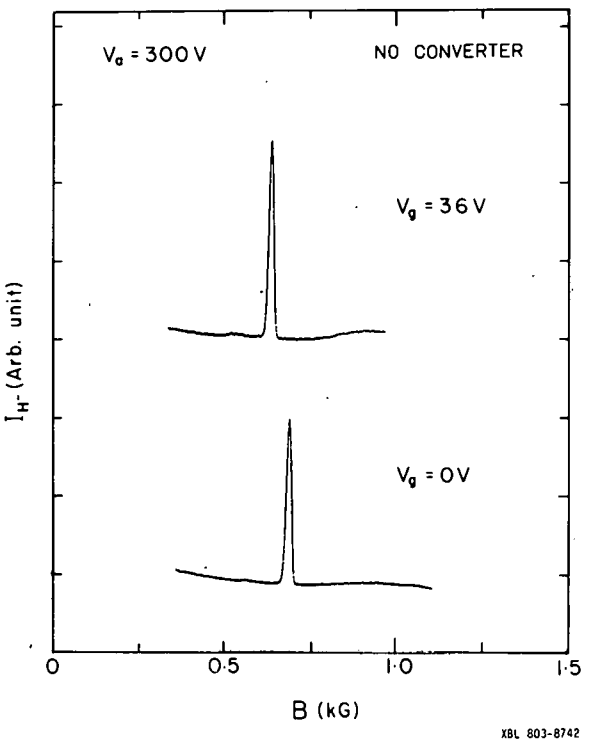

Fig. 5. The energy spectrum of the H^- ions for two different plasma grid bias voltages.

The amount of volume-produced H^- ions that can be extracted from the source depends not only on the acceleration voltage V_a, but also on the source pressure. With a constant discharge power, Fig. 6 shows that the H^- ion peak can increase substantially as the pressure is increased from 1×10^{-4} to 7×10^{-4} Torr.

When cesium was introduced into the hydrogen plasma and the converter is in place, a second group of H^- ions with energy $E \approx eV_a + eV_c$ appear in the spectrometer signal (Fig. 7). The characteristics of this second group of H^- ions can be summarized as follows: (1) The height of this second H^- ion peak increases as more and more cesium is added to the plasma. However, there is no appreciable change in the size of the volume-produced H^- ion peak. (2) As the converter bias voltage V_c is varied from 100 V to 300 V, the energy of this second group of H^- ions changes accordingly as shown in Fig. 8 but the energy of the volume-produced H^- ions remains unchanged. (3) When the acceleration potential V_a = 0, the volume-produced H^- ion peak disappears and only the second group remains. In fact, these H^- ions are now "self-extracted" from the source. The energy of this second group of

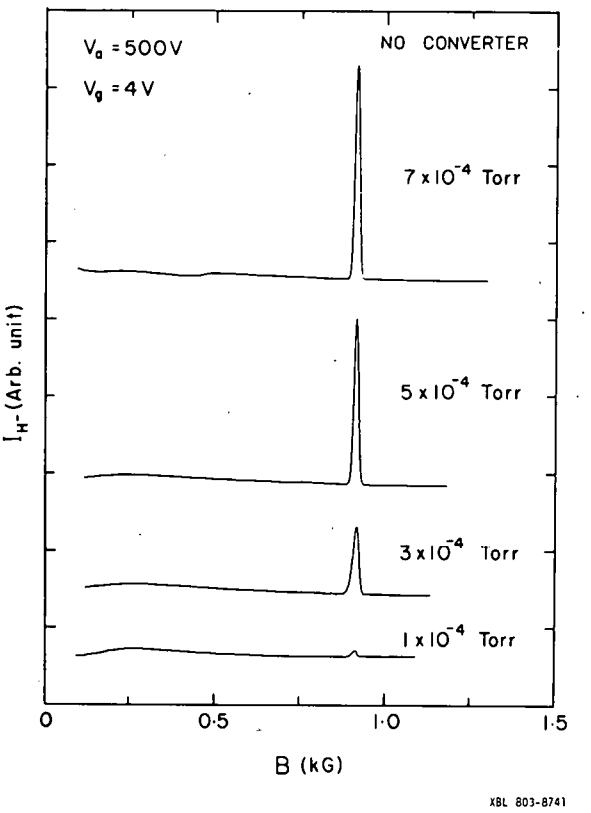

Fig. 6. The H^- ion spectrometer signal as a function of gas pressure at constant discharge power.

H^- ions again changes with the converter bias voltage V_c as illustrated in Fig. 9. On the basis of these results, one can conclude that the second group of higher energy H^- ions are generated at the surface of the converter. A detailed study on the formation of these H^- ions is presented in the next section. (4) Under the same cesium environment and discharge conditions, Figs. 8 and 9 also show that the amount of H^- ions in the surface-generated group increases as V_c is changed from 100 V to 200 V, and then decreases when V_c is further increased to 300 V. A similar optimum converter voltage V_c has also been found in the self-extraction negative ion source.[10] It is suspected that the best cesium and Hydrogen coverage that favors the formation of H^- ions may occur right at this optimum

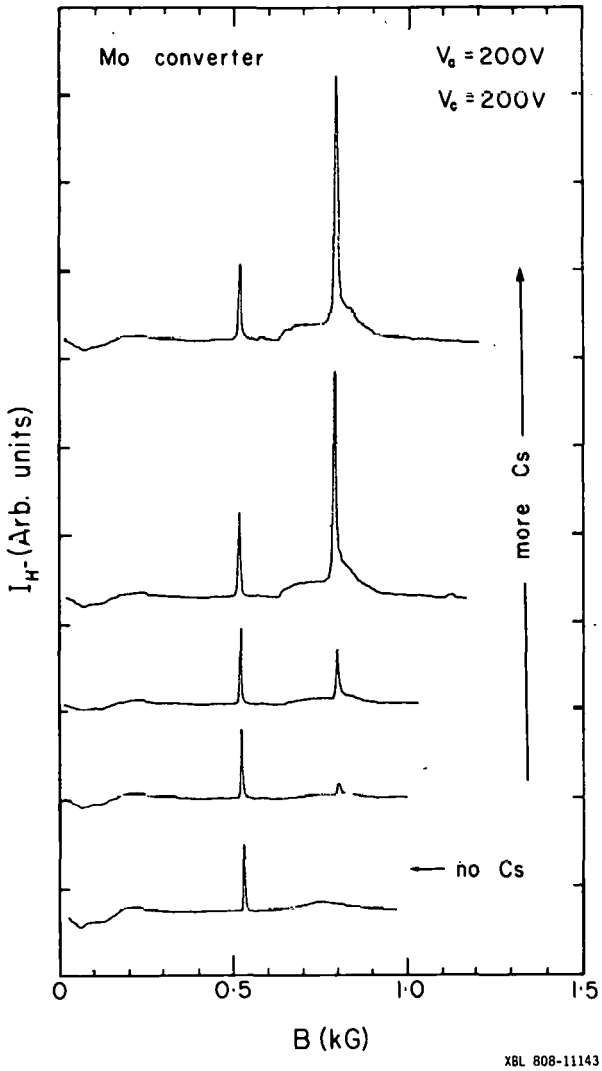

Fig. 7. The energy spectrum of the H^- ions when cesium is added to the discharge.

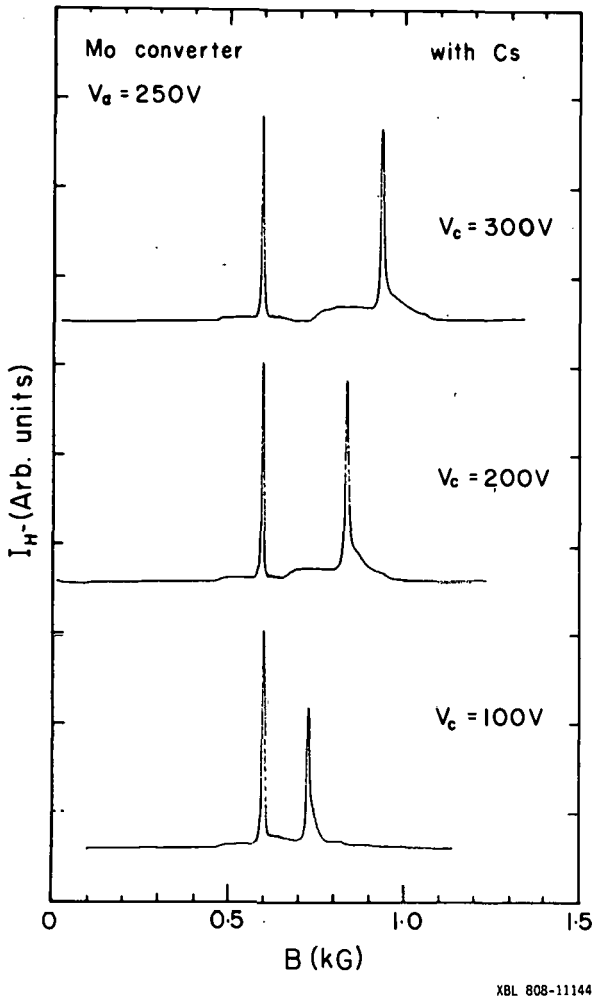

Fig. 8. The energy spectrum of the H^- ions as a function of converter bias voltages at constant discharge power.

converter bias voltage. (5) The energy spectrum of the second group of H^- ions has a steep rise at $E \approx eV_c + eV_a$, and then decays towards the higher energy side. This group of surface-generated H^- ions therefore have a larger energy spread than the volume-produced ones.

Figure 7 shows that the surface-generated H^- ion peak is about four times bigger than the volume peak. When the source is operated at a higher pressure and extraction voltage, the amount of H^- ions produced by volume and surface processes are approximately equal (Fig. 8). However, when there is no cesium in the hydrogen discharge, the number of surface-generated H^- ions will diminish by about two orders of magnitude.[11] The second H^- ion peak in the spectrometer output signal will therefore be much smaller than the first peak.

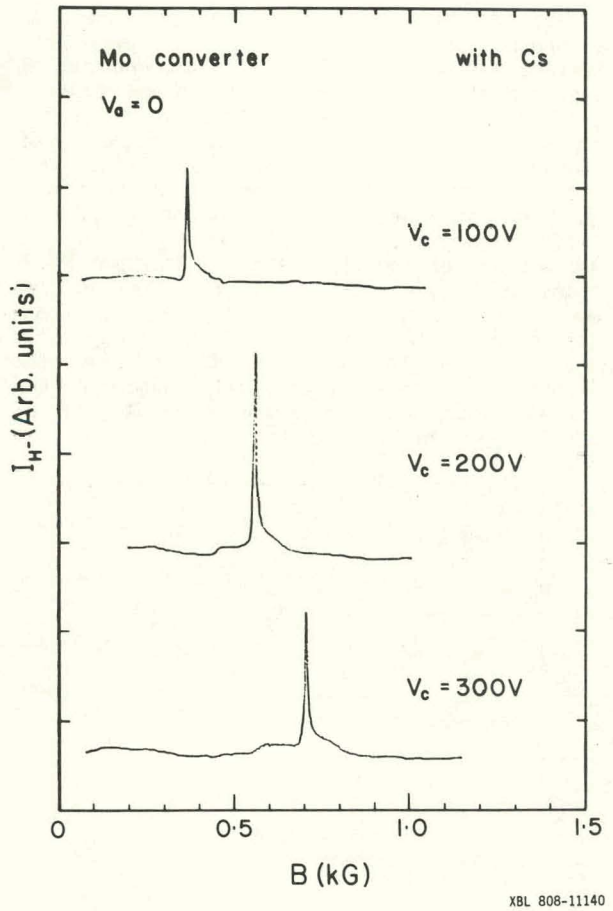

Fig. 9. The energy spectrum of the H^- ions as a function of converter bias voltages at constant discharge power with V_a=0.

It has been reported that there are two groups of H^- ions in the energy spectrum of the negative ion beam extracted from a planotron[12] or a duoplasmatron.[13] In both types of sources, the low-energy peak corresponds approximately to the anode potential while the high-energy peak corresponds to the cathode potential. The high-energy group appears only in the presence of cesium and is formed at the cathode surface of the planotron and at the tip of the center rod of the duoplasmatron. In both sources, the amount of H^- ions in the low-energy group depend only on the hydrogen content. This low energy group is interpreted to be produced by resonant charge exchange of fast H^- ion of the high-energy group with hydrogen atoms in the extraction gap of the planotron.[12] In the duoplasmatron however, it is believed that a volume process is responsible for the creation of the low-energy H^- ions.[13] The results of the present experiment seem to confirm the latter interpretation.

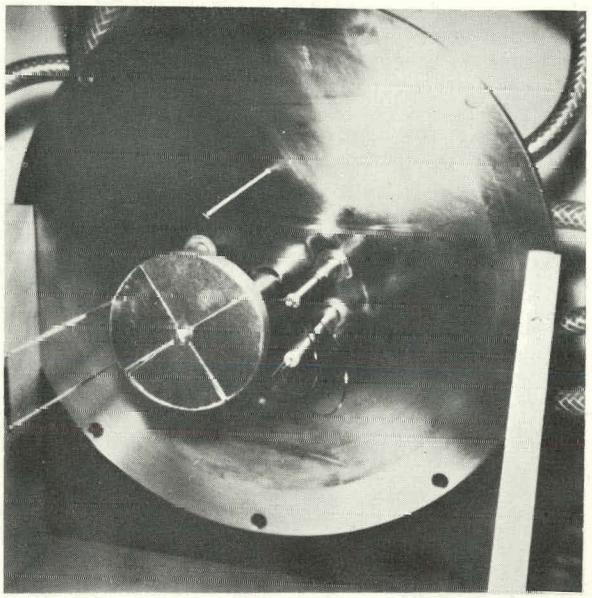

Fig. 10. A circular converter with four different materials brazed on the four quadrants.

Converter Material Study

In order to investigate different converter materials for use with the self-extraction negative ion source, a rotating converter disk with four different materials brazed on the four quadrants was employed (Fig. 10). This converter was installed in the multi-cusp ion source (Fig. 1) equipped with one exit aperture so that only the negative ions generated by one portion of the converter disk would exit from the source. The source was operated in the presence of cesium with V_a = 0 and the converter was biased at -200 V with respect to the anode. The energy spectrum of the "self-extracted" H^- ion beam was detected by the mass spectrometer. With this arrangement, the yield of H^- ions for each metal could be compared under identical conditions of gas pressure, discharge power, cesium coverage and converter potential.

Figures 11 - 13 show the energy spectrum of the H^- ions produced by Mo, W, Pt, Ni, Cu, Re, Ta and Pd. The shape of the spectrum differs from one material to the other. In general, two distinct groups of surface-generated H^- ions can be identified. The energy of one group is approximately equal to the sheath potential, indicating that the ions leave the converter surface with little or no energy. These H^- ions can be produced on the converter by a desorption process.[8,14-17]

The H^- ions can be desorbed from the converter when positive ions enter the surface layer provided the energy transferred in the collision is equal to or greater than the adsorption energy of hydrogen. In this case, the average energy gained by the H^- ions is usually small,[18] and their final energy should be approximately equal to the sheath potential. The cross-section for hydrogen sputtering by hydrogen incident upon metallic hydrides is small.[3] However, this cross-section increases quite rapidly with the mass of the projectile.[19] In addition to reducing the surface work function, which is essential for the efficient production of H^- ions, the Cs^+ ions in the plasma could also serves as a sputtering agent to enhance the hydrogen desorption rate.

It has been found that the coefficient of secondary H^- emission from a molybdenum surface exposed to Cs^+ ion bombardment can be improved if the surface loading of hydrogen is performed in a plasma rather than in a gas atmosphere.[17] However, the degree of hydrogen adsorbed on a cesiated surface may depend on the substrate material. Perhaps this is the reason why the very low energy H^- ion yield is typically higher for Mo and Re. Reflection of neutral atomic hydrogen with energy $E > \phi - E_a$,[20] where ϕ is the surface work function and E_a is the electron attachment energy of the H^- ion, may also lead to the formation of H^- ions.[21] The importance of this process will depend upon the concentration and the energy distribution of atomic hydrogen in the source.

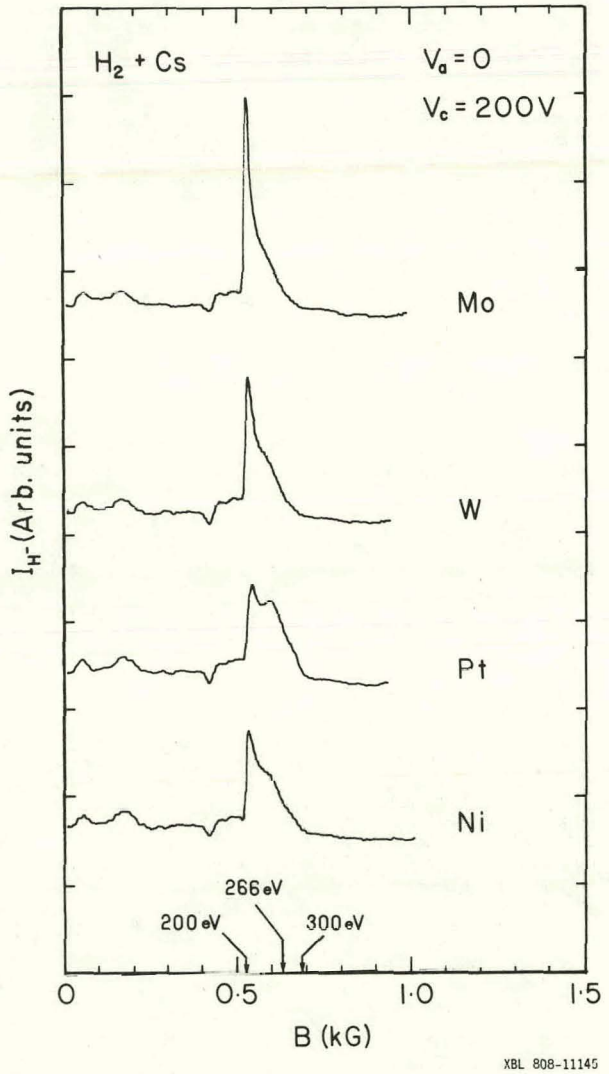

Fig. 11. The energy spectrum of the H^- ions produced on Mo, W, Pt and Ni at constant converter voltage.

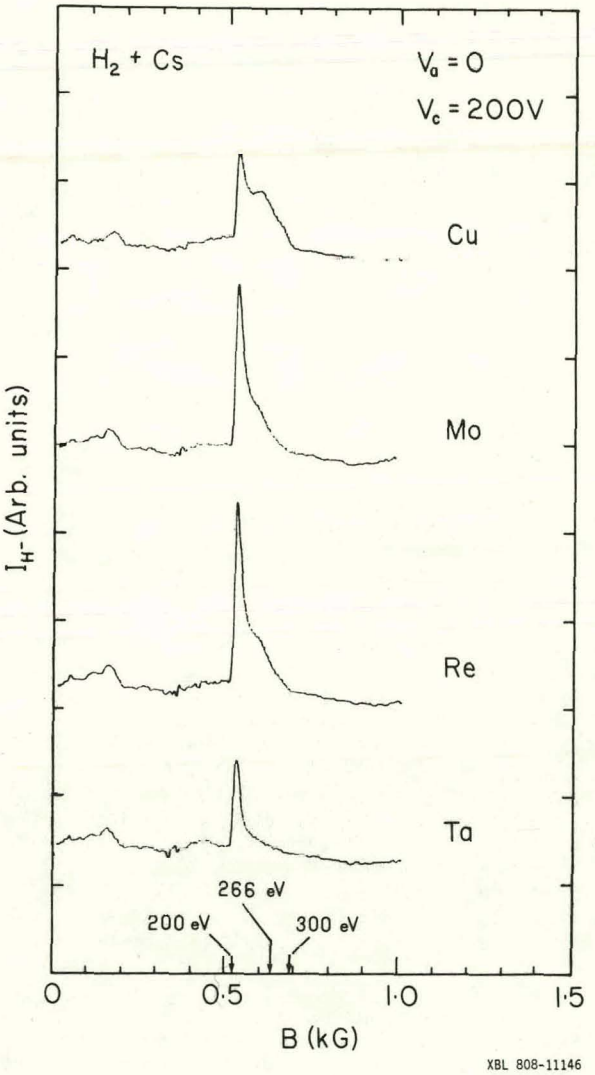

Fig. 12. The energy spectrum of the H^- ions produced on Cu, Mo, Re and Ta at constant converter voltage.

The second group of H^- ions have a higher energy and appear to be produced by a reflection process.[20] An incoming H^+ ion strikes the converter surface with energy E = 200 eV after falling through the sheath. The molecular species (H_2^+ and H_3^+) are fragmented to form atomic hydrogen particles with energy $E/2 \approx 100$ and $E/3 \approx 66$ eV respectively.[22] If the H^- ions are converted from the three groups of backscattered atomic hydrogen particles by capturing the additional electrons, then their average energy at the detector should be close to the limiting valves, 2E ($\approx$400 eV), E + E/2 ($\approx$300 eV), or E + E/3 ($\approx$266 eV). In the presence of cesium, the species current distribution $H^+ : H_2^+ : H_3^+ = 7 : 33 : 60$. Thus the dominant species is H_3^+ and most of the H^- ions formed by reflection of positive hydrogen ions should have energy equal to or less than 266 eV which is illustrated by the energy spectra of Figs. 11-13. In case of Pd, the group of H^- ions formed by the reflection of H_2^+ ions is distinguishable.

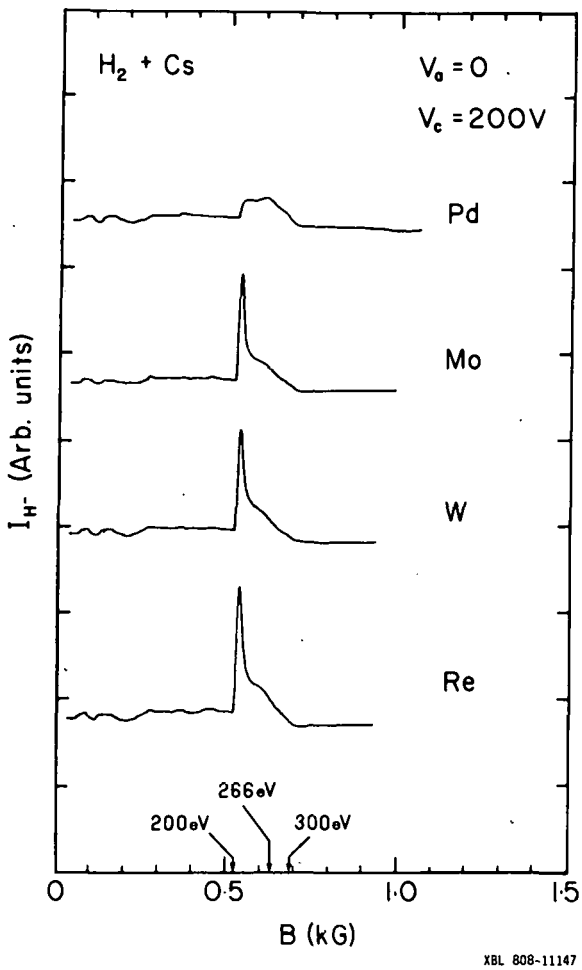

Fig. 13. The energy spectrum of the H^- ions produced on Pd, Mo, W and Re at constant converter voltage.

The energy spectra of Fig. 11 also demonstrate that Pt produces the biggest number of H^- ions formed by reflection. This result agrees with the Marlowe code calculation which shows that at a given energy, the fraction of reflected particles increases with the Z of target material.[23] Both Mo and Re give the highest total H^- yield at optimum conditions with the majority of the H^- ions belonging to the low energy group. Re is a better choice when used as a converter material because it has lower sputtering coefficient than Mo. In addition, its electron affinity for negative ion formation is lower than that of Mo.[10] Both elements give a maximum H^- yield with a converter bias voltage of about 200 V.

References

*This work is supported by the Fusion Energy Division, U. S. Department of Energy, under contract W-7405-ENG-48.

1. K. H. Berkner, R. V. Pyle, and J. W. Stearns, Nucl. Fus. 15, 249 (1975).

2. E. B. Hooper, Jr., Lawrence Livermore Lab. Report UCID-18067 (Feb. 1979).

3. John R. Hiskes, invited paper presented at the XIVth International Conference on Phenomena in Ionized Gases, Grenoble, France (July, 1979).

4. M. Bacal, and G. W. Hamilton, Phys. Rev. Lett. 42, 1538 (1979).

5. K. N. Leung et. al., Rev. Sci. Instrum. 49, 321 (1978).

6. K. N. Leung, T. K. Samec, and A. Lamm, Phys. Lett. A 51, 490 (1975).

7. K. W. Ehlers, K. N. Leung, and M. D. Williams, Rev. Sci. Instrum. 50, 1031 (1979).

8. M. L. Yu, Phys. Rev. Lett. 40, 574 (1978).

9. P. Schneider, Ph.D. Thesis, University of California, Berkeley, CA (1980).

10. K. W. Ehlers and K. N. Leung, (paper presented at this Symposium).

11. K. W. Ehlers and K. N. Leung, Rev. Sci. Instrum. 51, 721 (1980).

12. G. I. Dimov, Proceedings of the Second Symposium on Sources and Formation of Ion Beams, Berkeley (1974).

13. K. Wiesemann, K. Prelec and Th. Sluyters, J. Appl. Phys. 48, 2668 (1977).

14. Yu I. Bel'chenko, G. I. Dimov, and V. G. Dudnikov, Nucl. Fus. 14, 113 (1974).

15. M. Siedl and A. N. Paragellis, Bull. Am. Phys. Soc. 23, 804 (1978).

16. K. Wiesemann, Proceedings of the Symposium on Production and Neutralization of Negative Hydrogen Ions and Beams (Brookhaven Nat. Lab., Sept. 1977).

17. Ye. D. Bender, M. Ye. Kishinevskiy and I. I. Morozov, Proceedings of the Symposium on Production and Neutralization of Negative Hydrogen Ions and Beams (Brookhaven Nat. Lab., Sept. 1977).

18. G. D. Alton, IEEE Trans. Nucl. Sci. NS-26, 1542 (1979).

19. C. R. Barnett et. al., "Atomic Data for Controlled Fusion Research," ORNL-5207, p.D.1.63 (1977).

20. J. R. Hiskes, A. Karo, and M. Gardner, J. Appl. Phys. 47, 3888 (1976).

21. W. G. Graham, Phys. Lett. A 73, 186 (1979).

22. D. V. McCaughan, R. H. Sloane, and J. Geddes, J. Appl. Phys. 51, 4426 (1980).

23. J. R. Hiskes and P. J. Schneider, Lawrence Livermore Lab. Report UCRL-84261 (May, 1980).

DISCUSSION

HOPMAN I want to point out, that this morning we have heard in the talk by Los that formation of negative ions is not limited to the case that the work function minus the electron affinity is larger than 0. You get, easily, a yield of 40% of negative ions when low energy atomic hydrogen atoms strike the surface. So, I understood from your talk, that you denied the possibility that the atomic hydrogen forms the low energy peak of the H^- but I think it is the major cause.

LEUNG Well, I do not think anybody has really measured the cross section for this kind of production.

HOPMAN I have measured a yield of 40%.

LEUNG In this experiment it depends on the concentration of atomic hydrogen.

HOPMAN I think the concentration of atomic hydrogen in such a source must be very large.

LEUNG No. Not in this type of source. We did some source analysis and we found not too many atomic neutrals. It is a low arc power source with a density of 6×10^{10}.

BACAL I would like to ask about the comparison between volume production and surface production. I can not understand that volume production is as powerful, if not more powerful, as the surface production under normal extraction conditions.

LEUNG In some operation conditions those two peaks are comparable. I have not mentioned that I ignored the first part of the spectrum because of the large percentage of electrons coming out of the source: a couple of thousand times more. So, it is true that in some situations those two types of production could give us almost the same amount of H^- ions.

BACAL I think we got here a very important information, which we never got before, namely, that inspite of the difference in the number of electrons which we extract, which is a separate problem which can be handled, volume production can be a very powerful method of producing negative ions without cesium.

LEUNG If we can solve the electron problem.

BACAL You and I know that we can solve it. So we have here a method without cesium and which can be scaled. So please remember this figure for the rest of the conference and include it in any program you will start in the future.

CRANDALL I think, everybody who was here in '77 remembers those two peaks in the energy analysis.

GRAHAM I have two questions. The first one is, did you change the cesium densities when you switched from one target to the next?

LEUNG No.

GRAHAM So, you are assuming then that for each target you were getting optimum coverage with the same cesium density?

LEUNG Yes.

GRAHAM But it could be that you, for instance, when you changed from one target to the next, you did not in fact get the minimum or the best optimum work function condition?

LEUNG That is possible.

GRAHAM The second question is: did you measure the electron temperature while you were making these measurements?

LEUNG Yes, 1.5 eV.

GRAHAM And it remained constant, 1.5 eV, with and without cesium?

LEUNG Yes. The addition of cesium in the plasma would not change the electron temperature much.

ANDERSON I can not imagine why you would think that you would get the same cesium coverage when you simply rotate one surface to the other and then expect the same cesium vapor and the same temperature, surely the coverage would depend on how the cesium binds the surface.

LEUNG Maybe.

HOLMES You showed that the volume production went up very rapidly with the gas pressure inside the source. Could you have changed the arc conditions, or do you think it is something else?

LEUNG That increase is probably due to the density increase. We found out that the plasma density increased to a certain point and then stopped increasing. If you look at Dimov's results, you also find, that as they increase the gas pressure, the low energy peak increases while the other one drops.

HOLMES What is the maximum pressure then?

LEUNG Well, I measured the pressure downstream. I do not have any measurement right at the source. At the source, I think it is around 2 or 3 microns.

HAGENA How do you compare the yield for the optimum conditions for surface production of negative ions and under optimum conditions for the volume processes, in your device. How do the two peaks compare? And do you have any quantitative control about the partial density of cesium ions in the discharge, because you mentioned that cesium ions hitting the target are essential?

LEUNG Your first question is quite complicated because it depends on your operation condition, not only your gas pressure, but also your extraction voltage, the amount of cesium etc. It is possible to have the area under both peaks almost equal, or one a little bit higher. For instance without cesium you can see that one peak is almost two orders of magnitude higher than the surface production peak.

CRANDALL These are at optimum conditions?

LEUNG No. To answer your second question. It is difficult to measure the partial density of cesium, but we know that cesium has the highest ionization cross section. So I suspect that a large percentage of the partial density is made up of Cs^+ ions.

EHLERS Could I just add one comment. I do not think you should compare the production from the two systems too close on this experiment because the optics of the two are different. We did not use a Faraday cup. This is a mass spectrometer and the optics from the converter versus the optics from direct extraction are not the same. So, to really get a comparison, we have to use a Faraday cup.

PETERSON This leads me to the question I wanted to ask: how do the optics compare for the two different species.

EHLERS I can not answer you that, because the optics for the volume produced ions are very definitely affected by the amount of voltage you put on where the plasma is, just like you would in a volume or in a positive ion source. The optics for the surface produced is quite different. That converter is some distance back, so it is really not a very fair comparison. A better comparison would be that if you bought the fact that Dimov's work showed volume and not charge exchange ions along with surface produced ions, then there might be a comparison there.

FORRESTER I was puzzled; you had those peaks at 100 and 266 and 300 eV. How do you explain the fact that there is 66 eV of difference in energy from the ions formed from molecular ions, striking it and atomic ions striking it? I do not understand that big difference that comes from whether an H_2^+ or an H strikes it?

LEUNG Between the plasma sheet and the converter there is approximately 200 V. When H_3^+ moves into the surface it will be broken up into three particles, so each one would carry 66 eV. When they backscatter, they pick up an additional electron or two electrons and form H^-. So 66 eV is the maximum energy of the negative ion and when it comes out, it picks up another 200 eV. So 266 eV is the maximum but most particles, when they reflect, can have lower energies, instead of 66 they may have 60, 50 etc.

FORRESTER How come there is not some H^+ that go there with 200 and reflected at 200 and come off with 400 eV?

LEUNG That is right, but you may remember the distribution of the positive ions, they shift when you put in cesium. H_3^+ is completely dominated and each H_3^+ particle can form three H^-.

FORRESTER I am puzzled by the fact that you think you go to a cesium plasma without changing the electron temperature. That surprises me, I would expect the cesium plasma to have a much lower temperature than the hydrogen.

LEUNG I found practically the same temperature.

RELAXATION OF H_2 VIBRATIONAL MOTION BY WALL COLLISIONS*

A. M. Karo, T. M. DeBoni, and J. R. Hiskes
Lawrence Livermore National Laboratory
Livermore, California 94550

Abstract

We have applied the method of computer molecular dynamics to an important technological problem where experimental data may be extremely difficult to obtain: collisional de-excitation at surfaces of vibrationally highly excited hydrogen molecules. Our calculations have been carried out primarily for vibrational states about the v = 6 level. We illustrate the technique by means of a specific example and demonstrate the detail that can be obtained from such calculations concerning the dynamics of the interaction. Molecular states excited to the v = 4, v = 6, and v = 11 vibrational levels and the J = 1 rotational level have been examined. The translational temperature of the molecules is chosen to be 500K, and the wall is given thermal motion characteristic of a temperature of 500K. Different angles of approach have been studied, and different impact points on the surface have been selected. After the first collision, the impact point becomes random because of the stochastic nature of subsequent molecular trajectories. For any given collision with the wall, the molecule may pick up or lose vibrational, rotational, and translational energy. Careful sampling and averaging of the results of many trajectory runs is needed in order to arrive at meaningful conclusions about the probability of de-excitation as a function of such parameters as the number of wall collisions, the residence time, the wall temperature, and the microscopic nature of the wall itself.

The results that we have obtained strongly indicate that simplistic models will not be adequate for obtaining trustworthy answers to the collisional de-excitation problem. We anticipate that our present calculations as they are refined will provide such answers; certainly they can provide insight into the detailed microscopic dynamics.

I. Introduction

Satisfactory progress in the development of present designs for negative ion sources depends on a thorough understanding of the physical processes involved in three general areas: double charge-exchange processes such as occur when protons are passed through cesium vapor; electron-volume processes in which low-energy electrons interact with molecular species, leading to negative ion products by means of recombination or dissociative attachment; and the generation of negative ions in surface interactions, mainly by means of desorption and backscattering. Our attention in this paper will focus on the second of these three areas and will be concerned with reporting preliminary results for computer calculations of the scattering from a wall of iron atoms of vibrationally excited hydrogen molecules, using the method of computer molecular dynamics. In the following section, we will discuss briefly the nature and significance of the problem itself; and in following sections we will outline the method of molecular dynamics, the molecule-wall simulation studies being carried out, and the results of our preliminary work. In summarizing what we have learned up to this point in the final section, we will outline possible directions for future work.

II. Electron-Volume Processes

It has been shown in the study of electron-molecule collisions occurring in hydrogen discharges that the negative ion density increases with the third power of the electron density.[1] A tentative scenario for the enhanced negative ion concentration has been proposed as follows:[2]

$$e + H_2(v = 0) \rightarrow H_2^{\ddagger}(v) + 2e \quad (1)$$

$$H_2^{\ddagger}(v) + H_2(v = 0) \rightarrow H_3^{\ddagger}(v) + H \quad (2)$$

$$H_2^{\ddagger}(v) + M \rightarrow H_2(v \geq 6) + M \quad (3)$$

$$e + H_3^{\ddagger}(v) \rightarrow H_2(v \geq 6) + H \quad (4)$$

$$e + H_2(v \geq 6) \rightarrow H_2^- \rightarrow H^- + H \quad (5)$$

$$H_2(v > 6) + M \rightarrow H_2(v \geq 6) + M \quad (6)$$

$$H_2(v) + M \rightarrow H_2(v - 1) + M \quad (7)$$

The processes (1) and (2) lead to $H_3^{\ddagger}$ and $H_2^{\ddagger}$ fractions in hydrogen discharges of the order of 90 percent and 5 percent, respectively. Auger neutralization of $H_2^{\ddagger}$ ions in wall collisions, shown in (3), and the process of dissociative recombination, indicated in (4), are known to have large cross sections.[2,3] These are two processes giving rise to the vibrationally excited molecules, $H_2(v)$. Kulander and Guest[4] have studied the products formed in step (4) and have concluded that the hydrogen molecules are formed with a substantial fraction in the higher vibrational states. It has been estimated that Auger neutralization of $H_2^{\ddagger}$

*Work performed under the auspices of the U.S. Department of Energy by Lawrence Livermore National Laboratory under contract No. W-7405-Eng-48.

ions in wall collisions may yield populations for levels $v \geq 6$ which are greater than 30 percent of the total $H_2(v)$ distribution.[2]

Recently, these processes have been supplemented by the important additional processes of wall collisions[5]

$$H_3^+(v) + M \rightarrow H_2(v \geq 6) + M \qquad (8)$$

and the excitation from the ground state of hydrogen to higher singlet states by energetic electrons followed by radiative decay to the ground electronic state:[6]

$$e + H_2(v=0) \rightarrow e + H_2^* \rightarrow e + h\nu + H_2(v \geq 6). \qquad (9)$$

Careful analysis indicates that the most probable process for the production of H^- negative ions is the dissociative attachment to vibrationally excited hydrogen molecules indicated in step (5).[2] Cross sections greater than 2×10^{-16} cm^2 have been estimated[2,7] for both $H_2(v)$ and $D_2(v)$ for the upper levels $v \geq 9$. However, for the density of $H_2(v \geq 6)$ to rise sufficiently high for steps (1) through (9) to be a credible scenario for explaining the observed negative ion yields, the vibrationally excited molecules must survive from 10 to 20 wall collisions, step (6), before vibrational de-excitation occurs, as shown in step (7).

In an attempt to obtain some insight into the transient behavior of vibrationally excited H_2 and D_2 during a collision with an appropriate surface and to estimate at least qualitatively the probability of survival of these highly excited molecules as a function of the number of wall collisions and the residence time at or near the surface, we have carried out some computer experiments based on the method of molecular dynamics. An advantage of this technique is that it allows us to begin with some initial simple approximations and gradually to refine the calculations as our understanding of the problem increases.

III. Molecular Dynamics

Molecular dynamics provides a very powerful technique for examining the microscopic details of a wide variety of phenomena, subject to practical computational restrictions on time and scale. For example, practical limits on the number of particles in an ensemble currently range from 10^3 to 10^4, and the period of time over which the evolution of the system can be followed can range from 10^3 to 10^4 in units of time natural to the problem being considered (in general this implies from 10^5 to 10^7 integration steps). Thus, as an example, molecular vibration frequencies are typically of the order of 10^2 to 10^3 cm^{-1}, and correspond to vibrational periods of tenths to hundredths of picoseconds (10^{-12} seconds). Rotational periods are typically around a hundred times longer. In real units of time, then, computer runs requiring a few minutes of time allow us to examine the evolution of our ensemble for up to several hundred picoseconds. Within these constraints, a virtually unlimited variety of computer simulations can be explored.

For the molecule-wall simulation studies we are concerned with here, specification of initial conditions for the computer experiment can include: variations of temperature and temperature gradient of the wall; detailed specification of the particle, its internal modes, and its interaction with the wall (e.g., the velocity and angle of impact, the isotopic composition, and the degree of excitation of the molecule); and the crystallographic orientation and the type of lattice simulated (e.g., monatomic, diatomic, or polyatomic, with configurational regularity or irregularity).

The method of molecular dynamics has evolved to a more sophisticated level because of the dramatic revolution in large-scale computer technology. Simply stated, computer molecular dynamics involves the numerical solution by computer of Newton's equations of motion for all the atoms comprising the active region of the assembly. As a result, the coordinates and velocities of the particles are obtained as functions of time.[8]

The set of coupled nonlinear second-order differential equations that represent the forces acting on the particles are reduced to a doubled set of first-order ordinary differential equations by standard procedures. The initial positions and velocities of the particles represent the initial conditions on these equations. For the numerical solution of this set of equations, we have employed the EPISODE software package, written by A. C. Hindmarsh and G. D. Byrne at the Lawrence Livermore National Laboratory.[9] This package utilizes the variable-step, variable-order, implicit Adams method with functional (or fixed point) iteration; this is a generalization of the classical Adams-Bashforth-Moulton method.[10] Relative error buildup is controlled by an error tolerance parameter, so that numerical error is typically kept to less than 10^{-6} for times up to 10 to 50 picoseconds (in the real time units for the evolving system) during the simulation. Estimation of these errors is made as a function of the time step-size, and the step-size is chosen so as to maintain the errors below the chosen level. Symmetry checks of the output are routinely made to verify the accuracy of control.

IV. Molecule-Wall Simulation Studies

Dimensionality and Regularity

The study of energy transport and decay in discrete systems can be carried out in two-dimensional systems as well as in three-dimensional, "more realistic" situations. Although care must be exercised in allowing for

the purely two-dimensional character of the results obtained, such studies can lead to valuable insights, large numbers of parameter variations can be easily made, and the general characteristics of an evolving system can be observed with minimal expenditure of computer time. Surfaces with which the molecule will interact can be designed with irregularities and with variations in mass and potential. Questions that can be given detailed examination include the nature of the particle-surface interaction as a function of different initial conditions; the general nature of interparticle momentum transfer and its dependence on the effective interaction potential; the stability of the vibrational-rotational state of the molecule and its dependence on the discrete nature of the mass array in the wall; and the importance of the nonlinear or chemical nature of the interatomic forces.

Three-dimensional lattices are inherently more realistic, with the increased dimensionality adding translational, vibrational, and rotational degrees of freedom and opening channels for relaxation processes not otherwise present in two-dimensional systems. We anticipate that our three-dimensional studies of the dynamical response of vibrationally excited molecules to wall collisions will complement in an important way the two-dimensional calculations we are presenting here and can, if it should prove necessary, supplant them entirely. For the rather simple situation we are looking at here, it is very possible, however, that the general features we see in the two-dimensional calculations contain almost all of the qualitative information that will be found in the three-dimensional simulations.

Potentials

The force acting on any one particle in the ensemble is the resultant of all interactions with other atoms in its neighborhood and is obtained as a derivative of an effective many-body potential. However, any molecular dynamics calculation which would in fact attempt to include most or all of a complete potential energy hypersurface represents a Herculean task far beyond present considerations. Fortunately, our experience to date indicates that much can be learned within the framework of a suitably generalized pair-potential approximation. In going beyond this simple treatment at some later stage, we are likely to find it possible to deal only with those portions of the hypersurface that are relevant to the trajectories of the particle and the chemical dynamics of the evolving system.

Initial Conditions

We have considered in these initial calculations simple two-dimensional simulations of the type depicted in Fig. 1. At some initial time, t = 0 (in units of 10^{-14} seconds), a hydrogen molecule is set in motion toward a lattice composed of iron atoms. As can be seen, this lattice represents a surface layer and four interior layers. We have chosen a [110] plane of the body-centered cubic phase of Fe for these initial computer studies, as this particular two-dimensional configuration most closely matches the lattice used in extensive shock propagation studies carried out for two-dimensional face-centered cubic structures.[11] At the time, t = 8, of Fig. 1 the molecule has not yet approached near enough to the surface for long-range interactions to be included in the equations of motion.

The initial translational velocity of the H_2 molecule has been chosen equal to the average molecular speed associated with a gas temperature of 500K; at this temperature the J = 1 rotational state also predominates. In most of our computer runs, the initial vibrational energy is that associated with the v = 8 vibrational level, about 28,000 cm^{-1} above the potential energy minimum. A few calculations have also been carried out for the v = 4 and v = 11 levels as checks on the overall procedure. For the v = 8 level, a Morse curve fit predicts the left turning point to be at 0.423 Å and the right turning point to be at 1.757 Å. For the wall, the Fe atoms have been given initial thermal motion characteristic of a temperature of 500K. Because of the small number of atoms comprising the wall, this is more properly related to a local kinetic temperature rather than a true thermodynamic temperature. For the dynamics of our problem, this distinction is not important. The two-body potential for FeH has been adapted from the work of Scott and Richards,[12] and the Fe potential from the two-body potential derived by Johnson[13] in which experimental elastic-constant data were used. Although there are unpublished calculations for the ground electronic state of FeH indicating that this state may not be the $^6\Delta$ found by Scott and Richards, their potential is very likely sufficiently accurate for our present calculations. For the molecular dynamics simulations we are reporting here, these two-body potentials form the framework within which the interrelated particle and chemical dynamics of the system must be described. In the equations of motion, masses are in atomic mass units, and the units of time are in 10^{-14} seconds.

V. Discussion

Although our results are at this stage very preliminary, it is rather instructive to follow one example in some detail. A typical sequence is shown in Figs. 1 and 2. In Fig. 1, the molecule is shown moving toward the wall at the time, t = 8 (8 x 10^{-14} seconds). Its initial vibrational excitation is equivalent to a molecule in the v = 6 level, and it has been given rotational motion characteristic of the J = 1 level. In Fig. 2a, the system is shown at t = 21 as it begins to interact with the wall. This interaction is initially very weak

and is depicted by dashed lines indicating those bonds which the code itself recognizes as having been formed between the hydrogen atoms and the iron atoms of the wall. The two hydrogen atoms are seen to be momentarily near the inner turning point, i.e., in the close-in or helium-like configuration. In Fig. 2b, one can see that the molecule has approached quite near the surface; the code now recognizes additional, but rather weak, bonding. At the moment shown in Fig. 2b, the molecule is in its stretched or hydrogen-atom-like configuration, so that the potential appropriate for the Fe-H interaction is the weak, long-range part of the Fe-H pair potential. Rapid changes in electronic structure now occur associated with the rapidly varying spatial conformation and, at t = 32, shown in Fig. 2c, a strong bond has formed between one of the hydrogen atoms and an Fe surface atom, all other interactions remaining weak. The result of a sequence of strong dynamical interactions occurring between t = 32 and t = 40 is shown in Fig. 2d where the molecule is now moving away from the surface, with only a few weak, long-range bonds remaining, indicating a rapidly diminishing interaction with the surface.

As we follow the motion of the molecule relative to the surface, we monitor a number of interesting dynamical quantities, some of which are shown in Fig. 3. When the molecule is far from the surface, we are able to factor its internal energy into rotational and vibrational kinetic energy and vibrational potential energy. The translational motion is also monitored, and the sum of these energies, or the total energy of the molecular unit, is plotted. We have also found that plotting the center-of-mass position relative to the surface provides not only information about the position and velocity of approach of the molecule with respect to the wall but also provides very useful information about the "residence time" on the surface. As the molecule nears the surface, changes in the translational kinetic energy can be seen as well as changes in the slope of the center-of-mass plot. During the time of strong interaction with the surface, the molecular vibrational and rotational energies are not well-defined, and these quantities should only be used as a vivid indication of the rapidly varying dynamics occurring at the surface. Following separation of the molecule from the surface, changes in these quantities from values possessed by the incoming particle can be readily observed. For the example we have used in Fig. 2, we show in the sequence given in Fig. 3 the corresponding dynamical quantities plotted from t = 24 to t = 44. During the collision with the wall, the initial vibrational energy of -2.50 eV (the sum of the vibrational kinetic and potential energy components) decreases to around -3.25 eV, but the molecule at the same time has picked up both rotational and translational energy.[14] Overall, the total energy of the molecule has increased after collision with the wall from about -2.44 eV to -2.14 eV. From Fig. 3, we can also see that the residence time of the hydrogen atoms at the surface for this collision was of the order of $7 - 8 \times 10^{-14}$ seconds, i.e., from 7 to 8 vibrational periods for the isolated molecule in its v = 6 state. Subsequent collisions of this hot molecule with the wall will give rise to further changes in the vibrational and rotational energy. For any given collision with the wall, the molecule may pick up or lose vibrational, rotational, and translational energy. It is the statistical averaging of these events that we are now carrying out that will provide a more complete answer to the question of collisional de-excitation.

VI. Conclusions

In this report we have discussed the application of computer molecular dynamics to an important technological area where experimental data may be very difficult to obtain: collisional de-excitatin at surfaces of vibrationally highly excited molecular systems. Here our interest is specifically in H_2, D_2, and HD, vibrationally excited above the v = 6 level. We have illustrated the technique by means of a specific example and have demonstrated the detail that can readily be obtained from such calculations. We have also pointed out that there is work to be done in characterizing as realistically as possible changes in the effective potentials, and therefore the resulting forces, as the molecular species approach and interact with the surface. In addition, we have indicated the necessity of sampling and averaging the results of many trajectory runs in order to arrive at meaningful conclusions about the probability of de-excitation as a function of the number of wall collisions, the residence time, the wall temperature, and the nature of the wall itself, as well as other variables that will undoubtedly show themselves to be important as the calculations proceed. Finally, results obtained from two-dimensional simulations will have to be checked carefully against statistically weighted series of three-dimensional trajectories to remove uncertainties about a two-dimensional bias in the results.

Our work up to the present time strongly indicates that simplistic models that have been occasionally used in the past will not be adequate to obtain trustworthy answers to the collisional de-excitation problem. It may be that for the near future the combining of a generalized pair potential approach with parametric fitting to known experimental data may be most effective for obtaining realistic answers for this problem. We anticipate that our present calculations as they are refined will provide such answers; certainly they can provide insight into the detailed microscopic dynamics involved.

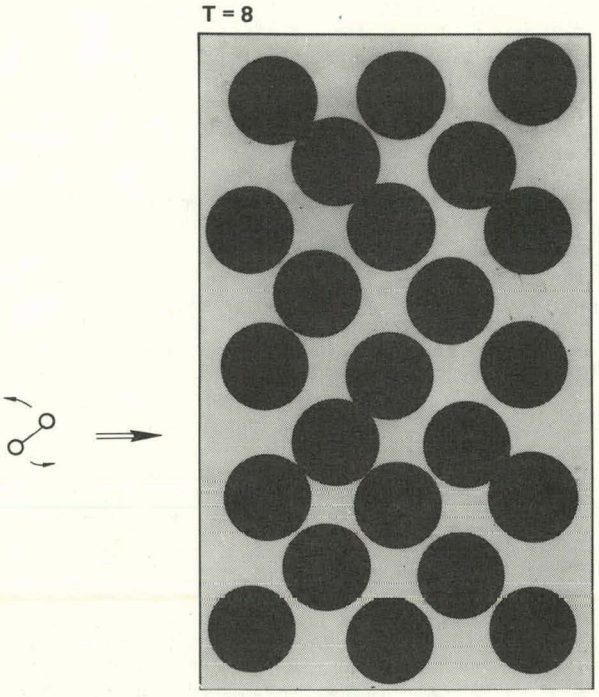

FIGURE CAPTIONS

Fig. 1. Configuration at t = 8 for an H_2 (v = 6, J = 1) molecule in motion toward a lattice composed of Fe atoms. The translational velocity is characteristic of a gas of H_2 molecules at 500K, and the lattice has been given initial random motion appropriate to a temperature of 500K.

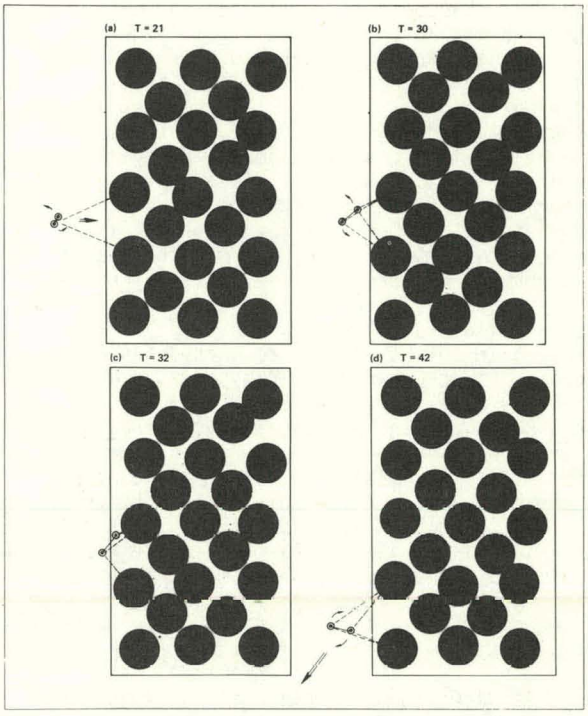

Fig. 2. Configurations of an H_2 molecule, as described in Fig. 1, within range of interaction with an Fe lattice: (a) the H_2 molecule near its inner turning point; weak, long-range interactions are shown by dashed lines; (b) the molecule near its outer turning point; additional long-range, weak interactions are evident; (c) the molecule in contact with the surface; a strong chemical bond has formed as indicated by the solid line; and (d) the molecule leaving the surface; only weak, long-range interactions remain. The corresponding time, t, is shown in each figure.

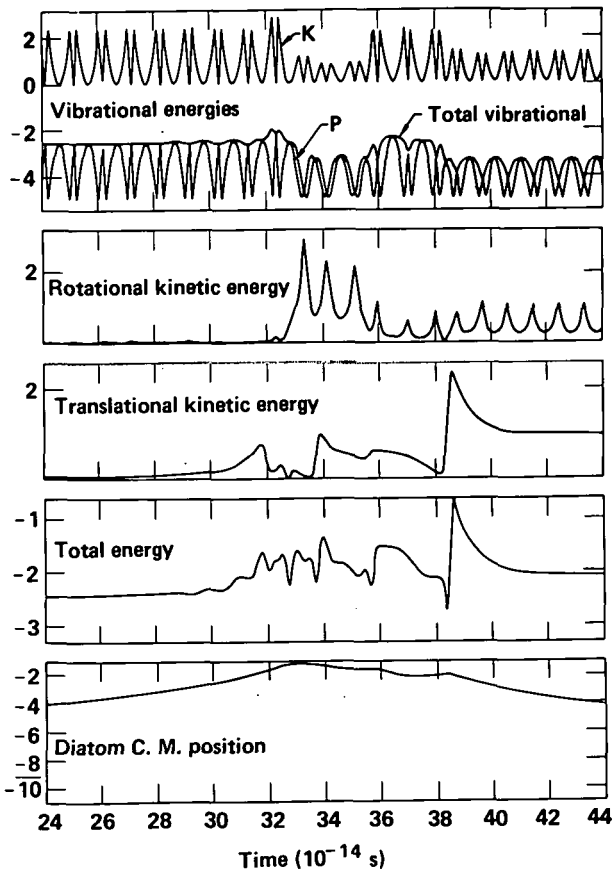

Fig. 3. Vibrational, rotational, and translational energies, and the center-of-mass distance normal to the surface plotted against time. The vibrational energy has been additionally separated into its kinetic and potential energy components, and the total molecular energy has been plotted.

References

1. M. Bacal and G. W. Hamilton, Phys. Rev. Lett. 42, 1538 (1979).

2. J.R. Hiskes, J. de Physique, Colloque C7, suppl. 7, 40, C7-179 (1979).

3. B. Peart and K. T. Dolder, J. Phys. B. 7. 1948 (1974).

4. K. C. Kulander and M. F. Guest, J. Phys. B. (to be published).

5. M. Bacal, I. M. Bruneteau, W. G. Graham, G. W. Hamilton, and M. Nachman, J. Appl. Phys. (1980) (to be published).

6. J. R. Hiskes, J. Appl. Phys. (1980) (to be published).

7. J. M. Wadehra and J. N. Bardsley, Phys. Rev. Lett. 41, 1795 (1978), and Private Communication.

8. B. J. Alder and T. E. Wainwright, J. Chem. Phys. 27, 1208 (1957); 31, 459 (1959); 33, 1439 (1960).

9. A. C. Hindmarsh and G. D. Byrne, "EPISODE: An Effective Package for the Integration of Systems of Ordinary Differential Equations," Lawrence Livermore National Laboratory Report UCID-30112, Rev. 1 (April 1977).

10. C. W. Gear, Numerical Initial Value Problems in Ordinary Differential Equations (Prentice-Hall, Englewood Cliffs, New Jersey, 1971), Chapter VII.

11. A. M. Karo and J. R. Hardy, Proc. of the NATO Adv. Study Inst. on Fast Reactions in Energetic Systems, Ioannina, Greece, 1980, C. Capellos, Editor (D. Reidel Publishing Co., Dordrecht-Holland, Boston-U.S.A., 1981).

12. P. R. Scott and W. G. Richards, J. Chem. Phys. 63, 1690 (1975).

13. R. A. Johnson, Phys. Rev. 134A, 1329 (1964).

14. The negative sign appears because, by convention, we have defined the asymptotic energy of the separated H_2 molecule to be 0; our value for the dissociation energy D_e for H_2 is -4.745 eV.

DISCUSSION

LOS I am interested how you treat the interaction between the molecule and the surface? Do you treat that interaction like a physisorption interaction or do you include the possibility that there is a precursory state between physisorption and eventual a second state, which is chemisorption? I mean, do you include the possibility that different potential surfaces are important?

KARO Yes, what we have done basically, is to consider this within the framework of a pair of potential approximations. But, in generalizing this, one has to account for the fact that chemical bonds can form or you may just have a physical interaction with the wall. In this generalized pair approximation one is able to consider the possibility of a bond forming or if you want to say a physisorption sort of thing, where it comes in as very weak interaction with the surface and bounces off. This process has to be taken into account.

LOS Did you do it?

KARO We have done sort of a general precursor to this point in that we varied the potential to see just what effect all of this would have. The code itself is being set up to include that type

of direct switching when you have, say a chemical interaction with the surface.

LOS At what separation of the hydrogen molecule would it dissociate at the surface?

KARO Meaning if it is in residing near the surface, at what point would it probably separate the two? We only have one or two runs in which we have seen this occur so far. I think we need again the statistical sampling to sort of give a general picture for that. Certainly, as the hydrogen molecule separates to the far point, in a $v = 8$ stretch, we are getting very close to the point where interaction between the two hydrogens are very weak and things can happen to it.

PETERSON What was the vibrational energy content and the kinetic energy in this particular example?

KARO This one was in the $v = 6$ level and it had a translational speed approximate to 500° K.

LIMITING SECONDARY PLASMA EFFECTS IN CESIUM CELLS OR JETS USED IN THE DOUBLE CHARGE EXCHANGE METHOD FOR D^- BEAM PRODUCTION

J. M. Dolique
Université de Grenoble I, France

Abstract

One of the two principal presently developped methods of producing the intense D^- beams required for magnetic fusion plasma additional heating, is the double charge exchange. On a cell or jet of an electropositive gas such as cesium, a D^+ beam is partially transformed into a D^- beam by D^+ Cs Cs/D° Cs^+ Cs/D^- Cs^+ Cs^+. At the same time a Cs^+, e^- secondary plasma is formed which in its turn gives rise to inelastic collisions with the beam : some D^- ions are destroyed. Production and dynamics of that reactive plasma are studied theoretically for the cell case. An axial magnetic field is present, as in the major existing double charge exchange D^- source[1]. The D^- efficiency is discussed. Finally preliminary results for the jet case are presented which emphasize the interest of this method.

I. Introduction

Figure 1 schematically shows a (D^-, D°) beam line for MF plasma additional heating, based on the cell double charge-exchange method of producing the D^- beam. An axial guiding magnetic field may be added.

If the secondary (Cs^+, e^-) plasma effects are neglected, the charge-exchange processes $D^{(m)} + Cs \rightarrow D^{(p)} + Cs^+ + (p + 1 - m)\, e^-$ only being considered, the theoretically predicted axial density profiles for D^+, D°, D^-, with a gaussian axial density profile for Cs : $n(Cs) = n_n(z) = n_{no} \exp(-z^2/2\ell^2)$, will be those shown by Fig.2

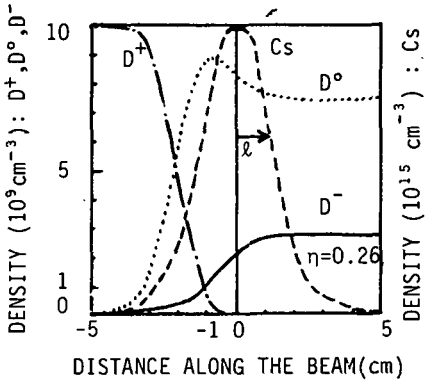

Fig. 2. D^+, D°, D^- axial density profiles if the secondary plasma effects are neglected. $n_{no} = 10^{15}$ cm^{-3}, ℓ = 1.17 cm, $n_{D^+}{}_{in} = 10^{10}$ cm^{-3}, D^+ energy = 1 keV ($J_{D^+}{}_{in}$ = 50 mA/cm^2). $\eta = n_{D^-}{}_{out}/n_{D^+}{}_{in} = |I_{D^-}{}_{out}|/I_{D^+}{}_{in}$

But one has to expect a very high Cs^+ or e^- density and therefore important and possibly unfavorable secondary plasma effects.

In fact, for the particle flux pattern at the beam-cell interaction zone border shown in Fig.3a

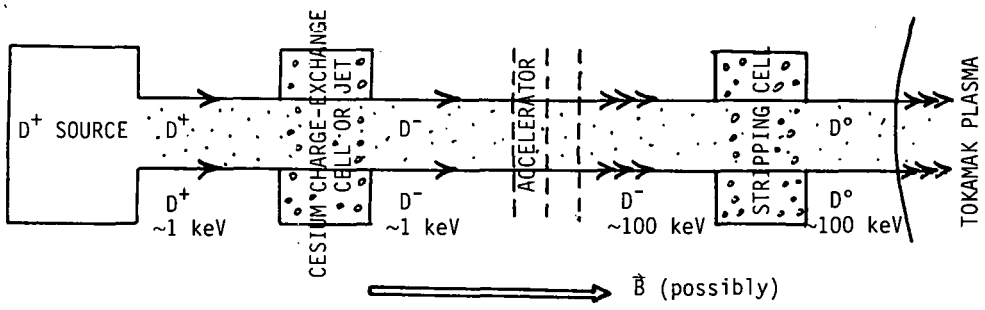

Fig. 1. Schematic of a (D^-, D°) beam line with double-charge exchange produced D^-

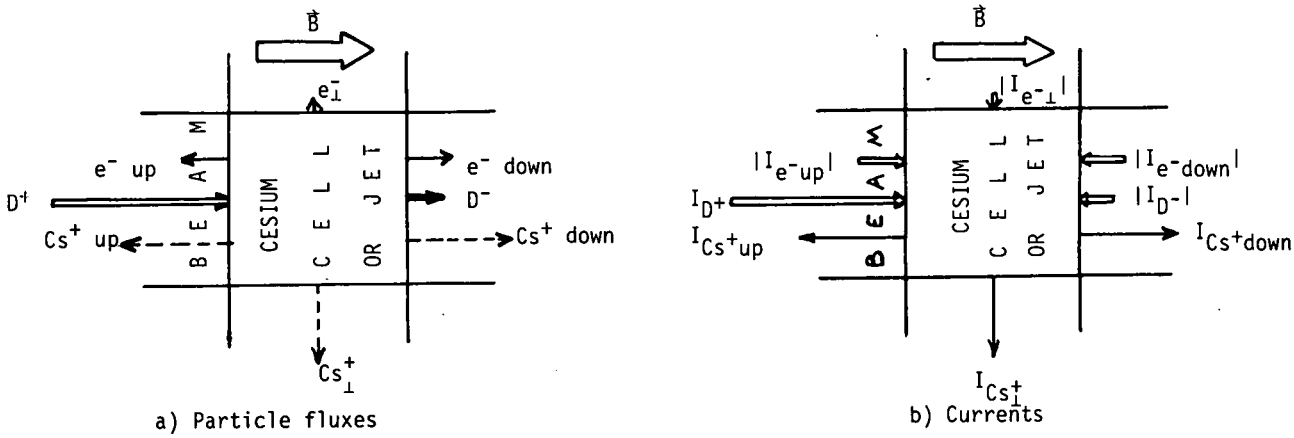

a) Particle fluxes b) Currents

Fig. 3. Particle flux (a) and current (b) patterns at the beam-cell interaction zone border.

the corresponding current pattern is that of Fig. 3b, for which the KIRCHHOFF law tells us that $I_{D^+} + |I_{D^-}| + |I_{e^-}| = I_{Cs^+}$, and therefore $I_{Cs^+} > I_{D^+}$.

One can roughly estimate I_{Cs^+} at $I_{Cs^+} \approx 2\pi R(R + 2\ell)\, en_{Cs^+} v_{Cs^+}$ where R is the beam radius, n_{Cs^+} and v_{Cs^+} some mean Cs^+ density and fluid velocity at the surface of the cell-beam interaction zone. Therefore, with $R \approx \ell$: $6\, n_{Cs^+} v_{Cs^+} > n_{D^+} v_o$, where n_{D^+} and v_o are respectively the incoming D^+ beam density and velocity. As it will be seen later, the Cs^+ fluid dynamics is a Cs collision dominated diffusion. Accordingly $v_{Cs^+} < v_{T_i}$ where v_{T_i} is the Cs^+ ion thermal velocity. For $T_i \sim 0.1$eV, $v_{T_i} \sim 250\ m.s^{-1}$. With the above mentioned values $n_{D^+} = 10^{10} cm^{-3}$, 1 keV D^+ : $n_{Cs^+} \gtrsim 10^{12}\ cm^{-3} >> n_{D^+}$.
This paper summarizes calculations on the secondary plasma effects.

II. Involved inelastic processes. Source terms. Conservation laws

Many of the inelastic processes likely to be involved have negligibly small cross sections. The processes taken into consideration are :

a) Cell-beam charge exchanges :
$D^+ + Cs \rightarrow D^\circ + Cs^+$
$D^\circ + Cs \rightarrow D^- + Cs^+$

b) Cell ionization by the beam :
$D^+ + Cs \rightarrow D^+ + Cs^+ + e^-$
$D^\circ + Cs \rightarrow D^\circ + Cs^+ + e^-$
$D^- + Cs \rightarrow D^- + Cs^+ + e^-$

c) Beam ionization by the cell :
$D^\circ + Cs \rightarrow D^+ + Cs + e^-$

d) Beam-cell electron detachment :
$D^- + Cs \rightarrow D^\circ + Cs + e^-$

e) Beam-secondary plasma charge exchange :
$D^\circ + Cs^+ \rightarrow D^+ + Cs$

f) Beam-secondary plasma electron detachment :
$D^- + Cs^+ \rightarrow D^\circ + Cs^+ + e^-$

g) Beam-secondary plasma mutual neutralization :
$D^- + Cs^+ \rightarrow D^\circ + Cs$

h) Recombination in the secondary plasma :
$Cs^+ + e^- \rightarrow Cs$

i) Cell secondary ionization :
$e^- + Cs \rightarrow Cs^+ + e^- + e^-$

For each of the six involved species : D^+, D°, D^-, Cs, Cs^+, e^-, the preceding inelastic processes give rise to a source term S : number of particles created or destroyed per unit time and volume.

For the deuterium species $D^{(m)}$ $(m = -1,0,1)$, $S_{D(m)}$ is an algebraic sum of terms like $n_a n_b v_o \sigma_{ab}(v_o)$ where $\sigma_{ab}(v_o)$ is the total cross section attached to the $D^{(m)}$ creating or destroying a-b reaction.

Besides this type of term there are, in the Cs, Cs^+ and e^- source terms, contributions due to recombination 1'e/0' and secondary ionization e0'/1'ee. In order to be able to describe the recombination for any secondary plasma density, a source term of the most general form $[\alpha_r(T_e) + \beta_3(T_e)\, n_e]\, n_e\, n_i$ has been used, where α_r is the radiative coefficient, β_3 the collisional three-body coefficient, n_e and n_i the electron and Cs^+ ion density respectively. α_r and β_3 are both strongly dependent on the electron temperature T_e. It is also the case for $I(T_e)$, the secondary ionization coefficient, in the corresponding $I(T_e)\, n_e\, n_n$ source term.

The six source terms S_{D^+}, S_{D°, S_{D^-}, $S_i \equiv S_{Cs^+}$, S_e, $S_n \equiv S_{Cs}$ are not independent. They are connected by three conservation laws :

a) charge conservation : $\Sigma q_a S_a = 0$,

b) Mass conservation : $\Sigma m_a S_a = 0$,

where q_a and m_a are the a-particle charge and mass respectively.

c) Total deuterium conservation : $\Sigma S_{D(m)} = 0$. More explicitly :

$$S_{D^+} - S_{D^-} + S_i - S_e = 0 \qquad (1)$$

$$m_{D^+} S_{D^+} + m_o S_{D^o} + m_{D^-} S_{D^-} + m_i S_i + m_e S_e + m_n S_n = 0 \qquad (2)$$

$$S_{D^+} + S_{D^o} + S_{D^-} = 0 \qquad (3)$$

According to (1) and (3)

$$S_i + S_n = 0, \qquad (4)$$

which expresses the total cesium conservation.

To be selfconsistent, any set of chosen inelastic processes must satisfy these conditions. It is the case for the above mentioned set.

III. Current regimes

Let us now turn from the local to the total source terms

$$S_a = \int S_a(\vec{r})\, d\vec{r},$$

the integration being extended to the whole beam-cell interaction zone. Within the frame of a steady state, to which the present model is restricted, it follows from the continuity equation for particle a

$$\vec{\nabla}.(n_a \vec{v}_a) = S_a$$

that S_a is also the total a-particle flux across the interaction zone border

$$S_a = \oint n_a \vec{v}_a . d\vec{\sigma}$$

$S_a > 0$ for a net outcoming flux, $S_a < 0$ for a net incoming flux.

The charge or electricity conservation law (1) gives

$$S_{D^+} - S_{D^-} + S_i - S_e = 0 \qquad (1bis)$$

$S_i \geq 0$ since the Cs^+ are produced inside the interaction zone. Anticipating the forthcoming result that the outflowing D^+ current is small as compared to the inflowing current I_{D^+}, one has $S_{D^+} \approx - I_{D^+}/e$. Finally $S_{D^-} = |I_{D^-}|/e$. Therefore

$$S_i = \frac{1}{e}(I_{D^+} + |I_{D^-}|) + S_e \geq 0$$

$$S_e \geq - \frac{1}{e}(I_{D^+} + |I_{D^-}|)$$

If the secondary plasma density $n_e \approx n_i = n$ were considered as an independent parameter, the variation of S_e as a function of n, for given $n_n = n_{Cs}$, T_e and I_{D^+}, could be shown as rapidly decreasing around the point $S_e = 0$ [Fig. 4], due to the fact that we are now moving into the high density $S_e \propto - n^3$ recombination dominated regime.

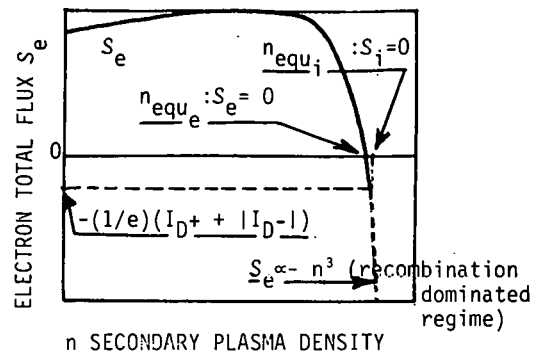

Fig. 4. Electron total flux across the interaction zone border, versus the secondary plasma density considered as an independent parameter.

The ion equilibrium regime ($S_i = 0$: no Cs^+ flux across the interaction zone border) and the electron equilibrium regime ($S_e = 0$) correspond to very close densities. Figure 5 compares the current patterns for various regimes : $S_i = 0$; $S_e = 0$; S_e, $S_i > 0$.

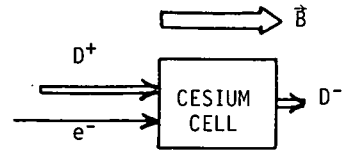

a) $S_i = 0$: ion equilibrium regime

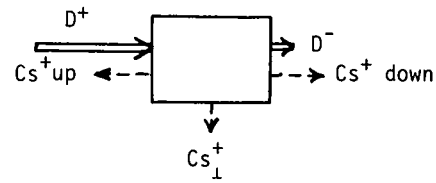

b) $S_e = 0$: electron equilibrium regime

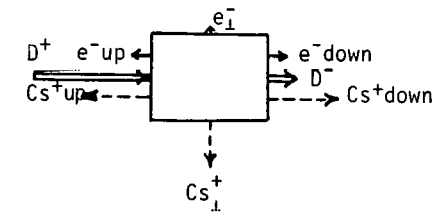

c) $S_e > 0$, $S_i > 0$: regime with net electron and ion production.

Fig. 5. Current pattern for various regimes.

But of course n is not an independent parameter. Its value is both conditioned by the electron current possibly injected into the interaction zone, and by the boundary conditions. In order to favour a steady-state regime where n is

as small as possible, it is advantageous to ensure boundary conditions for which both electron and ion current collection are allowed (regime c in Fig.5).

IV. Basic equations and assumptions

a) Steady state and cylindrical symetry around the beam are postulated.

b) The deuterium beam is assumed to be radially homogeneous ; angular dispersion and slowing down are neglected :

$$n_{D(m)}(r,z) = n_{D(m)}(z)\ \mathcal{T}(R-r),$$

$$\vec{v}_{D(m)}(r,z) = \vec{v}_o = v_o \vec{u}_z$$

($\mathcal{T}$: unit step function, R : beam radius)
($\vec{u}_z$: unit vector along the axial z coordinate)

The only equations taken into consideration for the three deuterium species are the three continuity equations :

$$v_o \frac{\partial}{\partial z} n_{D(m)} = S_{D(m)}[n_{D^+}, n_{D^\circ}, n_{D^-}, n_n, n_i, n_e] \qquad (5)$$

c) Electrons are assumed to be in BOLTZMANN equilibrium with temperature T_e. To take into account a possible small electron diffusion out of the interaction zone ($S_e > 0$), a small TONKS - like correction $\phi^{(1)}$ to the BOLTZMANN potential has to be considered :

$$\phi(\vec{r}) = (k_B T_e/e) \ln[n_e(\vec{r})/n_{eo}] + \phi^{(1)}(\vec{r}) \qquad (6)$$

For the ion dynamics study, $\phi^{(1)}$ will be neglected.

d) As for the Cs^+ ion fluid, its dynamics is described on the one hand by a continuity equation

$$\frac{\partial}{\partial z}(n_i v_{iz}) + \frac{1}{r}\frac{\partial}{\partial r}(r n_i v_{ir}) = S_i[n_{D^+}, n_{D^\circ}, n_{D^-}, n_n, n_i, n_e] \qquad (7)$$

and on the other hand by a motion equation. To choice the latter it is important to point out that the physical situation is not at all the free fall situation considered in similar problems by various authors (HOOPER et al. [2], HOLMES [3],..). For a Cs neutral density at the cell middle $n_{no} = 10^{15} cm^{-3}$, and a Cs^+ ion temperature $k_B T_i \sim 0.1$ eV, the Cs^+ mean free path for elastic Cs^+ - Cs collisions is $\lambda_{in_o} \sim 0.1mm \ll R \sim 1$ cm, the beam radius.

So a diffusion equation for ion-neutral collision-dominated motion, in the presence of both the electric ($\vec{E}(\vec{r}) = -\vec{\nabla}\phi(\vec{r})$) and the magnetic fields, will be used :

$$n_i \vec{v}_i = n_i \overleftrightarrow{\mu}_i \cdot \vec{E} - \overleftrightarrow{D}_i \cdot \vec{\nabla} n_i \qquad (8)$$

$\overleftrightarrow{\mu}_i$ and $\overleftrightarrow{D}_i$ are the conventional mobility and diffusion tensor coefficients

$$\overleftrightarrow{\mu}_i : \begin{pmatrix} \mu_{i\perp} & -\mu_{iT} & 0 \\ \mu_{iT} & \mu_{i\perp} & 0 \\ 0 & 0 & \mu_{i//} \end{pmatrix} \quad (//, \perp : \text{with respect to } \vec{B})$$

$\mu_{i//} = e/m_i \nu_{in}$, $\mu_{i\perp} = \mu_{i//}/(1+\omega^2_{ci}/\nu^2_{in})$ (PEDERSEN mobility), $\mu_{iT} = (\omega_{ci}/\nu_{in})\mu_{i\perp}$ (HALL mobility). ν_{in} is the macroscopic Cs^+ - Cs elastic collision frequency, ω_{ci} the Cs^+ cyclotron frequency.

$$\overleftrightarrow{D}_i = (k_B T_i/e)\overleftrightarrow{\mu}_i \quad \text{(EINSTEIN)}$$

For B = 4 000 gauss and $k_B T_i \sim 0.1$ eV, $\omega_{ci}/\nu_{in} \sim 0.1$: at the middle of the cell the anisotropy introduced in the ion dynamics by the magnetic field is small. (For the electrons, with $k_B T_e \sim 0.1$ eV, $\omega_{ce}/\nu_{en} \sim 300$: the anisotropy is very important). Of course near the cell border the anisotropy becomes important for the ions too.

e) Quasineutrality, electric field.
For $n_e \sim 10^{12}\ cm^{-3}$ (cf. introduction) and $k_B T_e \sim 0.1$ eV, the DEBYE length is $\lambda_D \sim 1\ \mu m$: the assumption of quasineutrality is quite adequate

$$n_{D^+} + n_i - n_{D^-} - n_e \approx 0$$

or, with $n_i, n_e \gg n_{D^+}, n_{D^-}$

$$n_e \approx n_i = n \qquad (9)$$

The BOLTZMANN electric field $\vec{E}(\vec{r}) = -\vec{\nabla}\phi(\vec{r})$ where $\phi(\vec{r})$ has the above mentioned expression (§ 4.c) is associated to a small space charge density $|n_e - n_i| \ll n$.

f) Beam radial homogeneity. This assumption has already been made for the deuterium species. It will be extended to Cs^+ and e^- :

$$n_i(r,z) \equiv n(r,z) = \begin{cases} n_i(z) & 0 \le r \le R \\ n_i(r,z) & R < r \end{cases}$$

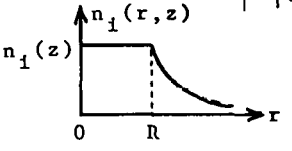

V. Electron temperature

T_e has a drastic influence on secondary ionization ($e^- + Cs \rightarrow Cs^+ + e^- + e^-$), on recombination ($Cs^+ + e^- \rightarrow Cs$), and hence on the secondary (Cs^+, e^-) plasma steady state density. Care should be taken in its calculation.

The steady state electron energy balance equation can be written

$$\vec{\nabla}.\left[\frac{1}{2} n_e m_e \vec{v}_e^{\,2} \vec{v}_e + \frac{5}{2} n_e k_B T_e \vec{v}_e + \vec{q}_e \right] =$$

$$- n_e e \vec{v}_e . \vec{E} + \sum_{b=i,n} n_e m_e \nu_{eb} \left\{ \frac{3 k_B (T_b - T_e)}{m_e + m_b} + \frac{m_e \vec{v}_e + m_b \vec{v}_b}{m_e + m_b} . (\vec{v}_b - \vec{v}_e) \right\} + \sum_{m=-1,0,1}$$

$$P_{D^{(m)}e} \; n_{D^{(m)}}$$

+ inelastic source terms

where $\vec{q}_e$ is the heat flux, ν_{eb} the e - b macroscopic collision frequency, $P_{D^{(m)}e}$ the power transfered to the electrons by one slowed down $D^{(m)}$ ion or atom.

It can be shown that the leading terms are, at the lhs, the heat flux term $\vec{\nabla}.\vec{q}_e$ and, at the rhs, the e-i, e-n collision heat exchange terms and the energy transfer terms from $D^{(m)}$ to electrons. For the latter one has

$$P_{D^\circ} = m_D \nu_{D^\circ e} v_o^2$$

$$P_{D^\pm} = m_D \vec{v}_o . \vec{F}_{D^\pm e}(\vec{v}_o) + \frac{1}{2} m_D \, Tr \, \vec{\vec{D}}_{D^\pm e}(\vec{v}_o)$$

where $\vec{F}_{D^\pm e}(\vec{v}_o)$ and $\vec{\vec{D}}_{D^\pm e}(\vec{v}_o)$ are the $D^\pm$ - electron friction and diffusion FOKKER-PLANCK coefficients respectively. In its turn $\vec{F}_{D^\pm e}$ is a sum

$$\vec{F}_{D^\pm e}(\vec{v}_o) = - \frac{e}{m_D} \vec{E}_{ind} - \frac{1}{2} \frac{\partial}{\partial \vec{v}_o} . Tr \, \vec{\vec{D}}_{D^\pm e}(\vec{v}_o)$$

of a polarization term $- (e/m_D) \vec{E}_{ind}$ (where $\vec{E}_{ind}$ is the induced polarization field) and of a fluctuation term.

VI. Results when the Cs^+ axial diffusion is neglected (cell case)

For $\vec{v}_i(r,z) = v_{ir}(r,z) \vec{u}_r + v_{i\theta}(r,z) \vec{u}_\theta$,

the Cs^+ continuity and motion equations come down to

$$\frac{1}{r} \frac{\partial}{\partial r} (r n_i v_{ir}) = S_i[n_{D^+}, n_{D^\circ}, n_{D^-}, n_n, n_i, n_e]$$

$$n_i v_{ir} = \mu_{i\perp} E_r - D_{i\perp} \frac{\partial n_i}{\partial r}$$

Outside the beam, the source term S_i may be neglected : the characteristic time of diffusion to the wall is much smaller than any inelastic collision time.

As boundary condition, the usual $n_i(R) = 0$ is used where R is the radius of a cylindrical wall coaxial with the beam. After integration between R and R, $v_{ir}(R,z)$ is obtained as a function of R, R, T_i, $\nu_{in}(z)$, ω_{ci}.

In view of the beam homogeneity assumption, the Cs^+ ion continuity equation, as integrated between 0 and R, gives

$$\frac{2}{R} n_i(z) \, v_{ir}(R,z) = S_i[n_{D^+}(z), n_{D^\circ}(z), n_{D^-}(z), n_n(z), n_i(z), n_e(z)] \qquad (10)$$

(10), (9) and the 3 deuterium species continuity equations (5), yield the 3 deuterium densities n_{D^+}, n_{D°, n_{D^-} and the secondary plasma density $n = n_i \approx n_e$ as a function of z, for a given impinging D^+ beam density n_{D^+in}.

Fig. 6 shows a sample result (Appendix).

Fig. 7 emphasizes the drastic influence of T_e on the D^- efficiency

$\eta = |I_{D^-out}| / I_{D^+in}$.

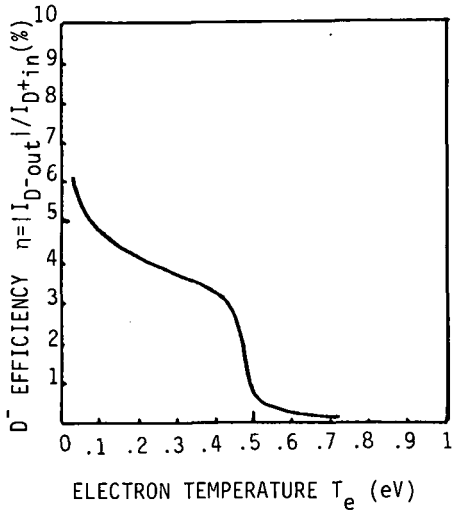

Fig. 7. D^- efficiency : $\eta = |I_{D^-out}| / I_{D^+in}$. as a function of the electron temperature T_e.

VII. Cs^+ axial diffusion taken into account (cell case)

Between beam and wall, the Cs^+ diffusion is assumed to be still purely transverse (1 D 1/2 approximation). The Cs^+ continuity equation can be written as :

$$\frac{d}{dz}(n_i v_{iz}) = S_i[n_{D^+}, n_{D^\circ}, n_{D^-}, n_n, n_i, n_e] - \frac{2}{R} n_i v_{ir}(R) \qquad (11)$$

where $v_{ir}(R)$ has been previously calculated (cf. 5) as a function of R, R, T_i, T_e, $\nu_{in}(z)$ and ω_{ci}. From the system (11), (5), (9), n_{D^+}, n_{D°, n_{D^-}, $n_i = n_{Cs^+} \approx n_e$ and $v_{iz} = v_{Cs^+z}$, the axial Cs^+ fluid velocity, are deduced as a function of z.

Fig. 8 shows a sample result (Appendix).

VIII. Preliminary results concerning the Cs jet case. Comparison with the cell

As neutralizing target, alkaline cells such as those considered in the previous theoretical treatment, were tested, in particular at LLL. Another type of neutralizing target consists in a cesium jet perpendicular to the deuterium beam (Fig.9). Such a jet is at the heart of the

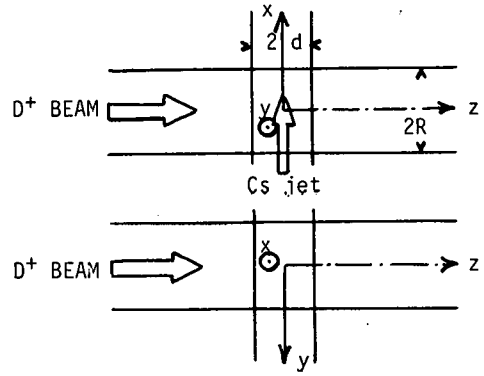

Fig. 9. Cs jet as neutralizing target.

APOCALYPSE double charge exchange source recently put into service at the GRENOBLE-CEA-SIG Laboratory.[1] In the latter an axial (z) confining magnetic field B = 4 000 gauss is added.

In the corresponding theoretical model the cylindrical symetry $\partial/\partial\theta = 0$ is broken. For a monokinetic cesium jet

$$\vec{v}_n(x,y,z) = v_j \vec{u}_x,$$

with a gaussian profile

$$n_n(x, y, z) = n_{no} \exp(-z^2/\ell^2),$$

preliminary calculations, where the Cs^+ axial diffusion is neglected, give, for the densities of the three deuterium species and of the secondary plasma, z,x variations of the type shown in Fig. 10, 11, 12 (Appendix).

Conclusion

With the express reserves due to the insufficient knowledge of several inelastic collision cross sections, these findings seem to condemn the cell*double-charge exchange method, even in a presence of an axial magnetic field.

On the other hand, if the preliminary results obtained in the jet case, with rather crude approximations, are confirmed by a superior model, radical improvement in the D^- efficiency could be obtained when the secondary plasma is jet blown.

*This conclusion is restricted to the collision dominated Cs^+ motion regime to which the present model applies, i.e. for sufficiently dense Cs cell: $n_{no} \gtrsim 10^{14}$ cm^{-3}; and hence for intense D^+ beam to be transformed: $J_{D^+_{in}} \gtrsim$ 10 mA.cm^{-2} at $\sim$ 1 keV.

Acknowledgement

A part of the programming and numerical computations is due to Dr. F. ZADWORNY. The author wishes to thank him for this helpful assistance. Discussions with the APOCALYPSE team members and in particular with Dr. GELLER and Dr. JACQUOT are gratefully acknowledged.

References

1. C. Jacquot, M.Delaunay, R. Geller, P. Ludwig, F. Mahzari, J.C.Rocco, P. Sermet, F. Zadworny, These Proceedings.
2. E.B. Hooper Jr., J.O. Anderson, P.A. Willman, Phys. Fluids 22, 2334 (1979).
3. A.T. Holmes, Phys.Rev. A,19, 389 (1979)

Appendix

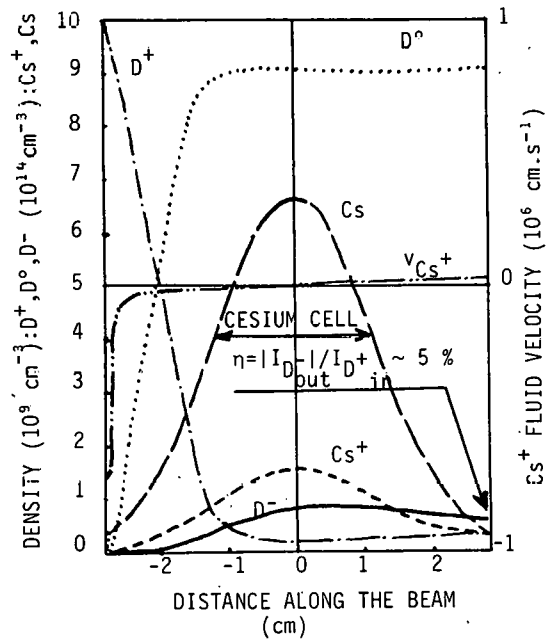

Fig. 8. Cs^+ axial diffusion taken into account. n_{D^+}, $n_{D°}$, n_{D^-}, and $n = n_{Cs^+} \approx n_e$ versus z, distance along the beam. D^+ energy : 1 keV, $n_{D^+_{in}} = 10^{10}$cm^{-3} ($J_{D^+_{in}} \approx$ 50 mA/cm^2); R = 2.25 cm, $\mathcal{R}$ = 5 cm ; ℓ = 1.17 cm.

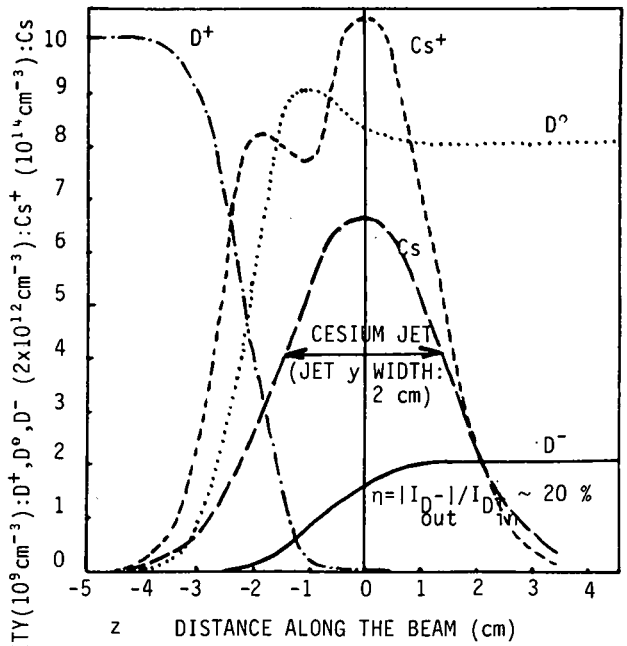

Fig. 10. As a comparison : a sample result for the jet case, with the same Cs density axial profile and T_e as in Fig.6. Jet y width : 2 cm, cesium jet fluid velocity : $v_j = 230$ m.s^{-1}.

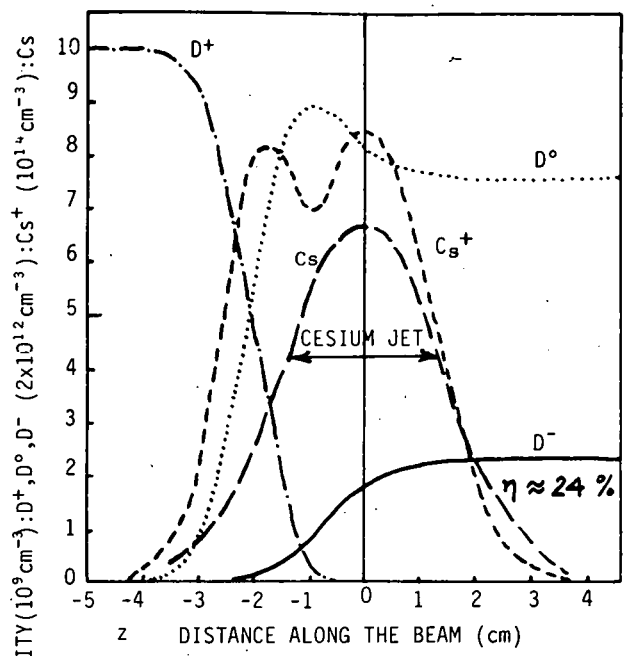

Fig. 11. Jet case : same parameters as in Fig.10, but with a cesium jet fluid velocity $v_j = 520$ m.s^{-1}

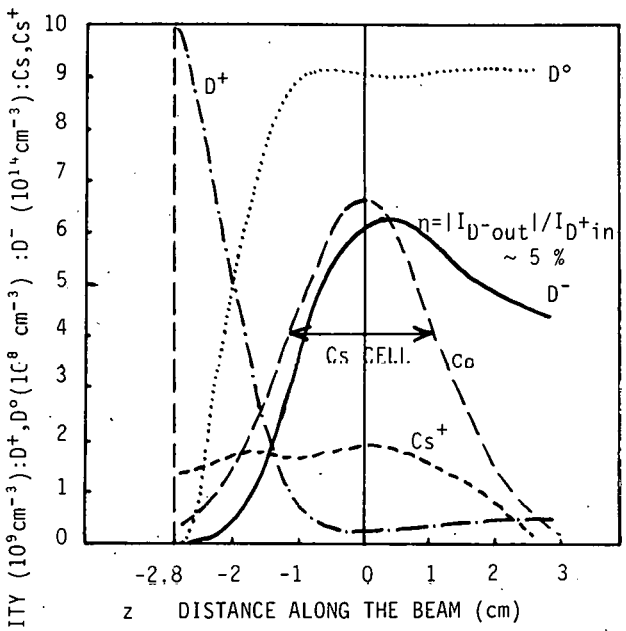

Fig. 6. Cs^+ axial diffusion neglected. n_{D^+}, n_{D°, n_{D^-}, and $n = n_{Cs^+} \approx n_e$ versus z, distance along the beam. D^+ energy : 1 keV, $n_{D^+in} = 10^{10}$cm^{-3} ($I_{D^+in} \approx 50$ mA/cm^2); R = 2.25 cm, R = 5 cm ; ℓ = 1.17 cm.

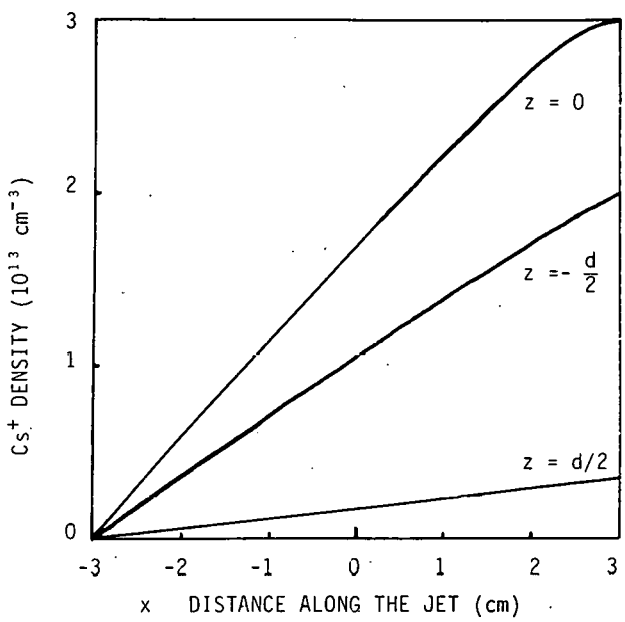

Fig. 12. Jet case. $n_{Cs^+}(x,z)$. R = 3 cm, d = 5 cm $v_j = 520$ m.s^{-1}

DISCUSSION

HOPMAN You gave so many processes in the equation, that I am curious now, what is the real physical mechanism that decreases the efficiency of the cesium cell?

DOLIQUE Cross section measurements, such as were presented by Schlachter, are relative to very low density incident beams. In that case, the secondary plasma effects probably are negligible. But for high density incidence D^+ beams, we have important secondary plasma effects with many destructive reactions between the Cs^+, the electron and deuterium species. Some D^- are destroyed by the secondary plasma.

CRANDALL The question is can you put your finger on what the dominant mechanisms were. There were so many included in the model that we might feel a little bit lost.

DOLIQUE I can not answer this particular point. There are many, many different processes.

HOOPER I just might say that in the studies that I have done the dominant destruction mechanism for the D^- is charge exchange between D^- and Cs^+. I am not completely certain that this is still true in the regime you studied, although I suspect it is. D^- charge exchanging with the Cs^+ has a very large cross section.

DOLIQUE It is one of the most important processes, sure.

HAGENA I think for practical purposes, one would not consider using a cesium cell for the beam apertures which are necessary for high intensity negative ion sources. Therefore, I think everyone has to use a cesium jet. As I understand it, most ion sources have not a D^+ beam incident into the jet, but a mixture of D^+ and D^0. This will change all your conservation laws, the current balance etc. What kind of an effect would it have, if you have no positive ions incident into your target but neutrals?

DOLIQUE The current balance would be modified.

HAGENA The secondary plasma would change. Is it good or bad?

DOLIQUE Probably good.

HAGENA That is good news.

GELLER It would be good, but if you have a majority of neutral particles which diverge before entering the cell you may lose those particles.

HAGENA Only if you have a divergent beam.

GELLER That is correct.

DOLIQUE In the experimental situation there is a magnetic field all along the beam, a widening magnetic field. It is possible that there is a large angular divergence for the D^0.

FORRESTER Does the magnetic field play a major role in the whole consideration?

DOLIQUE Sure, as in all transport systems.

FORRESTER Are your conclusions apt to be quite different if there is no magnetic field?

DOLIQUE Absolutely.

FORRESTER So one may better be able to approach the theoretical limit of 30 or 35% if there were no magnetic field than you can in the case of a magnetic field?... You do not know. Is it better to have a dense narrow jet or a broader jet which would cut down the space charge effect of the D^+? And, have you taken into account focusing of the D^- ions by D^+ ions which will make a trough for the D^-?

DOLIQUE In my opinion, the comparison would not have great meaning because in this theoretical model we neglect any angular dispersion. With a guiding magnetic field these assumptions are valid but without magnetic field we have an angular scattering and with a broad cell, angular scattering is not desirable.

FORRESTER Worries about angular scattering may not enter, because you are focusing (to some extent) those negative ions that are formed by the fact that you have a positive ion dominated space charge situation. The ions which are drifting out radially provide a through in which the negative ions are funneled to the acceleration region.

DOLIQUE Sure, the magnetic field has also an unfavorable effect on the beam as some electron and some Cs^+ ions are pulled towards the accelerator.. It is a problem to separate the species before you accelerate. But the overall effect is positive; that is the confinement of the beam from the positive ion source to the jet, and to avoid angular scattering for these ions.

BACAL I wanted to comment on the fact that we have built both systems jets and cells and I think that the discussion was relevant to a particular situation, relevant to an experiment in Grenoble. I would not support the statement made by Hagena that there is no chance for cells to be used. We know now that small beams will be accelerated like in the MEQALAC system and with the cell it may become a very good and easy solution for producing negative ions. I think that a further analysis should be made in conditions relevant to other systems. We should not transfer the conclusion (which is relevant to the Grenoble system) to any cell in any circumstances. I think the cell technology is well known, reliable, used in most laboratories and in some accelerators and we should continue using them when it is suitable.

DOLIQUE The comment of Mrs. Bacal is a very good comment, because in fact the conclusion that seems to condemn the cell system is relative to the high

density in the cell (we consider the cell with a peak density of 10^{15}) and probably for lower peak density in the cell, D^- conversion efficiency would have a much better value. It is a limited conclusion for high density cells.

HAGENA I agree completely with you about the prospective merit of gas cells and gas jets. One is for small apertures and the other one is for these apertures. For these big apertures, used for example in Livermore, nobody would consider using a gas cell for obvious reasons.

HAMILTON I disagree with that statement. I am from Livermore and we are planning big gas deuterium cells. Not for negative ion production, but for large diameter beams we use large diameter gas cells.

HAGENA I was talking about cesium gas cells, where the flux of cesium in the beam direction is undesirable.

JAQUOT My comment on the supersonic cesium cell is that for low energy positive ions in the magnetic field it seems to be better to use a very narrow and dense cesium cell. I will explain that on Thursday morning.

EHLERS Does this also say that we should use a jet for the double charge exchange but a gas cell for the stripper?

CRANDALL I think you should use a laser for the stripper.

MEASUREMENT OF H^- and D^- DENSITY IN PLASMA BY PHOTODETACHMENT

G. W. Hamilton*, M. Bacal, A. M. Bruneteau,
H. J. Doucet and M. Nachman+
Laboratoire de Physique des Milieux Ionisés
Groupe de Recherche n°29 du Centre
National de la Recherche Scientifique
Ecole Polytechnique
91128 Palaiseau Cedex, France

Abstract

A technique for measuring the density of H^- and D^- ions in a plasma by photodetachment is described. Photodetachment is detected by the increase in electron density with no change in positive ion density after a light pulse from a ruby laser. The authenticity of photodetachment signals can be assured by their comparison with known cross sections for photodetachment of H^-, and by mass analysis of extracted ions. The choice of photon energy, laser pulse energy and laser beam diameter will be discussed.

Introduction

Previous work at Ecole Polytechnique has shown that the H^- density in a hydrogen plasma is about 100 times larger than the density computed from the cross sections then known for H^- production and loss.[1] However these results were questioned because of the method for measuring H^- density by Langmuir probes. The purpose of the present work is to confirm by an alternative method the existence of large densities of H^- ions in hydrogen plasmas and to extend the measurement to a deuterium plasma and to higher density plasmas where probe measurements are not possible. This subject is of interest because of the need for sources of D^- ions for neutral injection into controlled fusion devices.

Photodetachment, i.e. the stripping of negative ions by photons, has previously been used to measure negative ion densities in oxygen plasmas.[2] We applied this technique to the measurement of H^- density in plasmas[3], since it has several advantages over the alternatives. The interpretation of photodetachment signals can be verified by comparison with known cross-sections and by mass-analysis of extracted ions.

Photodetachment in a plasma produces an increase in electron density n_e, equal to the reduction of the negative ion density, without an immediate increase in the positive ion density n_+.

If the light flux is sufficient to destroy all the negative ions present in the illuminated plasma column then the change in electron density is equal to the initial negative ion density.

$$n_{-0} = \Delta n_e \qquad (1)$$

The change in electron density can be determined by probes or microwaves, depending upon the geometry and plasma density. Thus, the measurement of the negative ion density is reduced to a measurement of electron density, which is effected using a cylindrical probe, coaxial with the laser beam.

The fraction of the plasma negative ions destroyed by the light pulse (which we will call the photodetachment fraction) can be presented as a function of laser energy per unit area, with the cross section for photodetachment and the photon energy as parameters.

$$\frac{\Delta n_-}{n_-} = 1-\exp\left[-\frac{\sigma}{h\nu} \times \frac{\text{laser pulse energy}}{\text{area}}\right] \qquad (2)$$

This relation is fundamental, since it guides the choice of the photon and laser energies.

Choice of Photon Energy

The photon energy should be higher than the electron affinity of H (0.75 eV) to detach the electron from H^-. We used the light pulse from a ruby laser which has a photon energy of 1.8 eV. At this photon energy the photodetachment cross section is near its maximum (4×10^{-17} cm^2).

Although most single-photon interactions are excluded by the low photon energy, photodetachment of certain other negative ions (OH^-, O^- or O_2^-) is possible with cross sections one or two orders of magnitude smaller than the photodetachment cross-sections of H^- or D^-. To eliminate these possibilities from consideration we have magnetically analyzed the negative ions extracted from the plasma and also verified that our measurements agree with the theoretical photodetachment cross section for the photodetachment of H^-, but not with that for other ions (Fig. 1). This test should be repeated whenever the experimental conditions change.

The light from a neodymium glass laser (1.06 μm) seems more suitable than that of a ruby laser, since its photon has a lower energy

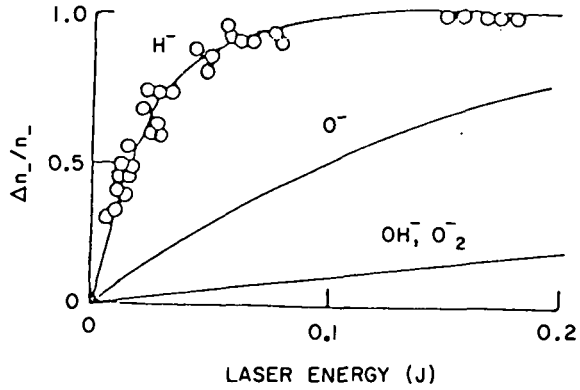

Fig. 1. Photodetachment of several negative-ion species by ruby laser light as a function of laser pulse energy, according to the theory of Eq. (2). Experimental data points are superimposed upon the theory of Eq. (2) for H^-, where $\sigma/h\nu$ = 139 cm^2/J and the area of the laser beam is 3 cm^2.

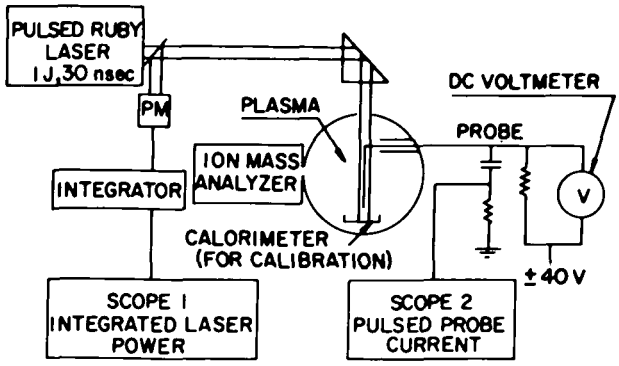

Fig. 2. Equipment diagram for measurement of H^- density by photodetachment.

(1.2 eV); the cross section for photodetachment at this photon energy has the same value as in the case of light from a ruby laser.

Choice of laser pulse energy

Figure 1 shows that for laser pulses above 0.1 J the photodetachment fraction is essentially unity and we can determine the relative density of H^- from the relative increase in n_e, i.e. from the relative increase in the probe electron current:

$$\frac{n_-}{n_e} = \frac{\Delta n_e}{n_e} = \frac{\Delta i^-}{i_{dc}^-} = \alpha \qquad (3)$$

The apparatus used for the photodetachment measurement consists of a ruby laser capable of delivering pulses of 1J energy and 30 ns duration, a probe circuit measuring the relative increase in n_e due to the laser pulse, and a calibrated light monitor measuring the energy of each pulse (Fig. 2). Various tests were applied to assure the authenticity of the photodetachment signals, such as operating the system with and without plasma, with and without an open window, with and without a trap cooled by LN_2.

Two types of cylindrical tungsten probes were used to measure the densities of electrons and ions. For absolute measurements of n_e and n_+ it is necessary to measure the complete probe characteristic and to analyze it either by the Langmuir theory (if the probe radius is less than 3 Debye distances) or by a theory for larger probes.[4] We used for absolute measurements a thin probe 5 x 10^{-2} mm dia.

On the other hand, for measurements of changes in n_e and n_+ it is sufficient to use large-area probes of which the radius may be more than the Debye distance. Measurements of pulsed relative changes in density may be made without measuring the complete current-voltage characteristic. We chose to work with a positive probe bias of 40 V. When the probe bias voltage was varied from +10 to +50 V we found that the probe currents were affected by no more than 20%.

Tungsten was selected for its high melting point and high work function, but other materials were also tested. Probes were cleaned by electron bombardment at 300 V before being used for data. The best probe geometry is such that the probe is coaxial with the laser beam and the probe area within the primary laser beam is larger than the probe area outside the laser beam (Fig. 3). For measurements of relative densities (not using the Langmuir theory) it was convenient to increase the probe diameter to 0.5 mm so the probe would be self-supporting and so the pulsed probe currents would be easier to measure.

A typical oscilloscope trace showing the pulsed probe current is presented in Fig. 4.

Choice of Laser Beam Diameter

The relative negative ion density n_-/n_e is obtained by comparing the amplitude of the transient current pulse (Δi^-), following the laser pulse, with the current drawn from the plasma by the positively biased probe under stationary conditions (i_{dc}^-) (Eq. 3). Therefore it is important to illuminate the entire region around the probe, from where the electrons are collected. The diameter of the cylindrical region around the probe where from

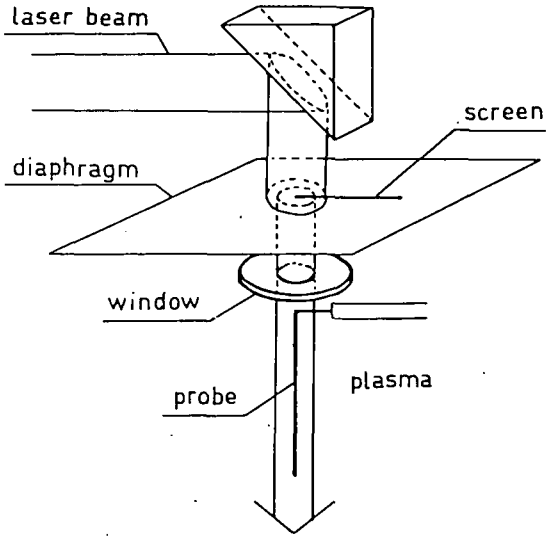

Figure 3. Details of the equipment used in photodetachment measurements: a cylindrical screen (1 mm dia) is preventing the laser light from hitting the probe surface. A diaphragm is limiting the laser beam diameter.

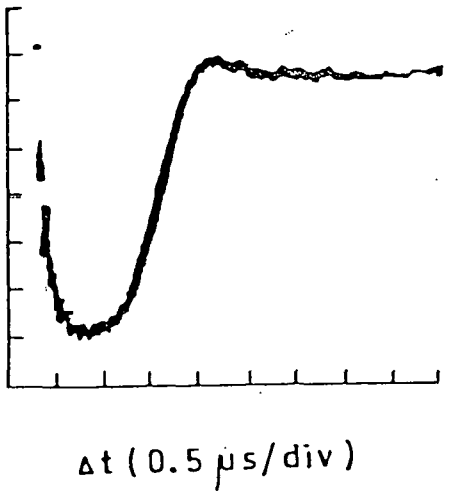

Figure 4. Oscilliscope trace of photodetachment signal.

the probe collects electrons has been determined experimentally;[5] for the conditions of the present experiment (probe voltage + 40 V, n_e in the range 10^9 to 10^{10} cm^{-3}) this diameter is not greater than 9 mm.

Taking into account Eq. 3 and the neutrality of the plasma,

$$n_- + n_e = n_+ \qquad (4)$$

the negative ion and electron densities can be easily obtained from the measured values of α and n_+:

$$n_e = \frac{n_+}{1 + \alpha} \qquad (5)$$

and

$$n_- = \frac{\alpha\, n_+}{1 + \alpha} \qquad (6)$$

A difficulty occurred when studying the dependence on laser energy of the photodetachment signals: we found some large spurious signals at higher laser energies. This "noise" interfered with the measurements, especially at lower n_e, and imposed an upper limit upon the laser energy to be used for stripping the negative ions. We observed that these large spurious signals were correlated with the high laser power density (2 to 10 MW/cm^2); therefore a laser giving longer pulses with the same energy could have been more suitable. We found that these spurious signals are due to the interaction of the laser light with the probe surface and with surfaces at the plasma boundary, when they are close to the probe.

The interaction of the laser light with the probe surface could be avoided by inserting a small screen (1 mm wide) between the laser and the probe (Fig. 3).

Simultaneous measurements of n_- were carried out by photodetachment, mass spectrometry and thin Langmuir probes. The variation of the H^- current through the mass filter with electron density is very similar with the n_- vs n_e dependence measured by photodetachment. This similarity indicates that the amplitude of the photodetachment signals is indeed proportional to the density of H^- ions in the plasma. The measurement of n_- using a thin Langmuir probe indicates higher n_- values than photodetachment, especially at low n_e.

Several reasons have been mentioned which could lead to an over-estimate of n_- in the measurement by thin Langmuir probes: secondary electron emission due to ion or metastable atom bombardment, presence of fast electrons, unprecise knowledge of plasma potential, oversimplified probe theory. It is not clear, however, if any of these effects can explain the large discrepancy at low electron density.

Since the experiments and the calculations have shown that with a laser beam diameter of 9

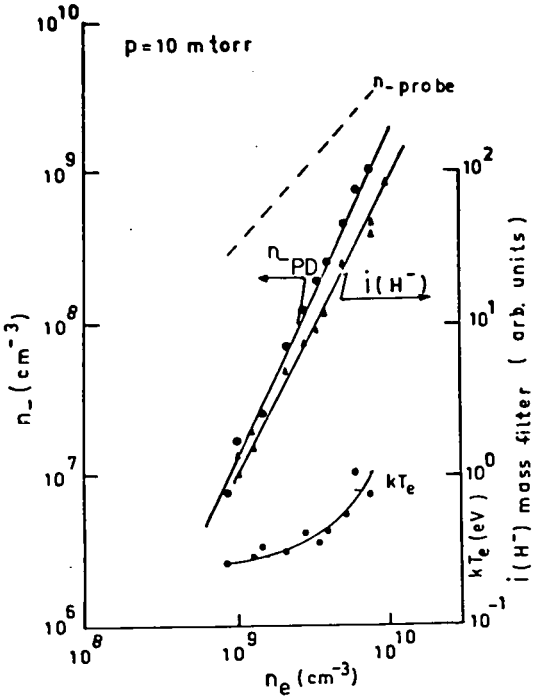

Figure 5. Comparison of n_- measured by photodetachment (probe biased at V_p = + 40 V, laser beam diameter 9 mm) and by thin Langmuir probe, with the current of H^- ions through a 60° magnetic sector mass filter. The variation of the electron temperature is also shown.

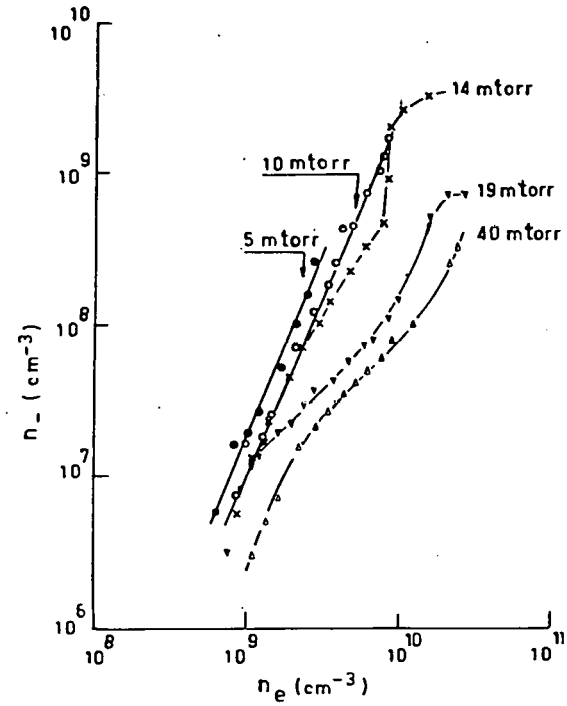

Figure 6. Effect of gas pressure upon the n_- vs n_e dependence, as measured by photodetachment. Probe biased at V_p = +40 V.

mm, as used in the present experiments, allthe photodetached electrons should be collected by the probe even at the lowest n_e studied, and since the results obtained by photodetach- ment are confirmed by mass spectrometery, we conclude that photodetachment gives the correct measurement of n_-, while measurements by thin Langmuir probes give an overestimate of n_- which is particularly important at low plasma density (10^9 cm^{-3})but which is reduced to a factor of 2 only for $n_e > 10^{10}$ cm^{-3}.

Though the thin Langmuir probe measurements give a distorted shape for the n_- vs n_e dependence, they still reflect some important changes of these dependences, due to change in neutral density, as it can be inferred from a comparison of Figures 6 (photodetachment) and 7 (thin Langmuir probes).

The measurements by the photodetachment technique were reproducible and independent of the probe diameter, showing n_- increasing in

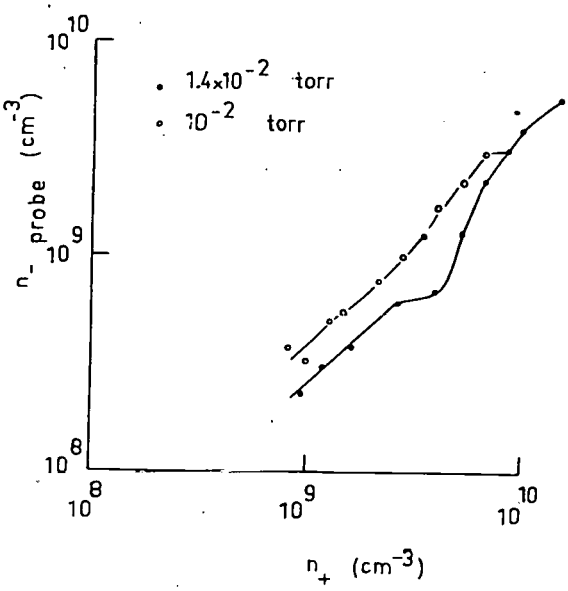

Figure 7. Effect of gas pressure upon the n_- vs n_e dependence, as measured by thin Langmuir probes.

proportion to n_e^3 in the range of n_e between 10^9 and 10^{10} cm^{-3}, when the pressure is below 10^{-2} Torr. The results for deuterium indicate no isotope dependence.

References

* Permanent address: Lawrence Livermore National Laboratory, Livermore, CA. 94550.

\+ Permanent address: Ecole Polytechnique, University of Montreal, Montreal, Canada.

1. M. Bacal, E. Nicolopoulou and H. J. Doucet, Proc. of the Symposium on the Production and Neutralization of Negative Hydrogen Ions and Beams, September 26-30, 1977, Brookhaven National Laboratory, BNL-50727 p. 26.

2. J. Taillet, Compt. Rend., Paris, 269, série B, 52 (1969).

3. M. Bacal, G. W. Hamilton, A. M. Bruneteau, H. J. Doucet and J. Taillet, Rev. Sci. Instrum., 50, 719 (1979).

4. L. S. Hall and R. P. Fries, Proc. 7th Intl. Conf. Phenomena in Ionized Gases, Beograd (Gradevinska Knjiga, Beograd, 1965), Vol. III, p. 15.

5. M. Bacal, A. M. Bruneteau and M. Nachman, submitted for publication to J. Phys. Lettres, Paris.

DISCUSSION

LEUNG Are the results sensitive to the bias voltage on the probe?

HAMILTON Yes, they are. I should say that the relative results are not sensitive, that is one of the tests we had to make. The bias voltage for everything I mentioned is +40 volts, but we have operated with other bias voltages and we chose 40 volts because that is in a range where the ratio is not affected by the probe voltage.

LEUNG What happens when you change the gas from hydrogen to say helium or argon?

HAMILTON I do not think we did that. In any case we have so much absorbed gas on the surfaces that we could not make that change easily. When we did change from hydrogen to deuterium we found photo-detachment due to both H and D. To my knowledge we never operated with helium or argon. Now we did do some tests to make sure we were looking at H^- and not at other types of negative ions, such as O^- and O_2^-, and I have already told you one of the tests we have made by the exponential curve and also by comparing our photo-detachment measurements with the mass analysis.

LEUNG What happens when you go up to high density and the probe becomes emissive? Would that change your results, because at the same time when you go up to 10^{12} you emit electrons from the probe?

HAMILTON Yes, we did not get that high. At 10^{11} we do not have that problem. One remedy is to pulse the probe bias voltage. It is not necessary to leave this 40 V bias voltage on continuously and the electron bombardment, of course, would depend upon that.

BACAL I wanted to answer Leung's questions about other gases. We have had a very difficult test. It is very important when you work with hydrogen plasmas and look for negative ions to use liquid nitrogen traps. We used liquid nitrogen in the experiment and whenever we did not have the liquid nitrogen we had only few negative ions and there was no photo-detachment. Only when we filled the liquid nitrogen trap we did have negative hydrogen ions indicated by the mass spectrometer and also by photo-detachment. We thought this experiment is very significant and we do not have to go to other gases like argon.

H^- AND D^- PRODUCTION IN PLASMA

M. Bacal, A. M. Bruneteau, H. J. Doucet, W. G. Graham* and G. W. Hamilton+

Laboratoire de Physique des Milieux Ionises
Groupe de Recherche n°29 du Centre
National de la Recherche Scientifique
Ecole Polytechnique
91128 Palaiseau Cedex, France

Abstract

The density of negative ions in a low pressure hydrogen plasma has been investigated as a function of neutral gas pressure, plasma density and electron temperature, using the photodetachment technique. A new multifilament, metal wall device was used to extend the plasma density range up to 10^{11} cm^{-3}. The transition to the regime where ion-ion recombination dominates negative ion loss has been observed at $n_e \sim 2x10^{10}$ cm^{-3}. Measurements by coherent anti-Stokes Raman scattering (CARS) and calculations of the vibrational population distribution will be discussed. The comparison of the experimental data with theoretical results derived from computed reaction rates, seems to indicate that hydrogen negative ion production occurs, mainly, through the process of electron attachment on vibrationally excited hydrogen molecules.

Introduction

In the previous paper[1] a photodetachment technique for reliable measurement of H^- and D^- densities in a hydrogen plasma has been described. This technique has established that negative hydrogen ions are present in sizeable fractions ($n_-/n_e \leq 0.35$) in a low pressure, low density plasma.[2-4]

The purpose of the present paper is to
1) review the progress made in understanding the processes leading to H^- production in such plasmas;
2) describe work in progress to attain the higher negative ion densities required for a useful neutral beam injection ion source.

H^- and D^- Production in a low density plasma

Basic Processes

We define our low density plasma as one with a gas density of more than 10^{14} cm^{-3} and plasma densities in the range 10^9 - 10^{10} cm^{-3}.

After consideration of various possible processes, it has become apparent that the collision mechanisms most likely to lead to H^- production in plasmas are[2]:

$$e + H_3^+ \rightarrow H^- + H_2^+ \quad (1)$$

$$e + H_2(3\pi_u) \rightarrow H^- + H \quad (2)$$

$$e + H_2(v^*) \rightarrow H^- + H \quad (3)$$

where $H_2(v^*)$ represents a hydrogen molecule in an excited vibrational state.

From recent cross section measurements[5,6] and theoretical calculations[7,8,9], it appears that process (3) might be the one responsible for the large fractions of H^- found in these plasmas.[10,11] Consequently, attention has been focussed on assessing the density of $H_2(v^*)$ in the plasma.

Hiskes et al[10] evaluated the equilibrium density of $H_2(v^*)$ using the reaction rates for a number of processes and found

$$H_2^+(v^*) + H_2(v=0) \rightarrow H_2(v^*) + H_2(v^*) \quad (4)$$

$$H_2^+(v^*) + e(wall) \rightarrow H_2(v^*) \quad (5)$$

to be dominant amongst those they considered.

The main $H_2(v^*)$ loss process is de-excitation in wall collisions. Hiskes et al[10] concluded that, to account for the H^- densities which had been measured experimentally, the $H_2(v^*)$ would be required to survive a number of the order of 50 collisions with the wall of the containing vessel.

Bacal et al[12] considered several other possible mechanisms which they thought might be important for $H_2(v^*)$ production.

E-V singlet excitation: The vibrational excitation of the ground state hydrogen molecule can occur by radiative decays from higher singlet electronic states excited by collisions with energetic electrons[13,14]:

$$e + H_2[X^1\Sigma_g^+ (v=0)] \rightarrow$$

$$H_2 (B^1\Sigma_u^+, C^1\pi_u.., v') + e$$

$$\rightarrow h\nu + H_2[X^1\Sigma_g^+ (v'')] + e \qquad (6)$$

The cross section for reaction (6) has been calculated by Hiskes[15] who found that the effective cross section for excitation into the upper ten vibrational levels ($5 \leq v \leq 14$) is approximately 3×10^{-17} cm^2 at 100 eV.

$H_3^+(v^*)$ processes: it is known that H_3^+, by far the dominant ion species in these plasmas[4], is formed through the reaction

$$H_2^+ + H_2 \rightarrow H_3^+ + H \qquad (7)$$

It has also been found that a substantial fraction of the H_3^+ so formed has an internal energy in excess of 2 eV[16,17]. This energy can be transferred to H_2 by wall collisions (Eq. 8) and proton transfer (Eq. 9)

$$H_3^+(v^*) + e(\text{wall}) \rightarrow H_2(v^*) + H \qquad (8)$$

$$H_3^+(v^*) + H_2(v=0) \rightarrow H_2(v^*) + H_3^+ \qquad (9)$$

Taking into account the additional processes (6), (8) and (9), the dependence of the negative hydrogen ion density on gas pressure, electron temperature and plasma density can be obtained from the equilibrium rate equations for the ionic and neutral components of the hydrogen plasma, in a manner similar to that described by Hiskes et al.[10]

A brief description of this analysis and a comparison with experimental results is presented below. A more detailed description can be found in Ref. 12.

Theoretical Model

The theoretical model developed to predict the negative ion density in the plasma assumes that dissociative electron attachment to highly vibrationally excited molecules (of density $n(v^*)$) is the dominant production process, while H^- loss is due to ion-ion recombination (rate $\overline{\sigma v}$ (ii) $= 2 \times 10^{-7}$ cm^3/sec) and wall diffusion (lifetime τ_d). Thus

$$n_- = \frac{n_e\, n(v^*)\, \overline{\sigma v}\ (DA)}{n_+\, \overline{\sigma v}(ii) + 1/\tau_d} \qquad (10)$$

E-V singlet excitation (Eq. 6) and H_3^+ processes (Eqs. 8 and 9) are considered for the production of highly vibrationally excited molecules.

It can be shown[12] that for these production processes, the density of vibrationally excited molecules is proportional to the plasma density (n_+):

$$n(v^*) = A\, n_+ \qquad (11)$$

Taking into account Eq. (11), the negative ion density is

$$n_- = \frac{A\, n_e n_+\, \sigma v\ (DA)}{n_+\, \sigma v(ii) + 1/\tau_d} \qquad (12)$$

A is proportional to the number, b, of wall collisions a vibrationally excited molecule can survive before de-excitation.

$$A = b\, \frac{v(3+)}{v^*} \left[\frac{\sigma(E,V)}{\sigma(2+)} + p(v^*)\right] \qquad (13)$$

Here $\sigma(E,V)$ is the cross section for E, V singlet excitation (Eq. 6); $\sigma(2+)$ is the cross section for ionization of H_2^+ in collisions with electrons. For 100 eV electrons, $\frac{\sigma(E,v)}{\sigma(2+)} = 0.326$

$p(v^*)$ is the percentage of H_3^+ population contributing to vibrational excitation of $v > 5$ by reactions (8) and (9).

The ratios $v(3+)/v^*$ of the velocities of the H_3^+ ions and $H_2(v^*)$ molecules is uncertain by a factor of three; it can have a range of values between 0.8 (assuming that the thermal energy of the ions and excited molecules is the same) and 2.5 (assuming that the ion temperature is higher than that of the neutrals). This leads to an uncertainty in the value of b, inferred from Eq. (13).

Several important observations can be made from Eq. 12. For the plasma conditions under consideration the negative ion density is

a) independent of the neutral gas density
b) dependent on the plasma density
c) dependent on the electron temperature

through the dependence of the reaction rate for dissociative attachment and possibly of the lifetime for diffusion.

Further study of Eq. 12 shows that for the low plasma densities in the present experiment the diffusion term should dominate over that for ion-ion recombination, leading to an n_e^2 to n_e^3 dependence for n_-. It is interesting to note that at higher plasma densities, when ion-ion recombination becomes more important, then n_- should increase linearly with n_e. This prediction is based

on the assumption that reactions between charged particles and neutral hydrogen molecules (such as Eq. 6, 8, or 9) are dominating in the formation of $H_2(v^*)$. However, at high plasma density, other reactions (e.g. dissociative recombination of H_3^+) can become important and lead to a stronger dependence of n_- on n_e.

It has been estimated[18] that at most 20% of the H_3^+ population has sufficuent internal energy to contribute to H_2 ($v \geq 6$) production through proton transfer or wall collisions. Therefore, the contribution of H_3^+ processes to $H_2(v^*)$ production through reactions 8 and 9 is estimated to be at most 60% of that due to E-V singlet excitation.

Experimental Results

The apparatus used for these measurements, previously described by Bacal et al[12], is a 15 l glass vessel with grounded end plates; it contains an electron gun, consisting of a negatively biased hot filament and a grounded grid. A plasma is created when the hydrogen pressure, exceeds 5 mTorr. Two types of probes were used to measure the ion and electron densities. A thin Langmuir probe (5×10^{-3} cm dia) was used for measuring the positive ion density (n_+) and the electron temperature. A thick probe was used for measuring n_-/n_e by the photodetachment technique.[1]

At pressures below 10 mTorr, the negative ion density was found to have between an n_e^2 and n_e^3 dependence. Figure 1 illustrates the n_e^3 dependence in plasmas produced in hydrogen and deuterium at the same gas pressure. The observed n_e^3 dependence indicates that the plasma is in a regime controlled by diffusion loss of negative ions, in agreement with the prediction of the theoretical model.

Figure 1 also indicates that the negative ion density is not isotope dependent, i.e. the negative ion density does not depend whether hydrogen or deuterium is used. The absence of an isotope dependence supports the idea that the production of H^- is due to dissociative attachment to highly vibrationally excited molecules ($v > 6$ for hydrogen, or $v > 8$ for deuterium) for which the theoretical calculations indicate no isotope effect.[9]

The effect of gas pressure has been examined under the following conditions: constant filament current (Fig. 2), or constant plasma density, maintained by varying the filament thermionic emission (Fig. 3). In both cases, a sudden decrease in n_- is observed when the pressure is about 10 mTorr. However, the electron temperature also decreases when the gas pressure is increased and it seems possible that the mentioned decrease of n_- is due to the variation of the electron temperature.

We succeeded in increasing the electron temperature at constant pressure and plasma density by reducing the discharge voltage and simultaneoulsy increasing the filament thermionic emission. Again, the negative ion density goes down with the electron temperature, but now the pressure is constant.

Using this method we obtained the dependence of n_- upon the electron temperature, for two values of the plasma density (Fig. 4). Note that for given plasma density and electron temperature, n_- is pressure independent.

While it first appears that the H^- density strongly depends on the neutral density, our experiment indicates that this variation of n_- is the result of the pressure dependence of the electron temperature, which, with the plasma density, dominates the variation of n_-. In other words, the negative ion density is found to be independent of the neutral gas density, but dependent upon the plasma density and electron temperature as predicted by the theoretical model.

Comparison of the theoretical model with the experimental data.

In order to further test the validity of the model outlined above, it is useful to present the experimental data in a form compatible with Eq. 12. According to Eq. 12 we have:

$$\frac{n_-}{n_e n_+}\left[n_+ \,\overline{\sigma v}(ii) + 1/\tau_d\right] = A\,\overline{\sigma v}(DA) \qquad (14)$$

The variation with electron temperature of the expression of the left-hand-side of Eq. 14, calculated using experimentally obtained values for n_-/n_e and n_+, can be compared to the theoretically derived variation of $\overline{\sigma v}(DA)$ since A should not depend on electron temperature.

Fig. 5 shows the data of Fig. 4 normalized according to Eq. 14. n_+ has been measured separately with the thin probe. The value $\tau_d = 10^{-3}$ s estimated in Ref. 4 was used. The most significant feature in this figure is that this normalization brings close to a single curve all the data shown in fig. 4, although these data correspond to different plasma densities and pressures.

Figure 5 also shows that the experimentally obtained temperature dependence is similar to that of the theoretical rate for dissociative attachment, for $v = 8$. In fact, a wide range of vibrational levels is to be expected, however, the general shape of the reaction rate

or a summation of these vibrational levels ould not be dissimilar to those for the ndividual state represented here.

In order to fit the experimental data ualitatively to the theoretical rate for v=8, i value of A ~ 5 must be assumed. This indicates that, if E-V singlet excitation (Eq. 6) only is considered in calculating A, then the $H_2(v^*)$ molecules would be required to survive between six and nineteen wall bounces lepending on the value assumed for $v(3+)/v^*$. Considering the contribution to A of the H_3^+ processes [Eqs. (8) and (9)] would reduce by 30% the required number of wall bounces.

It is interesting to note that the wall deactivation coefficient, measured for vibrationally excited hydrogen molecules with v = 1 on quartz by J. Villermaux (see Table I in Ref. 21) is 5.1×10^{-4}.

The Vibrational Population Distribution in Low Pressure Hydrogen Plasma

The solution of the problem of negative ion formation in hydrogen plasma requires the knowledge of the populations of H_2 molecules on different vibrationally excited levels. Recently, coherent anti-Stokes Raman scattering (CARS) has been used[20] to measure the populations of vibrational states v = 0, 1 and 2 in a hydrogen plasma produced in a magnetic multipole at a pressure of ~ 0.1 Torr. CARS is a non-obtrusive method, using the non linear interaction of two laser beams with the gas sample; it measures concentrations, rotational temperatures and vibrational populations.

The plasma conditions were optimized for obtaining the maximum anti-Stokes signal for v = 1. They were as follows:

Gas density:	2×10^{15} cm^{-3}
Electron temperature:	0.4 eV
Electron Density:	2×10^{11} cm^{-3}
Gas temperature:	475 ± 10°K

In addition to the measurement of gas temperature, CARS has provided the relative populations for v = 1 and v = 2 levels:

$$\frac{n_0}{n_1} = \frac{H_2(v=0)}{H_2(v=1)} = 41$$

$$\frac{n_0}{n_2} = \frac{H_2(v=0)}{H_2(v=2)} = 418$$

Hiskes[22] has analyzed the CARS data for the lower vibrational levels. The equilibrium solutions for the rate equations were used with the above data, to determine b, which is in the range seven to fourteen. Note that this value of b is relevant to the lowest vibrational levels, v = 1,2.

An insight to the b values for the higher vibrational states, which are relevant to the negative-ion hydrogen discharge experiment, can be obtained from the analysis of the parameters of this experiment:[4,10]

$n_0 = 4 \times 10^{14}$ cm^{-3}
$n_e = 2 \times 10^{10}$ cm^{-3}
$n_- = 4 \times 10^{9}$ cm^{-3}
$n_+ = 2.4 \times 10^{10}$ cm^{-3}
$n^f(e) = 3 \times 10^{7}$ cm^{-3}
$E^f = 100$ eV
$T_g = 500$°K

An effective value $n_{eff}(v^*) = 1.5 \times 10^{11}$ cm^3/s can be estimated from Eq. (10) using the mentioned above parameters (with a maximum value for $\overline{\sigma v}(DA) = 8 \times 10^{-9}$ cm^3/s, with $\overline{\sigma v}(ii) = 2 \times 10^{-7}$ cm^3/s and $\tau_d \approx 10^{-3}$s). The average population of each of the ten levels ($5 \leq v \leq 14$) is thus 1.5×10^{10} cm^{-3}, or an average population of about 4×10^{-5} relative to v = 0.

Hiskes[22] has calculated the distribution of relative vibrational populations in the negative-ion hydrogen-discharge experiment. In order to fit the average relative population, found in this experiment, to the calculation of Hiskes[22], a value for b between 9 and 18 has to be assumed, which is within the range of uncertainty of b found from the analysis of Fig. 5.

High Plasma Density Operation

In order to increase the negative ion density it is necessary to go to higher plasma densities since a linear dependence with n_e is expected. The previous apparatus was limited by the glass walls with no water cooling and the single filament electron source. Accordingly a plasma device able to produce and operate at higher plasma densities has been constructed. This device can also be operated as a multipole, which should further increase the plasma density by electron confinement. Whether this is a desirable feature for negative ion confinement must be determined.

Experimental Apparatus

The experimental apparatus (Fig. 6) consists of a cylindrical stainless steel vacuum vessel 23.6 cm high with a radius of 13.3 cm. The walls of the vessel (3 mm thick) could be water cooled and could accommodate 20 columns of magnets with an appropriate, radial, magnet configuration on the end plates. One end plate supported an assembly which could hold up to ten filaments; both tungsten and thoriated tungsten filaments have been used. The grounded walls of the vacuum vessel act as an anode and various negative potentials of up to 60 V could be applied to the filaments; this voltage determined the primary electron energy.

Facilities for pumping and pressure measurement were similar to those in the previous apparatus[1-4] with a cold trap in direct contact with the plasma to prevent water vapor contamination. Plasma diagnostics consisted of the thick probe for photodetachment measurements and a plane probe for measurement of electron density, electron temperature and plasma potential.

Diffusion Type Plasma in Metal Wall Device

Measurements were made with the metal wall system operating without magnets, with 10 filaments made of thoriated tungsten (0.4 mm dia, 10 cm long). The variation of n_- with n_e was studied at various pressures in the range 3-10 mTorr (Fig. 7). The multifilament operation meant that higher plasma density (up to 10^{11} cm^{-3}) could be achieved. The corresponding variation of electron temperature and plasma potential is also plotted on Fig. 7.

An important new feature in the n_- dependence upon n_e is the sudden change in slope which occurs at an electron density of about 2×10^{10} cm^{-3}: at electron densities below 2×10^{10} cm^{-3}, n_- varies as n_e^3 or n_e^2 (depending on the pressure and on the behavior of the electron temperature). At electron densities above 2×10^{10} cm^{-3}, n_- varies linearly with n_e.

This change in slope is interpreted as the change from a regime dominated by diffusion loss of negative ions (below 2×10^{10} cm^{-3}) to a regime where negative ion loss is dominated by ion-ion recombination[4] (see Eq. 10).

In the low plasma density regime, where negative ion loss by diffusion dominates, the results obtained in the multifilament metal wall system are qualitatively similar to those obtained in the glass system.[4,12] However, the maximum relative density n_-/n_e observed in the metal wall system (12 %) is lower than that observed in the glass vessel (35%). In this regime, the negative ion density increases as n_e^2 to n_e^3, the n_e^2 dependence tending to become n_e^3 at the lowest gas densities (3 mTorr) where operation was possible (Fig. 7). It is interesting to note that the n_e^2 dependence is observed at 6 mTorr, when the electron temperature stays constant at about 1 eV over the whole range of n_e variation. The n_e^2 dependence is in agreement with Eq. 12, for the case when electron temperature, and consequently $\sigma v(DA)$ and τ_d, are constant. According to Fig. 5, the electron temperature of about 1 eV corresponds to the maximum effective rate for dissociative attachment.

The n_e^3 dependence, observed at 3 mTorr, corresponds to a situation where the electron temperature increases from 2.0 eV to 2.8 eV, when n_e is increased; in this range. we do not expect the rate for dissociative attachment to increase with electron temperature (Fig. 5). The n_e^3 dependence observed in these conditions may indicate the important contribution of τ_d as discussed in Ref. 4.

It is interesting to note that the plasma potential is always positive with respect to the metal wall and attains a value as high as +6.5 V at the lowest pressure, where, at given n_e, the negative ion density is the highest (Fig. 7). Increasing the gas pressure tends to reduce both the electron temperature and the plasma potential; at given n_e, the negative ion density also goes down when the pressure is increased in the mentioned range.

The plasma potential measured in the metal wall device is higher than that measured in the glass device. However the present measurement is more relaible since all the walls are metal.

Hybrid multipole plasma

Following the measurements without magnets, ten columns of magnets were installed on the cylindrical surface of the stainless steel vessel, to produce a hybrid multipole arrangement. No magnets were installed on the end plates. The hybrid multipole could be operated at lower pressure than the diffusion type plasma; therefore, we investigated first the dependence of the negative ion density on gas pressure in the range 0.4-8 mTorr. We found that the negative ion density attained a broad maximum at 1-3 mTorr.

We therefore compared the operation with and without magnets at a gas pressure of 3 mTorr (Fig. 8).

With ten magnet columns it was possible to extend the plasma density at the mentioned pressure from 10^{10} cm^{-3} to 10^{11} cm^{-3}, using the same filament power.

The hybrid multipole operation has the effect to reduce the electron temperature from about 2.5 eV to an apparently more desirable value of 1.3 eV. However, the plasma potential, which determines the negative ion confinement, is seen to drop from +6.5 to + 3 eV.

The negative ion density produced in the hybrid multipole is higher compared to that produced in the metal device without magnets.

In the low density regime (below 2×10^{10} cm^{-3}) n_- varies as $n_e^{1.15}$; a change in slope is observed at an electron density of 2×10^{10} cm^{-3} indicating the transition to the regime dominated by ion-ion neutralization. n_- varies then linearly with n_e, up to 7×10^{10}. A maximum n_- density

of 10^{10} cm^{-3} is obtained, while n_-/n_e attains a higher value (20%) than in the same device operated without magnets.

It is important to note that the negative ion density in the metal wall device is very sensitive to the conditioning of the device and to the type of electron emitter used. Therefore, we presented on Figs. 7 and 8 data taken with Thoriated Tungsten filaments only. A better control of gas and wall temperature, wall surface condition and ion species in the plasma is necessary for a full understanding of the observations.

Conclusion

Since the 1977 Symposium on the Production and Neutralization of Negative Hydrogen Ions and Beams, a considerable insight into the physical processes related to the volume production of H^- in plasmas has been obtained.

The use of the photodetachment technique confirmed the presence of a high proportion of H^- ions in low pressure, low density, ($<10^{10}$ cm^{-3}) hydrogen plasmas, and established that the negative ion density is not isotope dependent, does not depend on the neutral density, but strongly depends on the electron density ($n_- \sim n_e^3$) and the electron temperature.

Recently, we extended the density range studied up to 10^{11} cm^{-3} by the use of a multifilament stainless steel device, which can be operated either as a diffusion type plasma (without magnets) or as a hybrid multipole plasma (with magnets). A change in slope in the n_- vs n_e dependence is observed at an electron density of about 2×10^{10} cm^{-3}. We interpret this change as the transition from a regime where the negative ion loss is due to diffusion, to one dominated by ion-ion recombination.

In the high density regime, n_- varies linearly with the electron density.

The hybrid multipole operation leads to an increase in negative ion density, electron density and n_-/n_e, compared to the diffusion type plasma.

A theoretical model for the processes in the plasma is proposed, based on the idea that dissociative electron attachment to highly vibrationally excited hydrogen molecules is the main negative ion formation process. This model predicts the experimentally found behavior of the negative ion density.

The formation of highly vibrationally excited molecules has been analyzed both theoretically and experimentally. The main production process is through E-V singlet excitation[13-15] (collisions of energetic electrons with molecules); the main loss process is de-excitation in wall collisions. Measurements by CARS of the vibrational population of the lowest levels has been effected. From these results, it was inferred[22] that the number of wall collisions a vibrationally excited molecule can survive before de-excitation is in the range seven to fourteen.

Acknowledgments

This work was supported by Ecole Polytechnique, Palaiseau, France, by Commissariat a l' Energie Atomique and by the U. S. Department of Energy. Valuable consultations were provided by W. B. Kunkel and J. Taillet. The authors are grateful to J. N. Bardsley, C. Bottcher, B. D. Buckley, J. R. Hiskes and J. M. Wadehra for the theoretical study of processes related to H^- production in plasmas and for communicating their results in advance of publication.

References

1. G. W. Hamilton, M. Bacal. A. M. Bruneteau, H. J. Doucet, and M. Nachman, Proceedings of this Symposium.

2. E. Nicolopoulou, M. Bacal and H. J. Doucet, J. Phys. (Paris), 38, 1399 (1977); also in Proc. Symp. on the Production and Neutralization of Negative Hydrogen Ions and Beams, BNL-50727, K. Prelec,. Editor, September 26 - 30, 1977, p. 26.

3. M. Bacal, G. W. Hamilton, A. M. Bruneteau, H. J. Doucet and J. Taillet, Rev. Sci. Instrum., 50, 719 (1979).

4. M. Bacal and G. W. Hamilton, Phys. Rev. Lett., 42, 1538 (1979).

5. M. Allan and S. F. Wong, Phys. Rev. Lett., 41, 1791 (1978).

6. B. Peart, R. A. Forrest and K. Dolder, J. Phys. B, 12, 3441 (1979).

7. C. Bottcher and B. D. Buckley, J. Phys. B, 12, L497 (1979).

8. J. M. Wadehra and J. N. Bardsley, Phys. Rev. Lett., 41, 1795 (1978).

9. J. N. Bardsley and J. M. Wadehra, Phys. Rev. A, 20, 1398 (1979).

10. J. R. Hiskes, M. Bacal and G. W. Hamilton, LLL UCID-18031 (1979).

11. J. R. Hiskes, J. Phys. (Paris), Colloque C7, Suppl. au n° 7, 40, C7-179 (1979).

12. M. Bacal, A. M. Bruneteau, W. G. Graham, G. W. Hamilton and M. Nachman, J. Appl. Phys., to be published.

13. W. B. Kunkel, private communication,1979.

14. R. W. Wayant, J. D. Shipman, R. C. Ellen and A. W. Ali., Proc. IEEE, 59, 679 (1971).

15. J. R. Hiskes, J. Appl. Phys., to be published.

16. D. L. Smith and J. H. Futrell, J. Phys. B, 8, 803 (1975).

17. J. K. Kim, L. P. Thread and W. T. Huntress, Jr., Intern. J. Mass. Sprectrom. Ion Phys., 15, 223 (1974).

18. W. G. Graham, P.M.I. Report (1980), to be published.

19. J. M. Wadehra, Appl. Phys. Lett., 35, 917 (1979).

20. M. Pealat, J. P. E. Taran, J. Taillet, M. Bacal and A. M. Bruneteau, J. Appl. Phys. (submitted for publication).

21. G. Black, H. Wise, S. Schechter and R. L. Sharpless, J. Chem. Phys. 60, 3526 (1974).

22. J. R. Hiskes, Report P.M.I. 1045, July 1980.

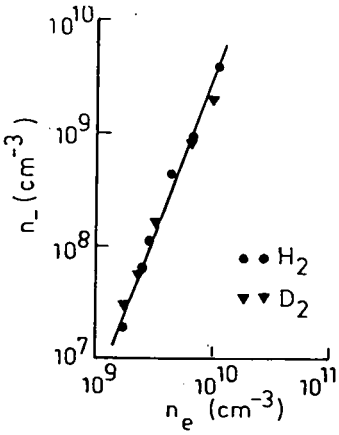

1. Dependence of the negative ion density on the electron density in hydrogen and deuterium plasma.

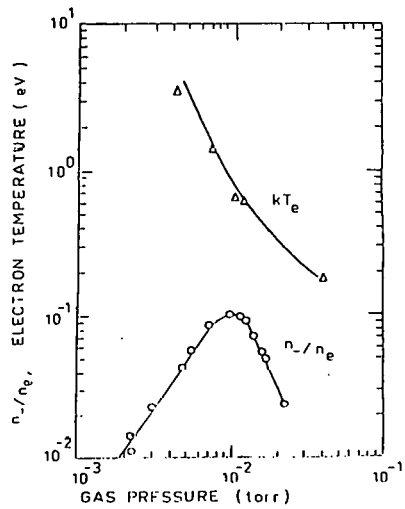

2. Pressure dependence of n_-/n_e and electron temperature at constant filament current.

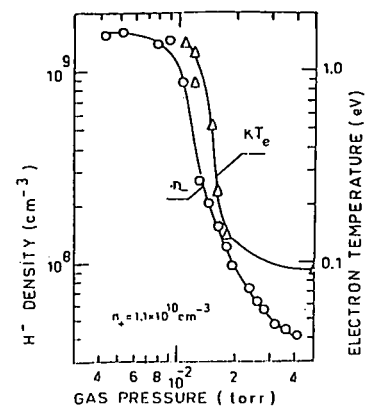

3. Pressure dependence of H^- density and electron temperature at constant plasma density.

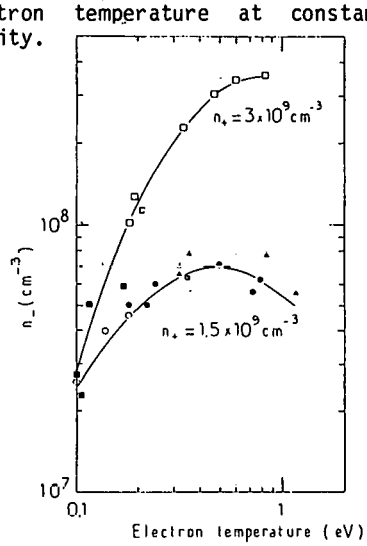

4. Variation of the negative ion density with electron temperature, for two constant plasma densities. The data were taken by varying the energy of the primary electrons at several constant values of gas pressure. ▲ 10mTorr; ● 14 mTorr; ○ - 21 mTorr, □ 16 mTorr; ■ 34 mTorr.

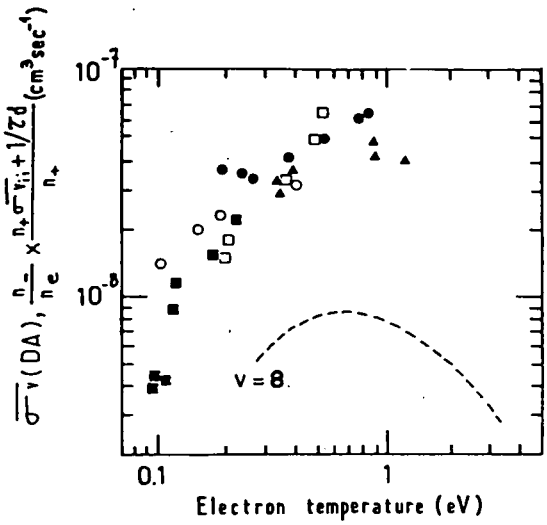

5. Dependence upon the electron temperature of the left hand side of Eq. 14, calculated using the data of Fig. 4. Dotted line: theoretical rate for dissociative attachment to $H_2(v=8)$, calculated by Wadehra (Ref. 19).

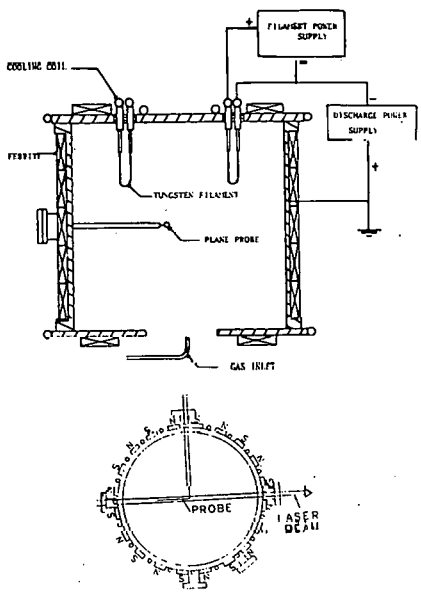

6. Multifilament stainless steel multipole device.

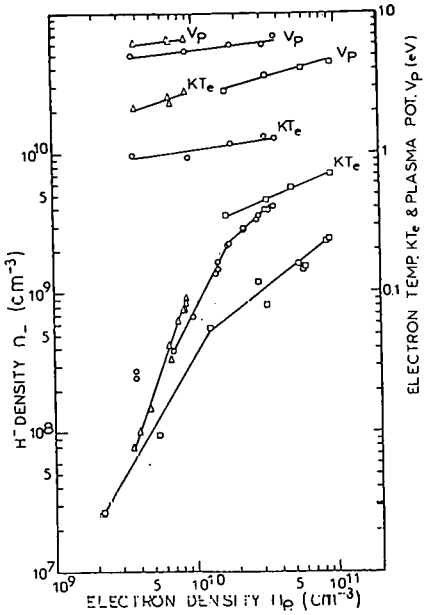

7. Variation of H^- density, electron temperature and plasma potential with electron density, for various gas pressures, in a diffusion type plasma, produced in the multifilament metal apparatus (no magnets). Discharge voltage: 35 V; 10 Thoriated Tungsten filaments. ▲ 3mTorr; o 5.7 mTorr; □ 9.5 mTorr.

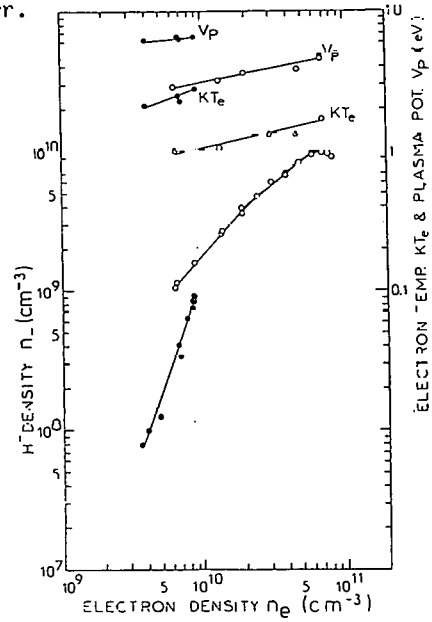

8. Comparison of diffusion type and hybrid multipole plasma, produced in the multifilament metal apparatus. ● no magnets; O 10 columns of magnets. Discharge voltage 35 V; 10 thoriated Tungsten filaments.

DISCUSSION

EHLERS Both your theory and your results seem to show no isotope effect and that worries me because I always see one. Did you see an isotope effect with your mass spectrometer data?

BACAL No. Where do you see it?

EHLERS If you run deuterium and you run hydrogen in a PIG source, you always see an isotope effect, factors of 2. In that case the emission currents are emission limited, so it is not Child's law that makes a difference.

BACAL Are we sure that the PIG source is the same thing as our plasma? We have many differences; for instance is it pressure dependent?

EHLERS I do not know, that is why I am asking the question.

BACAL I do not know whether the PIG discharge is the same as the discharge we are dealing with, because it optimizes at much higher pressure and it has an isotope effect.

HISKES The lack of an isotope dependence follows from the calculations of Wadehra and Bardsley. If you are in the high vibrational levels and the cross sections are within a factor of 2 of each other, you are above the 5 or 6 level and that seems to be the basis for that. Now in the PIG discharge what is the dominant formation process of the negative ions? I am not sure but they may be different.

HOOPER One other comment. Martha is measuring density and I believe you are measuring current and for given density and temperature, there ought to be at least a square root of 2 difference because of the thermal velocity of the ions involved.

EHLERS When you reach space charge emission limited current, than that should fall out. I mean you could run the voltage up factors of 2, 3 or 4 and it would not change that current; you have taken out all that is there.

BACAL We are talking about only a factor of 2, I would not argue very much about that.

HISKES If it was only the ground vibrational states that were populated, one would expect an isotope effect which is a factor of 10 or 100.

BACAL 10^3.

HISKES 10^3 even and you are seeing less than a factor of 2.

OETTINGER Was your CARS work done in a steady state plasma or a pulsed plasma?

BACAL It was a steady state plasma with a hot filament and operated at the highest pressure, because increasing pressure reduced the vibrational excitation due to a drop of the electron temperature.

OETTINGER It was interesting that your first and second vibrational levels had almost the same population...

BACAL No, they were different by a factor of 10, sorry.

OETTINGER Were they?

BACAL Yes, that would be too nice. They do not have the same population, the first one is 4.10^{13} and the second one is 4.10^{12}, so there is a factor of 10 difference, but there was a factor of 40 between 0 and 1, which shows that our populations are highly non-Boltzmannian. Bill Bailey made the estimate of what the Treanor distribution should be and this V = 2 is higher than the Treanor distribution predicts, so it is a very non-Boltzmannian population.

HAMILTON I would like to go back to this isotope effect and support what Hooper said about the effect on the ion mass on the emission limited current density, because we are talking about the ion saturation current which is a function of ion mass and that is part of the effect that Ehlers is talking about.

BACAL I agree with what was said.

PETERSON I see here you have the population of V = 3 jumping up again?

BACAL No, we did not measure the population of V = 3. We could not measure it. When you work with CARS, you measure the signal which is proportional to the difference of population of V = 2 and V = 3. It may be possible to estimate the population of V = 3 for instance from the Treanor distribution. But do not consider it, we do not know V = 3.

PETERSON But what you are saying is that the population of V = 3 is higher than V = 2.

BACAL No, I said that V = 1 is higher than V = 2. Sorry, I made then a mistake. I have another plot which probably gives the right value.

PETERSON I think that if you are exciting by cascade from higher states using a high energy electron then you can have some inversions where you actually do have some of the higher vibrational levels.

BACAL We did not observe them. I wish we would observe an inversion that would be easy to measure. We could not see V = 3 because we could not spend more time or maybe we did not look at the right level of sensitivity. You always need something which you did not measure in order to estimate the last one you measured. So you have to go back from V = 3 up to V = 0 to make any calculation from the data you record.

HISKES I would like to make a comment. The experiment is sensitive to the difference in the number between the population of 2 and 3 and I

think essentially 3 has been set equal to 0 in this interpretation. The excitations of these first 4 or 5 levels is dominated by the V-V' excitations which Bardsley and Wadehra calculated and reported yesterday. If we take these numbers and use their cross sections we would predict 3 is down by a factor of 10 or 100.

PETERSON Yes, I was talking about the fact that if you really are being excited in your plasma by some high energy electron component, you actually get the higher vibrational levels and you could have some inversions.

BACAL Yes, in fact John Hiskes made a calculation and he got an inversion but the inversion is about 6, V = 6. At 3 we have no inversion yet.

CRANDALL This is a different subject. You made a statement comparing H_3^+ destruction with electrons and collisions with neutral molecules. You said that the collisions with neutral molecules should be more important because the density was much higher, like three orders of magnitude higher than the electron density. But that depends not on just the density but also on the collision frequency. Can you say what the collision frequency is between H_3^+ and neutrals compared to H_3^+ and electrons.

BACAL I have compared not the cross sections but I just multiplied the rate by the densities. I know that the limit is 10^{10} and below 10^{10} I do not have to consider these processes.

McGEOCH But, in the photo-detachment experiment you referred to, you measured the rate of recovery of negative ion densities.

BACAL Yes, but that is not the rate of recovery but the rate of diffusion. I mean the rate of recovery is much slower, it is in the order of ms probably. We were looking at microseconds. So we consider the rate of diffusion of negative ions from the area surrounding the beam into the laser beam. We have just a modest laser which does not allow us to measure the formation times or the rate of recovery.

JACQUOT Have you an idea of the optimum pressure of the neutrals in the source to produce 10 mA/cm^2 of D^-?

BACAL The optimum pressure is not related to the current we want to produce, increasing the pressure does not help. I have shown that an increasing pressure leads, at a certain point, to a drop in negative ion density. So that is not the solution to go to higher pressure, we have to stay at low pressures.

JACQUOT Have you tried to test at 10^{-3} mm?

BACAL Not in this apparatus, but in another one, yes. I know the pressure dependance and there is an optimum between 1 and 3 millitorr. This is the reason why I am saying that I am not sure we deal with the same phenomena as in the PIG discharge of Ken Ehlers, because he requires higher pressures while we know that higher pressures do not help us. Maybe just because the electron temperatures become unsuitable, maybe another way of excitation...

OETTINGER Because cascading excitation of the high vibrational state versus maybe a V transition from the ground state is so important. Could you run a pulsed discharge, because if you observe the time dependence of the populations of those lowest vibrational states, you would be able to determine whether they were coming down through cascading processes or upward through a simple vibrational interaction process?

BACAL We can run a pulsed discharge. Now the question is, do we want to run the pulsed discharge at the same pressure or at a very high pressure?

OETTINGER No, at the same pressure.

BACAL I think we can run a pulsed discharge. It is a question of synchronizing the pulsed discharge.

OETTINGER You can gain some information from that.

BACAL We were considering using a pulsed discharge just to go up in pressure and investigate the whole distribution, but that would mean a different job. What you propose is just passing the discharge at the same level. It increases the difficulty of the CARS experiment but that is maybe something we can handle.

SLUYTERS Can you elaborate a little bit on your recent experiments in Berkeley?

BACAL We studied a bucket ion source which was operating very good in the range up to the 5 x 10^{11} level. We saw a very strong dependence on the negative ion density extracted from this plasma, I would say an n_e^2 dependence. We were working above a point where mutual neutralization occurs. I can not tell you exactly what the proportion of negative ions was, so I can not tell you whether it was much or not. We have to work out the results; it is not straight-forward to compare these densities with the extracted currents. But what is so encouraging is that I saw the negative ion density going up very fast with the electron density, no sign of saturation, no sign of unpleasant effects due to mutual neutralization. Well, I could also tell you that we were experimenting with something which would help us not to extract electrons but that is something on which we have to work more to optimize the system and to understand it better.

HOPMAN You have shown that the density of vibrationally excited neutrals is very dependent on the fraction of electrons above 20 eV. Because you have a hot filament producing an electron beam one would expect also a strong electron beam gradient. Therefore one would expect in the negative ion density also a density dependence that is difficult to trace.

BACAL There is no gradient in the bucket source. I think that with the bucket ion source which we studied in the CARS experiment and which we used in our high density experiments, the distribution of fast electrons is very homogeneous.

HOPMAN You have checked this?

BACAL Everybody has checked that. That is the advantage of the bucket ion source, isn't that true? When you extract a lot they become non-homogeneous but when the bucket is closed it is very good.

HOPMAN I agree on normal electron densities, etc. but if it is true for the high energy tail in the electron distribution, I doubt it.

BACAL Well, it is true for the electron beam density. Anyway, we know that the plasma density in the bucket sources, which depends on the beam density, is very homogeneous compared to any other type of plasma source. So, there is no reason for us to assume that there is a big gradient.

H^- PRODUCTION IN H^+ AND H^o COLLISIONS WITH ALKALINE-EARTH METAL VAPORS

M. Mayo, J. Stone and T. J. Morgan
Department of Physics, Wesleyan University
Middletown, Ct. 06457

I. Alvarez and C. Cisneros
Instituto de Fisica, México, 20, D. F.

Abstract

This paper presents recent data on H^- negative ion formation in H^+ and H^o collisions with alkaline-earth metal vapor targets. Data on H^- formation in multiple-collision thick targets is reported, as well as H^- formation via single and double electron capture in a single collision. Low energy angular scattering data is also presented for the double electron capture process $H^+ \rightarrow H^-$ in Mg.

Introduction

There is an active and continuing interest in providing the atomic physics data base necessary for understanding and modeling ion sources and neutral injection beam lines. Since neutral beam injection energies are expected to be large in a fusion device (> 150 keV), emphasis has been placed on methods of producing intense H^- beams, since they can be efficiently neutralized at high energies.[1] Since the 1977 Negative Ion Symposium[2] considerable new information has become available and this paper presents new results for H^- (D^-) formation in collisions of H^o (D^o) atoms and H^+ (D^+) ions with Mg, Sr, and Ca alkaline-earth metal vapor atoms.

The attractiveness of alkaline-earth atoms as possible effective charge exchange targets for double electron capture negative ion sources dates back to Hiskes,[3] who exploited trends in known cross sections and energy defect arguments. In 1975 Olson[4] performed the first double electron capture calculation using an alkaline-earth metal atom target. The results of his Landau-Zener calculation for $H^+ \rightarrow H^-$ in Mg indicated that alkaline-earth targets behave quite differently than alkali targets. Since that first calculation Olson and Liu[5] have performed several theoretical investigations of the collision mechanisms responsible for H^- formation and destruction in alkaline-earth metal vapor targets.

The complimentary experimental work has been carried out primarily by the Berkeley group[6] and the group at Wesleyan University[7]. During the period 1977-1980 measurements have been made of H^- equilibrium fractions, and cross sections pertinent to the formation and loss of H^-. These results — some recently published and some still preliminary — are presented and discussed in this paper. In particular, H^- equilibrium fractions in Mg, Sr, and Ca are presented as well as preliminary cross section data for the negative ion collision processess $H^+ \rightarrow H^-$ (σ_{1-1}) and $H^o \rightarrow H^-$ (σ_{0-1}) in Ca and Sr.

In order to assess completely the potential of alkaline-earth metal vapors as targets in neutral beam injection lines, angular scattering information must be available also. Consequently, we present the first data on differential scattering in alkaline-earth targets. In particular, differential cross sections and cone acceptance angles are presented for the collision $H^+ \rightarrow H^-$ in Mg.[8]

Experimental

The experimental techniques required to perform multiple-collision, single collision, and

angular scattering measurements are, of course, quite different. Typical experimental concerns associated with measuring multiple-collision (thick target) H^- formation data deal with insuring that the post collision products (H^+,H^o, and H^-) are all collected with equal efficiency. For single collision (thin target) cross section measurements experimental concerns are numerous. Accurate results depend on detailed knowledge of the target vapor pressure along the effective collision length of the target, and on reducing the effects associated with impurities. Impurity problems result primarily from two causes, metallic impurities in the sample, and oxidation of the sample. For a target of strontium, a small percentage of magnesium may greatly increase the number density in the target, since at a given temperature the vapor pressure of maguesium is much larger than that of strontium. (The primary metallic impurities found in an alkaline-earth metal sample are other alkaline-earth metals.[9]) Also, strontium is very reactive and oxidizes quickly in air. Since the vapor pressure of strontium oxide is very small compared with that of strontium, the number density in the target can be much smaller than expected. Experimental signs of the above impurity problems have been observed in our experiments, and until these effects are completely understood and demonstrated to be negligible, our data for total cross sections must be treated as preliminary. Besides the problems mentioned above there are experimental details specific to low energy angular scattering measurements. In particular, energy resolution and detector efficiency are possible sources of error.

Thick Target Results

H^- production via multiple-collisions in a thick target can be discussed in terms of the H^- fraction of the beam F_-^∞ after charge-state equilibrium has been attained. If we assume that the equilibration of H^- ions is determined primarily by collisions involving H^+, H(1s), and H^- only, and that we may neglect double charge exchange processes, and that at low energies single electron capture by H^+ is large compared to single electron loss from H^o, then

$$F_-^\infty = (1 + \sigma_{-10}/\sigma_{0-1})^{-1} \qquad (1)$$

where σ_{-10} and σ_{0-1} are the single electron detachment and attachment cross sections respectively. Also, a measurement of two of the three quantities F_-^∞, σ_{-10}, and σ_{0-1} allows the third to be determined. In Fig. 1 we present measured D^- equilibrium fractions versus incident D^+ energy for Mg, Ca, and Sr targets. Based on Eq.1, the rise in F_-^∞ at low energies is due to an abrupt change in the energy dependence of σ_{-10},σ_{0-1},or both.

Total Cross Section Results

We have recently measured the cross sections σ_{0-1} and σ_{1-1} for Sr and Ca. Fig. 2 presents our data versus impact energy. It can be seen from Fig. 2 that σ_{0-1} rises sharply at the same energy (~ 5 keV) as F_-^∞ (See Fig. 1). Consequently, the collision mechanism responsible for the abrupt increase in the negative ion equilibrium fraction at 5 keV is due to an increase in the cross section for single electron attachment, $H^o \rightarrow H^-$. Molecular curve-crossing arguments are presently being invoked to explain the structure in σ_{0-1} but as yet no quantitative calculation is available. In Fig. 3 we have plotted the cross section σ_{-10}, deduced from Eq.1. The cross section is rather insensitive to energy over the present range, but it is expected that at lower energies this cross section would drop dramatically due primarily to the lack of a charge-transfer electron-detachment channel in the alkaline-earths.[10] This fact, coupled with the rising cross section σ_{0-1} intimates a very large

value of F_-^∞ at lower energies.

Angular Scattering Results

We have recently measured angular differential cross sections $d\sigma_{1-1}/d\Omega$ for the process $H^+ \rightarrow H^-$ in Mg. These results constitute the first available angular scattering information on H^- ions using an alkaline-earth target. In Fig. 4 we present preliminary results for $d\sigma_{1-1}/d\Omega$ at four different energies. At high energies the H^- ion angular distribution is highly forward peaked. For example, at 4 keV the distribution has fallen by four orders of magnitude within one degree. As the energy is reduced a wide-angle shoulder appears, and pronounced large angle oscillations are evident at 500 eV. A series of molecular curve crossings involving hydrogen atom intermediate states ($H^+ \rightarrow H^0 \rightarrow H^-$) is presently under study to explain the structure. Also, integration of the measured differential scattering cross sections yields total cross sections in agreement with previous measurements[7].

Of importance in maximizing the overall efficiency of neutral beam production is the acceptance angle required to collect a certain fraction of the scattered beam. Preliminary values for the acceptance angles required to collect several different fractions of an H^- beam formed from $H^+ \rightarrow H^-$ collisions in a thin target of Mg are presented in Fig. 5 as a function of H^+ energy. Even with the presence of a low-energy wide-angle shoulder in the differential scattering cross section, about 90% of the 500 eV H^- ions can be collected within 1 degree.

Summary

Since the 1977 Negative Ion Symposium a considerable amount of data on H^- formation in alkaline-earth metal vapors has been obtained. Equilibrium fractions, total cross sections, and angular differential cross sections have been measured. The results show that an abrupt increase in F_-^∞ occurs at low keV energies in the heavier alkaline-earths Ca and Sr (and Ba), and is due to structure in the single electron attachment cross section σ_{0-1}. Based on the present results, and the predicted behavior of σ_{-10} at low energies, it is expected that F_-^∞ will be very large for energies < 700 eV.

Acknowledgments

This work was supported by the Fusion Energy Division of the U.S. Dept. of Energy and by the Instituto de Fisica, México.

References

1. L. W. Anderson, C. J. Anderson and A. M. Howald, in the proceedings of the present conference, The Second International Symposium on The Production and Neutralization of Negative Hydrogen Ions and Beams, 1980, edited by T.Sluyters(Brookhaven National Laboratory, 1980).

2. Proceedings of the First International Symposium on the Production and Neutralization of Negative Hydrogen Ions and Beams, 1977, edited by K. Prelec (Brookhaven National Laboratory, 1977).

3. J. Hiskes (private communication, 1974),

4. R. E, Olson, Phys. Letts. 55A, 83 (1975).

5. R. E. Olson and B. Liu, Phys. Rev. A 20, 1366 (1979); Chem. Phys. Letts. (to be published).

6. K. H. Berkner, D. Leung, R. V. Pyle, A. S. Schlachter, and J. W. Stearns, Nucl. Instrum. and Methods, 143, 157 (1977); Phys. Lett. 64A, 217 (1977).

7. T. J. Morgan and F. J. Eriksen, Phys. Rev. A 19, 1448 (1979); Phys. Rev. A 19, 2185 (1979); T. J. Morgan, J. Stone, M. Mayo, and J. Kurose, Phys. Rev. A 20, 54 (1979).

8. The angular scattering measurements were done at the Instituto de Fisica, México as part of a collaborative effort between I. Alvarez, C. Cisneros, and T. J. Morgan.

9. Powell Metals, Rockford, Il. (private communication, 1980)

10. R. E. Olson, Proc. of this Symposium.

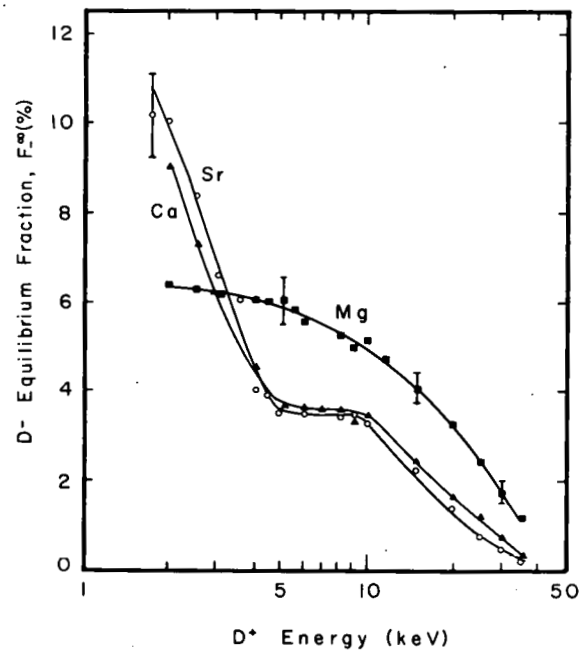

Fig. 1 Measured D^- equilibrium fraction F_-^∞ for Mg, Ca, and Sr.

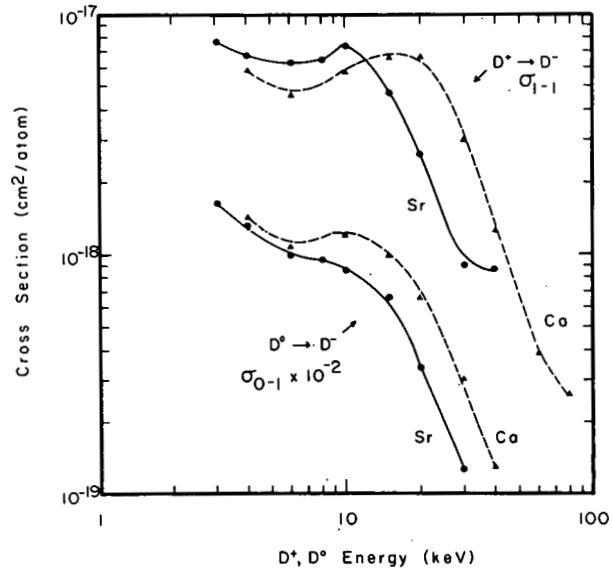

Fig. 2 Measured cross section for D^- formation via single (σ_{0-1}) and double (σ_{1-1}) electron capture collisions in Ca and Sr.

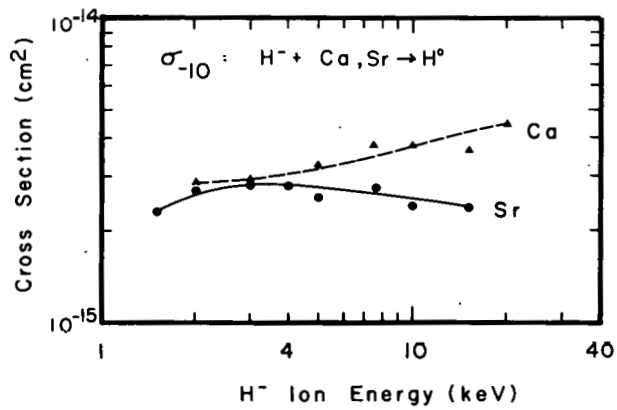

Fig. 3 Electron detachment cross section for Ca and Sr.

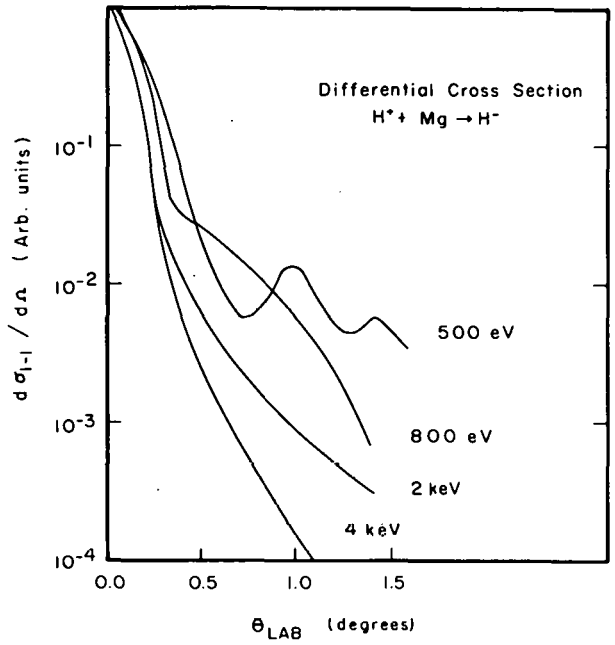

Fig. 4 Measured angular differential scattering cross section for H^- formation via double electron capture collisions in Mg.

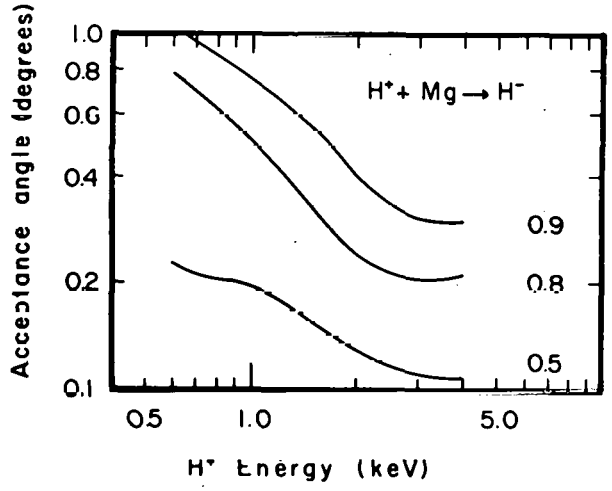

Fig. 5 Acceptance angle required to transmit 50, 80, and 90% of the H^- ions formed from double electron capture collisions in Mg.

DISCUSSION

CRANDALL You did not say concretely whether or not you were going to do some measurements at lower energy which looked most interesting.

MORGAN Well, that depends on many things. Some subtle and some not so subtle. Depending on what other things there are to do, money and so on. It is a complicated question.

CRANDALL You are not committed.

MORGAN That is right.

EMISSION OF NEGATIVE HYDROGEN IONS FROM METAL HYDRIDES BOMBARDED WITH CESIUM IONS

Milos Seidl, Andrew N. Pargellis, James Greer
Department of Physics, Stevens Institute of Technology
Hoboken, New Jersey 07030

Abstract

Measurements of secondary emission yields of negative hydrogen ions from some metal hydride targets bombarded with positive cesium ions are presented. The following targets have been investigated: LiH (max. yield 0.07), CsH (max. yield 0.4), VH (max. yield 0.4), CsOH (max. yield (0.18). The maximum yields occur for bombardment energies from 6 to 10 keV. The yields of electrons, impurity ions and neutrals are also presented. Formation of H^- ions by backscattering of thermal H atoms from a cesium surface has been observed with an efficiency of 10^{-4} H^- ions per incident H atom. Emission of exoelectrons accompanying chemisorption of H atoms on cesium occurs with an efficiency of 10^{-2} electrons per incident hydrogen atom.

1. Introduction

The bombardment of solids with ions results in the emission of various secondary particles such as photons, electrons, neutral atoms and molecules, positive and negative ions. Secondary emission of negative ions was apparently first observed in the early thirties.[1] The yields measured in the early experiments[2-4] were very low, 10^{-3} to 10^{-4} secondary ions per primary ion, until Krohn discovered that cesium coverage of the target increased the yield considerably.[5] This effect has been used for the construction of practical sources of negative ions (including H^- ions) with currents ranging from 1 to 100 microamperes.[6-9] The potential advantage of these "sputter ion sources" is the fact that they operate at pressures several orders of magnitude lower than gas discharge sources. On the other hand, it is not clear whether they can be scaled up to higher currents. In order to answer this question more information is needed about absolute yields not only of the desired ions but also of the impurity ions as well as of electrons and neutral atoms. The yield (or secondary emission coefficient) of the atomic species A is defined by the equation

$$\gamma(A) = n_A/n_P \qquad (1)$$

where n_A is the number of particles A ejected from the surface of the target and n_P is the number of primary ions hitting the surface of the target.

In this paper we present measurements of absolute yields of negative and neutral particles emitted from some metal hydride targets bombarded with positive cesium ions. The choice of hydrides for the target material was dictated by the objective to obtain high yields of negative hydrogen ions. The following target materials are discussed: LiH_x, CsH_x, and VH_x. Lithium hydride was chosen because it is the most stable alkali metal hydride having a hydrogen equilibrium pressure smaller than 10^{-6} torr at a temperature of 300°C in the plateau region that corresponds to a stoichiometry $x \approx 0.5$.[10] Cesium hydride is interesting because cesium is the best electron donor. Its poor stability[11] requires special methods of preparation as described in Section 4. Secondary emission of H^- ions from cesium hydride was previously studied by the Novosibirsk group[12,13]. Our interest in vanadium hydride was motivated by the remarkably large diffusion coefficient of hydrogen in vanadium[14] at relatively low temperatures.

While the sputtering of neutral particles under ion bombardment is relatively well understood, there is no concensus on the mechanism of ion formation during sputtering. The physics and application of secondary emission of negative ions will be briefly discussed in the last section.

2. Experimental Apparatus

The central part of the experiment is an approximately planar diode shown in Fig. 1.

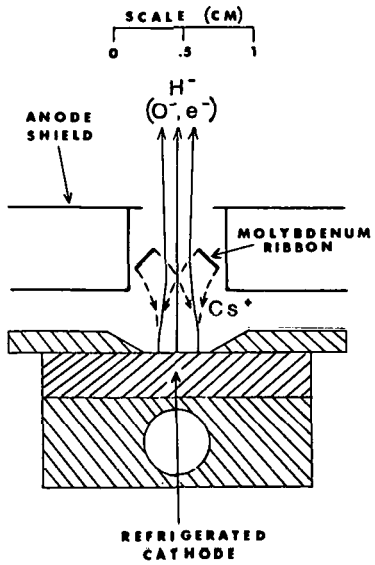

Fig. 1. Schematic diagram of the vacuum diode. The dashed lines indicate Cs^+ trajectories, the solid lines correspond to sputtered negative ions and electrons.

The anode of the diode consists of two 2-by-40 mm molybdenum ribbons separated by a 3 mm wide extraction slot. The ribbons are heated to a temperature of 1200° C and are the source of

Cs^+ ions. The latter are produced either by thermionic emission (when the ribbons are coated with Cs-Mordenite[15]) or by surface ionization of Cs atoms produced in the cesium oven described below.

The cathode of the diode is a 2.5-by-2 cm molybdenum base plate mounted onto a cooling block whose temperature can be maintained from +20°C to -85°C using refrigerated methanol as coolant. On top of the base plate are two stainless steel wedges used to focus the beam of secondary particles from the cathode through the extraction slot in the anode. Only a small central part of the cathode of 4 mm-by-4 mm area is hit by the Cs^+ beam which passes through an aperture in the shield surrounding the anode. The surface of the cathode is coated with the appropriate hydride that forms the target exposed to Cs^+ bombardment. Methods used for the preparation of the hydrides are described in the next two sections.

The anode of the diode is grounded and the cathode is negatively biased from -500 V to -20 kV. Either DC or pulsed operation, with pulse length ranging from 50 μs to 1 ms, have been used. More than 90% of the secondary negatively charged particles originating on the cathode are extracted through the extraction slot in the anode. They are collected by the cathode cup located behind the anode. The cup is positively biased to retain secondary electrons.

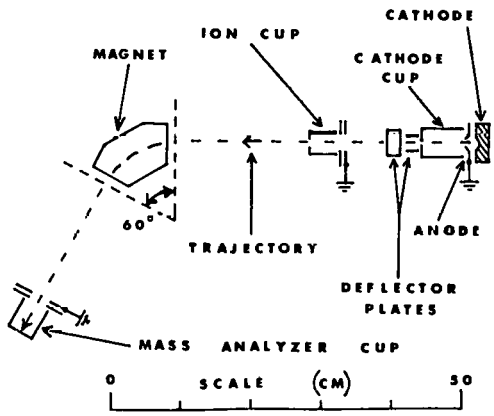

Fig. 2. Experimental setup for measuring absolute secondary emission yields of negative ions and electrons.

Fig. 2 shows the experimental setup for measuring the fractions of the electrons and ions in the extracted beam. About 1 percent of the beam exits through a small opening in the back of the cathode cup and is intercepted by the ion cup. A transverse magnetic field of 10 to 20 gauss applied along the path between the cups deflects the electrons from the ion cup, enabling us to measure the ratio of the electron to ion component. About 1 percent of the remaining beam exits through a small slot in the rear of the ion cup and is mass analyzed by a magnetic sector mass spectrometer. In this way one obtains the fractions of the electron and ion components in the beam. To obtain the absolute secondary emission yields, these fractions are multiplied by the ratio I_S/I_p where I_S is the total secondary current collected by the cathode cup and I_p is the Cs^+ ion current emitted by the molybdenum ribbons. Measurement of the cathode current, which should be equal to (I_S-I_p), gives a convenient check of the collection efficiency of the secondary particles in the cathode cup.

The vacuum system was evacuated by a six inch oil diffusion pump and LN_2 trap to a background pressure in the 10^{-8} torr range, the residual gas being predominantly water vapor.

3. Lithium Hydride Target

The LiH target was prepared by applying LiH powder onto the surface of the cathode of the vacuum diode, Fig. 1, and melting it in a 600 torr H_2 atmosphere. The measured secondary emission yields of H^- ions and electrons are shown in Fig. 3 for two different bombarding ions, Na^+ and

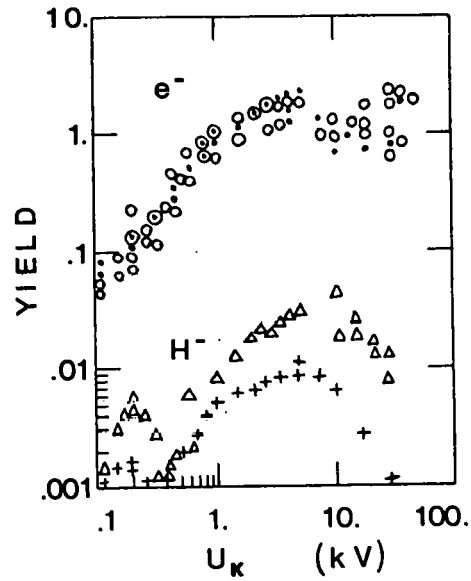

Fig. 3. Secondary emission yields of electrons and H^- ions as function of bombarding voltage for LiH target. The (Δ,O) are H^-, e^- yields for incident Cs^+ ions. The (+,•) are H^-, e^- yields for incident Na^+ ions.

Cs^+. They were produced by thermionic emission from a sodium or cesium mordenite[15] coating applied to the molybdenum ribbons of the diode. The optimum H^- yield reaches $\gamma(H^-) = 0.01$ for Na^+ bombardment at 5 kV and $\gamma(H^-) = 0.07$ for Cs^+ bombardment at 15 kV. The cathode temperature was 300°C and hydrogen gas pressure in the chamber was 10^{-5} torr.

4. Cesium hydride target

Because of the high reactivity of cesium hydride, the target must be prepared in vacuum by atomic beam deposition techniques. Cesium vapor, produced in a small oven, is directed onto the cathode surface by means of a heated feeder tube shown in Fig. 4. A typical Cs atom flux at the cathode is $\phi(Cs) = 10^{15}$ atoms cm^{-2} s^{-1} for an oven temperature of 150°C. Some Cs atoms are also hitting the molybdenum ribbons and are surface ionized when the ribbon temperature is about 1000°C. This effect has been used for producing the primary Cs^+ current.

Atomic hydrogen is produced by thermal dissociation of hydrogen gas in a tungsten tube of 3.2 mm diameter heated to 2500°k by electron bombardment. The atomic hydrogen (and some residual H_2 molecules) effuses from the tube through a hole 0.7 mm in diameter onto the cathode as shown in Fig. 4. The atomic hydrogen flux at the

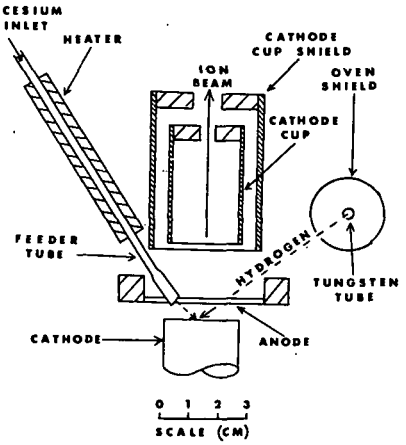

Fig. 4. View of the vacuum diode with the cesium feeder tube and hydrogen oven.

surface of the cathode has been calculated as a function of the tube temperature and vacuum chamber pressure, assuming thermal equilibrium in the tungsten tube. As an example, for a W-tube temperature of 2500°k and a vacuum chamber pressure of 10^{-5} torr, the H flux at the cathode is $\phi(H) = 10^{16}$ atoms cm^{-2} s^{-1}.

The deposition of Cs atoms on the cathode was observed by means of secondary ion mass spectroscopy. The molybdenum cathode was gold plated and the intensity of the Au^- current in the secondary ion spectrum was used as an indication of the thickness of the cesium coating. This method proved to be more convenient than direct observation of Cs^- ions, because their yield is very low while the Au^- yield is high, $\gamma(Au^-) = 0.5$ for 5 keV Cs^+ ions. Starting with a clean gold surface and observing the disappearance of the Au^- signal with time, it was found that the sticking probability of cesium atoms is close to unity when the cathode temperature is lower than a certain critical temperature T_{cr}. The latter reasonably well agrees with the formula

$$T_{cr} = 3840/(27.37 - \log \phi) \qquad (2)$$

which is obtained from eqn. (51) of ref. [16]. The temperature is in °K and the cesium flux ϕ is in atoms cm^{-2} s^{-1}. Conversely, by observing the time needed to sputter away a cesium layer of known thickness, the sputtering yield of neutral Cs atoms was found to be $\gamma(Cs) = 17$ for bombardment with Cs^+ ions of 5 keV energy. This value agrees well with formula (96) of Sigmund's theory[17] using $U_0 = 1.7$ eV for the surface binding energy. Because of this high sputtering yield, the H^- ion yield measurements were done in pulsed regime.

The appearance of H^- ions in the secondary ion spectrum, when the cathode is bombarded with Cs^+ ions, indicates hydrogen absorption in the cesium layer. No hydrogen absorption was observed when the cesium coating of the cathode was done in an atmosphere of molecular hydrogen gas at 10^{-5} torr pressure and -50°C cathode temperature. This is in agreement with a study [18] of hydrogen adsorption on a cesium covered tungsten surface. The sticking coefficient of molecular hydrogen was found to decrease by four orders of magnitude when the cesium coverage increased from 0 to 0.3.

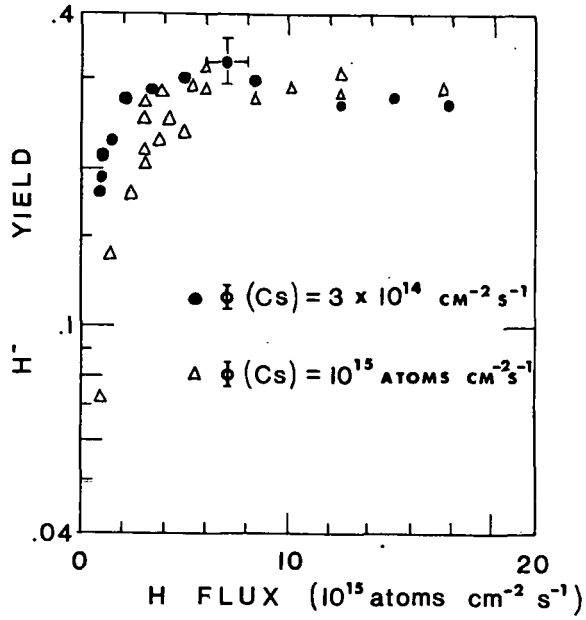

Fig. 5. Yield of H^- ions as function of atomic hydrogen flux for two cesium fluxes. Cathode temperature -50°C, bombardment voltage 5 kV in 0.25 ms pulses. Hydrogen oven temperature 2400°K.

Fig. 5 shows that the yield of H^- ions increases rapidly with the flux of atomic hydrogen and reaches a saturation value when the H flux is about 5 to 10 times larger than the flux of

cesium atoms. This is consistent with a sticking coefficient equal to unity for cesium atoms and 0.1 to 0.2 for hydrogen atoms.

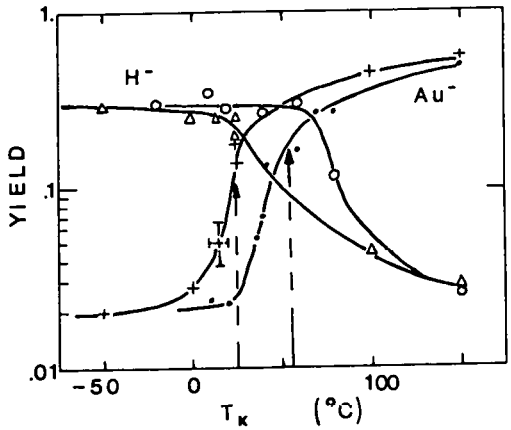

Fig. 6. Yields of H^- and Au^- ions as function of cathode temperature. The (O,·) are (H^-, Au^-) yields for $\phi(Cs) = 5 \times 10^{15}$ atoms cm^{-2} s^{-1} and the (Δ,+) are (H^-, Au^-) yields for $\phi(Cs) = 3 \times 10^{14}$ atoms cm^{-2} s^{-1}. Bombardment with Cs^+ ions of 5 keV energy in 0.25 ms pulses, $\phi(H) = 10^{16}$ cm^{-2} s^{-1}. The critical temperatures, eqn. (2), are indicated.

Fig. 6 illustrates that the H^- yield saturates at the highest value when the cathode temperature is lower than the critical temperature, eqn. (2). This indicates that the highest H^- yield occurs when the cathode is coated with a thick layer of cesium and when the hydrogen is dissolved in cesium to form cesium hydride. The fact that the yield saturates with hydrogen flux, as shown in Fig. 5, makes us believe that the concentration of hydrogen in the target is close to the stoichiometric value, $Cs/H \tilde{\sim} 1$. It should be noted that a thick target means thick as compared to the penetration depth of Cs^+ ions. According to LSS theory[19], the penetration depth of 10 keV Cs^+ ions in cesium target is about 350 Å (58 monolayers).

The yields of electrons and H^- ions from a CsH target optimized with respect to Cs and H fluxes and cathode temperature are shown in Fig. 7. The H^- yield reaches a maximum of $\gamma(H^-) = 0.35$ for a Cs^+ bombarding energy of 10 keV. The yield at 1 keV is less than 0.1. This is about 10 times smaller than the yield reported in [13]. The reason for this discrepancy is not clear.

A Cs^+ current of 16 mA, corresponding to an incident current density of 100 mA/cm^2 at the 4 x 4 mm area of the cathode, produces H^- ions with a current density of 35 mA/cm^2 and 100 mA/cm^2 of electrons, at 10 kV bombarding voltage. In a 0.25 ms pulse, 3.4×10^{15} cesium and hydrogen atoms (about 8 monolayers) are sputtered from the

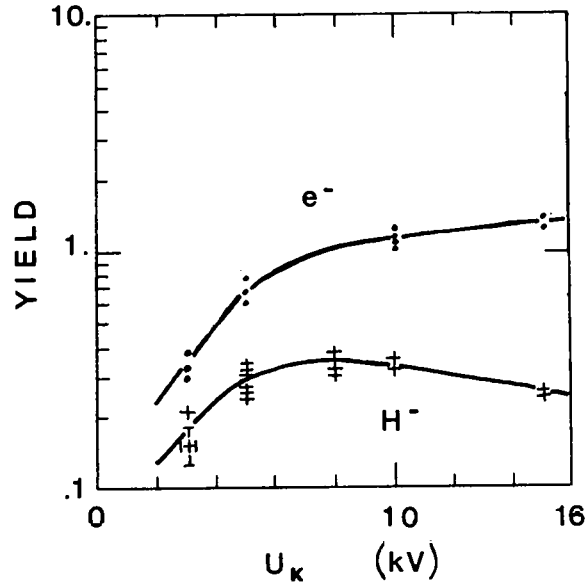

Fig. 7. Secondary emission yields of electrons and H^- ions from CsH target bombarded by Cs^+ ions as function of bombardment voltage. $\phi(Cs) = 10^{15}$ atoms cm^{-2} s^{-1}, $\phi(H) = 5 \times 10^{15}$ atoms cm^{-2} s^{-1}, cathode temperature -50°C, 0.25 ms pulses.

target. They are replaced in about 3.5 seconds with a typical Cs flux of 10^{15} cm^{-2} s^{-1}.

Because of the high reactivity of cesium with water, any residual water vapor in the system will produce a certain amount of CsOH in the target. This will result in the presence of O^- and OH^- ions in the spectrum of secondary ions. To keep their yields small, the arrival rate of water molecules onto the target must be much smaller than the arrival rate of Cs atoms. For example, for a Cs flux of 10^{15} cm^{-2} s^{-1} and a partial pressure of 10^{-8} torr of H_2O, the water molecule flux will be about 1 percent of the cesium flux and the yield of O^- ions will be at least 10 times smaller than the H^- yield. On the other hand, the target turns into cesium hydroxide in a few minutes after the supply of cesium has stopped. This is accompanied by a reduction of H^- yield and an increase of O^- and electron yields. To prove this point, we have measured the secondary ion yields from a pure CsOH target that was prepared by coating the cathode with a CsOH solution and evaporating the excess water. The yields shown in Fig. 8 are very similar to the yields obtained from a cesium target exposed to residual water vapor in the vacuum chamber. Notice the relatively high yield of 0.1 for the Cs^- ion whose yield from Cs or CsH targets is smaller than 10^{-3}.

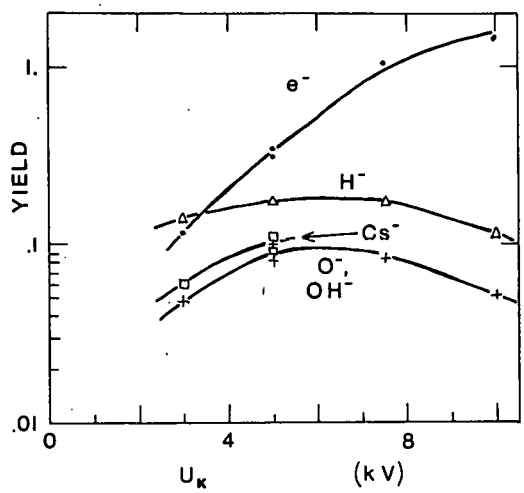

Fig. 8. Yields from CsOH target bombarded with Cs^+ ions as function of bombardment voltage. Cathode temperature +30°C.

5. Formation of H^- ions and electrons by interaction of atomic hydrogen with cesium.

While working with the CsH target, we have noticed a small residual current even when the molybdenum ribbons of the diode, Fig. 1, were cold and no positive ion bombardment of the cathode could occur. The current consists of electrons and H^- ions emitted from the cathode of the diode. The absence of any other ions is a proof that this is not a sputtering effect. Both electrons and H^- ions are emitted only when the beam of atomic hydrogen is incident on the cathode. The current goes to zero when the hydrogen oven is hot and no hydrogen is admitted. It is also equal to zero when the oven is cold and hydrogen gas is admitted. Both electron and H^- ion currents are proportional to the atomic hydrogen flux incident onto the cathode. Fig. 9 shows the formation efficiency, defined as the number of electrons (or H^- ions) produced per incident H atom.

The formation of H^- ions is apparently due to backscattering of thermal hydrogen atoms from the cesium surface. This effect was first observed by Graham[20] in a similar experiment. The theory was developed by Hiskes et al[21,22] for incident energies exceeding 10 eV. Extrapolating the theory to thermal energies we may approximately write for the formation efficiency

$$\frac{J(H^-)}{J(H^0)} = \int_{v_0}^{\infty} \left(\frac{2}{v_t^4} v^3 e^{-v^2/v_t^2}\right) e^{-\beta/v}(1-e^{-\alpha/v})dv \quad (3)$$

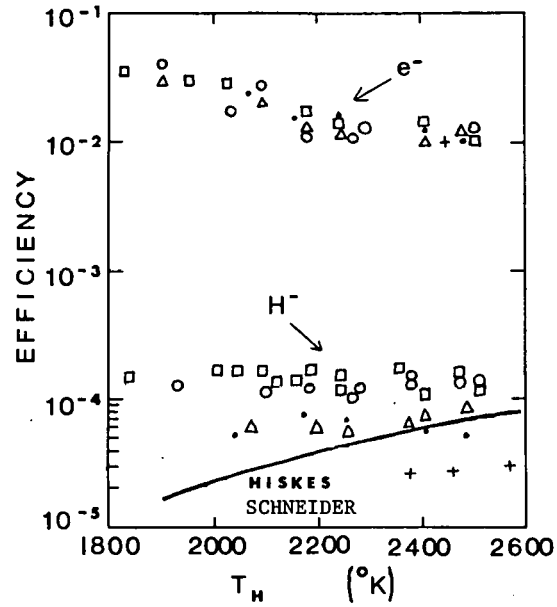

Fig. 9. Formation efficiency = number of electrons (H^- ions) produced per incident H atom as function of hydrogen oven temperature. $\phi(Cs) = 10^{15}$ cm^{-2} s^{-1}, $\phi(H)$ is proportional to hydrogen pressure $p(H_2$ in the chamber. (+) $p(H_2) = 7 \times 10^{-6}$ torr, (·) 1.4×10^{-5}, (Δ) 2.4×10^{-5}, (0) 7.2×10^{-5}, (□) 1.4×10^{-4}.

where the first expression in parenthesis is the velocity distribution in the effusion flux of the hydrogen atoms with $v_t = (2kT/m)^{\frac{1}{2}}$ corresponding to the temperature T of the hydrogen oven. This is multiplied by the production probability, eqn. (6) in[22] where the parameters α,β are given in Table II of [22]. The integration is extended over all atoms whose kinetic energy is larger than the difference between the work function of the thick Cs layer, W = 1.9 eV, and the electron affinity of the H atom, A = 0.75 eV,

$$\frac{1}{2} m v_0^2 = W - A = 1.15 \text{ eV} \quad (4)$$

The formation efficiency calculated from eqn. (3) is drawn by a full line in Fig. 9. The agreement with measurements is not too bad, indicating that chemical effects can be neglected down to thermal velocities for a theory of backscattering.

In contrast to this, the production of electrons appears to be due to chemisorption of hydrogen atoms onto cesium. Although the emission of electrons due to chemical reactions (exoelectrons) has been studied by many authors, we are not aware of any specific observation of electron emission accompanying formation of cesium hydride. On the other hand, electron emission has been observed when halogen gases were adsorbed on sodium[23] and for oxygen adsorbed on magnesium.[24]

6. Vanadium Hydride Target

Of all pure metals, vanadium has the largest diffusion coefficient for hydrogen at temperatures smaller than 100°C.[14] It also has a relatively high solubility for hydrogen[25] and one of the lowest sputtering rates for neutrals.[26] These features make vanadium an interesting target for H^- ion sputtering experiments. The most attractive feature is that the hydrogen oven from Section 4 can be eliminated since hydrogen can be supplied to the surface of the target by diffusion through the target.

The experiments with the vanadium target were done in a modified vacuum diode shown in Fig. 10. The cathode consists of a vanadium foil 0.5 mm thick that is brazed to a stainless steel tube. A hydrogen gas pressure of a few torr is maintained at the back side of the vanadium foil. A gas discharge between the positively biased hydrogen inlet tube and the vanadium foil removes any oxide layer that could block hydrogen absorption in vanadium. The remaining parts of the diode are the same as in Section 4.

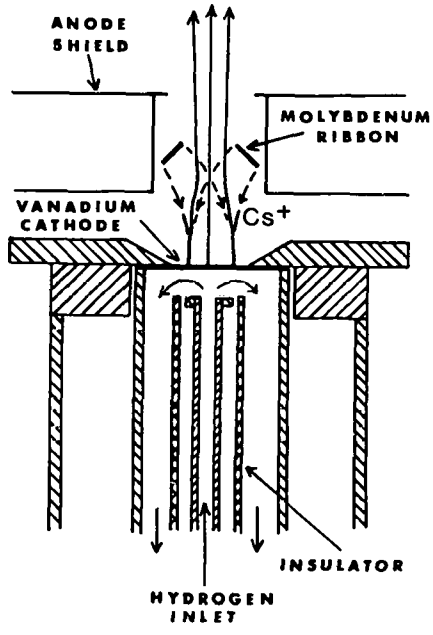

Fig. 10. Diagram of the vacuum diode with vanadium target.

The value of the diffusion coefficient of hydrogen in vanadium is[14]

$$D = 3.1 \times 10^{-4} \exp(-522/T) \text{ cm}^2 \text{ s}^{-1}$$

where T is the temperature in °K. For a temperature of T = 373°K the diffusion coefficient is $D = 7.6 \times 10^{-5}$ cm^2 s^{-1}. Using eqn. (12.46) for the solubility of hydrogen in vanadium[25] one obtains that a pressure of 3.3 torr at the rear side of the vanadium target gives a hydrogen concentration H/V = 0.6 at the rear side and HV = 0.1 at the front side and a diffusion flux $\phi = 5 \times 10^{19}$ H atoms cm^{-2} s^{-1}.

In the experiment, the discharge heated the vanadium target to a temperature close to 500°C so that only intermittent operation was possible. With the discharge on (300 V, 0.1 A, 100 torr H_2), the target was loaded with hydrogen at a temperature of 500°C. Yield measurements under Cs^+ bombardment were done after the discharge had been switched off and the target had cooled down to about 50°C. The hydrogen concentration in the target was estimated close to $H/V \approx 0.1$. Yields were measured in DC operation with Cs^+ current density up to 10 mA/cm^2. The pressure in the vacuum chamber did not exceed 10^{-7} torr.

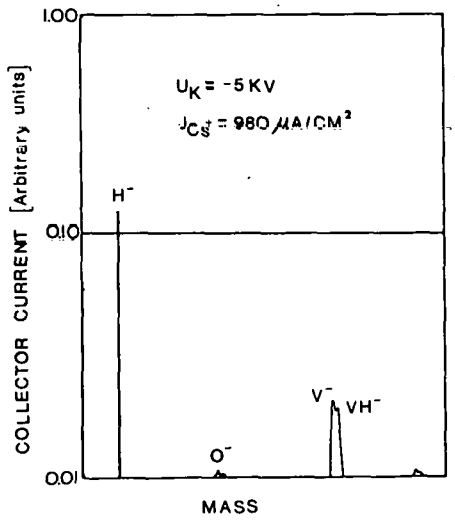

Fig. 11. Secondary ion spectrum from VH_x target ($x \sim 0.1$) bombarded with Cs^+ ions of 5 kV energy. DC operation.

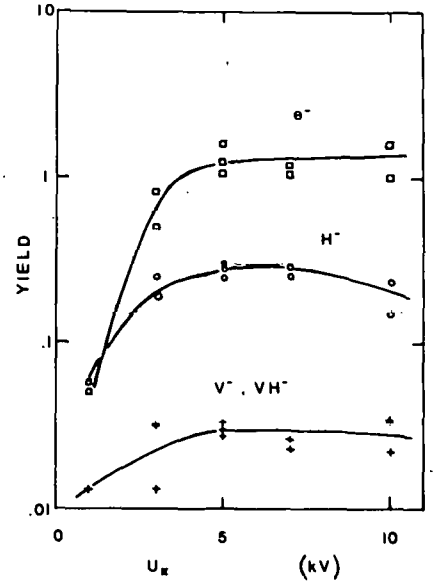

Fig. 12. Yields of electrons and dominant ion components from VH_x target bombarded with Cs^+ ions. DC operation.

Fig. 11 shows that H^- is the dominant component and V^- and VH^- is the only significant impurity. Fig. 12 shows that H^- yield reaches a maximum of about 0.4 for a 6 kV bombardment energy. The sputtering yield of neutral vanadium is about 2.7 for 5 keV Cs^+ ions according to Sigmund's formula (96) in [17]. This is in agreement with experimental observation.

7. Summary

Secondary emission data obtained for the cesium and vanadium targets at the optimum bombardment energy of Cs^+ ions are summarized in Table 1. The atomic concentration, x, of hydrogen is a rough estimate only. $\gamma(n)$ is the neutral sputtering yield of the target with no hydrogen.

	CsH_x	VH_x
x	~ 0.5	~ 0.1
Cs^+ energy (keV)	8 (pulsed)	6 (DC)
$\gamma(H^-)$	0.35	0.4
$\gamma(e)$	1.0	1.2
$\gamma(n)$	23	3
$\gamma(H^-)/\gamma(n)$	0.015	0.13

Table 1

We are not aware of any published measurements of absolute yields from vanadium hydride. On the other hand, H^- yields from cesium hydride have been measured by Bender et al.[12,13] They reported a yield of $\gamma(H^-) = 1.45$ for Cs^+ ion energy of 1.7 keV[13]. This is about 15 times larger than our value shown in Fig. 7. The cause for this discrepancy may be sought either in the measurement technique or target preparation. Numerous checks of our measurements make us confident that we have measured the yield correctly. Bender et al[13] prepared their target by exposing the cesium surface to a hydrogen arc discharge while we used a thermal source of atomic hydrogen. This may result in a different hydrogen content in the target. To account for the large discrepancy, the atomic concentration of hydrogen in our target could have been only a few percent.

In conclusion we wish to make a few remarks on the application of ion sputtering for negative hydrogen ion sources in view of our results. Obviously, the desired ion (H^-) should be the dominant component in the beam of particles produced by the source. This can be easily achieved as far as charged particles are concerned. The yield of impurity ions (mainly O^- for Cs target and VH^- for vanadium target) can be kept below 10 percent of the H^- yield with relative ease. Since the yield of the electrons is only 3 times larger than the H^- yield, they may be eliminated from the beam by applying a modest transverse magnetic field. On the other hand the sputtering yield of neutrals is relatively large. The ratio $\gamma(H^-)/\gamma(n)$ is analogous to the gas efficiency of a gas discharge source. Table 1 shows that this ratio is so low for the Cs target that it practically excludes it from DC operation. The vanadium target gives a somewhat better value $\gamma(H^-)/\gamma(n) = 0.13$ because of its smaller sputtering yield.

Neutral sputtering is well described by Sigmund's theory[17], at least for simple targets. Any drastic changes in the values of $\gamma(n)$ are unlikely. On the other hand, the process of ion formation during sputtering is not yet well understood but is very actively investigated.[27] Further work may lead to a substantial increase in the H^- yield.

8. Acknowledgments

This work was supported by the National Science Foundation.

References

1. J. S. Thompson, Phys. Rev. 38, 1389 (1931).

2. F. L. Arnot, J. C. Milligan, Proc. Royal Soc. A156, 538 (1936).

3. F. C. Arnold, C. Beckett, Proc. Royal Soc. A168, 103 (1938).

4. R. H. Sloane, R. Press, Proc. Royal Soc. A168, 284 (1938).

5. V. E. Krohn, J. Appl. Phys. 33, 3525 (1962).

6. M. Mueller, G. Hortig, IEEE Trans. Nucl. Sci. NS-16, 38 (1969).

7. K. H. Purser, IEEE Trans. Nucl. Sci. NS-20, 136 (1973).

8. R. Middleton, Ch. T. Adams, Nucl. Instr. and Methods 118, 329 (1974).

9. R. Middleton, IEEE Trans. Nucl. Sci. NS-23, 1098 (1976).

10. W. M. Mueller, J. P. Blackledge, G. G. Libowitz (Editors), Metal Hydrides (Academic Press, N. Y. 1968) p. 175.

11. Ref. 10, p. 179.

12. E. D. Bender, G. I. Dimov, M. I. Kishinevskii, Preprint IYaF 75-9, Novosibirsk, 1975, BNL-TR-607.

13. Y. D. Bender, M. Y. Kishinevskii, I. I. Morozov, Proc. Symp. on the Production and Neutralization of Negative Hydrogen Ions and Beams, K. Prelec, Editor (Brookhaven Natl. Laboratory 1977) BNL 50727 p. 60.

14. G. Alefeld, J. Völkl, Editors, Hydrogen in Metals, (Springer, 1978) Vol. 1, p. 333.

15. A. N. Pargellis, M. Seidl, J. Appl. Phys. 49, 4933 (1978).

16. J. B. Taylor, I. Langmuir, Phys. Rev. 44, 423 (1933).

17. P. Sigmund, Phys. Rev. 184, 383 (1969).

18. C. A. Papageorgopoulos, J. M. Chen, Surf. Sci. 39, 283 (1973).

19. P. D. Townsend, J. C. Kelly, N. E. W. Hartley, Ion Implantation, Sputtering and their Applications (Academic Press, New York, 1976) Chpt. 2.

20. W. G. Graham, Phys. Letters, 73A, 186 (1979).

21. J. R. Hiskes, A. M. Karo, M. A. Gardner, J. Appl. Phys. 47, 3888 (1976).

22. J. R. Hiskes, P. J. Schneider, Lawrence Livermore Laboratory Preprint UCRL-83688, June 1980.

23. B. Kasemo, L. Wallden, Surf. Sci. 53, 393 (1975).

24. T. F. Gesell, E. T. Arakawa, T. A. Callcott, Surf. Sci. 20, 174 (1970).

25. Ref. 10, p. 600.

26. Ref. 17, p. 184.

27. Secondary Ion Mass Spectrometry, A. Benninghoven, C. A. Evans, Jr., R. A. Powell, R. Shimizu, H. A. Storms, Editors (Springer, New York 1979) p. 2-76.

DISCUSSION

LEUNG I saw in one of your slides that you changed the oven temperature but your H^- yield remains constant. Can you explain that?

SEIDL The slide that refers to the backscattered hydrogen? The explanation is simple, I do not understand it. You know, the thing is that what you rally have to keep in mind is that this is not a pure cesium target. It is cesium with a large fraction of hydrogen desolved in it. So, it may well be that the work function is different. It somehow changes as the energy of the incoming flux changes.

LEUNG When Bill Graham changed the oven temperature he saw an increase in H^- yield.

SEIDL That is poooible.

LOS You have any idea with what energy the H^- is emitted from the surface?

SEIDL No, we have not done it yet.

LOS Not a single guess?

SEIDL Well, one can refer to many measurements people did. When they looked at the velocity distribution of the particles they found a typical energy spread of a few eV like 5-6 eV.

TSAI Could you give an explanation for the electron emission that decreases with the temperature?

SEIDL I have no theory at all for those electrons. I really could not find anything in the literature where the people treated this case. In fact, even those cases I mentioned, they did not have any theory, they just did some measurements.

LEUNG There was an experiment done at Brookhaven and reported during the last symposium. They used Ne^+ to bombard a molybdenum crystal. Have you compared your results with that experiment?

SEIDL Well, they did not change the work function. We had a thick cesium layer, so we never measured the dependence of this yield on the work function. We intend to do that.

HISKES Do you have a means of measuring the work function?

SEIDL We can arrange it; it does not seem to be that difficult.

HISKES You can measure partial coverages of cesium?

SEIDL Yes, what we shall do, we replace our cooled cathode by a ribbon and heat it; in this way we can clean the target and control the coverage.

LOW WORK FUNCTION SURFACE FOR IMPROVING THE YIELD OF NEGATIVE HYDROGEN IONS

F.N. Huffman and P.E. Oettinger
Thermo Electron Research and Development Center
Waltham, Massachusetts 02154

Abstract

Measurements at Lawrence Berkeley Laboratory show an excellent correlation between increasing yield of negative hydrogen ions and decreasing electrode work function. Surfaces with work functions less than 1.6 eV (typical minimum for cesium on clean metals) are almost always associated with compositions involving cesium and oxygen. Usually, low work function surfaces can be attained only by critical adjustment of separate cesium and oxygen sources. However, in work related to thermionic energy conversion at Thermo Electron, Briere and Sommer have reported on a reproducible surface with a work function of 1.1 eV that can be formed without separate oxygen and cesium sources. The properties at this surface have been found to be insensitive to substrate composition, film thickness, and hydrogen exposure. Such a surface should be useful in enhancing the yield of negative ions from direct extraction sources. A thermal spike model is used to interpret the experimental data.

I. Introduction

Fusion experiments utilizing neutral beam injectors have given promising results. Since the neutralization efficiency for negative ions is much higher than for positive ions for deuteron beam energies in excess of 100 keV, there would be marked advantages if such a beam could be generated by utilizing a direct extraction negative hydrogen ion source.

After the demonstration of dramatically increased negative ion emission from cesiated sources by Bel'chenko, Dimov and Dudnikov,[1] other investigators[2,3,4] have studied negative hydrogen ion production from alkali-coated electrodes. Since the yield increases with the mass of the alkali metal, one immediately suspects that the negative ion production is related to the work function of the surface. This suspicion is confirmed by plotting Schneider et al. measurements of negative hydrogen ion yield (i.e., mean fractional yield per incident nucleon for positive ion energies between 100 and 400 eV) versus the work function of the five alkali metals studied (see Figure 1). These results are consistent with the yields determined by Ehlers and Leung[5] relative to copper from a cylindrical multiline-cusp source. Their results are summarized in Table I. Thus, there appears to be an inverse dependence between negative hydrogen ion yield and surface work function. The lower the work function of the surface, the greater the generation of negative ions.

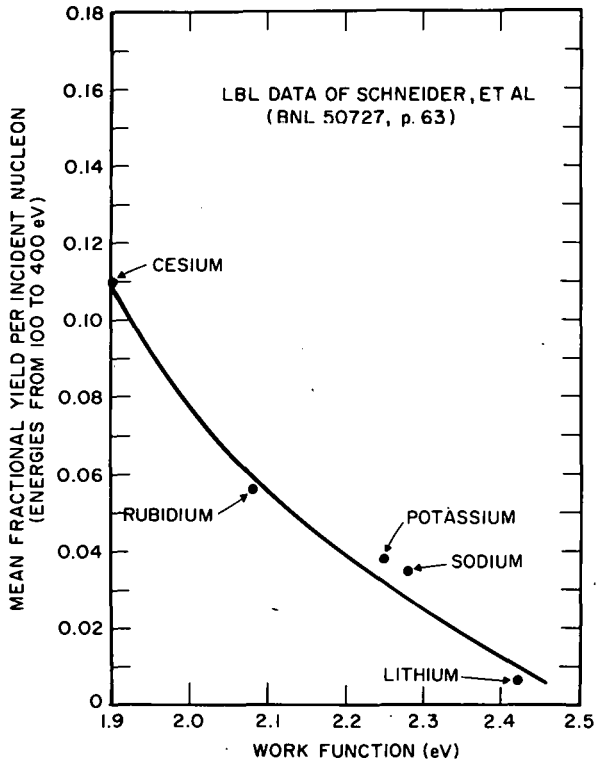

Figure 1. Measured Negative Ion Yield Versus Surface Work Function

TABLE I

NEGATIVE HYDROGEN ION YIELD RELATIVE TO COPPER*

Electrode	Relative Yield	Work Function (eV)
Copper	1	1.65
Lithium	~10	< 2.42
Sodium	~50	< 2.28
Cesium	~100	< 1.90

* K.H. Ehlers and K.N. Leung, "Characteristics of a Self-Extraction Negative Ion Source," Paper 5P1, 21st Annual Meeting of the Division of Plasma Physics, Boston (1979).

Research in thermionic energy conversion has long concentrated on developing cesiated and cesiated-and-oxygenated surfaces with low work functions. Since the literature in this technical area is reported mostly in specialist publications, it should be of interest to first summarize the primary results relative to cesiated electrode work functions. Then the characteristics of a low work function surface produced by cesium carbonate decomposition will be described. The properties of this electrode would appear to be well suited for application in negative hydrogen ion sources. Finally, the expected yield from such a surface will be estimated by use of a "thermal spike model" (TSM).

II. Cesiated Work Function Summary

A. Converter Fundamentals

The thermionic energy converter transforms heat into electricity without moving parts. Such a converter is illustrated in Figure 2. It consists of a hot electrode (the "emitter") facing a cooler electrode (the "collector") inside a sealed enclosure containing a controlled atmosphere of vapors. Electrons vaporized from the hot emitter move across the interelectrode gap to the cooler electrode where they condense and then return to the emitter via the electrical load. In effect, the temperature difference between the emitter and collector drives the electrons through the load. Various geometries are possible, with electrodes arranged as parallel planes or as concentric cylinders. The gap spacing between the emitter and the collector electrodes is typically less than a millimeter.

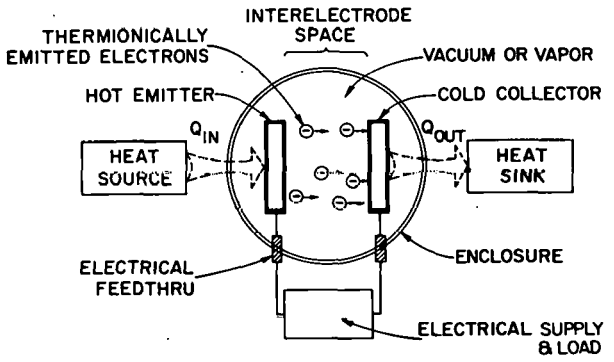

Figure 2. Identification of Thermionic Converter Components

A motive diagram of a thermionic energy converter is shown in Figure 3. The diagram gives the spatial variation of the electrostatic potential between the electrodes. Since the potential energy of the electrons in the collector is greater than that in the emitter, the collected electrons can perform work as they flow back to the emitter through the electrical load. The load voltage is given by the difference in the Fermi levels between the emitter and the collector. In the conventional "ignited mode" thermionic energy converter, cesium is introduced into the interelectrode space at a pressure of approximately one torr. The cesium pressure is adjusted by varying the temperature of a cesium reservoir.

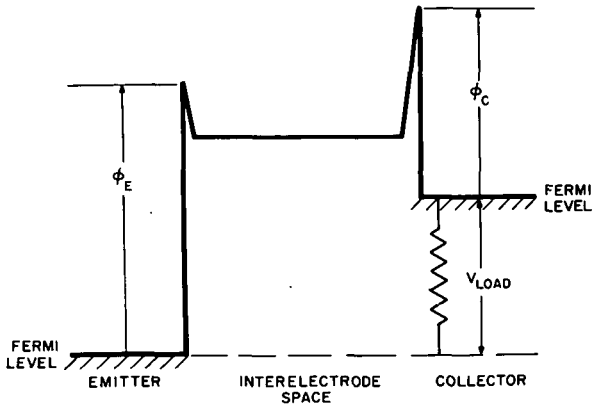

Figure 3. Potential Diagram of Ignited Mode Thermionic Converter

The cesium serves two purposes. First, it adsorbs on the electrodes to reduce their work functions. Second, it provides positive ions for space charge neutralization by electron impact ionization of the cesium between the electrodes. Sheath regions couple the emitter and collector to the interelectrode plasma where the ion and electrode densities are roughly equal. Typically, the output of a thermionic converter is about 0.5 V at a current density of 10 A/cm^2, for an emitter temperature of 1700 K.

For a given current density, it is clear from inspecting Figure 3 that the lower ϕ_C the higher the output potential. For this reason, a great deal of effort has been expended on reducing the cesiated work function of the collector in thermionic converters. This experience is quite relevant to the problem of direct extraction negative hydrogen ion sources.

B. Cesiated Work Functions

Well-known experimental results[6] have indicated that the adsorption of cesium vapor atoms on a metal surface produces a change in the work function of the surface. For less than a monolayer, coverage studies[7,8] show that the surface work function is a sensitive function of the ratio of surface temperature, T, to that of a cesium reservoir, T_R, which supplies the cesium atoms for the surface coverage. A graph of work function versus T/T_R is shown in Figure 4, parametric in substrate bare work function. For T/T_R ratios between 2 and 6, the higher the bare work function the lower the cesiated work function. Typically, the minimum cesiated work function (corresponding to a coverage of around two-thirds of a monolayer) on any metal is approximately 1.6 eV.

If lower work functions are desired, it is necessary to add oxygen to the surface. Pronounced improvements in thermionic converter performance have been demonstrated with controlled addition of oxygen.[9,10,11] A variety of additive techniques have been explored. Thus far, the most successful converter operation has been achieved by using collectors formed by depositing tungsten oxide or molybdenum oxide on a suitable substrate. Often, the

converter characteristics correspond to a collector work function of about 1.4 eV at temperatures ranging around 800 K. Unfortunately, the simple relationship between work function and T/T_R (cf. Figure 4) does not hold for oxygenated systems.

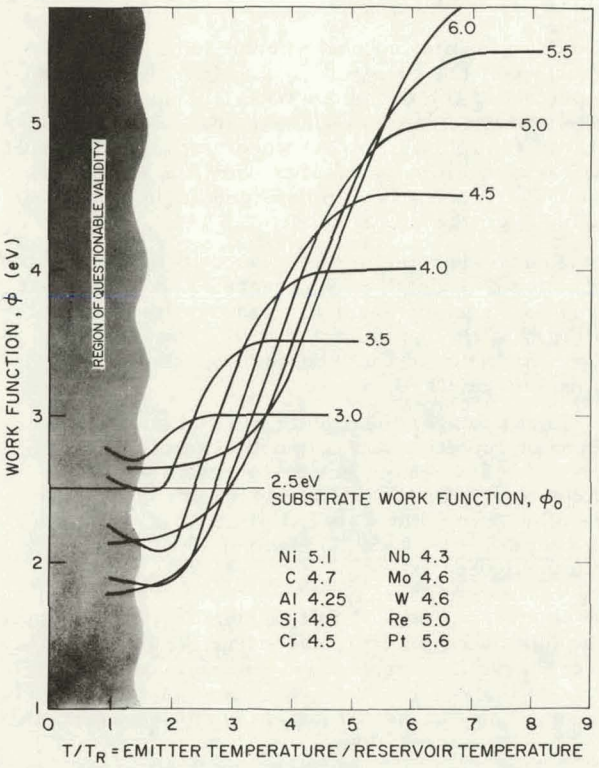

Figure 4. Effective Work Functions of Cesiated Metals as a Function of Surface Temperature to Cesium Reservoir Temperature Ratio for Various Bare Work Functions

Significantly lower work functions are possible outside the converter environment. Studies by Sommer, Briere, and Huffman[12] have demonstrated that cesiated-oxygenated work functions of around 1.15 eV (measured by thermionic emission at 450 K) can be formed on a wide variety of substrates by alternating doses of cesium and oxygen. An abbreviated list of substrates investigated at Thermo Electron is given in Table II. Similar results have been obtained using codeposition of cesium and oxygen.

Inspection of the diverse substrate studies listed in Table II shows that the cesiated-oxygenated work functions at 450 K are remarkably similar. This agreement implies that if a low work function cesiated-oxygenated surface can be formed on a substrate, the composition formed is essentially identical to that on the other substrates. Other investigations indicate that these cesium-oxygen surfaces have a thickness greater than 30 Å. Thus, it is not surprising that the work function of such coatings is essentially independent of the substrate. Sommer[13] has speculated that such surfaces may correspond to layers of the semiconductor Cs_2O which are doped by small amounts of Cs_2O_2 to form a donor level close to the conduction band.

TABLE II

WORK FUNCTIONS OF SCREENED MATERIALS
(Electrode Temperatures in Parentheses)

MATERIAL		WORK FUNCTIONS (eV)		
CLASS	COMPOSITION	BARE	MINIMUM CESIUM	MINIMUM CESIUM-OXYGEN
Rare Earth Oxides	Lanthanum Oxide	>3 (1200 K)	>1.50 (450 K)	1.12 (450 K)
	Europium Oxide	>3 (1200 K)	1.43 (525 K)	1.14 (450 K)
	Ytterbium Oxide	>3 (1000 K)	1.52 (600 K)	1.05 (450 K)
Rare Earth Sulfides and Hexaborides	Lanthanum Sulfide	>3	>3	>3
	Lanthanum Hexaboride	2.57 (900 K)	1.68 (600 K)	1.12 (450 K)
	Cesium Hexaboride	2.75 (1100 K)	>1.8 (600 K)	1.24 (450 K)
Tungsten Metal Borides	Tantalum Diboride	>3	>1.7 (550 K)	1.06 (450 K)
	Zirconium Diboride	>3	>1.7 (550 K)	1.25 (450 K)
	Titanium Diboride	>3	>1.7 (550 K)	1.10 (450 K)
Refractory Metals (Not Atomically Clean)	Tungsten	-	1.40 (500 K)	1.21 (450 K)
	Platinum	-	1.65 (600 K)	1.25 (450 K)
	Tantalum	-	-	
	Molybdenum	-	1.43 (500 K)	1.25 (450 K)
Alkaline Earth Oxides	(Ba,Sr,Ca)O	1.56 (600 K)	1.34 (500 K)	1.16 (450 K)
	Strontium Oxide	2.0 (800 K)	1.4 (500 K)	1.4 (500 K)
III-IV Compounds	p-GaAs	-	2.00	1.13 (450 K)
	p-GaP	-	1.57 (570 K)	1.22 (450 K)

It is also possible to form fractional monolayer coverages of cesium and oxygen on tungsten which have work functions ranging around 1.1 eV. However, the stability of such surfaces during sputtering in an intense discharge is highly questionable.

Unfortunately, all of the foregoing surfaces require critical adjustment of cesium and oxygen exposures in order to obtain the indicated low work functions. In addition, few of the surfaces are stable at temperatures above 450 K.

III. Surface Produced by Cesium Carbonate Decomposition

In the course of thermionic energy conversion studies at Thermo Electron, Briere and Sommer[16] found that when Cs_2CO_3 is heated to the decomposition temperature of approximately 875 K and the resulting carbon dioxide is removed by pumping, the nonvolatile decomposition products condensed on a nickel substrate have a work function of approximately 1.1 eV. To our knowledge, this is the only means of forming a thick surface with a work function less than 1.25 eV without the critical adjustment of separate cesium and oxygen sources!

The experimental arrangement is illustrated in Figure 5. All experiments were performed in an ULTEK (Model TNB-X) vacuum system. After a 200 C bake, a vacuum in the range of 10^{-10} torr was established. The substrate was a radiation-heated RCA-Vidicon gun assembly with a nickel surface area of 0.07 cm^2. A thermocouple was welded to the sample to monitor the temperature for thermionic emission measurements. A platinum ribbon filament, spray-coated on both sides with a Cs_2CO_3 powder suspension in an organic binder solution, was mounted about 1 cm above the sample. The temperature of the platinum ribbon was measured with an IRCON (Model 300 LC) infrared pyrometer. A

Sloan Digital Thickness Monitor 200 was mounted at about the same distance below the sample. The operation of this instrument is based on the frequency change of a quartz crystal with increasing mass of the deposit. Therefore, the thickness of the cesium oxide layer can be derived if the density of the deposited material is known. A cesium "channel" was provided as a source of elementary cesium which was used in an attempt to modify the work functions obtained from the evaporated cesium oxide.

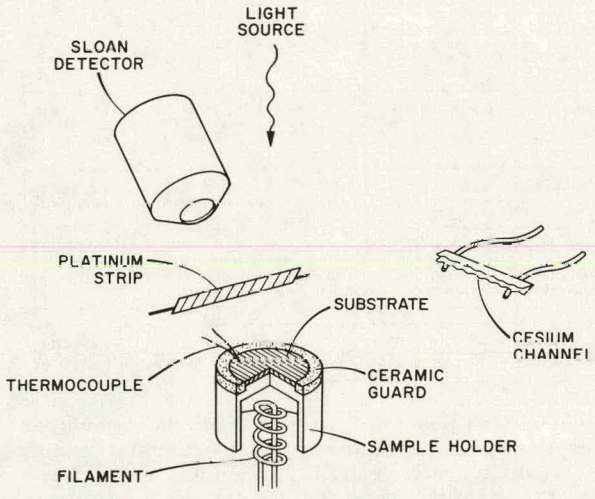

Figure 5. Experimental Arrangement

A window in the pump system allowed the sample to be exposed to a light source for measuring photoemission. Both thermionic and photoelectric emission currents from the sample were measured. The variation of work function and photoemission with deposit thickness is shown in Figure 6. The thickness measurements are approximate because of geometry problems which make it uncertain whether equal amounts (per unit area) of material are deposited on both sample and monitor. Moreover, the chemical composition and, hence, the density of the deposit are not known. For deposits over 200 Å, the work function is independent of thickness.

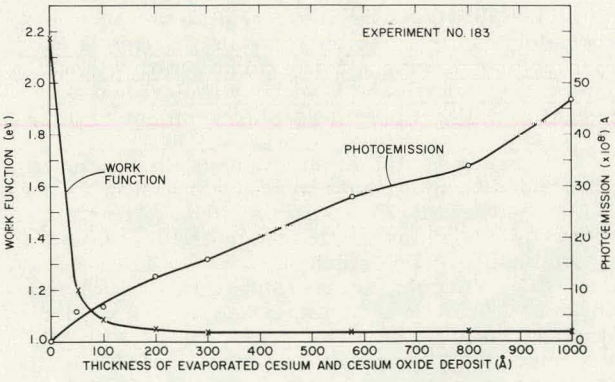

Figure 6. Work Function and Photoemission Characteristics of Cesium Oxide Deposition (Formed by Decomposing Cesium Carbonate) Versus Thickness

Attempts were made to lower the work function below 1.1 eV by exposing the sample to small amounts of cesium vapor released from the cesium channel. In all cases, both thermionic and photoelectric emission decreased, but recovered on heating the sample to between 400 and 450 K.

Experiments were also performed to determine the effect of the substrate material on the emission properties of the deposited material. In addition to nickel, silver and sprayed (Ba, Sr, Ca)O-cathode material (supplied by RCA) were used as substrates. The results, after evaporation from the Cs_2CO_3-coated Pt-ribbon, were indistinguishable from those produced on the nickel substrate.

The interpretation of the described experiments is discussed in detail in Reference 13. For present purposes, it is sufficient to summarize results by stating that the low work function material is probably a thick film of Cs_2O containing small amounts of cesium and/or Cs_2O_2.

Furthermore, the stability of the surface to hydrogen exposure was tested by means of a palladium leak. No change in work function was evident after exposure of the surface to a hydrogen pressure of 10^{-6} torr for a period of about 10 minutes at a temperature of 450 K. Longer periods were not investigated.

Surfaces produced in this manner, from cesium carbonate decomposition, are attractive for use in a direct extraction negative ion source because:

- The film work function is much lower than for cesium alone.
- The film is easy to form (relative to techniques requiring separate adjustment of cesium and oxygen exposure).
- The film properties are insensitive to substrate.
- The film characteristics are reproducible.
- The film is stable to hydrogen exposure (at least, for the order of 10 minutes at a pressure of $\sim 10^{-6}$ torr).
- The film may be thick (i.e., thousands of molecular layers) so that it might be expected to withstand sputtering in an intense discharge for an extended period.

Several cesium carbonate sources have been delivered to Lawrence Berkeley Laboratory for evaluation in their multiline-cusp source.

IV. Thermal Spike Model

A simple analytical model is used to estimate the potential enhancement of negative hydrogen ion yield that may be associated with using the surface produced by cesium carbonate decomposition. This model is based on pseudoequilibrium thermodynamic concepts rather than on microscopic nonequilibrium surface interaction mechanisms as, for example, in

the analytical models developed by Hiskes and Karo[17] and by Bel'chenko, Dimov, and Dudnikov.[18] In these models, negative ion production is the product of the atom reflection (or desorption) coefficient times, the probability of negative ion formation at the surface times, and the probability that the negative ion can escape intact from the surface fields. In the model proposed by Bel'chenko et al., the probability of negative ion formation is unity, so that the dominant factor in establishing the negative ion yield is the product of the surface desorption and escape probabilities. In contrast, the most recent model of Hiskes and Karo suggests that the escape probability is almost unity, so that the dominant factor in determining the negative hydrogen ion yield is the product of the reflection and formation probabilities. Both models are conceptually and mathematically complex.

However, a far less complex "thermal spike model" (TSM) of the surface can provide agreement with experiments, as well as give an interpretation of the electrode properties. In addition, the model allows quantitative predictions of likely improvements. The TSM is based on the Saha-Langmuir equation which describes the temperature dependences for positive surface ionization. This equation is derived considering the thermodynamic equilibrium (in the absence of electric fields and particle reflectivities) of a mixture of ideal atomic, ionic, and electron gases at the surface of a metal under the assumption that the equilibrium concentration of the electrons is determined by the thermionic emission of electrons from the surface. The derivation for negative surface ionization is formally analogous to that for positive surface ionization.[19] In this case, the ratio, β, of the negative flux evaporating from the surface to the total particle impingement rate is given by the expression:

$$\beta = \left[1 + A \exp\left(\frac{\phi - S}{kT}\right)\right]^{-1}$$

where:

ϕ = Electron work function of the surface

S = Electron affinity (0.75 eV for hydrogen)

k = Boltzmann constant

T = Surface temperature

A = Statistical weight ratio of the atomic and ionic states of the adsorbed atom (2 for hydrogen)

The rate and charge state of the evaporating species are independent of the sign of the impinging particles. The validity of the equation as it applies to surface ionization has been demonstrated many times.

Clearly, the conditions in the cesiated ion sources or in the negative hydrogen ion production experiments from alkali metal surfaces by Schneider et al. are far from thermal equilibrium with the ambient temperature. However, if an effective temperature, T_E, can be assigned to the surface which accounts for the kinetic energy of the particles impinging on the surface, the foregoing equation can provide insight into the negative ion emission properties.

The thermal spike concept assumes that the impinging particle will lose a large fraction of its energy within a very small volume. This energy (regardless of whether removed as atomic translation, vibration, or electronic excitation) will be rapidly converted to heat. The result will be the formation of a small volume around the track of the particle which is at a temperature much higher than ambient for a very short period. Such a thermal spike mechanism has proven useful in accounting for radiation damage from nuclear particles. Kapitza has suggested a similar model for the secondary electron emission due to fast ions. In this model, the secondary electron emission can be regarded as thermionic emission arising as a result of intense local heating by the kinetic energy of an incident ion. In addition, Hippel has developed an interpretation of cathode sputtering based on a theory of intense local heating.

An essential feature of the TSM is the use of an effective temperature that is inferred from the experimental data. Such an effective temperature will only be useful if it can be shown to be independent of the details of the surface as well as the incident particle over a restricted range of bombardment energies. The validity of the effective temperature concept will be examined using the data of Schneider et al. In these data, the peak negative hydrogen yields occur at a bombardment energy of the positive hydrogen ion between 100 and 400 eV. In the TSM, higher energies are associated with greater penetration depth rather than increased temperature. As the penetration becomes deeper, the reflection probability would be expected to decrease.

Effective temperatures calculated from Equation 1 using the experimental data of Schneider et al. are given in Table III. For each surface, the table also gives the mean fractional yield per nucleon of hydrogen with incident energies from 100 to 400 eV and the work function assumed for that surface. In all cases, the electron affinity of hydrogen is taken as 0.75 eV. The effective temperatures are seen to be relatively high, except for lithium which would be expected to dissipate the particle energy more rapidly and, hence, result in a lower effective temperature than the other bombarded surfaces. For estimating the work function of the cesiated molybdenum surface in the experiments of Dudnikov, the effective temperature was taken as the mean of the values for molybdenum and cesium (i.e., 9219 K). Typically, cesiated metal surfaces have minimum work functions around 1.6 eV. From Equation 1, one would expect substantially higher negative ion yields from such partially coated surfaces than from thick targets (most results in Table III). This expectation is in good agreement with experiment. Specifically, the maximum negative hydrogen yield from Dudnikov's observation of a cesiated molybdenum surface was 0.22. Using an effective temperature of 9219 K, Equation 1 implies a surface work function of approximately 1.20 eV. This low value suggests that the molybdenum surface was oxidized.

TABLE III

EFFECTIVE TEMPERATURES FROM EXPERIMENT*
Electron Affinity of Hydrogen - 0.75 eV

SURFACE	β^{**}	ASSUMED WORK FUNCTION (eV)	EFFECTIVE TEMPERATURE*** (K)
Molybdenum	0.0055	4.20	8890
Cesium	0.11	1.90	9547
Rubidium	0.056	2.08	7240
Potassium	0.038	2.25	6959
Sodium	0.035	2.38	6767
Lithium	0.0065	2.42	4470

* P.J. Schneider, K.H. Berkner, W.G. Graham, R.V. Pyle and J.W. Stearns, "D⁻ Production by Backscattering from Clean Alkali-Metal Surfaces," Proc. of the Production and Neutralization of Negative Hydrogen Ions and Beams, Sept. 26-30, Brookhaven National Laboratory Report No. BNL 50727, p. 63.

** Mean fractional yield per incident nucleon of hydrogen with energies from 100 - 400 eV.

***Calculated from Equation 1.

Based on the data from the cesium carbonate decomposition surface discussed previously, work functions can be obtained as low as 1.05 eV. The corresponding negative hydrogen yield is 0.26 (assuming an effective temperature of 9219 K). Note that a highly improbable surface work function equal to the electron affinity of hydrogen (i.e., 0.75 eV) would increase this yield only to 0.33.

In summary, the TSM provides a simple means of correlating negative hydrogen yields from cesiated surfaces in good agreement with experiment.

The TSM identifies the work function as the critical parameter. An effective temperature of 9219 K appears to suitably explain negative ion production from partially cesiated surfaces over an incident hydrogen energy range from 100 to 400 eV. Calculations based on this model suggest that the partial cesium coverage on molybdenum data of Dudnikov correspond to an oxidized substrate.

V. Summary

Based on the data discussed in this paper, it appears that:

- Negative hydrogen ion yield is inversely related to the surface work function.
- Oxygen is required in combination with cesium to obtain work functions less than 1.5 eV.
- A surface with a work function of approximately 1.1 eV can be conveniently formed from the decomposition products of cesium carbonate.
- The TSM is a simple and useful means of estimating negative hydrogen ion yields.
- Based on the TSM, the cesium carbonate decomposition surface should provide a negative hydrogen ion yield of around 0.26.

References

1. Yu.I. Bel'chenko, G.I. Dimov, and V.G. Dudnikov, Nuclear Fusion 14, 113 (1974).
2. K. Prelec and Th. Sluyters, Rev. Sci. Instrum. 44, 1451 (1973).
3. P.J. Schneider, K.H. Berkner, W.G. Graham, R.V. Pyle, and J.W. Stearns, Proc. Symposium on the Production and Neutralization of Negative Hydrogen Ions and Beams, Brookhaven Nat'l Lab., 1977 (BNL 50727), p. 63.
4. K. Prelec, Proc. Symposium on the Production and Neutralization of Negative Hydrogen Ions and Beams, Brookhaven Nat'l Lab., 1977, (BNL 50727), p. 111.
5. K.W. Ehlers and K.N. Leung, Bull. Am. Phys. Soc. 24, 1015 (1979).
6. J.B. Taylor and I. Langmuir, Phys. Rev. 44, 433 (1932).
7. N.S. Rasor and C. Warner, J. Appl. Phys. 33, 2589 (1964).
8. G.N. Hatsopoulos and F. Rufch, Energy Conversion 10, 135 (1970).
9. D. Lieb and F. Rufeh, Proc. 3rd Int'l Conf. on Thermionic Electrical Power Generation, Juelich, 1972, p. 1091.
10. D. Lieb, B. Gunther, M.C. Richmond, and F. Rufeh, Proc. Thermionic Conversion Specialists Meeting, Eindhoven, 1975, p. 11.
11. D.M. Ernst, Record of 1970 Thermionic Conversion Specialist Conf., Miami, 1970 (IEEE, New York) p. 492.
12. A.H. Sommer, R.R. Briere, and F.N. Huffman, Proc. Thermionic Conversion Specialists Meeting, Eindhoven, 1975, p. 43.
13. A.H. Sommer, J. Appl. Phys. 51, 1254 (1980).
14. J.L. Desplat and C.A. Papageorgopoulos, Surface Science 92, 97 (1980).
15. B. Gunther and F.N. Huffman, Proc. 15th Intersociety Energy Conversion Eng. Conf., Seattle, 1980 (AIAA ISBN 0-915928-42-6, New York) p. 2103.
16. T.R. Briere and A.H. Sommer, J. Appl. Phys. 48, 3547 (1977).
17. J.R. Hiskes and A. Karo, Proc. Symposium on the Production and Neutralization of Negative Hydrogen Ions and Beams, Brookhaven Nat'l Lab, 1977 (BNL 50727), p. 42.
18. Yu.I. Bel'chenko, G.I. Dimov, and V.G. Dudnikov, Proc. Symposium on the Production and Neutralization of Negative Ions and Beams, Brookhaven Nat'l Lab, 1977 (BNL 50727), p. 79.
19. E.Ya. Zandberg and N.I. Ionov, Soviet Physics Uspehki 67, 255 (1959).

DISCUSSION

SEIDL I would like to mention that we tried to apply this local equilibrium model to our results and what we see is that the ratio of the electrons to ions agrees reasonably well, but what does not agree at all is the ratio of the neutrals to the ions. Obviously, there is something which has to be included, and maybe it is a formation of some potential sheath or something that makes the emission of negatives much more difficult.

HUFFMAN That is an interesting result. I can not comment on it any more. They say necessity is the mother of invention and I invented this in order to come up with an estimate and I will not defend it anymore than I have already.

LOS Would it not be that the Saha-Langmuir is a formula based on thermodynamic equilibrium between vapor and surface while the thermal spike is a thermodynamic equilibrium in the surface and that they are two different things. The thermal spike concept seems, in first instance, to be attractive but it has nothing to do with the equilibrium between the vapor phase and surface.

HUFFMAN Well if the electron density outside the surface would be related to the thermal spike temperature then I think there would be a rational for it. That is a fundamental assumption of derivation.

BACAL You mentioned the highly improbable value of .75 for the work function. I think it is interesting to mention that a value as low as .9 eV has been obtained and that was reported ten years ago at a thermo-ionic conference by myself. This was made with oxygen and cesium on tungsten single crystals and to my knowledge this result has been reproduced recently by Laser Associates. There is place for invention below the values which have been obtained so far.

HUFFMAN I am familiar with both pieces of work. The point that I would like to make here is that we are dealing with a layer that can be quite thick, whereas I have the impression that these other surfaces were not nearly so thick as what I am describing. Consequently, this has the possibility perhaps of lasting longer in a more intense discharge. Certainly, a number of people have measured work functions as low as 1.0 but usually by techniques which are far more tricky than what I have described.

HERSHCOVITCH How resistant would a surface like this be to bombardment of, let us say, plasmas of 10^{14} and electron temperatures of 9 eV?

HUFFMAN I have no idea.

LEUNG I want to make a comment. We have not measured the work function of our converter while the source is running, but Pyle and his group are planning to do that. So the number you quoted on your first slide is with an assumed work function.

HUFFMAN What I meant to indicate there was just the order of the thick film work functions. In the paper we used little symbols "less than". A minimum alkali coverage work functions will have the same order as the thick film work functions.

HAGENA Your surface with cesium and oxygen, do you know the exact composition of the surface as far as mol. fraction of oxygen and mol. fraction of cesium?

HUFFMAN We do not. From a number of arguments that involve chemistry and photo-cathodes, we believe that they are predominantly Cs_2O. We are quite confident there is also free cesium.

EHLERS I suppose it is the appropriate time that we comment on the results of our preliminary tests with these converters. We feel that it is difficult for our source to be a good test for this low work function converter, because we do have sputtering as a problem. If we are interested in dc conditions it makes it difficult for us to utilize them. That does not say it does not have a use elsewhere. We find that if we apply surfaces such as tungsten on a converter with thicknesses like a half mill, it will last for such a short time that they are really not of interest to us. Although we are exceedingly interested in low work function materials, we are also forced to be interested in things that have good integrity for sputtering and thus far we have not gotten that data on this material.

PROPERTIES OF ALKALI METALS ADSORBED ONTO METAL SURFACES

W. G. Graham
The New University of Ulster,
Coleraine BT52 1SA
Northern Ireland

Abstract

Experimental measurements of the work function of metal and alkali metal covered surfaces are reviewed.

A method for producing surfaces of different known work functions for backscattering experiments is described.

INTRODUCTION

It has been established that the surfaces in many present day negative ion sources play an important role in the production of negative ions. While no direct measurements of surface conditions in these sources have been reported, the enhancement of the negative ion output when an alkali metal is added to the discharge is seen as indirect evidence that the work function of the surfaces is an important parameter.[1] This has been confirmed in separate studies of sputtering[2] and backscattering[3] from metal surfaces with alkali metal coverage.

This paper will discuss two aspects of alkali metal coverage of metal surfaces. The first section will be a discussion of recent literature on this topic, accompanied by a compilation of some work function values which may be relevant to those interested in negative ion source development. In the second section I will discuss attempts to produce known and reproducible work function surfaces for future backscattering experiments.

At this point it is useful to summarize some of the experimental work relating to the surface effects in negative ion sources. In the early stages of negative hydrogen ion source development various cathode materials were tried, - molybdenum, tantalum, titanium, stainless steel and tungsten, along with various alkali metal additives, - cesium, potassium and sodium.[1] However, the use of a molybdenum cathode with cesium was found to be the most successful[1] and now seems to be the most widely used combination.[4] It has been argued that ion source operating conditions are such as to favour a cesium coverage which for a Mo cathode, results in a minimum work function value.[5]

Measurements of negative ion formation by sputtering from a Mo (100) surface with Cs coverage have been reported by Yu.[2] These have shown that the maximum yield of negative ions from the bulk (Mo^-) and from absorbed layers of hydrogen (H^-) and oxygen (O^-) correlates closely with the minimum in the surface work function.

Investigation of negative hydrogen ion formation from positive hydrogen ions backscattered from a variety of surfaces, polycrystalline metals with thick and partial coverages of alkali metals, has demonstrated that the H^- yield produced in this manner is also maximized at or near the coverage at which the surface work function is a minimum.[3]

WORK FUNCTIONS OF METAL AND ALKALI-COATED METAL SURFACES

There is a vast amount of work published in the measurement of the work functions of the surfaces of elements and alloys, both clean and with known surface adsorbates. A wide variety of techniques have been employed in these measurements, under differing experimental conditions. It is outside the scope of this paper to provide an indepth survey. It is therefore intended to use the published literature to collect together work function measurements which could be relevant to future negative ion source development. The values selected are from the more recent measurements. In some cases only early work is available and while cleaning techniques are described the analysis of the surface conditions may not be as reliable as present techniques permit. It is left to the reader to consult the individual references for a description of the techniques used, both to make the work function measurement, and to ensure that the surface conditions are known.

1. Work Functions of the elements.

Several extensive compilations of work function data have appeared in the literature. Particularly interesting is that by Riviere,[6] who critically reviews the various work function measurement

techniques and presents values reported in the literature up to 1966. A more recent compilation is that by Michaelson.[7] He presents the work function of 44 elements which he assesses, by examining the experimental technique, are the best available from the literature up to 1976. In Table I some selected work function values from this compilation are presented.

Element	Work Function eV	Reference
Cu	4.65	8
Fe	4.5	9
Mo	4.6	9
Nb	4.3	9
Ni	5.15	9
Re	4.96	10
Ta	4.25	10
Ti	4.33	9
W	4.55	11
Cs	2.14	12
K	2.30	13
Li	2.9	14
Na	2.75	15
Rb	2.16	16

Table I. Work function values for polycrystalline samples.

In applying these values, measured on polycrystalline samples, it is necessary to assume that materials commonly used in practise have the same surface condition as that of the specimens used in the measurements. The highest reported polycrystalline work function values are for Se (5.9),[17] Pt (5.65)[9] and Ir (5.27),[10] while the lowest values are those for the alkali metals.

Michaelson[7] also includes measurements on various crystal planes for 21 of the elements. While initially it might appear unlikely that single crystal planes could be used for the large cathode surfaces of ion sources, it is known that with suitable treatment certain polycrystalline substrates can be converted into pseudo single crystals.

For example, Tracy and Blakely[18] have shown that W(100), W(112) and W(111), heated in the presence of O_2 will facet to {110} planes, while an initial flat (110) surface is stable against facetting. In Table II some crystal values are presented. These serve to illustrate the magnitude of the work function differences which are to be typically expected between various crystalline surfaces of the same metal, although differences of up to 1 eV have been recorded.[7] The highest reported single crystal work functions are for Ir(111),[23] 5.76 eV; Re(1011),[4] 5.75 eV; Pt (111),[24] 5.7 eV.

Single Crystal Face	Element Cu[19]	Mo[20]	Nb[21]	Ni[22]	W[23]
(100)	4.59	4.53	4.02	5.22	4.63
(110)	4.48	4.95	4.87	5.04	5.25
(111)	4.98	4.55	4.36	5.35	4.47
(112)	4.53	4.36	4.63		

Table II. Work function values, in electron volts, for single crystal faces.

2. Work function change with alkali metal coverage.

The general behaviour of the surface work function as a function of alkali metal coverage is illustrated in Fig. 1.

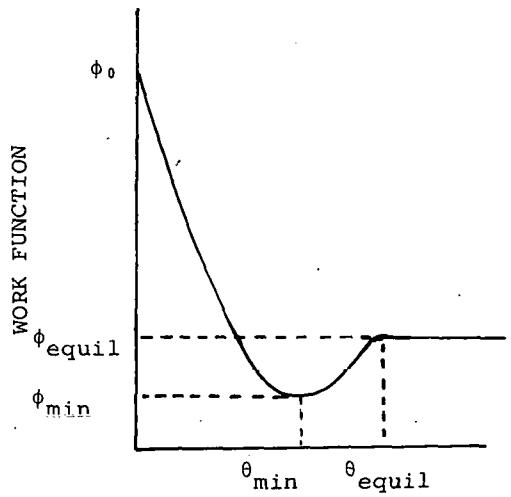

Fig. 1 Schematic diagram of work function dependence on alkali coverage.

The work function of the bare metal substrate, ϕ_0, is found to decrease with increasing alkali metal coverage, to a minimum value, ϕ_{min}, corresponding to a coverage θ_{min}. The work function then increases with increasing alkali metal coverage until a value ϕ_{equil}, at which no further change in the work function is observed, either because no further alkali metal atoms stick to the surface, or the work function of the bulk adsorbate material has been reached. This corresponds to a coverage denoted by θ_{equil}. From the point of view of negative ion studies the quantities ϕ_{min}, ϕ_{equil}, θ_{min} and θ_{equil} are all of interest.

Two distinct methods are used for investigating this behaviour. In one a constant flux of alkali metal is incident on a substrate. Control of the substrate surface temperature then determines the amount of alkali metal coverage. In the other, coverage is built up as successive evaporations of alkali metal are applied to the metal substrate, which is generally at room temperature or lower. The first type of measurement is particularly relevant to ion source conditions, while the latter is of interest in experiments investigating backscattering or sputtering processes.

Several studies of alkali metal coverage of polycrystalline metals have been made. In Table III measurements for some polycrystalline surfaces in cesium vapour are presented.

Absorbate/ Substrate	ϕ_{min} eV	ϕ_{equil} (eV)	Ref.
Cs/Cu	1.64	1.64	26
Cs/Mo	1.54	1.82	25
	1.61	1.77	27
K/Mo	1.76	2.14	28
Cs/Ni	1.37	1.80	25
Cs/Re	1.45	1.77	25
	1.51	1.56	27
Li/Re	2.8	3.05	30
Cs/Ta	1.69	1.70	27
K/Ta	1.73	2.26	28
Cs/W	1.52	1.80	25
	1.60	1.64	27
K/W	1.65	2.20	29
Na/W	2.16		31
Cs/304 Stainless Steel	1.52	1.60	26

Table III. Minimum and Equilibrium work function values for alkali metal coverage of polycrystalline substrates.

These measurements serve to illustrate differences in techniques. Wilson[26,27] employs a thermionic emission technique which means that the surface is at elevated temperatures throughout the measurement, while Swanson and Strayer's[25] field emission measurements are made with a target at around 200°K. It is worth pointing out at this time that Swanson and Strayer also report measurements of ϕ_{min} and ϕ_{equil} for cesium of single crystal tungsten surfaces (W (100) and W (110) which are in excellent agreement with the more recent values presented in Table IV.

However Wilson's field emission S curves provide useful values of ϕ_{min} for a wide range of materials - Be, Ti, Cr, Ni, Cu, Pt, 304 stainless steel, Nb, Mo, Ta, W, Ke, Os and Ir in cesium vapour and also allow us to compute the cesium flux/surface temperature combination required to attain this minimum work function value.

Measurements for polycrystalline metal surfaces with other alkali metal vapours are not as plentiful. Several authors, using a field emission apparatus to measure work function changes on single crystal faces, also report average values for the entire probe, which is polycrystalline.[28,29,30,31] Some measurements obtained in this manner are also presented in Table III.

Recently, most work has concentrated on measurements of single crystal surfaces, since the nature of the alkali metal adsorption can be more readily studied in this case. Many measurements have been reported on the cesium-tungsten system, probably due to early theoretical work on this system.[42] However, other systems have been studied and some representative data is presented in Table IV.

Generally, where two or more measurements of ϕ_{min} have been made for the same system, the agreement between the different measurements is quite good. Most reported measurements quote an uncertainty of ±0.05 eV and, with a few exceptions, the recent measurements, agree within ± 0.1 eV. However, wider differences, as large as 0.3 eV, are found in the recorded values for ϕ_{equil}, even when the recorded values for ϕ_{min} agree. For Cs on W surfaces the sticking probability at room temperature is found to be zero after the first monolayer is formed,[43] and so the work function ceases to change in the presence of more adsorbate atoms, yielding the value ϕ_{equil}. The value for ϕ_{equil} is generally not the same as that reported for the bulk material, probably because in this layer the Cs atoms are arranged in a different manner than in the bulk.[33]

When the target is cooled to 77K, a second layer can form. In this case the value for ϕ_{equil} is that of the work function of the bulk material.[38] It has been reported that a second layer of Na can form on W, even at room temperature, although the sticking probability is low.[44]

The alkali metal coverage can be defined in several ways. Some authors quote the adsorbate atom surface density, others define the coverage in terms of the fractional monolayer coverage in one of two ways - 1) $\theta_a = N_a/N_{equil}$, where N_a and N_{equil} are the number of adsorbate atoms per unit area at any particular coverage and for monolayer adsorbate coverage respectively 2) $\theta_a = N_a/N_s$ where N_a and N_s are the number of atoms per unit of the absorbate and the first layer of the substrate respectively. The latter definition will be used herein.

Substrate	ϕ_{min} eV	ϕ_{equil} eV	Reference
Cesium			
Cu (100)	1.65	2.07	32
Cu (111)	1.60	2.00	33
Mo (110)	1.60	2.10	34
Ni (100)	1.60	2.00	35
Ta (110)	1.76	2.00	36
W (100)	1.6	1.78	37
W (110)	1.45	2.15	38
W (111)	1.57	1.80	39
W (112)	1.57	1.85	39
Re (10$\bar{1}$1)	1.48		40
Re (2$\bar{1}$10)	1.55		40
Re (2$\bar{1}$11)	1.60		40
Re (2$\bar{1}$12)	1.53		40
Sodium			
Ni (100)	2.02		41
Ta (110)	2.29	2.46	36
W (100)	2.32		31
W (110)	2.0		31
W (111)	2.4		31
W (112)	2.6		31
Re (10$\bar{1}$1)	2.2		31
Re (1120)	2.51		31
Re (1$\bar{1}$12)	2.40		31
Re (11$\bar{2}$2)	2.36		31
Potassium			
Mo (110)	1.70	2.5	28
Mo (112)	1.98	2.25	28
Mo (100)	1.85	2.2	28
Mo (111)	1.98	2.4	28
Ni (100)	1.62		41
Ta (110)	1.92	2.26	36
Ta (011)	1.71	2.6	29
Ta (112)	2.02	2.3	29
Ta (100)	2.02	2.3	29
Ta (111)	1.93	2.2	29

Table IV. Minimum and equilibrium work functions values for cesium, sodium and potassium coverage of single crystal faces.

It is generally agreed that the minimum value for the work function occurs at partial monolayer coverage of the substrate. The onset of the equilibrium work function value occurs when an ordered monolayer of the adsorbate has been reached. Representative values for θ_{min} and θ_{equil} respectively are, for Cs/W (100) 0.25, 0.43;[45] Cs/W (110) 0.23, 0.6;[38,46] Cs/W (112) 0.5, 0.75,[47] Cs/Cu (111) 0.14, 0.25.[33] Adsorbate atom surface densities at the minimum and equilibrium work function have been reported for Cs, K and Na on Ta (110) and W (100)[36] and K on W, Ta and Mo.[28,29]

3. The effect of impurity species.

The presence of impurities, both initially on the substrate and subsequently deposited during or after alkali metal evaporation, has been the subject of several investigations. The general effects of adsorption onto surfaces with H_2 and O_2 present are -1) A lowering of the minimum work function value and the alkali metal coverage at which this value occurs 2) An increase in the density of the equilibrium alkali metal layer and a corresponding increase (eg. (Cs/W(100[38])) or decrease (eg. Cs/Cu (100[37])) in ϕ_{equil}.

The cesium - oxygen - tungsten combination has been widely studied in the hope of producing work functions of around 1 eV.

Work functions of this value have been reported for Cs on oxygenated W (110).[38] While the problems of O^- contamination probably preclude the use of such surfaces in negative hydrogen ion sources, it is interesting to note that when cesium is adsorbed on hydrogen covered W (100), θ_{min} is reduced to a value of 1.42 eV.[45]

While most investigators detail the process by which carbon contaminants are removed from the substrate material, the author has been unable to find a quantitative description of the effect of carbon contamination on the work function of alkali metal covered metal substrates.

4. Conclusion

At present negative hydrogen ion sources are generally operated with polycrystalline Mo cathodes with cesium added to the hydrogen discharge. If, as is suggested, these sources operate under conditions of optimum Cs coverage, and the bombardment of the cathode by plasma particles ensures clean surfaces, then the cathode work function would be between 1.54 and 1.6. eV. However, it is possible the cathode operates with some hydrogen, oxygen or carbon coverage, in which case the cathode work function could be substantially different.

Present measurements suggest that a change to a different alkali metal would not produce a lower work function. However, a change to a different polycrystalline cathode material e.g. Ni or Re, or to a single crystal cathode e.g. W (110), could lead to a reduction in the cathode work function, provided the plasma condition and cathode temperature can be adjusted to provide an optimum coverage on these materials.

Whether such work function changes will substantially change the negative ion yield from the surface, requires further experimental investigation of sputtering and backscattering processes from surfaces with known and reproducible work functions.

PRODUCTION OF SURFACES

The requirements to produce a clean and reproducible alkali metal covered surface are a clean substrate and a method for applying the alkali metal which is free from impurities. Surface diagnostic techniques are required to check if these conditions are met. In a backscattering experiment, at present under construction, it is proposed to incorporate a work function measuring system and secondary ion mass and energy analysis. Experiments are underway to determine if these diagnostics are sufficient to ensure that known surfaces are reproduced. This will be accomplished by comparing measurements made using these techniques with the results of Auger Electron Spectroscopy (AES) and X-ray Photoelectron Spectroscopy (XPS) measurements.

As discussed earlier, it is known that the work function of alkali metal covered surfaces is sensitive to small concentrations of impurities. The work function change with alkali metal coverage has also been measured for several adsorbate/substrate combinations. It would therefore appear that an absolute measurement of work function, combined with a mass analysis of sputtered particles, could provide the necessary information about surface conditions. Measurements have started to confirm this for the various substrate/alkali metal combination to be used in the backscattering experiments.

There are several work function measuring techniques,[6] the photoemission technique has been chosen for the present experiment since the ion and light beam can be coincident on the surface, hence

measuring the work function at the point of ion impact. The alkali metals are evaporated onto the surface using a Cs getter.[4,8] The substrate is cleaned by heating, in an oxygen environment to remove carbon impurities and then in U.H.V. to remove oxygen. These components are mounted in a U.H.V. vacuum chamber with A.E.S. or X.P.S. facilities.

The present experimental work has so far been concerned with the production of clean substrates, initially polycrystalline Mo. The major problem in this case is, that after the apparent removal of carbon in successive oxygen cycles, subsequent heating to remove O_2, unless carefully controlled, will result in more carbon segregating to the surface.

If these impurities persist after the oxygen cycling the measured work function is found to be 4.3 ± 0.1 eV. While this is in accord with earlier polycrystalline Mo measurements, a measurement by Eastman,[9] in which Mo was evaporated onto a clean substrate, yields a higher value of 4.6 eV.

Evaporation of Cs and Na onto these surfaces also showed a markedly different behaviour than that reported for clean substrates. With the work function not going through a minimum and saturating at a value of about 2.5 eV. As the amount of carbon and oxygen on the surface changed, as monitored by the A.E.S. intensities, changes in the measured work function were observed.

These initial results indicate that careful preparation of surfaces is required if they are to be reproducible. However, work function measurements can be used to indicate the presence of impurities, if a particular system is first studied using A.E.S. or X.P.S. Considering the marked work function changes associated with small amounts of impurity it would seem desirable to study the surface condition in present day ion sources.

ACKNOWLEDGEMENTS

This work is supported by the New University of Ulster. The author is grateful to the members of the Surface Studies group of the University for their assistance and advice.

References

1. Yu. I. Belchenko, G.I. Dimov and V.G. Dudnikov, Izu. Akad. Nauk. SSSR Ser. Fiz., 37, 2573 (1973).

2. M.L. Yu, Phys. Rev. Lett. 40, 574 (1978).

3. P.J. Schneider, K.H. Berkner, W.G. Graham, R.V. Pyle and J.W. Stearns, Submitted to Phys Rev. B.

4. Proc. of the Symposium on Production and Neutralization of Negative Hydrogen Ions and Beams, Brookhaven (1977).

5. Yu. I. Belchenko, G.I. Dimov and V.G. Dudnikov Pages 79-96 in Ref. 4.

6. J.C. Riviere, in Solid State Surface Science, edited by M. Green (Dekker, New York, 1969), Vol. 1.

7. H.B. Michaelson, J. Appl. Phys. 48, 4729 (1977).

8. J. van Laar and J.J. Scheer, Philips Res. Rep. 15, 1 (1960).

9. D.E. Eastman, Phys. Rev. B2, 1 (1970).

10. R.G. Wilson, J. Appl. Phys. 37, 3170 (1966).

11. B.J. Hopkins and J.C. Riviere, Phys. Proc. Soc. (London) 81, 590 (1963).

12. G.A. Boutry and H. Dormont, Philips Tech. Rev. 30, 225 (1969).

13. Th. G. J. van Oirschot, M. van den Brink, and W.H.M. Sachtler, Surf. Sci. 29, 189 (1972).

14. A.P. Ovchinnikov and B.M. Tsarev, Soc. Phys. - Solid State 9, 2766 (1968).

15. R.J. Whitefield and J.J. Brady, Phys. Rev. Lett. 26, 380 (1971).

16. V.B. Lazarev and Yu. I. Malov, Fiz. Met. Metalloved. 24, 565 (1967).

17. R.H.Williams and J.I. Polanco, J. Phys. C7, 2745 (1974).

18. J.C. Tracy and J.M. Blakely, Surf. Sci. 13, 313 (1969).

19. P.O. Gartland, Phys. Norv. 6, 201 (1974).

20. S. Berge, P.O. Gartland and B.J. Slagsvold, Surf. Sci. 43, 275 (1974).

21. R.P. Leblanc, B.C. Vanbrugghe and F.E. Girouard, Can. J. Phys. 52, 1589 (1974).

22. B.G. Baker, B.B. Johnson and G.L.C. Maire, Surf. Sci. 24, 572 (1971).

23. R.W. Strayer, W. Mackie and L.W. Swanson, Surf. Sci. 34, 225 (1973).

24. J.E. Demuth, Chem. Phys. Lett. 45, 12 (1977).

25. L.W. Swanson and R.W. Strayer, J. Chem. Phys. 48, 2421 (1960).

26. R.G. Wilson, J. Appl. Phys. 37, 3161 (1966).

27. R.G. Wilson, J. Appl. Phys. 37, 4125 (1966).

28. M. Blaszczyszyn, Surf. Sci. 59, 533 (1976).

29. R. Blaszczyszyn, M. Blaszczyszyn and R. Meclewski, Surf. Sci. 51, 396 (1975).

30. A.P. Ovchinnokov and B.M. Tsarev Sov. Phys. Solid State 9, 2766 (1968).

31. A.P. Ovchinnikov and B.M. Tsarev Sov. Phys. Solid State 9, 1519 (1968).

32. C.A. Papageorgopoulos, Solid State Commun, 27, 1069 (1978).

33. S.A. Lindgren and L. Wallden, Solid State commun. 25, 13 (1978).

34. E.V. Klimenko and A.G. Naumovets Sov. Phys. Tech. Phys. 24, 710 (1979).

35. C.A. Papageorgopoulos and J.M. Chen. Surf. Sci. 52, 40 (1975).

36. D.L. Fehrs and R.E. Stickney. Surf. Sci. 24, 309 (1971).

37. J.M. Chen and C.A. Papageorgopoulos, Solid State Commun. 11, 999 (1972).

38. J.L. Desplat and C.A. Papageorgopoulos, Surf. Sci. 92, 97 (1980).

39. A.P. Ovchinnikov and B.M. Tsarev Sov. Phys. Solid State 8, 1187 (1966).

40. A.P. Ovchinnikov Sov. Phys Solid State 9, 1508 (1968).

41. S. Anderson and U. Jostell Surf. Sci. 46, 625 (1974).

42. N.D. Lang, Phys. Rev. B4, 4234 (1971).

43. L.D. Schmidt, J. Vac. Sci. Tech. 9, 882 (1972).

44. J.M. Chen and C.A. Papageorgopoulos Surf. Sci. 21, 377 (1970).

45. C.A. Papageorgopoulos and J.M. Chen. Surf. Sci. 39, 283 (1973).

46. A.G. Federus and A.G. Naumovet Surf. Sci. 21, 426 (1970).

47. C.A. Papageorgopoulos and J.M. Chen J. Vac. Sci. Tech. 9, 570 (1971).

48. S.A.E.S. Getters, Milan, Italy.

DISCUSSION

EHLERS When you say that impurities affect the work function, you really can not say in which direction however, is that correct?

GRAHAM Well, it looked as if in my case, it lowered the substrate work function, but I could not get to this minimum value, which is a characteristic problem that I had before. I was sort of relieved that I saw it again to some extent. Now we are hoping to start a systematic study of this for surfaces that are particularly of interest to ion source people.

HISKES Some of the light mass impurities would tend to reduce the reflectivity of the surface too.

MEYER You made a comment about the equilibrium work function and the bulk work function not being the same under certain conditions. Could you elaborate on this?

GRAHAM I thought I was elaborating on that. I will take the example of cesium, which is probably the easiest for me to explain. If you get to that equilibrium value then you probably have a mono-

layer coverage of cesium on the surface. If you look at the work function value that people generally measure you get a value of something like ..8. Apparently the reason that that is not the bulk value is because, first of all, you have only one monolayer there. If you have got more than one monolayer then you would probably start to see the bulk material. But, when there is only one monolayer the spacing between the hydrogen atoms is different when it is sort of confined by the surface rather than sort of free in the bulk. I gather that is the general idea.

CRANDALL It seems that part of your point is that very subtle things can happen to work functions. For instance by making Ca^+ in 1971, we had a rhenium surface spot welded to a bulk tungsten surface and suddenly the source started working much better. We got a lot of Ca^+ data and then we found out, when we took the source apart, that the rhenium had fallen off, so we were using bulk tungsten. Well, we liked that, so we put the source back together and we never saw another ion. We have to find out some of these subleties about heating and oxygen atmospheres to produce the right surface. Those changes are pretty subtle and really waste a lot of time in your laboratory. At that time we did not know anything about these things, and the kind of work you are doing should be useful for people who really try to design and build ion sources.

GRAHAM I am planning to go to single crystals because I think it is so complicated to do anything with the polycrystals. I think all these phenomena can really affect results. It is easier to start with single crystals and then find out the problems afterwards about the polycrystals.

BACAL We also had all these problems when studying absorption of oxygen and cesium on tungsten, ten years ago. We dealt with a single crystal and the single crystal was really clean. We understood we had this absorption of cesium but it did not allow oxygen to absorb on the surface before carbon was removed. So we have to clean the surface by heating in order to remove the oxygen. The important point is however that this carbon does not originate probably from the sample, but from the stainless steel of the vessel. When you heat again the sample to remove the oxygen you somehow heat the walls and the problem comes back. So everybody should take care of that in his own way and just try to avoid the stainless steel when you do not want carbon on the surface.

GRAHAM I think I agree with Martha. My conclusion was that it was not in fact segregating from under the bulk after a while, it was coming from some other source. But, I think it makes one very weary of people who report atomically clean surfaces, who have not in fact done some sort of analysis on that surface to begin with, but have used a recipe they find published somewhere.

HUFFMAN I guess my first comment is that I wished I had given my paper after yours instead of before. The second is that we have had similar results with tungsten as far as getting the carbon out, and I agree completely with your last comment. Unless people have done Auger spectroscopy on the surface and at the same time doing their work function measurement, you really do not know what has been measured. I want to reinforce another point that you made earlier in regard to large areas with preferred orientation. We chemically vapor deposit from tungsten floride and you can then grind that surface and get preferred tungsten (100) or electro-edged that surface to get preferred (110). You can also deposit tungsten-hexachloride and grind it off and get preferred tungsten (110) and you can do this on curved surfaces also.

CRANDALL Some other people at Oak Ridge have told me recently that you never get tungsten free of carbon. That all commercial tungsten that you buy in bulk form will have carbon in it from the way it is made. They have tried and tried and never got rid of the carbon. The only way you can get tungsten free carbon is to vapor deposit it.

OETTINGER This question of carbon, I would like to ask you why you do not think it came from the bulk?

GRAHAM Well, I think, just because after several heat treatments, we could see that we sort of reached an equilibrium value as I mentioned before and you know as we kept cycling we would get the oxygen-carbon combination coming and going back. The carbon peak or intensity seemed to reach an equilibrium value after a while and I thought that perhaps that was due to the fact that we got everything out of the bulk and that there was a second constant source of carbon coming from somewhere else. Maybe that was a misinterpretation.

OETTINGER I think it could very well be continually coming from the bulk and you might want to consider using very thin foil targets and heating them for long periods of time to get the carbon out.

GRAHAM Well it actually were thin foils. But it could be that my patience gave right up after a while. You know I had to meet a deadline for my paper so you understand. I hope to get all these problems ironed out in the near future.

THIS PAGE

WAS INTENTIONALLY

LEFT BLANK

SURFACE CONVERSION SOURCES

THIS PAGE

WAS INTENTIONALLY

LEFT BLANK

SOME EFFECTS OF SURFACE-PLASMA MECHANISM FOR PRODUCTION OF NEGATIVE IONS*

V. G. Dudnikov
Institute of Nuclear Physics
Novosibirsk, USSR

Abstract

The effects attributable to production of negative ions via the surface-plasma mechanism are analyzed and their use in the production of negative ion beams and accelerated atoms is discussed.

I. Introduction

To determine the mechanism for enhanced production of negative ions as a result of addition of cesium to the discharge chamber of an ion source,[1] special experiments were carried out,[2,3] which made it possible to formulate basic concepts about the surface-plasma mechanism for production of negative ions. The hypothesis of the dominating role of surface-plasma mechanism for production of negative ions in discharges due to addition of cesium, which was developed on the basis of initial investigation of the enhanced emission of negative ions, contradicted in many ways the established ideas about the relative role of known elementary processes of negative ion production. At that time, the ambiguous information on the parameters of the discharge plasma in ion sources made it very difficult to uniquely explain the observed effects.

In the subsequent experiments, the surface-plasma mechanism for negative ion production has been verified experimentally and satisfactorily described theoretically.[3-5] In many cases, however, clearly manifested effects of surface-plasma mechanism are strongly masked by other effects, especially by a highly effective destruction of negative ions in a dense plasma. In complicated situations, which are most typical, an identification of the mechanisms for negative ion production and selection of methods for their optimization are difficult. This problem was discussed at the first Symposium on production and neutralization of negative hydrogen ion beams.

In view of this, we consider it appropriate to analyze the past and current experiments in which the surface-plasma mechanism for negative ion production can be clearly identified.

II. Main Features of the Surface-Plasma Mechanism for Negative Ion Production

The general diagram of the surface-plasma mechanism for negative ion production is shown in Fig. 1. The positive hydrogen and cesium ions are produced in the discharge plasma, after introducing into it a working material (hydrogen) with an addition of cesium. The produced ions, which are accelerated by electric fields in the plasma or in the layers adjacent to the electrode, appear on the surface of the emitter electrode as fast ions or neutral particles. As a result of momentum exchange between the incident particles and the particles in the condensed phase a flux of sputtered and reflected particles is leaving the surface with high velocities. If the work function ϕ of the surface, which is reduced due to adsorption of cesium, does not exceed by much the electron affinity S of the sputtered and reflected particles, then it is very likely that these particles will go beyond the surface potential barrier as negative ions after capturing the emitter electrons in the electron-affinity levels. A strong electric field, which accelerates the negative ions from the surface to the ion beam forming and accelerating system, is usually produced near the emitter surface.

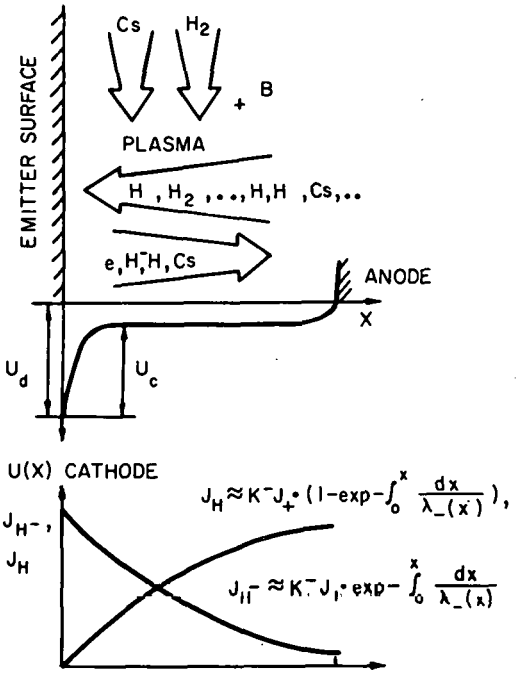

Fig. 1. General diagram of the surface-plasma mechanism for production of negative ions in a gas discharge.

However, since the negative ions are rapidly destroyed as a result of passing through the plasma and gas, the majority of accelerated negative ions will not lose an electron to become an accelerate atom only when the layer of plasma and gas between the emitter and the beam-forming system is very thin. The flux of accelerated atoms in turn can again be converted to negative ions as a result of bombardment of the elements of the beam-forming system, if their work function can be reduced due

* Translated by S.J. Amoretty, TID, Brookhaven National Laboratory.

to cesium adsorption.

The mentioned processes were analyzed in detail in the review articles.[3-5] Under optimized conditions the effective coefficient of secondary emission of negative ions is $K^- \approx 0.3$–0.8 H^- ions per incident ion with an energy of $\sim 10^2$ eV. The effective cross section for the destruction of H^- ions with an energy of $\sim 10^2$ eV in a plasma is $2 \times 10^{-14} \lesssim \sigma_d \lesssim 7 \times 10^{-14}$ cm^2, the cross section of resonant charge exchange is $\sigma_r \approx 7 \times 10^{-15}$ cm^2, and the cross section for the destruction in molecular hydrogen is $\sim 10^{-15}$ cm^2. These initial data allow us to estimate the attainable production efficiency of negative ions and the permissible thickness of the gas and plasma layers through which they can be transmitted.

III. Investigation of Surface-Plasma Mechanism for Negative Ion Production in Discharges with a Planotron and Penning Electrode Configuration

1. An efficient production of negative ions via the surface-plasma mechanism was achieved for the first time in discharges with a planotron electrode configuration.[1]

The schematic of the source is shown in Fig. 2. A discharge chamber shaped like a plane magnetron-planotron was filled with hydrogen to a pressure of ~ 5.0 Pa through a pulsed electromagnetic valve 4. A high current glow discharge was ignited in a narrow (~ 1 mm) gap between the flat central cathode plate 10 and the square anode window surrounding it. The magnetic field ($B \sim 0.1$ T) produced by the poles 1 prevented the direct drift of electrons from the cathode to the anode 3 before interactions with the gas in the chamber have ocurred. The discharge gap was limited by cathode side shields II, which prevented the electron drift to the anode along the magnetic field lines. This arrangement made it possible to hold the fast electrons in the discharge gap until they would spend most of their energy on ionization. The produced positive ions were accelerated in the region of the cathode potential fall U_c (see Fig. 1) and bombarded the cathode while maintaining the discharge via secondary electron emission from the cathode. The cathodes made from refractory metals (molybdenum, tungsten, tantalum), which were cleaned and conditioned by arc discharges, produced steady 400 to 500 V glow discharges up to arc currents of ≈ 100 A (the cathode area was $S_c \approx 2$ cm^2, the pulse duration was ~ 1 msec). The negative ion beam 9 was extracted through 0.5 mm x 10 mm emission slit 7 oriented at normally to the magnetic field by the extraction voltage of up to 20 kV; this voltage was applied between the insulated body of the discharge chamber 3 and grounded plates of the extracting electrode 14. The beam current was measured by the collector 8. A reduction of the length of the emission slit along the magnetic field greatly reduced the yield of the accompanying electrons. To eliminate the discharges caused by oscillating electrons in the extraction gap, a curved magnetic field was formed by the pole tips 1. Its effect was to rapidly remove the electrons along the magnetic field lines and dump them on the magnet poles or on a special electron collector.

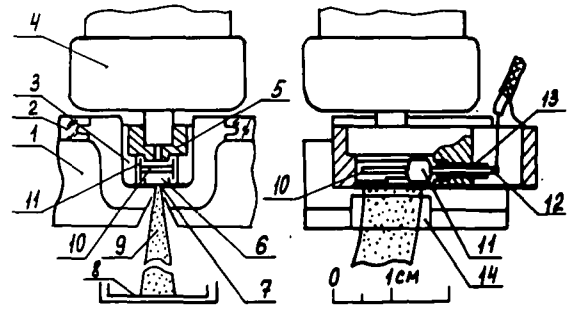

Fig. 2 Schematic of a negative ion source with a planotron geometry of the discharge chamber. 1, magnet poles; 2, high voltage insulators; 3, body of the discharge chamber (anode); 4, pulsed hydrogen supply valve; 5, anode insert; 6, equipotential slot; 7, emission slit; 8, beam collector; 9, negative ion beam; 10, central cathode plate; 11, cathode side shields; 12, cathode holders; 13, cathode insulators.

The described experimental setup was used as a prototype for many modifications of the surface-plasma sources.

In 1971, these sources with discharges in pure hydrogen were used to obtain beams of negative hydrogen ions with an emission current density j_e^- up to 250 mA/cm^2, which exceeded several fold the emission current density of other plasma sources, but was consistent with the limiting possibilities of the dominant mechanisms for production of negative ions in a discharge plasma.[7]

2. It was concluded in July 1971 that the emission of negative ions can be greatly increased by adding a small amount of cesium into the discharge chamber of such a source. In initial experiments, tablets were prepared by pressing a mixture of cesium chromate with titanium; they were put in the anode or placed in a cavity in the central cathode plate. The mixture was heated by the discharge in hydrogen to reach the temperature for the release of cesium, and cesium vapors were injected into the discharge chamber. The glow discharge voltage in this case was reduced from 400-500 V to 100-150 V, and the intensity of the extracted beam of H^- ions increased by several factors.

By optimizing the configuration of the electrodes and their geometric dimensions and the supply of hydrogen and cesium vapors, we were able to increase the emission current density of H^- ions from discharge chambers (Fig. 2) with molybdenum cathodes to 1.5 A/cm^2. The beam intensity increased proportionally to the area of the emission slit, from 75 mA for a 0.5 mm x 10 mm slit to 230 mA for a 1.5 mm x 10 mm slit.

3. The estimates showed that those elementary processes known at the time for production of negative ions in a discharge plasma via the interaction of electrons with hydrogen molecules,[7] which were considered the most efficient, can produce a much smaller emission current density of H^- ions even under most favorable conditions.

Thus, a search began for a new, efficient mechanism,not considered earlier, for production of negative ions in a gas discharge.

The experience obtained from studies of the source showed that the density of cesium in a discharge is fairly small, so that volume processes with cesium cannot appreciably affect the net production efficiency of negative ions. A large reduction of the discharge voltage as a result of introduction of cesium into the cell uniquely shows that the emission properties of the cathode change significantly. The intensity and composition of the produced beams depended on the cathode material: the best results were obtained by using cathodes made from pure molybdenum; tungsten and tantalum cathodes produced large impurities of heavy negative ions, primarily oxygen.

4. The most attractive hypothesis attributed the increase in intensity of H^- ion beams to an increase of the coefficient of secondary emission of negative ions at the cathode as a result of decreasing its work function due to cesium adsorption.

The most convincing confirmation of this hypothesis was obtained by studying the energy spectra of negative ions extracted from these sources.[2]

A system for measuring the energy spectra is shown in Fig. 3. The beams of H^- ions, which were extracted from the planotron and accelerated by the extraction voltage U_0 up to an energy eU_0, were separated from the heavier ions in the magnetic field of the source and analyzed by the electric field of the plane condenser 10. The negative ions were injected into the condenser at an angle of 45° with respect to the electrostatic field lines. The ions rotated 90° and were recorded either by the collector 11 or by a secondary electron multiplier. The 0.05 mm width of the analyzing condenser slits with a 20 cm spacing between them corresponded to a resolution of ~ 5 eV for $eU_0 = 10$ keV. The extraction voltage and the analyzing voltage of the condenser were stabilized with a relative accuracy of $\sim 10^{-4}$ and accurately measured by digital voltmeters.

The characteristic energy distribution of H^- ions is illustrated in Fig. 4, which also shows oscilloscope traces obtained from the collector 11 by modulating the analyzing voltage with a sawtooth voltage. The energy scale was determined form the shift of the spectra produced by slightly varying the extraction voltage.

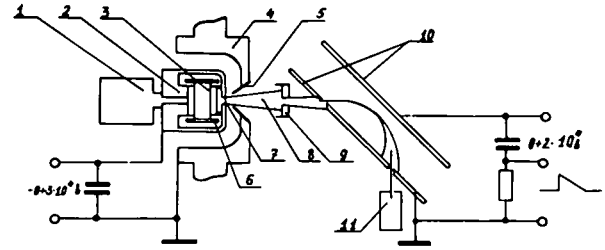

Fig. 3 A device for recording the energy spectra of negative ions. 1, Pulsed valve; 2, body of the discharge chamber (anode); 3, central cathode plate; 4, magnet poles; 5, extractor plates; 6, cathode side shields; 7, emission slit; 8, negative ion beam; 9, beam collector; 10, analyzing condenser; 11, analyzer collector.

The ion spectra from a planotron usually have two peaks separated by a valley. The location of the first peak coincides with the accuracy of the measurement (±10 eV) with the energy eU_0 imparted to the negative ions by the extraction voltage. The ion energy of the second peak is higher than that of the first peak by an amount close to eU_d. The oscillograms in the upper part of Fig. 4 illustrate the change in the spectrum as a result of increasing the discharge voltage U_d from 120 V (1) to 210 V (4) by reducing the cesium supply.

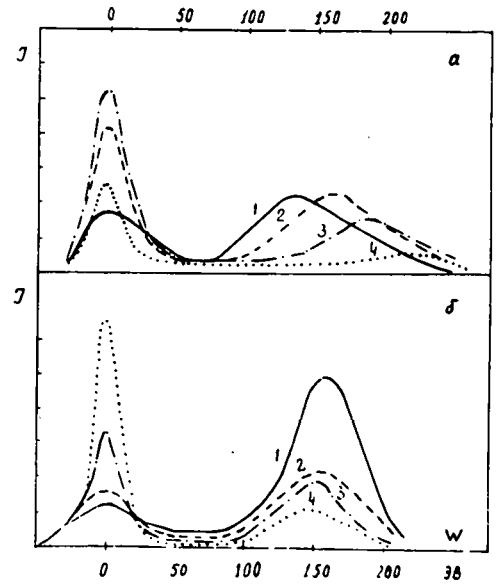

Fig. 4 Energy spectra of H^- ion beams from hydrogen-cesium discharges in a planotron (discharges with noise): upper part, for different discharge voltages: 1, 120 V; 2, 150 V; 3, 160 V; 4, 210 V. Lower part, for different hydrogen supplies (molecules per pulse): 1, 10^{16}; 2, 1.2×10^{16}; 3, 1.7×10^{16}; 4, 2.2×10^{16}.

The oscillograms (1-4) in the lower part of Fig. 4 illustrate how the spectra vary as a result of increasing the hydrogen supply to the discharge chamber. When the hydrogen supply is the lowest and the cesium supply is optimum, a large fraction of ions from planotron discharges will be accelerated by the full discharge voltage, but the amplitude of the peak with the higher energy will rapidly decrease with increasing hydrogen supply and the amplitude of the first peak will increase.

5. On the basis of the observed characteristics, we have concluded that the main mechanism for primary production of negative ions in the conditions we consider, is their emission from the central plate of the planotron cathode. The negative ions are emitted from the central cathode plate, are accelerated by the cathode potential, pass through a thin layer of gas and plasma to the emission slit, and are extracted by the extraction voltage. The energy of a substantial fraction of ions is higher than the sum of energies $e(U_o + U_d)$ imparted by the extraction and discharge voltages, because the cathode emits fast negative ions; they are produced as a result of electron capture at the level of electron affinity by sputtered and reflected particles which have conserved a substantial fraction of the initial energy. A very intense flux of sputtered and reflected particles can be produced by adsorption of atomic hydrogen from the discharge, by intense bombardment of the cathode by positive ions from the discharge plasma which have been accelerated to an energy eU_c in the potential fall at the cathode, and by fast, secondary atoms produced as a result of neutralization of accelerated ions on surfaces and in the volume. A large increase of the negative ion emission due to addition of cesium may be attributed to a higher probability of sputtered and reflected particles to leave the cathode in the form of negative ions as a result of reduction of the cathode work function because of cesium adsorption.

6. The production mechanism of slower ions in the first peak required further discussion. The slow H^- ions can be produced as a result of collisions of electrons with hydrogen molecules in a plasma. Until recently, the emission current densities of H^- ions, which can be obtained from plasma sources under optimum conditions, greatly exceeded the rated current densities, calculated with allowance for the known reaction rates for creation and destruction of negative ions in a plasma.[7]

The new data for the cross sections for production of H^- ions in the interaction of electrons with vibrationally excited hydrogen molecules, which were given in Hiskes's review article,[5] would make it possible to reconcile the calculated production rates of H^- ions with those observed experimentally. However, even under optimum conditions the maximum current density of H^- ions from plasma sources ($j_e^- \sim 0.1$ A/cm^2) is an order of magnitude smaller than that obtained from a discharge in a planotron. Moreover, the conditions in the discharges we studied are not optimal for H^- ion production via volume processes. In order to reach the region of the emission slit, hydrogen gas has to pass through a discharge gap filled with a dense plasma and is almost completely dissociated. As the direct measurements of gas flow from a planotron have shown,[8] the hydrogen is vigorously pushed out of the plasma after the ignition of the discharge, so that the minimum hydrogen density in front of the emission slit decreases to $n_H \simeq 2 \times 10^{14}$ cm^{-3}.

The collisions of electrons with hydrogen molecules account for only a very small fraction of the ion flux of the first peak. This is confirmed indirectly by an almost monotonic decrease in intensity of the extracted H^- ion beam as a result of increasing the hydrogen supply, whereas the beam intensity from plasma sources is the highest at higher pressures.

7. The maximum cross section for production of H^- ions due to collisions of hydrogen atoms with cesium atoms, according to the data of Ref. 21, does not exceed $\sim 10^{-15}$ cm^2; hence, this process can play a key role only at a very high density of cesium. However, the probability for production of H^- ions in the collision with the excited cesium atoms may be much higher.

However, in the discharges under consideration, cesium is very effectively trapped in regions around[9,10] the cathode so that the concentration of neutral cesium in the discharge plasma is very small ($n_{Cs} \sim 10^{12}$ cm^{-3}). Therefore, the charge exchange of hydrogen atoms by cesium atoms cannot play an important role in the generation of negative ions.

8. The production of "slow" ions of the first peak can be more adequately explained by a resonant charge exchange of H^- ions of the second peak in atomic hydrogen occuring in the equipotential cavity 6 in front of the emission slit (see Fig. 2). Since the cross section for resonance charge exchange is $\sigma_r = 7 \times 10^{-15}$ cm^2 for an H^- ion energy of about 100 eV, a 2 mm deep cavity and a minimum hydrogen density of 2×10^{14} cm^{-3} correspond to a charge exchange probability of $\sim$30%, roughly consistent with the oscillograms 1 in Fig. 4. A further increase of hydrogen supply rapidly increases the probability of charge exchange to 100%. This process also accounts for the redistribution of the intensities of the peaks on the oscillograms in the upper part of Fig. 4 (the minimum hydrogen density for a stable discharge increases as the cesium supply decreases). The intensity of the second peak in the discharges without cesium is a factor of 10^1 smaller than that of the first peak for a minimum hydrogen supply and minimum discharge currents; the second peak vanishes when these parameters increase.

9. The H^- ions accelerated by the cathode potential fall and the fast atoms produced as a result of destruction of the ions in a plasma bombard the walls of the discharge chamber near the emission slit. If the work function of these surfaces is reduced because of cesium adsorption,

then the secondary emission of H^- ions from these surfaces will contribute significantly to the intensity of the extracted beam. The H^- ions emitted from the surface with a large energy loss due to desorption and reflection will be recorded as ions of the first peak. The contribution from this process is apparently most pronounced when the cesium supply is maximum and the hydrogen supply is minimum (oscillograms 1 in Fig. 4 with an increased width of the first peak), but the resonance charge exchange begins to dominate as the hydrogen supply increases.

The energy of a large fraction of the ions of the second peak is lower than $\langle eU_d \rangle$, whereas the ions emitted from the cathode should have higher energies. It is true, however, that these spectra were obtained from discharges with large voltage fluctuations whose amplitudes are sufficiently large to justify the large width of both peaks. The H^- ions, whose energy is slightly lower, can be produced in the scattering of accelerated H^- ions and fast atoms at small angles as a result of grazing collisions with the walls of the emission slit. A contribution from this process increases with increasing wall thickness of the emission slit.

In the experiments of Bel'chenko et al.,[2] the investigators were able to clearly separate the peaks of the "fast" and "slow" particles, despite strong fluctuations of the discharge voltage. Minimization of the thickness of the plasma layer and the small wall thickness of the emission slit (0.2 mm) helped them to achieve this. As a result of a more pronounced destruction of fast ions in the plasma and an increase in the fraction of H^- ions produced due to collisions of fast particles with the walls of the emission slit, both peaks widen toward one another and may overlap, forming a broad peak that is shifted in the direction of lower energies.

Such transformed spectra were observed in an energy analysis of negative ion beams from a duoplasmatron with a hollow discharge. The characteristics of these spectra were discussed in a review article.[4]

10. The energy spectra of H^- ions extracted from the discharges with a Penning geometry of electrodes, which are obtained by removing the central cathode plate 10 (Fig. 2), have only the first, "slow" ion peak. The ion energy spectra obtained from discharges with noise are identical to low energy regions of the spectra on the oscillograms in Fig. 4. It was possible to produce in the Penning geometry discharges without fluctuations. An energy spectrum of H^- ions from such a discharge without noise is shown in Fig. 5. The location of the narrow peak corresponds to an energy imparted by the accelerated voltage. Its width is comparable with the resolution of the analyzer. The small, low energy peak is apparently attributable to the energy loss of accelerated ions in the double charge exchange process while moving between the source and the analyzing condenser.

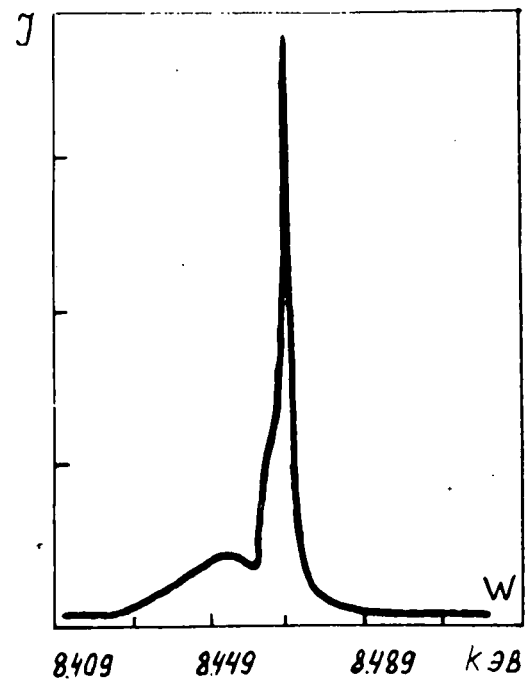

Fig. 5 Energy spectrum of an H^- ion beam from a noise-free, hydrogen-cesium discharge in a Penning source. The extraction voltage is 8.47 kV.

The fast H^- ions emitted from the cathodes of a Penning discharge cannot reach the emission slit directly. In the case under consideration, only the ions produced by the resonant charge exchange in the equipotential cavity 6 can be extracted through the emission slit. The production efficiency of negative ions can be increased due to secondary emission from the walls of the emission slit by removing the anode protrusions that shield the emission slit from the fast particles; however, the energy dispersion in this case also increases appreciably.

11. The dependence of the intensity of the obtained beams of H^- ions on the discharge current are in agreement with the examined mechanisms for production of negative ions. In planotron discharge chambers with a minimized gap between the central cathode plate and the anode,[12,13] the intensity of the extracted beam is proportional to the discharge current in the initial region. The emission current density of H^- ions is more than 10% of the cathode current density in this region, before the destruction of fast H^- ions as a result their motion through the plasma becomes more pronounced. At high discharge currents the intensity of the extracted beam continues to increase slightly. This is attributable to negative ion production at the walls of the emission slit due to bombardment by fast atoms. The initial production efficiency of negative ions is much smaller in Penning sources than in an optimized planotron, but it remains almost constant up to very high discharge currents (up to 300 A for a 0.5 cm^2

cathode area).[14,15]

IV. Surface-Plasma Mechanism for Production of Negative Ions in a Semi-planotron

The surface-plasma mechanism for production of negative ions can be used most effectively in sources with a semiplanotron geometry of the discharge chamber, reported in Ref. 16-18. The geometry of the discharge gap in a semiplanotron is shown in Fig. 6. The fast electrons can be contained only in a semicylindrical cathode located opposite the emission slit, and the electron oscillations must be carefully eliminated in the remaining parts of the gap. Negative ions can be extracted through the narrow emission slit by localizing the discharge near it and by geometrical focusing of the accelerated ions by a cylindrical cathode. The sputtering trace on the anode, due to the bombardment by negative ions from the cathode, has a width of less than 1 mm for a 3 mm wide cathode. The angular divergence of an accelerated flux of negative ions from the cathode is estimated to be ±0.2 rad. Under optimized conditions the maximum ratio of the intensity of an extracted beam to the discharge current approaches 0.1, and the energy expended for generation of negative ions in a discharge approaches 1.5 keV/ion.[18] An effective extraction of the ion flux from a wide cathode through a narrow emission slit justifies the use of multiaperture beam forming systems.

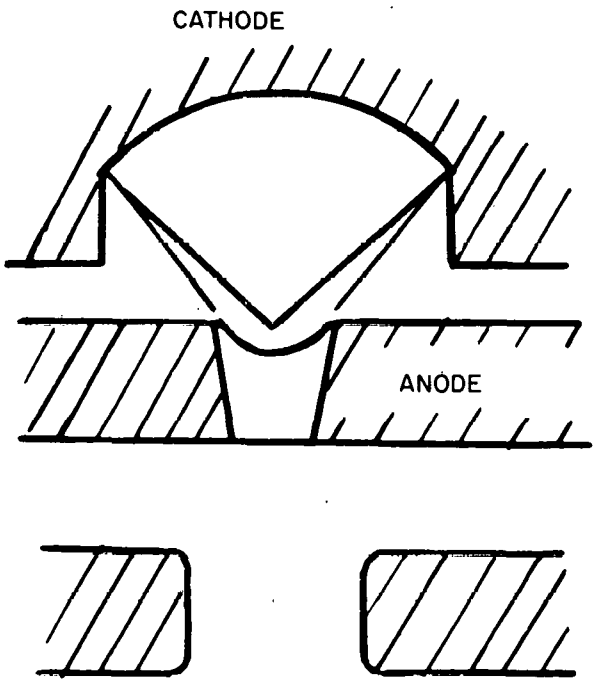

Fig. 6 Schematic of the discharge gap of a single-channel semi-planotron.

Negative ions can be produced in a semiplanotron with thick emission slit walls by bombarding with fast particles from the cathode: at large discharge currents the intensity of the beam continues to increase proportionally to the discharge current, but the proportionality factor was several times smaller than for small currents when the destruction of negative ions in the plasma is small. In some cases the dependence of the H^- beam intensity on the discharge current is N-shaped. The intense, negative ion beams can also be extracted from discharges in an inverted semiplanotron when the electrode of the discharge chamber with the emission slit is used as a cathode. But the maximum production efficiency in this case is several times smaller, and the intensity of the flux of accompanying electrons increases appreciably.

V. Surface-Plasma Mechanism for Production of Accelerated Atoms

As was noted, the accelerated atoms with an energy $E \geqslant eU_c$ can be produced as a result of destruction of negative ions accelerated by the cathode potential fall in the discharge. A direct study of the flux of accelerated atoms from a surface-plasma source was done by Dudnikov and Fiksel'.[19-20]

The flux of atoms through the emission slit of a source with a planotron geometry, which was described in Refs. 12 and 13, was recorded by a diagnostic system shown in Fig. 7. The intensity of the beam and the distribution of the current density of accelerated atoms were recorded by a secondary-emission detector and a bolometer with a heated foil. The pulsed heating of the foil by a beam of accelerated atoms was recorded from the current variation of the photodiode which monitored the foil radiation. The characteristic distribution of the current density of accelerated atoms is shown in Fig. 8. The angular divergence of the produced beam is ±0.1 rad.

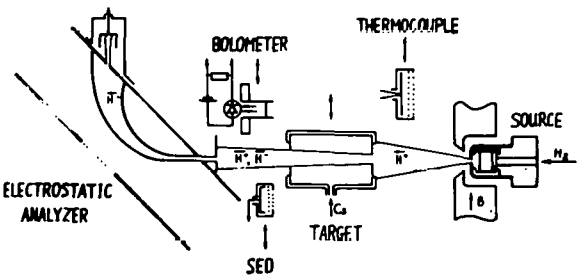

Fig. 7 A device for recording and energy analysis of a flux of accelerated hydrogen atoms from the planotron.

To measure the energy distribution of accelerated atoms, we converted them into H^- ions by using a thin, cesium vapor target (Fig. 7). The produced ions were analyzed according to their energies by using a plane condenser with a resolution of ∿ 10%. The efficiency of conversion of the atoms into H^- ions was ∿ 1%. The oscillogram in Fig. 9 illustrates the characteristic energy

spectra of accelerated atoms, which are analogous to the high-energy part of the spectrum of the oscillograms in Fig. 4. A beam of accelerated atoms with an intensity up to 3 A at an emission current density up to 3 A/cm^2 was obtained from a source with a semiplanotron geometry.

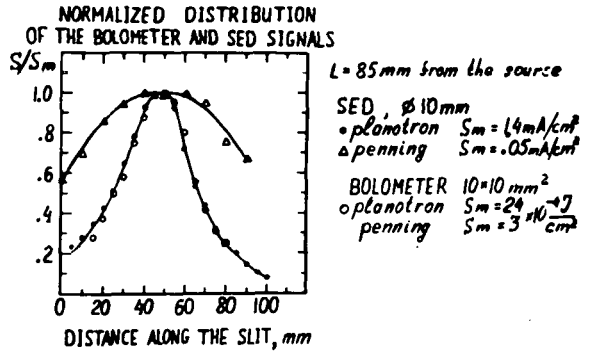

Fig. 8 One-dimensional distributions of the flux density of accelerated hydrogen atoms from the planotron and background radiation from the Penning cell.

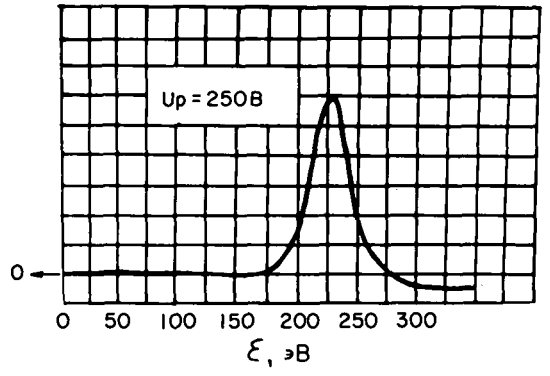

Fig. 9 Oscillogram of the energy distribution of H^- ions obtained by charge exchange of accelerated atoms from the semiplanotron on a thin cesium target.

The average energy of accelerated atoms and the relative efficiency of their production are plotted in Fig. 10 as a function of the discharge voltage which is changed by varying the cesium supply. This dependence is analogous to the dependence of the production efficiency of H^- ions on the discharge voltage as described in Ref. 3.

In these measurements the average energy of accelerated atoms turned out to be slightly smaller than $\langle eU_d \rangle$. This conclusion requires additional experimental verification, although it can be fully accounted for by the finite drop of the discharge voltage near the anode and by the strong interaction of recorded particles with the lattice walls, through which the accelerated atoms leave the discharge chamber.

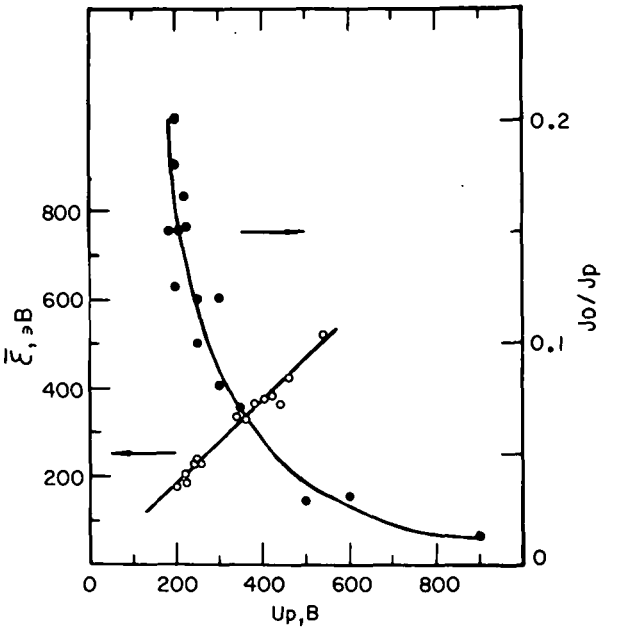

Fig. 10 Average energy of accelerated atoms and ratio of the emission flux density of accelerated atoms to the average cathode current density as a function of discharge voltage (cesium supply).

VI. Conclusion

In the described experiments the emission of negative ions from a cathode is an important effect which ensures the production of an intense flux of negative ions and accelerated atoms. Under optimized conditions more than 10% of the discharge power can be converted into the energy of negative ions from the cathode. Such a strong effect can play a large role not only in the negative ion sources but also in other cases involving bombardment of surfaces by accelerated particles.

A considerable progress in understanding the processes of negative ion production has been achieved during the last decade. However, the relative contribution of sputtering and reflection in the gneration of negative hydrogen ion beams remains uncertain. The calculated efficiency of H^- ion production due to reflection of bombarding particles is comparable with that observed experimentally in the surface-plasma sources. On the other hand, the efficiency of heavy, negative ion production as a result of sputtering in discharges in inert gases with the addition of cesium is sufficiently high. An activation of hydrogen adsorption by a discharge greatly enhances the production of H^- ions due to sputtering. However, measured spectra of accelerated hydrogen atoms generally correspond to distributions of the

normal component of the velocity of scattered particles. The width of the energy spectrum can be relatively small due to a low probability of single scattering at large angles and a high concentration of light atoms at the surface. A structure in the spectra, which could be interpreted as a narrower peak of sputtered particles, has not been observed.

References

1. Yu. I. Bel'chenko, G.I. Dimov, V.G. Dudnikov, and A.A. Ivanov, Dokl. Akad. Nauk SSSR 213, 1283 (1973). Preprint IYaF 81-72, Novosibirsk, 1972.

2. Yu. I. Bel'chenko, G.I. Dimov, and V.G. Dudnikov, Izv. Akad. Nauk SSSR, Physical series, 37, 2573). Preprint IYaF 39-73, Novosibirsk, 1973.

3. Yu. I. Bel'chenko, G.I. Dimov, and V.G. Dudnikov, Proc. Symp. Production and Neutralization of Negative Hydrogen Ions and Beams, BNL-50727, pp. 79-96, 1977.

4. K. Wiesemann, Proc. Symp. Production and Neutralization of Negative Hydrogen Ions and Beams, BNL-50727, pp. 97-104, 1977.

5. J.R. Hiskes, Journ. de Physique C7, T.40, p. C7-179-192 (1979).

6. Yu. I. Bel'chenko, G.I. Dimov, and V.G. Dudnikov, Zh. Tekh. Fiz. 43, 1720 (1973). Preprint IYaF 76-72, Novosibirsk, 1972.

7. K. Prelec and Th. Sluyters, Rev. Sci. Instrum. 44, 1451 (1973).

8. A.N. Apolonskii, Yu. I. Bel'chenko, G.I. Dimov, and V.G. Dudnikov, Pis'ma Zh. Tekh. Fiz. 6, 86 (1980). Preprint IYaF 80-17, Novosibirsk, 1980.

9. Yu. I. Bel'chenko, V.I. Davydenko, G.E. Derevyankin, A.F. Dorogov, and V.G. Dudnikov, Pis'ma Zh. Tekh. Fiz. 3, 693 (1977). Preprint IYaF 77-18, Novosibirsk, 1977.

10. P.W. Allison and H.V. Smith, IEEE Trans. Nucl. Science NS-26, N3, 4006 (1979).

11. K. Wiesemann et al., J. Appl. Phys. 48, 2668 (1977).

12. Yu. I. Bel'chenko, G.I. Dimov, and V.G. Dudnikov, Zh. Tech. Fix. 45, 68 (1975).

13. Yu. I. Bel'chenko, G.I. Dimov, and V.G. Dudnikov, Proc. Sec. Symp. on Ion Sources and Formation of Ion Beams, Berkeley, 1974 (LBL-3399) rep. VIII-1.

14. V.G. Dudnikov, Proc. IV All-Union Conf. on Charged Particle Accelerators, Moscow, Nauka, Vol. 1, p. 323, 1975.

15. G.I. Dimov, G.E. Derevyankin, and V.G. Dudnikov, IEEE Trans. Nucl. Sci., NS-24, N3, 1545 (1977).

16. Yu. I. Bel'chenko and V.G. Dudnikov, Preprint IYaF 78-95, Novosibirsk, 1978.

17. Yu. I. Bel'chenko and V.G. Dudnikov, Journ. de Physique 40, C-7, pp. 501-502 (1979).

18. Yu. I. Bel'chenko and V.G. Dudnikov, Preprint IYaF 80-34, Novosibirsk, 1980.

19. V.G. Dudnikov and G.E. Fiksel', Journ. de Physique 40, C-7, p. 479 (1979).

20. V.G. Dudnikov and G.E. Fiksel', Preprint IYaF 80-44, Novosibirsk, 1980.

21. R.E. Olson, Phys. Lett. 77A, 143 (1980).

PROGRESS IN THE DEVELOPMENT OF HIGH CURRENT, STEADY STATE H^-/D^- SOURCES AT BNL*

K. Prelec
Brookhaven National Laboratory
Upton, New York 11973

Abstract

Several recent studies have shown that negative ion based neutral beam systems may become competitive at energies as low as 50 keV/nucleon. As part of its long range program, the Neutral Beam Development Group at BNL is actively engaged in the development of an H^-/D^- ion source capable of delivering about 1 A of beam current, at an energy of several tens of keV, operating in long pulses (5-30 s; thermodynamically this corresponds to a steady state operation) and having properties that would allow a scaling up to 10 A and subsequent use in a neutral beam line. Of the two models recently designed and fabricated, a Penning and a magnetron, the latter is the more promising one and efforts will be concentrated on its studies.

I. Introduction

Three methods for negative ion production are presently under consideration:[1] volume production via several processes leading eventually to the dissociative attachment of electrons to vibrationally excited molecules ($\nu \geq 6$), double electron capture of positive ions in cesium or sodium vapors, and surface formation processes. Of these three methods, surface formation seems to be the most promising. It is the basis of several similar approaches for the development of a negative ion source, including BNL designs (Penning, magnetron) where the converter surface serves also as a cathode to maintain the discharge, LBL and ORNL designs[2,3] where the source plasma is produced independently of the converter electrode, and those where a surface is bombarded by a beam of accelerated particles.[4]

BNL sources belong to the group of surface-plasma devices - a term introduced by the Novosibirsk group, inventors of the first models. This term describes the mode of operation: in the close vicinity of the converter a plasma is established that serves as the source of charged and neutral particles to bombard the converter. If the converter surface has a work function low enough and if the energy of primary bombarding particles is in the proper range, a combination of surface - particle interactions (desorption, backscattering) will result in a substantial flux (relatively to the primary flux) of negative ions leaving the surface. Energy spectrum of negative ions when reaching the plasma is wide, up to the twice the value of the potential difference between the converter and the plasma; the width depends on the production mechanism and primary particle species and energy. Negative ions formed in this way may reach the extraction aperture directly or after exchanging charge with slow atoms;[5] in the latter case they have the energy corresponding to the atom energy spectrum.

Until about a year ago BNL sources were of the standard design,[6] without electrode cooling. Beam currents of 1A have been obtained from magnetron sources, with a pulse length of 10 ms. Yields from smaller Penning sources were lower, up to 0.5 A. Due to a rather low cathode surface utilization (< 10%), source power efficiency was not better than 0.03 A/kW; also for an H^- beam current density of 0.5 A/cm^2 in the extractor aperture, more than 1 kW/cm^2 would have to be removed from the cathode surface in a long pulse mode of operation. Gas efficiency of sources was poor, 2-3% at most. Still, at that time that was the state-of-the-art and cooling methods using nucleated boiling were contemplated.

Late 1979 there was a breakthrough in the design of magnetron sources. First, geometrical focusing of negative ions, formed on the cathode, into the extraction slits (suggested independently in Refs. 7 and 8) has been tried on the BNL Mk III magnetron source[9] and a substantial improvement in the performance observed. Second change in the design was the widening of the back side of the racetrack discharge gap;[10,11] these two new features resulted in an overall improvement by almost an order of magnitude.[9] As a consequence electrode cooling requirements for a long pulse source could be relaxed by up to a factor of ten and a source could be designed using simple water cooling. Another benefit of these changes has been an improvement in the gas efficiency,[9] alleviating problems related to high voltage breakdowns as well as to the pumping of the gas streaming out of the source. This paper will deal mostly with the background analysis of sources utilizing geometrical focussing and then describe the design of the Mk V, 1A, long pulse magnetron source. In a separate paper,[12] presented to this Symposium, future plans for plasma injection from a hollow cathode discharge into a modified version of the Mk V magnetron will be described; if successful, this design should improve the gas efficiency of the source by an order of magnitude so that even He^- and T^- sources could be considered as feasible.

II. Efficiency of H^- Sources With Geometrical Focusing

Improvements in the source performance resulting from geometrical focusing of fast, surface produced negative ions and from an asymmetric discharge chamber[9] justify some analysis of related phenomena in the source. The analysis will be done assuming that the source operates in the emission limited mode. Effects of the focusing

are either direct, due to a change in trajectories of fast primary H^- ions, or indirect, due to a change in interactions of such ions with the plasma in the source. Only one type of focusing will be considered, i.e. when cylindrical grooves are perpendicular to the magnetic field (Fig. 1).

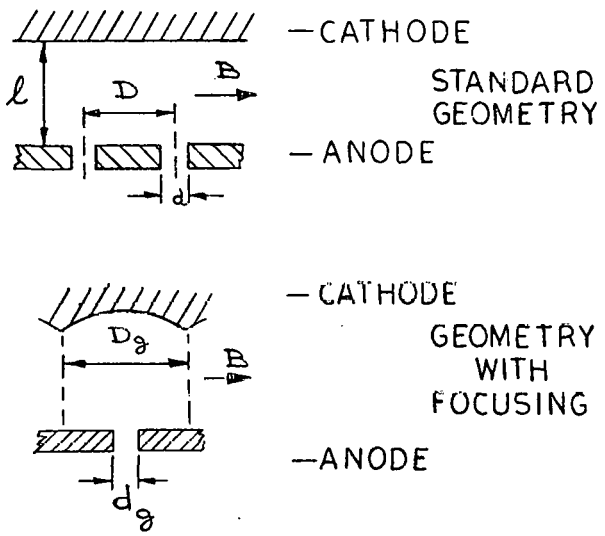

Fig. 1: Source geometry; standard and with focusing

While the focusing has been suggested quite some time ago, it has been successfully tried first on a semiplanotron type of an H^- source[13] and then on the BNL magnetron.[9] Use of cylindrical grooves, which are parallel to the magnetic field lines, has been tried as well,[9] but the source performance was a factor of two lower.

Following notations will be used in the text:

- I_c - total discharge current
- J_c - cathode current density
- I^- - total extracted H^- current
- J^- - H^- current density in the extraction slit
- j^- - average H^- current density ($j^- = \kappa J^-$)
- V_c - discharge voltage
- D,d - pitch and width, respectively, of extraction slits
- g - subscript denoting the source with focusing
- p - source neutral gas pressure
- β - utilization of the cathode surface ($0 < \beta < 1$)
- κ - transparency of the active part of the source cover (= d/D)
- ℓ - distance between the cathode surface and extraction slits
- λ - mean free path of fast H^- ions
- η - gas efficiency of the source
- η_p - power efficiency of the source

As shown in Ref. 14, if extracted H^- current density is the same in both cases, without and with focusing, then the ratio of cathode current densities should be

$$\frac{J_{cg}}{J_c} = \kappa_g \exp\left(\frac{\ell_g}{\lambda_g} - \frac{\ell}{\lambda}\right); \; J^- = J_g^- \qquad (1)$$

The geometrical factor contributing to the reduction in the required cathode current density is equal to κ_g, the transparency of the source cover, as defined above; the exponential factor is due to a different mean free path for fast ions while passing through the plasma. However, if the same average H^- current density j^- is required, which may be more relevant for a beam line, then

$$\frac{J_{cg}}{J_c} = \kappa \exp\left(\frac{\ell_g}{\lambda_g} - \frac{\ell}{\lambda}\right); \; j^- = j_g^- \qquad (2)$$

The geometry factor κ is usually larger than κ_g, implying that the reduction in J_c in the latter case will be smaller. It is evident, that in the situation described by Eq. 1 the improvement results from the focusing of particles formed over the width D_g into a slit with the width d_g, while in the other case the improvement results from a virtual opening of the source cover up to d = D.

Source power requirement $1/\eta_p$ (or the energy cost to produce an H^- ion and bring it to the edge of the extraction field) has to take into account those parts of the cathode not contributing to the beam, i.e. the cathode utilization factor β becomes relevant. In a standard magnetron source its values may at best reach 0.3 to 0.4, while in a semiplanotron type of a source[13] (with no return path for $\underline{E} \times \underline{B}$ electrons) values between 0.6 and 0.8 are possible.[13] The improvement in the source power efficiency will be[14] (assuming that the surface production efficiency remains the same)

$$\frac{\eta_{p,g}}{\eta_p} = \frac{V_c}{V_{cg}} \cdot \frac{\beta_g}{\beta} \cdot \frac{1}{\kappa} \exp\left(\ell/\lambda - \ell_g/\lambda_g\right) \qquad (3)$$

If discharge voltages V_c and V_{cg} do not differ, then the geometrical focusing will contribute to

the improvement through the factor $1/\kappa$ (virtual opening of the source cover up to d = D); additional improvement may be achieved by using the semiplanotron geometry (higher β).

Gas efficiency of the source is determined by the pressure gradient along the slit depth, gas conductance of the slit and H^- current density. Assuming that the pressure gradient is approximately equal to the source pressure p, which among others is a function of the cathode current density, and that the flux of H^- ions is small compared to the flux of neutrals, gas efficiency will be proportional to the ratio

$$\eta \propto \frac{J^-}{p(J_c)}$$

If the two systems on Fig. 1 are compared at equal extraction slit current densities ($J^- = J_g^-$), then the improvement in the gas efficiency is due only to a lower source pressure $p(J_{cg}) < p(J_c)$

$$\frac{\eta_g}{\eta} = \frac{p(J_c)}{p(J_{cg})} \quad ; \; J^- = J_g^- \tag{4}$$

However, if sources are compared so that $j^- = j_g^-$, then

$$\frac{\eta_g}{\eta} = \frac{\kappa}{\kappa_g} \cdot \frac{p(J_c)}{p(J_{cg})} \quad ; \; j^- = j_g^- \tag{5}$$

In Eq. 4 and Eq. 5, the cathode current densities are given by Eq. 1 and Eq. 2, respectively. Generally, a lower J_c requires also a lower source pressure, although the dependence is less steep than linear.

It is much more complex to consider the indirect, plasma effects in a source with focusing grooves on the cathode surface. As both, the cathode current density and the source pressure, are lower in such a source, the mean free path λ_g for the loss of a fast H^- ion will be longer due to a lower density of all plasma components (atoms, molecules, electrons, ions). However, without knowing the density and energy distributions of individual components it is not possible to do much more than estimate this contribution to the source improvement. Although it has been previously assumed that at cathode current densities of the order of 10 A/cm^2 and more the attenuation of fast ions, while travelling toward the anode, would be very pronounced so that their contribution to the extracted beam would be relatively small (the main component being slow ions originating in charge transfer collisions with atoms), semiplanotron results contradict this assumption. There, a focusing effect on fast ions has been observed at even higher cathode current densities.[13] One is lead to conclude, that in the range of operating parameters of BNL H^- sources, without and with focusing, both energy groups, fast primary and slow secondary ions, contribute significantly to the extracted beam; it is the ratio of the two that varies from case to case. This feature has also been confirmed experimentally.[15]

An estimate of the importance of various collisions along the path of a fast ion[14] has shown that under normal operating conditions dominant losses inside the source are due to collisions with atoms and molecules; part of the former will result in the formation of a slow ion. A reduction of the source pressure should therefore reduce stripping losses, favoring in this way focusing effects. Moreover, in a source geometry with focusing grooves there should be a favorable effect on slow ions as well. The production rate of slow H^- ions depends on the density of fast ions. As one approaches the anode, the density of fast ions increases due to the focusing, so that the production rate of slow ions will increase in the same way if the distribution of atoms is more or less uniform. If this is so, the energy spectra of extracted ions should show an important contribution of slow ions (see e.g., Ref. 5, 14 and 15).

There is another effect that may be important for the operation of sources with cathode grooves. Secondary electrons emitted from the cathode are focused toward the anode the same way as negative ions, but the magnetic field bends their trajectories and they drift around the cathode. If the groove is perpendicular to the magnetic field, that component of the electric field in the cathode voltage fall region, which is parallel to the magnetic field due to the cathode curvature, may act as a restoring force for electrons, resulting in slow oscillating component of the motion around the longitudinal plane of symmetry. This effect may reduce the losses of fast electrons and contribute to the improvement of the gas efficiency due to a more efficient ionization. If the groove is parallel to the magnetic field, there is no focusing effect, which may offer a partial explanation for a less favorable performance in this case.

Finally, there is the effect of a wider chamber in the back of the source. This widening has been suggested as a means to facilitate the initial breakdown of the discharge gap[10,11] as well as to sustain the discharge at a lower pressure[10] due to a longer effective electrode distance. It is, however, doubtful that this simple picture could explain the observed improvement in the source performance:[9] a cathode current density about 40% lower for the same H^- current density. If one assumes that the efficiency of H^- production on the front surface of the cathode (opposite extraction slits) is not particularly affected by processes in the back of the source, then two phenomena could be offered as a possible explanation: a reduction in plasma losses due to a lower operating pressure and a cathode current density which is lower in areas with a wider gap. The latter effect would result in a lower overall cathode

current density, while still keeping a higher value in the front part of the discharge. Furthermore, if this is the case, one may contemplate to use a nonhomogeneous cathode surface, with a higher work function in the back.[14]

III. Summary of Mk III and Mk IV Magnetron Results (no electrode cooling)

Two models of the magnetron source have been investigated at BNL over the past year or two: a smaller version, Mk III with a total cathode surface area of 12.5 cm^2, and the larger one, Mk IV, with 38 cm^2 of cathode surface area. The former has been studied most extensively, without grooves,[6] with subsequent acceleration of the beam to 120 keV,[16] and more recently, with grooves and an asymmetric chamber.[9] The mode of operation was pulsed, most experiments having been done with pulse lengths 10-25 ms. The larger source, Mk IV, was designed for about the same H^- current, but to operate with several slits and in pulses longer than 0.1 s. There were many problems encountered with this source (and eventually solved), problems related basically to a much longer pulse duration, especially those due to electrode and extractor heating. Still, the operation of the source has not yet been optimized; systematic studies have, however been slowed down somewhat to give a higher priority to the design and studies of sources with electrode cooling.

Table I shows some of Mk III source parameters; preliminary results from experiments with Mk IV model have also been included.

Comparison of experimental results of MK III studies with scaling equations (Eq. 1 to 3) shows that plasma effects together with the effect of the asymmetry of the discharge gap contribute at least a factor of two to the improvement of source parameters (required cathode current density; power efficiency; a possible explanation lies in an overheating of the cathode surface during long pulse operation resulting in a loss of cesium from the surface follwed by an increase in the work function. Still, even under conditions far from an optimum, it was possible to achieve a beam density of 0.5 A/cm^2 with a cathode power density of only 0.25 kW/cm^2.

A very interesting result was obtained with the Mk III source:[9] at cathode current densities of several A/cm^2 there was no isotope effect observed. This is in contrast with a strong effect observed in a semiplanotron source,[13] but at current densities an order of magnitude higher.

IV. Design Parameters and the Design of the Mk V Magnetron Source

Based on Mk III parameters and taking into account requirements as defined in the general neutral beam program, the decision was made about the next source to be designed, fabricated and studied. This source has to deliver about 1 - 2 A of negative ions, extracted with a voltage of 10 kV or higher, and operate with pulses of at least several seconds duration. To cool the electrodes, water should be used, which limits the power density to about 0.2 kW/cm^2. The H^- current density

Table I

	Mk III (Standard design)	Mk III (1 groove, asymm.)	Mk IV (3 grooves, asymm.)		
I^-	1	0.6	0.35	0.5	A
V_{beam}	15	15	10	10	kV
J^-	0.7	2.2	0.35	0.5	A/cm^2
Δt	0.01	0.01	0.1	0.05	s
$j^-(=\kappa J^-)$	0.2	0.29	0.047	0.065	A/cm^2
J_c	20	3.6	1.3	2.1	A/cm^2
P_c	1.6	0.45	0.16	0.25	kW/cm^2
κ	0.3	0.13	0.13	0.13	-
β	0.3	0.17	0.25	0.25	-
η_P	0.03	0.075	0.04	0.035	A/kW
η	2	6	-	-	%

in the extractor plane will probably be limited by the grid heat load and not by source emission or space charge effects. Still, for the design purposes it will be assumed that the current density is 0.5 - 1 A/cm^2. There are two more parameters to be chosen, the transparency κ and the utilization of the cathode surface β. The first of them, κ, should not be much different from the value in Mk III and Mk IV sources, i.e., about 0.12; the utilization of the cathode surface obviously should be as high as possible and $\beta = 0.25$ should be achievable. To summarize, Table II shows the parameters above.

Table II

Desired H^- current	1 - 2 A
H^- current density	0.5 - 1 A/cm^2
Extraction voltage	> 10 kV
Pulse length	> 5 s
Max. power density on electrodes	0.2 kW/cm^2
Transparency	0.12
Cathode utilization factor β	0.25

From Table I, for Mk III source, by linear scaling

$$J_c' = \frac{P_c'}{P_c} \; J_c = \frac{0.2}{0.45} \cdot 3.6 = 1.6 \text{ A/cm}^2 \qquad (6)$$

The parameters with an apostrophe correspond to the Mk V model. With a cathode current density of 1.6 A/cm^2 one should get an H^- current density of

$$J^{-\prime} = \frac{P_c'}{P_c} \cdot \frac{\kappa}{\kappa'} \cdot J^- = \frac{0.2}{0.45} \cdot \frac{0.13}{0.12} \cdot 2.2 =$$

$$1.06 \text{ A/cm}^2 \qquad (7)$$

which is higher than the assumed upper limit of 1 A/cm^2, implying that the cathode power density could be somewhat lower than 0.2 kW/cm^2. The extraction slit area follows from $I^{-\prime}$ and $J^{-\prime}$, i.e. it should be about 2 cm^2. If a slit width of 0.5 mm is chosen, which is close to the size used in Mk III and Mk IV sources (a wider slit may result in a disproportionally higher gas load, while a narrower slit would require a lower κ, which means either a higher J^- or a lower j^-), the total length L of the slit is

$$L = \frac{2}{0.05} = 40 \text{ cm} \qquad (8)$$

Multiple slits have to be used to avoid a very long and narrow source; as a compromise a set of 5 slits, 8 cm long was chosen. The value of the average H^- current density follows from

$$j^{-\prime} = \kappa \, J^{-\prime} = 0.12 \, J^{-\prime} \qquad (9)$$

or between 0.06 and 0.12 A/cm^2. The power efficiency and the required source power may also be estimated. From Eq. 3, for equal plasma parameters (discharge voltage, mean free path)

$$\eta_P' = \frac{\beta'}{\beta} \cdot \eta_P = \frac{0.25}{0.17} \cdot 0.075 \approx 0.11 \text{ A/kW} \qquad (10)$$

The power efficiency η_P is in the range of interest independent of the H^- current, so that the total power for $I^- = 2$A will be

$$P_{tot} = \frac{2}{0.11} = 18 \text{ kW} \qquad (11)$$

The power density to be removed by water cooling from the anode is not higher than 50% of the cathode power density, i.e. less than 0.1 kW/cm^2.

The power load on the first grid consists of the electron component (plasma electrons, electrons from stripped H^- ions, electrons produced by ionization in the extraction gap) and intercepted H^- ions. Although measurements on the Mk III source show that the grid current may be as low as 25% of the H^- current, it is not known what the real power load is (some particles may have an energy lower than that corresponding to the extraction voltage). The line H^- current density (for L = 40 cm) should be between 0.025 and 0.05 A/cm; if the extraction voltage is 10 kV, this would correspond to a grid line power density of betwen 60 and 120 W/cm. If grids with 3 mm o.d. are used as the extractor, an average (over the surface of the grid) power density of between 65 and 130 W/cm^2 would result. Of course, any increase in the extraction voltage or (if required by the design) reduction in the size of the grid would result in a higher grid power density but still within the range of the present state-of-the-art.

Table III summarizes the design parameters of the Mk V magnetron source. A comment on the assumed value of the discharge voltage: it is quite possible that it may be lower than 180 V; this would result in lower power and cooling requirements.

Table III

$H^-(D^-)$ extracted current	1 to 2 A
$H^-(D^-)$ current density (in the extraction slits)	0.5 to 1 A/cm^2
Average $H^-(D^-)$ current density	0.06 to 0.12 A/cm^2
Extraction voltage	> 10 kV
Pulse length	> 5s
Cathode surface area	60 cm^2
Cathode current density	0.8 to 1.6 A/cm^2
Cathode current	50 to 100 A
Discharge voltage	180 V
Cathode power density	0.1 to 0.2 kW/cm^2
Anode power density	0.05 to 0.1 kW/cm^2
Total source power input	9 to 10 kW
Cathode cooling system (full load)	
Inside wall temperature	90°C
water velocity	35 m/s
pressure drop	4.5 kg/cm^2
Anode cover cooling system (full load)	
inside wall temperature	75°C
water velocity	26 m/s
pressure drop	4.5 kg/cm^2
Extraction slit area	2 cm^2
Total # of slits	5
Slit length	8 cm
Source power efficiency	0.11 A/kW
Source gas efficiency (Mk III)	6%

Fig. 2 shows a cross section of the source. Cathode material is molybdenum, including the supports, while the rest of the source is stainless steel. The shape of the cathode side supports is such that in all regions close to the discharge plasma there is a component of the electric field parallel to the magnetic field. Such a shape has proved[13] to be efficient to prevent the diffusion of electrons out of the discharge gap and initiation of sparks or parasitic discharges. The gap in the back of the source is wider, a beneficial modification discovered on the Mk III source. At the time of this symposium there were two methods for cesium injection under consideration: either a cell using pure metal or a container with a mixture Ti - Cs, which has been successfully tried on Mk IV model. Figure 3 represents an isometric view of the source; anode base, cathode, and anode cover are visible as well as the assembly method.

The extraction grid has not been shown on the drawing; as the first design a solid structure is contemplated, with no cooling capabilities and operating in a pulsed mode (0.1s); this would serve to optimize the design and lead to the proper cooled grid. In the design of the grid support structure (supports, shields, insulators) extensive use has been made of computer field calculations in order to avoid high field concentrations.[17]

The status of the source fabrication should allow first source tests in October 1980, and beam extraction tests in November 1980.

V. Ion Source Test Stand

In order to be able to test sources operating with very long pulses or steady state it was necessary to build a new test stand.[18] The existing test stand, with a pumping speed of less than 10,000 ℓ/s, depended on volume pumping and was therefore suitable for pulsed operation only (< 0.1 s). The parameters of the new test stand were chosen so that the gas load from a 1 A, H^- source can be handled. If the gas efficiency of the source is assumed to be 5%, the gas flow is about 1.6 torr ℓ/As; a vessel pressure of 2×10^{-5} torr would require a pumping speed of 80,000 ℓ/s. The test stand was designed by using two (NASA surplus) 35" diffusion pumps, attached to a 1.2 x 2.1 x 2.7 m^3 box; the pumps should be sufficient for such a gas load. If, in the future, a higher pumping speed becomes necessary, (a larger source with the same gas efficiency), there is space enough in the box to install a cryopumping system. The electrode cooling system, using deionized water, is capable of pressurization to 250 psi; present pumping capacity allows for a pressure drop of 60 psi and a total flow rate of 17ℓ/min. Two heat exchangers have been installed with a rated capacity of about 50 kW. The system has all the instrumentation necessary to read the flow rate, pressure and temperature at various points in the system. A water cooled beam stop has been designed with a rated capacity of 25 kW, at 200 W/cm^2.

The discharge power supply, used for continuous mode of operation, delivers 25 A at 850 V; for pulsed operation (pulses up to 30 s duration) a battery system will be used, delivering from 100 A (10% duty cycle) to 500 A (4% duty cycle) at voltages up to 450 V. The extractor power supply is rated 25 kV, 2.5 A d.c. or 20 A in 0.1 s pulses. In addition to the beam stop, the beam current can be monitored by using a beam transformer, having an aperture of 17 cm diameter, a sensitivity of 200 mV/A, current range up to 2 A and a frequency band from d.c. to 6 MHz.

The test stand is in operation, except for the battery power supply (scheduled for November 1980); a Penning source with water cooled cathodes[19] has been used to check all the systems, mechanical, electrical and electronic, and 10 s operation with a 90% duty cycle has been achieved.

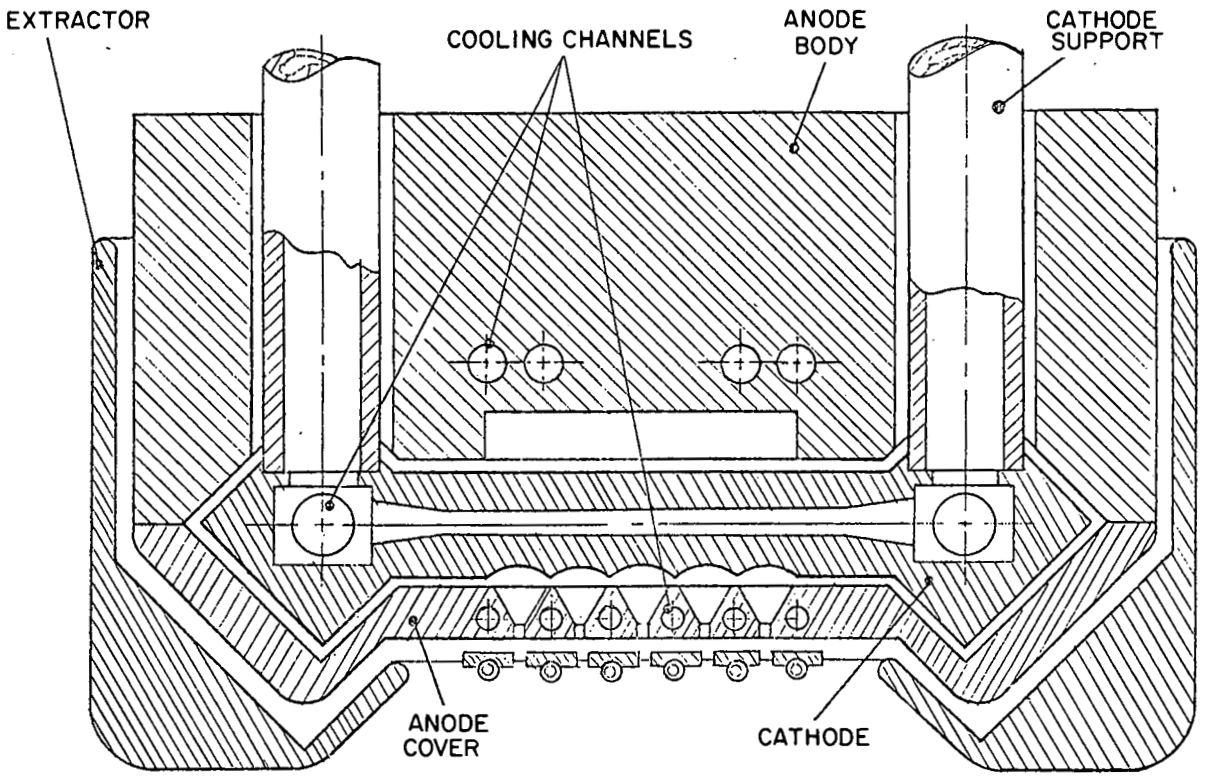

Fig. 2: Cross section of the Mk V magnetron

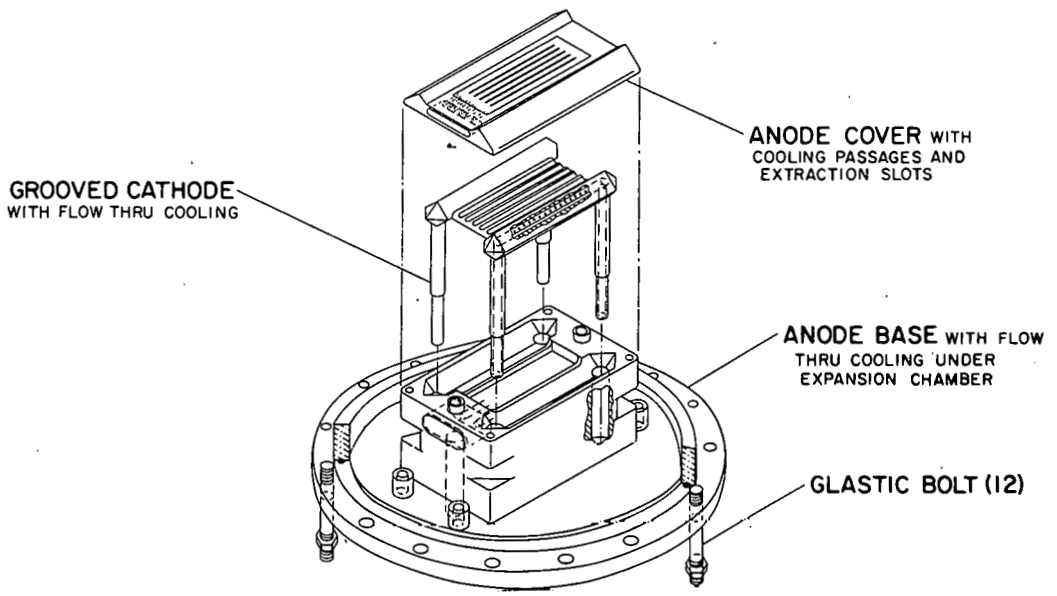

Fig. 3: Isometric view of the Mk V magnetron

References

1. J.R. Hiskes, Journal de Phys., Colloque C7, suppl. to No. 7, tome 40, p. C7 - 179 (1979).
2. K.W. Ehlers, and K.N. Leung, presented at this Symposium.
3. W.L. Stirling, et al.; C.C. Tsai, et al.; ibid.
4. H.J. Hopman, et. al., ibid.
5. K. Prelec, BNL Rep. 22847 (1977).
6. K. Prelec, Proc. Symp. on Phys. of Ionized Gases, Dubrovnik, 1978, R.K. Janev, editor.
7. T. Green, private communication.
8. Z.W. Sternberg, BNL Int. Rep. AGS 77-4 (1977).
9. J.G. Alessi, and Th. Sluyters, to be published in the Review of Scientific Instruments.
10. K. Prelec (unpublished, 1976).
11. K. Wiesemann, Proc. Symp. on the Production and Neutralization of Negative Hydrogen Ions and Beams, K. Prelec, editor, BNL 50727 (1977).
12. A Hershcovitch, and K. Prelec, presented at this Symposium.
13. Iu. I. Belchenko and G.V. Dudnikov, Preprint I Ia F 78-95, Nososibirsk (1978).
14. K. Prelec, AGS Div, H^- Tech. Note 52 (1980).
15. J.G. Alessi, and Th. Sluyters, presented at this Symposium.
16. Th. Sluyters and C. Lam, Proc. Symp. on the Production and Neutralization of Negative Hydrogen Ions and Beams, K. Prelec, editor, BNL 50727 (1977).
17. V. Kovarik, to be published.
18. R. Larson and R. McKenzie-Wilson, to be published.
19. J. Alessi, J. Fink, A. Maschke, K. Prelec, and Th. Sluyters, Proc. 2nd Joint Grenoble-Varenna Int. Symp. on Heating in Toroidal Plasmas, Como (1980)

*Work done under the auspices of the U.S. Department of Energy.

DISCUSSION

GELLER What is the position of the pumping system with respect to the gas flow coming out of the source? In other words, what is the conductance between the pumps?

PRELEC It is wide open. Basically the box is just a manifold to attach the pumps to the source. There are two diffusion pumps, one on each side. On the other side of the box there is a flange with the source attached to it and the gas streams freely into the box and is pumped away through two valves.

GELLER The gas expands in the box?

PRELEC Yes, but it is a very short path.

LEUNG How do you feed cesium into the source?

PRELEC We have been using two methods. The first one is the cesium cell, just metallic cesium which we are using presently on the Mk V Penning source. The second method is by using a container where we put a mixture, a paste of cesium metal and titanium powder; this we have been using on the small sources. This corresponds more to the standard cesium bichromate-titanium pellet method except that the cesium is already mixed with the powder, without having to heat it up to 500°.

LEUNG And in the new source?

PRELEC One of these two methods.

LEUNG Can you show me the location in the picture?

PRELEC In the back of the source.

EHLERS Can you make a rough guess of your source pressure, and second what is your arc voltage?

PRELEC The details of the operation of sources with grooves will be given by Jim and Theo, but it is roughly 120 to 180 V and the pressure is 100-200 mTorr.

REGULAR AND ASYMMETRIC NEGATIVE ION MAGNETRON SOURCES WITH GROOVED CATHODES*

J. Alessi and Th. Sluyters
Brookhaven National Laboratory
Upton, New York 11973

Abstract

The performance of the BNL Mk III magnetron source has been improved by geometrically focusing H^- ions produced at the cathode into the anode emission slit. In addition, an asymmetric configuration, with a large anode to cathode spacing in the back of the source, has allowed operation of the source at lower pressures. The result of these two changes is a gas efficiency of approximately 6% and a power efficiency of 8 kW/A. No isotope effect has been observed. Measurement of the energy of H^- ions shows that one extracts both slow ions and ions with an energy equal to the cathode voltage. The ratio of electrons to H^- ions can be as low as 0.5.

I. Introduction

The use of geometrical focusing in magnetron sources had been proposed by Green[1] and Sternberg[2], who suggested curving the cathode in order to focus H^- ions into the anode emission slit. It was not clear that geometrical focusing would work because of the relatively high pressure in the source, which resulted in the extraction of primarily "slow" H^- ions, some formed between the cathode and anode by symmetric charge exchange collisions between "fast", surface produced H^- ions and H atoms, and others possibly coming from volume production of H^- ions. Subsequently, Belchenko, et. al. applied the principle successfully in a semiplanotron surface plasma source.[3] They observed sputtering on the anode from ions focused by a groove in the cathode.

A cylindrical groove was added to the cathode in the BNL Mk III magnetron source. This has allowed us to reach desired H^- current densities (0.5 - 2.0 A/cm^2) with almost an order of magnitude lower arc currents than required without the groove.

To further enhance performance, an asymmetric magnetron source was tested, having a relatively wide gap in the back of the cathode, as suggested by Prelec[4] and Wiesemann[5]. The idea of such a source is that this wider gap allows ignition of the discharge at lower gas pressures.

In addition to a discussion of source performance with the above mentioned modifications, results of measurements of the energy of H^- ions extracted under various operating conditions will be given. Finally, some experimental observations related to the ratio of extracted electrons to H^- ions will be discussed.

*Work done under the auspices of the U.S. Dept. of Energy.

II. Grooved Cathode and Asymmetric Configuration

The cathode-anode region of the magnetron, as well as the detail of the grooved region, is shown in Figure 1.

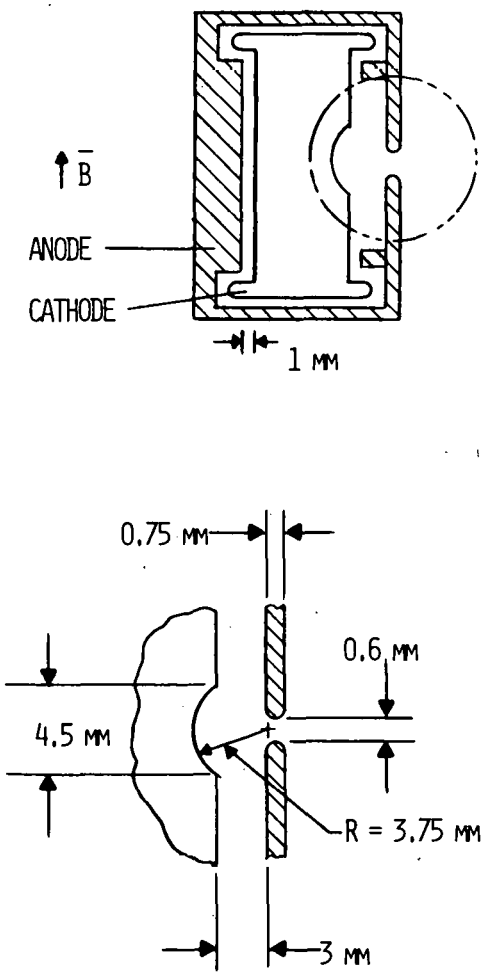

Fig. 1: The placement and dimensions of the groove put in the cathode of the Mk III magnetron.

The groove was directed perpendicular to the magnetic field, along the full front of the cathode (5 cm). The radius of curvature of the groove was 3.75 mm, and the width was 4.5 mm. In general, the emission slit was 0.6 x 45 mm^2. Figure 2 shows H^- current density versus arc current for the magnetron with the groove, as well as the previous performance with a flat cathode. Within

the range of arc currents shown in Figure 2, we could typically operate the source with 10 to 25 ms pulse lengths, and a repetition rate of 15 to 20 pulses per minute. Beam currents were measured on a Faraday cup approximately 8 cm from the source. The extraction voltage was always high enough to insure that the H^- output current was emission limited (typically 12 kV or 80 kV/cm). In general, after running one could observe a line 0.5 - 0.7 mm wide on the inside of the anode (opposite to the groove) which had been sputtered clean by the focused H^- ions. Therefore, with the groove one could extract H^- ions coming from an area of the cathode which was 7.5 times larger than the anode emission slit.

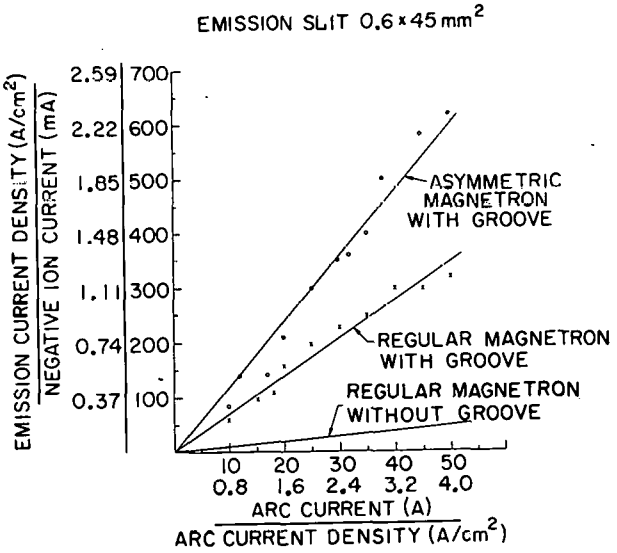

Fig. 2: H^- current versus arc current for the normal magnetron with flat cathode, normal magnetron with grooved cathode, and asymmetric magnetron with grooved cathode.

The H^- output was quite sensitive to the source pressure and Cs coverage. One obtained maximum H^- output when operating at the lowest pressure possible without losing the discharge. An increase from this pressure by a factor of two would result in a 50% reduction in H^- current, due to the increased destruction of ions between the cathode and anode. For a given H^- current density, we observed a reduction in the source pressure by at least a factor of three over that required with the flat cathode. This is primarily due to the fact that the lower arc currents can be sustained at lower pressures.

In an attempt to further reduce the source pressure (and therefore the destruction of H^- ions), the anode to cathode spacing on the back side of the magnetron was increased from 1 mm to 5 mm, while leaving the front side unchanged (see Fig. 3). The idea is that ignition of the discharge may occur at lower pressures with the increased gap. The results with this asymmetric configuration (and grooved cathode) are shown in Figure 2. The H^- output was increased by 70% over that with the normal grooved magnetron. The source seemed to operate with a more stable discharge at somewhat lower pressures than the normal grooved magnetron. We now estimate the gas efficiency of the source (H^- ions/neutral atoms) to be at least 6%. Experiments with a 10 mm gap in the back of the source are now under way.

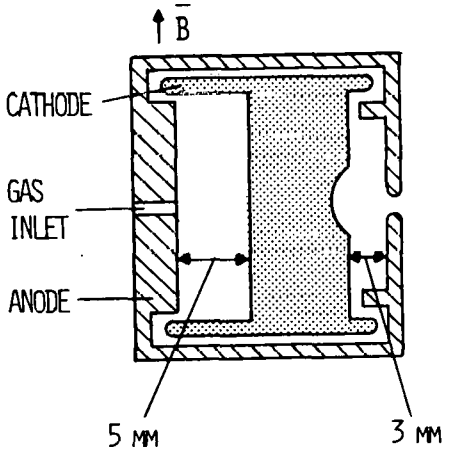

Fig. 3: The asymmetric magnetron configuration

In the Cs mode, the source operates with an arc voltage of 120 - 180 volts, the lower voltage being obtained when a larger amount of Cs is supplied. A decrease in arc current is often accompanied by some increase in arc voltage. One must then increase the Cs supply rate to reduce the arc voltage at this lower current. Also, as one reduces the source pressure one reaches a point where the arc voltage begins to rise (and arc current drops). Again, additional Cs will get one back to lower arc voltages.

Emittance measurements, taken with an on-line minicomputer, gave an emittance perpendicular to the emission slit which was a factor of three lower than the emittance with the flat cathode at the same H^- current density.[6] Presumably, this is due to the lower arc current required with the groove. The normalized emittance perpendicular to the slit is approximately 0.1 π cm-mrad for a 0.5 to 1.0 A/cm^2 beam (135 - 270 mA). The current distribution was uniform in the direction of the slit.

An asymmetric magnetron with a series of grooves in the cathode parallel to the source magnetic field was tried. The anode emission

slits were offset slightly with respect to the grooves to compensate for the deflection of ions between the cathode and anode by the source magnetic field. While we did observe sputter marks indicating that the H^- ions were again being focused, the output with this configuration was less than 50% of that obtained with the groove and slit perpendicular to the magnetic field. The most likely explanation seems to be a spreading out of the ions at the slit by the magnetic field, preventing one from focusing the H^- ions as well into the slits.

It has been suggested that since the curvature of the groove provides an electric field component directed toward the center of the groove, this may tend to increase the concentration of electrons in the groove when its orientation is perpendicular to the magnetic field.[7] This could result in a higher discharge current density in the groove. In an attempt to enhance this effect, if it exists, a groove was put all around the cathode. This gave no noticeable difference in source performance.

With two grooves and emission slits (approximately 10% anode transparency), we have been able to extract 380 mA of H^- with a 25A, 120 V discharge. This corresponds to a power efficiency of 8 kW/A, an improvement by about a factor of four over that with a flat cathode (with four emission slits and 50% anode transparency).

III. Operation with Deuterium

With the asymmetric magnetron operating in the Cs mode, the pulsed gas was changed from hydrogen to deuterium. A residual gas analyzer was monitored and confirmed the change in gas, but no change was observed in the operation of the source. One had the same arc current, arc voltage, and negative ion current as had been obtained with hydrogen. D^- output versus arc current fell along the same line as that obtained for H^- ions, while operating with arc current densities up to 4 A/cm^2. Semiplanotron results[3] indicated maximum D^- currents which were only 50-70% of maximum H^- currents. In that case, however, the source was operating at arc current densities in excess of 20 A/cm^2. The results in Ref. 3 seem to indicate a reduction in the isotope effect at lower densities, so our failure to observe an isotope effect may not be in conflict with their results. This might suggest that in magnetron sources the isotope effect is related to the destruction of ions between the cathode and anode rather than being a surface production effect.

IV. Energy Analysis of H^- Ions

An energy analyzer was constructed in order to determine the relative importance of the fast and slow H^- components under typical operating conditions for the grooved, asymmetric magnetron. Figure 4 shows a schematic of the energy analyzer. The source was operated in a uniform magnetic field. H^- ions coming from a 0.75 mm diameter hole were deflected by 180°, and detected by a monitor containing thirty small metal strips, collecting ions with Larmor radii from 3.0 to 4.5 cm. Thirty sample/hold circuits allowed one to get the complete energy spectrum at any time during the beam pulse. A 0.5 - 1.0 kV extraction voltage was applied across a 0.25 mm gap, while the magnetic field was within the range required for operation of the source (0.9 - 1.6 kG).

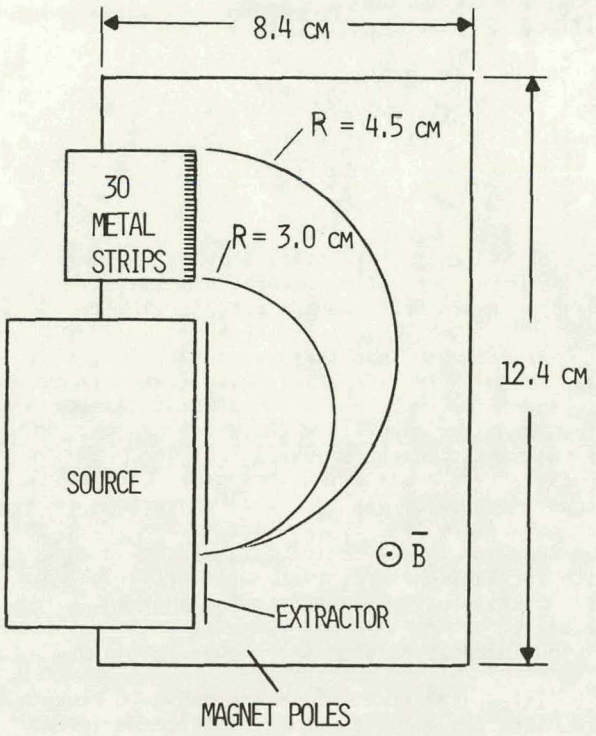

Fig. 4: Schematic of the H^- ion energy analyzer

Fig. 5 is a typical energy spectrum, containing two peaks - the left peak is at the extraction voltage (V_E) and the right one is at V_E plus the cathode voltage (V_c). In the hydrogen mode, one observed only the peak at V_E. As Cs was added, the second peak, at $V_E + V_C$, appeared. With increasing amounts of Cs, this second peak grew, and moved toward the first peak as the cathode voltage dropped.

By shifting the extractor voltage by an amount equal to the cathode voltage, one could clearly see that the energy difference of the two peaks was equal to V_C. We did not observe peaks at higher energies, as one might have expected if reflection of atomic and molecular ions at the cathode was occuring. The spectra differ somewhat from that measured by Belchenko, et.al.[8]. While they also observed two peaks, one at V_E and one around $V_E + V_C$, the tail on the high energy peak extended up to $V_E + 2V_C$. In the present spectra the peak at $V_E + V_C$ has no such tail.

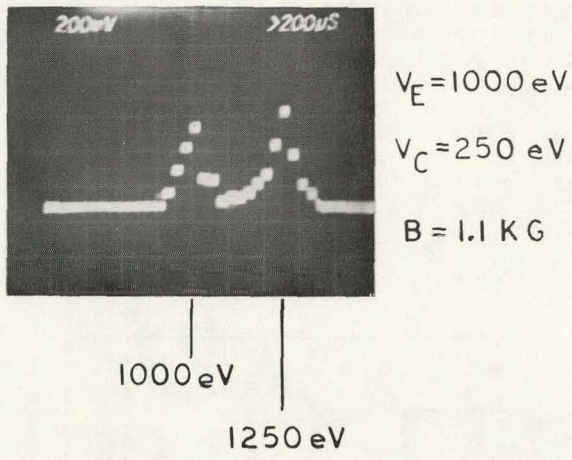

Fig. 5. H^- energy spectrum, showing a peak at the extractor voltage, and one at the extractor plus the cathode voltage.

As one went into the proper Cs mode, the fast ion peak ($V_E + V_C$) increased. With decreasing source pressure the ratio of fast ions to slow ions increased (less charge exchange), while at the same time the magnitude of both peaks increased (less destruction of ions). Figure 6 shows a series of spectra taken at various arc currents (V_E = 1000 V, V_C = 150 V, B = 1.1 kG). The decrease in the ratio of fast to slow ions with increasing arc current could be due to more dissociation of hydrogen at the higher arc currents, resulting in an increased fraction of fast H^- ions undergoing charge exchange collisions.

It appears that, while the ratio of fast to slow ions changes with source conditions, we do not normally operate in a regime where either component is less than 20% of the total beam. Even with a large slow ion component the cathode groove enhances the source output by increasing the concentrations of slow ions around the emission slit.

V. The Electron Component

In going from the normal magnetron with the flat cathode to the asymmetric magnetron with grooves, we were able to extract a given H^- current density at approximately an order of magnitude lower arc current. Somewhat suprisingly, however, the ratio of electrons to H^- ions extracted showed no dramatic improvement. This seemed to indicate that most of the extracted electrons were not the result of diffusion from the main plasma. Subsequent experiments seem to confirm this conclusion.

Typically, the anode emission slit was 0.6 mm wide, and the anode wall was 0.5 mm thick. Electrons should diffuse much more easily parallel to the source magnetic field than perpendicular to it, and so tend to run into the slit walls rather

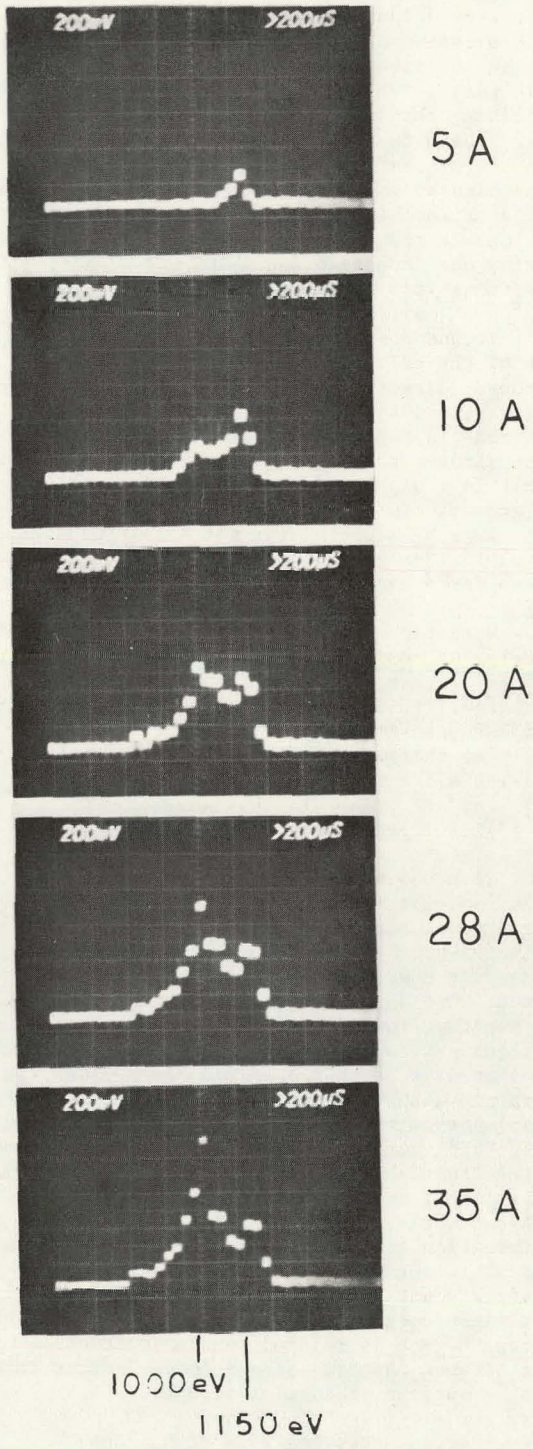

Fig. 6: H^- energy spectra for various discharge currents. The discharge voltage was 150 V, extraction voltage was 1000 V, and B = 1.1 kG. The pressure and Cs coverage was the same in all cases.

than diffuse out of the source. In switching to an anode slit 0.25 mm wide and 0.75 mm thick (a configuration which should have reduced diffusing electrons) we obtained the expected reduction in H^- current, but the e^- current dropped by the same fraction, maintaining the same e^-/H^- ratio. Going to the other extreme, with the anode slits oriented parallel to the source magnetic field, one still obtained approximately the same e^-/H^- ratio. Finally, for source magnetic fields from approximately 1.0 to 1.7 kG, the e^-/H^- ratio does not change (nor do the magnitudes change). Thus, this seems to rule out the possibility of the extracted electrons coming from the main plasma. (In the hydrogen mode, where the H^- density is low, the extractor field may penetrate through the anode slit. In this case, one may be extracting plasma electrons. In the Cs mode, however, the H^- ion density inhibits the penetration of the extractor field).

Under optimum conditions of source pressure, Cs coverage, and extractor voltage, one can attain the ratio $e^-/H^- = 0.5$ (i.e., H^-/total extractor supply load = 0.67). The best ratio is obtained when the pressure is as low as possible. Figure 7 shows various currents as a function of source pressure. The increase in pressure decreases the H^- current, but the electron current (extractor supply load - H^- current), remains essentially constant. The grid and magnet pole currents (electrons) are also constant.

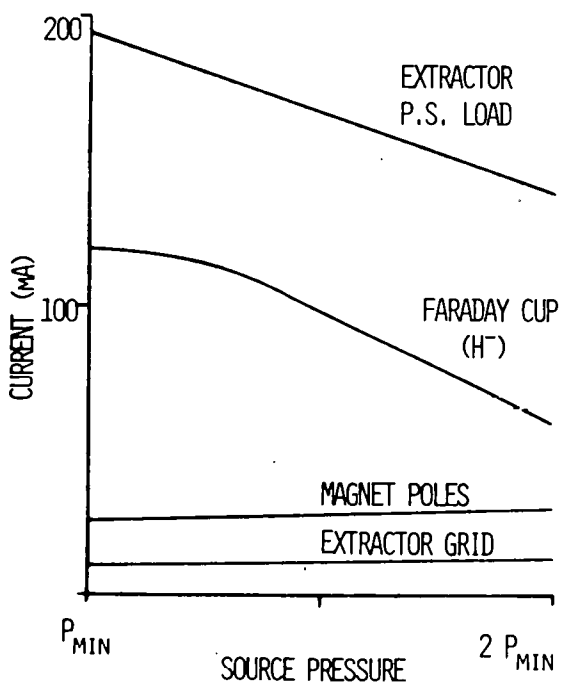

Fig. 7: Dependence of various currents on the source pressure. P_{min} is the minimum pressure at which the source will operate.

Therefore, one may conclude that ionization in the extractor gap is not the primary contributor to the elctron load. Destruction of H^- ions in the extraction gap should be very small. A likely origin of some of the electrons is through destruction of fast and slow H^- ions in the emission slit, or by electrons released in collisions of ions with the walls of the anode slit. There is also the possibility that photoelectrons are produced in and around the anode slit (enhanced by any Cs coating). Light reflected from the front of the mirror - like cathode is focused at the anode slit by the groove, so it is not unreasonable that photoelectrons produced in the slit region were increased in going from the flat to the grooved cathode along with the increased H^- current. Extraction of photoelectrons would be consistant with the observed constant electron current versus pressure in Figure 7. A simple calculation of the rate of H^- destruction in the emission slit as a function of pressure indicates that it is also possible to explain Figure 7 by claiming that the electrons originate from H^- destruction. The pressure dependence of this rate of H^- destruction (i.e., rate of electron creation) goes as $K_1 P e^{-K_2 P}$, where K_1 and K_2 depend on H^- destruction cross sections, ratio of H to H_2, etc., and P is the source pressure. This function can have a relatively flat region around its maximum. When one puts numbers into a more careful calculation one finds that the flat part of the curve can indeed be in the range of pressures where we are operating the source. The position of this maximum does shift depending on the H to H_2 ratio, among other things, so one can only conclude that electrons arising from H^- destruction cannot be ruled out on the basis of Fig. 7.

VI. Summary

The performance of the BNL Mk III magnetron has been improved significantly by the use of geometrical focusing of H^- ions and by increasing the anode to cathode spacing in the back of the source. We can now extract almost all H^- ions reaching the front anode plane, even with a low anode transparency. We have extracted 1.0 A/cm^2 of H^- ions (270 mA) with an arc current density of less than 2 A/cm^2 (25 A arc current). This is an order of magnitude lower arc current than what was required with the normal magnetron and flat cathode. The fact that one can operate at lower arc currents allows one to decrease the pressure in the source, which in turn reduces the destruction of H^- ions. The net result is an improvement by about a factor of three in gas efficiency (to 6%), and a factor of four in power efficiency (to 8 kW/A).

The H^- energy spectrum contains only two peaks, one corresponding to slow ions produced by charge exchange of the fast ions with neutral atoms, and one at an energy equal to the cathode voltage. Peaks at higher energies, coming from reflection of ions at the cathode, are not observed.

Under optimum conditions we can obtain a ratio of electron to H^- current equal to 0.5. The electrons are not diffusing from the main plasma, but seem to be produced in and around the anode emission slit, by either H^- destruction or photoemission.

References

1. T. Green, Culham Laboratory, private communication, 1975.

2. Z.W. Sternberg, BNL Int. Report AGS 77-4, 1977.

3. Iu. I. Belchenko, G.V. Dudnikov, preprint 1 YaF-78-95.

4. K. Prelec, BNL Log Book 1976, p. 28.

5. K. Wiesemann, Proc. Symp. on the Production and Neutralization of Negative Ions and Beams, BNL 50727, p. 97, 1977.

6. Th. Sluyters and V. Kovarik, BNL 26881, 1979.

7. K. Prelec, AGS Division H^- Tech. Note 52, 1980.

8. Iu. I. Belchenko, G.I. Dimov, V.G. Dudnikov. "Izvestiya of USSR Acad. of Sci." ser. physical XXXLII, 2573, 1973.

DISCUSSION

HOOPER I did not understand your last argument that the photoelectrons would be independant of the gas pressure. Naively, I would have thought it was just the opposite, that they were originating in the gas and therefore as you increase the pressure you would get more of them.

ALESSI I was thinking more that the emission electrons would be coming from around the emission slit itself. If we get a cesium coating on the exit slit of the source, we may get photoelectrons coming from that surface.

HOOPER But where are the photons originating?

ALESSI From the discharge.

HOOPER And that would not be proportional to the gas pressure?

ALESSI This is at the same arc current, the pressure is changing but the arc current practically remains constant.

LEUNG What is the ratio of electrons to extracted H^-?

ALESSI That is 1:2.

TSAI You said the ratio of electrons to H^- is always ½. Because the gas pressure is so high, is it possible that it is just gas particle effects in the extractor gap itself?

ALESSSI We can not rule that out, but I think some of the indications, for instance the fact that it is independant of magnetic field, would kind of go against that assumption.

FORRESTER When you talk of the cesium mode, are you operating this as a cesium discharge, primarily, with hydrogen mixed through it?

ALESSI When we have hydrogen gas only, the arc voltage is maybe 400 or 500 V and the arc current is low and as we add the cesium the arc voltage will drop to between 120-200 v. In general, we operate with this low arc voltage and that is what I have called the cesium mode.

FORRESTER I see, but it is primarily a hydrogen discharge, I suppose?

ALESSI Yes.

FORRESTER How does the cesium get around to the front, just migrates over the surface?

ALESSI In this source we put cesium bichromate in the cathode and the discharge heats the cathode and the cesium comes through cracks under the cathode surface. The cesium bichromate get a certain temperature that emits pure cesium and this creeps out.

FORRESTER There are cracks around that carried them by just surface tension leading it through cracks?

ALESSI Yes.

PETERSON I have two questions. One is that you mentioned that the ratio of the fast ions and the slow ions vary with the current. I would think it would also be a pressure variation.

ALESSI Right, in general, as we increased the pressure we would get more of the slow ions.

PETERSON The other question is if you are talking about photo-emissions from the slit surfaces, I would think that, unless the discharge is confined to an area very close to the cathode, that there would not be any focusing of that light.

ALESSI If you illuminate the front of the cathode with light, you could see that the grooves themselves will focus the light into narrow strips of light illuminating the front of the anode.

DAGENHART Can you comment further on the gas sensitivity of the output? The destruction mechanisms or whatever is happening there to reduce the output?

ALESSI The pressure in the source at the minimum value is maybe 0.1 torr. If you use the cross sections for destruction in the neutral gas it can explain this kind of drop in the output as a

function of pressure, not taking into account destruction in the plasma.

CRANDALL I am trying to figure out if I am jumping to the right conclusions. In comparison of your energy spectra with what Leung showed yesterday, it looks like you have a volume process and a surface production process. A surface production process, according to your spectrum, must arise from neutral particles, at least they did not become charged until they came off the cathode, is that what you are implying.

ALESSI The only difference may be whether the low energy peak is really volume production or charge exchange. In our source our pressure is a lot higher than the pressure in Leung's source. So, I think it is possible that his low energy peak may be volume production while our low peak may be charge exchange. We can not really tell, although in our source it is likely charge exchange.

CRANDALL I am still confused about that.

HOLMES Can you tell me some details about the extraction system, the extraction gap in this particular experiment?

ALESSI Usually, we had maybe 1½ millimeter gap and we would run anywhere from 10 to 20 kV.

HOPMAN Even though the density will be very low, you have in your plasma neutral cesium. I am wondering what is the equivalent current density of the cesium that is streaming out through the anode slit?

ALESSI The loss of cesium from the front of the source?

HOPMAN Yes.

ALESSI We have not measured that. I think in Novosibirsk in the past they have made some measurements on the cesium flow out of the source but off hand I can not remember what their number is.

MARK V MAGNETRON WITH H.C.D. PLASMA INJECTION *

A. Hershcovitch and K. Prelec
Brookhaven National Laboratory
Upton, New York 11973

Abstract

An experiment designed to test the feasibility of negative ion sources based on plasma injection from a hollow-cathode discharge is described. From the plasma column up to 2.3 Amp/cm^2 of positive ion current were drown onto a cesiated Mo converter. Strong evidence was found for an H^- production at a conversion efficiency of 25%. Based on these encouraging results a 2 Amp/H^- source has been designed.

I. Introduction

Hollow-cathode discharges (HCD)[1,2,3,4] can produce plasmas which have ideal characteristics for negative ion sources: (1) very high ionization, (2) high plasma densities ($n \approx 10^{13}$ - 10^{14} cc^{-1}), (3) capability to operate dc, (4) HCD plasmas follow the contour of magnetic field lines, (5) background pressure of 10^{-4} - 10^{-5} torr., (6) some cathodes run well in cesium.[4]

The implication of these characteristics is clear: one would hope to construct a negative ion source which would be fed with HCD plasmas, thus producing negative ion beams with a very high gas efficiency. This source would have a very low background pressure and it would run dc. In addition, since the plasma is injected into the source, the bias on the cesium covered grooved converter could be independently adjusted to optimize the conversion efficiency.[5]

II. Feasibility Questions

Theoretically, an HCD fed negative ion source should work very well. One envisions a source in which HCD plasmas are injected along magnetic field lines between two biased plates with a potential difference of 50-100 volts. To test for physical feasibility we must verify that

(1) The bias on the plates won't have an adverse effect on the operation of the HCD.

(2) At least 1 Amp/cm^2 of ion current can be collected on the plate which acts as a converter.

(3) Cesium, which reduces the arc voltage and improves the power efficiency, does not have adverse effects on the system.

(4) Tantalum HCD runs well in H_2.

(5) H^- ions are efficiently produced

(6) A test of a lanthanum hexaboride converter doped with cesium.

Theoretically, the discharge should not be affected by the presence of biased plates. The plasma which streams out of the HCD will be subjected to an $\underline{E} \times B$ drift which is negligible compared to the thermal velocity of the electrons; e.g., in a gap of 0.5 cm at 80 volts and 1 kG, the $\underline{E} \times \underline{B}$ drift is 1.6×10^7 cm/sec, while the thermal velocity corresponding to a temperature of a 9 eV electron is 1.3×10^8 cm/sec.

The current drawn by the converter should easily exceed 1 Amp/cm^2 since the ion saturation current that can be drawn from a hydrogen plasma with a density of 10^{13} cc^{-1} and an electron temperature of only 4 eV is 1.77 Amp/cm^2.

III. The Experiments

A number of experiments were performed at MIT on an HCD device[1] which has been used to train students in basic experimental techniques in plasma physics. The vacuum chamber is basically a cylindrical tube which is 2.5 feet long and about 5 inches in diameter. It is pumped by three diffusion pumps with a pumping speed of close to 2,000 liter/sec. The axial magnetic field is produced by six coils which have 4 inch gaps between them. Thus, the maximum field strength varies from 640 G in the center of a coil to 430 G in the center of the gap (where the experiments were done). On one end of the machine the cathode is mounted on an insulated plate, the rest of the chamber is at ground potential. The cathode itself is a 3 inch long tantalum tube with an i.d. of 3 mm.

Two flat electrodes, a converter and a collector were mounted on opposite windows in the center of the device, i.e. about 12 inches "downstream" from the cathode. Both the converter and collector could scan the discharge radially. The converter consists of a water cooled Mo block with a surface area of 1 cm x 3 cm facing the plasma. Provisions were made to mount small cesium pellets and getters on this block; the getters and pellets were to be heated by the discharge itself. The collector consists of an Al block 2.5 x 5 cm with provisions to attach extension plates on top and bottom. The collector has a hole in it, and it is mounted on a hollow rod such that additional gas could be fed through the collector. Hollow cathode discharges of noble gases in the MIT device[1] and a similar device at RPI[6] produced cylindrical plasmas whose peak density of 2×10^{14} cc^{-1} falls off to 1×10^{13} cc^{-1} in 1.5 cm. The electron temperature in the center is about 9 eV.

(1) Disturbance of the HCD operation. In the first experiment, the converter and collector were brought within .75 cm from each other; the

collector was at ground potential, the converter at -80 volts, and the magnetic field at 430 G. There was no evidence of disruption nor were there any adverse effects other than a physical obstruction which caused a slight rise in the anode to cathode voltage.

(2) Operation in the hydrogen mode. Up until this set of experiments the MIT machine was operated in Argon, with only small traces of hydrogen. In our experiment this tantalum HCD ran very well in hydrogen. The "hot spot" on the cathode stayed at the tip (unlike in Argon where the hot spot is in the middle). This fact indicated that the projected lifetime of a Ta cathode operating in this mode should be far greater than the 20-25 hours of operation in Argon. The arc current in the hydrogen mode was 22-29 Amp and the arc voltage was 60-90 volts. Electric probe measurements indicate that n and T_e are the same as in noble gas discharges.[1,6] Hydrogen HCD discharges seem to be more quiescent than Argon discharges.

(3) Cesium injection through the cathode. Traces of Cs were injected through the cathode. The results were spectacular: the arc voltage dropped to about 50 volts and the arc current could be varied from 3 to 100 Amp with the arc voltage being almost constant.

(4) Positive ion current collected by the converter as a function of the converter bias and radial position, arc current and gas feed. Figure 1 shows the converter current density versus bias and radial position. The maximum current density collected by the converter was 1.3 Amp/cm^2.

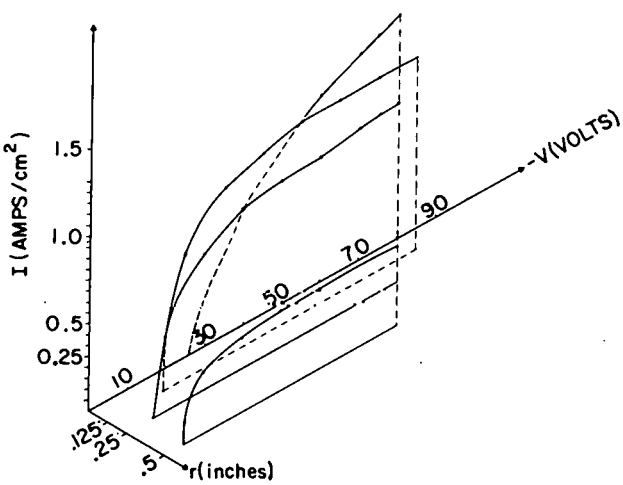

Fig. 1: Current density collected by the converter as a function of its radial position and bias. The arc voltage and current were 66 volts and 27 Amp respectively, and the magnetic field was 430 gauss. About 25% of the gas was fed through the collector.

In this case, part of the gas was fed through the collector. When the gas was fed through the cathode only, slightly less than 1 Amp/cm^2 were collected. Next, a MACOR shield was placed around the the converter to insure that contributions to the current collected from the side are negligible, as one would expect from the steep density gradient. Indeed, the current collected by the converter with the MACOR shield in place was over 80% of the current collected without it. Finally, traces of Cs were injected through the cathode, and the converter current was measured as a function of arc current at a fixed radial position. As expected (Fig. 2), the converter current increased linearly with the arc current.

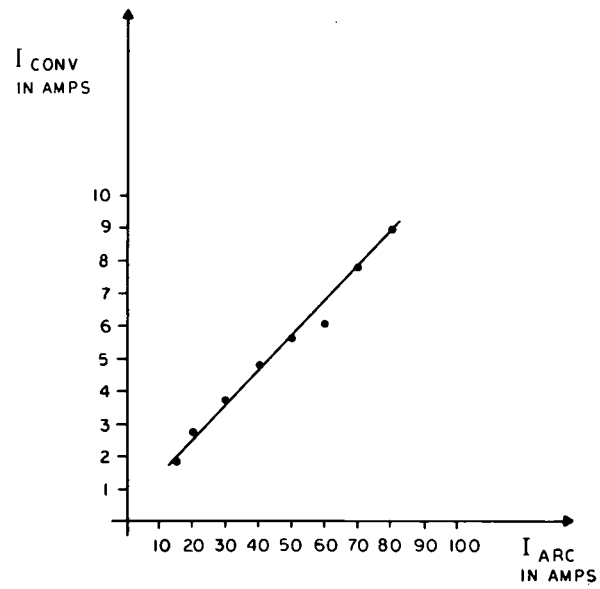

Fig. 2: Total current collected by the converter at a fixed radial position versus the arc current. Hydrogen and traces of cesium were fed through the cathode only. The converter bias was fixed at -74 volts.

(5) Cesium coated converter. In an attempt to detect H^- ions, cesium getters and pellets (composition 75% Ti, 25% $Cr_2 Cs_2 O_7$) were placed on the converter, which was then immersed in the plasma. The pellets heated up and the released cesium was seen flowing from the pellets and getters on the converter surface. A marked increase in the converter current was observed. With some gas feed through the collector, the converter current density was recorded to be 2.3 Amp/cm^2. Next, the converter was pushed in until its surface reached the center of the plasma and the collector block was inserted far enough such that the plate extended beyond the converter. Figure 3 is a schematic representation of the experimental setup. The converter was biased to -82

volts with respect to ground, and measurements were made of the collector current with the plate above and below the converter.

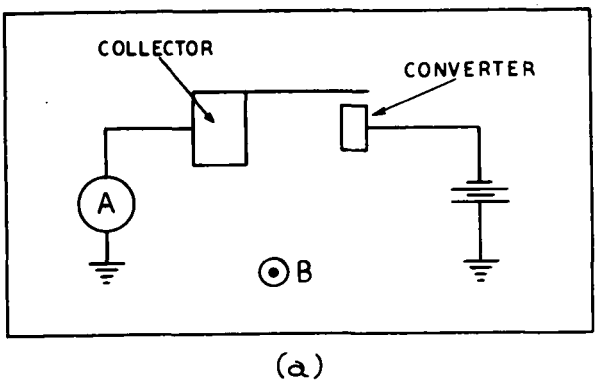

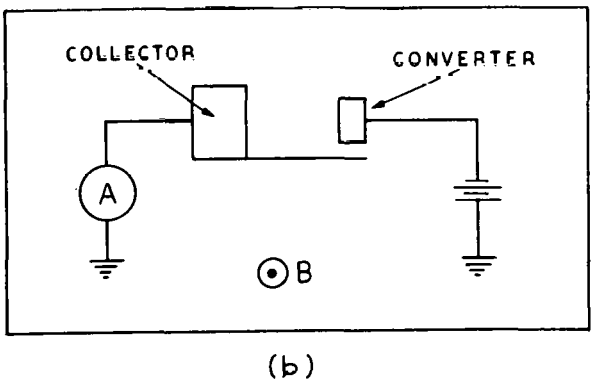

Fig. 3: Schematic of the experimental setup. Discharge conditions: arc current 26 Amp, arc voltage 67 volts, partial gas feed through the cathode, cesium covered converter biased to -82 volts, and background pressure 3 x 10^{-4} torr. With the converter at the center of the discharge, the collector current was (a) 0.8 Amp, (b) 2.9 Amp.

The negative potential of an HCD plasma and the direction and strength of the magnetic field are such that with the plate above the converter, the collector, when connected to ground draws only electrons. In this configuration (Fig. 3a), 0.8 Amp were recorded. With the plate at the bottom negative ions can be collected as well. Indeed, by flipping the plate to the bottom (Fig. 3b), 2.9 Amp were collected. Next, with the plate in the "bottom" position, the converter was retracted. Figure 4 displays the collector current versus the converter current for various radial positions. The collector current is strongly dependent on the converter current. Since the HCD plasma is symmetric, the top and bottom electron densities can be assumed to be the same, and therefore, the electron contribution to the current collected by the collector with the plate in the bottom position can be assumed to be 0.8 Amp.

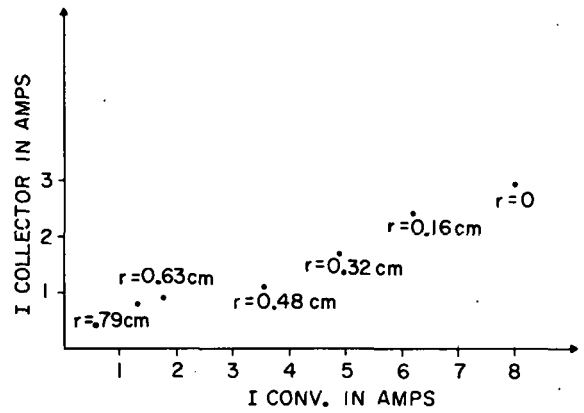

Fig. 4: Collector current versus converter current and radial position.

Thus, with the plate in the bottom position, the negative ion current $I_- = I_{collector} - 0.8$. Figure 5, which is a plot of $I_-/I_{conv.}$ vs the radial position of the converter, is indicative of strong attenuation of the negative ion current.

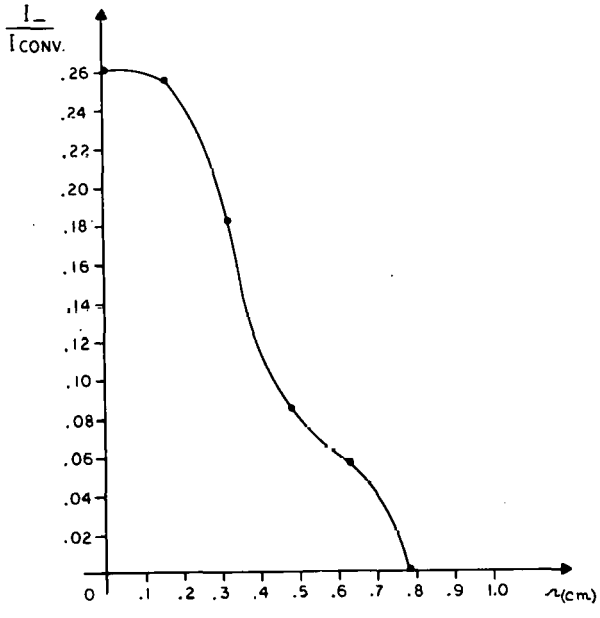

Fig. 5: The ratio of negative ion current to converter current versus the radial position of the converter. With the collector in the "top" position, the current collected by the collector was constant regardless of the converter position.

(6) LaB_6 converter doped with cesium. The previous experiment was repeated with a LaB_6 converter doped with cesium. This converter was exposed to air for a prolonged period of time before it was used. Therefore, it had to be immersed and baked in the plasma to remove surface oxidation. Initially, 0.8 Amp of current were drawn by the collector with the plate in either the top or the bottom position. After 1.5 hours of baking the collector current with the plate at the bottom started to incrase and reached a value of 1.5 Amp, while the current collected with the plate in the top position remained constant.

IV. Conclusion

This set of experiments strongly suggests that a substantial H^- current was produced by the converter from the plasma injected from the HCD. The strongest evidence comes from the fact that the H^- current collected is consistent with the field direction and strength and from the appearance of the H^- signal only after the oxidation was removed from the LaB_6 surface. Also, in the case of the Cs coated Mo surface, the effect reduced in time as the Cs was depleted. It was not measured quantitatively since the Cs depletion could only be observed visually through a window. The remaining question, which cannot be solved without a radical alteration of the device, is what fraction of the negative ion current is due to H^-. The system is dirty and F^- and O^- currents are possible. However, it is hard to imagine that they would amount to more than 10-20%.

Nevertheless, these experiments indicate that a negative ion source based on plasma injection from a hollow-cathode discharge may work well at the expected parameters. Furthermore, due to low background pressure and high gas efficiency, a source based on this principle seems ideal for the production of $_3He^-$ and T^- ions.

V. Design of a 2 Ampere Negative Ion Source

Our next step is to build a dc negative ion source based on HCD plasma injection as it was previously suggested.[7] For our purpose, a desired plasma is to be shaped into thin sheet which is very differenct from the shape of the plasma in the MIT device. To reach this objective, five tantalum cathodes are to be mounted inside a pole piece which is shaped to produce a magnetic field configuration designed to form the plasma into a sheet of 3 cm x 10 cm with a thickness of 0.5 cm. If the planned experiment is successful, Mark V magnetron will be modified to include plasma injection. Figure 6 is a possible design of such a source. The cathode in the original Mark V becomes a converter.

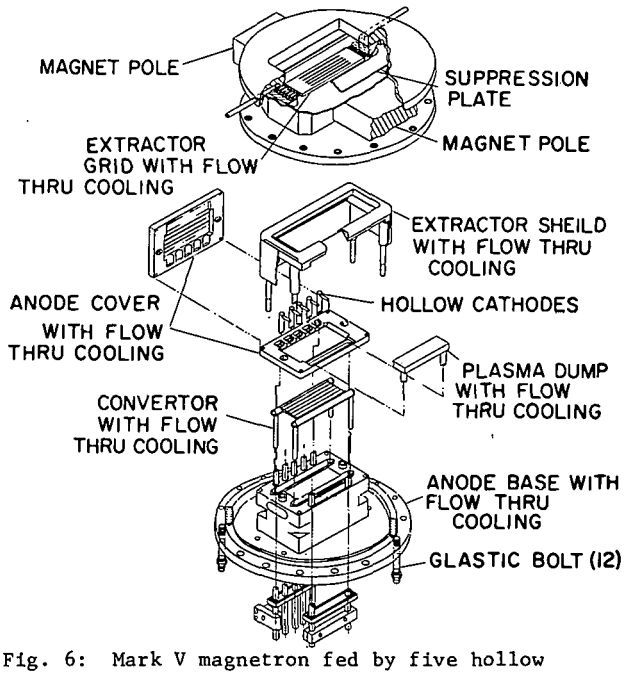

Fig. 6: Mark V magnetron fed by five hollow cathodes.

In a plasma density of 10^{13} cc^{-1}, 2 Amp/cm^2 can be easily drawn by a cesiated converter as we have shown experimentally. Since we have 30 cm^2 of surface area, 60 Ampere of ion current can be drawn on the converter surface. This can be accomplished by plasma injection from five cathodes each yielding 50 Ampere. If we assume conservatively a conversion efficiency of 10%, converter area utilization of 50% and 30% losses in transport, the H^- current extracted from such a source should reach 2 Ampere.

Acknowledgments

We wish to thank Prof. L.M. Lidsky for helpful discussions and for allowing us to use the HCD. All members of the H^- group at BNL teamed up to help with this experiment. One of us (A.H.) would like to acknowledge Jim Alessi's helpful advice in the critical stage of the experiment. Last but not least, Ken Rettman provided enthusiastic highly professional support at every stage of the experiment.

References

1. L.M. Lidsky, S.D. Rothleder, D.J. Rose, S. S. Yoshikwa, C. Micheleson and R.J. Mackin, Jr., Journal of Appl. Phys. 33, 2490 (1962).

2. D.M. Goebel, J.T. Crow and A.T. Forrester, Rev. Sci. Instrum. 49, 469 (1978).

3. A.T. Forrester, D.M. Goebel and J.T. Crow, Appl. Phys. Lett. 33, 11 (1978).

4. D.P. Grdlichko and R.B. Shihikh, Teplofizika Vysokikh Temperatur 15, 708 (1977).

5. J.R. Hiskes and P.J. Schneider, Lawrence Livermor Laboratory report UCRL-84261, May 1980.

6. R.E. Reinovsky, W.C. Jennings and R.L. Hickok, Phys. of Fluids 16, 1772 (1973).

7. K. Prelec, presentation at the DOE program review meeting, Oct. 4, 1979.

* Work done under the auspices of the U.S. Department of Energy.

DISCUSSION

FORRESTER Tell me something about the operation of the cathode. What temperature does this cathode run at and what was the temperature distribution along it when you said a little bit of cesium went through?

HERSHCOVITCH All I can do is to quote you numbers from Lidsky's paper. The temperature is about 2200 to 2500°.

FORRESTER But the cesium was introduced at some place else through a hole?

HERSHCOVITCH This cesium oven was connected to the cathode. This was very difficult to do; we could not get much cesium in.

FORRESTER Apparently a minute cesium can make a spectacular difference in the operation of the cathode.

HERSHCOVITCH One of the references in my paper refers to a Russian paper where they ran hollow cathode discharges in cesium and they were able to drop the discharge voltage all the way from 60 V to 15 V as a function of cesium pressure.

FORRESTER I have run hollow cathodes in cesium too, but you have the cathode operating at the front, at 2200° or something like that.

HERSHCOVITCH There is one thing I did not mention in my talk. In argon discharges, if you are familiar with Lidsky's machine, the famous hot spot of the hollow cathode sits on some distance from the tip and this area eventually burns and the cathode breaks. Now in hydrogen, for some reason, the hot spot moves up to the front so it may be a bit cooler when it runs in hydrogen.

FORRESTER How much current were you running? It depends somewhat on the current. We run hollow cathodes as well, but they do not look like that. With hydrogen we do have the hot region á la Lidsky but it depends on the mode somewhat. Lidsky makes the point that it is operating properly in the high current mode.

HERSHCOVITCH We could not run for very long in this mode because they have cooling only on the anode. This machine was not designed to run at very high currents. During operation at 100 A the soldering joints started to evaporate so we could not run it for very long.

FORRESTER You turned the collector from top to bottom and you got much more current with the collector in the bottom position. When you do that the plate on the bottom is now in the direction of E x B. How do you know you are not collecting electrons?

HERSHCOVITCH For negative ions at 82 volts and 430 Gauss the Larmor radius is about 3 cm while the electrons have a tiny little Larmor radius; only electrons which are in very close vicinity can be collected.

FORRESTER Electrons from the converter could just migrate right down, little tiny loops and they E × B right over to that plate.

HERSHCOVITCH Since the HCD plasma is symmetric the top and bottom electron densities can be assumed to be the same. It would also tend to go around the corner. Another strong argument for having collected negative ions is our measurement with ceslated LaB_6 as converter.

STIRLING How did you measure your density of your plasma column?

HERSHCOVITCH I did not. Measurements were done before with a heavy ion probe and in noble gases by Lidsky and the RPI group. All I did, was to insert a probe as far as I could to see whether I could duplicate the region that could be probed by a probe, and this is what I measured in the hydrogen mode.

EHLERS Did you try this geometry in argon?

HERSHCOVITCH In argon I measured the current that was collected on the converter. I have the data if somebody is interested.

JACQUOT You speak about the neutral pressure in the source of 10^{-4} torr, correct?

HERSHCOVITCH Yes, that is correct.

JACQUOT That corresponds to a maximum of 3.10^{12} particles per cm^3 and you find an electron density more than 10^{13}?

HERSHCOVITCH All I can tell you is that we have an ionization gauge. Plasmas tend sometimes to act as a pump and actually suck gas from the surroundings. I have seen it in Tokamaks.

GELLER It is a fact that in a hollow cathode discharge the ionization rate is close to 100%. This is perfectly true. If I understand you, you try to avoid the heating on the cathodes by using a plasma gun, is that the real problem?

PRELEC The problem is not to improve the power efficiency of the source. The power efficiency would be comparable, it may be improved by a

factor of 2 at most, because you need power for the hollow cathodes, you need the power for the converter and so on. We would keep the power density on the converter at about the same level of 200 watts/cm^2, but what we hope to improve is the gas efficiency and this could be a factor of 10. It is not the power efficiency, it is the gas efficiency that would be improved.

GELLER That is very good.

LEUNG Do you know whether there is any impurity in the negative current you collect?

HERSHCOVITCH That is a good question. One of the things that worried me the most was the impurities. Before we did this experiment we had a macor shield around the converter. As we were doing that experiment, part of the macor oblated so we probably had lots of fluoride. However, it will be very, very hard to conceive of more than 10 or 20% of negative oxygen and negative fluoride. Also, because they move so slow they are more susceptible to destruction than the negative hydrogen. And that is why instead of saying that I have 0.7 A/cm^2, I report only 0.5 A/cm^2. I think it is a reasonable assumption that the impurities would not amount to more than that. In order to measure that accurately, the machine would have to be altered significantly. I think by now we have enough encouraging results to go ahead and design the source.

STEWART Back to the electron business again. At these very high plasma densities I would think that collisional diffusion would be even dominant and the Larmor radius would not even be very relevant, so electrons would just be going all over.

HERSHCOVITCH Collisional diffusion? The neutral density is very low so I do not think so, I disagree with you, I am sorry.

STEWART You are trying to keep electrons inside and they do not want to stay inside, they just want to go all over.

HERSHCOVITCH Are you referring to this experiment or to the source?

STEWART Yes, to this experiment. I am wondering if you are really getting negative ions?

HERSHCOVITCH The collisional diffusion should be symmetric, so why would we see that much more current is detected in one direction as opposed to the other?

FORRESTER It may be a combination of E x B and diffusion which will enable stuff to get to this plate below.

HERSHCOVITCH Yes, but then it does not explain the LaB_6 experiment. Before it became a low work function surface, we could not produce negative ions, the current registered in both the upper and lower position was identical. Only after the surface was heated up and the oxidation was removed, we measured the difference. I could not do a quantitative experiment, but I let the system run for about half an hour. When I came back and started to do the measurement again the negative ion current has dropped about 50%, which is due to the cesium depletion. So it was tested in more than one way.

PRELEC Just a comment to summarize what has been done. First, we know that we can draw a positive ion current onto a biased electrode with about the same density as we have in our sources. We know also that something happens when we put cesium onto that surface. It could well be that we have also electrons coming off that surface and it is possible that they do drift into the collector, but it is a fact, from our sources again, that when we cover molybdenum cathode with cesium, we do notice production of H^- ions together with some secondary electrons. So, we are not saying that we know for sure that we have 0.7 amps of H^- coming off that surface but there are indications, that there is a copious emission of negative ions and that is all. Now the second stage will be an experiment designed at Brookhaven and done in a more careful way, we hope to accomplish that by the end of the year and then we shall proceed with the design of a source itself.

EHLERS Why 82 volts?

HERSHCOVITCH That is as much as I could get from the power supply.

EXTRACTION AND TRANSPORT OF H^-, D^- BEAMS FROM MAGNETRON SOURCES+

Th. Sluyters and J. Alessi
Brookhaven National Laboratory
Upton, New York 11973

Abstract

Negative ion beam optical properties from regular and asymmetric magnetrons are described in single and double gap extractor structures. A significant reduction of beam emittance was observed when the regular flat cathode of the magnetron was replaced by the asymmetric source. The beam divergence could be reduced from 250 mradian in a single gap extractor to 75 mradian in a double gap extractor, but not without beam losses. The loading on the high voltage grid can be reduced to 10% of the total H^- current at an optimum extraction voltage. A 0.5A beam was transported and focussed in a 90° bending magnet with a field gradient n = 1.

I. Introduction

The purpose of the extraction and transport system is to accept negative ions coming out of the source, form a beam with satisfactory properties in current density and emittance, remove the accompanying electrons, transport the beam from the high pressure extractor region, and match it to the low pressure accelerator. In existing neutral beam systems, the acceleration to the final energy is done by electrostatic fields, because this is the best known technology today. Its application in the BNL injector is being studied in spite of some drawbacks (required high voltages, resulting large dimensions). A close coupled, 130 kV system was the only one studied in operation.[1] Although beam currents on the target of up to 1A were achieved in 3 ms pulses, this approach was abandoned because of great difficulties in maintaining high voltage gradients in the presence of a relatively high density background gas from the source. The alternatives are to separate the plasma source from the accelerator by a weak focussing bending magnet, or perhaps by a strong focussing periodic system consisting of electrostatic quadrupoles. These options provide not only independent control of the vacuum around the source and the accelerator, but they also separate the unwanted heavy components from the beam and eliminate possible source damage from backstreaming positive ions.

In this report we will discuss several extractor geometries, single and double gap structures with slits parallel or perpendicular to the magnetic field lines, and also the removal of the electron component of the beam extracted from the source. In addition, we will give the results of the beam transport through a weak focussing n=1 bending magnet, and an initial experiment with a strong focussing electrostatic quadrupole channel.

+Work done under the auspices of the U.S. Dept. of Energy.

II. Single and Double Gap Extraction

The simplest form of beam extraction is single gap extraction. It has been successfully applied in practically all laboratories which utilize magnetron and Penning type negative ion sources. With a computer controlled slit emittance monitor,[2] located about 8 cm from the source, we have analyzed the beam properties (density distribution, divergence and emittance) at an energy level up to 15 keV or a gradient of 75 kV/cm. Figure 1 demonstrates the resolution of the monitor. It illustrates an emittance of a magnetron with four emission slits (50% transparency). At this location of the monitor the emittances of the beamlets from each slit are still separated.

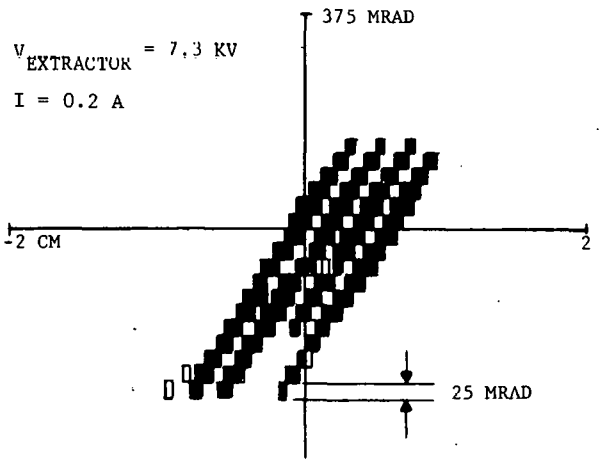

EXTRACTION GEOMETRY

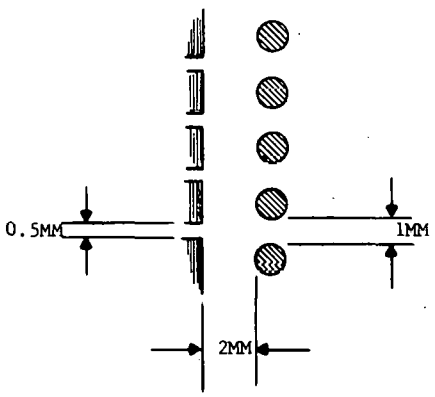

Fig. 1: The emittance from a magnetron with four emission slits. The monitor is located 4 cm from the source. The emittances from each slit are separated.

The divergence of the beam perpendicular to a single slit and in the direction of the magnetic field is in general about ± 250 mrad for beam currents around 200 mA (corresponding to about 1 A/cm^2 emission current density). The normalized emittance, defined as the total emittance area multiplied by $\beta\gamma$ is than about 0.3π cm-mrad for 85% of the beam. The divergence of the beam in the direction of the slit is about ±75 mrad. The emittance for Penning sources are in general smaller than from magnetrons. This difference in performance has been explained by the different origins of fast and slow H^- ions extracted from the magnetron, while only slow H^- ions are extracted from the Penning source. The fast component in the magnetron is directed from the cathode and the slow ions originate from charge exchange collisions.

When the regular flat cathode in the magnetron was replaced by the asymmetric magnetron with groove,[3] we observed a reduction of the total emittance by about a factor of three. This reduction in emittance from 0.3 to 0.1 π cm-mrad is most likely caused by the large reduction in arc current (almost an order of magnitude) for the same beam current output. Figure 2 shows the emittance of a 0.3A D^- beam from a single 0.6 x 45 mm^2 emission slit.

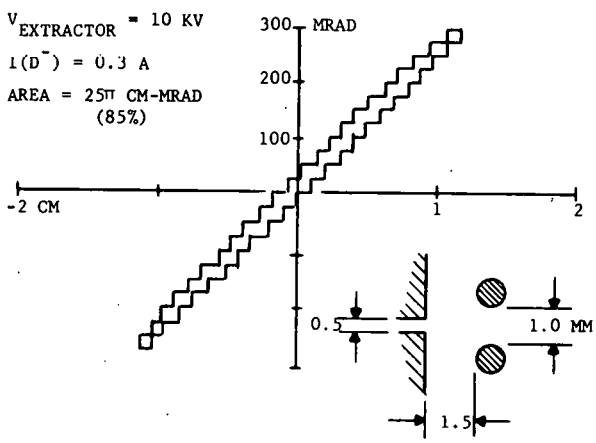

Fig. 2. The emittance of a 0.3A D^- beam from a single emission slit (0.6 x 45 mm^2)

In an effort to collect electrons at low energies and to reduce the divergence of the beam the single gap extractor was replaced by a double gap extractor. The divergence and emittance were indeed significantly reduced (see Figure 3), but not without losing beam current. Based on experiments and computer calculations with different electrode configurations we have concluded that the beam loss is probably due to the different beam optics for fast and slow ions emerging from the source: for example, focussing only the fast H^- component and scraping the slow ions. In an energy analysis of the H^- ions, the existance of significant amounts of both types of ions has been confirmed.[4]

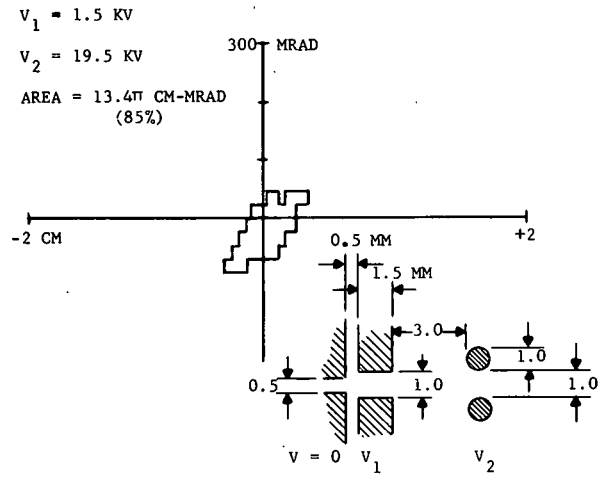

Fig. 3 The emittance of a 75 mA beam with a double gap extractor

III. Electron Removal and Grid Loading

In order to study the electron removal from the beam and the grid loading, the currents falling on all grids of the extractor were separately monitored, in addition to the current on the magnet poles, total power supply load and Faraday cups.

The electron component of the beam extracted from the source may consist of those diffusing out of the plasma itself, those produced by photoemission, by stripping of negative ions in the high pressure regions and those produced in the ionizing collisions of gas molecules. The electrons have to be collected as efficiently as possible after a path in the combined electrostatic and fringing magnetic field which is as short as possible (to reduce secondary ionization) and at an energy level as low as possible (to reduce power losses and heating of the grids).

Under optimum conditions the ratio of electrons extracted to H^- ions can be as low as 1:2. At a fixed arc current, one attains this under optimum Cs coverage and pressure, not because of reductions in the electron component, but primarily due to increases in the H^- component. Much of the electron current (30-50%) travels along the magnetic field lines and hits the source magnet poles. A small fraction E x B drifts out of the extractor gap, while relatively few electrons hit the grids.

Figure 4 shows some typical current parameters as a function of extraction voltage. Above a few kilovolts the total electron plus H^- current out of the source is often constant. The rise in Faraday cup current and drop in the extractor grid current are the result of improved focussing of the beam at higher voltages. At 7 kV practically all H^- ions leaving the source emission slit reach the Faraday cup. The ratio of grid loading to H^- current at this point is 10-20%. Above this voltage the grid loading rises slowly, this being an electron current, as is the loading on the magnet poles.

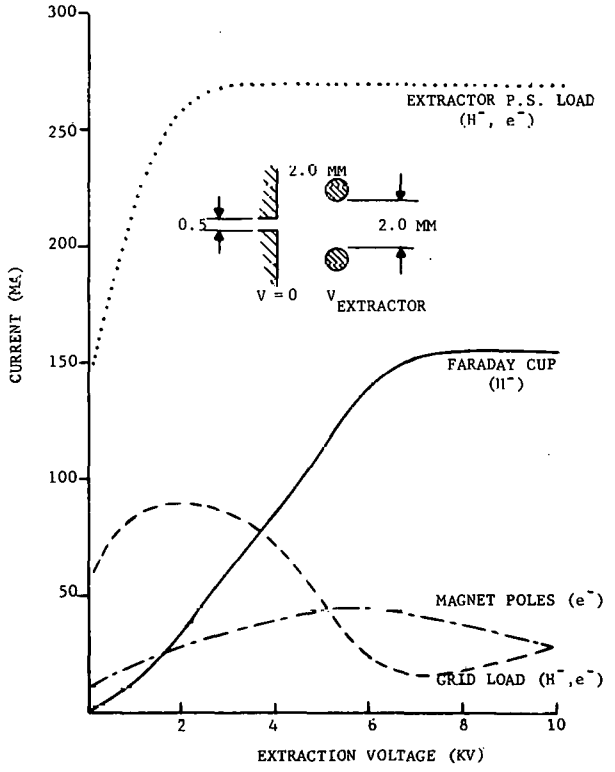

Fig. 4: Some typical current parameters as a function of extraction voltage.

Increasing the source pressure by up to a factor of two above its minimum operating pressure reduces the H^- current out of the source, while the electron current remains very nearly constant, (this fact allows us to determine which loads are electrons and which loads are H^- ions at any extractor voltage). Therefore, one gets the best e^-/H^- ratio at the lowest pressures. Attempts to further reduce the e^-/H^- ratio by making the anode emission slit deeper and narrower (to increase the number of electrons diffusing along B into the slit walls) were unsuccessful - both the e^- current and H^- current dropped, maintaining essentially the same ratio. In the switch from the regular magnetron with flat cathode to the asymmetric magnetron with grooves in the cathode the change in e^-/H^- at a given H^- current was much less than the corresponding change in arc current. From these observations one may conclude that a large fraction of the electrons emerging from the source originate from stripping of negative ions and ionization around the emission slits or from photoemission, and much less by diffusion from the main plasma.

When the cathode grooves and emission slits were placed parallel to the magnetic field, the H^- yield for similar source parameters was at best 50% of that obtained with slits and grooves perpendicular to the field. This reduction results from a higher angular dispersion of geometrically focussed ions inside the source, due to deflection in the magnetic field. However, for single gap extraction, the e^-/H^- ratio, and the ratio of grid loading to H^- current were essentially the same as values obtained with the grooves and slits perpendicular to the magnetic field.

Using a double gap extraction with a small first gap (intended for collection of electrons at low voltages), we obtained particularly low loading on the high voltage electrode when there was no voltage across the first gap. In this way we could sometimes reduce the loading on the final grid to 5% of the beam current, without too much reduction in beam current. This configuration seemed to eliminate some of the electrons, in addition to the possibility that the slow H^- component was reduced. The effect of the first gap with no voltage across it is similar to making the anode thicker, except that the pressure in the anode emission slit is high, while the pressure in the first gap is significantly lower.

The double gap system with the slits parallel to B consistently had low loading on the final grid, although, as mentioned previously, one sacrificed beam output. In this configuration the electrons would be deflected into the first grid by the source magnetic field.

IV. Beam Transport With Single Gap Extraction

The main purpose of the beam transport is to match the beam from the high pressure extraction region to the low pressure accelerator. This may be achieved by either a weak focussing bending magnet or by an array of strong focussing electrostatic quadrupoles.

A first attempt at transporting a 15 kV beam was made with a 20 cm radius, 90° weak focussing dipole magnet with a central gap of 8 cm and a field gradient n=1. A 0.5A beam, extracted from a magnetron with four emission slits (emission density $0.5A/cm^2$) was transported and focussed. Figure 5 shows an emittance measured after the bending magnet. The divergence is about ± 50 mrad. The transmission through the bending magnet was estimated to be better than 90% in a background pressure smaller than 10^{-4} Torr. The beam dimensions and low divergence was in good correspondence with the beam transport calculations assuming 100% space charge compensation. The beam density after the bending magnet was about 10-12 mA/cm^2.

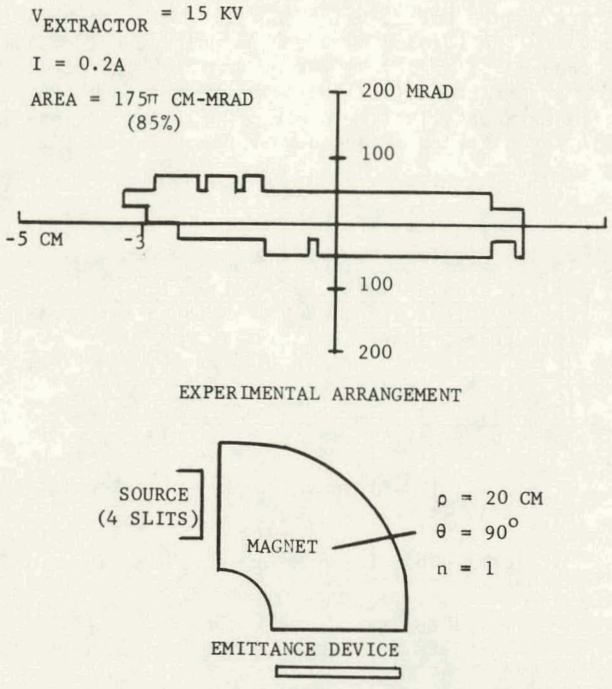

Fig. 5: Emittance after the 90° bending magnet for a 0.2A beam. The beam density after the bending magnet is 10-12 mA/cm^2

In collaboration with Al Maschke and the Heavy Ion Fusion group, a crude strong focussing electrostatic quadrupole channel was constructed to test its feasibility in applications for neutral beams. Figure 6 shows its principle and Table I some of its pertinent parameters. The quadrupole chain of 12 quadrupoles with a total length of 7.2 cm, a channel aperture of 3 mm and a quadrupole length of 3 mm was mounted on the poles of the magnetron (see Fig. 7). The voltage on the quadrupoles is ± 1.5 kV. With a source emission slit of 0.3 x 3 mm^2 a negative ion beam of 15 mA was injected into the channel. Although only 3.8 mA of beam was transported through these single aperture quadrupoles, the transmission of 55% of the calculated value is encouraging. Further exploration of this new method of beam transport seems to be justified.

TABLE I

Number of quadrupoles	12
Total length	7.2 cm
Length of each quadrupole	3 mm
Inner radius of quadrupole	1.5 mm
Voltage	±1.5 kV
Acceptance (normalized)	0.066π cm mrad
Source emission slit	0.3x3 mm^2
Extracted H^- beam	15 mA
Calculated transmission	46%
Transported beam (11 kV)	3.8 mA
Percentage of calculated value	55%

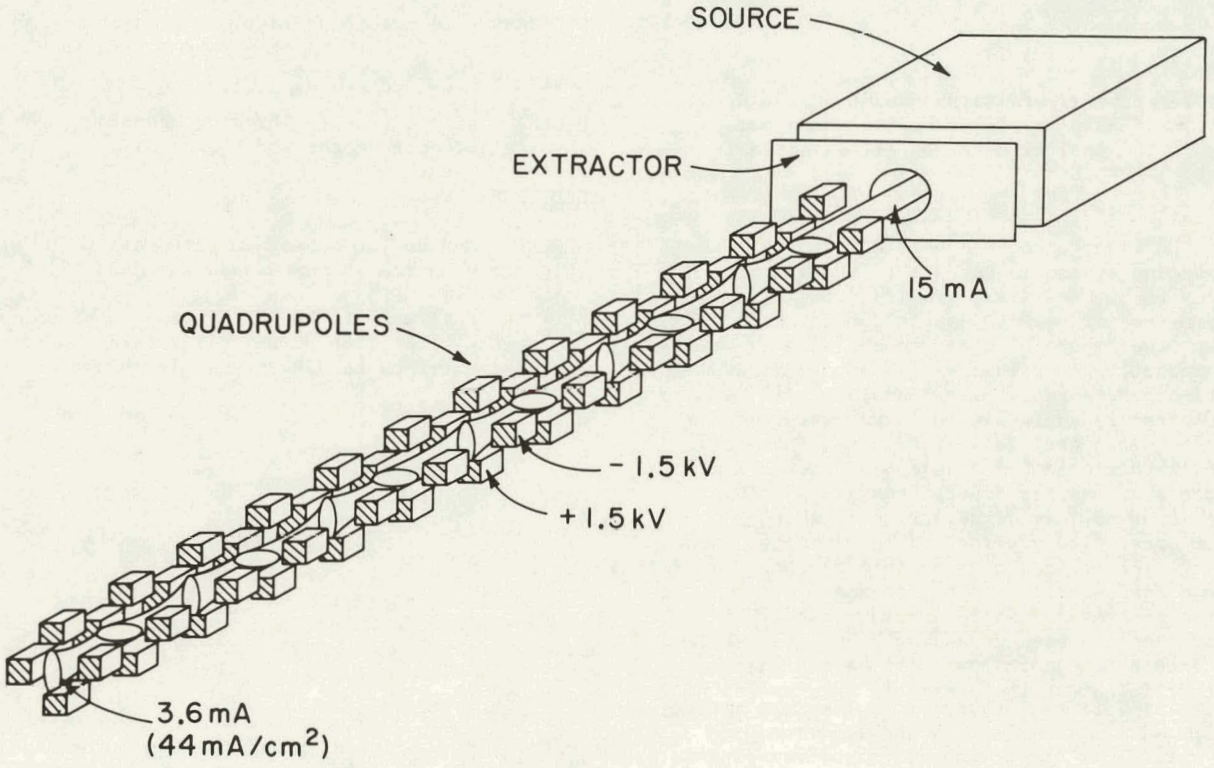

Fig. 6: Schematical layout of a strong focussing electrostatic quadrupole channel mounted downstream from a magnetron source.

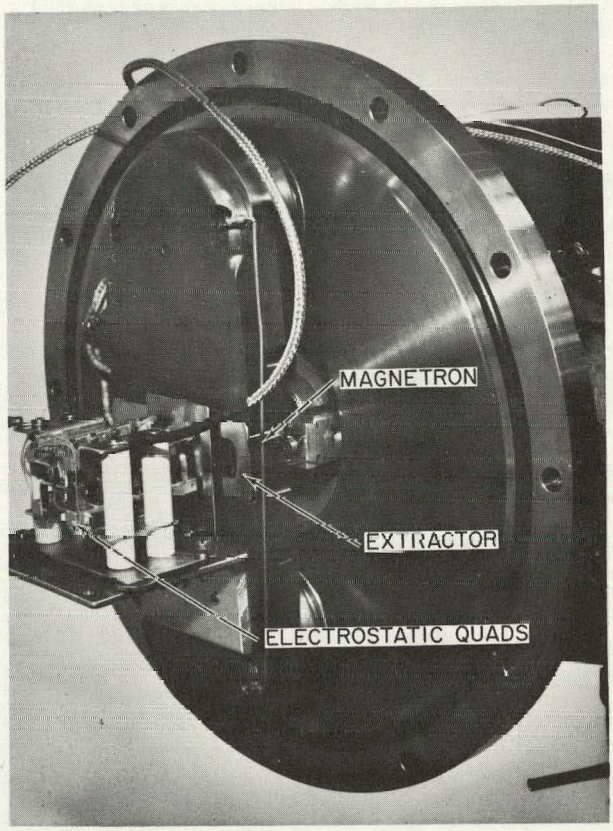

Fig. 7: Experimental arrangement of the strong focussing electrostatic quadrupole channel with the MK III magnetron.

V. Discussion

The divergence of a beam with a single grid extraction system is acceptable for a transport system which uses field gradient bending magnets. This method of beam transport can be scaled to one or two ampere H^- beams in a single gap bending magnet. For a multi-gap bending magnet and multi-ampere negative ion beams, it will be more convenient to apply simpler structures such as magnets with zero field gradients. The measurements with single and double gap extraction indicate that smaller divergences are possible with lower current densities and double gap structures. The precise configuration of such a system will depend on a possible further reduction of gas pressure in the asymmetric magnetron source to provide single species (fast) H^-/D^- ions. In case such pressures cannot be realized the double gap structure will be designed such as to eliminate the undesirable species in the most efficient way, namely on the lowest voltage electrode.

The grid loading is a less severe problem than anticipated. Most of the electrons (50%) are collected on an electron collector or on the source magnet poles, which therefore have to be cooled. The loading on the high voltage grid can be reduced to as low as 10% of the total H^- beam. With a heat removal capacity in the grids of 100 W/cm, extraction voltages of 15-20 kV are acceptable, even for emission current densities as high as 0.5 A/cm^2.

References

1. Th. Sluyters and C. Lam, Proc. of the Symp. on the Production and Neutralization of Negative Ions and Beams, Brookhaven National Laboratory, Sept. 1977, p. 211.

2. Th. Sluyters and V. Kovarik, Proc. of the 1979 Linear Accelerator Conference, Brookhaven National Laboratory, BNL 51134, p. 428.

3. J. Alessi, Th. Sluyters, to be published in Rev. Sci. Instr.

4. J. Alessi, Th. Sluyters (published in these proceedings).

DISCUSSION

HAGENA Assuming the improved gas efficiency of 6% with your grooved cathode device do you expect any problems with neutrals coming out of the source and interfering with the transport and extraction of the negative beams?

SLUYTERS In pulsed operation for pulses up to 10-100 ms we do not expect problems. For d.c. operation we do not know.

HAGENA If you take the bending magnet, you physically separate the two flows?

SLUYTERS Yes.

HAGENA And do you expect improvements by using this other source at much lower gas densities?

SLUYTERS If we get the hollow cathode discharge operational then I think we will return to close coupling where no bending magnet is involved.

H⁻ ION SOURCE RESEARCH AT LOS ALAMOS*

Paul Allison, H. Vernon Smith, Jr. and Joseph D. Sherman
AT-2 (MS-818), Los Alamos Scientific Laboratory, Los Alamos, NM 87545

Abstract

Up to 160 mA of H^- ions has been extracted at 20 kV from a 10 by 0.5-mm^2 slit in a Penning surface-plasma source. Typically, 70% of the beam can be transported through a bending magnet to a Faraday cup or emittance scanner. Up to 90% transmission has been observed for some neutralizing gases. Average and pulsed cesium flows from the source were measured with a surface-ionization gauge. Operating parameters of the source and measurements of the emittance are reported.

Introduction

Many medium- and high-energy accelerators, including those at Argonne,[1] LAMPF,[2] TRIUMF,[3] and Fermilab,[4] use H^- ions in lieu of or in addition to H^+ ions, for a variety of reasons. Accelerators producing beams with high average power (800 kW for LAMPF) require the lowest possible emittance to minimize beam losses and subsequent accelerator activation. The Penning surface-plasma source (SPS)[5] has low emittance and pulsed current suitable for use with these machines. Future accelerator applications may require intense dc sources of H^- ions.

Operation of the Penning SPS

The Los Alamos Scientific Laboratory (LASL) Penning source, adapted from the design by Dudnikov[5] for use with the USSR meson factory, is shown in Fig. 1. Electrons, confined by an ~0.2-T magnetic field oscillate between molybdenum cathodes, and ionize hydrogen gas at a nominal density of $4 \times 10^{15}/cm^3$. The ions drift to the cathodes, are accelerated through the plasma sheath, and impact on the cathodes, releasing secondary electrons and H^- ions. Only a low discharge current of 50-100 mA is produced at 650 V until cesium is added, usually from heating of a 2:1 mixture of titanium and Cs_2CrO_4 powders packed into the anode. When the cathode and anode temperatures are 400-500°C and the source housing is at 200°C, sufficient cesium is generated so that the discharge potential drops to 40-60 V for a 1-A dc current. Within the limitations of an ~50-W discharge power the uncooled source can be operated at any duty factor; for our purposes this is usually 7.5-Hz, 1-ms pulses of 100 A.

The cesium is believed to play two important roles:

1. It increases the secondary electron emission coefficient[6] $\gamma = j_e/j_+$ from about 0.1 for a pure molybdenum surface[7] to about 5.5.

2. It increases the secondary H^- ion emission coefficient[6] $K = j_-/j_+$ from a low value to about 0.7, where j_e, j_+, j_- are the electron, positive ion, and negative ion current densities at the cathode, respectively.

The large value of γ presumably accounts for the low discharge voltage, which is strongly dependent on cesium coverage of the cathodes.

Our discharge will not operate below a minimum magnetic field B_m. Because positive ions must reach the cathodes to sustain the discharge, we expect that B_m must be large enough that the Larmor radius of the ions is less than the half-width w/2 of the anode chamber. The value of B_m for 100-A discharges in H_2 and in D_2 for two chamber widths is consistent with H^+ and D^+ ion energies kT of about 2 eV (Table I), where $kT = (eB_m\, w/2)^2/2M$. Derevyankin[8] operates a similar source with a field as low as 0.05 T, more nearly consistent with confinement of primary electrons whose momenta transverse and parallel to the field are comparable. Discharge noise disappears at about our value of B_m for both sources, a desirable condition for the production of low-emittance beams.

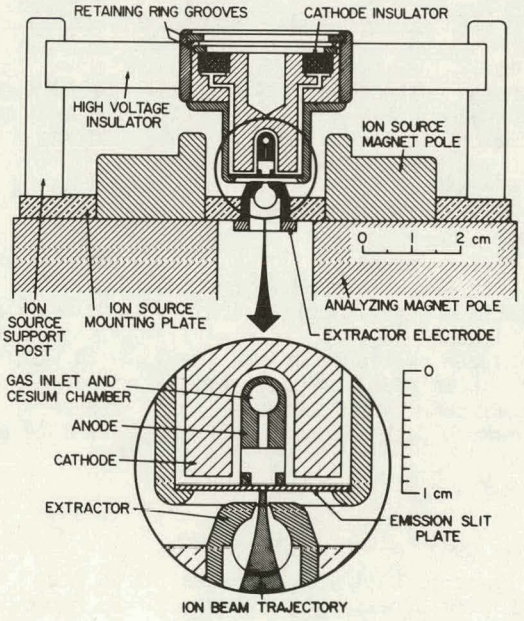

Fig. 1. Cross-sectional drawing of LASL Penning surface-plasma source.

*Work done under the auspices of the US Department of Energy

Table I. Minimum Magnetic Field B_m Needed to Sustain Pulsed Discharge

Gas	w(mm)	B_m(T)	kT(eV)
H_2	2	0.21	2.1
H_2	3	0.15	2.4
D_2	3	0.20	2.2

A 100-A discharge in the 2 by 12-mm^2 discharge area will produce a 100-mA beam through the 10 by 0.5-mm^2 emission slit for a dc gas flow of 100-atm-cm^3/min. The source volume is about 1 cm^3, and the gas flow is pulsed with a Veeco PV-10 piezoelectric valve. A time of 1-2 ms is required to stabilize the source pressure, primarily because of mechanical oscillations in the valve. Source gas density, measured in the absence of a discharge, was 4×10^{15}/cm^3.

From the values of K and γ and the total measured cathode current density we calculated the electron, H^-, and positive ion current densities there. We estimate the plasma density by assuming that the ion current to the cathode j_+ consisted of protons with a temperature kT = 4 eV, so that $j_+ = neV/4$ where $V = (8kT/\pi M)^{1/2}$. The measured, assumed, and calculated operating parameters of the source are summarized in Table II.

Cesium Flow Measurements

We measured[9] the cesium flow with a surface-ionization gauge (SIG) mounted on an insertable probe so that the distance between the SIG and the source emission slit could be varied.

Table II. Typical Source Operating Parameters

Measured	
Discharge voltage	40-120 V
Discharge current	100 A
H^- current extracted from 10 x 0.5-mm ^{2}emission slit	100 mA
Extraction gap	2.5 mm
Transport efficiency through 90° magnet	70%
Gas flow	100 atm cm^3/min
Magnetic field in discharge region	0.21 T
Extraction power supply current	200 mA
Duty factor	7.5 Hz, 1 ms
Normalized emittance of 40% of the beam (63% for each plane)	0.04 x 0.03 $(\pi$ cm-mrad$)^2$
Current density at cathodes	208 A/cm^2
H_2 density with discharge off	4×10^{15}/cm^3
Assumed	
$kT_e = kT_+ = 4$ eV	
K = 0.7	
γ = 5.5	
Calculated	
Ion current density at cathodes	29 A/cm^2
H^- current density at cathodes	21 A/cm^2
Electron current density at cathodes	158 A/cm^2
Plasma density	3×10^{14}/cm^3

Charged particles were kept from the SIG by a combination of the magnetic field and a biased electrode at the SIG entrance. The cesium atoms entered the SIG and impinged on a tungsten filament at a temperature of 1500 K, hot enough to ensure that they would be re-emitted within 10 μs as Cs^+ ions.[10] The filament bias of +60 V with respect to the collector was sufficient to collect all Cs^+ ions but low enough to avoid excessive secondary emission at the collector. Hydrogen neutrals had little or no effect on the SIG. The cesium evolution rates from 2:1 mixtures of titanium with $Cs_2Cr_2O_7$ and with Cs_2CrO_4 powders were measured and the rates doubled for temperature changes of 20° and 32° respectively at 450°C, but the rate from the latter mixture was about four times that of the former. Source operation is essentially identical whether these mixtures or cesium metal-vapor ovens are used.

Absolute cesium flow rates from the source were calculated by using the solid angle subtended by the SIG and by assuming a modified isotropic angular distribution of cesium atoms from the source. When the source is operated with a 1-A dc discharge, the cesium flow for optimum H^- current is 0.5 mg/hr. The variations of discharge voltage and H^- ion current with the equivalent cesium density are shown in Fig. 2, where this density is that which would produce the observed flow rate in the absence of a discharge and hydrogen flow. When the discharge is abruptly extinguished, the cesium flow jumps about a factor of three, showing that even at a low discharge-current density of 4 A/cm^2, cesium flow is retarded by ionization.

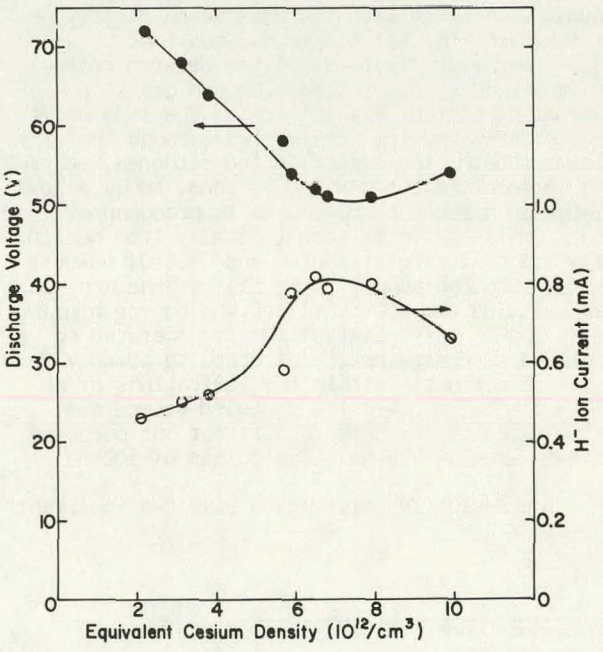

Fig. 2. Variations of the discharge voltage and extracted H^- current vs equivalent cesium density for a 1-A dc discharge.

Flow during pulsed operation is more complex. For a 60-V, 100-A discharge, the cathode power density F is 8.3 kW/cm^2, assuming that 1/3 of the power goes to each cathode and to the anode.[6] The temperature rise of a semi-infinite solid subjected to this surface heating would be[11]
$\Delta T = 2F(t/\pi K\rho C)^{1/2} = 140°C$ at t = 1 ms, where K = 1.38 W/cm°C, ρ = 10.2 g/cm^3, and C = 0.3 J/g°C for molybdenum.

For an average cathode temperature of 500°C and a fractional equilibrium coverage θ = 0.65, the evaporation rate of the cesium will be increased by a factor of ~100 for this temperature rise, which would lead to a new equilibrium value of θ = 0.45; however, we believe that θ actually increases during the pulse because of discharge pumping. As the cesium flow from an independently controlled oven is increased up to the optimum value, the discharge voltage and noise decrease and the H$^-$ current increases. The same trends are observed as a function of time for a 1-ms pulse when the average cesium flow is low. When the discharge is extinguished, cesium rapidly evaporates from the cathodes. From the evaporation rates given by Taylor and Langmuir[10] for cesium on tungsten, we estimate that θ decreases by 0.05-monolayer in the first 20 μs with a rapid drop in evaporation rate thereafter. The atoms are quickly readsorbed on cooler surfaces of the source so that there is a short burst of cesium flowing from the source.

We calculate that the cesium flux N as a function of time t at the SIG, at a distance d from the source, using the equations of flow for an ideal oven[12] for a short time δt is

$$N = N_0 (t_0/t)^5 \exp(2.5[1-(t_0/t)^2]) \qquad (1)$$

where

$$N_0 = Af\Omega n\delta tkT (5/e)^{5/2}/4\sqrt{2}\,\pi^{3/2}Md$$

$$t_0 = (Md^2/5kT)^{1/2}$$

A = emission area of source

f = flux distribution factor[9]

Ω = solid angle subtended by SIG

n = density of cesium atoms in source.

This calculated flux is compared with the measured data in Fig. 3, for which N_0 and t_0 have been adjusted to fit the data. A cathode temperature T of 730°C, near the value estimated at the end of the pulse, is calculated from the value of t_0. Scattering of the cesium atoms by the H_2 gas was not taken into account, but this would improve the fit for long times of flight. As first noted by Belchenko[13] the cesium consumption for a dc source might be much less than the typical 1 mg/hr used for pulsed operation.

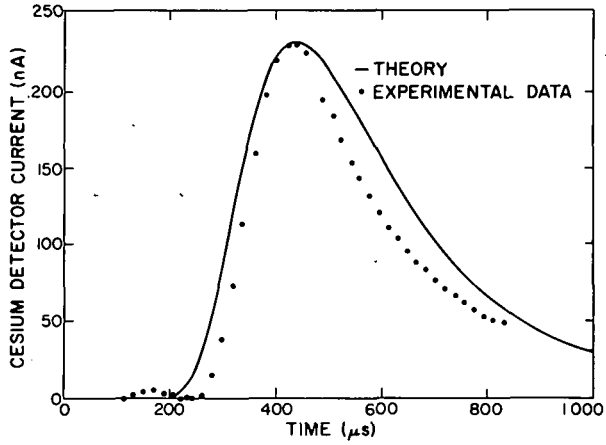

Fig. 3. Flow of cesium from source vs time after 100-A discharge is extinguished. The curve is a fit of Eq. 1, assuming a cathode temperature T of 730°C.

H$^-$ Plasma Losses

From the plasma densities given in Table II we can estimate the attenuation for an H$^-$ ion traveling a distance ℓ from the cathode to the emission slit. The factor a_e for attenuation by electron collisions is
$a_e = \exp(-\rho_e \langle \sigma_e v_e \rangle \ell/v_-) = 0.2$
for ℓ = 3 mm, 60-eV H$^-$ ions, and an electron temperature of 4 eV, for which
$\langle \sigma_e v_e \rangle = 2 \times 10^{-7}$ cm^3/s (Ref. 14). The factor a_+ for proton collisions is 0.2, whereas that for H_2 collisions is 0.6. The attenuation by collisions with slow H^0 atoms leads mostly to slow H$^-$ ions. Because ρ_0 is not known, we can only state that if it is 8 x 10^{14}/cm^3 (10% of the H_2 dissociated) then a_0 = 0.2. As H$^-$ ions are thermalized, a_e becomes the dominant factor. It seems clear that only a small fraction of cathode-produced H$^-$ ions would reach extraction. From Table II the H$^-$ current density from each cathode is 21 A/cm^2, whereas the extracted current density is only 2 A/cm^2; therefore, if the H$^-$ ions are produced at the cathode, the current density is attenuated by a factor of ~20 before extraction.

To get some measure of this effect, we varied the anode web thickness and measured the H$^-$ current under otherwise identical conditions. This web (Fig. 4) serves to partially filter plasma electrons from the emission area and is normally 1-mm wide. The H$^-$ current was found to be attenuated by e^{-1} in a distance of about 1.4 mm. If H$^-$ ions from the cathode had a similar attenuation the factor would be 8, over the 3-mm distance. The agreement with the above estimates is rough, but it seems clear that H$^-$ ions are subject to severe losses before extraction. Although the H$^-$ production efficiency increases for small web thickness, the electron loading of the extraction power supply increases

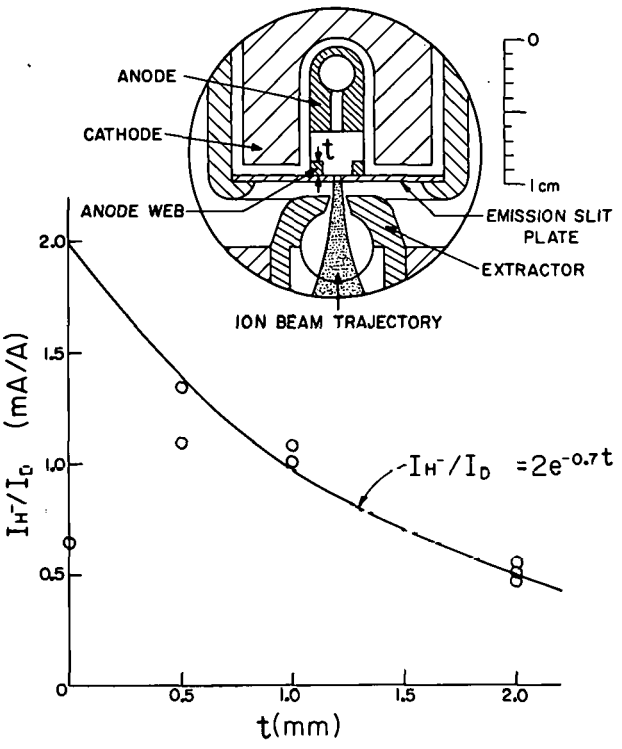

Fig. 4. H^- production efficiency (I_{H^-}/I_D) vs anode web thickness t. A curve with exponential dependence on t has been fit to the data.

from 100% of the H^- ion beam to about 300% for a web thickness change of from 1 mm to 0.5 mm, and for zero web thickness it becomes difficult to operate the extractor.

Extraction and Transport

Extraction is difficult if the extraction gap g is small enough to allow electrons to cross. In the presence of a magnetic field B, and extraction voltage ϕ, electrons cross the gap unless $g > (2m\phi/e)^{1/2}/B = 2.3$ mm for B = 0.21 T, ϕ = 20 kV. The extractor is made of molybdenum so that occasional overheating does not melt it. It is desirable to operate the extractor at a warm temperature to evaporate impinging cesium. A cooled extractor was unsuccessful because of cesium condensation.

The beam diverges strongly at the entrance to the 90°, n = 0.85, 8-cm-radius magnet but is reasonably well focused at the exit. Up to 160 mA has been extracted at 20 kV into the Faraday cup, 2 cm past the extractor [I(0°)], a current density of 3.2 A/cm^2 at extraction. Extraction from circular emitters has also been successful.[15] Table III lists parameters for extracted and transported beam for several different emission geometries, where I_D = discharge current, I(90°) is the H^- current transported to a Faraday cup, 6 cm past the 90° magnet, and j_{em} is the H^- emission current density.

Increasing the hydrogen feed rate beyond the minimum for stable discharge operation causes the H^- beam to be attenuated in a manner consistent with the cross sections for collisional detachment, both in the source and in the 90° magnet. If the gas is pulsed instead of flowed continuously the required flow of cesium is reduced. The transport efficiency through the 90° magnet improves, however, when some other gases are added to the vacuum system. Ion-optics calculations using the Kapchinskij-Vladimirskij equations[16] for beams with space charge and emittance show that an unneutralized beam of 100 mA at 20 kV would diverge in the magnet and be poorly transmitted, whereas 70% transmission is typically observed, implying at least partial neutralization. A neutralization monitor consisting of a biased collector plate shielded by a grounded screen was installed at the magnet exit with the 4 by 2-cm^2 collector plate parallel to the magnet poles so that slow electrons and ions would be collected. The energy spectrum of charged particles was measured by varying the bias voltage of the collector.

For low-energy H^- ion beams, the probability of ionizing the residual gas is much less than that for producing slow electrons by H^- stripping. The ionization cross sections for H^- and H^+ ions beam have been[17] found to be the same. The ratio R_c of electrons to ions produced in various gases at 20 keV was calculated from existing data[7,17,18] and is given in Table IV. Our measured value R_m is in rough agreement.

The electron energy distribution was approximately Maxwellian with a temperature of about 25 eV, twice that for electrons produced by proton ionization of gases.[19] Because the stripped electrons have kinetic energy (11 eV for 20 keV H^- ions) a higher temperature might be expected. Generally gases heavier than helium improved the H^- transmission by about 15%, resulting in up to 90% transmission. The optimum density in the transport region was about 10^{12}/cm^3 for all gases.

Table III. Extracted and Transported Beam

Emitter (mm)	Extractor (mm)	Gap (mm)	I_D (A)	I(0°) (mA)	I(90°) (mA)	j_{em} (A/cm^2)	ϕ (kV)
10x0.5	20x1	2.5	108	100	80	2	18
10x0.5	20x1	2.5	150	160	110	3.2	20
1 diam	1 diam	1.2	100	33	-	4.1	15
2 diam	2 diam	2	100	57	-	1.8	20

Table IV. Beam Transport with Neutralizing Gas Added

Gas	R_c	R_m	kT_e(eV)	Transmission Improvement over that for H_2
H_2	7.8	5	24	0%
N_2	5.1	-	-	19%
Ne	8.5	10.4	28	-
Kr	7.2	9	25	17%

Transmission efficiency is strongly dependent on beam-current noise. In a single pulse, the H^- current I(0°) may rise 30% during a transition from a noisy to a quiet discharge, and I(90°) may rise by 100% or more.[20] Probably the neutralizing plasma cannot track the fluctuating current, which, along with a fluctuating location of the plasma surface at the source, would lead to a time-averaged emittance increase. Measurements have shown that there can be a factor of 3 variation in emittance under these conditions.[15]

The 90° magnet used results in a circular beam at the exit with about 100 times lower density than at extraction, desirable for many subsequent accelerator applications. The magnet also induces substantial coupling between the x- and y-planes (the 1- and 0.05-cm directions along the emission slit respectively). There are two dominant aberrations[21] in this case, $\delta y' = A_1 x'y$ and $\delta y' = A_2 xy$. These arise from a combination of the sextupole components of the bending and of the exit fringe fields, the latter being essentially fixed but the former being adjustable by magnet pole design. The minimum net aberration is achieved by taking a finite value of the bending sextupole to partially cancel the effects of the exit fringe fields. If the beam size (about 2-cm diam) were smaller in the magnet, perhaps by means of better extraction optics and a quiet discharge, the aberration would be reduced. Even so the emittance is acceptably low.

Emittance

The emittance of an ion beam has as its origins

1. the temperature of the ions in the plasma and the size of the emitter,
2. ion-optical aberrations in the extraction and transport elements,
3. nonlinear space-charge forces, and
4. time-dependent fluctuations in the current, leading to time-averaged increase in emittance.

In a typical emittance scanner[20] phase space is mapped as a function of threshold t, where

$$t = (\partial^2 i/\partial x \partial \dot{x})/(\partial^2 i/\partial x \partial \dot{x})_{max}$$

averaged over y, $\dot{y}$ space. Then the fraction F of current within a normalized emittance ε is given by $F(t_o) = \iint_{t_o \leq t \leq 1} (\partial^2 i/\partial x \partial \dot{x}) dx d\dot{x} \Big/ \iint_{o \leq t \leq 1} (\partial^2 i/\partial x \partial \dot{x}) dx d\dot{x}$ and $\varepsilon(t_o) = 1/\pi \iint_{t_o \leq t \leq 1} dx d\dot{x}/c$.

As a simple model we assume that the ions at the plasma surface have uniform spatial density and a temperature T, and we neglect other sources of emittance (2,3,4 above). Then by Liouville's theorem[22], F and ε are invariant in transport, even in the presence of linear space-charge forces, so that the calculated dependence of F on ε at the plasma surface may be compared directly with that at the emittance scanner plane.

For a slit emitter, t is independent of x over the slit of width 2R, so that $t = \exp(-m\dot{x}^2/2kT)$ $|x| \leq R$. Evaluation of the integrals leads to

$$F = \mathrm{erf}(\pi\varepsilon/4R[\,2kT/mc^2]^{1/2}) \qquad (2)$$

The normalized rms emittance is defined by[22] $\varepsilon_{rms} = 4\,(\langle \dot{x}^2 \rangle \langle x^2 \rangle - \langle x\dot{x} \rangle^2)^{1/2}/c$ so that for the slit $\langle x^2 \rangle = R^2/3$, $\langle \dot{x}^2 \rangle = kT/m$, $\varepsilon_{rms} = 4R(kT/3mc^2)^{1/2}$ and $F = \mathrm{erf}(\pi\varepsilon/6^{1/2}\varepsilon_{rms})$. For a circular aperture t is no longer independent of x but is given by $t = (1-x^2/R^2)^{1/2} \cdot \exp(-m\dot{x}^2/2kT)$. Now F is not a simple function of ε, but the integrals were evaluated numerically, and the results are very close to those for the slit. It is still possible to evaluate ε_{rms} analytically, and the results are[22] $\varepsilon_{rms} = 2R\,(kT/mc^2)^{1/2}$. According to this model the rms emittance contains 93% and 91% of the beam for the slit and the circular aperture emitters, respectively.

The emittance of a 17-keV, 80-mA beam extracted from a slit was measured with a scanner having a pair of movable slits, between which are beam-deflecting plates so that the current distribution can be measured as a function of angle. The calculated fraction of the total current within a given normalized emittance is shown in Fig. 5, along with a fit of Eq. 2, using T as the adjustable parameter.

We believe that fast H^- ions from the cathodes make resonant charge-exchange collisions with H atoms in the discharge; therefore their temperature should be that of the H atoms. The latter temperature is not known, but the Franck-Condon energy for collisional dissociation[23] of H_2 is > 2 eV/atom. The temperature deduced from the fit for the x-plane (2R = 10 mm) is 5 eV, in the expected range. For the y-plane (2R = 0.5 mm) the deduced temperature is 820 eV; however, we know[21] that the bending magnet couples the x- and y-plane emittances so that the larger emittance of the x-plane masks that of the y-plane. The large effective ion temperature reflects the small initial plasma radius for the y-plane. The fit of the theory to the data shows that the velocity distributions are not exactly

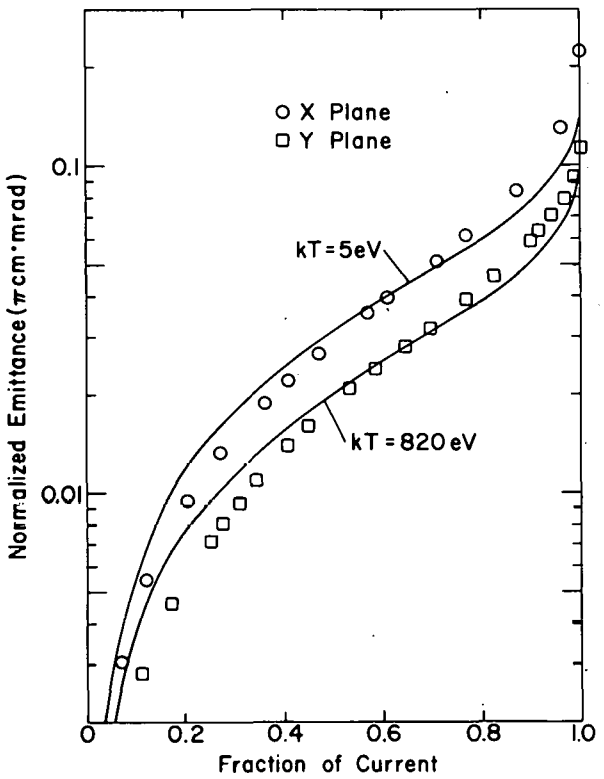

Fig. 5. Normalized emittance vs fraction of an 80-mA beam extracted from a 10 x 0.5-mm^2 slit. The curves are fits of Eq. 2 assuming kT = 5 eV and 820 eV in the x- and y-planes, respectively.

Maxwellian, and this is typical of all of our emittance measurements for beams extracted from slit emitters. Better fits have been observed for circular aperture emitters.[15]

Future Plans

The SPS principle using Penning geometry has been extended to a design with rotating electrodes to help dissipate the high power density required to produce 100 mA of H^- ion current dc. This concept is now being tested.[24] A 250-kV H^- injector is being built to provide beams for accelerator structure tests. This injector is designed to produce 100-mA beams with a pulse length of 1-ms and a frequency of 7.5 Hz.

References

1. John A. Fasolo, H^- Source Development at ANL, IEEE Trans. on Nucl. Sci. NS-24, No. 3, June 1977, p.1597.

2. P. W. Allison, E. A. Meyer, D. W. Mueller, and R. R. Stevens, Jr., "Performance of the LAMPF Injector," Proc. of the Second Symp. on Ion Sources and Formation of Ion Beams, LBL-3399, Berkeley, 1974.

3. John B. Warren, TRIUMF, March 1971, IEEE Trans on Nucl. Sci. NS-18, No. 3, 1971, p. 272.

4. Charles W. Schmidt, Cyril D. Curtis, "A 50-mA Negative Hydrogen-Ion Source," IEEE Trans. on Nucl. Sci. NS-26, No. 3, June 1979, p. 4120.

5. V. G. Dudnikov, "Surface-Plasma Source of Penning Geometry," IV USSR National Conference on Particle Accelerators 1974.

6. Yu. I. Belchenko, G. I. Dimov, V. G. Dudnikov, "Physical Principles of the Surface Plasma Method for Producing Beams of Negative Ions," Proc. of the Symp. on the Production and Neutralization of Negative Hydrogen Ions and Beams, BNL 50727, Sept. 1977, Brookhaven National Labs. p.79.

7. From the compilation by C. F. Barnett, J. A. Ray, E. Ricci, M. I. Wilker, E. W. McDaniel, E. W. Thomas, and H. B. Gilbody, "Atomic Data for Controlled Fusion Research," ORNL-5206, Oak Ridge National Lab, 1977.

8. G. E. Derevyankin, V. G. Dudnikov, "Formation of H^- Ion Beams for Accelerators in Surface-Plasma Sources," Novosibirsk Preprint IYaF 79-17, UCRL-TRANS-11549.

9. H. Vernon Smith, Jr., Paul W. Allison, "Measurements of the Cesium Flow from a Surface-Plasma H^- Ion Source," IEEE Trans. on Nucl. Sci. NS-26, June, 1979, p. 4006.

10. J. B. Taylor and I. Langmuir, "The Evaporation of Atoms, Ions, and Electrons from Caesium Films on Tungsten," Phys. Rev. 44, No. 6, Sept. 1933, p. 423.

11. H. S. Carslaw and J. C. Jaeger, "Conduction of Heat in Solids," Oxford, 1959, p. 75.

12. Francis Weston Sears, "Thermodynamics," Addison-Wesley, 1956, p. 241.

13. Yu. I. Belchenko, V. I. Davydenko, G. E. Derevyankin, A. F. Dorogov, V. G. Dudnikov, "Escape of Cesium from a Surface-plasma H^- Ion Source," Sov. Phys. Tech. Letters 3(7), July 1977, p. 282.

14. K. Prelec and Th. Sluyters, "Formation of Negative Hydrogen Ions in Direct Extraction Sources," Rev. Sci. Instr., Vol. 44, No. 10, Oct. 1973. p. 1451.

15. Joseph D. Sherman, Paul Allison, and H. Vernon Smith, Jr., "H^- Beam Formation from a Penning Discharge Surface Plasma Source Using Circular Emission-Extractor Electrodes," Proc. this Conf.

16. I. M. Kapchinskij and V. V. Vladimirskij, "Limitations of Proton Beam Current in a Strong Focusing Linear Accelerator Associated with the Beam Space Charge," Conference on High Energy Accelerators and Instrumentation, CERN, Geneva, 1959, p. 274.

17. Ya. M. Fogel, A. G. Koval, and Yu. Z. Levchenko, "Ionization of Gases by Negative Ions," Sov. Phys. JETP, Vol. 11, No. 4, Oct. 1960, p. 760.

18. Samuel K. Allison, "Experimental Results on Charge-Changing Collisions of Hydrogen and Helium Atoms and Ions at Kinetic Energies Above 0.2 keV," Rev. Mod. Phys. Vol. 30, No. 4, October 1958, p. 1137.

19. M. F. Rudd, "Energy and Angular Distributions of Secondary Electrons from 5-100 keV Proton Collisions with Hydrogen and Nitrogen Molecules," Phys. Rev. A, Vol. 20, No. 3, September 1979, p. 787.

20. Paul W. Allison, "Experiments with a Dudnikov-Type H^- Ion Source," Ref. 6, p. 119.

21. J. D. Sherman and P. W. Allison, "A Study of 90° Bending Magnet for H^- Beams," Ref. 9, p 3916.

22. J. D. Lawson, "The Physics of Charged Particle Beams," Oxford, 1977.

23. H. S. W. Massey, "Electronic and Ionic Impact Phenomena Vol. II," Oxford, 1969, p. 883.

24. H. Vernon Smith, Jr., Paul Allison, and Joseph D. Sherman, "A Rotating Penning Surface-Plasma Source for DC H^- Beams," Proc. this Conf.

DISCUSSION

HISKES The cesium density you quoted, is that the Cs^+ density or the cesium neutral density?

ALLISON That is neither.

HISKES What would the Cs^+ density be?

ALLISON I have no idea. What we measured is the flow. In the pulse mode it was ½ mg/hour and in the other it was 1 mg/hour. From that you can take your pick on how to figure out what the cesium density in the discharge is, since it is almost surely totally ionized and it would be governed by the evaporation rates of the cathode and things like that. By assuming that cesium flowed out in molecular flow, the density was chosen to match the flow we had measured.

HISKES Would you speculate on the density of cesium ions in the discharge?

ALLISON No.

HISKES Would you speculate on the ratio of cesium ion density to hydrogen ion density?

ALLISON I think I have figured that out but I can not think of it right now, I have estimated that it must be very small.

HISKES Do you think it is less than 1?

ALLISON A lot less than 1.

SMITH The problem is that while the discharge is running you have got no idea where the cesium is. It could be entirely on the cathode.

HISKES So the ratio could be 0.

SMITH Right.

ALLISON From the data of Langmuir and Taylor on the evaporation rates of cesium on tungsten you can try to make some estimates. If you assume that θ is at the minimum work function, it would take a cathode temperature equal to that to be measured. Then you can calculate what the density of the discharge would have to be and it is in the neighborhood of the equivalent cesium density that I quoted, but I do not have those numbers with me. That is the only way that we could estimate that.

PETERSON Does the cesium come out during the discharge or afterwards?

ALLISON During a discharge I am a bit skeptical of the measurement. I would say it is probably about the same or it could be less. The cesium burst that you see after the discharge is fairly spectacular, it jumps up a couple of orders of magnitude, however, the total amount of cesium that comes out during that burst is small compared with ½ mg/hr.

A ROTATING PENNING SURFACE-PLASMA SOURCE FOR DC H^- BEAMS*

H. Vernon Smith, Jr., Paul Allison, and Joseph D. Sherman
AT-2 (MS-818), Los Alamos Scientific Laboratory
Los Alamos, NM 87545

Abstract

We investigate the possibility of using a Penning surface-plasma source (SPS) with rotating electrodes to produce dc H^- beams. In this rotating ion source (RIS), the average power density on the electrodes is reduced by magnetically confining the discharge to a small region near the emission slit while maintaining the geometry and instantaneous power density of the fixed-electrode Penning SPS. H^- beam currents (2.5 mA at 100% duty factor, 104 mA at 1.5% duty factor) and two-dimensional normalized emittances (0.036 π cm•mrad x 0.009 π cm•mrad for 40% of a 1.5-mA, dc H^- beam) similar to those of the fixed-electrode Penning SPS are produced by the uncooled RIS reported in this paper. The scaling to a 100% duty factor, fully cooled RIS is briefly discussed.

I. Introduction

New linac structures, such as the radio-frequency quadrupole (RFQ)[1], may allow a substantial increase in the average beam current injected into particle accelerators. We are developing a rotating Penning surface-plasma source (SPS)[2] as a high current (~100 mA), dc H^- source for this application. We chose to build a Penning SPS because of (1) its low emittance and (2) its adaptability to a design employing rotating electrodes.

Using the source magnetic field we confine the rotating ion source (RIS) discharge to a small region near the emission slit, thereby reducing the average electrode heat load by the ratio of the discharge length to the electrode circumference, about a factor of 40. We built and tested the uncooled RIS described in this paper. We find that it produces H^- beams similar in quality to those generated by the fixed-electrode Penning SPS[3,4].

II. Source Design

In developing an ion source to produce ~100 mA of H^- at 100% duty factor and an emission density $J^- = 2$ A/cm^2, we find it necessary to add the complication of rotating electrodes because of power loading considerations. In our fixed-electrode Penning SPS[3], 110-mA H^- current pulses are produced by discharge current and voltage pulses of 60 A and 80 V, respectively, corresponding to $J^- = 2.2$ A/cm^2 through the 0.5-mm by 10-mm emission slit. Because the ratio of cathode power to anode power is about 2 at a discharge voltage of 100 V (Ref. 5), the 4.8-kW pulsed discharge power is equally shared by the anode and each of the two cathodes. The exposed cathode surface (0.48 mm^2) has a 6.7-kW/cm^2 heat load, about an order of magnitude too high for operation at 100% duty factor. The exposed anode surface (0.7 cm^2) has a 2-kW/cm^2 power load, still about a factor of 4 too high. It is desirable to reduce these heat loads to 0.5 kW/cm^2 or less. Reducing the electrode power loading by enlarging the source dimensions might lead to a reduced emission density and thus a lower H^- beam brightness.[6]

The RIS design (Fig. 1) maintains the geometry and instantaneous power density of the fixed-electrode source.[3,6] Because the SPS discharge will not operate below a minimum magnetic field B_m, the spatial extent of the RIS discharge is controlled by the magnet pole piece shape (1 cm by 1 cm) and the current in the electromagnet coils. The average RIS electrode power density is reduced by the ratio of the length of the discharge region (~1.2 cm) to the circumference of the electrodes (44 cm), about a factor of 37. The RIS design calls for a 100-V, 100-A discharge, resulting in anticipated power densities of 380 W/cm^2 for the cathodes and 150 W/cm^2 for the anode, well within the limits of cooling with present technology.

Initially, both RIS cathodes and the anode were rotated. For reasons discussed below, we presently rotate only the cathodes: the rotating anode (Fig. 2b) was replaced with a fixed structure (Fig. 2c). Ferrofluidic feedthrus[7], using magnetic-fluid seals, provide the rotating shaft seals. Discharge power is transferred to the shafts by carbon brushes. The shaft drive motor is at ground potential and has variable speed. The anode and cathodes are constructed from molybdenum, the source housing from stainless steel.

Because the fixed-electrode source operates for at least 1 ms with 100-mA H^- yields, the 1.2-cm-long arc slot results in an upper limit of 1200 cm/s for the electrode speed in the RIS. The 14-cm RIS electrode diameter sets the required rotational speed at < 1600 rpm. Measurements show negligible braking of the drive motor by eddy currents induced in the rotating electrodes (< 20 W at 1700 rpm). The magnetic field in the discharge region changes by < 5% when the source rotational speed is varied from 0 to 1700 rpm.

Four electrical cartridge heaters are used to heat the source body to 250°C, thereby limiting cesium condensation on the inner surfaces of the source housing. Cesium metal vapor is

*Work performed under the auspices of the U.S. Department of Energy.

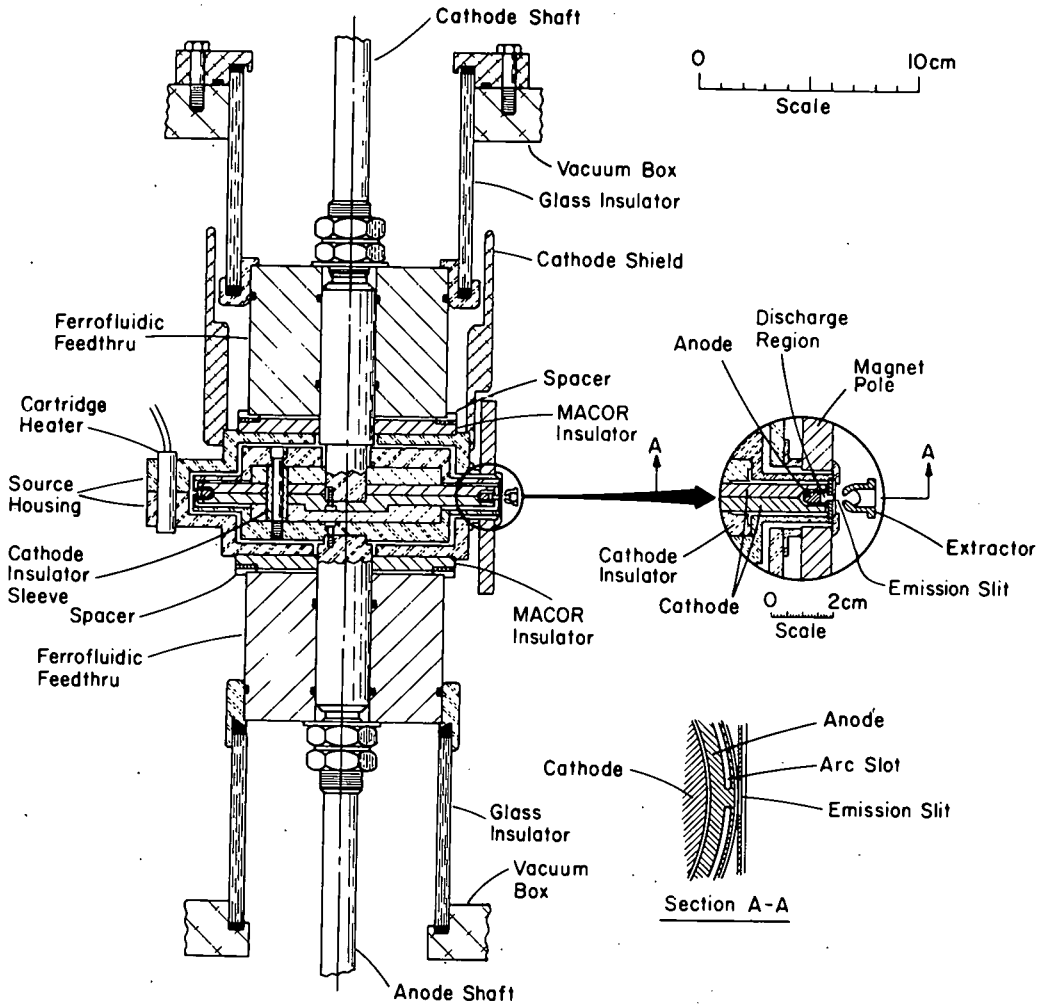

Fig. 1. The rotating ion source.

Table I. Design and Achieved H^- Performance Levels in the RIS.

	Design	DC	Pulsed
Discharge current, A	100	1.0	98
Discharge voltage, V	100	160	100
H_2 flow, sccm	-	36	115
Magnetic field, T	-	0.14	0.15
Rotational speed, rpm	-	120	15
Duty factor, %	1	100	1.5
Beam energy, keV	20	10.1	21
H^- current, mA	~100	1.5	104*
J^-, A/cm^2	~2	0.03	2.1*
ϵ_x (63%) x ϵ_y(63%), π^2 cm^2 mrad^2	-	0.036x0.009	-
B(40%), A/cm^2 mrad^2	-	0.91	-
H^- conversion efficiency, A of H^-/A of arc	> 0.001	0.0015	0.0011*
Thermal efficiency, kW of arc/A of H^-	< 100	107	94*

*Unanalyzed.

injected in the source housing 215° around the electrode wheel from the discharge region. The cesium metal feed (similar to that in Fig. 2 of Ref. 8) incorporates an all-metal, bellows-sealed needle valve for adjustment of the cesium flow rate. Presently we do not cool either the emission slit (0.5 by 10 mm^2) nr the extraction electrode. The ion source test stand and electrical supplies used to test[3,6] the fixed-electrode source are used for the RIS. The design H^- performance levels for the RIS are given in column 1 of Table I.

III. Results and Discussion

Because the RIS design relies on the discharge magnetic field to limit the length of the discharge region along the electrode periphery, it is important to confirm this effect. To do this, we constructed a special rotating anode, containing only two 2-mm-wide by 5-mm-long arc slots located 180° apart (Fig. 3a). We used pole pieces with 1-cm square faces. The source electrode wheel was rotated at moderate speed

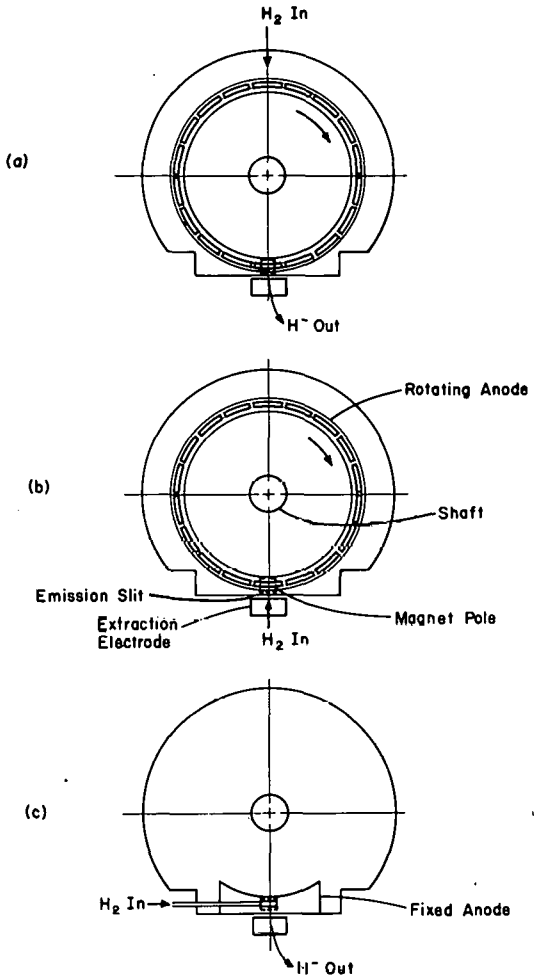

Fig. 2. (a) Schematic of the original H_2 gas feed, located 180° around the electrode wheel from the discharge region.
(b) Capillary H_2 gas feed through the emission slit.
(c) Fixed anode structure, with H_2 gas fed directly into the arc slot.

to pass the arc slots through the discharge region at 16 Hz. A timing pulse indicated a fixed location on the electrode periphery so that we could measure the rate of rotation. We then measured the discharge and H^- currents as a function of wheel location (Fig. 3b). These measurements were repeated for many different settings of the magnetic field. As shown in Fig. 3c, the width of the discharge region decreases monotonically with magnetic field. A 0.1-T field produced a 1-cm discharge width. Thus, the spatial extent of the RIS discharge can be controlled with the magnetic field for discharge currents near 1A.

We varied the location of the H_2 gas feed as shown in Fig. 2. Feeding H_2 gas into the

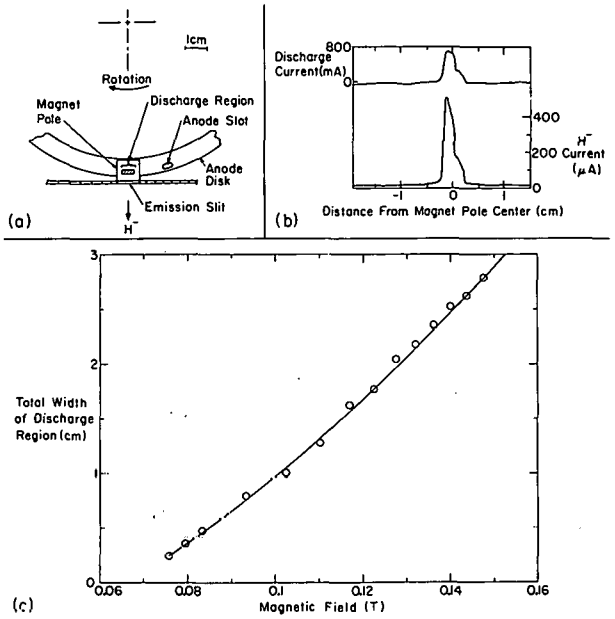

Fig. 3. (a) The magnet poles and the anode used to measure the width of the discharge region as a function of magnetic field strength.
(b) The discharge current (top) and H^- current (bottom) as a function of the location of the 5-mm-long arc slot for a 0.084-T magnetic field.
(c) The total width of the discharge region vs the discharge magnetic field strength. The curve serves only to guide the eye.

source housing 180° from the discharge region (Fig. 2a) is a satisfactory arrangement for dc operation at 1 A of discharge current. However, with this arrangement the RIS only operates stably for pulsed discharge currents $\leq$ 20 A. At higher discharge currents the voltage and current oscillate at ~ 10 kHz with 100% modulation. We calculate that at the higher currents the discharge can pump the H_2 gas away in < 10 μs. Perhaps this causes the instabilities. To investigate this possibility, a 0.4-mm-i.d. capillary tube was directed into the discharge region through the emission slit and used as the H_2 gas feed (Fig. 2b). Steady operation at discharge currents up to 80 A resulted. We then replaced the rotating anode with a fixed anode structure (Fig. 2c) and fed the H_2 gas directly into the arc slot as in the fixed-electrode source. This change allowed steady pulsed operation at discharge currents up to 120 A. All measurements reported below were obtained using the fixed-anode structure. The pulsed H^- current increased when the number of H_2 gas inlets in the fixed anode was increased from one to five, the five inlets being equally spaced along the 1.2-cm arc slot.

Because of the need to support the rotating anode, the drift distance t (see inset in Fig. 4) from the arc slot to the emission slit was 2 mm in the RIS compared to 1 mm in the fixed-electrode source. We studied the effect of varying t on the H^- output of the fixed-electrode source and found that it is an important parameter (open circles and curve in Fig. 4). Using two different fixed anodes, we measured the pulsed H^- output from the RIS with t = 2 mm and t = 1/2 mm and found that t = 1/2 mm gives the best H^- output (squares, Fig. 4). The RIS current and emittance measurements reported below were all obtained for t = 1/2 mm.

The cesium flow through the RIS emission slit is monitored using a cesium surface-ionization gauge (SIG) identical to that described in Ref. 9. Typically, the cesium flow from the RIS is identical to that measured for the fixed-electrode source (see Figs. 2-4 of Ref. 9), 1 mg/h for dc operation at 1 A discharge current.

The H^- current and two-dimensional, normalized emittance ($\epsilon = \beta\gamma A/\pi$, where A is the phase-space area of the beam and β and γ are the relativistic parameters) for dc RIS operation are shown in Table I. The largest dc RIS H^- beam we have observed is 2.5 mA, for which we have no emittance measurements. Figure 5 shows ϵ as a function of the beam-current fraction I/I_0 for the 1.5-mA dc beam. The x,θ direction is parallel to the 0.5-mm by 10-mm emission slit and in the bending plane of the n = 0.9 dipole magnet; the y,ϕ direction is perpendicular to the slit.

The data displayed in Fig. 5 were obtained in the following manner. The emittance scanner[3] was set at a fixed position x, then an oscillogram of the emittance scanner Faraday-cup current S_x vs the emittance scanner plate sweep voltage (proportional to θ) was recorded. The emittance scanner was stepped across the beam to record the three-dimensional plot of S_x vs x and θ. Because $S_x = \partial^2 I/\partial x \partial\theta$, the integral

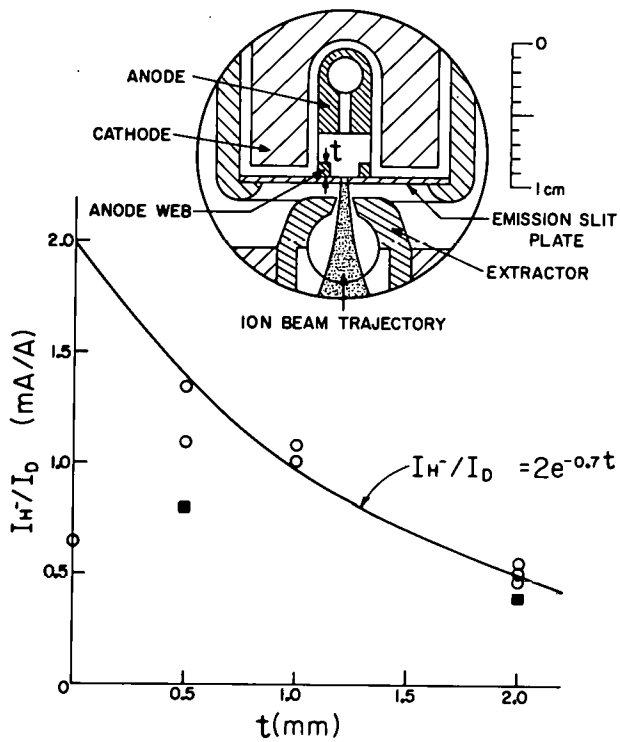

Fig. 4. The ratio of H^- current to pulsed discharge current (I_D ~ 100 A) vs the distance from the arc slot to the emission slit t (inset) for the fixed electrode source[3] (circles) and the RIS (squares). The curve is calculated assuming an exponential attenuation of H^- ions in the drift t. The 1/e attenuation distance is 1.4 mm.

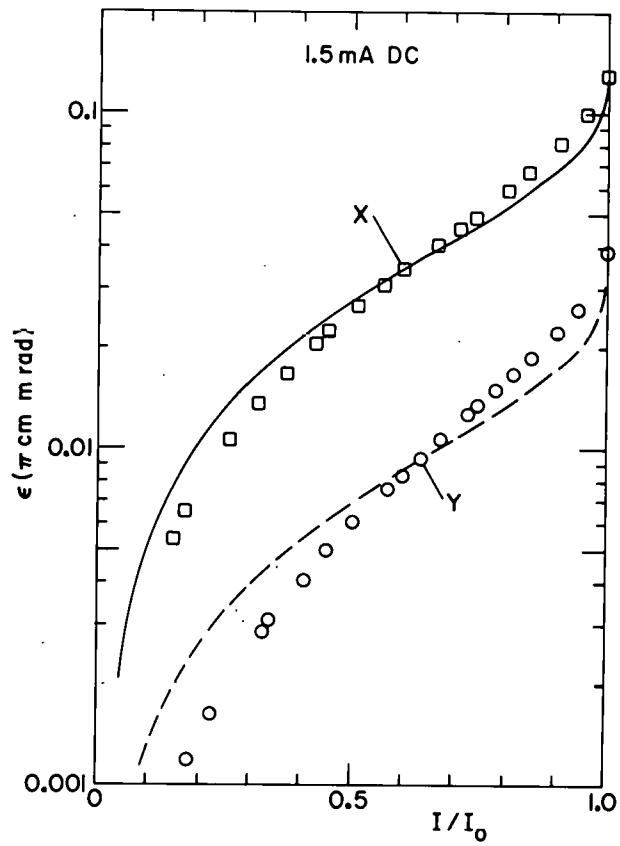

Fig. 5. Two-dimensional, normalized emittance ϵ vs the fraction of the total beam included in the emittance measurement I/I_0 for a 1.5-mA dc H^- beam from the RIS. The curves are calculated from Eq. (2) assuming kT_x = 3.7 eV (solid curve) and kT_y = 96 eV (dashed curve).

$I_1 = \int \partial^2 I / \partial x \partial\theta d\theta$ is the beam profile. The integral $I_2 = \int\int \partial^2 I / \partial x \partial\theta \, d\theta dx$ is proportional to the total beam current I_0. A computer program calculates the normalized emittance and beam current included at various threshold (brightness) levels. These results then permit plotting normalized emittance $\varepsilon(F)$ vs the beam current fraction ($F=I/I_0$). A second, identical emittance scanner is used to make the y,ϕ emittance measurements. The normalized brightness $B(F^2)$ is calculated from

$$B(F^2) = 2\, I_0 \,/\, [\pi^2\, \varepsilon_x(F)\, \varepsilon_y(F)] \qquad (1)$$

The values of ε given in Table I correspond to the emittance value that includes 63% of the beam in each plane, or 40% of the total beam. The discharge voltage noise to discharge voltage ratio was 0.14 for these measurements. The dc H^- current, emittance, and brightness values for the RIS and the fixed-electrode source (I_0 = ? mA, $\varepsilon_x \times \varepsilon_y$ = 0.044 x 0.016 π^2cm^{2}mrad^2, B=0.50 A/cm^{2}mrad^2, F=63%, Table IV of Ref. 10) are very similar at the ~ 2-mA level.

The largest pulsed RIS H^- beam we have measured is 104 mA (Table I). The maximum field strength provided by the dipole magnet is insufficient to bend a 21-keV H^- beam through 90° and into a Faraday cup for measurement. The 104 mA was recorded in a Faraday cup located 2 cm behind the extraction electrode, without magnetic analysis of the beam.

We have not yet obtained emittance measurements for the RIS pulsed beam. However, the dc current, emittance, and brightness values for the RIS are so similar to those for the fixed-electrode source that we expect a 100-mA pulsed H^- beam from the RIS to have nearly the same emittance and brightness as the fixed-electrode source (I_0 = 79 mA, $\varepsilon_x \times \varepsilon_y$ = 0.041 x 0.027 π^2cm^{2}mrad^2, B = 15A/cm^{2}mrad^2, F = 63%, Fig. 6 of Ref. 11).

From a model[11] that assumes the H^- ions are emitted uniformly from the rectangular emission slit with a Maxwellian velocity distribution of temperature T, the beam fraction vs normalized emittance is given by

$$F = \mathrm{erf}\,[\pi\, \varepsilon / \{4R\, (2kT/mc^2)^{1/2}\}] \qquad (2)$$

where R is half the slit dimension and m is the ion mass. The curves in Fig. 5 were calculated using Eq. (2), normalized to the values of ε at F = 63%. Using the values of ε_x (63%), ε_y (63%), and Eq. (2), we obtain estimates of the ion energy of kT_x = 3.7 eV and kT_y = 96 eV. We know[12] that the dipole magnet pole pieces couple the x- and y-plane emittances, so the larger emittance of the x-plane masks that of the y-plane. The larger effective ion energy reflects the small initial plasma radius for the y-plane.

The principal difference noted between the operation of the RIS and the fixed-electrode source is that for maximum dc H^- current, the discharge voltage for the RIS is 170 V, compared to 50 V for the fixed-electrode source. The difference in discharge voltage for pulsed operation is not so great; 100 V for the RIS compared to 80 V. We do not understand the difference in operating voltage. Understanding and controlling the voltage has clear implications for a fully cooled RIS, because a lowering of the discharge voltage reduces the electrode heat load by the same factor.

IV. Summary and Conclusions

We have shown that magnetic-field confinement of the Penning SPS discharge can be used to reduce the average heat load on the cathodes in a rotating source design. Using a fixed anode and rotating cathodes in our uncooled RIS, we have achieved performance levels at 1-mA H^-, 100% duty factor and 100-mA H^-, 1% duty factor which are comparable to those of the fixed-electrode Penning SPS described in Refs. 3 and 6.

A fully cooled RIS must have adequate cooling for the anode and both cathodes, the emission slit, and the extraction electrode. Taking our pulsed RIS measurements (Table I), correcting for 30% attenuation of the H^- beam when it is magnetically analyzed, and scaling up to 100 mA of analyzed H^- beam implies that each rotating cathode will have a power load of 0.5 kW/cm^2, the anode 0.16 kW/cm^2 if rotated and 6 kW/cm^2 if fixed. The power loading on the extraction electrode may be a serious problem because a 20-keV, 100-mA H^- beam having a 2-A/cm^2 current density has an average power density of 40 kW/cm^2. This scaling to a fully cooled, 100% duty factor RIS is acceptable, provided the anode and extraction electrode heat loads can be reduced.

References

1. R. H. Stokes, K. R. Crandall, R. W. Hamm, F. J. Humphry, R. A. Jameson, E. A. Knapp, J. M. Potter, G. W. Rodenz, J. E. Stovall, D. A. Swenson, and T. P. Wangler, paper presented at the XIth Int. Conf. on High Energy Accelerators, CERN, Geneva (July, 1980); and LA-UR-80-1855.

2. The physics of SPS sources is discussed in:Yu. I. Bel'chenko, G. I. Dimov, and V. G. Dudnikov, Proc. of the Symp. on the Production and Neutralization of Negative Hydrogen Ions and Beams, BNL-50727, pp 79-96 (September, 1977).

3. P. W. Allison, in Ref. 2, pp 119-122.

4. G. E. Derevyankin and V. G. Dudnikov, Institute of Nuclear Physics Preprint IYAF 79-17, Novosibirsk, 1979 (UCRL-TRANS-11549).

5. Yu. I. Bel'chenko and V. G. Dudnikov, Conf. on Interactions of Atomic Particles in Solid Bodies, Kharkov, 1976 (Scientific Translation Service Inc., 1976, Trans. 4 pp).

6. P. W. Allison, IEEE Trans. on Nucl. Sci. NS-24, 1594-1596 (1977).

7. Model No. SC-1000-N-W-Modified, manufactured by Ferrofluidic Corp., Burlington, MA 01803.

8. H. V. Smith, Jr., Nucl. Instr. and Methods 164, 1-10 (1979).

9. H. V. Smith, Jr., and P. W. Allison, IEEE Trans. on Nucl. Sci. NS-26, 4006-4008 (1979).

10. J. D. Sherman, P. Allison, and H. V. Smith, Jr., Proc. of this Conf.

11. P. Allison, H. V. Smith, Jr., and J. D. Sherman, Proc. of this Conf.

12. J. D. Sherman and P. W. Allison, IEEE Trans. on Nucl. Sci. NS-26, 3916-3918 (1979).

DISCUSSION

JACQUOT The beautiful violet light in the beam is due to the cesium, I suppose, because the cesium plasma is violet and do you have an idea of the density of the plasma in the beam?

SMITH We have not considered that at all. We have been looking at what goes on in the source and not what goes on after extraction from the source.

PETERSON That looks to me like an H_2 discharge. I think it is probably excitation of the hydrogen gas by the beam.

SMITH That is what we think it is. We do not know that for a fact.

PETERSON What is the pressure there?

SMITH That is in the order of 10^{-4} torr.

H^- BEAM FORMATION FROM A PENNING SURFACE PLASMA SOURCE USING CIRCULAR EMISSION-EXTRACTOR ELECTRODES*

Joseph D. Sherman, Paul Allison, and H. Vernon Smith, Jr.
AT-2 (MS-818), Los Alamos Scientific Laboratory
Los Alamos, NM 87545

Abstract

Circular emission-extractor electrodes are used to extract H^- ions from a Penning surface-plasma source, with the calculated space-charge limited current being observed. Emittance measurements are extended to include emittance as a function of beam fraction. Comparatively noise-free discharge voltages lead to factor of three reduction in emittance. Equal emittances in the transverse phase spaces are observed for the circular geometries.

I. Introduction

We study the possibility of using circular extractor geometries to simultaneously obtain both symmetrical and low-emittance H^- beams from a Penning surface-plasma source (SPS). Ribbon-type emission slits result in asymmetrical emittances in the two-dimensional transverse phase spaces.[1,2] First, operation of the Penning SPS with H^- extraction using circular emission-extractor geometries is summarized. Second, we present our results on emittance measurements for this geometry type. We discuss our technique of obtaining emittance versus beam fraction, and we show the importance of operating with a quiet discharge to achieve reduced emittances.

II. Source Performance

We have asked two questions. First, what is the fraction of the calculated space-charge limited current we can achieve with these geometries, and second, what is the efficiency of producing H^- ions in the extracted beam and then transporting this beam through a 90° dipole magnet.

These measurements used the H^- SPS in the pulsed mode, as described in Ref. 3. The H^- ion beam is extracted from the SPS, then immediately bent in a 90°, n = 0.5 dipole magnet. The 0° Faraday cup is located 2 cm behind the extractor, whereas the 90° Faraday cup is 6 cm from the exit edge of the dipole magnet.

Figure 1 defines our notation for the circular extraction geometries. Five measurements were done. Table I contains the measurement number, emission aperture radius (r_1), the extractor aperture radius (r_2), extractor gap (d), extractor voltage, and the 0° Faraday-cup current. The seventh column contains our experimental perveance and is compared with the calculated planar[4] and spherical[5] space-charge limited currents, as appropriate. We note that in measurements 1, 3, and 4 we have obtained from 78 to 110% of the theoretical space-charge limited current. Significantly less of the theoretical limit was obtained for measurements 2 and 5. This may be because of the extremes in geometry contained in measurement 2 (small extractor gap) and measurement 5 (large emission-extractor diameters).

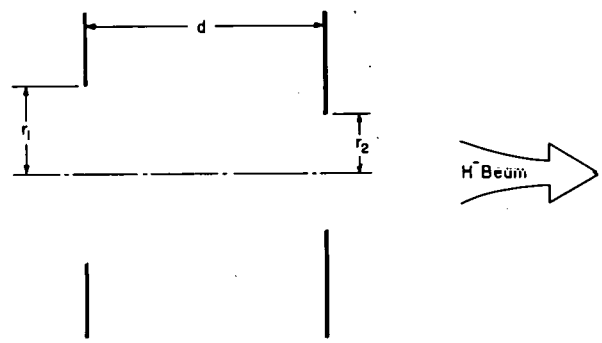

Fig. 1. The emission aperture (radius r_1) is separated from the extraction aperture (radius r_2) by the distance d.

*Work performed under the auspices of the U. S. Department of Energy.

TABLE I. Comparison of Measured H^- Beam Perveances Compared with the Planar and Spherical Diode Predictions. Geometrical Parameters are Defined in Fig. 1.

Measurement	r_1 (mm)	r_2 (mm)	d (mm)	V_{ext} (kV)	I_{H^-} (0°) (mA)	Perveance $(A/V^{3/2}) \times 10^{-6}$ Measurement	Theory Planar	Theory Spherical
1	0.50	0.50	2.0	15.0	21	0.012	0.011	---
2	0.50	0.50	1.2	15.0	32.5	0.018	0.030	---
3	0.75	0.50	2.0	16.5	20.5	0.0097	--	0.012
4	0.75	0.50	1.5	19.0	45.0	0.0172	--	0.022
5	1.0	1.0	2.0	20.	57.	0.020	0.042	---

Next we fixed the extractor voltage at 15 kV, and then checked H^- production efficiency by measuring H^- current in the 0° Faraday cup as a function of the pulsed discharge current. We have defined an H^- production efficiency, Y, at extraction to be

$$Y = \frac{I_{H^-}(0°)}{A_e \cdot I_D} \qquad (1)$$

where I_{H^-} is the H^- current (mA) in the 0° Faraday cup, A_e is the emitter area in cm^2, and I_D is the discharge current in amps.

Table II shows our results. Column 1 identifies the measurement and corresponds to measurements shown in Table I. Maximum H^- production efficiency, Y_{max}, occurs at $I_D \approx 50$ A for the planar cases ($r_1 = r_2$) and $I_D \approx 35$ A for the spherical ($r_1 > r_2$) cases, showing that the extracted H^- ion beam is apparently space-charge limited at these discharge currents for 15-kV extraction potential. The Y_{max} values listed in Table II are about the same as H^- production efficiency of 36 ($mA/A\text{-}cm^2$) derived from Table I of Ref. 3 for a 1.0 by 0.05 cm^2 ribbon slit.

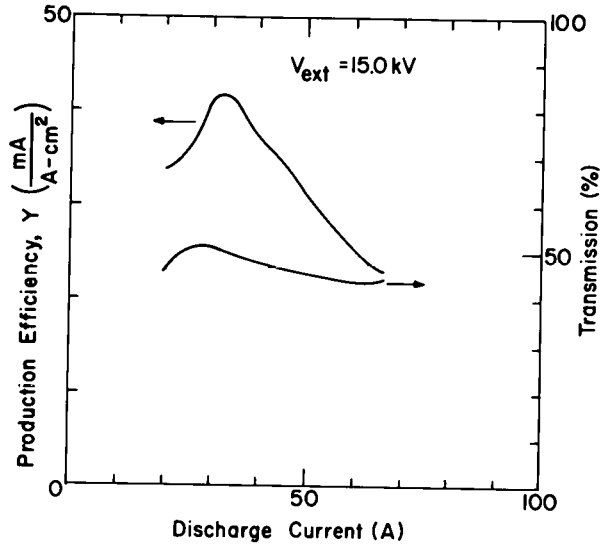

Fig. 2. Representative result for the production efficiency and H^- transmission efficiency to the 90° Faraday cup as a function of discharge current for measurement 4 with an extraction voltage of 15 kV.

TABLE II. Maximum H^- Production Efficiency (Y_{max}), Corresponding Discharge Current, and the Maximum Observed Transmission to 90° Faraday Cup.

Measurement[a]	Y_{max} ($mA/A\text{-}cm^2$)	I_D (A)	Maximum Transmission (%)
1	38	52	--
2	56	50	42
3	31	37	64
4	42	32	51

[a]The measurement number corresponds to that listed in Table I.

Maximum transmission from the 0° to the 90° Faraday cup is also shown in Table II. The best transmission occurred at a discharge current approximately 15% below that corresponding to Y_{max}. Figure 2 shows representative results for the H^- production efficiency and the transmission as a function of discharge current for measurement 4.

III. Emittance Measurements

Emittance measurements were made using the electronic scanner described in Ref. 1. However, to reduce background noise, for beam profile information, and for obtaining emittance as a function of beam fraction (I/I_0), current pulses from the emittance scanner Faraday cup were analyzed differently. We fixed the scanner at one position, and then swept the sampled beam current across the rear slit, using a voltage ramp on one of the two parallel plates. The waveform generated in the scanner Faraday cup is saved on a storage scope; it yields the angular spread in the beam at the fixed position vs a voltage that is proportional to the current density in phase space. A collection of these waveforms over the beam profile then yields a 3D plot where the axes are position, angle, and phase-space current density. Approximately 15 positions were recorded for each phase-space plane discussed below. The waveforms were computer analyzed to yield the emittance and the beam profiles as a function of beam fraction.

Five measurements were made using the SPS. The measurement number, geometry, dipole magnet n value, and mode (dc or pulsed) are shown in Table III. The first two measurements with dc and pulsed beams used the ribbon slits. The x-direction is in the bend plane along the 1-cm edge of the emission slit; the y-direction is perpendicular to the bend plane along the 0.05-cm edge. The ribbon slit emittance results at unity beam fraction (corresponding to threshold equal to zero in Ref. 1) agree with previously reported emittances.[1] Circular aperture measurements (cf Table III) include two cases where $r_1/r_2 = 1.5$ (measurements 8 and 9) and one case where $r_1/r_2 = 1.0$ (measurement 10). Figure 3, parts (A) and (B), shows the y-plane emittance diagrams and beam

TABLE III. Emission-Extractor Configurations for which the H^- Beam Emittance was Measured as a Function of Beam Fraction.

Measurement	Emission Slit	Extractor Slit	Accelerating Gap (cm)	Dipole Magnet	Mode
6	Rectangular 1.0 by 0.05 cm^2	Width = 0.1 cm	0.2	n = 0.9	dc
7	Rectangular 1.0 by 0.05 cm^2	Width = 0.05 cm	0.18	n = 0.9	Pulsed 7-1/2 Hz, 1.0 ms
8	Circular r_1 = 0.075 cm	Circular r_2 = 0.05 cm	0.15	n = 0.9	Pulsed 7-1/2 Hz, 0.8 ms
9	Circular r_1 = 0.075 cm	Circular r_2 = 0.05 cm	0.15	n = 0.5	Pulsed 7-1/2 Hz, 0.7 ms
10	Circular r_1 = 0.10 cm	Circular r_2 = 0.10 cm	0.20	n = 0.5	Pulsed 7-1/2 Hz, 0.6 ms

profiles for measurements 8 and 9 at the indicated beam fractions.

Table IV contains a summary of the data and derived theoretical results. The H^- beam energy was limited to 15.0 keV because the dipole magnet was not capable of bending a higher energy beam through 90°. Measurements 9 and 10 had quieter discharges than measurements 6, 7, 8 as indicated by the ratio of discharge voltage noise to the discharge voltage. The normalized emittance ε_0 contains 63% of the beam per plane. Our results show that quiet discharge voltages lead to a factor of three reduction in emittance, and that the emittances in the transverse planes are equal within errors of measurement. The quiet discharge voltage was induced by increasing the cesium vapor flow. Figure 4 is a comparison of the normalized emittance versus beam fraction (F) for the y-plane in measurement 8 (noisy discharge voltage) and measurement 9 (quiet discharge voltage). The data are represented by the circles and squares, respectively. Solid lines are theoretical calculations discussed below. The shift of the factor of three in emittance is seen clearly at all beam fractions. The same result is obtained for the x-plane. This improvement in emittance with a quiet discharge was previously observed in ribbon slit experiments.[2]

IV. Discussion

Our measured emittance versus F data have been related to an H^- ion energy by assuming that the H^- ions have uniform spatial distribution and a Maxwellian velocity distribution at emission. Details of the theory are contained in another paper published in these proceedings.[6]

The theoretical expression appropriate to rectangular slits for F is given by

$$F = \mathrm{erf}\left[\frac{\pi\varepsilon}{4R\sqrt{\frac{2kT}{mc^2}}}\right] \qquad (2)$$

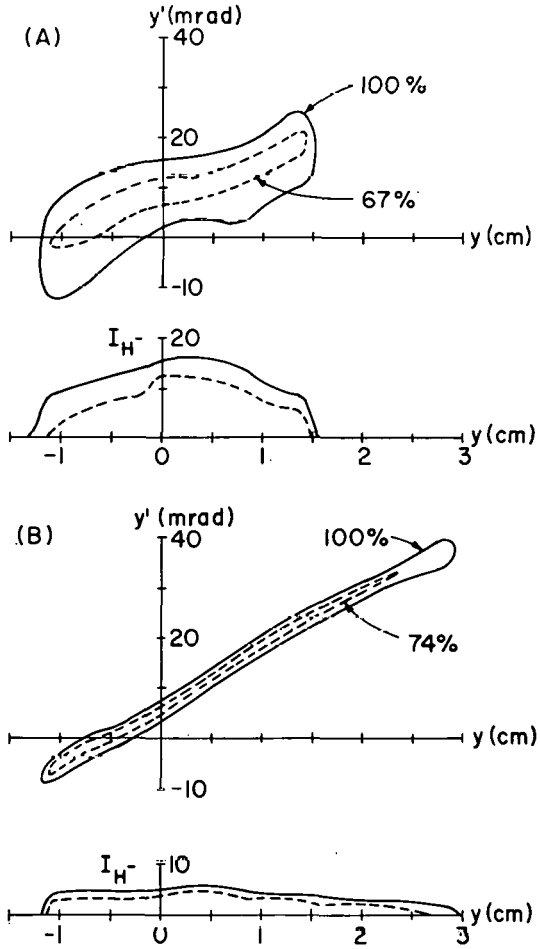

Fig. 3. The y-plane emittance diagrams and beam profiles, for measurements 8 (Part A) and 9 (Part B). The solid curves refer to 100% of the beam, whereas the dashed lines correspond to 67% and 74% of the beam, respectively.

TABLE IV. The H^- Beam Energy, Current, Discharge Voltage Conditions, Emittance at 63% Beam Fraction, and the Derived Ion Energy (see text).

Measurement[a]	Dimension	V_{ext} (kV)	$I_{H^-}(0°)$ (mA)	Discharge Voltage (V)	Ratio (Discharge Noise)/(Discharge Voltage)	ε_o (π-cm•mrad)	kT (eV)
6	x	15.0	2.0	53	0.38	0.044	5
	y					0.016	300
7	y	15.2	50	97	0.36	0.036	1500
8	x	15.0	25	105	0.38	0.018	50
	y					0.019	50
9	x	14.1	31	80	0.08	0.005	4
	y					0.007	7
10	x	15.0	35	100	0.06	0.010	8
	y					0.008	5

[a]The measurement number corresponds to that listed in Table III.

where F is the beam fraction, ε is normalized emittance, R is half the emission slit width, mc^2 is the H^- rest mass, and kT is the H^- ion energy. The theory thus gives a universal curve for emittance versus F, scaled by the ion energy. The derived kT values are shown in Table IV for the rectangular emission experiments. The comparatively large H^- energies in the y-direction reflect y-plane emittance growth because of aberrations and fringe field effects in the dipole bending magnet.[1,7]

The circular apertures case is slightly more complicated, requiring a numerical evaluation of F versus threshold. A theoretical universal curve $S_{Theory}(F)$ relating emittance and F is still obtained, with the curve being scaled to the experiment by

$$\varepsilon(F) = R \cdot \sqrt{\frac{2kT}{mc^2}}\, S_{Theory}(F) \qquad (3)$$

where R is now the emission aperture radius and the remaining parameters are defined as before. The solid lines in Fig. 4 show the universal curve scaled to the data. The kT values (see Table IV) were derived by normalizing measurement to theory at F = 0.63.

The larger emittances for noisy discharge conditions lead to a factor 10 increase in the derived H^- energies as compared to the quiet discharges (cf Table IV, measurements 8, 9, 10). The increased emittance may be caused by incomplete neutralization in the beam plasma or by H^- current variations that lead to varying focus conditions. Comparing measurements 9 and 10 to a model in which ion energy and aperture radius determine emittance, the emittance of measurement 10 would be given by scaling the emittance of measurement 9 by 1.33 (ratio of aperture radii given in Table III.) Using the arithmetic averages of the x- and y-plane

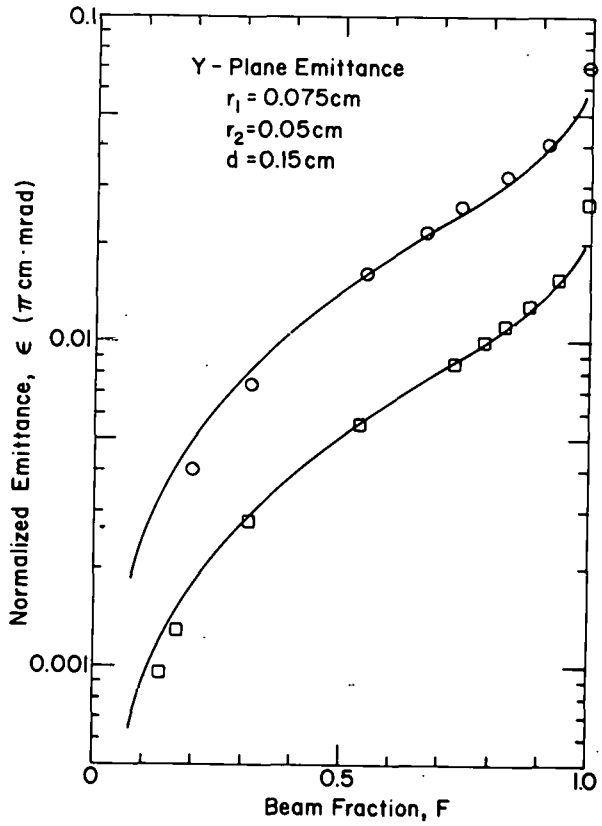

Fig. 4. A comparison of the y-plane emittances vs beam fraction for measurements 8 and 9. A factor of three reduction in the normalized emittance is observed when the noisy discharge (circles) is compared to the quiet discharge (squares). The solid curves are theoretical calculations discussed in the text.

emittances for measurements 9 and 10, this scaling is found within our errors, thus implying within this model that an ion energy of 6 eV would account for the quiet discharge emittance measurements.

Summarizing, we have investigated the use of circular extractor systems in a SPS. We have obtained the calculated space-charge limited H^- current in these geometries. Emittance as a function of beam fraction has been measured, and we have seen that the emittance versus beam-fraction curve is reasonably described by a uniform-in-space, Maxwellian velocity-distribution model for H^- ions. Finally, emittance is sensitive to the discharge voltage conditions, having observed a normalized emittance of 0.005 (π cm·mrad) under optimum conditions.

References

1. Paul W. Allison, "Experiments with a Dudnikov-Type H^- Ion Source," Proc. of the Symp. on the Production and Neutralization of Negative Hydrogen Ions and Beams, BNL-50727, pp. 119-122 (September 1977).

2. G. E. Devevyankin, V. G. Dudnikov, and V. S. Klenov, "Ion Optical Characteristics of Negative H^- Ion Beams Generated by Surface Plasma Sources," preprint IYAF 77-8, Nuclear Physics Institute, Siberian Branch, USSR Academy of Sciences, Novosibirsk 1977. UCRL-TRANS-11269.

3. Paul W. Allison, "A Direct Extraction H^- Ion Source," IEEE Trans. on Nucl. Sci., NS-24, No. 3, p 1594-1596 (June 1977).

4. C. D. Child, "Discharge from Hot CaO," Phys. Rev. 32 (1911), p. 492.

5. Irving Langmiur and Katharine B. Blodgett, "Currents Limited by Space Charge Between Concentric Spheres," Physical Review 24 (1924), p. 49.

6. Paul Allison, H. Vernon Smith, Jr., and Joseph D. Sherman, "H^- Ion Source Research at Los Alamos," these proceedings.

7. J. D. Sherman and Paul W. Allison, "A Study of a 90° Bending Magnet for H^- Beams," IEEE Trans. on Nucl. Sci., NS-26, No. 3, p. 3916-3918 (June 1979).

DISCUSSION

PETERSON Does this particular ion temperature of 5 eV imply a particular energy width in the extracted beam? You are talking only about emittance, what about the energy spread in the beam?

SHERMAN The power supply is regulated to 100 V.

SMITH I believe that the Novosibirsk records report a very narrow energy width along the longitudinal direction.

PETERSON Like what?

SMITH Just a few eV.

GELLER How did you measure the emittance versus the percentage of beam current?

SHERMAN That is kind of a long story: with this emittance scanner we recorded the shape of that current pulse versus the scan voltage and that gives us the angular spread of the beam. We essentially computerize those data and then set various thresholds and derived the emittance versus current that way.

FORRESTER Could you sketch that instrument roughly for us?

SHERMAN I have also a picture of it in the paper.

OPERATION OF THE FERMILAB H⁻ MAGNETRON SOURCE

C. W. Schmidt
Fermi National Accelerator Laboratory*
Batavia, ILL 60510

Abstract

A magnetron type ion source is being used at Fermilab to produce negative hydrogen-ions for acceleration in the Linac and charge-exchange injection in the Booster. Operation of the Linac, Booster and ion source is discussed.

Introduction

The decision to use negative ion injection into the Fermilab Booster was made in the spring of 1975. At that time the choice of an ion source was uncertain until a magnetron source[1,2] was obtained from the Brookhaven Neutral Beam Group in February, 1976. From this source the Fermilab magnetron source evolved. The Fermilab source was designed to minimize the source volume so that with a fast pulsed gas valve the gas consumption was small and could be handled by the existing preaccelerator vacuum system with the addition of a 400-l/sec turbopump located in the high voltage dome. The compactness and arrangement of the insulation between the cathode and source body gave a source with adequate cathode cooling to allow the needed duty factor (0.1%) (Fig. 1).[3]

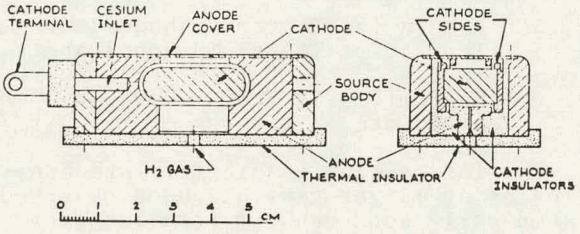

Fig. 1. Fermilab H⁻ Magnetron Ion Source

Early attempts to electrostatically focus the beam for direct extraction into the high voltage accelerating column were unsuccessful due to the large space-charge forces within the beam and the lack of neutralization in electrostatic fields. A 90° bending and focusing (n=1) magnet gave the desired beam focusing and provided the final design (Fig. 2).[4]

In the summer of 1977 the source was successfully tested on a Cockcroft-Walton accelerator and in October, 1977, H⁻ beam was accelerated through the Linac. In

*Operated by Universities Research Association Inc., under contract with the United States Department of Energy.

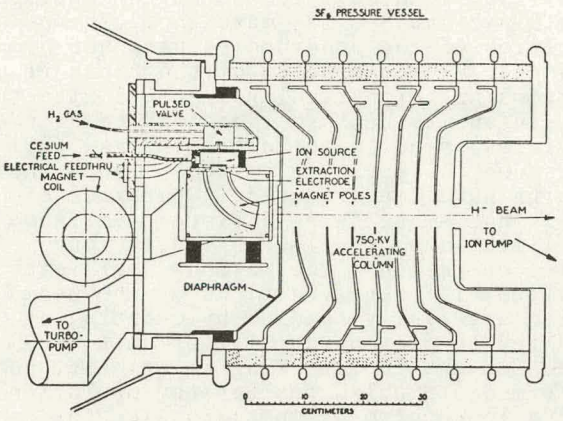

Fig. 2. H⁻ Ion Source Assembly

February, 1978, H⁻ beam was first studied in the Booster accelerator. Within eight days a record intensity was achieved so that in March, 1978, H⁻ multi-turn charge-exchange injection into the Booster was used for operation. The success and performance of this method has been sufficiently good that in the summer of 1979 the standby proton source was removed and replaced by a second H⁻ source to provide redundancy in the source and allow maintenance on the non-operating preaccelerator.

Booster

The use of H⁻ injection into the Booster has been important toward achieving major improvements in the operational program. Because of space charge limitations in the Booster higher intensities were not expected, however the present record intensity using H⁻ injection is 28% higher than previously obtained with protons. The injection efficiency is significantly higher than with proton injection and the step-wise growth of beam during injection into the Booster shows little or no loss of efficiency between the first and later injected turns. Up to sixteen turns have been injected for studies with the limit determined by the Booster acceptance. The Booster intensity is routinely adjusted by changing the number of injected turns. The emittance of the 8-GeV extracted Booster beam is equivalent to or better than that obtained with protons for similar intensity.[5,6]

Linac

In the Linac, operation with the low-intensity (25-40 mA) H⁻ beam was

achieved without difficulty. Except for the last four quadrupoles the same rf and quadrupole parameters as were used for high intensity (200-300 mA) proton operation were initially used for H^- operation. With continuous use of H^- the Linac has since been adjusted to better optimize the Linac and Booster matching. The polarities of the quadrupoles have not been changed. The operation of the Linac rf systems has dramatically improved with the low-intensity beam so that loading of the cavities is no longer a problem and failures due to operating systems beyond their design have been reduced. Operation of the Linac among three different users was facilitated by the low-intensity long-pulse operation. The various users each require different fractions of the beam which are easily handled by chopping at 750 keV to provide a pulse of up to 1 μsec for the Cooling Ring experiment, an intermediate pulse for Booster operation and a long pulse of up to 60 μsec (extracted at 66 MeV) for the Neutron Therapy Facility.[7]

Ion Source

Operation of the ion source during this time has been relatively good and has improved with understanding and experience. The design of the source has been essentially unchanged since it was last described in the first Symposium Proceedings.[3] Some improvements in the electronics along with some early operational understanding of the source was given in the last Particle Accelerator Conference.[8]

A source will operate at near maximum intensity (40-50 mA) for 4-6 weeks following a 1-2 day start-up and conditioning period during which the output current increases to the operating level. A typical method of failure has been caused by flaking of metal deposits on the anode which results from erosion of the cathode. As these deposits become thicker they eventually peel from the anode surface and into the plasma gap. This causes the plasma to become non-uniform and noisy. The effect on the source is to decrease the output and increase the low frequency noise (0.1-1 MHz) of the beam pulse. This deterioration of the source becomes noticeable after the initial 4-6 weeks of good operation and gradually increases. After another two weeks the beam intensity is about half the good operating value and the noise modulation may be $\pm$20%. It is usually in this period that the source is cleaned or a change is made to the other source. During a run, in which the arc would have been on for an integrated time of 1-1½ hours, 5-10 mils of the cathode erodes unevenly due to the arc current of 150 A. The arc current density is about 15 A/cm^2. In addition, a deeper depression (20-40 mils) occurs in the cathode behind the anode aperture when positive ions formed in the extraction gap are accelerated back into the source and strike the cathode (Fig. 3). Reusing cathodes that have been severely eroded has not affected the source operation. This implies that the anode-to-cathode spacing is not critical and possibly a larger spacing would reduce the effect of anode flakes on the plasma and give longer lifetimes.

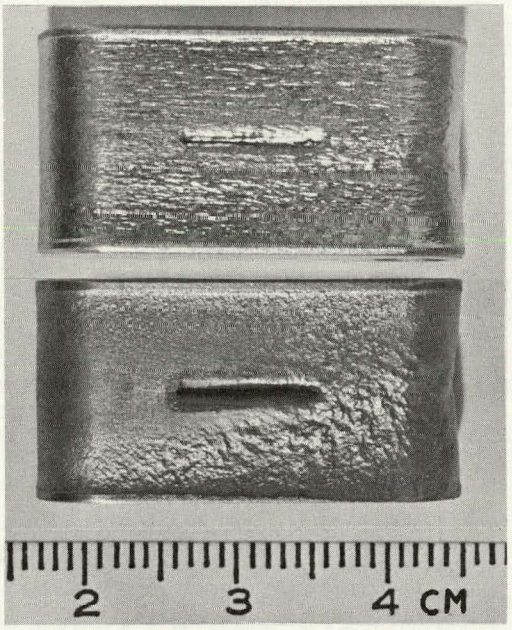

Fig. 3. Eroded Ion Source Cathodes
Top: Used Twice, ∿3 hours arc on time
Bottom: Used Four Times, ∿6 hours arc on time

The interesting possibility and benefit of using larger gaps has been observed in some early work done at Fermilab on a source with a 2 cm anode-to-cathode spacing. This source gave good plasma operation at lower pressure ($< 50 \times 10^{-3}$ torr) than in the standard magnetron with 1 mm spacing. Since this experiment was done in a bell jar under static gas pressure to observe the plasma conditions, beam parameters were not measured but visible streams of ionized gas energizing from the source aperture were exciting indications of beam.

Beam currents in the range of 50 mA are desirable though not necessary for the Fermilab use and some sources have achieved only 20-25 mA. The cause of most sources working poorly or having low beam current has usually been traced to contamination. Early sources became contaminated with a hydrocarbon from the gas supply system and would not condition to the proper plasma

operation. Purer hydrogen and a cleaner gas system were necessary for good operation. Several recent sources which were used with a new supply of cesium metal had proper plasma conditions but low beam current. It is believed that some contaminant from the cesium affected the cathode surface and caused the low H^- yield. Preheating this supply of cesium in a separate vacuum system to the operating temperature for several days gave improved H^- yield when later used on a source. Using a different supply of cesium also gave good intensity with the same source. Even though an analysis of the cesium has not been made, it would appear as though a volatile compound was in the cesium which poisoned the cathode surface.

In the three years that the source has been in operation on the high voltage accelerating column there has been no problem with cesium affecting the column. Cesium has been observed only around the source and nearby metal parts, predominantly on the refrigerated surfaces of the bending magnet poles and cooled box just beyond the source aperture.

Good operation of the source is critically dependent on several parameters. The best operation occurs with the arc (anode-to-cathode) voltage of 130-135 volts, a cathode temperature of 425-500°C, a hydrogen gas pressure just sufficient to maintain a good discharge, and an optimized cesium supply. Small changes in these operating parameters may severely affect the operation of the source and reduce the beam output. The magnetic field is not critical to the source operation over large changes above a critical field and is used to match the bending radius with the extraction voltage.

For the Fermilab source the operating parameters are:

Repetition Rate	15	Hz
Arc Voltage	130-135	V
Arc Current	150-160	A
Arc Pulse Width	∿60	μsec
Cathode Temperature	425-500	°C
Source Body Temperature	175-225	°C
Source Magnetic Field	1-1.5	kG
Extraction Voltage	18	kV
Extraction Current During Pulse	∿200	mA
Bending Magnetic Field (provides source magnetic field of 1.3 kG)	2.4	kG
Cesium Boiler Temperature	∿190	°C
Cesium Valve and Feed Tube Temperature	>300	°C
Estimated Source Hydrogen Pressure During Pulse	0.4	torr

With proper operation of the source the beam intensity from the 750-keV preaccelerator column is about 50 mA. The beam typically increases in intensity during the pulse and has about 10% or less high frequency modulation. A beam pulse of 50 mA x 80 μsec as observed by a current toroid following the 750-kV column is shown in Figure 4.

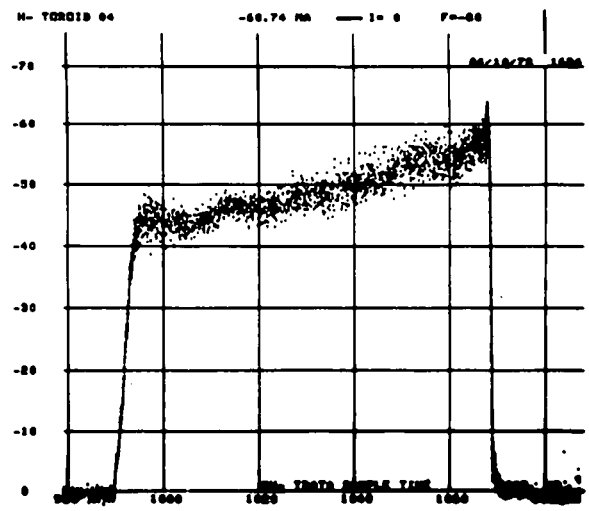

Fig. 4. H^- Ion Beam From Preaccelerator -10 mA/div x 20 μsec/div.

The normalized emittance for 90% of a 50-mA H^- beam emerging from the preaccelerator at 750 keV, as measured by a slit scanner, is:

$$E_{nh} = 0.088\pi \quad \text{cm-mrad}$$

$$E_{nv} = 0.15\pi \quad \text{cm-mrad.}$$

Significant improvements in the source could possibly be made by incorporating new ideas recently observed at Brookhaven.[9] Using grooved cathodes to decrease the arc current could greatly increase the lifetime or duty factor and may give a source with up to a 1% duty factor. The lower arc current may also produce a quieter plasma and smoother beam pulses. Asymmetric cathode spacings or larger anode-to-cathode gaps may further reduce the gas consumption and increase the lifetime.

References

1. Yu. I. Belchenko, G. I. Dimov & V. G. Dudnikov, "Surface-Plasms Source of Negative Ions," Proc. 2nd Sym. on Ion Sources and Formation of Ion Beams, Berkeley, Ca., VIII-1, LBL-3399, (1974).

2. K. Prelec & Th. Sluyters, "A Pulsed Negative Hydrogen Source for Currents Up to One Ampere," 1975 Particle Accel. Conf., IEEE Trans. Nucl. Sci., NS-22, No. 3, (1975) 1662.

3. C. W. Schmidt & C. D. Curtis, "An H^- -Ion Source for Accelerator Use," Proc. Symp. on the Production and Neutralization of Negative Hydrogen Ions and Beams, BNL, Sept. 26-30, 1977, BNL 50727, p. 123.

4. J. D. Sherman & P. W. Allison, "A Study of a 90° Bending Magnet for H^- Beams," 1979 Particle Accel. Conf., IEEE Trans. Nucl. Sci., NS-26, No. 3, (1979) 3916.

5. C Hojvat et al., "The Multi-turn Charge Exchange Injection System for the Fermilab Booster Accelerator," 1979 Particle Accel. Conf., IEEE Trans. Nucl. Sci., NS-26, No. 3, (1979) 3149.

6. C. Ankenbrandt et al., "H^- Charge Exchange Injection Systems," to be published in the Proceedings of the XIth Inter. Conf. on High Energy Accel., CERN, Geneva, July 7-11, 1980.

7. C. D. Curtis, et al., "Linac H^- - Beam Operation and Uses at Fermilab," 1979 Particle Accel. Conf., IEEE Trans. Nucl. Sci., NS-26, No. 3, (1979) 3760.

8. C. W. Schmidt & C. D. Curtis, "A 50-mA Negative Hydrogen - Ion Source," 1979 Particle Accel. Conf., IEEE Trans. Nucl. Sci., NS-26, No. 3, (1979) 4120.

9. J. G. Alessi & Th. Sluyters, "Regular and Asymmetric Negative Ion Magnetron Sources with Grooved Cathodes," Brookhaven Nat. Lab. Report, BNL-27942; also proceedings of this conference.

DISCUSSION

EHLERS It is a personal pleasure to me to see that the accelerator people finally recognize the advantage of negative ions. Fifteen years ago you could not sell one to an eskimo.

LEUNG You report that the cathode temperature is 450-500°C, so not much cesium will be sticking onto the cathode and most of it stays in the discharge?

SCHMIDT Yes, I would say there is quite a bit of cesium in this discharge. In fact if we let the cathode cool down and absorb the cesium, the discharge voltage does fall off. We do have a lot of cesium in the discharge to get that voltage.

FORRESTER At that temperature, 16 A/cm^2 is a remarkable emission. Did you say your cathode current was 16 A/cm^2?

SCHMIDT Yes.

FORRESTER You imagine some kind of a double sheath over there, so it has to be of the order of the electron emission. It seems like a remarkable number.

ALLISON In the Penning source it is another order of magnitude higher. It is 200 A/cm^2 there and I think the reason that that is true is that the secondary emission coefficient goes up from maybe 0.1 for a molybdenum surface to maybe 5 or 6 for a cesium surface. So there are a tremendous number of electrons that are knocked off by positive ions.

HOOPER What is the highest energy you have had the negative ion beam up to before you convert it to protons and how much current have you had at that energy?

SCHMIDT We extract from the linac at 200 MeV; we have had up to as high as 42 mA out of the linear accelerator.

HOOPER 42 mA at 200 MeV?

SCHMIDT That is right. I might point out that in the 200 MeV beam line it was necessary to change some bending magnets to reduce the stripping in those magnets. We had some rather high field bending magnets, so we had to lower those to below 10 kG to reduce stripping in there.

HOPMAN You mentioned that you had difficulties with the gas valves. I just want to mention that we are using a piezo-electric valve ourselves made by Balzer's. It works without any problem, only it is very sensitive for temperature, so you have to cool it locally.

SCHMIDT We are using a Veeco piezo-electric valve which is not intended for pulsed operation.

HISKES Can you make your cesium ion density more quantitative?

SCHMIDT No.

HISKES When you talk about the stripping you mean Lorenz detachments?

SCHMIDT Right.

SEIDL Have you analyzed your beam for other ions?

SCHMIDT No.

GELLER Do you take care when you open your ion source? I mean, are you afraid to admit air to the cesium inside?

SCHMIDT No, not at all. We use about a mg an hour or in a single run we will use a vile of about 5 grams of cesium. So the quantity of cesium is sort of small and it does deposit over fairly large surfaces. As soon as we take it out,

it becomes a hydroxide very quickly. There is no problem with that. Typically, if we have to change the source itself, we fill the vacuum tank with dry nitrogen, change the source unit, pump it down again and continue to run.

JACQUOT What is the average electric field in the accelerator?

SCHMIDT In the column the electric field gradient is 25 kV/cm.

JACQUOT Do you observe photo-emission due to the cesium on the electrodes?

SCHMIDT No, in fact we looked for radiation from the accelerator and compared it with the proton accelerator. We have less emission from the H^- accelerator than we have from the proton accelerator. Of course, the proton accelerator now looks directly into the cup of a duoplasmatron. In the negative ion column the beam is completely analyzed. We are injecting a clean beam. We are not going to get electrons streaming back and the radiation level from this accelerator was about a factor of 10 lower than in the other one. The radiation level in neither one was significant.

AN OVERVIEW OF THE LBL/LLNL NEGATIVE-ION-BASED NEUTRAL BEAM PROGRAM*

R. V. Pyle

Lawrence Berkeley Laboratory
University of California
Berkeley, California 94720

Abstract

The LBL/LLNL negative-ion-based neutral beam development program and status are described. The emphasis has shifted in some details since the first symposium in 1977, but our overall objectives remain the same, namely, the development of megawatt d.c. injection systems. Until last year we concentrated on a system in which the negative ions were produced by double charge exchange in sodium vapor. At present, the emphasis is on a "self-extraction" source in which the negative ions are produced on a biased surface imbedded in a plasma. A one-ampere beam will be accelerated to at least 40 keV next year. Studies of negative-ion formation and interactions help provide a data base for the technology program.

I. Introduction

The Lawrence Berkeley Laboratory and the Lawrence Livermore National Laboratory have a joint program to develop high-power neutral beam systems based on the production, acceleration, and neutralization of negative hydrogen and deuterium ion beams, for heating and fueling fusion devices. The rationale for negative-ion based systems was discussed in the first symposium[1] in 1977.

The work described here is supported by the Applied Plasma Physics Division and the Development and Technology Division of the Office of Fusion Energy. As the titles of papers in the first and Second Symposia indicate, the activities in this field include as much "physics" as "technology", indicative of the fact that the development of negative-ion-based systems for fusion still is in its infancy. Nevertheless, we shall see that substantial progress has been made since the previous meeting, and can expect to present the applications designer with some actual demonstrations of usable and scaleable components by the time of the Third Symposium.

The approaches and status of program components for meeting the R and D goals are outlined in the following sections. It will be indicated how the technical studies described here by other LBL and LLNL staff members fit into the overall program; these technical papers do not encompass all of our activities but they reflect the emphasis fairly well.

II. Program Elements - Status

Our research and development program must have the potential of producing neutral beam systems that will be used in the confinement programs. We anticipate, and users specify, parameters and development schedules, based on needs and perceptions of the state of the art. For example, LLNL has requested the development of high-current beams in the several-hundred keV range for use in its next generation of mirror devices.

The LLNL staff continues to devote a substantial effort to studies of systems needed for future experiments and reactors. These studies, an example of which is presented at this symposium[2], not only help define the basic parameters, but also help identify the engineering questions that must be answered as we move from the research to the application stage.

The discussion of the program elements and their present status is based on the neutral beam hardware system.

A. The negative ion source

This may be a double-charge-exchange or direct-extraction source.

1. Double-charge-exchange sources

Because the physics of producing negative ion beams by double charge exchange of positive ions in metal vapors was reasonably well understood, our first efforts toward a technology demonstration were based on this approach. Theoretical estimates and experimental measurements of yields of D^- ions are now fairly complete[3], except at low energies.

In a short-pulse experiment a beam of approximately 10 keV D^+ ions was converted to 2A of D^- ions in a supersonic sodium vapor jet, demonstrating one way to produce a useful negative ion source. The potentialities of this approach are discussed in an accompanying paper.[4] Although this system-approach has been carried farthest toward an actual neutral

beam system, it is in principle more complicated than the "direct extraction" sources now under investigation, and we are not planning to accelerate negative ions produced in this way, in the near term.

We shall continue studies of negative ion yields in vapors, especially at low D^+ energies.

2. Direct extraction Sources

a. Surface production

Our proposed technology demonstration currently is based on negative ion production on a biased surface immersed in a plasma produced in a "magnetic bucket". Positive ions striking the surface produce negative ions that are accelerated into the plasma and then emerge ("self-extract") through the magnetic field at a slot in the bucket walls. The production mechanisms have been studied as basic processes[5,6] and in an actual plasma device.[7,8]

The non-plasma experiments showed that production on low-work-function surfaces is small for incident energies of about 1 eV, but is rising rapidly with energy.[5] At higher energies, 200-300 eV/nucleon, the D^- yield from backscattering reached about 10^{-6}. Unfortunately, we don't have measurements for energies between ~ 1 eV and about 200 eV per nucleon. Measurements made with a source producing a dc, ~ 1/2A, beam of H^- ions[8], are generally consistent with the results of the energetic-ion studies, but also show a strong low-energy (< 10 eV) H^- component coming from the surface; the production mechanism has not been identified with certainty. Ions formed at low energy may have less transverse energy, and therefore permit better optics of the accelerated beam.

b. Volume Production

Large H^- densities in a plasma are reported by Bacal and co-workers[9,10]. Substantial H^- current densities from ions produced in the plasma also have been observed in the LBL experiment.[7] It is thought that accelerated electrons will be a greater problem with a volume-production source, than with a "self-extraction" surface-production source, but the possibilities of volume sources must continue to be examined.

B. The Accelerator

We have not built any accelerator structure for negative-ion beams yet, but optimized dc accelerators for beams from double-charge exchange and "self-extraction" sources have been designed for energies up to 200 keV.[11] These four-electrode slotted structures are not unlike those used in our positive-ion program,[12] except that the current densities are lower. For example, a 10-ampere system may require an accelerator array 50 centimeters on a side. One of the design boundary conditions is that accelerators for multiple beams must pack together closely.

Maschke's Meqalac proposal[13] has stimulated thinking about rf accelerators for energies above about 200 keV. We find the idea very attractive, but have not yet developed a conceptual design for an rf system.

In some cases it may be desirable to transport the negative ions from the plasma source to the accelerator, e.g. by a structure that permits transverse pumping of gas from the source.[14] Arrays of multipoles also might be used to transport high-energy negative-ion beams through the shielding of a reactor.

C. The Neutralizer

Gas, plasma, and photon targets are being considered as neutralizers. Gas targets, perhaps supersonic jets[4], are the most straightforward, and should give neutralization efficiencies of about 60%.

Fully-ionized plasma neutralizers have been estimated to give neutralization efficiencies of about 85-90%. Partially-ionized gases will give values somewhere between 60% and 90%. Several aspects of plasma targets were presented in the first Symposium.[15]

The prospect of making fully-ionized plasma targets for beams with large cross-sectional areas is not very attractive. On the other hand, a partially-ionized (e.g 20) target from many small beams might not be difficult. To bring some focus to this problem we have a program to study the interactions of 200-300 keV D^- ions with plasmas.[16]

Finally, photodetachment can be used as a method for converting the D^- beam to a D^0 beam.[17,18]

D. Other System Elements

As in the case for positive-ion beam systems, much of the size and cost of negative-ion beam systems will be in components other than the above: The vacuum system, power supplies and controls and beam dumps. Much of the technology being developed for positive-ion systems[12] will be applicable.

III. Status Summary

Substantial progress in understanding the principles of negative-ion-based neutral beam systems has been made since the first Symposium was held in 1977. In particular, a lot of the physics of negative ion formation in vapors, surfaces, and plasmas has been established, and negative ion beams with currents of the order of one ampere have been produced by both the

double-charge-exchange and the surface-interaction techniques. System studies have been carried far enough to identify important design features for both the developers and the potential users. Neither the research programs nor the development programs are in want of good ideas.

A rough schedule and cost estimate for a "proof-of-principle" one-megawatt CW D^0 beam has been prepared in anticipation of a program to have a prototype of a useful injector operating in about ten years. It is not surprising that the required time and funding appear to be about the same as required for development of a prototype positive-ion-based TFTR injector.

IV. Plans

A. Near-Term

By the end of 1981 we expect to demonstrate the quasi-steady-state operation of a one-ampere H^- beam accelerated to 40-100 keV with acceptable beam optics. The fairly basic studies of negative-ion formation in gases, surfaces, and plasmas will continue as required for the development data-base.

B. Longer-Term

We hope to build and demonstrate a megawatt neutral beam system based on negative ions in the 1980's.

References

* This work was supported by the Fusion Energy Division of the U. S. Department of Energy under contract No. W-7405-ENG-48.

1. Proceedings of the Symposium on the Production and Neutralization of Negative Hydrogen Ions and Beams, Brookhaven National Laboratory September 26-30, 1977; Brookhaven National Laboratory Report BNL-50727.

2. G. Hamilton, "Negative Ion Systems for Tandem Mirror Next Step and Tandem Mirror Reactor", this symposium.

3. A. S. Schlachter, "Atomic Physics in Negative Ion Based Neutral Beam Injectors," this sumposium.

4. E. B. Hooper, "Prospects for Negative Ion Systems Based on Charge Exchange", this symposium.

5. W. G. Graham, "Negative-Hydrogen-Ion Production by Low energy Hydrogen Atom Bombardment of Surfaces, LBL-9511.

6. J. Hiskes, P. Schneider, "Formation of H^- and D^- Ions by Particle Backscattering from Alkali Kransition Metal Complexes", this symposium.

7. K. N. Leung, K. W. Ehlers, "H^- and D^- Formation From a Surface Conversion Type Ion Source", this symposium.

8. K. W. Ehlers, K. N. Leung, "Characteristics of a Self-Extraction Negative Ion Source", this symposium.

9. M. Bacal, A. M. Bruneteau, H. J. Doucet, W. G. Graham, G. W. Hamilton, "H^- Production in Plasma", this symposium.

10. G. W. Hamilton, M. Bacal, A. M. Bruneteau, H. J. Doucet, M. Nachman, "Measurement of H^- Donsity in Plasma Photodetachment", this symposium.

11. O. A. Anderson, "High Perveance Negative Ion Accelerators", this symposium.

12. K. H. Berkner, et al., 'Development of 120 keV Neutral Beam Injectors, Proceedings of the 8th Symposium on Engineering Problems of Fusion Research, Nov. 13-16, 1979, IEEE Pub. No. 79 CH 1441-5 NPS.

13. A. W. Mashke, "MEQALAC, A New Approach to Low Beta Acceleratior," Brookhaven National Laboratory Report BNL-51029 (1979).

14. K. N. Leung, K. W. Ehlers, E. B. Hooper Jr., "Transport of Low Energy Positive and Negative Ion Beams by Permanent Magnets", this symposium.

15. M. W. Grossman, "Plasma Neutralizers for H^- Beams", See Reference 1.

16. K. Berkner, R. V. Pyle, S. A. Savas, and K. R. Stalder, "Plasma Neutralizers for H^- or D^- Beams", this symposium.

17. H. C. Bryant, P. A. Iovoi, and G. G. Ohlsen, "Production of Pulsed Particle Beams by Photodetachment of H^-", LASL Report 1971.

18. J. H. Fink, W. L. Barr, and G. W. Hamilton, "Efficient High-Power, High Energy Neutral Beams for the Reference Mirror Reactor", LLL Report UCRL-79205 (1977).

DISCUSSION

GELLER Why do you put emphasis on D^- current and not on D^- current densities? Because, it is well known that one can always make currents with geometrical expansion, whereas current densities are the most important thing for Tokamak injection.

PYLE In the final analysis it is the total current that counts as far as the Tokamak is concerned. But one does have to go through holes and things like that, so current density is an important thing. Current densities which we think about here, averaged over an array, are maybe of the order of 10 mA/cm^2 or something like that, whereas in the positive ion systems they are perhaps 25 times bigger. So going to high current density is desireable, but for the demonstration of something that is useful, for let us say a mirror reactor and the size holes that exist there, an average current density is 10 mA/cm^2. I should have mentined that, it is important. It is not at the moment our primary concern, it is a secondary concern.

GELLER When you talk about tens of amperes, that means a lot of gas through-put and you increase the difficulties. The strength of the negative ion injector is to work with little current and high voltage to make the MW. I think it is much more important to talk about kW/cm^2, which is limited in the Tokamak injectors. Now the philosophy is different, because you have less of a vacuum problem which is the big difficulty of injectors.

PYLE I did not understand where we have easy pumping. Under what conditions is there easy pumping?

GELLER If you have less current you have less gas through-put because particles are a gas, finally, somewhere. So, if you work with less current you need less pumping and I think this is the critical issue for the injector.

PYLE I think the safest thing for me to do is to refer this comment and/or question, as it may be, to people like Borchers or Hamilton. If I go to these people, then for the mirror program one wants not one ampere or even tens of amperes but hundreds of amperes. The mirror program needs them. Now with the Tokamak program, it is a matter of debate as to whether any are needed at all. Some people do not believe one needs a negative ion program or even a positive ion program. Eventually for the Tokamak program there is a case which I have mentioned, which has been put to us to study and that is the development of a few amperes of very high energy negative ion based neutral beams to drive steady state currents in Tokamaks by accumulation. That might fit in very well with what you are talking about as the easiest application. I think to go to a few MeV at a few amperes is not trivial, although the pumping will be easier. That would be a real incentive for us to go into the RF accelerator development. Thank you for your comment. By the way, I am hoping that I will (by this route) learn something about other people's programs and motivations as for example the European community. I do not know whether you plan to comment on that or not.

CHARACTERISTICS OF A SELF-EXTRACTION NEGATIVE ION SOURCE*

K. W. Ehlers and K. N. Leung

Lawrence Berkeley Laboratory
University of California
Berkeley, CA. 94720

ABSTRACT

A multi-cusp, self-extraction, negative hydrogen ion source has been designed and constructed. Several diagnostic techniques have been applied to study the operating characteristics of this type of source. Negative H^- and D^- ions are produced on a negatively biased converter surface, and are self-extracted from the system. With the addition of cesium, the source has been operated at a neutral pressure of 1 X 10^{-3} Torr to generate a steady-state H^- ion current greater than 400 mA. The generation of impurity negative ions has been investigated, as have methods for reducing the presence of background electrons in the ion exit region. Plans for a larger, next-generation device will be discussed.

INTRODUCTION

Subsequent to the first meeting of this Symposium,[1] we began the development of a concept for a negative ion source geometry which was conceived to produce continuous beams of self-extracted, surface produced, modest current density, negative hydrogen or deuterium ions. Because the self-extracted ion current density is not meant to be high ($\leq$50mA/cm^2) large ion exit apertures are required in order to obtain the multi-Ampere beams of negative ions that will eventually be required for neutral beam injection. This in turn, means that the plasma source must be capable of operating at a low pressure. With this requirement in mind, the multi-line cusp geometry,[2-3] which is known to operate with good gas efficiency, was chosen as the basic plasma generating system. The self-extraction feature was desired as it meant that no external electric fields would be required to extract the negative ions from the source plasma. The absence of such fields should greatly reduce the contamination of the beam with the unwanted electrons which are also extracted from the plasma when electric fields are applied.

APPARATUS

Fig. 1 is a drawing of the initial test geometry. The device is a cylindrical multi-line cusp arrangement (20-cm diameter and 23-cm long) with rows of samarium-cobalt

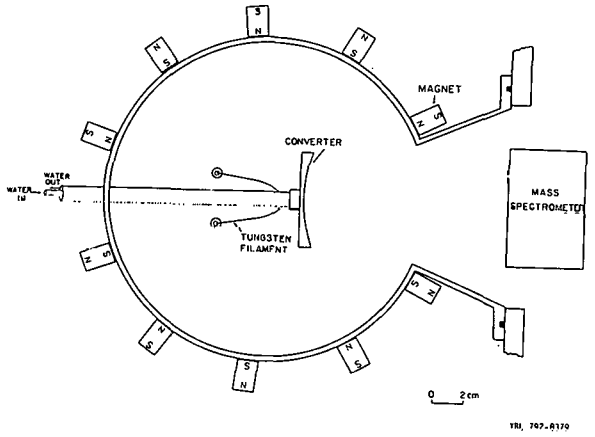

Fig. 1. Schematic diagram of the multi-line-Cusp Negative ion Source.

magnets (B max$\simeq$4 kG) placed externally around the chamber wall on all sides. In the region of the exit aperture, where the negative ions are to self-extract from the source, the spacing of the magnets has been increased. The magnetic field in this region is adjusted to be strong enough to contain all energetic electrons, which may have energies as high as 300 eV, yet weak enough to not seriously perturb the trajectories of the energetic negative ions, which are produced at the surface of the converter. The resulting cusp magnetic field pattern, mapped by iron filings is illustrated in Fig. 2 (A). A plot of the level of magnetic field, which shows the effect of the increased spacing of the magnets in the ion exit region, is shown in Fig. 2 (B)

A steady state hydrogen or deuterium plasma is generated by 60 to 70 eV primary electrons emitted from two 0.15-cm dia. tungsten filaments. The filaments are mounted on feed-throughs mounted on each of the two end plates. The entire chamber wall, which is at ground potential, serves as the anode for the discharge. The source pressure is maintained at 1 milli-Torr or less as measured by a Barocel. With an arc current of 45 A, plasma densities heigher than a few x 10^{12} can be generated. To produce negative ions, the converter shown in Fig. 1 (6 cm high and 10 cm long) is biased negative with respect to the

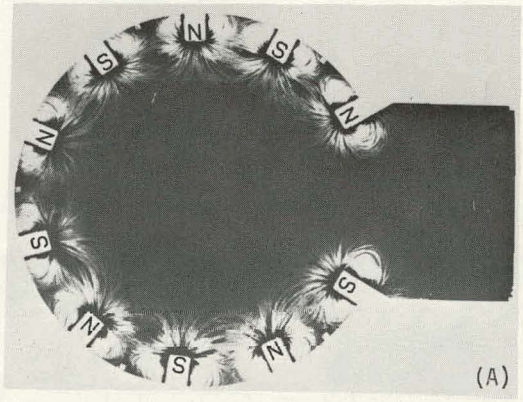

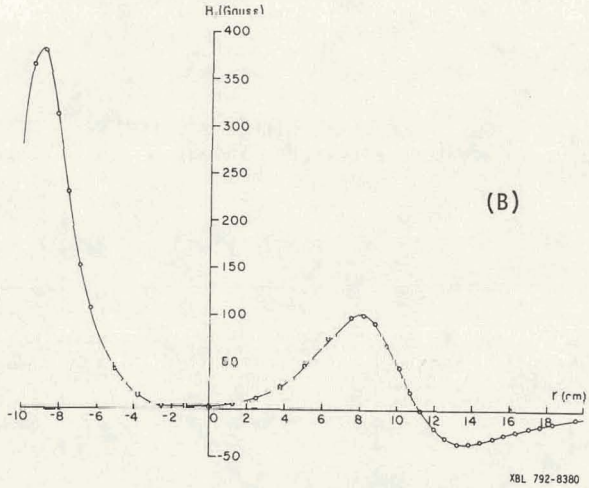

Fig. 2. (A) Magnetic field pattern generated by the line-cusp magnets. (B) A plot of the magnetic field as a function of radial position through the exit aperture of the source.

potential of the plasma by several hundred volts. Positive ions from the plasma strike the surface of the converter with this potential. Any negative ions that are produced at the surface of the converter are then accelerated back through the sheath by this same bias potential, and are directed through the plasma to the ion exit aperture. The bias potential on the converter thus becomes the ion extraction potential. In order to increase the number of negative ions produced, the area of the converter is increased by making the height of the converter larger than the height of the extraction aperture, and the converter is curved to geometrically direct the ions to a focus at the position of the extraction aperture.

In a preliminary study, the source was operated with a clean copper converter and negative ions which were generated by reflection from the uncesiated copper surface were monitored by a compact mass spectrometer. These results have been discussed by Leung at this symposium,[4] and a photograph of the source, and the spectrometer is shown in Fig. 3. The converter was operated with potential as high as -500 volts, but the spectrometer indicated that no energetic electrons, including secondaries from the converter electrode which would have energies equal to the converter potential, were escaping from the source.

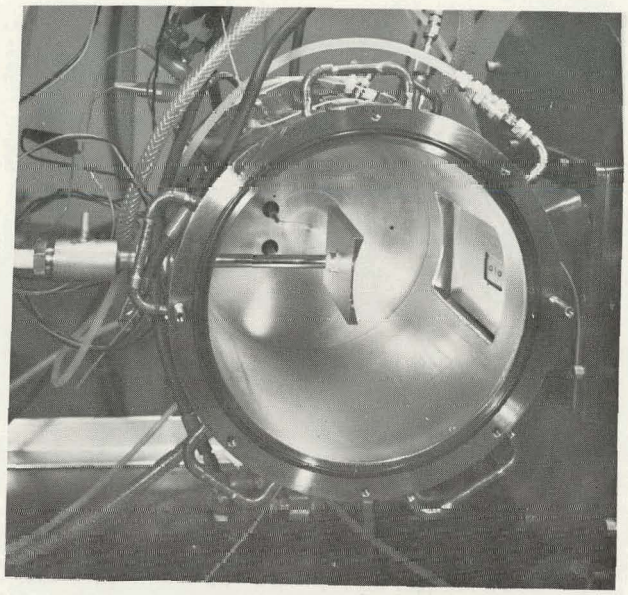

Fig. 3. Photograph of the test ion source.

With the spectrometer removed, a probe was installed in the ion exit region, and to our surprise, it indicated that there was a plasma present in this region. Although the plasma density was nearly 2 orders less than that of the discharge region, its presence was indeed a disappointment as it meant that should an electric field be applied to accelerate the negative ion beam, electrons too would become a part of the beam. The probe study further indicated that the electrons in the exit region were very cold (~1 eV), and that their numbers were a function of the potential of the plasma in the discharge region. This is illustrated in Fig. 4, where probe traces taken at the center of the discharge are compared to probe traces taken just outside the ion exit aperture for two slightly different levels of plasma potential. For the probe traces marked A, the plasma potential is ~6 volts positive in respect to the grounded chamber anode wall, and a plasma with a density of about two orders less exists in the ion exit region. When the potential of the source plasma was made just slightly negative in respect to the chamber wall, the density of the plasma in the ion exit region reduced by an additional two orders of magnetude, and this is shown in the probe traces marked B. These results pointed out the fact that while the confining magnetic field at the exit region is ample to return energetic electrons to the discharge, it is too low to

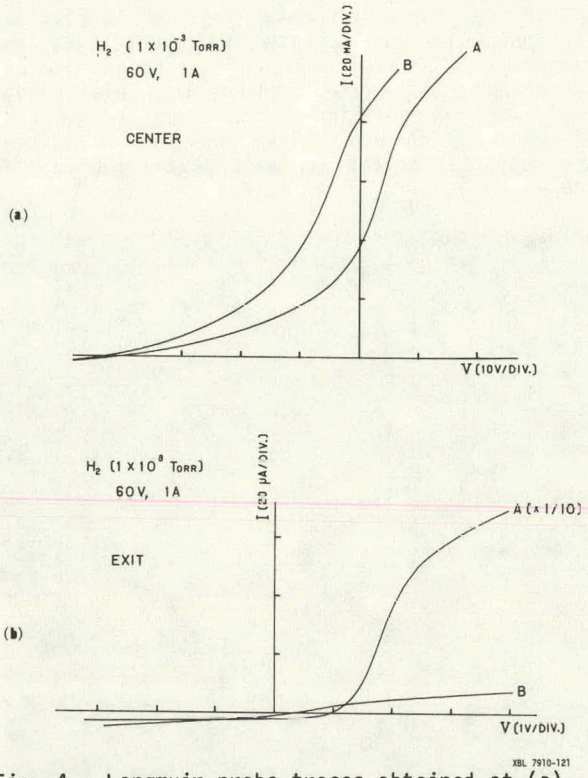

Fig. 4. Langmuir probe traces obtained at (a) the center and (b) the exit of the source for two different plasma potentials (A & B).

prevent the leakage of low energy ions from the discharge. Ion confinement by this magnetic field is not only a function of the charge, mass, and energy of the ion, but also a function of the magnetude and polarity of the electric field that exists between the volume of the plasma and the exit structure. The cold electrons found in this region could either diffuse across the magnetic field with the positive ions, or they might possibly be produced by photons that illuminate surfaces near the exit region. In either case, the electrons can be suppressed by a potential which would be expected to extract them from the discharge. In reality, the electrons are suppressed by preventing the entrance into the exit region of low energy positive ions from the discharge.

We did not wish to add to our list of operating requirements that the plasma potential be maintained negative to the chamber wall at all times. The results shown in Fig. 4 suggested that the same effect could be obtained by installing an exit aperture that could be baised slightly positive in respect to the potential of the plasma. Aperture plates were installed and the arrangement is shown schematically in Fig. 5. Probe traces, taken in the exit region as the bias of the exit aperture is changed, are shown in Fig. 6 The plasma density is only weakly affected as the

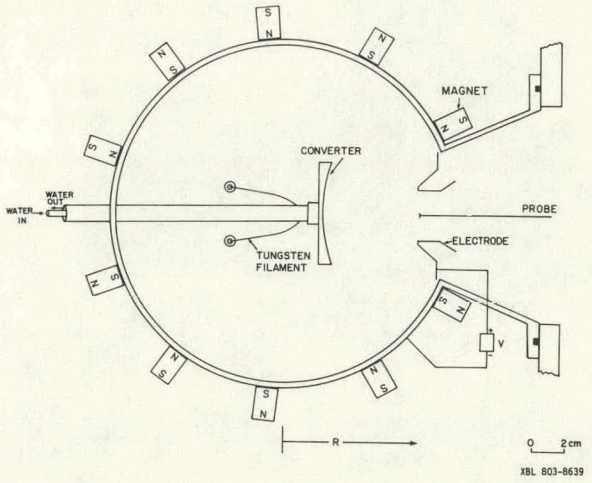

Fig. 5. Source geometry with the biased aperture electrodes added.

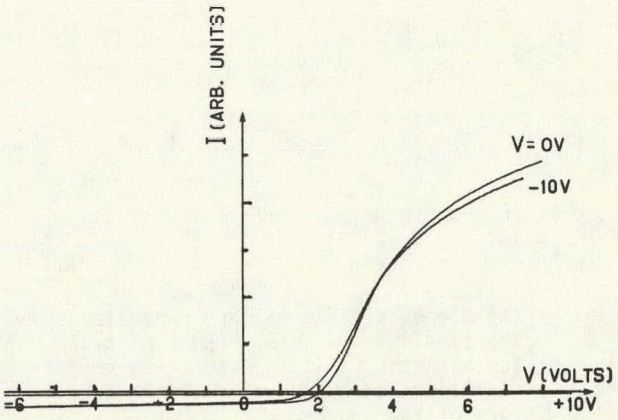

Fig. 6. Plasma density as indicated by probe traces with -10, 0, and +10 volts applied to the aperture electrode.

aperture bias is changed from 0 to -10 volts, but with a +10 V bias, the plasma in this exit region is essentially elinimated.

The data shown in Figures 4 and 6, were taken with the source operating with an uncesiated copper converter and with hydrogen gas. High mass ions can more easily penetrate the weak exit magnetic field and when cesium is added to the discharge, positive cesium ions (mass = 133) will be present. To determine whether the biased exit aperture would be effective in returning such large mass ions to the plasma, xenon gas (mass = 131) was added to the discharge. The results are shown in Fig. 7 where once again, no plasma exists in the exit aperture region when a positive bias of about +10 volts is applied to the exit aperture. When cesium is added and negative ions are produced, the potential in the exit region may become negative due to the space charge of the beam.

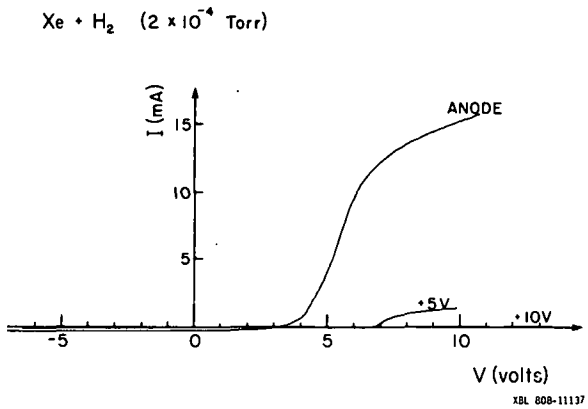

Fig. 7. Effect of aperture bias (0, +5, +10 volts) when xenon is added to the discharge.

In this case the presence of positive ions in the exit region will be desired, thus the bias on this electrode will be variable so as to allow the penetration of some positive ions.

When cesium is added to the discharge, the negative hydrogen or deuterium ion current increases dramatically.(5) Fig. 8 shows the H^- ion spectrometer signals obtained when the discharge is operated with and without the addition of cesium. The gain in H^- production from this copper converter (bias = -250 V) was approximately a factor of 100 with the addition of cesium.

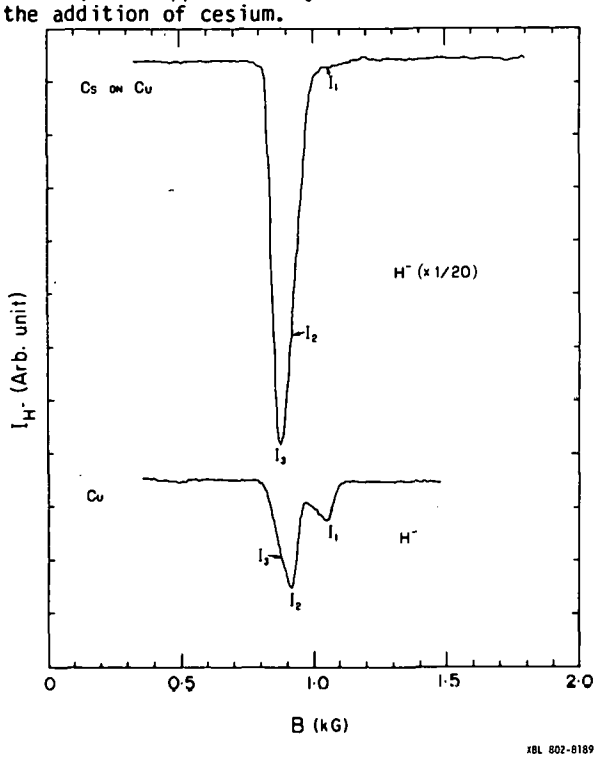

Fig. 8. The H^- ion spectrometer signal obtained when the source is operated with and without cesium in the discharge.

The mass spectrometer was also used to measure the H^- ion yield for several other alkali metals. It was found that the addition of lithium to the discharge increased the H^- ion yield by a factor of ten over the yield obtained from a clean copper surface, and for sodium, the yield increased by nearly a factor of fifty.

The change in the ion energy spectrum which is evident in Fig. 8, will be discussed by Leung at this Symposium(4).

IMPURITIES

Negative ions other than H^- and D^- can also be generated at the converter surface. While using the mass spectrometer and a copper converter, the impurities were found to be largely O^-, OH^-, and a mass 25, which is believed to be C_2H^-. The impurity level is directly related to the system cleanliness, and can be very high (typically 75%) when a new uncesiated converter is first employed. Higher impurity levels are also observed when the source has been inoperative for a period of time. We normally operate the source without cesium until the impurity level has decreased. When cesium is introduced into the discharge, the H^- ion current increases markedly, but there is generally no large increase in the impurity level. The electron binding energies of the main impurities observed are considerably higher than that of H^-. Thus these impurities can be formed more easily than H^- with an uncesiated converter. In addition, it is possible that impurities in the system may be pumped by cesium that is trapped on the walls of the source. Because impurities can represent a sizable fraction of the total negative ion beam, total beam current readings are taken in a manner in which the impurity level can be discerned. Fig. 9 is a drawing of the gridded Faraday cup that is used to read the total negative ion current. A 72% transparent fine mesh tungsten screen is biased approximately 15 volts negative to collect any low energy positive ions, and the collector plate is biased positive by 18 volts to collect any secondary electrons. These potentials were determined by varying the two bias potentials to obtain a zero reading on the cup in the presence of a plasma that contained no energetic negative ions. In addition, a portion of the beam is sampled by a small mass spectrograph constructed from a pair of iron shielded permanent magnets. The magnet is designed to bend both H^- and D^- ions so as to be received by one collector, and all other impurity ions from mass = >12 are received by a second collector. Figure 10 is a read out of the three currents taken as the source is started up and adjusted for maximum H^- output. As can be seen, the impurity level, which started out at about 40%, of the total negative ion current dropped to 1% or so in about 10 minutes when the reading was terminated. The total negative ion current,

which is now mostly H⁻ continued up to ~450 mA as source adjustments were continued.

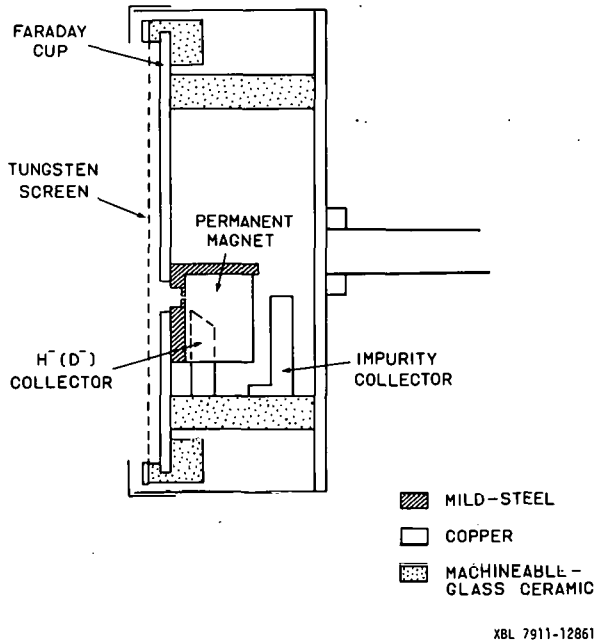

Fig. 9. Faraday collector including impurity analyser

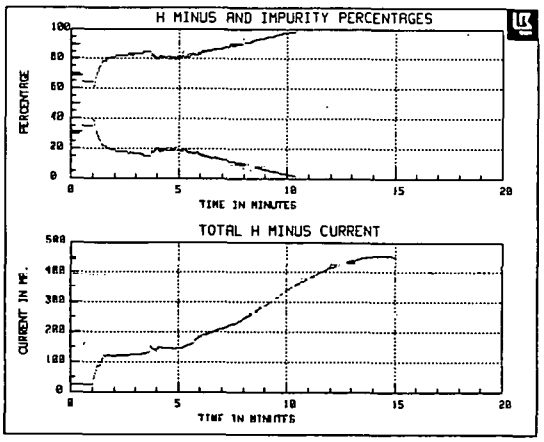

Fig. 10. Chart of total negative ion current and the change of impurity level with time.

CONVERTER

The mechanism by which negative ions are produced on the surface of the converter once cesium has been added to the discharge has yet to be fully understood. Thus one is unable to state the characteristics that the converter material should possess in order to obtain the best yield of H⁻ ions. Therefore, we conducted an imperical study, the results of which will be discussed by Leung.[4] In addition to producing the maximum yield, a number of other parameters deserve close consideration. The sputtering rate of copper for example, the first converter material that we tried, is very high, and only short periods of operation were required to completely coat the entire source system with a layer of copper. To minimize sputtering, the use of high mass elements in the region of tungsten[6] is best as they exhibit the least sputtering rate for ion energies in the range of a few hundred volts. The sputtering rate for 300 volt D^+ ions on copper (mass=63) is more than two order of magnetude larger than the sputtering rate for tungsten (mass=184) Cesium ions which strike the converter will have a sputtering rate that may be several orders of magnetude higher than that of deuterium, thus sputtering of the converter is an important consideration. In order to minimize sputtering, elements such as hafnium and tungsten would seem to be the best materials.

It is indeed possible that the converter material itself could appear as a contaminant negative ion. Thus one would desire the electron attachment energy of the converter to be low so as to minimize the probability of negative ion formation.

To minimize converter material as a negative ion contaminant on the basis of the electron attachment energy,[7] hafnium or rhenium would appear to be the best choice. One would not wish to choose platinum as it has a very high electron attachment energy. Work function is important as it may relate to the ability of the material to contain cesium on the surface. Of the metals tested we have selected rhenium and molybdenum our best converter materials. Rhenium is a high mass material, with a high work function, and a low electron attachment energy. In our tests, reproducibly rhenium and molybdenum were the materials that produced the largest yield of H⁻. Although we prefer rhenium, it is both very expensive and difficult to fabricate, thus the majority of our test data has been obtained using molybdenum converter surfaces.

Operating Characteristics

The arc power supply available for use with this experiment is a constant voltage type. Thus any changes in arc impedance are reflected as changes in arc current as the arc voltage is held constant at about 70 volts. Changes in arc power are therefore made by controlling the filament temperature, hence the arc current.

The converter potential, though adjustable, is generally maintained at about -200 volts. This is the approximate bias potential that is the most productive of negative ions, regardless of the material from which the converter is constructed. The sides, rear, and entrance support of the converter are covered with a floating quartz housing. Thus, the

converter current that we monitor is made up of positive ions striking, and negative charges leaving the curved front converter surface only.

The arc current and the converter current are sensitive to the mass of the gas. For example, if cesium is added to the discharge, the arc impedance becomes less and the arc current increases. Operation with deuterium as well reduces the arc impedance and the impedance will be further reduced as cesium is added.

Operating with hydrogen only, the converter current will read approximately 15% of the arc current. When cesium is added, the converter will read about 25% or less of the arc current. For example, with an arc current of 40 A, arc voltage of 70 volts, and a converter current of 10A, we typically read 400 mA of H^-. With a 3.5-cm high limiting exit aperture our best stable operation is with an H^- output of about 450 mA. Without a limiting aperture, 500 mA is readily obtained. We have on occasion, produced H^- outputs as high as 700 mA, but in general, these are not easily reproduced or available for long time, stable operation. Fig. 11 is a recorded output of the Faraday cup showing stable operation at the 450 mA level, dispite several sparks from the converter to the plasma.

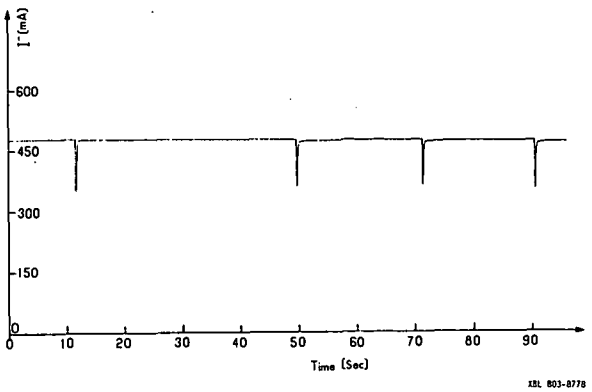

Fig. 11. Chart of Faraday output showing the effect of converter sparking.

Converter spotting will generally clean up, however one arc every few minutes is not unusual. We have a spot-detector circuit encorporated in the converter supply, which is designed to sense a spot or unipolar arc, reduce the voltage level for a few milli-seconds, and then reapply the voltage. Stable operation of the biased converter with cesium present in the discharge has not been as difficult a problem as we expected it to be.

In so far as the arc conditions change when one uses deuterium gas, it is difficult to make accurate comparisons between D^- and H^- yields. But if we use the converter current as a compative parameter, we do see a definite isotope effect. In general, the production of D^- is less than H^- by very roughly $\sqrt{2}$.

BEAM SHAPE

A small movable gridded Faraday cup was constructed which could scan the beam height to determine the effect of the geometric focussing. Fig. 12 is a plot of the ion beam shape taken at several distances from the converter. Fig. 13 compares the FWHM of these measured beam shapes with a geometric projection of the converter geometry.

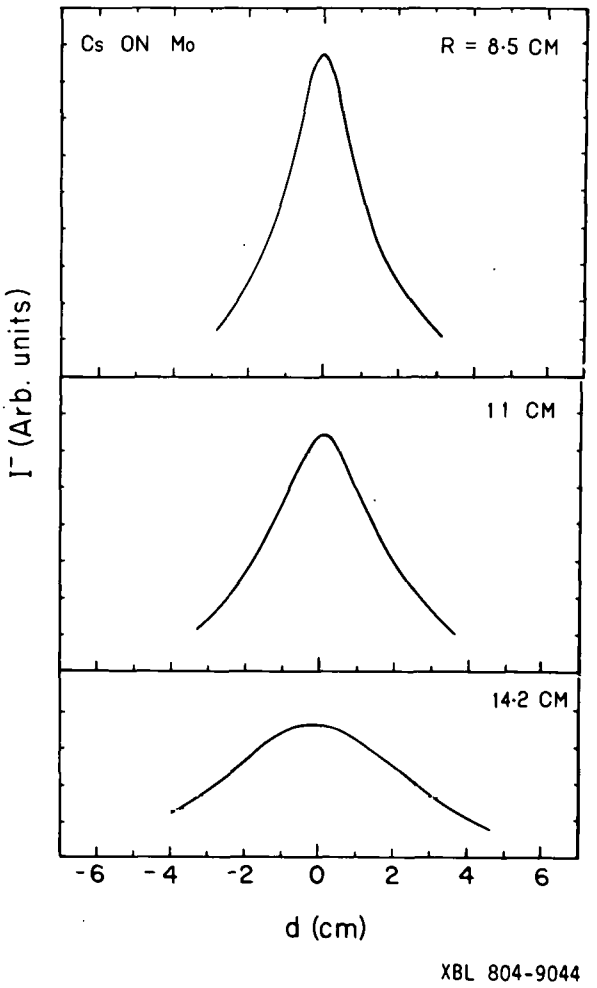

Fig. 12. Beam shape at several distances from the converter.

As can be seen, the beam rather closely follows the design geometry. If all negative ions formed on the converter surface left the surface with zero energy, the geometry should fully control the ion trajectories, however those ions which have appreciable initial

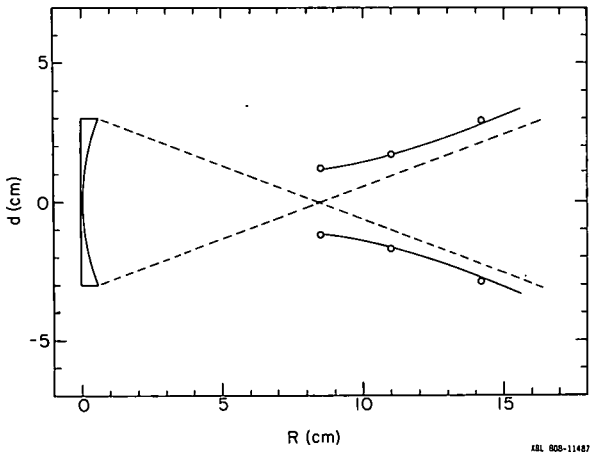

Fig. 13. Measured beam widths (FWHM) compared to the converter geometry.

energy, such as those produced by reflection, are not confined to the geometrically determined path.

The program goals, as established by the review panel of the recently convened Negative Ion Program Review, are to accelerate an H^- ion beam of ≥ 1 A to an energy of ≤ 50 keV with pulse lengths from 5 seconds to steady state. In order to meet these goals we are constructing a larger source, accelerator, and vacuum system. A stainless steel chamber (approx. 4' x 5' x 2') will serve as the main vacuum vessel and will be pumped by two turbo-molecular pumps for source operations. Two auxilliary liquid helium cryo-pumps (~12,000 L/sec ea.) will be added for beam acceleration studies.

Figure 14 is a drawing of the negative ion source. The shape of the source is designed to be scaleable in both x and y in order to obtain larger negative ion currents than from just the one converter shown. By increasing the vertical height, and maintaining the magnet spacing shown for the single exit aperture, additional ion exit apertures could be added, along with additional converter electrodes which would be placed above and below the single one shown. The magnet mounts, which also include the mechanical stiffeners needed to support the vacuum load, are sized to contain available ceramic or samarium cobalt magnets. This will allow us to adjust, by roughly a factor of two, the cusp magnetic field strength at the exit aperture. The use of the stronger magnets is detrimental only in that the ion beam is moved sideways farther in the direction of E x B. As can be seen in Fig. 2, the direction of the magnetic field changes as the ion moves through the exit aperture, and the E x B motion given to the ion on one side of the magnet is removed on the other side. Thus after passing through the magnetic fields at the exit aperture, the beam emerges with a trajectory that is normal to the converter, but moved sideways by an amount that is proportional to the magnetude of the magnetic field and the ion energy.

This can be as much as several centimeters, and thus a provision has been made to position the converter sideways by a like amount. The water cooled converter is 8 cm (the dimension shown) by 25 cm.

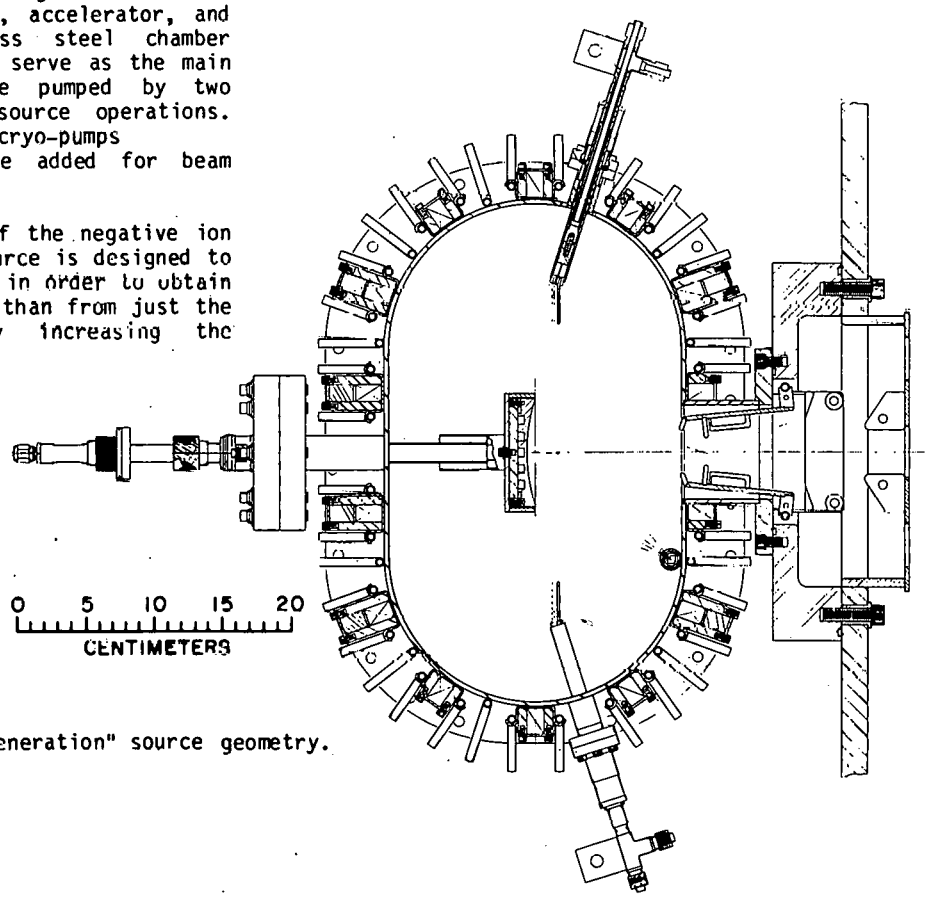

Fig. 14. Side view of "next generation" source geometry.

The exit aperture, which is electrically isolated so that a bias potential can be applied, is mechanically adjustable such that the width of the defining exit aperture can be changed from 3 cm. to nearly closed. The slit will be made as narrow as possible so as to reduce the gas flow rate, yet not so narrow as to impede the exit of optically useful negative ions.

The source design incorporates feedthroughs for 8 tungsten filaments (0.15-cm dia.) with four located at the top and four at the bottom of the chamber. The filaments are distributed so as to provide a uniform plasma illumination of the converter surface. Initially, cesium will be fed from an oven through a single, resistance heated, coaxial tube located below the ion exit slit. The cesium will be sprayed into the discharge rather than directly onto the converter surface.

The beam defining electrode of the single stage accelerator has an opening of 5 cm. The accelerator geometry was computer designed using the WOLF code,[8] and is designed for a uniform H^- ion density of 8 mA/cm^2 at 40 kV. The design, which will be refined when the beam shape has been fully determined, will be discussed by Anderson [9].

The design of source and beam diagnostics, including a water-cooled calorimeter is underway.

REFERENCES

*This work is supported by Fusion Energy Division, U. S. Department of Energy, under contract W-7405-ENG-48.

1. Proceedings of the Symposium on the Production and Neutralization of Negative Hydrogen Ions and Beams. Sept. 26-30, (1977). Brookhaven National Lab.

2. R. Limpaecher and K. R. Mackenzie. Rev. Sci. Instrum. 44 726 (1973).

3. K. N. Leung et. al. Phys. Lett. A 51, 490 (1975).

4. K. N. Leung - this Symposium - Second International Symposium on the Production and Neutralization of Negative Ions and Beams. Oct. 6-10, (1980). Brookhaven National Lab.

5. Yu I. Bel'chenko, G.I. Dimov, and V.G. Dudnikov, Nucl. Fus. 14, 113 (1974).

6. C.E. KenKnight, G.K. Wehner - Jour. Appl. Phys. Vol 35 #2 Feb. 1964 (322-326).

7. H. Hotop and W.C. Lineberger Jour. of Phys. and Chem. Ref Data 4 (1975).

8. W.S. Cooper et. al. - Proc. of the Second Symposium on Ion Sources and the Formation of Ion Beams - Berkeley, CA. (1974) p. 11-1.

9. O. Anderson - this Symposium - Second International Symposium on the Production and Neutralization of Negative Ion and Beams - Oct. 6-10, (1980) - Brookhaven National Lab.

DISCUSSION

PRELEC Do you have an estimate for the gas efficiency, for the overall power efficiency and the cesium loss rate?

EHLERS Yes, we have looked at the gas efficiency. For some time I have been worried that what we see would not be a fair answer and that it might be more of a systems problem. But, if you want to know our gas efficiency, I will whisper it to you. We have taken a look at the gas flow coming in and the negative ions going out and we see a gas efficiency, atomically that is, atoms in, atoms out, of about 35%. Well I do not tend yet to believe that and the reason I say that is, that we can shut the pumping off completely and still get negative ions and in that case our gas efficiency should be better than 100%. So really it is a systems problem, that is yet to be resolved. It looks encouraging, however, let me put it that way. And, what was the next question?

PRELEC What is the overall power efficiency?

EHLERS I could give you numbers of what we have got now, for example 35 A x 70 V, which is the power of the arc, and 200 V x 8 A and we get 0.5 A out. So the power efficiency is 8 kW/A.

PRELEC And the cesium loss rate?

EHLERS We have looked at the cesium loss rate and from what we can see it is very low. We did that by putting in a collector downstream while the arc was running. Inserting it after the arc was on and removing it before we turned the arc off. I do not remember the numbers but it was nanograms per cm^2 sec. Of course, as it was mentioned yesterday, if the arc is on all the time, your cesium has a difficult time getting out.

PETERSON Is your converter cooled?

EHLERS We have the temperature of the converter from essentially boiling on down. If we get too much cesium we turn the water off and help flush the cesium off the surface if you will; then we turn the water back on and look for changes in the negative ion current. On occasion we do. In other words we appear to have too much cesium at times.

PETERSON Are you looking for the best running conditions or that sort of thing too?

EHLERS That is something we will do too.

HOLMES Can you mention when you put those electrodes across the mouth of the source and bias them positive, the ion density in the drift region outside the source went right down. Is that nothing less than the 10 V negative ion extraction system?

EHLERS In essence yes. What you are really doing is telling the positive ions that they are not supposed to come in there. If they do not come in there, neither do the electrons. We read the electron current on the blade. I have some plots of that, and if you bias the blade as you would a Langmuir probe you see sometimes more ions than electrons and in other cases they are equal. We use that blade current to tell us the amount of cesium that is in the system. I should have mentioned that the system works nicely with high mass gasses (like cesium) as well. We used xenon to check that out. It works fine.

ALLISON Is the discharge affected by the introduction of cesium and by the operation of the converter?

EHLERS The discharge is affected by the gas you run. For example, the cesium is a higher mass, so it definitely affects the impedance of the arc; if you put in deuterium rather than hydrogen then you see an affect in the impedance of the arc. Therefore it is in a sense difficult for us to tell what the isotope effect is between H and D, but in general we see an isotope effect which is a good factor 2 down for D.

JACQUOT Have you done some calorimetric measurements of the beam?

EHLERS No, that will come when we accelerate the beam. You see, at the moment, the energy is 300 V.

JACQUOT You have 300 V continuously; with 0.5 A beam it is 1.5 kW.

EHLERS It would be easy if you were not so open looking at the light of the filaments. You could do it but it would be difficult.

JACQUOT I suppose that your self extracted D^- beam is space charge compensated. Is that true? Because if you have no compensation the blow-up is very important.

EHLERS Exactly.

JACQUOT Are you sure you have no electrons which go with the Cs^+ from the aperture to the Faraday cup.

EHLERS We feel quite optimistic that when we extract we are not going to see many electrons. There will be some, you can not stop them all because negative ions, that are charge exchanging in that region, will supply electrons. It takes a long time to explain some other experiments we have done. We feel rather confident that we are going to be in good shape electron wise. But, you never know until you try it and we will let you know next meeting.

SMITH In your probe measurements of electron density at the exit of the source, was that a H + Cs discharge or a H discharge?

EHLERS We have done it with both. I think the data I showed was hydrogen only.

SMITH Do you see a difference?

EHLERS We did a test with hydrogen and xenon rather then hydrogen only. Yes, you see a difference. You see a higher electron current collected at the cup but you see a decrease of the plasma density. I will show you those curves, I have got them with me.

TRANSPORT OF LOW ENERGY POSITIVE AND NEGATIVE ION BEAM BY PERMANENT MAGNETS*

K. N. Leung, K. W. Ehlers, and E. B. Hooper, Jr.+

Lawrence Berkeley Laboratory
University of California
Berkeley, California 94720

Abstract

An experimental investigation of low-energy ion beam guiding by a surface magnetic field generated by samarium cobalt magnets has been performed. It was found that magnets arranged in a multi-ring cusp configuration produced the best beam transport efficiency, in agreement with calculation of the charged particle trajectories for this particular magnet arrangement. This geometry is predicted to yield no distortion in the phase space of the beam. The effect is proportional to charge squared, and is therefore independent of the sign of the charge of the particle being transported.

Introduction

Recently, a dc self-extraction negative-ion source based on surface conversion of positive hydrogen or deuterium ions has been proposed for the production of high power neutral beams.[1] In this type of source, the H^- or D^- ions are formed on a concave, low work-function converter surface. They then accelerate radially across the plasma sheath and are self-focused at the exit aperture of the source. As a result, the H^- or D^- ions form a low energy (≈300 eV) divergent beam. Before these negative ions are accelerated to a much higher energy (>200 keV), some scheme may have to be introduced to transport the beam from the source exit to the accelerator without distorting phase space. Beam guiding by means of axial magnetic fields has been attempted.[2] Current produced cusp and surmac fields have also been proposed for guiding plasmas into confinement devices.[3,4] In this paper, an experimental investigation of beam guiding by permanent magnets is presented. Results show that some magnet arrangements can transport a low-energy divergent hydrogen beam quite efficiently.

1. Single Particle Consideration

Figure 1 shows the trajectory of a positively charged particle which travels with a velocity v from a field-free region into a uniform B-field region. In Figs. 1(a) and (b), the B field is pointing out of the paper (+x direction). The resulting $\vec{v} \times \vec{B}$ force tends to deflect the particle back into the B = 0 region. the distance of penetration into the B-field area increases with an increase of the angle of incidence (which is defined as the angle between v and the boundary of the two regions). If a wall is located at a distance greater than the deepest penetration, which occurs at normal incidence, the particle can return to the field-free region.

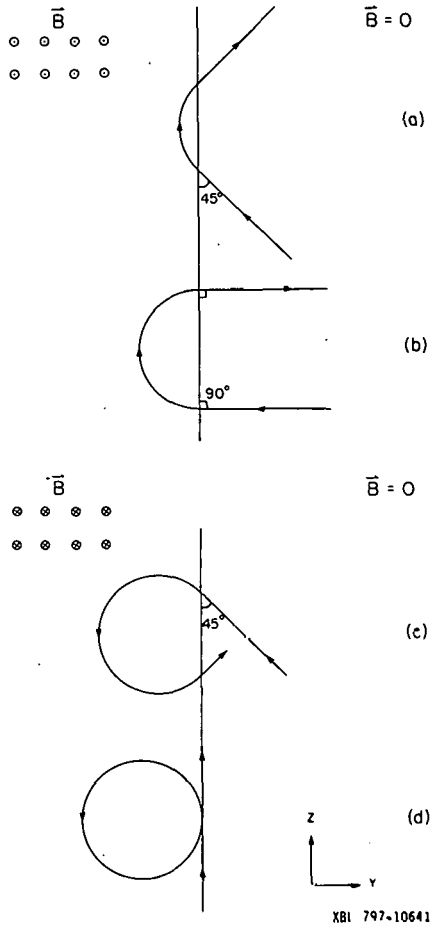

Fig. 1. Reflection of a charged particle by a uniform magnetic field.

In Figs. 1(c) and (d), the direction of the B field is reversed (-x direction). The $\vec{v} \times \vec{B}$

force deflects the same charged particle deeper into the B-field region. The distance of penetration is a minimum at normal incidence, but it increases with decreasing angle of incidence. The deepest penetration now occurs during a glancing incidence [Fig. 1(d)], provided that the magnitude of the B field is strong; otherwise the particle will be lost to the wall before it can return to the field-free region. Thus the direction of this B field is not "favorable" for transporting a divergent beam of positive charged prticles propagating in the z direction.

When permanent magnets are used to generate the multi-line-cusp fields along the beam edge, the effect on the motion of a charged particle is difficult to analyze due to the nonuniformity of the B field. However, for some magnet geometries (such as the configuration shown in Fig. 5), it is possible to estimate the maximum distance of penetration of the beam.

If A_z is the z component of the vector potential that characterizes the B field, m and q are respectively the mass and the charge of the particle, and the z axis is the direction of symmetry for the line-cusp fields, then the canonical momentum along this direction $P_z = mv_z + qA_z$ is conserved. In addition, the energy of the particle $E = mv^2/2 + q\phi$ is also a constant of the motion. Assuming the scalar potential $\phi = 0$ everywhere, then a charged particle coming from the $B = 0$ region with $P_z = 0$ cannot reach regions where $A_z > (2mE)^{1/2}/q$. On the other hand, a particle originating from the field-free region ($A_z=0$) can have a maximum value of $P_z = mv$. This particle cannot reach regions where $A_z > (8mE)^{1/2}/q$. Therefore, if the vector potential A_z of the given magnet geometry is known, the regions that are accessable to the beam particle can be found.[5]

In some magnet geometries, the line of symmetry is not along the direction of the beam propagation. The reflection of charged particles by the B field can be analyzed only by a computer. The ring-cusp magnet configuration shown in Fig. 8 has been studied in detail by Hooper[6] and Rowlands.[7]

We assume a beam is travelling in the z direction but with a finite divergence in the x direction. Consider the case in which the ring-cusps are generated by wires with currents flowing in alternating directions as shown in Fig. 2. A particle approaching the wires at a glancing angle will experience an alternating magnetic field with amplitude slowing increasing with time. If the field becomes strong enough, the particle will reverse its x direction and return towards the axis. The effect can be considered either as a reflection from a region of high magnetic pressure or as a second-order effect in which the v_xB_z force generates an oscillating v_y. The phase of y is such that the interaction with B_z reverses v_x. The v_zB_x forces alternate rapidly in time as the particle passes many wires, and thus average to zero. For the case of grazing incidence, Rowlands[7] has solved analytically the equation of motion. It was found that under appropriate conditions, the sign of v_x reverses during the interaction, with little exchange of energy between x and z motion. This result is in agreement with computer calculations shown in Fig. 2.[6]

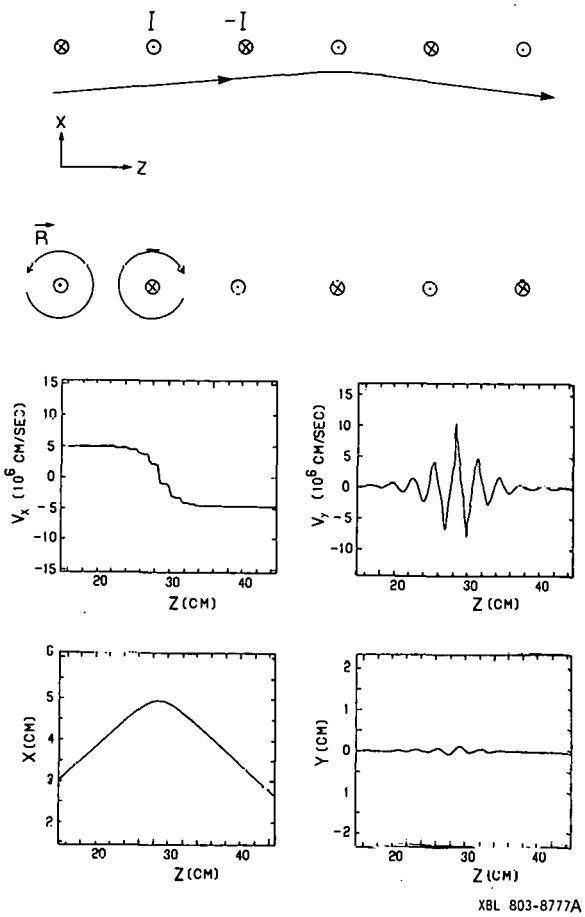

Figure 2. Particle-wire interaction. The velocities v_x and v_y plotted in the computer output are defined in the top figure. The wires are spaced 1 cm apart in z and 10 cm apart in x.

For a rectangular array of permanent magnets, the magnetic field can be approximated by that of a line dipole located a distance δ behind the front face. If q and m are the charge and mass of the beam particle, P is the dipole strength, $(d - \delta)$ is the distance from the z-axis to the magnet pole face and L/2 is the cusp spacing, then the maximum x-velocity (on axis) of contained particles, v_c, can be expressed as:

$$v_c^2 = \left(\frac{8\pi qP}{mcL}\right)^2 \sum_{n=0}^{\infty} \left[\frac{1 + 1/2(2n+1)\sinh\frac{4\pi d}{L}}{\sinh^2\left(\frac{2\pi d}{L}\right)} \left(e^{-(2n+1)2\pi d/L}\right) \frac{\sin^2\left[\frac{(2n+1)2\pi(d-\delta)}{L}\right]}{(2n+1)} \right]^2 \cdot \left[1 + (v_x^o/v_z^o)^2\right]^{-1}$$

For $\exp(2\pi d/L) \gg 1$, $\quad v_c^2 = \left(\frac{qP}{mc}\right)^2 \left(\frac{4\pi}{L\delta}\right) \left[1 + (v_x^o/v_z^o)^2\right]^{-1}$

As an example, if d = 10 cm, L/2 = 5 cm, P = 2260 gauss-cm^2 and δ = 0.64 cm, then for protons, $v_c \approx 3 \times 10^7$ cm/sec corresponding to 480 eV.

II. Experimental Apparatus

A schematic diagram of the experimental arrangement is shown in Fig. 3. The apparatus has three components; an ion source, an extraction system, and a drift pipe. The ion source is a water-cooled cylindrical stainless steel chamber (20-cm diameter by 28 cm long) with the open end enclosed by a three-grid extraction system. The chamber is surrounded externally by 10 columns of samarium cobalt magnets ($B_{max} \approx 4$ kG) to generate a line-cusp configuration for primary electrons and plasma confinement. A hydrogen plasma is produced by primary ionizing electrons emitted from two 0.05-cm diameter tungsten filaments which are biased at -60 V with respect to the source chamber (anode).

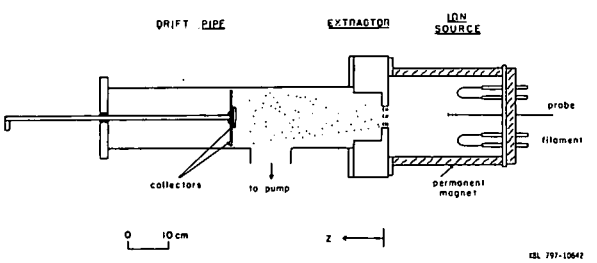

Fig. 3. Schematic diagram of the experimental apparatus.

The ion beam is extracted by means of a standard Berkeley accel-decel electrode system with the first (plasma) grid masked down to an extraction area of 5-cm diameter. This plasma grid is connected to the negative terminal of the filament and the source chamber is biased at a positive potential V_b (≈300 V) relative to ground. The center grid is biased at -60 V to extract the plasma ions and to retard any backstreaming electrons. The outermost grid is electrically grounded.

The drift pipe is a 15-cm diameter and 60 cm long thin-walled stainless steel cylinder. The beam collector is a 14-cm diameter circular copper plate with the center portion (5-cm diameter) covered by a second copper plate. Both copper collectors are mounted on a moveable shaft and are biased at +3 V with respect to the drift pipe (which is at ground potential) to retain the secondary electrons produced by the beam as it bombards the collectors. The beam current at the center or outer collector is measured by a X-Y recorder. The effect on the beam current from mounting samarium cobalt magnets on the external surface of the pipe has been investigated.

III. Experimental Results

In the experiment, the source plasma was operated at an overdense condition with V_b = 325 V. As a result, the extracted ion beam had a large angle of divergence. The gas pressure in the system was kept at 1 x 10^{-4} Torr so that neutralization of the beam in the drift pipe region could be minimized. Figure 4 shows the beam current at the center and outer copper plates as a function of collector position when there were no magnets on the drift pipe. The beam current at the center collector I_{in} drops monotonically as z increases from 8 to 60 cm. However, the current to the outer collector I_{out} goes up as z increases, reaching a maximum at z ≅ 22 cm, and then decreases gradually. Since the beam is divergent, I_{out} increases as the outer collector starts to intercept the beam. As soon as the beam strikes the wall of the drift pipe, the beam current received by the outer collector will decrease. The position where I_{out} reaches a maximum then corresponds to the location where the beam starts hitting the wall. In order to study the effect of beam guiding by surface magnetic fields, the permanent magnets are mounted starting z ≅ 22 cm on the drift pipe.

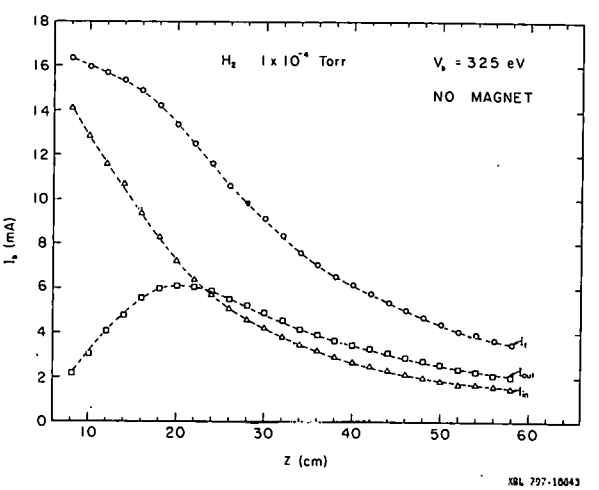

Fig. 4 Ion beam current versus collector position without the presence of permanent magnets on the drift pipe.

Four different magnet configurations have been tested. In the arrangement shown in Fig. 5, six columns of magnets are used to produce

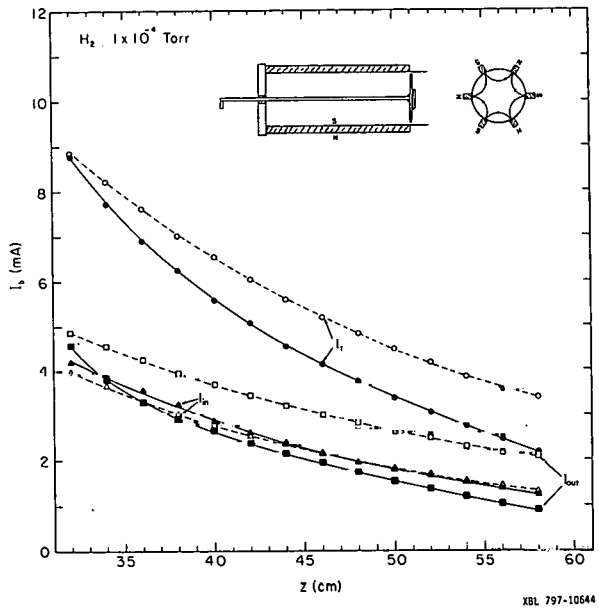

Figure 5. Ion beam current versus collector positoon with (▲■●) and without (△□○) six magnets columns on the drift pipe.

line cusps parallel to the direction of beam propagation. According to the charged particle trajectories shown in Fig. 1, one can conclude that half of the cusp field will tend to deflect the positive ion beam outward to the pipe-wall. The other half of the cusp field will deflect the ions inward. On the average, I_{in} is almost the same for the case with or without magnets. In the region where the outer collector is located, the ions have a larger angle of incidence. The B field with the favorable direction may not be strong enough to turn the ions ($B_{max} \cong 350$ G). Consequently, more ions will be lost, resulting in a drop of I_{out}. In fact for this magnet geometry, the total current $I_t = I_{in} + I_{out}$ is less than the case when there are no magnets.

In the arrangement of Fig. 6, 12 line cusps are formed parallel to the beam. The magnitude of the B field with an unfavorable direction is increased to a maximum of 2.5 kG by decreasing the separation between every two other magnet columns. However, the B field with the favorable direction now drops to a maximum of 150 G. The data shows that there is no increase in I_{out}, but I_{in} increases slightly. Overall the total beam current I_t increases by approximately 10% over the case with no magnets.

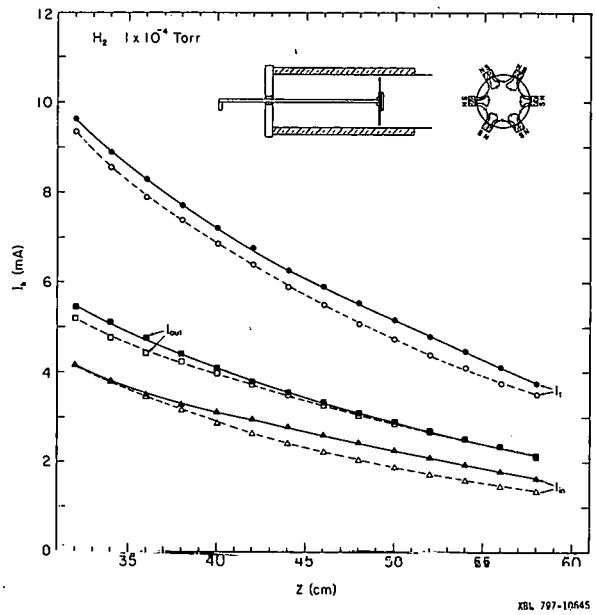

Figure 6. Ion beam current versus collector position with (▲■●) and without (△□○) 12 magnet columns on the drift pipe.

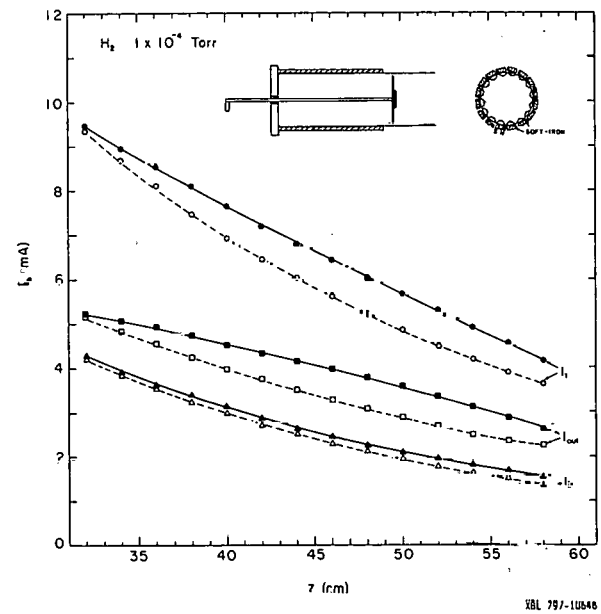

Figure 7. Ion beam curreent versus collector position with (▲■●) and without (△□○) 16 magnet columns on the drift pipe.

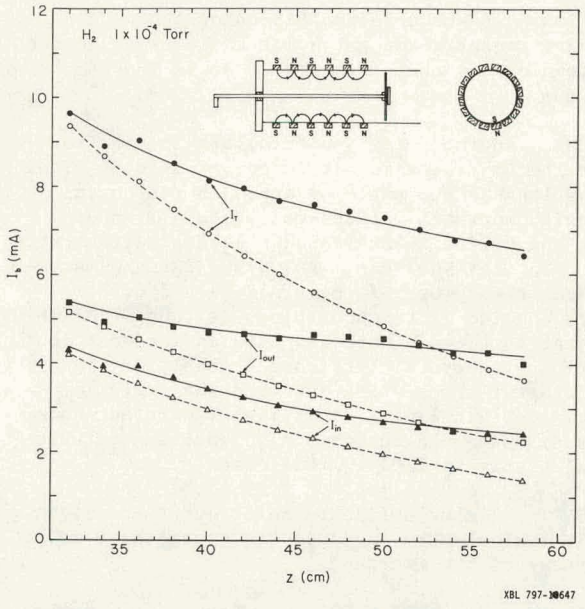

Figure 8. ion beam current versus collector position with (▲■●) and without (△□○) six rings of permanent magnets on the drift pipe.

In Fig. 7, the magnet columns are oriented with opposite polarity facing one another. The unfavorable B field that exists between two magnets is short-circuited through a strip of soft iron. Only the B field that has the favorable direction extends into the drift pipe. However, this B field does not penetrate very far and its magnitude is only 120 G at the wall. As a result, there is no improvement on I_{in}. But I_{out} in this case exceeds that when there are no magnets. An average increase of approximately 16% in I_t is observed with this geometry.

Figure 8 shows six rings of permanent magnets mounted normal to the beam in alternating polarity with a cusp spacing ≃ 5 cm. In this configuration, both I_{in} and I_{out} are found to be higher than when no magnets are used. In fact, a distance of 58 cm from the extraction grids, an increase of 75 in I_t is obtained. In fact, the exponential decrease in I_t as z increases (in Figs. 8 and for z < 18 cm in Fig. 4) is found to have a mean free path $\lambda \simeq 80$ cm as shown in Figs. 9 and 10. This corresponds to a cross section of 1.5×10^{-15} cm^2 which is approximately equal to that of the charge exchange reaction $H_2^+ + H_2 \rightarrow H_2 + H_2^+$. Thus the total beam current I_t corrected for charge exchange, is constant, in agreement with the numerical computation of charged particle trajectories described above. In order to show that this magnet arrangement yields no distortion in the phase space of the beam,

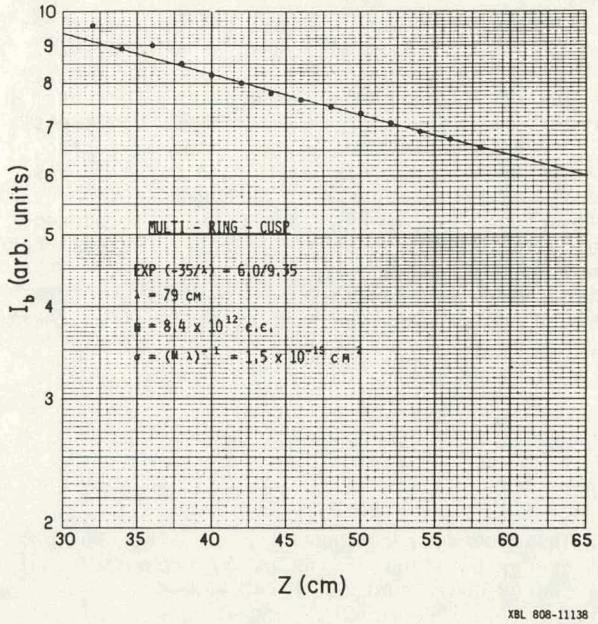

Fig. 9. A semi-log plot of the total beam current versus the axial distance for the magnet configuration in Fig. 8.

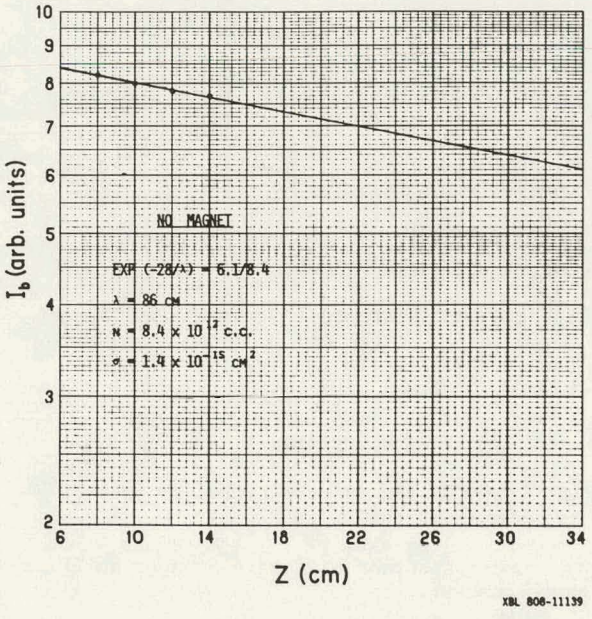

Fig. 10. A semi-log plot of the beam current versus the axial distance for z < 18 cm when there is no magnet.

further experimental investigation of the emittance of the beam will need to be conducted.

In conclusion, the effect on the beam current from mounting samarium cobalt magnets in different geometries on the external surface of the drift pipe has been studied. It was found that magnets arranged in a multi-ring-cusp configuration (Fig. 8) produced the best beam transport efficiency. Instead of mounting the magnets on the surface of the drift pipe, they can also be assembled to form an open system to allow pumping of gas from the beam line.

References

* This work was supported by the Fusion Energy Division of the U. S. Department of Energy under contract W-7405-ENG-48.

+ Permanent address: Lawrence Livermore National Laboratory.

1. K. W. Ehlers and K. N. Leung, Rev. Sci. Instrum. 51, 721 (1980).

2. H. P. Eubank and T. D. Wilkerson, Phys. Fluids 6, 914 (1963).

3. R. G. Tuckfield and F. R. Scott, Phys. Fluids 8, 1197 (1965).

4. R. A. Bruen, B. H. Rael, and A. Y. Wong, Rev. Sci. Instrum. 48, 1262 (1977).

5. T. K. Samec, Ph.D. Thesis, UCLA Report PPG-281 (1976).

6. E. B. Hooper, Lawrence Livermore Lab. Report UCID-16821 (1975).

7. G. Rowlands Lawrence Livermore Lab. Report UCID-16890 (1975); and J. Phys. A.: Math. Gen. (submitted for publication).

DISCUSSION

JACQUOT Why do you put the extractor just at the cross-over of the D^-?

LEUNG Oscar Anderson will have a paper on Friday on that geometry.

HOPMAN I want to point out that about 10 years ago we had a similar transport trouble as you described. We used a hexapole magnet, which was 1/2 meter long and we still lost the beam. Then we replaced the magnet for 25 cm long alternating magnet sections and the beam was transported very nicely.

ALLISON It seems to me that using such a non-linear transport you get quite an increase in the emittance. Is that true and if so is that bothersome?

HOOPER In fact when you calculate it you find that the emittance is not increased at all. That is as long as the angle of approach (the axial velocity approach) of the ions is small enough that the periodic lattice acts like a perfect mirror. In fact Rowlands, who worked out the mathematical theory of this several years ago, has since applied it to such things as tunnelling in crystal lattices, where you have an incident ion that hits a crystal lattice and sees a periodic electrostatic potential and when the angle is within certain limits, that ion is carried enormous distances in the crystal. The same mathematical theory applied in this case.

JACQUOT I should like to point out that with a periodical electro-magnetic structure there is no increase of the emittance.

BORCHERS About 15 years ago there were a number of papers published and quite a bit of work done on transmission of charged particles in plasmas and coaxial electrostatic geometries. Fine wire down the center of a pipe with a voltage on it, turns out to have similar properties and works out very well.

PROPOSED ELECTRODE DESIGN FOR DIRECT EXTRACTION OF NEGATIVE ION BEAMS

A.J.T. Holmes, T.S. Green and M. Inman
CULHAM LABORATORY
Abingdon, Oxfordshire England

Introduction

The major difficulty in the extraction and acceleration of a negative ion beam is the suppression of the unwanted electron beam. This problem is simplified by the double charge exchange technique which converts an initial H^+ beam into an H^- beam in a caesium cell, although the conversion efficiency is low.[1] An alternative technique is to accelerate both the electrons and negative ions together to a low energy and then deflect the electrons to a dump by a transverse magnetic field while the negative ions are accelerated to their final energy. Usually this magnetic field forms an integral part of the ion source as in the magnetron negative ion source[2,3], or more recently in the bucket type.[4] In these types of sources the electrons are reflected by the magnetic field back towards the discharge although they may not necessarily re-enter the extraction aperture.

Here we present a modification of this scheme, where the accelerating structure can be a multi-slit array and is combined with a transverse magnetic field localized in each slit. This type of structure has the advantage that it can in principle be scaled up to any size, as in the case of positive ions.

11. Mechanical Structure

The general layout of a direct negative ion source and extraction system is shown in Figs. 1 and 2. The plasma source is of the "bucket" type with the addition of a caesium oven and converter plate which can be biased to -400 volts relative to the hot tungsten cathodes following the design of Leung and Ehlers.[4] The permanent magnet array continues on to the extraction electrode which is at anode potential (unlike positive ion bucket sources).

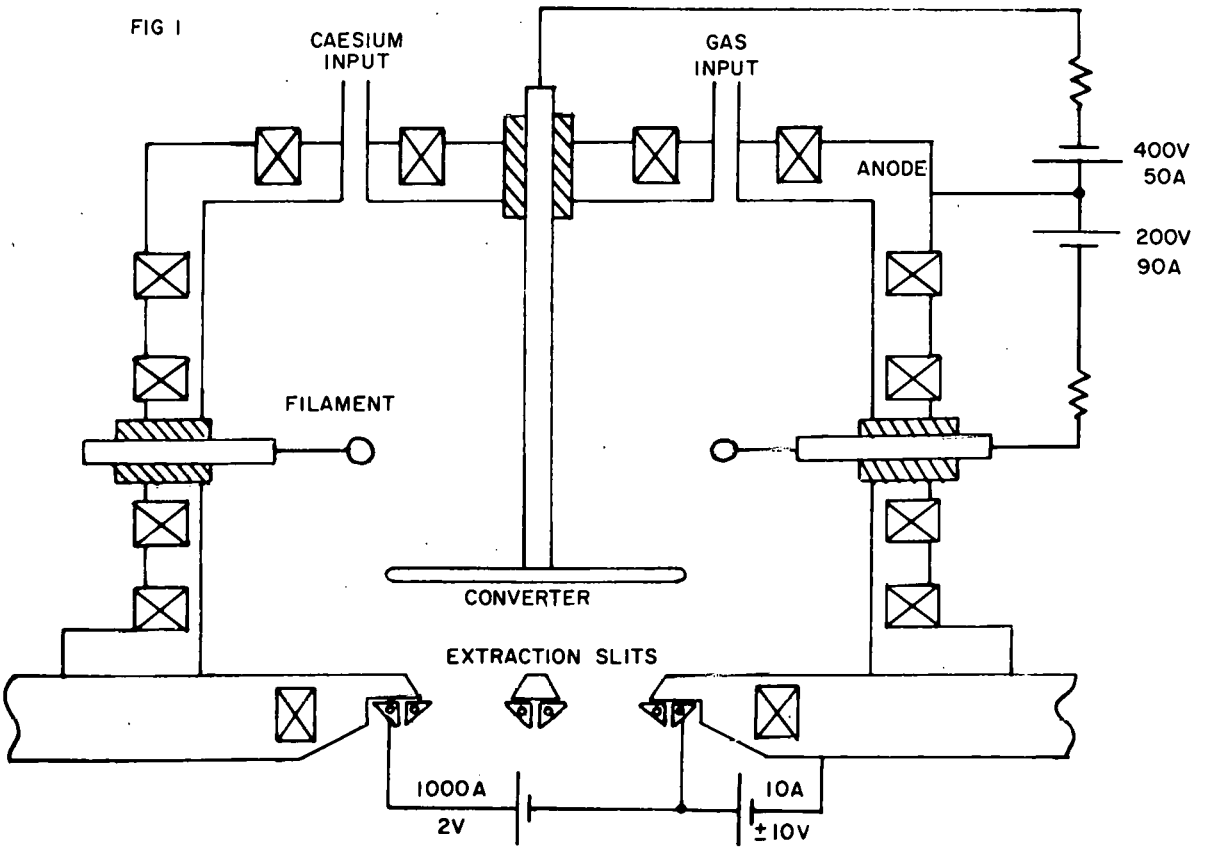

FIGURE 1.

FIG 2

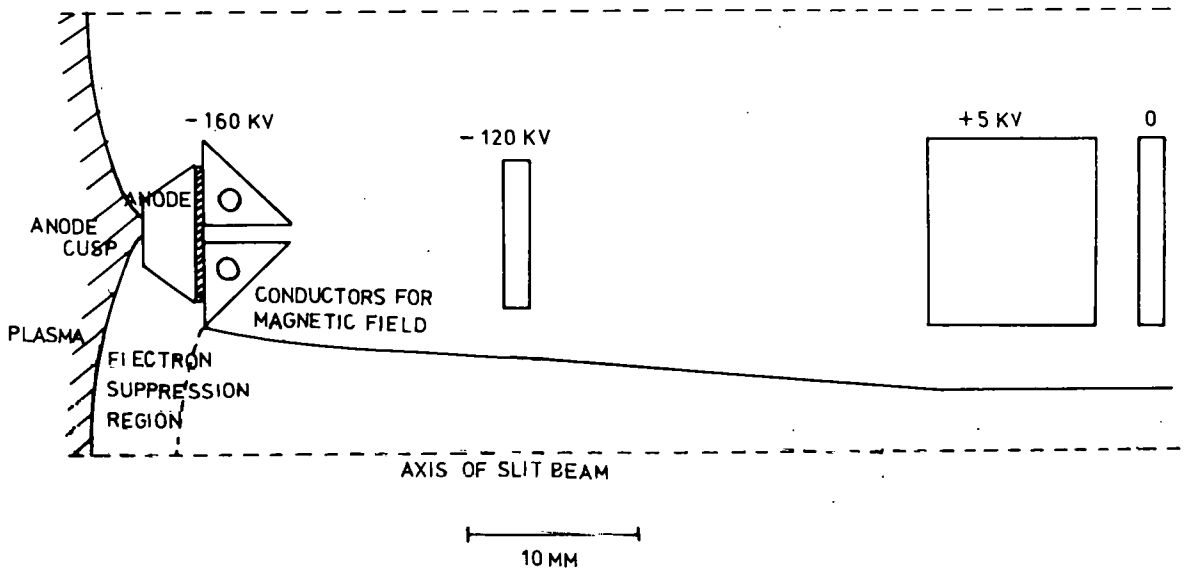

FIGURE 2.

However the central cusp lines next to the apertures are not formed by permanent magnets but instead are created by pairs of current-carrying conductors which also form the Pierce apertures. The design shown in Fig. 2 can generate two gauss/amp at the cusp. In addition these rods create a transverse flux across the extraction gap whose net value by symmetry is zero. This is an important feature in that the analysis in the next section shows that the change in total transverse beam velocity is proportional to the flux traversed by the beam. Electrons, however, are reflected by this field before they gain any appreciable energy.

An additional advantage of this type of extraction aperture is that the current carrying conductors also form the Pierce electrode and can be biased relative to the anode to control the local plasma potential (and hence plasma boundary). For example, if the busbars are negative with respect to the anode the plasma boundary would probably move towards the aperture with consequent effects on the beam optics and electron reflection.

The other acceleration electrodes are very similar to the positive ion design except that the potential are reversed, including the suppression (or third) electrode, which now prevents positive ions from the neutralizer from being accelerated back to the plasma source.

It should be noted that we propose to use slit apertures instead of holes because the negative ion beam trajectories will suffer a displacement along the slit axis (the y axis in the diagram) because of the magnetic field. This type of aperture is ideally suited to the Pierce bus-bars and also has the advantage of a high overall grid transparency which in this design is 55%.

III. Design Considerations

The motion of a charged particle under the influence of an axial electric field (the z direction in Fig. 1) and a transverse magnetic field (the x direction) is governed by the expressions:

$$m \frac{d^2z}{dt^2} = e \frac{d\phi}{dz} - e B \frac{dy}{dt}$$

and

$$\left(\frac{dz}{dt}\right)^2 + \left(\frac{dy}{dt}\right)^2 = \frac{2e\phi}{m} + \frac{2eU}{m}$$

where ϕ is the electric potential and eU is the initial energy. The above equations can be integrated and reduced to:

$$\frac{dy}{dt} = \frac{e}{m} \int B dz + \text{constant}$$

The product $\int B dz$ is the transverse magnetic flux, F, and the constant depends on the initial velocities of the particle. The corresponding equation for the axial velocity, dz/dt, is:

$$(dz/dt)^2 = \frac{2e}{m} (\phi + U) - \left(\frac{eF}{m} + \text{constant}\right)^2$$

In the case of plasma electrons, the initial electron distribution is maxwellian and isotropic. Hence if the initial velocity vector makes an angle θ to the z axis then:

$$\left(\frac{dz}{dt}\right)^2 = \frac{2e}{m}(U + \phi) - \left(\frac{eF}{m} + \left(\frac{2eU}{m}\right)^{\frac{1}{2}} \cos\theta\right)^2$$

if the transverse flux, F, is zero at the origin. The absolute maximum flux required to reduce dz/dt to zero is obtained when cos θ is -1, hence if the potential at the turning point is ϕ_o then this flux is given by:

$$\frac{eF^2}{2m} - \left(\frac{2eU}{m}\right)^{\frac{1}{2}} F = \phi_0$$

The effect of the maxwellian velocity distribution can be included by assuming that a certain fraction of these particles have to be reflected. For example, if 99% are to be reflected then:

$$eU = 5kT$$

and

$$\phi_0 = \frac{eF^2}{2m} - \left(\frac{10kT}{m}\right)^{\frac{1}{2}} \cdot F$$

The minimum flux required for electron reflection is that which would turn back thermal electrons. For a plasma temperature of 5 eV and no potential gradient, for example F equals $3.3.10^{-5}$T.m. For primary electrons in the plasma source at 100 eV, $1.4.10^{-4}$ T.m is needed. The effects of acceleration in the sheath could increase the flux required for reflection considerably.

The design shown in Fig. 2, where the current is carried by water cooled bars, can generate around 10^{-3} T.m easily and the flux pattern obeys the relation:

$$F = \frac{2\mu_0 I_0 s}{g} \cdot \frac{z^2}{(g^2 + z^2)}$$

where g is the distance between pairs of conductors and s is separation between the centres of a pair of conductors. The maximum allowable voltage at the reflection points would be 76 kV for electrons.

The negative ions are almost unaffected by this field, because of their higher mass. They would only be reflected if their energy was lower by a factor of m_e/m_i. Except in extreme cases, this much lower energy limit would allow the extraction of volume produced negative ions as well as those higher energy negative ions (200 - 400 eV) which come from the converter plate.[4] In principle, the range over which the suppression magnetic field could be varied would allow the comparison of the two types of production process, as the highest value of the suppression field would also reflect low energy negative ions.

The beam optics would be relatively unaffected by the magnetic field as the transmitted negative ions would experience no net flux (it cancels on each side of the busbars). Thus they would only be displaced in a direction at right angles to the field and beam axis, i.e., along the slit axis. This would neither steer the beam nor affect the electrostatic focussing providing the subsequent apertures were slightly longer than the beam forming aperture.

In view of the large degree of uncertainty in the available negative ion current density, the 2nd, 3rd and 4th extraction electrodes must be capable of being altered in position (possibly by inserting metal shims) over a wide range of extraction gaps if a collimated beam at a given energy is to be achieved. The general beam optics would then be very similar indeed to the optics of positive ion beams save that the current density would be an order of magnitude smaller and the space charge neutralization would obey different scaling laws.

Conclusion

The direct method of negative ion beam extraction through a transverse magnetic flux offers considerable advantages in simplicity and the ability to scale up to large arrays. In addition it allows the possibility of using both sources of negative ion production simultaneously and the possibility of optimizing the plasma boundary shape to suit the optics of the extraction geometry.

References

1. E.B. Hooper Jr., P.A. Pincosy, P. Pouben, C.F. Burrell, L.R. Graham and D.E. Post, Lawrence Berkeley Laboratory Report LBL 10448.

2. G.E. Derevyankin, V.G. Dudnikov and U.S. Klenov, Sov. Phys. Tech. Phy. 23, 239 (1978).

3. K. Prelec, Th. Sluyters, and M. Grossmann, Particle Accelerator Conference Chicago IU (1977).

4. K.W. Ehlers and K. Leung, Lawrence Berkeley Report No. LBL 10013.

DISCUSSION

JACQUOT You have an H^- of 100 eV of energy and an H^- of 0 eV and you think about the modification of the Child-Langmuir law?

HOLMES No, that is trivial, I quite agree. The only difference is that the negative ions in the plasma will have the same temperatures as the positive ions in the plasma and that is about 1/2 volt. The negative ions which would come from the converter will have 200 V when they leave the converter and they will be scattered as they travel through the plasma by Coulomb collisions to be the very least. This means these 200 electron volts will be randomized and it would appear as a transverse velocity which will be conserved all the way through the system.

GELLER Did you take into account the collisions between electrons and Cs^+ ions?

HOLMES The Cs^+ can not cross the plasma values in the same way as the H^+, because the electrostatic fields will stop them.

GELLER Yes, but the collision frequency....

HOLMES In the source? Yes, this will always randomize and I quite agree but I think all the plasma ions whether they be cesium or H^+ will all have a low temperature, they can not be that energetic. The only energetic ions in the plasma generator will be the ones coming from the converter plate.

HISKES I am a little bit confused about your randomization of those 200 V particles in one pass across the plasma. I will be surprised; you mean you are going to get a 90° deflection or a 10° deflection?

HOLMES No, I published a paper, I think last year, on the ion temperature of positive ions, that is H^+ in plasma generators, and we compared the ion temperature of helium ions in the discharge and hydrogen ions. We saw that the helium ions showed a steady increase of ion temperatures when you increased plasma density, almost linear. With hydrogen ions it is much faster because we have a dissociation break-up of H_2^+ involved, which feeds energy into the H^+ population which then really randomize among themselves. So, you have energy input into the ion population in a hydrogen discharge which does not exist in noble gas discharges and the H^- ions are also becoming involved with this because of their ion-ion collisions. It would not make a large effect, I agree. It raises temperatures a tenth or hundredth of volts.

HISKES I think a much more serious problem is going to be the angle distribution of backscattered particles when they come off the surface.

HOLMES Yes, that is another thing altogether, I quite agree. That may be much more dominant judging by the Berkeley work. There is an affect there. That would be conserved all the way through the system. Nothing we could do about that.

HAGENA Is there a definite time table for doing this experiment?

HOLMES Let me put it this way. We are building the beam line at the moment. We can not start immediately because we have other commitments, but I hope that towards the end of next year we should be in business. It is a hope more than anything else.

MODIFIED CALUTRON NEGATIVE ION SOURCE OPERATION AND FUTURE PLANS*

W. K. Dagenhart, W. L. Stirling, H. H. Haselton, G. G. Kelley, J. Kim, C. C. Tsai, and J. H. Whealton
Oak Ridge National Laboratory
Oak Ridge, Tennessee 37830

Abstract

Negative ion generation has advanced rapidly by employing the concept of surface ionization. The modified calutron has proven to be a successful tool to explore these concepts and provide solutions to the many problems which must be evaluated. Many features of the SITEX (Surface Ionization with Transverse Extraction) ion source are ideally suited for this exploration. Some of these features are; a ribbon-like plasma, electron control by transverse magnetic fields and the ability to separate the Cs oven parameters from those which control the positive ion generation.

I. Introduction

The advent of the surface ionization concept[1] for the production of negative ions has produced a flurry of ideas for negative ion generation.[2] The modified calutron[3] has shown itself to be a particularly useful and successful vehicle for developing concepts and experimental solutions for the many problems which must be confronted. The geometry of this source is ideally suited to exploitation of the surface ionization scheme. It permits intense bombardment of the cesium surface from a dense plasma which is nevertheless thin in the direction of negative ion escape. Further, the cross-field configuration provides for EXB removal of extracted electrons at low energy, and finally, the plasma generating hardware and the cesium oven hardware are effectively decoupled from the negative ion production region, permitting great flexibility in the design of both of those subsystems. We are contempleting the development of an intense-beam negative ion source based on the calutron, to be called SITEX for Surface Ionization with Transverse EXtraction.

Consider the list of descriptive parameters of a plasma generator for a negative ion based system in Fig. 1: (a) extracted beam current density, (b) CW capability, (c) gas efficiency, (d) electron energy losses, (e) impurity content, (f) optics, (g) grid loading, (h) cesium control and (i) scalability. We have investigated experimentally all of these parameters except grid loading and scalability. However, the calutron concept has been scaled by two orders of magnitude in other applications operating CW. This work is directly applicable to negative ion production. After a brief description of the modified calutron principle, we will discuss the performance of the modified calutron with respect to each of these parameters.

*Research sponsored by the Office of Fsuion Energy (ETM), U.S. Department of Energy under contract No. W-7405-eng-26 with Union Carbide Corporation.

Important Characteristics of a Negative Ion Plasma Generator

- Extracted Beam Current Density
- CW Capability
- Gas Efficiency
- Electron Energy Losses
- Impurity Content
- Optics
- Grid Loading
- Cesium Control
- Scalability

Fig. 1. List of important parameters of a plasma generator for a negative ion based system.

II. Source Operation

A schematic of the modified calutron used in these measurements is shown in Fig. 2. A discharge is ignited between the resistively heated filament and the 0.3 cm slit opening (anode) which is maintained by the power supply V_A. The gas feed, not shown, is in the filament region. Energetic electrons stream along the magnetic field ($\lesssim$1K gauss) and are reflected by the electrically isolated plate labeled reflector. Thus, plasma is produced everywhere along this electron ribbon which is 0.3 cm wide by 1.3 cm high by 15 cm long. A molybdenum converter surface on which cesium is deposited extends along one side of the plasma ribbon and is separated from it by about 0.2 mm. The power supply V_E is used to accelerate positive ions across a sheath onto the cesiated converter which then pass quickly through the thin ribbon to the extraction surface. In this manner of negative ion production, positive ions are produced by V_A and negative ions are produced by V_E in conjunction with an independently controlled cesium supply; negative ion losses are minimized by the geometry of the converter, plasma ribbon and extraction surface. As discussed in the section titled, Future Plans, this geometry may be easily varied to optimize negative ion output. In all extracted current measurements, the values given below are magnetically analyzed, whole beam values along with extracted j_{H^-}. As shown in Fig. 3, the modified calutron ion source and beam collector system are immersed in a uniform magnetic field. This type of test arrangement is well suited to measurements of impurities, beam optics and electron drain.

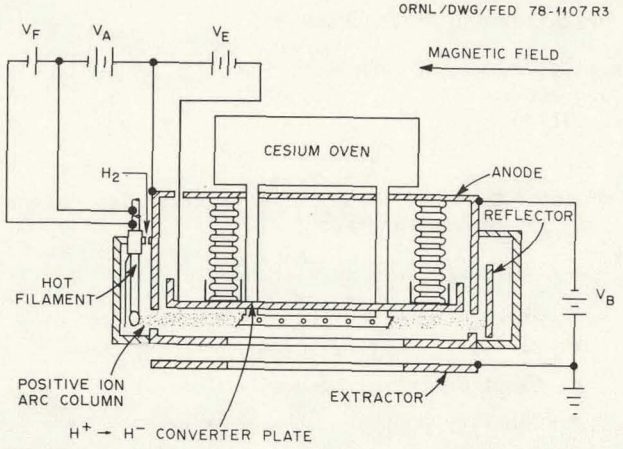

- Fig. 2. Sectional view of the modified calutron H^- source.

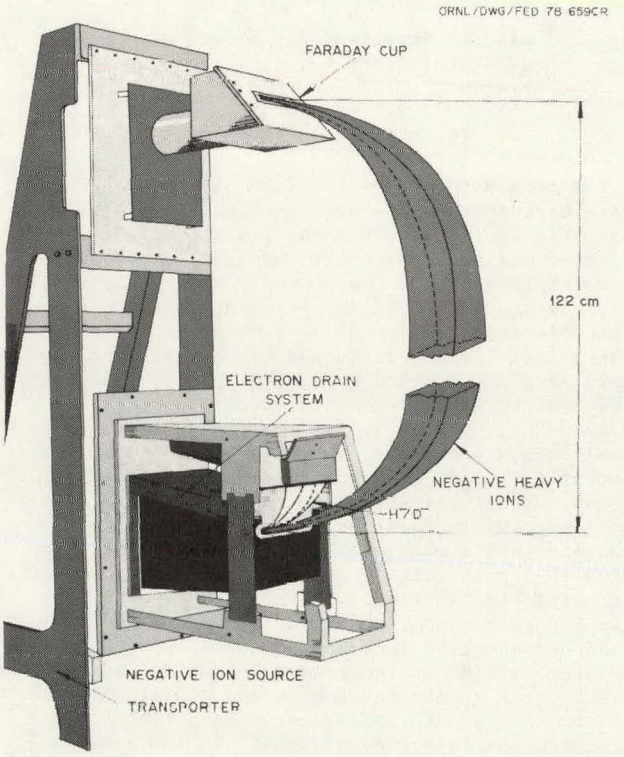

- Fig. 3. Calutron ion source and Faraday cup receiver shown illustrated on a carrier in relative operating positions along with ion beam orbits produced by uniform magnetic field.

After considering the questions of positive to negative ion conversion efficiency, extraction geometry and beam transport, we estimate the desired extracted beam current density for beam line applications to be ∿100 ma/A^2 at the extraction surface. To date, 90 ma/cm^2 at the extraction slit and 60 ma/cm^2 at the collector has been achieved for 100 msec pulses at 25 kV extraction. As shown in Figs. 4 and 5, current pulses of ∿5 sec have been achieved at ∿45 ma/cm^2 with a 0.4 cm^2 slit area. Figure 4 shows a current signal which is low initially due to application of the arc voltage alone without the converter voltage. After 10 sec the converter voltage is applied. The output climbs to a maximum and then falls to about one-fifth the maximum before the converter voltage is removed. The decrease is due presumably to depletion of the cesium layer. The gas efficiency measurements for the modified calutron are about 4% which is determined by measured gas flow into the source and analyzed beam current to the collector. Corrections for beam losses during transit have not been included. There has been no attempt to increase the gas efficiency or output current in the manner demonstrated by Dimov[4] and proposed independently by Dagenhart in 1978. A converter surface proposed by Whealton[5] is discussed in Future Plans below. Whealton calculates one order-of-magnitude improvement in gas efficiency for the modified calutron.

APPLICATION OF CONVERTER VOLTAGE PRODUCES LARGE INCREASE IN H^- OUTPUT

H^- 2 mA/cm (ANALYZED)

$V_{CONVERTER} = -130\ V_{DC}$

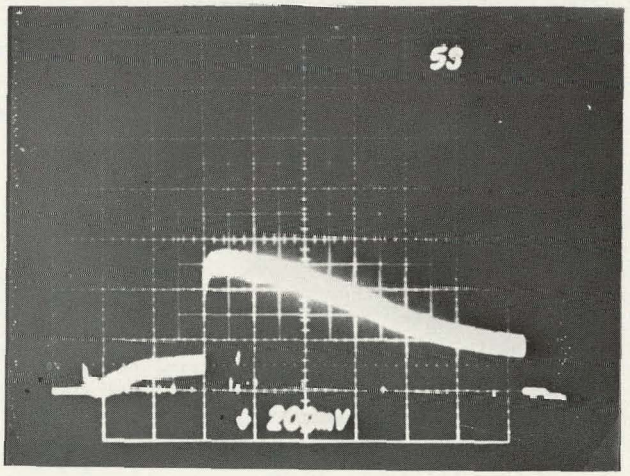

Fig. 4. Analyzed 25 keV H^- beam.

ORNL-DWG 80-3298 FED

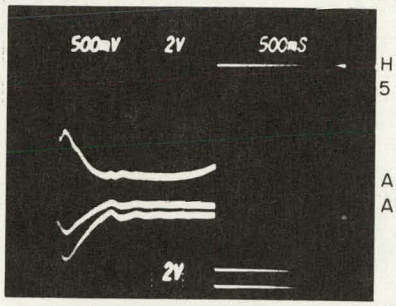

H^-
5 mA/cm (ANALYZED)

ARC NO. ONE (5A/div)
ARC NO. TWO (5A/div)

H^- ANALYZED BEAM
V_c = -90 V/9 A
V_{arc} = 100 V/22 A

Fig. 5. Analyzed H^- beam.

The power loss due to full energy electron extraction from the source is always undesirable and is intolerable for long pulse operation. The ratio of electrons to negative ions in the modified calutron is typically between four and six. However up to 94% of the extracted electron current has been recovered by the electron recovery system shown in Fig. 6. Electrons which are extracted from the source move up the face of the source due to the EXB drift present in this region. As the electrons approach the top of the source, the collector electrode potential forces the guiding center of the electrons to proceed under the collector electrode, at which point a component of E parallel to B is impressed upon the electrons. The electrons then drain off losing only the small energy supplied by the electron recovery supply. Figure 7 shows the variation of both the accel supply and electron recovery supply currents as a function of collector voltage. At low collector voltage some of the electrons escape to ground potential and are recorded by the accel current meter. Above about 1.5 kV collector voltage, essentially all of the electrons are being collected and the accel current is near zero. This same collection efficiency holds whether or not cesium is used in the discharge.

ORNL DWG 79-2612 FED

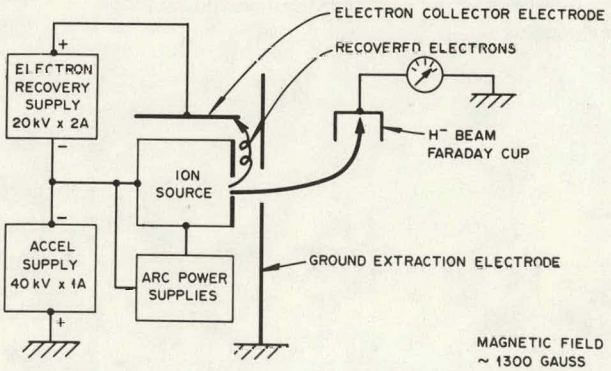

Fig. 6. Electron energy recovery system for the modified calutron H^- source.

ORNL DWG 79-2614A FED

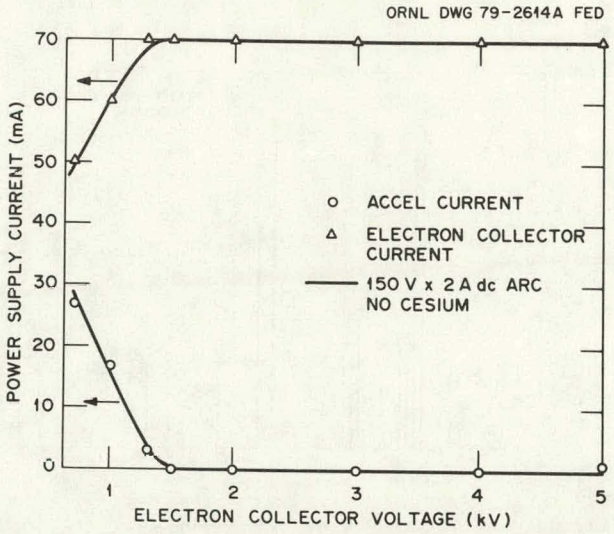

Fig. 7. Electron recovery efficiency variation with electron collector voltage.

The impurity content of the beam, shown in Fig. 8, can be mass identified by sweeping the magnetic field and monitoring the upper Faraday cup shown in Fig. 3. Total beam contamination has been reduced to <1% by careful source conditioning. It is estimated that the required change in magnetic field for mass identification has no more than a 30% effect on the negative ion output over the mass range scanned. In addition, an integral mass 12 → 20 amu impurity current measurement is made continuously during operation without changing the magnetic field. Many of the heavier masses detected are believed to be hydrocarbons arising from diffusion pump oil. Figures 9 and 10 show the variation of the impurity contaminants as a function of time for cesium dichromate and elemental cesium, respectively. The contaminants are summed from mass 12 to 20 amu which accounts for more than 75% of the impurities. A striking difference is the rapid decrease of the contaminant level with time using elemental cesium compared to cesium dichromate. These measurements are uncorrected for charge exchange losses along the path from source to collector; however, the entire beam is analyzed.

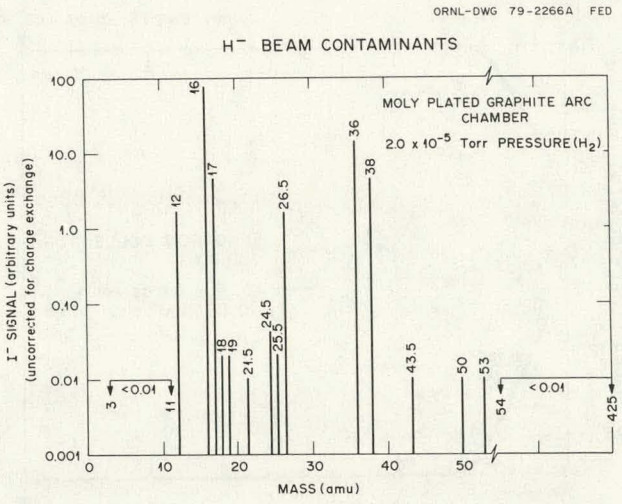

Fig. 8. Negative ion mass spectrum.

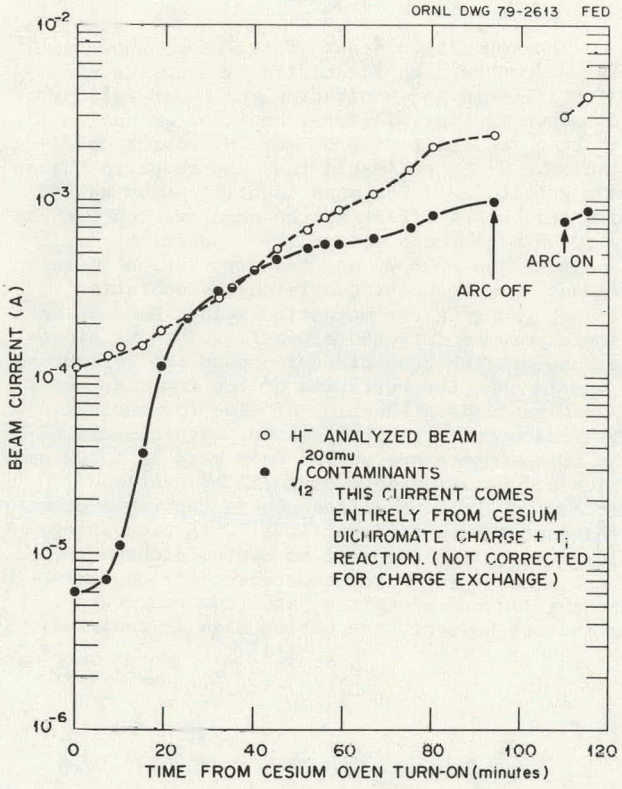

Fig. 9. Variation of heavy mass negative ion contaminants from cesium dichromate.

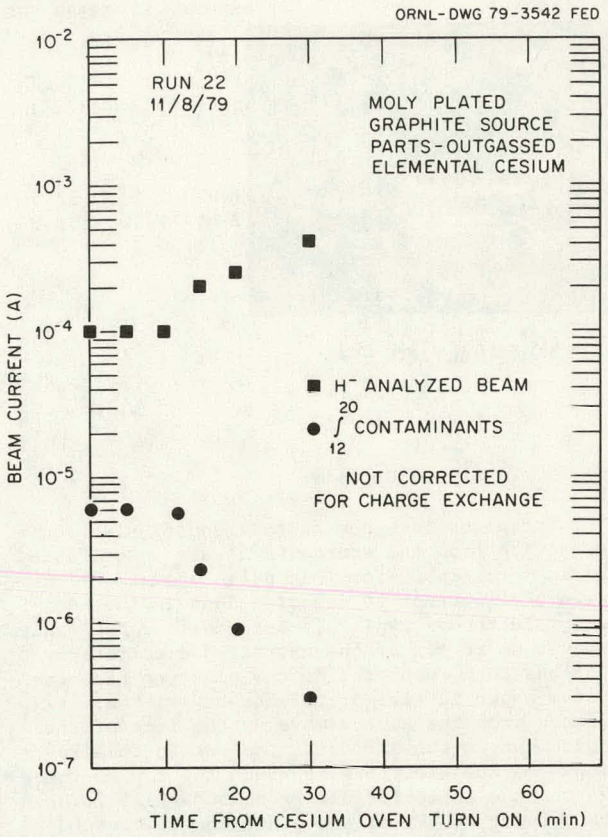

Fig. 10. Variation of heavy mass negative ion contaminants for elemental cesium.

No attempt has been made to optimize the electrode geometry. Existing parts from previous experiments were assembled producing the extraction geometry shown in Fig. 11. The space-charge-limited current density from this electrode configuration is about 95 ma/cm^2 at 20 kV. The only divergence measurement made is the angle subtended by the beam spot on the collector surface. The estimated one-half angle for $\Theta_\perp$ is approximately $\pm$ 2°, $\Theta_\parallel$ is very small. A segmented collector with an optimized electrode configuration will be forthcoming.

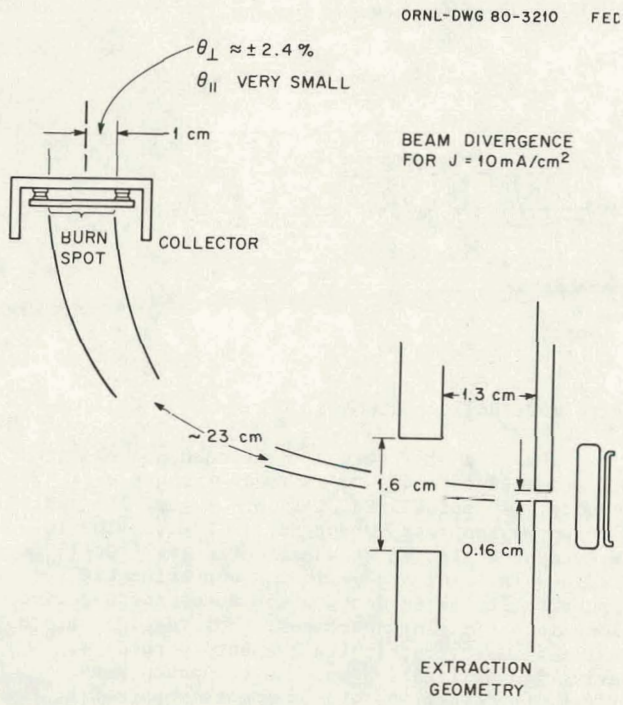

Fig. 11. Early extraction and acceleration geometry for the modified calutron H^- source.

We have started an investigation of the effect of a transverse magnetic field on the deflection and divergence of an ion beam emitted from a two stage accelerator. In these calculations, a TFTR slot geometry is used as a reference design. Two assumptions have been made: (1) the ions approach the meniscus with only about 4 eV and (2) the effect of electron space change in the accelerating gap is unimportant. Fig. 12 shows the deflection of the beam for 0 gauss, 1K gauss and 3K gauss. A plot of deflection versus magnetic field is linear. Figures 12 and 13 show that the divergence of the beam is minimally affected by the beam of the calutrons.

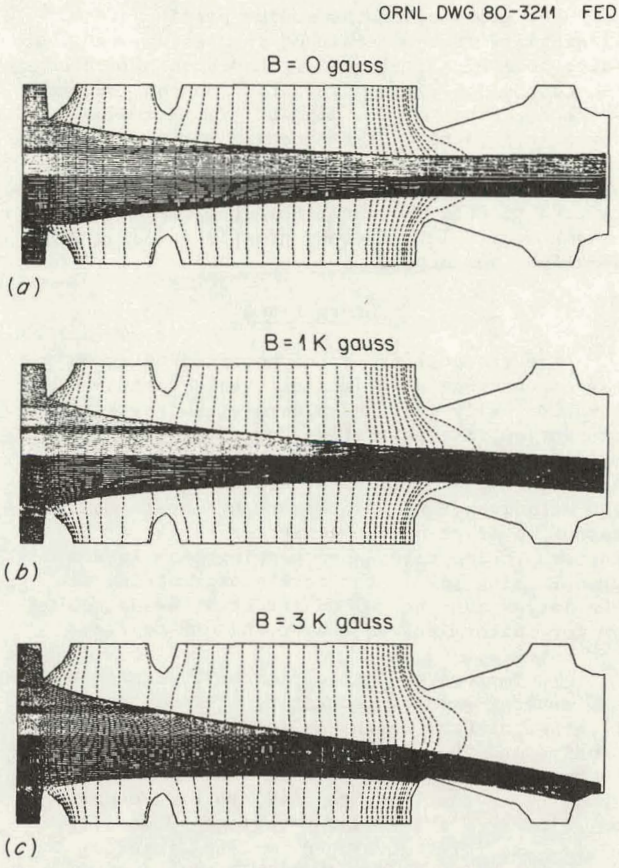

Fig. 12. Angular deflection of the H^- ion beam during acceleration from the modified calutron source.

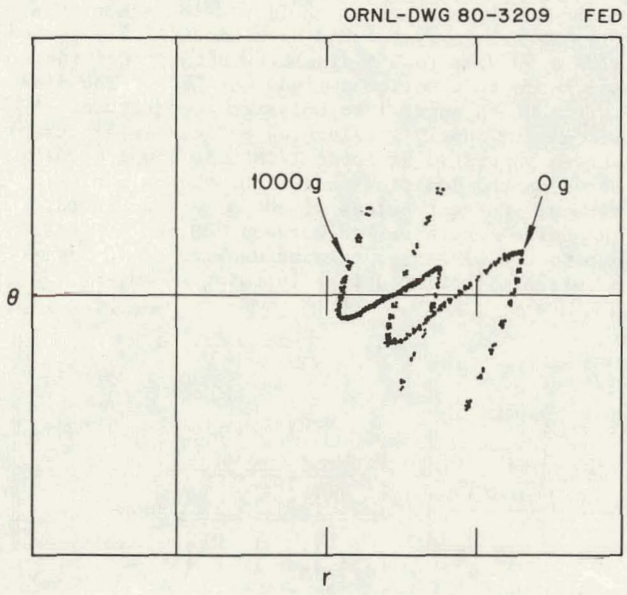

Fig. 13. Emittance plots for the beam acceleration cases of Fig. 12.

The geometry of the source permits great flexibility in the design of the cesium oven. To date, however, little effort has been allocated to the control of cesium deposition on the convertor surface. Since as the data of Fig. 4 indicate, there is depletion of the cesium surface with time using an uncooled substrate, we attempted to water-cool the surface. The temperature was lowered to such an extent that the cesium layer became very thick, thereby greatly reducing the negative ion output.

III. Future Plans

The versatility of the modified calutron and the encouraging experimental results obtained make a magnetically confined plasma with cross-field extraction very attractive for developing a negative ion source. The two major problems remaining in the development are improvement of the gas efficiency and maintenance of an optimum cesium coverage of the converter surface. The former problem relates to keeping beam losses and grid loading low in the accelerator structure. The latter must be solved for truly CW operation or for uniform pulses longer than ∿5 sec.

To improve the gas efficiency, we are studying several ways of generating intense, energetic electron ribbons which can increase the ion density and the ion-neutral ratio in the plasma. In Fig. 14, the anode slit is greatly lengthened compared to that used to date, to reduce neutral gas flow from the filament region. Such a discharge was first developed in 1963[6] in order to produce a plasma column having a plasma density greater than the neutral density of the surrounding gas. This goal was reached in a differentially pumped system. A second electron emitter under development is the hollow cathode shown in Fig. 15. This system has been successfully tested with a 50 V, 1 to 3 A discharge between Cathode 1 and Anode 1, a hollow cylinder of LaB_6. The discharge heats Anode 1 to emission temperature. A second arc supply accelerates an intense electron stream generated at Anode 1/Cathode 2 which will serve as the ionizing medium for the main plasma ribbon. Current pulses of 300 A were achieved. The pulse length varied between 100 and 400 msec due to the excessive current density of 40 A/cm^2. A current limiting device is being added.

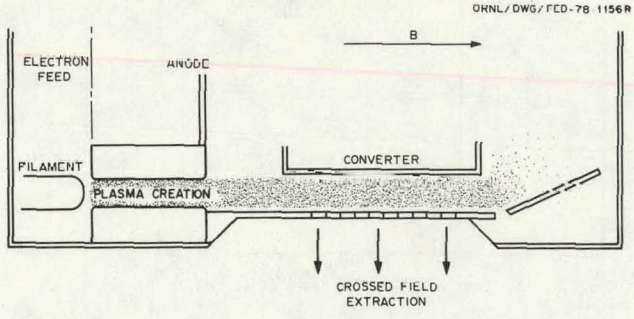

Fig. 14. Long anode high gas efficiency arc discharge.

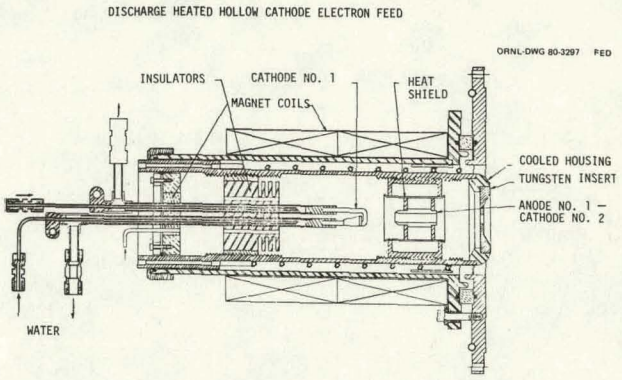

Fig. 15. Hollow cathode.

The idea of Whealton, mentioned above, which is intended as a way to increase the gas efficiency, is depicted in Fig. 16. Figure 16a and 16b shows the improvement due to Dimov. The improvement suggested by Whealton in Fig. 16c is to replace the slot groove in the converter with spherically-shaped dents which focus the negative ions into ciruclar apertures. This design retains earlier improvements with respect to total negative ion utilization and has two advantages. First, the electrons are even more repulsed at the extraction aperture since the negative ions are more highly concentrated due to the extra dimension of focusing. Second, the gas is inhibited from traversing the aperture since the transparency of the aperture is less that of a slot, which passes the same negative ion current.

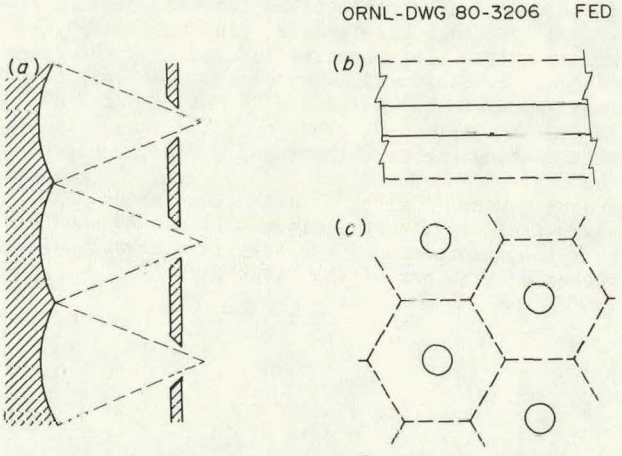

Fig. 16. Spherical focused H^- converter plate.

The problem of cesium control on the converter surface may well be the most difficult of all. Our preliminary attempts to deposit cesium on the surface by controlling oven temperature and by using a cesium flow control valve have not resulted in an optimun surface during long pulses. Even with finer cesium control, ion bombardment may prohibit the use of externally deposited cesium. An alternative measure is to permit the diffusion of cesium through a porous surface. We are starting now to consider the dynamics of such a design.

IV. Summary

The use of the modified calutron to study surface ionization and transverse magnetic field extraction has yielded results which are very promising. A performance summary of the characteristics listed in Fig. 1 are given below:

(a) extracted beam current density — 70 ma/cm^2 at the extraction grid; (b) CW capability — 5 sec pulses achieved and steady state believed to be achievable; (c) gas efficiency — 4% with unfocused converter; (d) electron energy loss — 94% of the electron current is recovered; (e) impurity content — <1% impurity in beam after conditioning; (f) optics — $\sim\pm2°$ subtended by burn pattern; (g) grid loading — not measured; (h) cesium not satisfactory; (i) scalability — a 1 A module called SITEX is in design and a 10 A module is feasible.

From these results, it is readily seen that the modified calutron is well suited to the study of negative ion plasma production.

With the completion of the experiments related to gas efficiency and cesium control discussed under Future Plans, we will be in a position to design a next generation source defined as SITEX which will embody all the concepts and improvements determined from the modified calutron experiments. The first version of SITEX will be an intense 1 A scalable module which will operate steady state at 40 kV extraction potential. An accelerating structure compatible with a 200 kV beam system will be designed with the aid of the 2D[7] and 3D[8] computational code of Whealton.

Acknowledgements

We would like to acknowledge the helpful disucssions and assistance of the members of the Isotopes Separation Section of the Chemical Technology Division, ORNL, and of Dennis Sparks of the Fusion Energy Division, ORNL, for assistance in setting up diagnostic equipment.

References

1. Yu I. Bel'chenko, G. I. Dimov, V. G. Dudnikov, A. A. Ivanov, Doklady An SSSR, 213, 1283 (1973). Preprint 1YaF 81-72, Novosibirsk, 1972. V. G. Dudnikov, Method for Producing Negative Ions, USSR Patent No. 411542, Int. CL. H01 3/04, Filed March 10, 1972, Published January 15, 1974, Bulletin No. 2.

2. BNL 50727, Proceedings of the Symposium on the Production and Neutralization of Negative Hydrogen Ions and Beams, September 26-30, 1977.

3. W. L. Stirling, The ORNL Negative Ion Program, Proceedings of the Plasma Heating Requirements Workshop, CONF-771241, Gaithersburg, Md., December 5-7, 1977, p. 320-344; W. K. Dagenhart, et al., Bulletin of the American Physical Society, 23 No. 7, September 1978, 4P6.

4. Yu I. Belchenko, G. V. Dudnikov, preprint 1 Yaf-78-95.

5. J. H. Whealton, April 1980, private communication (submitted for publication).

6. W. L. Stirling et al., A Low Density Plasma for Molecular Ion Dissociation, J. of App. Phy. 34, No. 12, 1963, pp. 3466-3469.

7. J. H. Whealton, Ion Extraction and Optics Arithmetic, Nuc. Instrum. and Methods, in press.

8. J. W. Wooten, J. H. Whealton, J. E. Akin, D. H. McCollough, R. W. McGaffey, and L. J. Drooks, 3D Asymmetric Electrostatic Accelerator Modeling Using Finite Elements, Bul. of APS 24 (1979) 999.

DISCUSSION

PRELEC You quoted an electron load which was 4 to 6 times higher than H^-. Do you think that this is due to the fact that your extraction slit is parallel to the B field?

STIRLING That is possible. That is one of the two things we can change, making slits perpendicular (like you are doing) and move the plasma discharge back from the extraction slit.

PRELEC Now, if you compare your SITEX source (I guess with perpendicular extraction) and the Penning source with the converter in the back, on which we have been working at Brookhaven, what is the fundamental difference between the two?

STIRLING I think the difference is in the flexibility. In this particular arrangement we can change the components in it. Both are reflex discharges. We will run the SITEX with the reflective plate at anode potential, as well as floating. So, now, if we change that potential on that plate then it will vary from a true Penning discharge. If we can run it at anode potential and make that a drifting plasma column, I am worried about being able to do that. I noticed that was part of the plans I think you fellows are proposing, to make that a drifting plasma column. I am afraid we can not maintain the density in it if we do that. It is going to be difficult to hold a 10^{12}, 10^{14} density when it is drifting.

FORRESTER I can not resist making a remark about the hexagonal array of spherical contoured surfaces. That is exactly what we used in the highly successful development of the porous tungsten sources, in the electric propulsion program; we call that the Sastruky ionizers for various reasons. It is a nice geometry.

HISKES Have you measured the plasma parameters, like electron temperature, ion density, etc.?

STIRLING In the source?

HISKES Yes.

STIRLING Electron temperature, no. The ion density we can infer what it is if we will take some reasonable conversion efficiency. The ion density then would be in the order of 10^{12}, 10^{13}.

HISKES How about the cesium ion density?

STIRLING I do not know.

ALLISON I think, it is worth pointing out that of the original surface plasma sources of the type very similar to the Novosibirsk ones, the only one that has been around CW, to my knowledge, is ours and we have run that at 80 mA/cm^2 for hours at a time. So I think the question about the cesium: cesium does change during pulses but it could also be controlled during steady state operation.

CHARACTERISTICS OF A MODIFIED DUOPIGATRON NEGATIVE ION SOURCE *

C. C. Tsai, R. R. Feezell, H. H. Haselton
P. M. Ryan, D. E. Schechter, W. L. Stirling and J. H. Whealton
Oak Ridge National Laboratory
Oak Ridge, Tennessee 37830

Abstract

A Cs converter in a duoPIGatron positive ion source is able to produce negative ions efficiently. The negative ions are accelerated by an electrostatic accelerator as that in the conventional positive ion source. The low energy ion beams of 1 keV/0.2A are being analyzed. The heavy impurity content in H^- beams is about 10%, that in D^- beams is more. The built-in electron suppressor can reduce electron fraction below 10%. In addition to these preliminary data, other significant results are reported and discussed.

Introduction

The state-of-the-art of tokamak plasma heating technology was recently assessed and reported in PPPL-1610 (1). The method of energetic neutral beam injection of hydrogen isotopes is recognized as the most successful technique to heat fusion plasma.

Neutral beams can be produced by either neutralizing positive ion beams or stripping negative ion beams. Currently, multi-mega-watt neutral beams are essentially produced from positive ion beams (2), but the neutralization and system efficiency of positive ion-based (PIB) systems is a decreasing function of beam-particle energy. The required particle energy for efficiently heating the ignition and reactor type of plasmas in both the mirror and tokamak devices can be increased above 100 keV/nucleon. The corresponding PIB neutral beam system efficiency could be below 30% even with an 80% recovery efficiency of full energy ions (3). On the other hand, the high stripping efficiency of negative ions at such high energy level is the motivating force for developing negative-ion-based (NIB) neutral beam systems (4).

At the moment, such negative-ion-based (NIB) systems are still in their infancy. For instance, an ion source capable of delivering ion beams at ten-ampere and multi-second levels is not available. Moreover, even assuming such negative ion sources can be developed, the potential advantage of high system efficiency can be realized only if the following losses can be reduced to those apparent in the PIB system. These losses are:

1. the reionization loss of neutral beams in the drift tube section,
2. the transmission loss due to space charge blow up or poor beamlet optics and
3. the electron loss of those created respectively in the extraction region and the acceleration column.

Obviously, the most critical task in developing an efficient NIB system is to develop an efficient 10 A negative ion source which is compatible with many restrictive and crucial parameters. During the last several years, the progress of negative ion technology has been spectacular. The representatives of the experimental and theoretical work can be found in the proceedings of this symposium and the previous one (5). The negative ion production by Cs-surface plasma method proved to be an efficient way (6-10). Employing such a production mechanism, various innovated ideas are proposed and pursued (6). One idea is to use a Cs converter to produce negative ions from low energy positive ions (11). The converter is used to modify a positive ion source such as a duoPIGatron for forming negative ion beams.

Figure 1 shows a sketch of this idea. It consists of a positive ion plasma generator, a Cs converter, and an electrostatic ion accelerator. The low energy positive ions from a source plasma created by the plasma generator impinge on cesiated surfaces of the Cs converter and become negative ions. The electrostatic accelerator then forms these negative ions into an energetic beam. The advantage of this method is that it can utilize the existing positive ion sources. With the addition of a Cs converter, a negative ion beam can be produced. If a conversion efficiency of positive ion to negative ion can be 10%, then a 100 ampere positive ion source will deliver a 10A negative ion beam.

Source Characteristics

To test the feasibility of this idea, we have performed a series of experiments. A Cs converter designed and used for the experiments is shown in Figure 2. It consists of a cesium oven and a positive ion (PI) to negative ion

*Research sponsored by the Office of Fusion Energy (ETM), U. S. Department of Energy under contract W-7405-eng-26 with the Union Carbide Corporation.

(NI) converter. The oven is made of thin tantalum sheet and is heated by the arc discharge of the plasma generator. The oven houses tablets of compressed powder of cesium dichromate and titanium. At high oven temperatures, it produces cesium vapor, which subsequently coats the relatively cold surface of tantalum vanes in the PI to NI converter. Figure 3 shows a better view of the vanes. In these figures, rectangular nickel plates are used for introducing a transverse magnetic field ($\sim$ 100 gauss) in the direction parallel to the vanes (see Figure 2).

Figure 4 shows a modified duoPIGatron negative ion source used in the experiments. The Cs converter is located in the recess-cup of the target cathode of an ORMAK 10 cm source. As described in the following, the initial results of this study are very encouraging. The source can be operated as reliably as that of the conventional positive ion source. Under normal operations with hydrogen gas, electrons emitted from the oxide filament produces a cathode plasma within the intermediate electrode. The cathode plasma supplies the ionizing electrons to the anode discharge. A dense anode or PIG plasma is formed right next to the Cs converter. By varying the power levels and duty cycle of the arc discharge, the temperature of the cesium oven can be controlled up to 450° C. Similarly, the cesium layer thickness in the vanes of the PI to NI converter can be varied for H^- production from positive ions originating from the anode plasma. Proceeding towards the grids, the H^- ions are extracted and formed into a negative ion beam. The electrons from the anode plasma and the converter region can be minimized by the built-in electrostatic and magnetic suppressor. The negative ion production and electron suppression have been studied initially by employing a crossed magnetic field Faraday cup to analyze the contents of negative ion beams. The preliminary results confirmed the Cs converter is capable of producing negative ions from low energy positive ions even at 10 to 15 eV (11, 12).

Some of the significant phenomena observed in the experiment are further described below. The negative ion production efficiency depends upon the condition of Cs surfaces in the converter. Usually, the production can decrease with time when the pulse length exceeds 300 ms, or when the duty cycle exceeds 10%. Moreover, after the converter surface is coated with a proper thickness of Cs layer, the negative ion can be produced even at surface temperature below 100° C. However, the negative ion production will be gradually diminished if the converter is water cooled. Hence, the Cs surface control will be an important task in the negative ion source development.

In addition to the H^- or D^- ions, the negative ion beams so formed probably contain some other undesired particles such as electrons and heavy impurities. The electron can produce x-ray hazards, waste acceleration energy, and eventually lower the overall NIB system efficiency. On the other hand, the heavy impurities such as O^-, OH^-, H_2O^-, and others can reduce the plasma heating efficiency. Hence, the negative ion source development should concentrate on optimizing H^- or D^- production and minimizing the yield of undesired particles. To this end, a reliable charged particle analyzer is needed for studying ion beam contents.

Figure 5 shows a charged particle analyzer designed and installed for the beam study. The analyzer consists of a wien filter to select the proper charged particle and two Faraday cups to measure the particle current. The charged particle such as H^+, H^-, their isotopes, and electrons entering the analyzer can be identified and measured. The heavy impurities can be measured as a whole but not individually identified at the moment. Figure 6 shows typical curves of measured signals plotted against the analyzer voltage of the wien filter. The area under each hump of the curve can be used to estimate the contents of various beam species. For instance, areas A_1, A_2, and A_3, are respectively for heavy impurities, H^- ions, and electrons.

A filter coil (Figure 7) located between the PI to NI converter and the first grid is used for calibrating electron measurement and studying electron suppression. This coil will introduce a transverse magnetic field. The electron content in the negative ion beams is a sensitive function of the magnetic field. Particularly at zero field, the electron fraction in the beam is above 95%. The measured values of I_E and A_3 can be utilized for calibrating A_3 measured at any beam condition. After the electron fraction is estimated, the fractions of H^- and heavy impurity ions can also be estimated. For example, the typical value of H^- ions in Figure 6 is about 80%, and that of heavy impurities is about 10%. A similar impurity content was observed in the calutron study when the cesium dichromate was used as a source of cesium. However, it has been demonstrated that the impurity content can be suppressed to below 1% by utilizing elemental cesium (13).

The other curve in Figure 6 is for a D^- beam. Under similar conditions as that of H^- ions, the D^- fraction is $\sim$ 67% and the heavy impurity content is $\sim$ 28%. This may be caused by either lower conversion efficiency or higher destruction probability of D^- ions. The latter could be the main cause, since the charged particle analyzer is located about 65 cm down stream and the vacuum pressure is about 8×10^{-5} Torr. In fact, when helium was used as the working gas, the charged particle detector hardly measured He^- ions, although the drain current is about 0.1 A at 1 keV.

Currently, we are studying the characteristics of the PI → NI converter by utilizing the charged particle analyzer to determine negative ion production and electron loss. We have also initiated a study of the conversion mechanism in this particular converter geometry. We have observed that the negative ion production is a sensitive function of arc condition and Cs surface condition. For instance, an optimal gas pressure range can be found for the maximum yield of negative ions. Similarly, the arc voltage and arc power can be tuned for the maximum negative ion production. Usually, the arc condition will influence the temperature of Cs oven and PI → NI converter. The resulting variation of the Cs layer thickness may explain the variation of negative ion production.

Apart from its use for optimizing negative ion production, the charged particle analyzer is also a useful tool for studying the electron suppression. We found that when the filter coil is biased positively in respect to both the PI → NI converter and the first grid, the electron content in the beam can be suppressed well below 10%.

Conclusion

The above study confirms that the modified duoPIGatron is a novel and viable negative ion source. The experimental results are summarized in Table 1. We believe, by utilizing the elemental cesium, the heavy impurity will be minimized. Hence, the most important tasks in the negative ion source development will be the beam optics and the negative ion production. In the coming year, we will use a 28 cm diameter converter to produce negative ions from a PDX/ISX-B 100 A positive ion source. We expect to produce a negative ion beam of 50 kV and up to 10 A, if the conversion efficiency of 10% can be achieved. We will carefully study the beam properties such as transmission efficiency of negative ions and electron content. In addition, we will pursue cesium surface control and geometry optimization for improving negative ion production. For example, we have a novel converter design (Figure 8) which will be developed for high negative ion beam density, good beam optics, low electron losses and high gas efficiency. The details of converter electrode shape and the distributions of electrons, positive and negative ions are shown and are valid even in the zero Debye length limit. With the above aggressive program, we expect the technology of the negative ion source development to be greatly enhanced.

Acknowledgements

We would like to thank our other colleagues in the ORNL Plasma Technology Section who made this experiment possible. Particularly, we thank G. E. Barber, N. S. Ponte, D. O. Sparks, and R. E. Wright for their assistance in the area of electrical and electronics. We appreciate C. F. Barnett and J. A. Ray who designed and developed the charged particle analyzer. We also would like to acknowledge the valuable discussions with W. K. Dagenhart and G. G. Kelley.

References

1. D. J. Jassby, PPPL-1610, (1979).
2. H. H. Haselton, Proc. of the Plasma Heating Requirement Workshop, Gaithersburg, Md., (1977).
3. W. L. Stirling et al, Appl. Phys. Lett. 35, 104 (1979).
4. J. W. Beal and H. S. Staten, BNL 50727, p. 259, (1978).
5. Proc. of Symp. on the Production and Neutralization of Negative Hydrogen Ions and Beams, BNL 50727, (1978).
6. K. Prelec, BNL 50727, p. 111, (1978).
7. Y. I. Belchenko et al, BNL 50727, p. 79, (1978).
8. J. R. Hiskes and A. Karo, BNL 50727, p.42, (1978).
9. M. E. Kishinevskiy, Interactions of Atomic Particles With A Solid, Kharkov, 1976, Vol. 3, p. 22-25.
10. R. K. Janev and S. B. Vojvodic, Phys. Lett. A 75, p. 348, (1980).
11. C. C. Tsai et al, BNL 50727, p. 340, (1978).
12. W. L. Stirling, Proc. of the Plasma Heating Requirements Workshop, Gaithersburg, Md. Conf-771241, p. 321, (1977).
13. W. K. Dagenhart, this symposium.

A DUOPIGATRON NEGATIVE ION SOURCE CONSISTS OF A POSITIVE ION PLASMA GENERATOR, A NEGATIVE ION CONVERTER, AND AN ELECTROSTATIC ION ACCELERATOR

ORNL-DWG 80-3167 FED

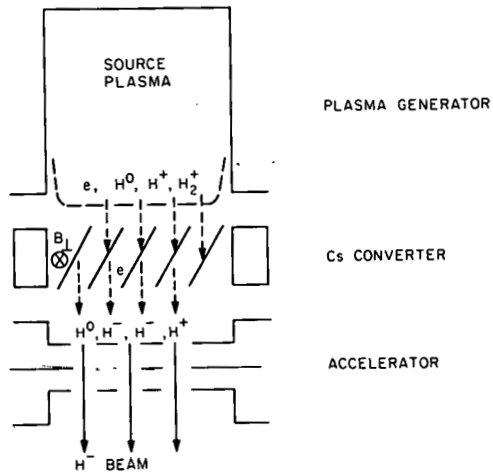

Figure 1.

ORNL/DWG/FED-77570R2

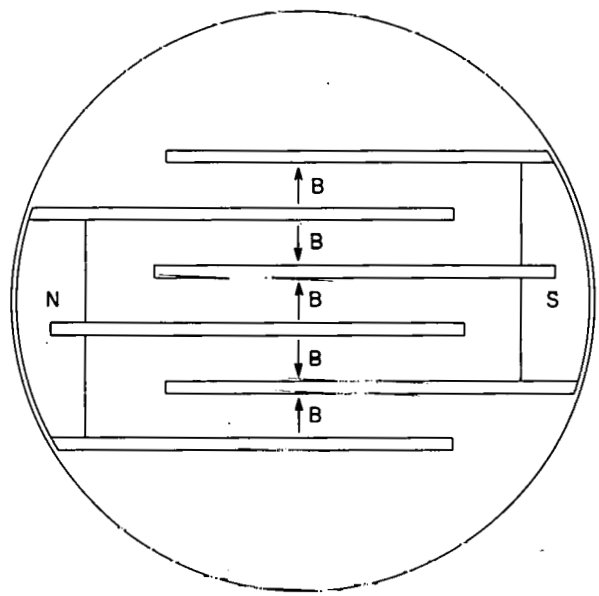

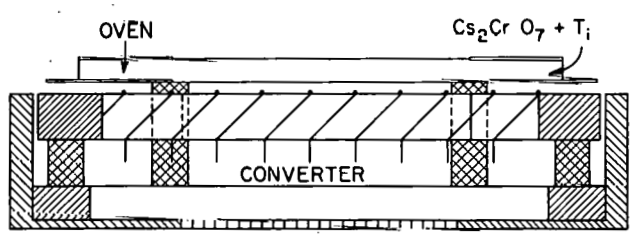

Figure 2.

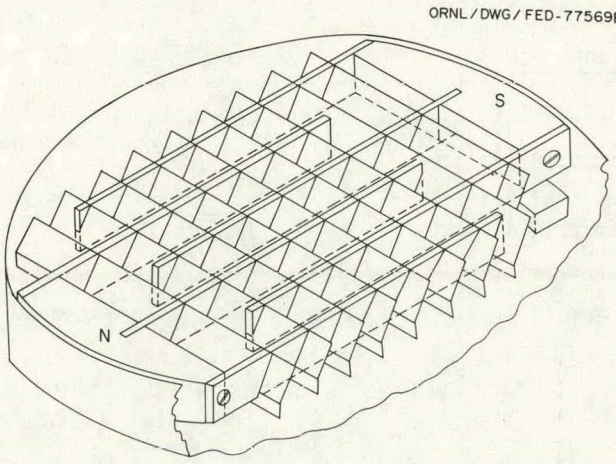

Figure 3.

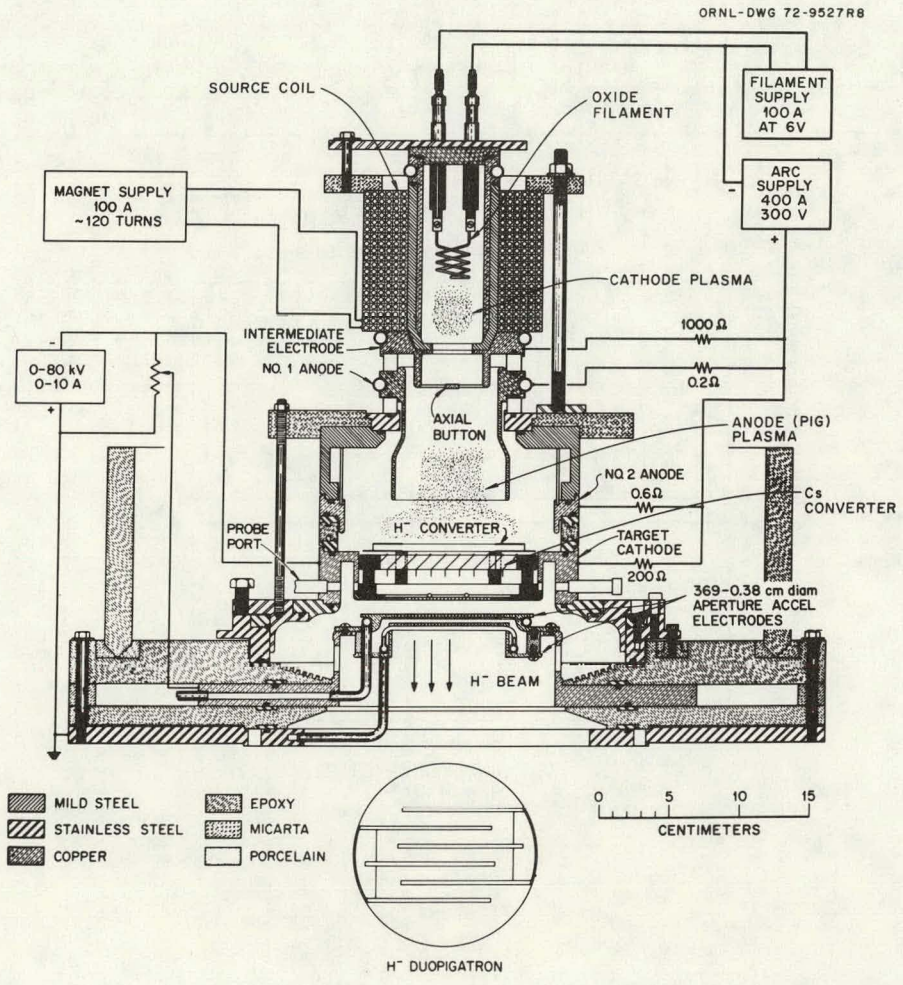

Figure 4.

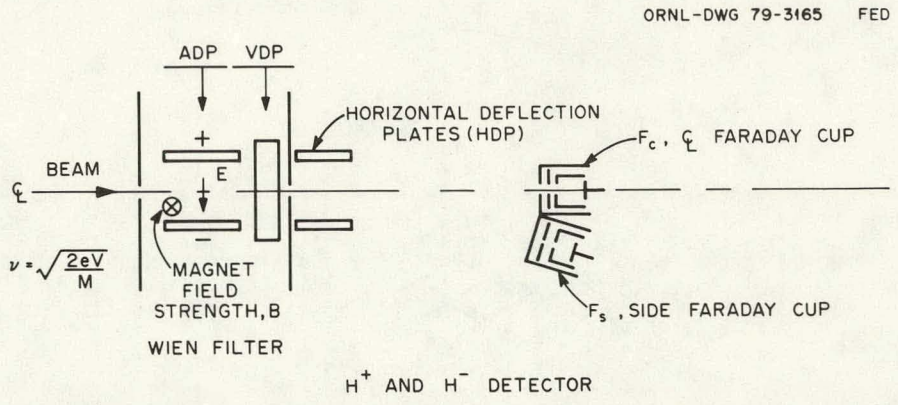

Figure 5.

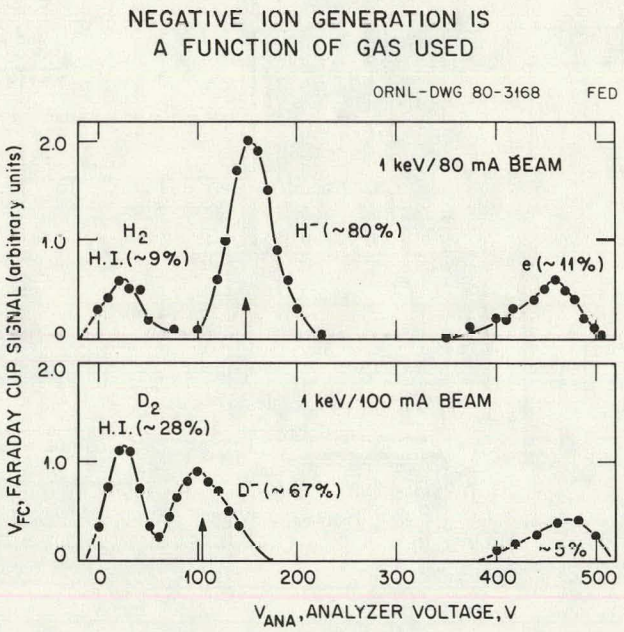

Figure 6.

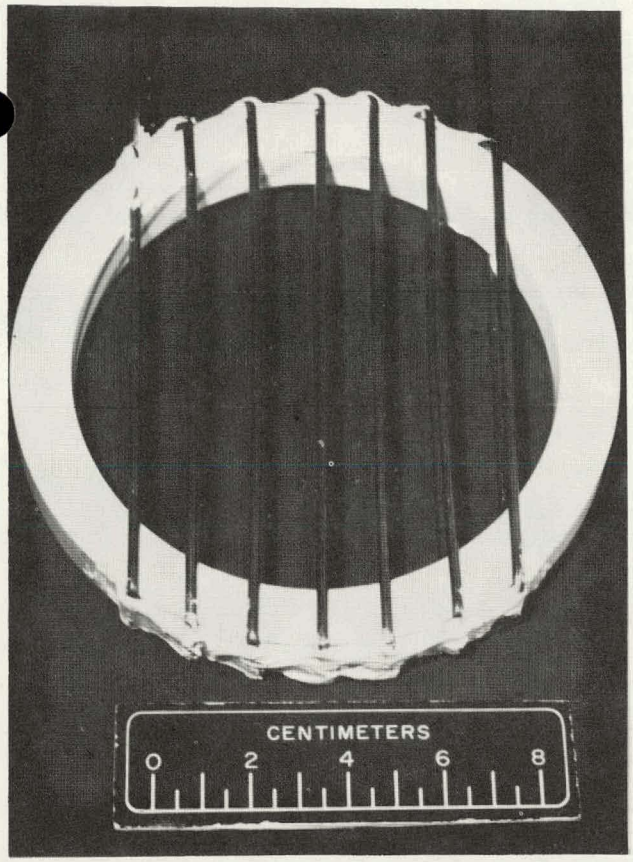

Figure 7.

Table 1

Modified DuoPIGatron is a Novel and Viable Negative Ion Source

1. Produced H^- or D^- beams with current below 0.5A.
2. Achieved beam current density < 20 mA/cm^2.
3. Observed conversion efficiency < 10%.
4. Estimated gas efficiency 3∿5%.
5. Suppressed electron fraction below 10%.
6. Detected heavy impurity content of ∿10%.

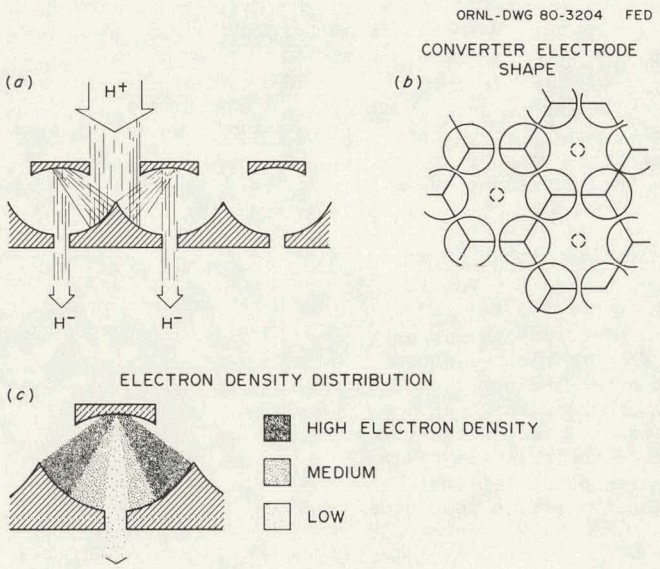

Figure 8.

DISCUSSION

GELLER Can you tell me, where did you measure the one ampere D^-?

TSAI The 1 A is the drain current of the power supply. We did not analyze the beam.

GELLER So it is not sure that they are all D^-?

TSAI I do not say that. I say probably it is 1A.

GELLER Do you worry about the impurities you may have in the beam?

TSAI Yes, I worry about that. As it has been mentioned in the previous paper we are studying that. When we change the cesium bichromate to pure cesium, the impurity may be eliminated. We will continue to study that.

EHLERS Perhaps I am confused but I can not see how any negative ion formed on that converter can arrive at the extraction region?

TSAI That is a good question. One has to go back to the theory of negative ion production, namely sputtering by positive ions approaching cesium covered surfaces; they pick up electrons and become negative ions. Now the Hiskes theory says: when the negative ion approaches a surface, it can be reflected back and I hope this source will prove that theory.

EHLERS But, there is a sheath, is that right, a plasma sheath?

TSAI No, not in this scheme. It depends on how you operate the source. The plasma density is very low.

HAGENA What is the energy of the positive ion incident on your converter? And what is the field strength to extract the negative ions? And, finally, how do you make sure that you have an even coverage on the surface? Perhaps an uneven coverage explains why the efficiency was not very high.

TSAI The energy of the positive ion is about 10 eV. The cesium is cesium bichromate put in a container and heated up by the discharge. So, the cesium coverage on this electrode is not optimized, I agree with you. When we tie all those electrodes together, first grid, the coil, the converter and the anode, then the plasma can come down. Only the negative ions created in the lower surface area will come out. When this electrode is about 40 V below the plasma potential (which is very low) then the incident positive ions have an energy of 30-40 V.

LEUNG Well if the plasma density is very low, then I assume that the positive ions are coming in at an angle; then they will bounce at least one time, two times, before they can come out as a negative ion. So there will be an attenuation, because 40% conversion is the biggest number.

TSAI Yes, I agree with you. Attenuation will be there but on the other hand you can increase production. There is another neutral that can come in on the other side and it has a chance to become a negative ion. Also the back surface may contribute to the negative ion production.

LEUNG You can find out whether these positive ions are really coming in at an angle by measuring the plasma densities. When it is coming in perpendicular then you can bounce many, many times before they can come out.

HOPMAN I think you make a mistake in your reasoning, the percentage of H^- that is coming out is independant of the incoming channel. After the first collision 60% becomes neutral but in that second collision these neutrals have again 40% chance of getting negative. So, it is only the final collision that counts.

LEUNG But those particles that are coming out, they are coming from the back side. They are not coming directly to their final surface and then bounce out, they are bounced twice....

STEWART Can you quote a power efficiency for producing the negative ions?

TSAI My 10 cm source is not a very efficient source, 10 kW for 0.5 A beam.

STEWART 20 kW/A? What is the efficiency when you run it as a positive ion source?

TSAI You know, we expect about 5 A positive ions out of this source.

STEWART With the same power?

TSAI Yes.

STEWART You think it is converting 5 A of positive tions into half an ampere of negative ions?

TSAI Yes.

A CONCEPTUAL D^- SOURCE EXPLOITING NEGATIVE SURFACE IONIZATION OF DEUTERONS

H.J. Hopman, P.J. van Bommel, P. Massmann, E.H.A. Granneman

Association EURATOM-FOM
FOM-Institute for Atomic and Molecular Physics,
Kruislaan 407, 1098 SJ Amsterdam, The Netherlands

Abstract

Under conditions of grazing incidence (θ = 75 - 85°) deuterons are specularly reflected from cesiated monochrystals of W, even at energies of a few keV[1]. A fraction of 10 to 45% is charged negatively during the process. These features suggest an improved concept of a D^--source in which the extraction of a high quality beam is separated from the formation of D^--ions. We shall discuss an experiment designed to test the above ideas at high current densities (250 mA cm^{-2}). The aim is the development of a source delivering a 50 mA cm^{-2} negative hydrogen beam at 20 kV having a divergence of 6°.

1. Introduction

The most widely encountered method to obtain negative deuterium ions is double electron capture by positive deuterium ions. Two principles are applied: the D^+ beam is passed through a gas target or is collided with a surface of low work function. In both techniques predominantly Cs and other alkali metals are used. In the first technique the Cs is in the form of a gas jet, in the second it is a fractional monolayer condensed on a metal substrate to produce a low work function surface[1]. In both cases the Cs target thickness seen by the D^+ ions is of the same order of magnitude. The principle advantage of using solid surfaces is the high density, which allows extremely short target thicknesses. Consequently the beam expansion over the target thickness can be made arbitrarily small if a suitable technique is developed. An additional advantage is the higher yield for the fundamental process of double electron capture, which is 45% on a cesiated solid[1] versus 35% in a Cs gas jet[2]. Moreover Cs gas jets are costly and bulky and any chance to dispense of these must be investigated.

In the Dudnikov type D^- source the low workfunction surface is placed in the plasma chamber where the D^+ ions are created. Such an arrangement hampers controll and diagnosis of the surface conditions. We think the maintenance of a low workfunction is easier accomplished when the surface is placed outside the plasma chamber. In the following we describe the design of a D^- source in which D^+ ions are first extracted from a classical ion source before they interact with the low workfunction surface. Many details of this setup are based on the measured reflection properties of hydrogen from a monochrystalline tungsten [110] surface covered with half a monolayer of cesium. Within the total energy range of the incident hydrogen ions, $50 \leq E \leq 10.000$ eV, these properties can be summarized as follows[3],

1a. specular reflection,
1b. mean energy loss less than 5% at grazing incidence,
1c. mean energy spread in the specular direction less than 8% at grazing incidence,
1d. mean angular spread around specular direction less than 5° at grazing incidence.

2. Design Criteria

Figure 1 presents a sketch of the electrode arrangement we intend to investigate in our concept for a D^- source. Also indicated is the potential distribution on axis. The following considerations led to this design.

2.1. Fusion application of D^- sources necessitates a high current density and accordingly an extraction voltage $V_b \gtrsim 10^4$ V, for the positive ion beam.
2.2. The optimum energy $E_\perp$, perpendicular to the low workfunction surface, for the conversion of D^+ to D^-, is $E_\perp \approx 5$ eV. This property holds in a range of total energies $100 \lesssim E \lesssim 600$ eV [1]. Therefore optimum efficiency can only be obtained for grazing incidence, $\theta \simeq 80°$, where θ is the angle between the beam velocity and the normal on the surface.
2.3. The surfaces are positioned parallel to the beam axis, to preserve the symmetry of the beam space charge field.
2.4. The beam is decelerated just in front of the surfaces to increase the beam divergence and to allow beam particle to collide with the surface.

The electrodes (1), (2), (9) in Fig. 1 therefore form a strong accel-decel lens, from which the beam emerges with energies around 1 keV.

2.5. The charge exchange surfaces [(10) in Fig. 1] are positive with respect to neighbouring electrodes to assure electrostatic confinement of secondary electrons produced at these surfaces.

The voltage V_e between electrodes (10) and (11) in Fig. 1 poses a potential hill for the D^- ions. Therefore $|eV_e|$ must be smaller than the kinetic energy of the D^-, which is equal to $|eV_{10}|$, if V_{10} is the potential of the surfaces (10), in Fig. 1. The measured negligible energy loss of the hydrogen ions, at reflection from the low workfunction surface, is a crucial property in the design of our negative ion source. In other words,

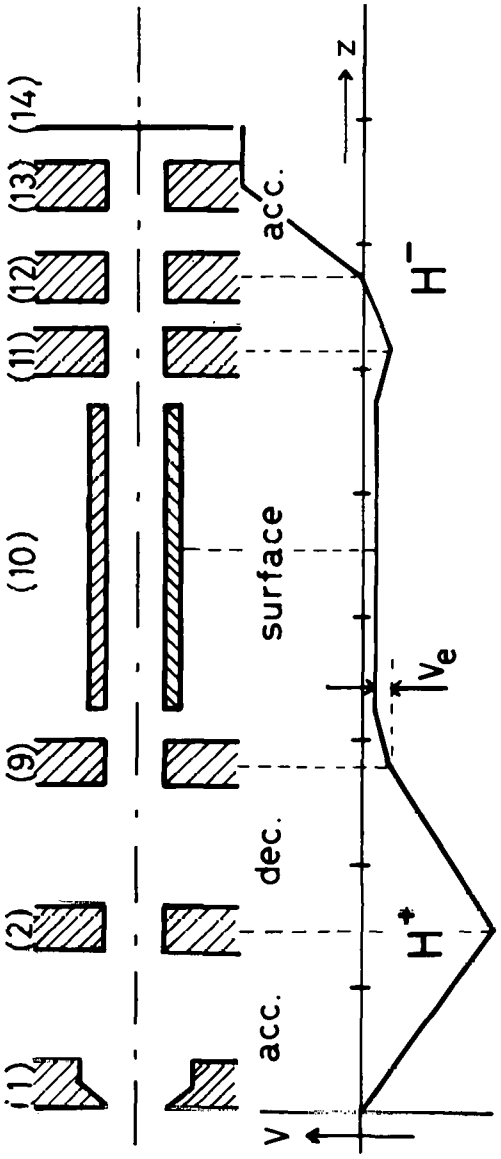

Fig. 1. Sketch of the electrode configuration and the axial potential distribution in Amsterdam negative deuterium source DENISE. Electrode (2): D^+ extraction; (9): D^+ deceleration; (10): low work function surface; (11): electron repeller; (12): ion repeller; (13): D^- acceleration; (14): termination/collector. Total length of the system is 3 to 4 cm.

2.6. Discrimination between D^- ions and electrons before acceleration of the negative ions, is possible because of their different kinetic energy at birth on the surfaces and no additional perpendicular magnetic fields are required.

Because an optimum D^- yield in the fundamental process of negative surface ionization is found for ion energies smaller than 600 eV and because we expect as a first guess that $V_e \approx 0.5|V_{10}|$, it is important to investigate in the actual experiment, whether V_e can be reduced to values below 300 V.

2.7. Beyond the electron repeller is placed a positive ion repeller.

The choice to position the surfaces parallel to the beam implies that a fraction of the D^+ ions does not touch the surfaces. They will be reflected, bombard the back of electrode (11) in Fig. 1, and will produce secondary electrons. These electrons are accelerated toward electrode (13) and their power must be minimized. Electrode (12) must have the minimum possible potential, which is $V_{12} \approx 0$. Actual acceleration of the negative ions is done between electrodes (12) and (13) in Fig. 1.

2.8. The surfaces (10), in Fig. 1, will be the most stable [110] plane of monochrystalline tungsten, covered by half a monolayer of cesium to minimize the workfunction.

Because of the specular reflection, surface roughness will play an important role in determining the final beam divergence. Monochrystalline surfaces are the ultimate solution. It remains to be investigated whether they are needed. The problem to maintain the Cs coverage is as yet unsolved. Sputtering ratios of Cs are not reported in literature for grazing incidence. With a sputtering ratio of 3×10^{-2} the lifetime of a monolayer is estimated to be ≈ 1 s, which is too short for fusion applications. Presumably Cs must be supplied to the surfaces during each extraction pulse. The quoted sputtering ratio is based on measurements by Taglauer et al.[4], who observed a maximum sputter coefficient of 2.5×10^{-2} for sputtering of sulfur adsorbed on a Ni substrate by H^+ ions at an angle of incidence of 60^0. The sputtering coefficient decreases with larger angles. The lower binding energy of Cs on W will tend to increase the sputtering but this is more or less compensated by the larger mass of Cs as compared to S.

3. Experimental setup

In Amsterdam we are assembling an H^- source experiment based on negative surface ionization on low workfunction surfaces mounted outside the H^+ source plasma. The construction is according to the set of guidelines reviewed in section 2.

The aim of the experiment, called DENISE (= DEnse Negative Ionbeam Surface Experiment), is a 20 kV, 0.2 A, 10 s pulselength H^- beam with a current density of 50 mA cm^{-2}. To realize this we intend to extract a 20 kV, 250 mA cm^{-2} H^+ beam from a 0.2 x 10 cm^2 single slit bucket source. Later we also intend to prove the stackability of our approach by working with three parallel slits.

3.1. Electrical Circuit

In the electrode geometry sketched in Fig. 1 the target surfaces are bombarded by the energetic H^+ ions and at the same time by the hot atomic hydrogen gas flowing out of the source. To separate effects due to both types of projectiles we required in the experiment the possibility to place the target close to the source or at a distance of $\approx$ 50 cm. The latter position would mean a severe loss of current density in the H^+ beam at the target. Therefore an accelerating einzellens is planned to focus the positive ion beam onto the target area. The latter electrode configuration is sketched in Fig. 2, together with the main power supply scheme.

Indicated in Fig. 2 are the 100 V power supply for the arc creating the source plasma, a 5 kV supply which regulates the energy with which the H^+ ions collide with the charge exchange surfaces, a 20 kV supply which provides the main H^+ extraction voltage, a 20 kV supply to accelerate the H^- ions and a 50 kV power supply for the focusing lens. In comparison to Fig. 1 the electrodes (3) to (8) are extra; electrodes (3) and (7) have the usual function to confine the plasma electrons to the drift space in between these electrodes. To facilitate diagnostics we have chosen to put the charge exchange surfaces on earth potential.

A fully automated control system has been developed. A central microprocessor switches the power supplies in the correct timing sequence and monitors the currents and voltages in the circuit. It further commands the regulator tube, which also serves to protect the electrodes in case of breakdown and which is connected in series with the 20 kV high voltage power supply.

3.2. The Hydrogen Source

With the charge exchange surfaces outside the source, one can use the well developed technique of positive hydrogen sources. After drawings of the "DITE" bucket source, kindly provided by the Culham Laboratories, we have constructed

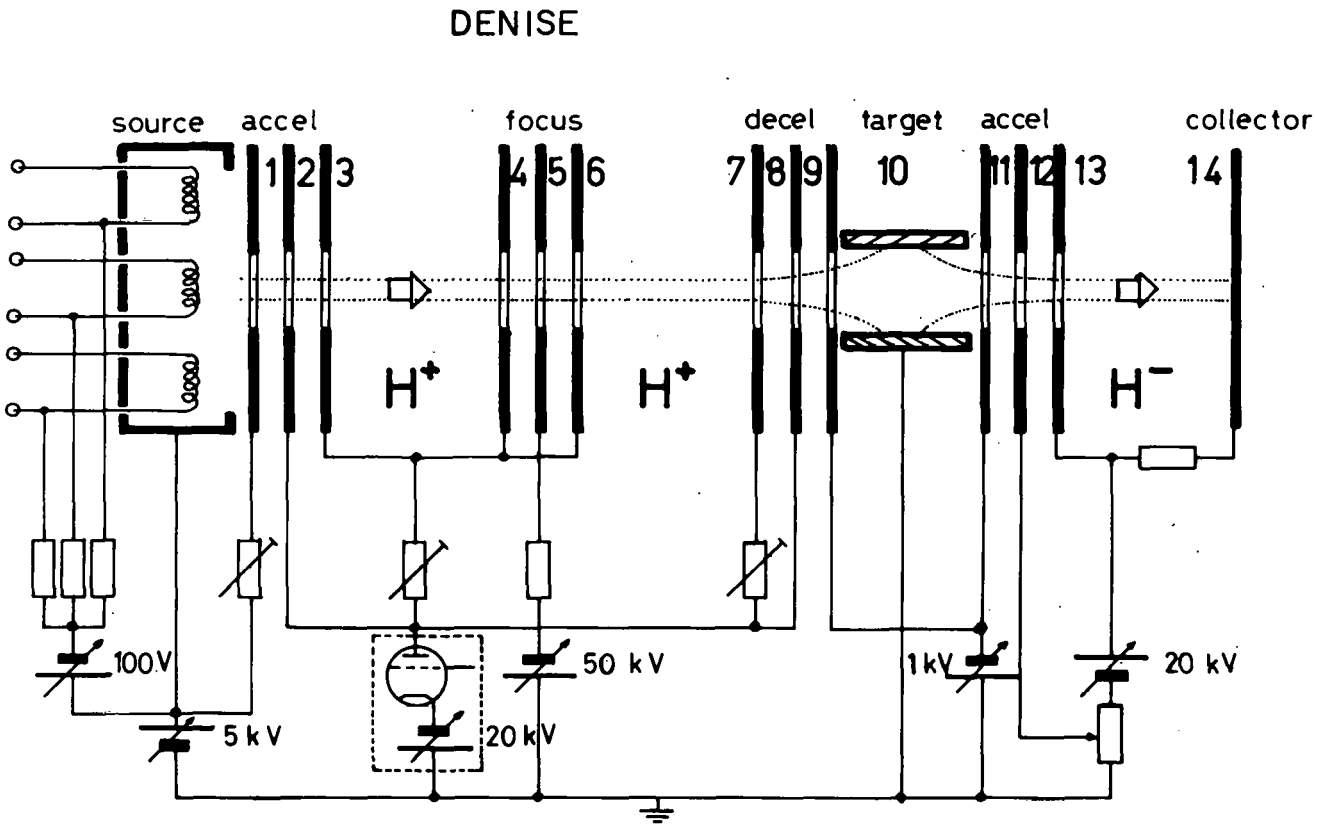

Fig. 2. Main power supply scheme of the H^- project DENISE.

a source plasma chamber with an area of 14 × 19 cm^2. Rotation of the source about the beam axis allows alignment of the source slit with respect to the target surfaces. Rotation about the axis through the extraction slit permits aiming of the beam onto the target area. The plasma chamber has been tried out and proved to function well for the full 10 s pulse duration. We are now in the stage of mounting the electrode system and will study the extraction of the H^+ beam in the last quarter of 1980.

3.3. Vacuum System

Fig. 3 presents the overall design of the experiment. Two 10^4 l/s cryo-sorption pumps readily give a base pressure better than 10^{-8} Torr. The cryo pumps are supported by a 270 l/s turbo pump. The target surfaces are placed in a separate compartment with its own pump, to keep the pressure as low as possible during source operation, when the pressure rises to 10^{-6} Torr in the source compartment. On top of the experiment is planned a small UHV compartment for preparation of the target surfaces. Pressure should be better than 10^{-9} Torr by use of a Ti sublimation pump and a 100 l/s turbo pump.

The targets will be mounted on retractable rods. This way it is possible to give the surfaces of the target the necessary treatment, such as flash cleaning, oxygen removal, cesium deposition etc., under well controlled conditions. Careful surface treatment is thought to be crucial to the reproducibility of the H^- yields.

The symmetry in the mounting of the turbopump and the UHV compartment allows an interchange of their respective positions. This way it is possible to have the target surfaces in front of the positive ion source or at a greater distance.

3.4. Diagnostics

The most relevant parameter in the experiment is the state of the target surface during bombardment. Due to continuous sputtering of the adsorbed Cs, the surface workfunction is a dynamic parameter. A tunable pulsed dye-laser will be applied, permitting time resolved measurement of photoelectron currents. Short pulses (4 ns) at a sufficient repetition time (20 ms) should facilitate the measurement of the photo-electron current (≈ 0.1 A mm^{-2}) in an environment dominated by space charge potentials.

The same diagnostic technique will be used to monitor the surface condition before the targets are lowered into position from the UHV compartment. The philosophy is first to start measurements on the production of H^- with surfaces prepared in the UHV compartment. If the lifetime of the Cs layer is too short, a method will be chosen to supply Cs during the beam pulse.

Other diagnostics are a mass spectrometer and multi channel calorimeters and Faraday cups to obtain power and current profiles of the H^+ and H^- ion beams.

4. Numerical trajectory calculations

To support the design and operation of the ion optical system in our apparatus we use a modified version of a computer program, originally developed by W.B. Herrmannsfeldt.[5] This code calculates the trajectories of charged particles in a potential distribution generated by potentials applied to the boundary and by the space charge of the beam.

The program is modified in order to incorporate the charge transfer surfaces on which the ions are reflected (specularly). The present version of the code allows to calculate the trajectories of H^+ (D^+) and H^- (D^-) ions simultaneously. Because of the relatively small H^- current density (about 20% of the incident H^+ current density) addition of negative space charge does not lead to numerical instability. The program treats the interaction of ions (H^+) and the surface according to the following set of rules.

-4.1- Specular reflection of the incident particles.

-4.2- (Double) electron capture by the incident particles (H^+).
The two appearing reactions leading to a charge transfer are:

$$H^+ + e \rightarrow H^0 \quad (1)$$

$$H^+ + 2e \rightarrow H^- \quad (2)$$

-4.3- The efficiency of the charge transfer process (reaction 2) is a function of incident angle and energy, as was measured by Van Wunnik.[3] All H^+ ions, not transfered to H^- ions, are assumed to be neutralised after interaction with the surface. The trajectories of these neutrals are not calculated.

-4.4- The loss of energy in one interaction with the surface is 5%.[3]

-4.5- If an H^- ion interacts with the surface then it is reflected as an H^- and loses 5% of the incident energy according point 4.4.

With this modified code we calculated the trajectories of the H^+ and H^- ions in the geometry drawn in figure 1. The accel-decel lenssystem is similar to the system designed by Hooper et al.[6] The geometry of the lenssystem is rectangular. The width of the infinitely long slits in the lenses is 2 mm. (Since in our apparatus the width to height ratio is 0.02, the influence of the slitheight is neglected).

The H^+ current density extracted from the source plasma is 250 mA/cm^2, the rms divergence of the H^+ beam beyond the accel-decel lens is about 10^o. Although in the present approach the calculated H^- beam does not yet have the wanted property, i.e. J = 50 mA/cm^2, the present calculations give already the right order of magnitude. The current density of the H^- beam is 13 mA/cm^2, the rms divergence is 6^o at 23 keV. In figure 4a an example of the trajectories in the lenssystem is given. (When H^+ ions hit the surface they proceed as H^- ions). Figure 4b gives the potential along the axis of symmetry. The figure is just a demonstration that the program works.

ACKNOWLEDGMENTS

The authors thank Dr. T.S. Green for fruitful discussions at a very early stage in the design of our D^- source . The second author expresses his gratitude to Dr. Ph. Raimbault for making him familiar with the code performing trajectory calculations. The authors are greatful to the UKAEA Culham Laboratories for the permission to copy parts of the DITE source.

This work was performed as a part of the research program of the association agreement of Euratom and the "Stichting voor Fundamenteel Onderzoek der Materie" (FOM) with financial support from the "Nederlandse Organisatie voor Zuiver-Wetenschappelijk Onderzoek" (ZWO) and Euratom.

REFERENCES

1. J. Los, Contribution to this conference.
2. A.S. Schlachter, Report Brookhaven Nat. Lab. BNL 50727 (1978), p. 11.
3. J.N.M. van Wunnik, B. Rasser, J. Los, Proc. ECOSS-3, Cannes (1980), vol. II, p. 849.
4. E. Taglauer, U. Beitat, G. Marin, W. Heiland, Surface Sci. 63 (1977), 507.
5. W.B. Herrmannsfeldt, Report SLAC-166 (september 1973).
6. E.B. Hooper, O.A. Anderson, T.J. Orzechowski, P. Poulsen, Report Brookhaven Nat. Lab., BNL 50727 (1978), p. 163.

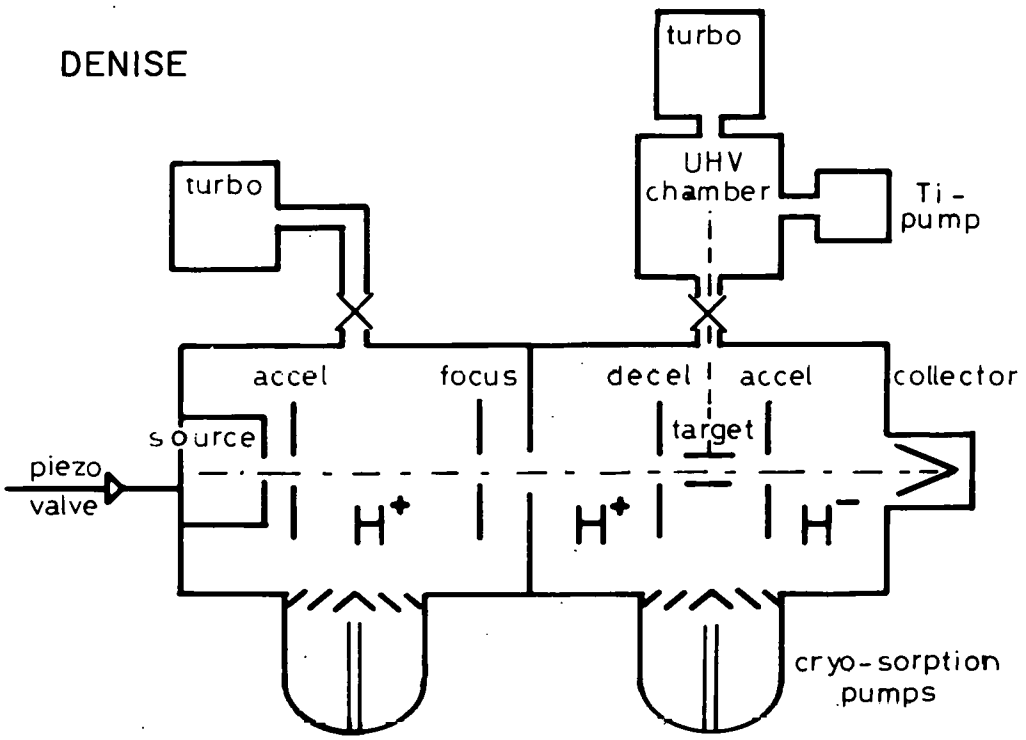

Fig. 3. Mechanical design of DENISE and vacuum system.

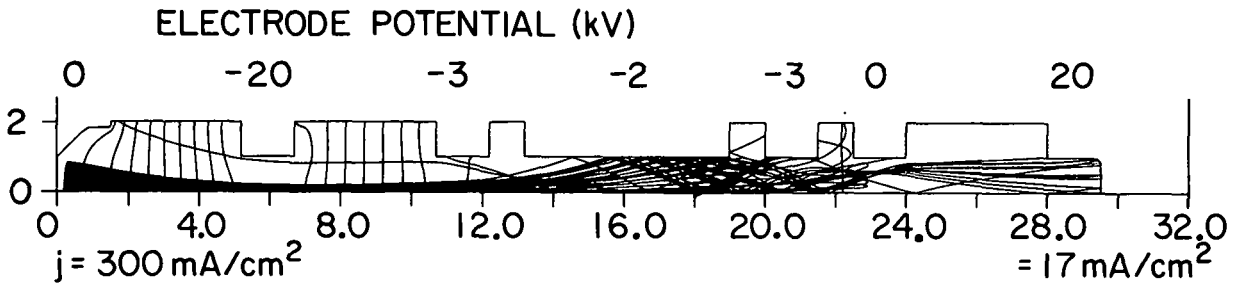

Figure 4a. Calculated trajectories of H^+ and H^- ions in DENISE.

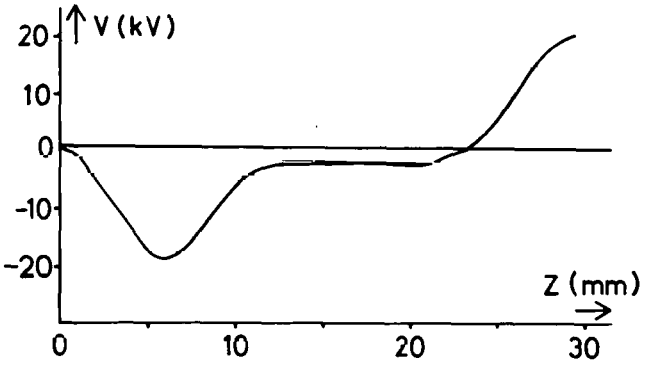

Figure 4b. The calculated potential on axis.

DISCUSSION

PRELEC First comment is, I would be a little bit apprehensive in how to get a nice low emittance beam after those collisions with the surface and conversion for two reasons: space charge spreading of the primary beam and angular dispersion at the conversion.

HOPMAN Los has measured an angular spread of about 6° dispersion at say 1 keV, that means that once you extract the beam at 300 keV beam, then the 6° decreases to something like 2° and according to Tokamak people this is acceptable.

PRELEC You assumed that you would have more than 0.25 A/cm^2 current density at the converted surface?

HOPMAN No, it is the extraction current density because the surface is parallel to the beam...

PRELEC One of the tables shows that one of the objectives was to study surface bombardment at 0.25 A/cm^2. My question is, if that is the case, what would be the primary extracted positive ion beam density if you want to have 0.25 A on the tungsten surface?

HOPMAN This table was too much shortened and some figures were left out. No, we extract 0.25 A/cm^2 positive ion beam. Then this is spread out and reaches the surface at 80°. So, the current density on the surface will be less. I should note that there is an energy reduction on the surface of 5%. This means that at 1 keV the energy loss is 50 eV/ion. For a current density in the order of 100 mA/cm^2 the heating of the surface will not be of importance. I think it increases by something like 10°.

HAGENA Do you have any estimates of what the conversion efficiency will be if you have not an incident proton beam but incident molecular ions or neutral molecules assuming the same velocity?

HOPMAN Van Wunnik and Los measured only what happens to incident positive ions. They are setting up measurements to repeat it with incoming negative ions. So, if the result is the same, you know for sure that if you use neutrals you will have the same result again.

HAGENA Neutral molecules?

HOPMAN Neutral atoms. Normally if a molecule hits the surface it will break apart and Van

Wunnik has measured the divergence with an H_2^+ beam. I think to remember that the angular spread is large in that case but I am not sure about it.

LAGENA The reason I am asking this is that the cluster beams would provide a good possibility for intense particle currents of neutral molecules in the energy range of interest for surface conversion. It is only a problem of efficiency.

HOPMAN Yes, the idea is that the outcome is independant of the type of the incoming particles, so if it comes in as an H_2 molecule it will fall apart and each atom will then give the same yield, only the velocity will be reduced by a root of 2. However in the acceleration structure maybe they are lost again, therefore we are glad that we have a current source with very high H^+ yield compared to H_2^+. So, in our experimental set-up the fraction of H_2^+ will be of the order of 10%.

HOLMES I noticed the conversion efficiency is a very rapid function of the angle with which the incoming ion strike the surface. I see from this calculation of Rambeau the beam sort of blow up.

HOPMAN They are calculations by VanBommel. Van Bommel took over the program from Rambeau and implemented the surface collision.

HOLMES The question really is: do you think you have a problem because the beam is expanding very rapidly when you try to accelerate it? So, the space charge force will try to fling the ions out radially and you will not be able to achieve a very grazing incidence. It would be much more close to normal.

HOPMAN The results should be convincing. This is taking into account the space charge.

HOLMES Yes, that angle, when it is hitting that W-Cs surface it looks like 20^o.

HOPMAN It is indeed large in this case but we use in this example 2 keV at various angles. If we are able to make the incidence more grazing, maybe by playing with the potential, we have a chance of increasing the final negative ion current.

SCHLACHTER My first question: is your geometry cylindrical or planar?

HOPMAN We use slits in our source of 10 cm long and 2 mm wide.

SCHLACHTER What gas pressure do you anticipate in the region of the converter electrode in operation?

HOPMAN Culham people say that the gas efficiency is 50%. We start with a very open structure and that means that in the chamber we estimate pressures of about 10^{-5}. When we increase the number of slits it is very well possible that the gas becomes a severe problem.

SCHLACHTER Well, if I understood the results that Dr. Los presented several days ago, this yield of 30-40% is quite critically dependent upon clean surface conditions that are, as you said today, a half a monolayer and this would be difficult to achieve in a pressure of 10^{-5}, is that correct?

HOPMAN Yes. It is one of the things we have to solve.

SCHLACHTER Have any tests made of what the conversion efficiency might be at hydrogen pressures of 10^{-5} assuming that was the only other thing present?

HOPMAN If you let in hydrogen gas it is molecular and you will see no change in the yield, but if it is not molecular but atomic hydrogen that surely will attack the cesium on your surface. This is a completely different problem.

DOUCET Can you accommodate a cesium layer thicker than a monolayer?

HOPMAN Well, the most difficult thing is to have a monolayer so once you achieve this you can go to a thicker layer, sure.

DOUCET The question is, do you think that your monolayer will remain a monolayer with that gas pressure and under bombardment of the ions?

HOPMAN No. At the moment our estimates of the lifetime of a monolayer is of the order of 1 second. We want to accept 10 second pulses.

DOUCET Under what conditions?

HOPMAN Under working conditions.

DOUCET Say 15 mA/cm^2 of proton beam.

HOPMAN Yes.

DOUCET A second question. You have shown the curve of the yield of negative ions per positive ion and from that qualitative value, it seems to be very close to what you can expect from double charge exchange. Could you check these values and compare the two curves?

HOPMAN It is even more astonishing. Geller remarked it already on Monday, the yield is the same, the velocity is the same but also the target thickness is the same. Half a monolayer is $5 \times 10^{14}/cm^2$, now in cesium vapor you have two times more, 10^{15} atoms/cm^2, so it is remarkable.

DOUCET My first question was, can you accommodate the thicker layer of cesium?

HOPMAN Yes, we can.

DEVELOPMENT OF NEGATIVE ION SOURCE AT THE IPP NAGOYA UNIVERSITY

T. Kuroda*, H. Okamura, O. Kaneko and Y. Oka
Institute of Plasma Physics, Nagoya University
Nagoya 464, Japan

Abstract

Preliminary experiments have been made to develop a high current H^- ion surface for a neutral beam injector. Initially, an H^- ion source of the magnetron type has been investigated in order to determine its physical and technical problems. A second plasma source for negative ion production is under construction, which is based on controlled plasma production. This paper describes preliminary experimental results of the magnetron ion source and some features in the new type of plasma source.

I. Introduction

As neutral beams with energy of higher than 150 keV will be required in future fusion reactors, it is necessary to develop the high current negative ion source. However, it seems that there are a lot of problems to be solved before negative ion sources can be applied in neutral beam injectors; even with the magnetron ion source, which seems presently the most developed one. The purpose of our preliminary experiments with negative ion sources is not only to study the physical phenomena of negative ion production in the source, but also to develop the proper means for high current beam formation.

We have started experiments with two different types of sources, one is a pulsed magnetron type H^- ion source and the other is a new type of dc plasma source.

II. The Magnetron Source

As a source of negative ions, a magnetron type source was chosen, because so far the most promising results were obtained with this source. The main purpose of our experiment is the following:

1. to obtain the operating characteristics of the source with and without cesium and to obtain its fundamental characteristics;

2. to determine the physical and technical problems which must be solved to use it for a high current negative ion source suitable for neutral beam injectors;

3. to obtain data which are required for a scaled up model.

A schematic diagram of the source is shown in Fig. 1. It is similar to the source developed in Novosibirsk[1] and BNL[2] except for the cesium supply system. The anode and the cathode are made of stainless steel and the gap between them is 1 mm.

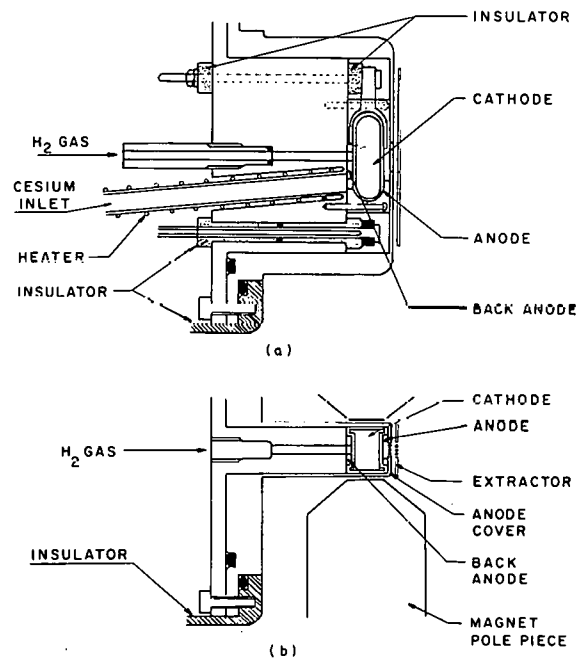

Fig. 1. A schematic diagram of the magnetron type negative ion source (a) cross section perpendicular to the magnetic field; (b) cross section parallel to the magnetic field.

The extractor electrode is a thin stainless steel plate of 1 mm with four slits. Each slit in the extractor electrode is aligned with each slit in the anode cover. The assembly of the source is floating from the ground by an insulator. The magnetic poles are on ground potential. Hydrogen gas is fed through a hole in the center of the back anode and cesium vapor is directed into the discharge chamber through another hole in the back anode. The quantity of cesium vapor flow into the discharge chamber is controlled by changing the temperature of the cesium oven. A high speed piezo-electric valve is used as the gas shutter. The source parameters and typical beam yield are shown in Table 1.

The discharge can be sustained above a critical magnetic field strength, where the value of $\omega_c \tau_c$ for electrons is estimated about 1 for the present experimental parameters (ω_c is the cyclotron frequency of the electron and τ_c is the collision time of electrons). It seems that the source is operated in the mode of the magnetron discharge.

*On leave at Brookhaven National Laboratory, Upton, New York.

TABLE 1

Source Parameters and Typical Beam Yield

	H_2 mode	$C_s + H_2$ mode
Total beam yield	4.4 mA	46 mA
H^- component	3.9 mA	40 mA
Heavy component	0.5 mA	6 mA
Discharge current	100 A	100 A
Discharge voltage	~500 V	~180 V
Source magnetic field		1.8 kG
Extraction voltage		14 kV
Pulse duration		1 ms
Cathode current density		13 A/cm^2
Repetition rate (H_2 mode)		0.3 Hz
($C_s + H_2$ mode)		1 Hz
Extraction electrode gap		1.7 mm
Number of emission slits		4
Each emission slit size		0.5 mm x 10 mm
Cathode stem temperature		240 - 260°C

The negative ion current is measured by a movable shielded Farady cup which has an entrance aperture of 1 mm in diameter. It is located a distance of 23 cm downstream from the source as shown in Fig. 2.

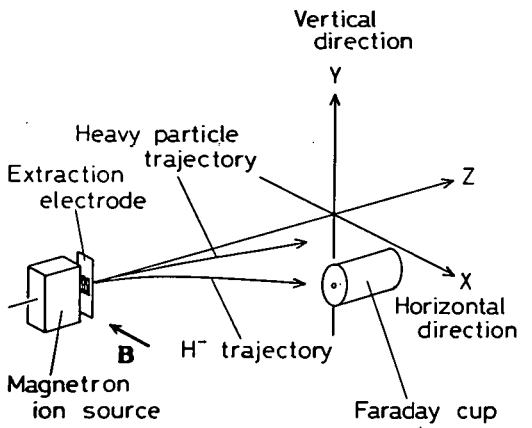

Fig. 2. Spatial configuration of the source and the Faraday Cup.

The negative hydrogen yield is investigated as a function of the discharge current and the hydrogen gas flow rate. The results show that the negative ion is destructed not only by the attenuation due to the charged particles in the plasma, but also by the neutralization due to the neutral particles in the source as predicted by reports.[3,4]

Although no special abnormality has been observed, the divergence of the beams are worthwhile to mention. A typical example of the H^- current density profile in the direction vertical to the magnetic field is shown in Fig. 3 for a 14 keV beam and for both the hydrogen mode and the hydrogen-cesium mode. The peak which is slightly displaced from the axis of the source, corresponds to a negative ion of heavy species, which originate most likely from the electrode material but this species is not identified yet. The second peak which is much more deflected from the axis of the source corresponds to the hydrogen negative ions. The profile is broader in the cesium mode than in the hydrogen mode. The e-folding half width of the profile is about 4.5 cm, which is much larger than the width observed in the hydrogen mode.

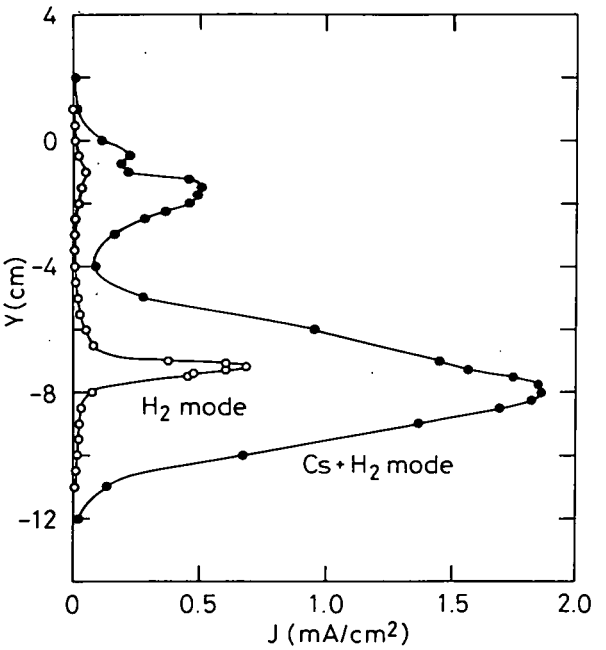

Fig. 3. A typical example of H^- current density profiles in the direction vertical to the magnetic field.

On the other hand the profile parallel to the magnetic field does not change much in both modes except for the scale. It is affected rather by the accuracy of the alignment of the extraction slit with respect to the anode slits.

The large divergence in the direction vertical to the magnetic field can be explained by: a) the nonuniform plasma density distribution along the slit b) the large energy spread of H^- ions emitted from the cathode surface c) the energy deflection angle of the ion in the magnetic field and d) space charge effect of H^- ion. These phenomena will be studied in more detail in future experiments.

III. The Sheet Plasma Negative Ion Source

The phenomena in the magnetron source are complex and it is very difficult to study the physical problems individually because the parameters of the plasma and the discharge cannot be changed independently. In order to investigate

each physical problem independently by changing the parameters of the source, for example, plasma density or thickness of the plasma without changing other conditions may lead to the possibility of a new type of dc negative ion source. We are preparing a dc plasma source which is called the "sheet plasma source."

This source is designed on the basis of the experience and the knowledge of dc plasma production and applying some principles of the surface plasma ion source. The requirements of the the source design are as follows:

1. Formation of a plasma sheet which is the least destructive for negative hydrogen ions.

2. Independent variation of individual plasma parameters.

3. Controlled temperature of the H^- emitter.

4. The plasma should be large in size in order to measure easily the plasma parameters, H^-, etc.

A schematic diagram of this source is shown in Fig. 4. It consists of two discharge chambers which produce the plasma by an electrical discharge. They are located on both sides of the beam extraction region. Furthermore, there is the emitter of negative hydrogen ions, the extractor, and two coils which provide the axial magnetic field confining the plasma.

The plasma produced by the discharge between the hot cathode and the anode is shaped into a narrow rectangular channel. The plasma flows into the beam extraction region from the source along the magnetic lines of force. The cross section of the plasma in the beam extraction region is approximately determined by the anode slit size, the magnetic field configuration and the diffusion rate across the magnetic field. The size of the cathode surface, the cross section of the anode slit, the relative position of the anode, and the cathode are chosen as to satisfy the following magnetic flux conservation:

$$\int_{S_1} B_1 ds = \int_{S_2} B_2 ds$$

where S_1 and S_2 are respectively the cross section of the cathode surface and the anode slit, and B_1 and B_2 are respectively the magnetic field near the cathode surface and the anode slit. In this situation the magnetic field lines started from the cathode periphery pass through the anode. The cathode with large electron emitting surfaces can be used by setting the cathode in the weak magnetic field. On the other hand, the anode is located in a strong magnetic field. The electron emitted from the cathode is converged towards the narrow anode region. Thus, the high density plasma is obtained as in the TPD plasma source[5] by a high current dc discharge.

The plasma source operates at high pressure but the pressure in the extraction region is kept low because it is differentially pumped through the narrow and long anode channel. It is desirable to operate at low pressures near the extractor region in order to minimize the losses of H^- by charge exchange with neutral particles and to prevent extractor breakdown.

Operating the cathode in a weak magnetic field and at high gas pressure prevent the cathode from hot spots. The cathode is an oxide coated concave cathode and it has a rectangular shape of 1.5 cm x 8 cm. The anode slit is 0.2 cm x 3.0 cm.

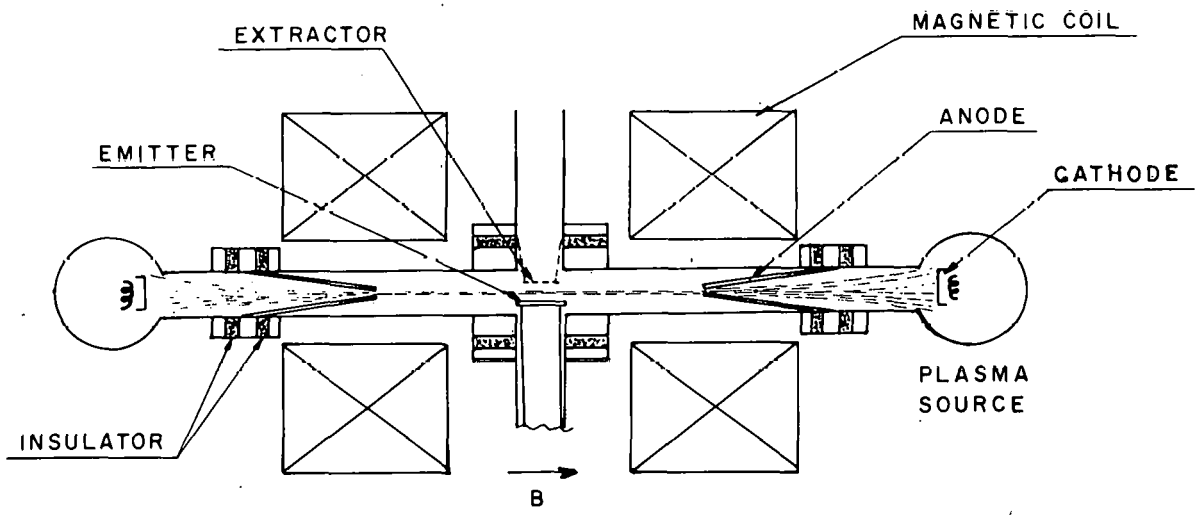

Fig. 4. A schematic diagram of sheet plasma source.

High pressure operation of the plasma source maintains the discharge at low cathode potential with high discharge current and very low noise. The cusp magnetic field will be applied to make the source condition better in the future. The design value of the discharge current is about 30A. These operating conditions guarantee a long lifetime of the oxide coating.

Primary electrons from the cathode oscillate between the cathodes and it enhances the ionization degree in the extraction region.

The emitter has holes to inject cesium vapor into the plasma and to cover the emitter surface. Its surface is rectangular, 4.0 cm x 1.6 cm.

The purpose of the experiment is:

1. To study problems of the emitter, the efficiency of formation of negative ions on the surface as a function of several parameters such as the temperature of the emitter surface, the material of the emitter, etc.

2. To study the transport and decay of H^- for defined plasma conditions by independently changing the plasma parameters (plasma density, plasma thickness, etc.).

3. To study the extraction of beams.

4. To resolve the technical problems in the dc high current negative ion source.

This source will operate in the near future.

References

1. Yu.I. Belchenko, G.I. Dimov, V.G. Dudnikov, Proc. 2nd Sym. on Ion Source and Formation of Ion Beams, Berkeley, Calif., VII-1, LBL-3399 (1974).

2. K. Prelec, Proc. Symp. on the Production and Neutralization of Negative Hydrogen Ions and Beams, Brookhaven National Laboratory, p. 111 (Sept. 1977).

3. Yu.I. Belchenko, G.I. Dimov, V.G. Dudnikov, Sov. Phys. Tech. Phys. 18, No. 8, 1083 (1974).

4. T.S. Green, Nucl. Inst. and Methods 125, 345 (1975).

5. Annal Review of Inst. Plasma Phy., Nagoya Univ., p. 55 (1967), p. 104 (1975),

THIS PAGE

WAS INTENTIONALLY

LEFT BLANK

DOUBLE CHARGE EXCHANGE SOURCES

THIS PAGE

WAS INTENTIONALLY

LEFT BLANK

PROSPECTS FOR NEGATIVE ION SYSTEMS BASED ON CHARGE EXCHANGE*

E. B. Hooper, Jr. and P. Poulsen
Lawrence Livermore National Laboratory, University of California
Livermore, California 94550

Abstract

Experiments on the production of H^- and D^- by charge exchange in alkali metals are reviewed. It is shown that the results can be calculated accurately from knowledge of the positive-ion characteristics and atomic cross sections. D^- sources for injection into a high voltage accelerator are considered as a function of positive-ion energy. Minimum dimensions are obtained at energies of 1.5-2 keV with conversion in rubidium.

Introduction

Negative ions of hydrogen and deuterium have been produced in alkali metals with currents as large as 1.4 and 2.2 amperes, respectively. Furthermore, analysis of the data from these experiments demonstrates that the characteristics of the resulting beam can be predicted to within 20% from the characteristics of the initial positive-ion beam and pertinent atomic cross sections. No "anomalous" effects have been found that caused the negative ions to be lost, spread in angle of propagation, or otherwise be affected in a manner which would prevent them from being used in a high-energy neutral-beam system. Finally, because the beam is well directed and propagates in a region of low gas pressure, it has many characteristics that make it suitable for such a system.

There are some features of charge-exchange systems that may cause difficulties in application. In particular, the apparatus is large and gas efficiency is low, although the consequences are minimized because the gas is shielded from the region in which the negative ions propagate. The use of alkali metals causes possible hazards because large quantities are required, and possible plasma problems if even small quantities reach the fusion device.

This paper describes experiments using charge exchange, with particular attention to our recent experiment in which detailed calculations were made to compare results with prediction. A general charge-exchange system is modeled in a simple way and its characteristics discussed as a function of the size. Optimums are found, in the sense of minimizing the area or linear dimensions of the source, and can serve as a basis for more detailed engineering design.

*Work performed under the auspices of the U.S. Department of Energy by the Lawrence Livermore National Laboratory under contract number W-7405-ENG-48.

The results are not applicable to magnetized beam lines or to systems using clusters, except to the extent that confidence in predictive capability is useful.

Charge-Exchange Experiments

Charge-exchange experiments on a scale large enough to be of interest for neutral-beam systems have been done in cesium[1-3] and in sodium.[4-8] The work by Osher et al.[1] was the first demonstration of an intense beam: 50 mA of D^-. In other work at LLNL,[2,3] up to 0.3 A was produced at 1 keV; 0.1 A was post-accelerated to 60 keV, demonstrating that the density of electrons in the negative-ion beam can be made low enough that they do not prevent efficient post-acceleration.

The sodium experiments of Semashko et al.[4,5] and of Hooper, Poulsen, and coworkers[6-8] were on a still larger scale. In the latter work, for example, as much as 2.2 A of D^- was produced at 12 keV. The beam pattern was elliptical, with distances from the peak to the e^{-1} points of 4 cm by 14 cm.

The current density predicted for our experiment was calculated from the known output of the positive-ion source and cross sections. Details of the calculations can be found in Refs. 7 and 8. The positive-ion current (D^+) is plotted as a function of sodium line density in Fig. 1; comparison with the σ_{+0} cross sections is excellent. The measured D^- current is compared with prediction in Fig. 2. Note that the calculation includes the three energy components originating from the molecular ion mix in the original source.

Beam profiles are very close to those of the positive ions and neutral atoms. The profiles across the narrow direction of the beam are shown in Fig. 3. The solid dots are obtained from a Gaussian ($\pm$ 0.7°) in transverse velocity at the source, projected to the detectors. Similar results are found in the wide direction (across the source slots) where a half-width of 2.75° is measured. Angular broadening of the D^- beam relative to the initial beam is quite small.

The total predicted and measured currents are shown as a function of beam energy in Fig. 4. This global measurement is also in good agreement with prediction.

For purposes of scaling sources, we note that the compounds with highest conversion efficiency to D^- in the keV range are cesium, rubidium, and sodium; the conversion efficiencies are known.[9-11]

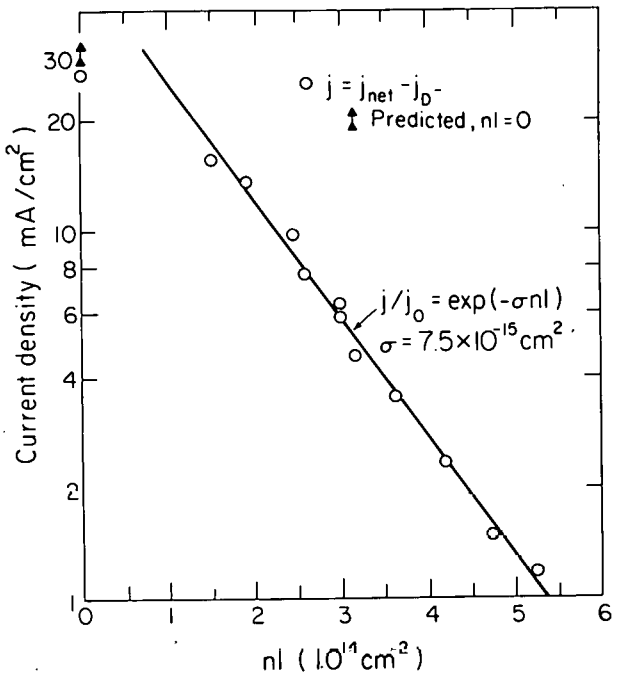

Fig. 1. Positive-ion current density (D^+ at 10.5, 5.3, and 3.5 keV originating in the positive-ion source) as a function of sodium line density. The discrepancy at low line densities probably originates from changing sodium axial profile. The decay corresponds to a cross section 7.5×10^{-15} cm^2; accurate measurements[9] yield $(6.1 \pm 1.5) \times 10^{-15}$ cm^2.

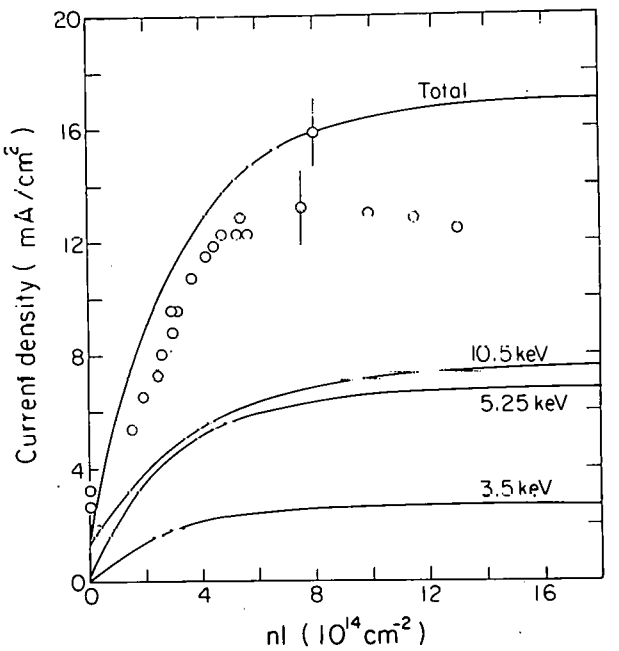

Fig. 2. Negative-ion (D^-) current density as a function of sodium line density. The error bars do not include uncertainties in the cross sections. Cross sections are from Refs. 9-11.

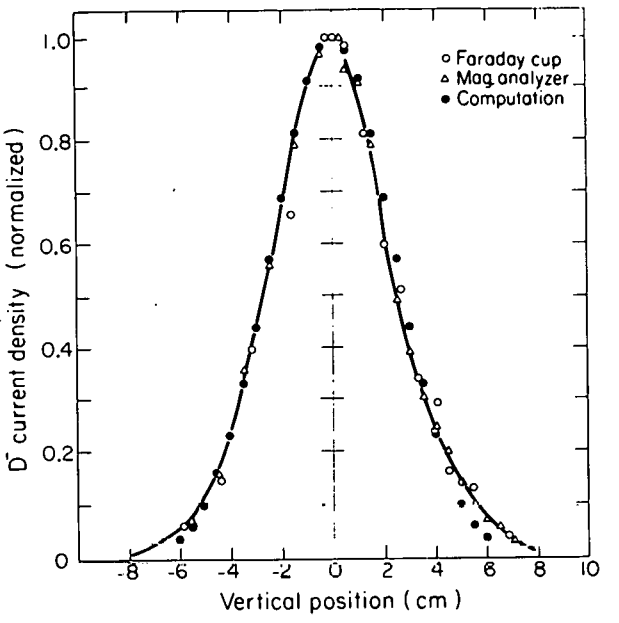

Fig. 3. Negative-ion current profile. Measurements were made with a Faraday cup and an analyzer using a magnetic field to ensure that there was no contribution from negative impurity ions.

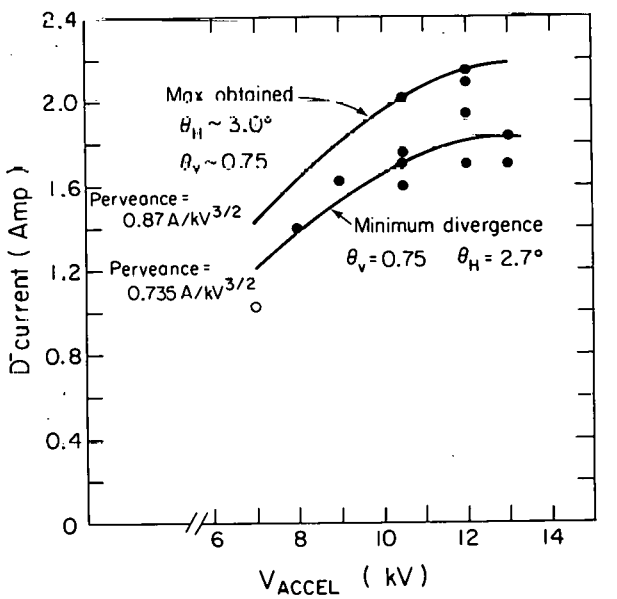

Fig. 4. Total D^- current. Measurements are compared with predictions for different positive-ion source operation.

The peak current density of negative ions which can be obtained in a charge-exchange system is[12]

$$j_- = F_-^\infty \frac{j_s A_s}{\pi} \left(\frac{180}{\pi L_f}\right)^2 \frac{1}{\theta_\parallel \theta_\perp} \qquad (1)$$

where F_-^∞ is the equilibrium fraction, j_s the current density at the source, A_s the source area, L_f the focal length of the source (both planes), and $\theta_\parallel$ and $\theta_\perp$ the half-widths of the current angular distribution. To good approximation[12], $\theta_\parallel = 2.1\ E_b^{-1/2}$ degrees and $\theta_\perp = 7.0\ E_b^{-1/2}$ degrees, with the initial positive-ion energy, E_b, in keV. Using the measured values[10,11,13] of F_-^∞, we obtain the prediction shown in Fig. 5, which also includes results from cesium[2,3] and sodium.[6-8] The measured results are slightly low because the beams contain fractional energies, whereas the calculation assumed only full-energy ions; nevertheless, the agreement is good.

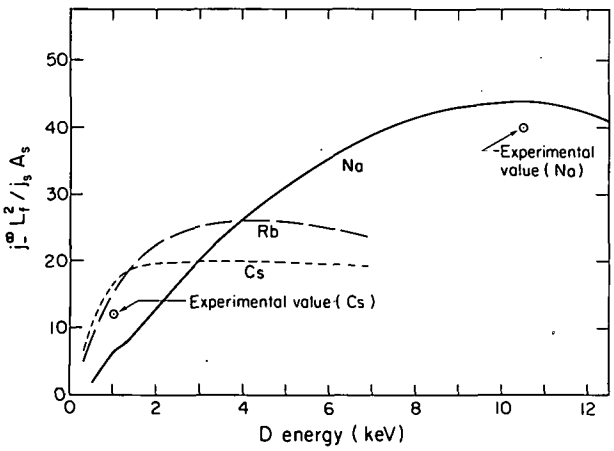

Fig. 5. Current density of D^- obtainable from a source focused in both directions. Experimental results are shown.

These experiments have several other important results. Recent work with charge-exchange jets has yielded excellent control of the metal vapor. We use our experiment as an example. Figure 6 shows the fall off of sodium density along the beam axis. Even better control is expected in future designs. Because of this drop in sodium density, the plasma density (measured by Langmuir probes) also drops rapidly along the axis as predicted by calculation.[14] Angular scattering during the beam formation is small even to energies as low as 1 keV.[7,8]

Extrapolation and Optimization[12]

Preliminary Considerations

The positive-ion source can be operated with some fraction of its current in molecular ions. Because the perveance of an accelerator is proportional to $(m_i)^{-1/2}$, with m_i the ion mass, whereas the ratio of the accelerator voltage to the energy per nucleus is proportional to m_i, the available current of nuclei for the positive-ion

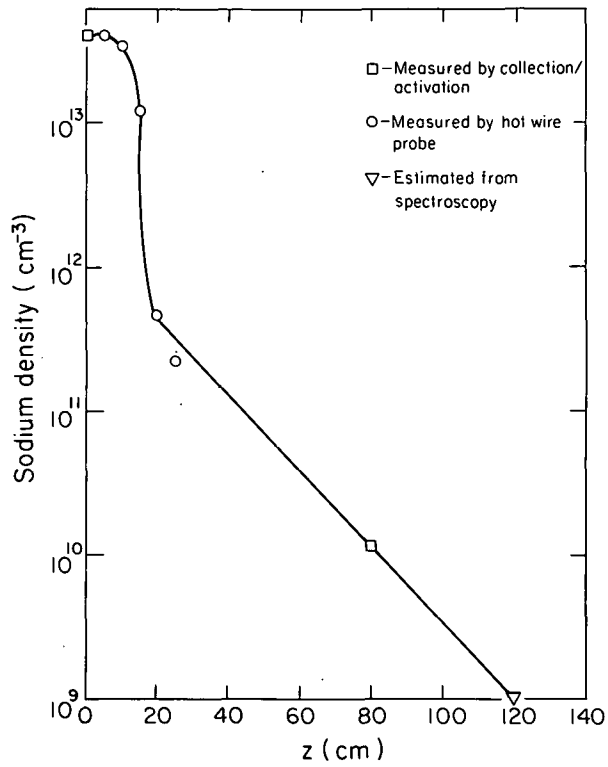

Fig. 6. Axial dependence of sodium density. Measurements were made with hot wire probes, with samples which were activated in a reactor, and with spectroscopy.

source can be increased by $(m_i)^{1/2}$. This can yield an increase in the current density of negative ions.

To utilize this current density, however, the molecular ions must be dissociated before conversion to negative ions. In both deuterium and charge-exchange vapors, a line density of about 10^{16} cm^{-2} is required for complete dissociation. The deuterium line density could be provided by a "neutralizer" tube downstream from the source, but: (a) the gas density in the source grid region is high, and (b) the neutralizer tube will be quite long, an estimated 80 cm, thus lengthening the system considerably. These penalties indicate that breakup of a large fraction of molecular ions in deuterium would be difficult to implement, especially in a dc system.

Alternatively, the charge-exchange medium can dissociate the molecules as was done in sodium by Semashko et al.[4,5] However, the H^- current produced from atomic deuterium reaches its full value at a line density of 10^{15} cm^{-2} to 2×10^{15} cm^{-2}, so that breakup implies 5-10 times more vapor flow than necessary to produce D^-. This excess vapor causes scatter in the D^- beam, more background plasma that can flow to the high voltage accelerator, larger losses of material from the charge-exchange region, and a larger inventory of material.

Because of these complications, we conclude that the use of molecular ions is unwarranted. It is best to design for a single-energy system, especially since present deuterium sources yield more than 75% D^+ in the initial beam at an energy cost of 0.9 keV per ion.[15] Contributions to the D^- current from molecular ions are useful but will not be included in the present analysis.

We assume that the negative-ion (post) accelerator is electrostatic in nature. One would like to work with a single large aperture in order to avoid losses due to incomplete grid transparency (typically 50%). In principle, a slot can be scaled to arbitrarily large currents by increasing its length; the optics of the resulting beam are unaffected. On the other hand, a circle cannot be increased to arbitrarily large radius. Therefore we chose to use a narrow slot.

The entrance geometry of an accelerator whose aperture is a long slot is approximately matched by the beam pattern of LBL ion sources.[15] The divergencies of the output particles create an elliptical current-density profile near and beyond the source focus if the grids are designed to focus the beam. However, analysis of an accelerator which accepts an elliptical profile is inherently three dimensional, and thus extremely difficult. In our design the accelerator is placed as near the source as possible and the beam focused in only one direction (the narrow width) to provide a long, slot-like beam. The beamlets from the wide ends of the source can be aimed inward to maximize the amount of beam with constant current density along the slot length.

The gas streaming from the positive-ion source must be pumped rapidly to minimize secondary effects within the source grid region, stripping of the negative ions once they are formed in the alkali-metal vapor, and generation of downstream plasma. The charge-exchange vapor assists in this situation by acting as a barrier to gas flow from the source region to downstream.[5,7,16] Thus most of the gas can be handled by a cryopump placed upstream of the charge-exchange jet. Gas which leaks through the jet and gas generated on surfaces downstream from the jet can be handled by additional cryopumping.

Condit[17] has pointed out that the binary and ternary alloys of the alkali metals[18] have very low melting points. An extreme example is an alloy consisting of 10.0 mole % Na, 47.5 mole % K, and 42.5 mole % Cs with a melting point of -73°C. At that temperature the vapor pressures are negligible, and even in less extreme alloys, vapor pressures of 10^{-9} Torr and below are common. Systems which would utilize these materials for liquid flow and extract the desired component for a vapor jet have yet to be developed, but it is clear that dc operation at low vapor pressures is possible for the candidate materials Cs, Rb, and Na.

System Design

For the "one-dimensional" (slot) design considered here, the peak current density at the accelerator aperture is

$$j_- = F_-^{\infty}\, j_s\, W_s (180/\pi\theta_{\parallel}\, L_f) \quad , \tag{2}$$

with W_s the width of the positive-ion source. The result is plotted in Fig. 7. Note that in this limit the current density is almost independent of energy; as total current is greater at low energy, the system optimum can be expected at low energy.

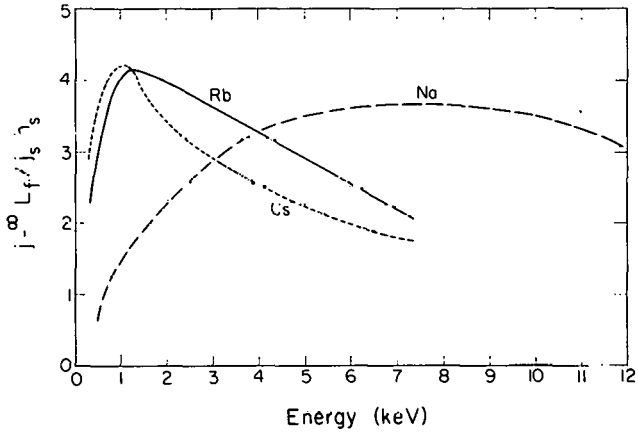

Fig. 7. Current density of D^- from a source focused in one direction.

Using the above conditions, the total current accepted in the accelerator is

$$I^- = F_-^{\infty}\, (j_s W_s l_a)\, \mathrm{erf}\left(\frac{45}{\pi}\frac{W_a}{L_f} E_b^{1/2}\right) \quad , \tag{3}$$

with W_a the accelerator width and l_a its length.

The geometry of the negative-ion source is constrained by the entrance aperture requirements of the accelerator. For a slot-type accelerator, the optics is determined by the "perveance per square", $P_s = jW_a/V^{3/2}$, with j the average current density and W_a the width of the entrance slot. Good optics have been obtained up to[19]

$$P_s^{max} = 1.6 \times 10^{-8}\ A - V^{-3/2}$$

$$= 5.1 \times 10^{-4}\ A - (kV)^{-3/2} \quad ,$$

for deuterium in an accel-decel system at 10 keV. For this design, the temperature of the ions injected with the acceleration causes only corrections to the divergence.

The perveance condition can be written as

$$\frac{l_a}{W_a} \geq \frac{1}{P_s^{max}} \frac{I^-}{V^{3/2}} \quad , \tag{4}$$

with I^- the total current and V the acceleration voltage. The condition to neglect end effects is

$$\frac{l_a}{W_a} \geq 10 \quad . \tag{5}$$

Condition (4) constrains the system first if

$$I^- > I_o = 10\ P_s^{max}\ V^{3/2} \quad . \tag{6}$$

Because of the angular divergence of the initial beam, the source is longer than the accelerator slot. The current density at the accelerator can be made uniform in the dimensions along the slot by choosing the source length l_s as

$$l_s = l_a + 2\alpha\ L_f\ \theta_l$$

$$= l_a + 2\alpha\ L_f(7\pi/180\ E^{1/2}) \quad . \tag{7}$$

The source is curved near its ends to focus those beamlets inward. Preliminary calculations indicate that $\alpha = 0.5$ is possible.

In the limit of high source energy, the initial beam is well focused. There is no need to make the argument of the error function in Eq. (3) greater than 1.5, at which point the function is 0.97. Thus, in the limit of large E_b, we set

$$W_a = \pi\ L_f/30\ E_b^{1/2} \quad . \tag{8}$$

The energy above which this is valid is found by combining the above equations:

$$\frac{F_-^\infty}{E_b^{1/2}} = \frac{30\ I^-}{0.97\ \pi\ j_s W_s L_f} \qquad I^- \leq I_o \quad , \tag{9a}$$

and

$$\frac{F_-^\infty}{E_b^{1/2}} = \frac{30\ P_s^{max}\ V^{3/2}}{0.97\ \pi\ j_s W_s L_f} \qquad I^- \geq I_o \quad . \tag{9b}$$

We consider numerical examples with V = 200 keV, $j_s = 0.15$ A/cm^2, 5 cm $\leq W_s \leq$ 10 cm, L_f = 250 cm and I^- = 5 A, 10 A, and 20 A. The high energy approximation is valid for:

$E_b \geq 12.0$ keV $I^- = 5.0$ A

$E_b \geq 8.5$ keV $I^- = 10.0$ A

$E_b \geq 6.2$ keV $I^- = 14.4$ A

At lower initial beam energies the appropriate limiting condition must be included. There are essentially two options: (a) Reduce $j_s W_s$, thus reducing the current density into the accelerator and compensating by lengthening the source and accelerator. To the extent that it can be done by reducing W_s, this will lead to a minimum area of the source. (b) Reduce W_a while keeping the current density as high as possible but reducing the current accepted into the accelerator per unit length. This will lead to a design of minimum length. One could, of course, design a system between these limits.

Consider the results for the three different currents:

(a) I^- = 5 A. The system is constrained at all energies by the condition $l_a/W_a \geq 10$. The design for minimum l_a has a weak minimum at 6-8 keV (sodium operation), whereas that for minimum area has a weak minimum at 3 keV (rubidium operation), as seen in Fig. 8. The minima are quite shallow, however, and considerations such as ease of handling the particular charge-exchange vapor could be dominant.

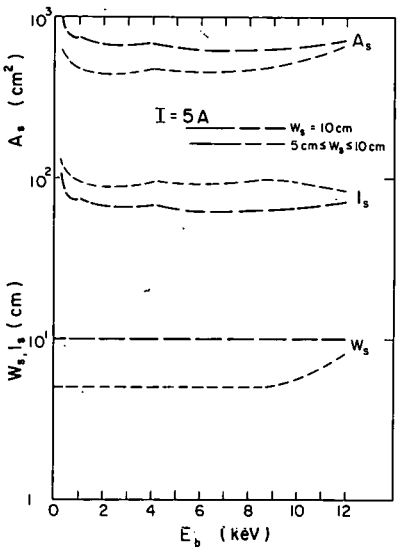

Fig. 8. Source area, length and width for 5 A of D^- at a final energy of 200 keV, as a function of initial beam energy.

(b) I^- = 10 A. Here the system is limited by available current at energies $\geq$ 8.8 keV and by $l_a/W_a \geq 10$ at lower energies. The design for minimum l_a has a weak minimum at about 2.5 keV (rubidium), but the results are almost independent of energy; as shown in Fig. 9. The design for minimum area, on the other hand, has a pronounced minimum at 1.5-2 keV (rubidium).

(c) I^- = 20 A. The system is limited by available current above 6.2 keV and by the accelerator perveance at lower energies. The minimum-length design has a definite minimum at 1.5-2 keV (rubidium) and that for minimum area optimizes at 1-1.5 keV (cesium or rubidium) as shown in Fig. 10.

These designs are far from voltage holding limits. The fields in the accelerator are comparable to those in a Child-Langmuir design; at 0.02 A/cm^2 and 200 kV, the field is only 15 kV/cm.

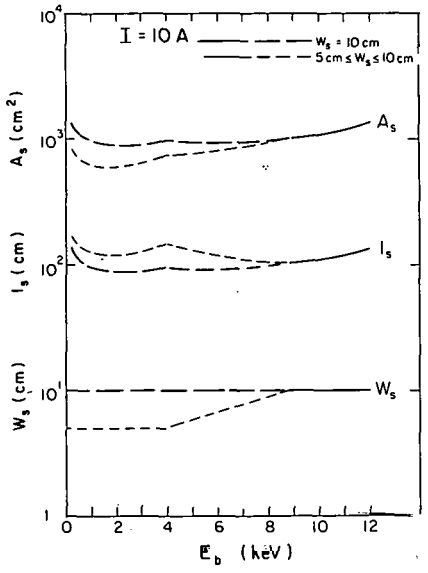

Fig. 9. Source area, length, and width for 10 A of D^-.

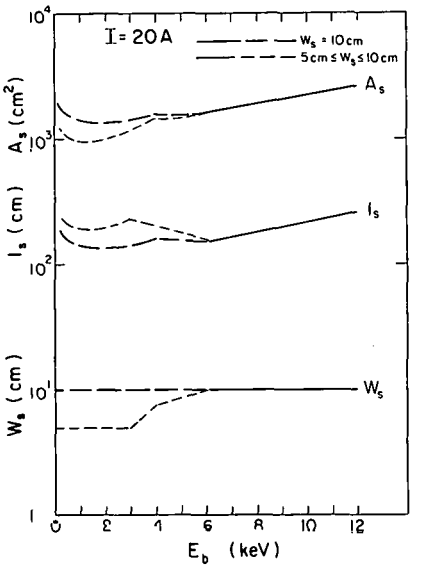

Fig. 10. Source area, length, and width for 20 A of D^-.

The beam parameters for a 20 A D^- beam are summarized in the two limits in Table 1.

Note that the energy cost per ion is quite small (6.4-9 keV) in all cases, so that the electrical efficiency of a final system can be quite large. Pumping calculations (not given here) show that the gas flow can be handled by cryogenic pumps in the region between the positive-ion source and the charge-exchange jet. It is clear that the beam angular divergence is large enough that considerable D^- current is missing the accelerator in both cases. To take more advantage of the high production at low energies, there are four options:

(a) Decrease L_f, minimizing angular divergence. However, as the acceleration is perveance limited at the design energy, this will not significantly reduce the accelerator length.

(b) Learn how to relax the constraints on a single-slot system.

(c) Use a multi-aperture system for the the accelerator. The utilization of available current at low energies is low enough that competitive multi-aperture sources may be possible.

(d) Operate at higher (>200 keV) final energies.

Table 1. Designs for a 20 A, D^- source for injection into a 200-kV accelerator.

	Minimum length design		Minimum area design	
	D^+ source	D^- beam	D^+ source	D^- beam
Accelerator dimensions	10 cm x 134 cm ($1340\ cm^2$)	7.9 cm x 110 cm ($870\ cm^2$)	5 cm x 190 cm ($950\ cm^2$)	11.6 cm x 160 cm ($1860\ cm^2$)
Beam energy	1.5 keV	1.5 keV	1.5 keV	1.5 keV
Current	200 A	20 A	143 A	20 A
Average current density	150 mA/cm^2	23 mA/cm^2	150 mA/cm^2	11 mA/cm^2
Peak current density	300 mA/cm^2	26 mA/cm^2	300 mA/cm^2	14 mA/cm^2
F_-^∞ (Rubidium)	-	21.5%	-	21.5%
Net conversion efficiency	-	10%	-	14%
Energy cost/ion	0.9 keV	22.5 keV	0.9 keV	15.6 keV
Gas efficiency	35%	3.5%	35%	4.9%

These options will not be explored further here, but should be considered in future development efforts.

Conclusions

We have described experiments that produced H^- and D^- beams by charge exchange in alkali metals. The results can be predicted accurately from knowledge of the initial (positive ion) source parameters and of pertinent atomic cross sections. This then permits interpolation of the results to energies in the range 1.0-12 keV.

Given these interpolations, systems for fixed final negative currents are considered. The characteristics of the sources are calculated as a function of source dimensions, and examples given. Optimum systems will operate with an initial energy of 1.5-2 keV and use rubidium as the charge-exchange medium. Detailed engineering considerations are outside the present analysis.

Acknowledgments

We wish to thank R. V. Pyle and the members of the LBL Neutral Beam Group for their hospitality during the course of this work.

References

1. J.E. Osher, F.J. Gordon, and G.W. Hamilton, Proc. 2nd Int. Ion Source Conf., Vienna, 1972.

2. P. Poulsen, O.A. Anderson, E.B. Hooper, Jr., T.J. Orzechowski, and R.J. Turnbull, Proc. 7th Symp. Eng. Prob. Fusion Research, (1977), p. 1408.

3. E.B. Hooper, Jr., O.A. Anderson, T.J. Orzechowski, and P. Poulsen, Proc. Symp. Prod. and Neut. Negative Hydrogen Ions and Beams, Brookhaven, 1977, K. Prelec, Editor, p. 163.

4. N.N. Semashko, V.V. Kusnetsov, and A.I. Krylov, Proc. Symp. and Neut. of Negative Hydrogen Ions and Beams, Brookhaven, 1977, K. Prelec, Editor, p. 170.

5. N.N. Semashko, V.V. Kuznetsov, and A.I. Krylov, Proc. 8th Symp. Eng. Prob. Fusion Research, (1979).

6. P. Poulsen and E.B. Hooper, Jr., Proc. 8th Symp. Eng. Prob. Fusion Research, (1979).

7. E.B. Hooper, Jr., P. Poulsen, P.A. Pincosy, O.A. Anderson, and T.J. Duffy, Lawrence Berkeley Laboratory Report LBL-10454 (1980).

8. E.B. Hooper, Jr., P. Poulsen, and P.A. Pincosy, to be published.

9. A.M. Howald, L.W. Anderson, and C.C. Lin, Bull. Am. Phys. Soc. 24, 1186 (1979).

10. A.S. Schlachter, K.R. Stalder, and J.W. Stearns, Proc. 10th Int. Conf. Phys. Elec. and Atomic Coll., Paris, 1977, p. 870.

11. C.J. Anderson, A.M. Howald, and L.W. Anderson, Nucl. Instr. Meth. 165, 583 (1979).

12. E.B. Hooper, Jr. and P. Poulsen, to be published.

13. A.S. Schlachter, K.R. Stalder, and J.W. Stearns, submitted to Phys. Rev. A.

14. E.B. Hooper, Jr., O.A. Anderson, and P.A. Willmann, Phys. Fluids 22, 2334 (1979).

15. K.H. Berkner, C.F. Burrell, W.S. Cooper, K.W. Ehlers, A.F. Lietzke, H.M. Ohren, J.A. Paterson, R.V. Pyle, and J.W. Stearns, IEEE 8th Symp. Eng. Prob. Fusion Research, 1979.

16. O.A. Anderson, Lawrence Livermore Laboratory Report UCID-16914 (1975).

17. R. Condit, private communication.

18. M. Hansen and K. Anderko, Constitution of Binary Alloys (McGraw-Hill, N.Y., 1958).

19. O.A. Anderson in Ref. 7.

DISCUSSION

JACQUOT You observe a small decrease of the current density when the line density in the sodium is greater than 10^{15}. Do you think that this is due to a destruction by the sodium plasma?

HOOPER I do not believe so, we were never quite certain whether it was real or not. It was within the instrumental uncertainties, which is one of the reasons I would have liked to have gone to even higher densities. As far as I could tell it was not due to plasma or due to angular scattering.

CRANDALL Do you know what is happening at Kurchatov?

HOOPER I have heard nothing from them since last fall and I do not think anybody has, as far as I know. Perhaps Dr. Geller?

GELLER They do not work presently on the beam line.

FORRESTER I did not exactly get what you envisioned as post acceleration.

HOOPER In the model I have assumed a single slot with a width which has been adjusted in order to accept as much of the beam as the accelerator can handle and with a length that is at least 10 times the width in order that it behaves like a slot. So depending upon the current that you are working with, it might be a meter long or

more than that. Now the point I want to make is that if you go to energies below about 1.5 keV that I described as a sort of optimum (which put you in rubidium where, as far as I know, nobody has really worked before) than in order to get the beam into a 200 keV accelerator, you would have to throw away more than half of the beam. Now if the acceleration voltage were greater than 200 keV you could accept more current because then your perveance would permit you to handle a larger current density at the entrance to the accelerator. If you are only going to something like 200 keV, I suspect that a better system at lower energies would use a multi-aperture source, but then you have to throw away roughly 40-50% of the beam.

HAGENA In your optimization, with the result that you go to 1.5 keV, did you have space charge limitation of the incident positive ion beam?

HOOPER We assumed that the initial positive ion beam was the maximum you could obtain. However, when you went to the higher currents you found that under certain conditions you had to reduce the size of that source because you are putting more current into the accelerator than you could handle. So in fact we either drop the current density in the positive ion beam or reduce the length of the slots to reduce the total current of the high voltage accelerator.

HAGENA In your last table, there was a net conversion efficiency of, I think 14% and the gas efficiency was only 5%; could you explain the difference?

HOOPER Well, to get the gas efficiency you have to take into account the initial gas efficiency of the positive ion source. One thing I did not mention is, that we measured the transmission of gas through the charge exchange vapor jet because as Oscar Anderson and the people of Kurchatov have proposed some time ago, the vapor acts as a very good block to the flow of gas from your positive ion source to the beam line. In fact, for our conditions operating at a line density of 1.5×10^{15}, we found that there was a factor of 50 reduction in the conductance of the beam line so the gas is very well confined up in the positive ion region of your beam line where it can be pumped without damaging the region where you have negative ions.

DOLIQUE Did you measure the Na^+ ion flowing downstream?

HOOPER We did not separate the Na^+ from any D^+. What we did measure was the plasma density downstream and once you got about a meter downstream it was in good agreement with what we predicted from the deuterium background gas pressure. I can not say for certain that it did not contain a large fraction of Na^+ but the plasma density was down by several orders of magnitude from the density in the sodium cell itself.

TSAI Could you give us an impression on the size of this 20 A source?

HOOPER It would be quite large, and this is one of the reasons why people have been worried about using this in an actual system. The D^+ source, for this particular design and current density, would have an average height of 5 cm and almost 2 meters long. The D^- beam at the entrance of your accelerator is then approximately $11\frac{1}{2} \times 160$ cm long.

PRODUCTION OF D^- IONS BY DOUBLE CHARGE EXCHANGE OF D^+ ON CESIUM

M. Delaunay, J.L. Foucher, R. Geller, C. Jacquot, P. Ludwig,
F. Mazhari, E. Ricard, J.C. Rocco, P. Sermet, F. Zadworny
Association EURATOM-CEA
Département de Recherches sur la Fusion Contrôlée
Service IGn - Centre d'Etudes Nucléaires
85 X - 38041 GRENOBLE CEDEX (France)

Abstract

A D^- beam immersed in a high uniform magnetic field has been produced by a double charge exchange of D^+ in a supersonic cesium target. The average D^- current density is 10-12 mA/cm^2 with a pulse duration of 1 s. With a beam of 750 mA of D^+ a total D^- current of 160 mA at 1 keV is obtained. The physics of the production and destruction of D^- will be discussed later.

Introduction

An alternative method to generate high energetic neutral beams ($\geq$ 200 keV) for additionnal heating in thermonuclear fusion reactors is the production and the acceleration of negative deuterium ions, with which monoenergetic neutral beams are established. There are various methods to produce an intense negative ion beam ; among which the double charge exchange of D^+ ions on an alcali target (Cs, Na) is of the greatest interest for its productibility of D^- ions beams in d-c operation. The main difficulty with this method is getting an intense negative ion current density ($\sim$ 10 mA/cm^2) with the minimum power consumption in the source, and also a better gas efficiency. In addition, the electrons should not be accelerated with the D^- ions and the background pressure in the accelerator must be kept very low ($\sim 10^{-5}$ Torr). Generally with deuterons passing through the cesium metal vapor one obtains the largest equilibrium yield (Fig. 1). Nonetheless, the designers of negative ion sources who use the double charge exchange method prefer a sodium metal target, where the transportation of D_0 neutral in the energy range of 10 keV is easier [1][2]. Indeed, the neutrals created near the positive ion source extraction, are far from the alcali target and have a lowest divergence angle ($\theta \sim (E_b)^{-1/2}$). Consequently, the D^- current density is sufficient for application of high energetic neutral injectors. However, the power density and the gas pressure in the positive arc ion source has to be enhanced as a consequence of which the d-c production of D^- ions create difficulties. The goal of our D^- production project is to use the cesium as charge exchange target in order to decrease the thermal difficulties of a d-c production of negative ions. But, one has to develop a new technic in order to avoid unwanted divergence of low energetic particles in the 1 keV energy range [3].

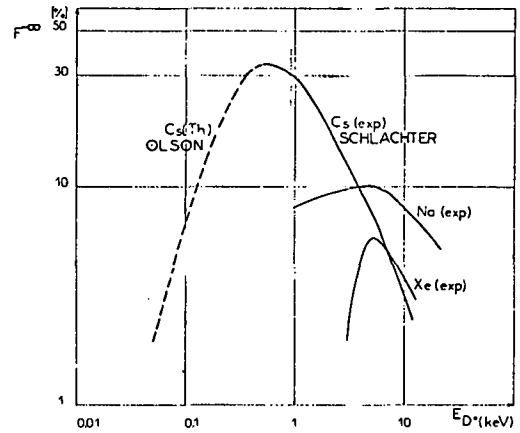

Fig. 1- D^- conversion factor versus neutral energy

Theoretical aspects of the new technic

In general, to enhance the D^- current density at low energy (1 keV) with a minimum D^+ current density, it is absolutely necessary to minimize the path of transportation of the low energetic neutrals. In the classical double charge exchange method (Fig. 2a), the neutrals are not only produced in the alcali target, but are also created near the positive ion source extractor by charge exchange on the background gas. As the D_0 atoms diverge far from the alcali target with an angle proportional to $(E_b)^{-1/2}$, the neutrals current density decreases along the axis according to the formula :

$$j_{D_0} \propto j_{D^+} E_b \qquad \text{where :}$$

E_b is the D^+ energy and j_{D^+} is the D^+ current density.
Furthermore the D^- current density created in the target diverges with the same angle. In this case at the entrance of the accelerator the D^- current density is not sufficient to built a neutral injector based on negative ions acceleration.

In our experiment, we have avoided these difficulties by following the conditions (Fig. 2b) 1) the background gas pressure (deuterium and cesium) has to stay low ($< 10^{-4}$ Torr) such that a few percent of D^+ ions are converted into D_0 in

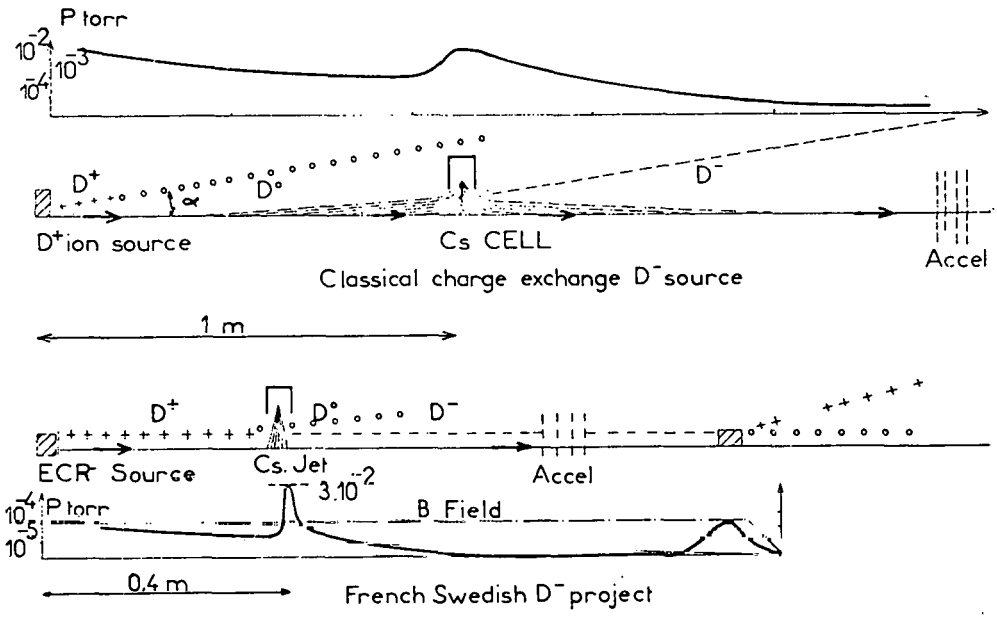

Fig. 2- Classical charge exchange D^- source and French Swedish project

the drift space of the D^+ ions (40 cm).
2) the width of the cesium target must be narrow and dense so that the D_0 path is minimized (few cm) before the conversion of D^- ions.

The first condition is achieved with high gas efficiency in the source using the mechanism of electron cyclotron resonance to produce the plasma [4]. A better gas efficiency and therefore, a low background pressure less than 10^{-4} Torr are obtained in the ion extraction region. The charge exchange of D^+ is almost canceled. The low background pressure is sufficient to get a good space charge compensation of the D^+ beam if the positive ion beam is immersed in a uniform magnetic field. The contribution of the B field is such that the electrons produced by ionization of the background gas are being confined radially. Then, the plasma density is determined by the parallel diffusion rate. The minimum neutral density is decreased in order to give a value according to the formula

$$N_o = \frac{V_s^+}{\sigma_i V_f^+ z}$$

where V_s^+ is the velocity of the slow particles.
V_f^+ is the velocity of the fast D^+ or D_0 particles,
σ_i is the ionization cross-section.
z is the distance along the axis.

As an example : at 1 keV and z = 40 cm, the minimum critical pressure is 10^{-4} Torr.

With a good space compensation of the D^+ beam in the drift space, the ionic current density immersed in the B field is kept constant. Indeed, if one considers a thermal positive ion beam with a radial distribution of perpendicular energy at the extraction, and a uniform radial density totally immersed in a high B field, then the radial profile of the positive ion beam can be calculated by the relationship [5] :

$$J(r) = \frac{J_{D^+}}{2}\left[1 + \mathrm{erf}\left(\frac{r_b - r}{2\rho_L}\right)\right]$$

where J_{D^+} is the emission current density assumed uniform.
r_b is the beam radius.
ρ_L is the Larmor radius : $\frac{m \langle V_L \rangle}{eB}$

The important parameter which determines a good transportation of the positive beam is

$$\frac{r_b}{2\rho_L}.$$

If this parameter is greater than 1, the current density profile is kept roughly constant at a great distance from the ion source. In our case, the perpendicular velocity of the positive ions corresponds to a maximum half angle of 10° at 1 keV for the neutrals. Then the value of the parameter $\frac{r_b}{2\rho_L}$ is roughly 5 for r_b = 2 cm. The D^+ beam is well collimated in the uniform B field and a small part

of the D^+ ions converted into neutrals (< 10 %) are lost by a diverging effect.
The divergence half angle for these neutrals is given by :

$$\tan \alpha = \frac{V_\perp}{V_{//}} = 10° \text{ at } 1 \text{ keV}.$$

Then the charge exchange target for the conversion of D^+ into D^- should be very narrow. However, the direct conversion of D^+ into D^- is negligible ; therefore the production of D^- is obtained by D_0 charge exchange on cesium. The mean free path of D_0 should be minimized (1 - 2 cm).
Therefore $n_{cs} \geq (\lambda \sigma_{0^-})^{-1}$ where

λ is 2 cm in this example.

σ_{0^-} is the cross-section to produce D^- from D_0 ($4.10^{-16} cm^2$).

Getting $n_{cs} \geq 10^{15}$ at/cm^3.

Thus the main parameters of the cesium target are a density of 10^{15} at/cm^3 and a width of 2 cm. At the exit of the target the D^- are confined in the magnetic field and the current density is kept constant. These two conditions are summarized in Fig. 3. The experimental cesium profile is gaussian. Under these conditions, the D_0 mean free path is small and consequently the D_0 divergence effect is negligeable. The enlargment of the D^- beam size is 10 % of the D^+ beam size.
The consequence of the totally immersed, low energy

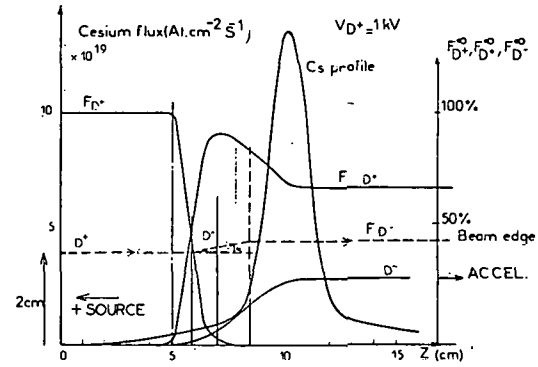

Fig. 3- D^0, D^- conversion in the cesium target along the axis.

D^- ions in a high uniform B field is, that one has to maintain the magnetic field in the D^- accelerator. In order to avoid an azimutal rotation of the beam. The magnetic field is cancelled after the neutralization of the high energetic D^- (Fig. 2b).

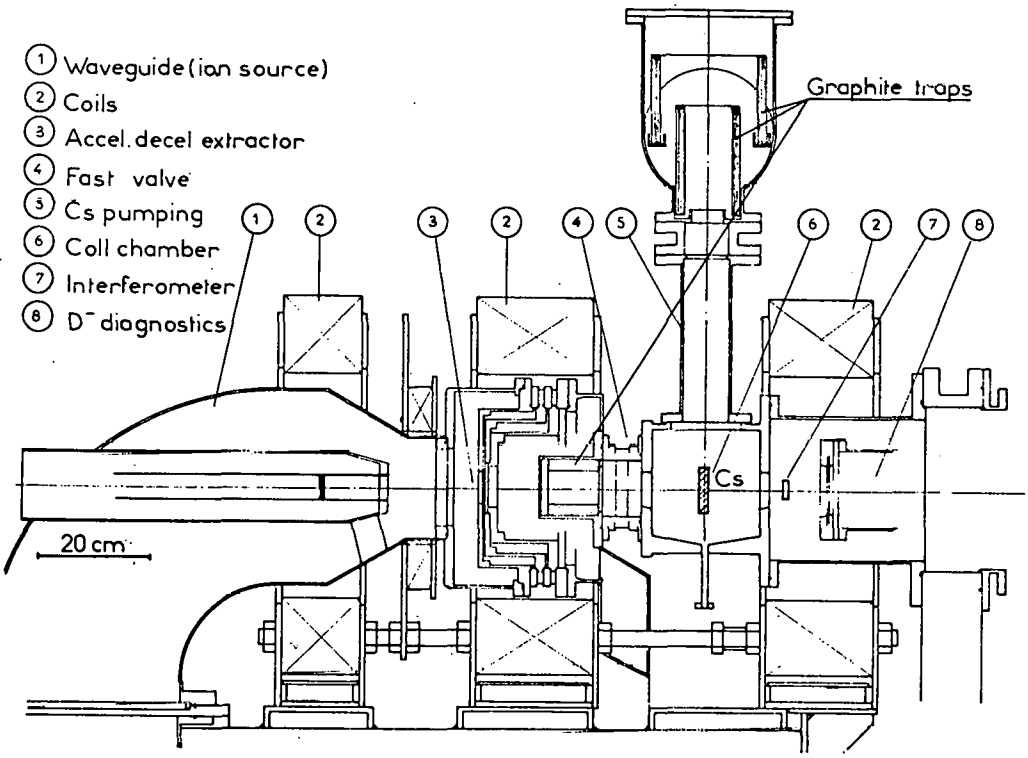

Fig. 4- Schematic view of the D^- source

Experimental Device

Fig. 4 is a schematic sketch of the double charge exchange D^- source. The two main elements of this apparatus are the following :

1) The positive ion source of the electron cyclotron resonance model [4] has a positive voltage (1 to 2 kV). The extractor is a classical accel. decel. system with slots. The acceleration voltage depends on the D^+ current density, to optimize the perveance the voltage range should be of the order of - 1 KV to - 4 KV. The total beam size is 16 cm^2. A d-c current of 2A of positive ions can be extracted from the source with 2 KW of RF power at 10 GHz. The average source pressure is 6.10^{-4} Torr D_2 ; and the maximum current density is 120 mA/cm^2. The last electrode (decel. electrode) is grounded. The background pressure in the drift space immersed in a uniform B field is less than 10^{-4} Torr. A graphite trap is located between the positive ion source and the collision chamber, where it pumps the parasite Cs flux and shapes the initial D^+ beam. A fast shutter valve separates the collision chamber from the ion source, and is located at 25 cm from the electrodes. A d-c current of 1.3 A of D^+ ions with the best performance is transmitted through the collision chamber. The maximum average density is 80-90 mA/cm^2 and the energy range is 1-2 keV.

2) The cesium target must be narrow and dense. These conditions has been provided by building a high density cesium supersonic jet at high Mach number (10-20).

The supersonic jet of cesium has been built in collaboration with Ecole Polytechnique (6), and it is located at 40 cm from the source. This supersonic jet is made by the expansion of a thermal cesium vapor through a Laval nozzle and a cooled skimmer. The cesium is contained in a boiler (T_{Max} = 650°C) and two condensers collected the cesium vapor. The maximum mass flow of cesium through the nozzle is high (few g/s). A recirculating system with a magnetohydrodynamic pump, valves and a level detector was used. Hence, the stability of the jet was established. At the optimum target thickness (2.10^{15} at/cm) the jet profile is quasi gaussian with a 2 cm half width and a maximum flux of cesium atoms of 1.4 10^{20} $at/cm^2/s$. The line density can be regulated from 0.8 to 3.5 10^{15} at/cm^2 by adjusting the boiler temperature. The profile exhibits a symmetrical form. The wings on each side are measured. These wings are probably due to an increase of the temperature in the skimmer. They also corresponds to a small flux of cesium which escapes along the axis of the beam and it is trapped in the graphite. In this case less than 10^{15} $at/cm^2/s$ flows into the positive ion source extractor.

Different diagnostics were used to verify the D^+, D^-, D_o beams characteristics and the cesium plasma parameters. In particular, by means of interferometry and Langmuir probes the plasma density and temperature were estimated.

The spatial profile of the energetic particles (D^+, D_o, D^-) (7) was obtained by using a high sensitive calorimeter composed of thermal transductors associated with a minicomputer. In this part of experiment, the acceleration of D^- is not being considered, so the energy of the negative ions is the energy of the positive beam.

Experimental Results

By keeping constant the potential of the positive ion source and the D^+ current, the D^- ion current is measured for differents cesium target pressures in the line density range of 0.8 - 3.5 10^{15} at/cm^2 The range of the positive ion current is 200-750 mA and the differents D^+ energy range is 1-2 keV. As an example a typical result is shown for the total incident D^+ current in the collision chamber of 0.6 A (Fig. 5).

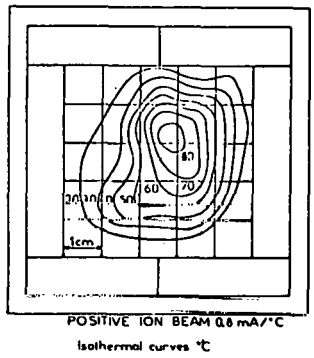

Fig. 5- D^+ spatial distribution

The pulse length is 1 s and the D^+ energy is 1 keV There are no neutrals signal detected on the calorimeter. The radial distribution is not exactly the same for the parallel and perpendicular plane of the extraction slots. By changing the line density of the cesium target, the D_o atoms are produced in the collision chamber. Due to their initial perpendicular velocity, they produce a uniform background signal corresponding to 15-20 % D^+ ions (Fig. 6).

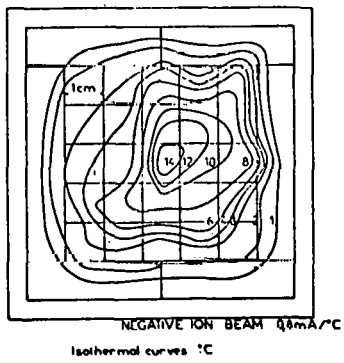

Fig. 6- (D^-+D_o) spatial distribution

The radial profiles are determined from the isothermal level curves (Fig. 7 and 8) and for the case of $1.5.10^{15}$ at/cm^2 line density. One can compare the D^+ and the $D^-(\eta^-)^{-1}$ profile (η^- is the conversion factor for the charge exchange D^+, D^-). The following conclusions were achieved : the profile of the beams were roughly the same with the exception that the halfwidth of the D^- was

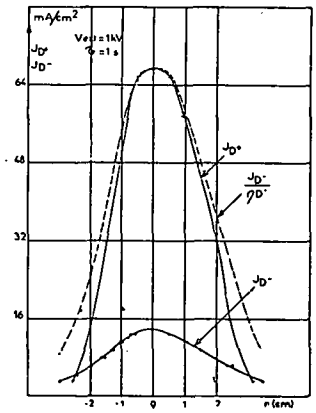

Fig. 7- D^+ and D^- radial profile parallel to the slots.

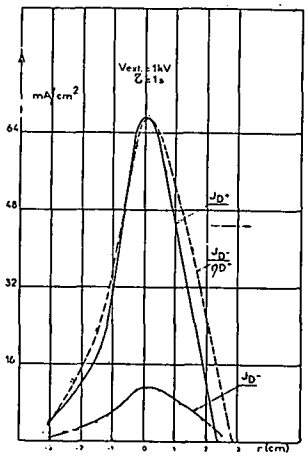

Fig. 8- D^+ and D^- radial profile perpendicular to the slots.

slighly greater than the D^+ profile. The small increase in the halfwidth is due to the divergence of the neutrals within the short distance in the supersonic jet before the trapping of D^- ions in the magnetic field. The peak D^- current density is 14 mA/cm^2 (D^+ peak current density 64 mA/cm^2), and the average D^- current density is 10 mA/cm^2 in 9 cm^2. The total D^- current is 160 mA, and the average conversion factor ηD^- at 1 keV is 22 % ± 2 % Instabilities are not observed during the one second pulse duration. For the optimum line density of the cesium target, the plasma density in front of the diagnostics is 2-3 10^{11} cm^{-3} with T_e < 1 eV. Fig. 9 shows the production of the D^- current and the average D^- current density for the two different values of the D^+ energies (1-2 keV) versus the D^+ current and also the optimum line density of the cesium target is of the order of 1.5.10^{15} at/cm^2. The maximum D^- current detected is 160 mA (750 mA of D^+ current) at 1 keV. At 2 keV, for 0.8 A of D^+ current, a D^- current of 115 mA is measured ; the explanations regarding the D^- current limitation will be given later. The average current density at 1 keV is roughly linear with the D^+ current and maximum of 12 mA/cm^2 average D^- current density could be obtained with 1 A of D^+.

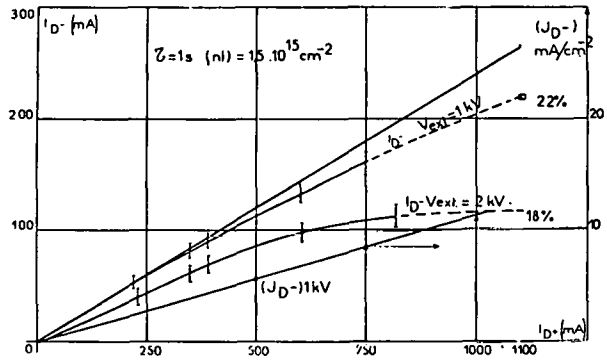

Fig. 9- D^- current and D^- current density versus D^+ current.

The ηD^- conversion factor at the optimum target thickness of 1.5.10^{15} at/cm^2 is 18 % for 2 keV and 22 % at 1 keV D^+ energy. For a given positive ion energy (1 keV) and a D^+ current of 0.5 A, the ηD^- conversion factor were obtained for different line densities in the explored range (0.8 - 3.5 10^{15} at/cm^2) (Fig. 10).

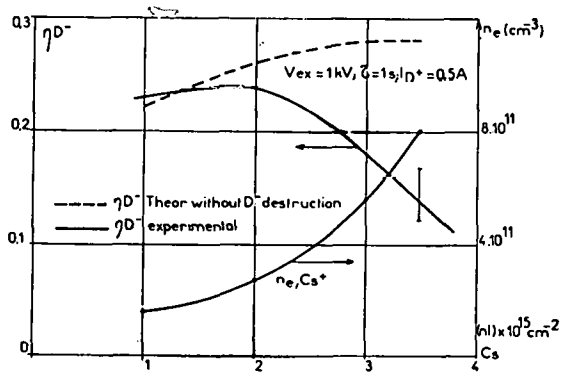

Fig. 10- ηD^- conversion factor versus the cesium line density.

The data indicates an optimum target thickness (1.5 10^{15} at/cm^2) for which the ηD^- reaches a maximum value of 22 %. At the wider target thickness ηD^- decreases by a factor of 2 for the ultimate target thickness of 3.5.10^{15} at/cm^2. The expected ηD^- linear model without any destruction of the D^- ions is plotted on the same graph. This is in agreement with the small line densities but not for the thick targets. Moreover, the cesium plasma density plotted against the line density exhibits a large increase with the neutral cesium pressure. The same behaviour was observed when the D^+ current or the positive ion energy were increased. As an

example at 2 keV, the D^- current limitations were observed whenever the D^+ current in the target was increased (Fig. 9). In this case, the probability of ionization of the cesium gas is greater at 2 keV D^+ than 1 keV D^+ and also the plasma density is greater for the same D^+ current.

Discussion

Different results could be drawn from the experimental data. First of all, for a given D^+ current value, Fig. 10 exhibits an optimum cesium line density ($<nl> = 1.5.10^{15}$ at/cm^2) where the conversion factor is maximum ($\eta D^- = 22$ % at 1 keV). According to the measurements, an estimated relative error of ηD^- is about 2 %. Therefore in the vicinity of the optimum target thickness a fair agreement exits between the ηD^- and the conversion efficiency obtained from the linear model. Where, on the other hand for large target thickness, the values of ηD^- are not satisfactory and the theory of the linear model without D^- destruction is not functionable. Different physical reasons are responsible for the decreasing of the value of ηD^-. Firstly, for a large line density, the geometry of the cesium jet could deteriorate as a consequence of which the flight distance of the D_0 becomes larger. The divergence and the scattering on the cesium are responsible for a decrease of the D^- current density. But this effect is small and does not explain the large discrepancy for the wide target thickness. According to a large plasma density growing with the cesium line density, it seems that the cesium plasma is the main factor responsible for the D^- destruction mechanism. The different reactions of destruction could be :

the mutual neutralization $D^- + Cs^+ \rightarrow D_0 + Cs$

the electronic detachment $D^- + e \rightarrow D_0 + 2e$

the three body recombination with an high cesium pressure : $D^- + Cs^+ + Cs \rightarrow D_0 + 2\,Cs$

The cross-section in the first reaction is large and the electronic temperature of the cesium plasma is an important parameter in determining the electrons contribution to the D^- detachment. The increasing of the plasma density shows that the electrons could be the main factor of the cesium ionization mechanism and dominate at high neutral pressure the ionization of the fast particles (D^+ or D^-). On the other hand, the excitation mechanism contributes to change the ionization rate by electrons. From the experimental data, preliminary theoretical interpretations are suggested :

A first theoretical approach taking into account the axial and radial diffusion of the cesium plasma in a cesium cell gives the following conclusions : for an electronic temperature of 0.3 eV, the final ηD^- is 8 % for a cesium neutral profile:

$nCs = 2.8\ 10^{15}(\exp -0.7\ z^2)$ [8] (Fig. 11).

Far from the cell the plasma density is 10^{12} cm^{-3} which is comparable to the experimental value. The Cs^+ velocity towards the positive ion source is high and low in the opposite direction. A second theoretical model bi-dimensional count the effect of a flow velocity for the cesium jet (Fig. 12). The mean flow velocity is 520 m/s and the profile is gaussian. For the same electronic temperature ($T_e = 0.3$ eV) the ηD^- conversion factor decreases slowly along the axis (28 % to

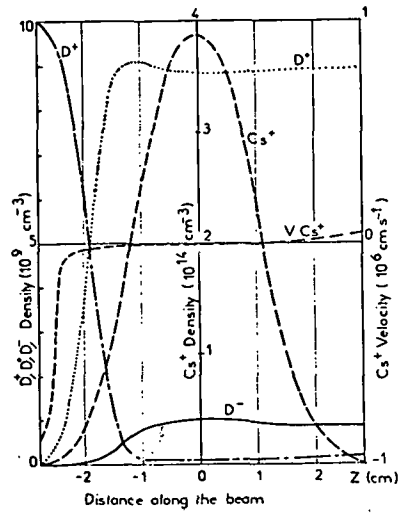

Fig. 11- Cesium cell model with longitudinal and transverse diffusion.

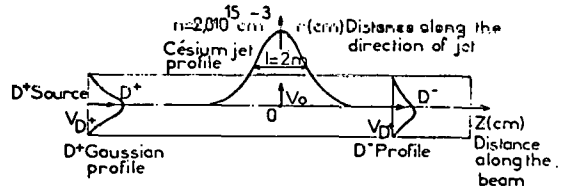

Fig. 12- Jet model geometry

19 %) (Fig. 13). In this model, the divergence of the D_0 atoms is not taken into account. Because the Cs^+ ions have a mean flow velocity, consequently the radial D^- profile is a little bit out of the mean axis of the D^+ beam. All these models are based on different hypotheses for the electronic

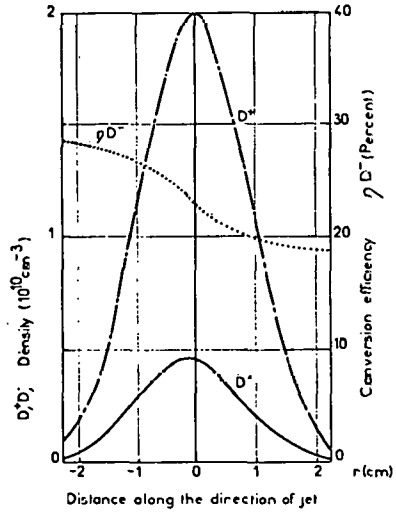

Fig. 13- Cesium jet model

temperature and cross-section. In order to understand which of fundamental parameters in the plasma are dominant a further speculation of the experimental plasma measurements in the jet is necessary (for example : spectroscopic measurements).

Secondly, up to now an important limitation to produce more D^- current density, is the maximum D^+ current density injected in the cesium target. To increase the positive current density for a given D^+ energy, it is necessary to increase the voltage of the accel electrode to maintain the optimum of perveance. As the cesium plasma density is not negligible, the Cs^+ current on this electrode is also high and therefore the secondary electrons emission occurs whenever the accel voltage is greater than 2 kV. These secondary electrons are responsible for the breakdowns in the accel gap and they limit the pulse duration, they produce also a larger plasma density. Different solutions will be envisaged to overcome this difficulty (magnetic trap or new electrode configuration).

Conclusion

The observed conversion efficiency to negative ions is 18 % at 2 KV and 22 % at 1 KV for an optimum target thickness of $1.5\ 10^{15}$ at/cm^2. For the optimum conditions, a 160 mA D^- current is obtained with 750 mA of D^+ incident on the target with a time duration of 1 s. The average D^- current density is 12 mA/cm^2 and a total surface of 9 cm^2. The peak current density is 14 mA/cm^2. For high D^+ current, breakdown limitations occurs due to secondary electrons emission. Overcoming these limitations, it will be possible to obtain 200 mA of D^- ions for 1 A of D^+ (D^- power efficiency : 1 A D^-/5 KW RF power). The background pressure in the accelerator is 10^{-5} Torr and no instabilities on the D^- current are observed.
Different D^- destruction processes seem to occur when the target thickness is increased up to 3.10^{15} at/cm^2. The cesium plasma is the main factor in this destruction and a more advanced theory and supplementary measurements are necessary to understand these phenomena. Finally an electric field of 40 KV/cm is applied without breakdowns in the positive ion extractor during 1 s period.

Acknowledgements

We would like to thank Drs M. BACAL, H. DOUCET, G. LABAUNE, for their useful collaboration in the realization of the supersonic cesium jet and Mrs L. DEOLA and J. GUALANDRIS for their technical assistance.

References

1. E.B. Hooper, and al., Proceedings of the Symposium on the production and neutralization of negative hydrogen ions and beam, sept. 26-30, 1977, Brookhaven Nat. Lab., p. 163.

2. N.N. Semashko, and al., Proceedings of the Symposium on the production and neutralization of negative hydrogen ions and beam, sept. 26-30, 1977, Brookhaven Nat. Lab., p. 170.

3. M. Delaunay, and al., "Heating in Toroidal plasmas", Joint Grenoble-Varenna Conference, Como (Italy), 4-12 sept. 1980.

4. R. Geller, and al., Proceedings of the Symposium on the production and neutralization of negative hydrogen ions and beam, sept. 26-30, 1977, Brookhaven Nat. Lab., p. 173.

5. R. Geller, and al., Low Energy Ion beams conference (2), University of Bath (England), 14-17 April 1980.

6. H.J. Doucet, and al., This conference.

7. L. Deola, Thesis (in preparation), 1980.

8. J.M. Dolique, F. Zadworny, "Heating in Toroidal plasmas", Joint Grenoble-Varenna Conference, Como (Italy), 4-12 sept. 1980.

DISCUSSION

EHLERS I know you explained it to me but I did not really understand it. I do not see how your Cs^+ that is left over in the charge exchange can get across the magnetic field to empty itself in the cesium cell.

JACQUOT That is because of the cyclotron frequency, or if you like the Larmor radius of the Cs^+ in the magnetic field. You have so many collisions between Cs^+ and Cs that the Cs^+ has no time to move away in that magnetic field, because at a pressure of $10^{1.5}$ atom/cm^2 in the jet, we have so many charge exchange collisions that the Cs^+ flows with the cesium.

EHLERS So the cesium get swept?

JACQUOT Yes.

HOOPER Did you change the area of the beam? Because if you decrease the area of the beam the density of cesium would drop and you would see a reduction in the drop-off of your negative ion current due to the plasma and this would be a check on that mechanism. Did you do tests like that?

JACQUOT No. As Doucet will explain in his paper the height of the beam should be kept in the order of the thickness of the target.

HOOPER What is the rate of axial drop-off of the cesium plasma as you move away from the jet?

JACQUOT Very sharp. In steady state operation we could maintain 40 kV on the extraction electrode of the source so our conclusion is that no cesium is deposited on these electrodes. In addition I suppose that the temperature of the electrode is so high that the cesium which arrives on these electrodes evaporates. I think that at 30 cm from the jet the cesium flux is probably lower than 10^{15} atoms/cm^2/sec.

EHLERS Knowing that the Grenoble sources grew famous as producers of multiply charged full stripped ions for example, may I ask you what is your atomic percentage in deuterium?

GELLER We can vary it. The best is something like 80% of D^+ but we can change it up to 60% of D_3^+. It is a question of temperature of the electrons and pressure inside the source. Here we are working with 70% of D^+.

LEUNG Is your experiment done in one second pulses or d.c.?

JACQUOT One second pulses.

LEUNG What prevents you from going to complete d.c.?

JACQUOT Nothing. We have operated for more than 1 second. We are sure we can operate in steady state because the cesium jet is steady state. For us 1 second is the beginning of the steady state.

GELLER In reality the diagnostics are limiting us.

TSAI Could you explain the operation of the ECR ion source?

JACQUOT The principle of the ECR source is very simple. We have a magnetic field mirror with the condition that in the waveguide you inject the power with the cyclotron frequency of the electrons equal to the frequency of the rf generator. You have no cathode, we have just a waveguide. We have a nice plasma with high efficiency and no pollution due to filaments as in other sources.

TSAI How large a source is possible?

JACQUOT It depends on the size of the waveguide. The dimension of one waveguide is 2.5 cm x 2.5 cm at 10 GHz. We can use another size waveguide for 1 m x 1 m at 10 GHz. For example, to produce 5 A D^- ions we expect to use 25 A of D^+ ions. We need a generator of 25 kW at 10 GHz to produce that beam.

HACENA Do you expect any problems with the energetic neutrals which pass your cesium jet? At your energies the neutral fraction is 80% which represents quite some power.

JACQUOT It is critical if you have neutrals of 10 kV. But soon we expect to work at lower energies than 1 kV. We expect to work at 400 V or lower for the D^+ because our beam line does not take into account the divergence of the neutrals and we can conserve the small angle of the D^+ ions in the magnetic field. Then I think that the thermal effect by the neutrals should be minimized. The difficulty is to construct a low energy positive ion source with the same perveance.

NEGATIVE ION PRODUCTION BY CHARGE EXCHANGE OF HYDROGEN CLUSTERS WITH A CESIUM VAPOR TARGET-STATUS REPORT

O. F. Hagena, P.R.W. Henkes, R. Klingelhöfer, B. Krevet, H.O. Moser
Kernforschungszentrum Karlsruhe, Institut für Kernverfahrenstechnik
D-7500 Karlsruhe 1, Federal Republic of Germany

Abstract

It has been shown that negative hydrogen ion production through charge exchange of cesium vapor with the neutral molecular fragments of accelerated hydrogen clusters is similar to that from molecular or atomic positive ions (double charge exchange). Based on this result the Karlsruhe negative ion project will use the cluster method to obtain 1 A negative current from a 5 cm diameter cluster beam. The paper presents data for the primary cluster beam and discusses the design and construction of the cesium jet target. The description of the apparatus includes data for two types of LHe cryopumps to be used in the charge exchange chamber.

I. Introduction

Present concepts of next-generation fusion experiments ask for neutral injection heating at particle energies of above 150 keV per atom. In this energy range neutrals are best obtained from negative ions which have an energy-independent neutralization efficiency upward of 60 %. One of the standard techniques to produce the necessary negative ion beams is by double charge exchange of low energy positive ions on alcali vapor and subsequent acceleration of the negative ion beam.[1] The highest conversion efficiency of $\gtrsim$ 30 % has been reported for Cs and positive deuterium ions with energies $\lesssim$ 500 eV.[2] Due to the difficulty of producing multi-ampere ion beams in this energy range (space-charge limitations), one has used Na and ion energies of 10 keV. In this case the conversion efficiency is $\lesssim$ 10 %.[2,3,4]

As discussed in the previous symposium on negative ion beams[5] the problem of low intensities of low-energy ion beams can be overcome by using cluster acceleration as a means to obtain intense hydrogen beams in the energy range required for negative ion formation in a cesium target.[6] There are considerable advantages of being able to use cesium: The higher conversion efficiency (e. g. 30 % vs. 10 %) together with the lower energy of the primary beam (0.5 vs. 10 keV) lead to big savings in the gas load (factor 4) and unused beam power (factor 80). This will result in corresponding simplifications in the design of the subsequent beam line elements, i. e. the acceleration of the negative ions and the subsequent neutralization.

In a first experimental test with a highly collimated, low current cluster beam and a Cs vapor target we have demonstrated, that negative ion production from the molecular fragments of accelerated clusters is similar to that from molecular positive ions.[7] Based on the success of this experiment we next started to design and build a beam source for 1 A negative ion current. It will use the Karlsruhe cluster injector as source for the intense energetic cluster beam.[8] A schematic of the principal components of the beam line up to the formation of the negative ions is shown in Fig. 1:

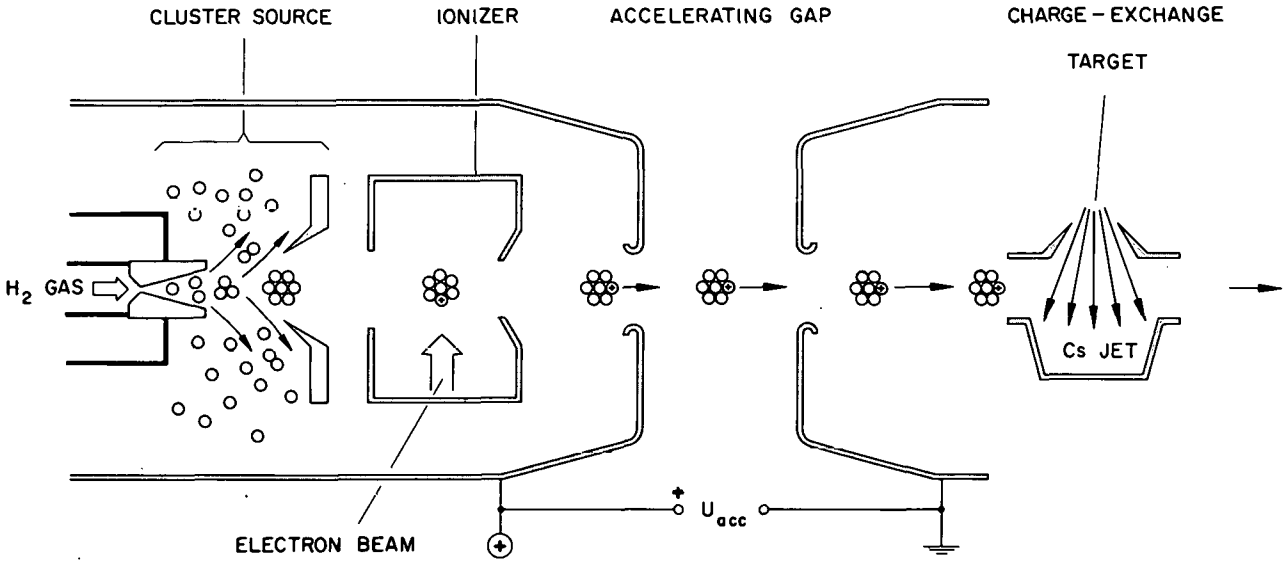

Fig. 1. Negative ion production by charge exchange of accelerated hydrogen clusters, schematic.

Hydrogen expands out of a miniature nozzle into vacuum, and clusters are formed by partial condensation of the expanding gas flow.[9] These clusters are transferred to a high vacuum region, ionized by electron impact, and accelerated in an electric field. Next the energetic cluster beam passes a cesium jet, where negative hydrogen ions are produced as result of collisions between clusters and cesium atoms.[7] This paper gives a status report about the Karlsruhe negative ion project, with special emphasis on the cesium jet target.

II. Cluster Ion Beam Source

The Karlsruhe cluster accelerator was designed for supplying particle currents of about 50 A_0 for refueling experiments at the ASDEX tokamak.[8] The negative ion source, however, requires much lower beam intensities at energies between 100 and 500 eV/atom. From the design data of $i^- = 1$ A and assuming conversion efficiencies between 0.2 and 0.3, the necessary intensity is between 5 and 3.5 A_0. Based on past experience with negative ion sources[1,3,4] the beam diameter is 5 cm to give a neutral flux between 0.25 and 0.175 A_0/cm^2 and a negative current density of 0.05 A/cm^2.

A schematic of the present beam line for the cluster ion beam with diagnostics is given in Fig. 2. A discussion of the performance charac-

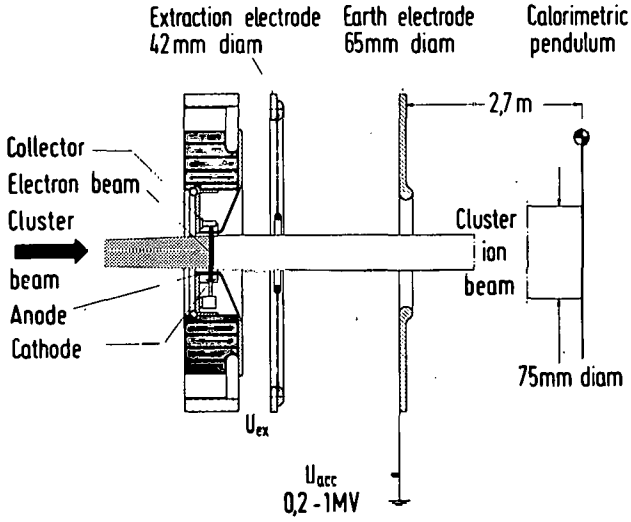

Fig. 2. Scheme of cluster beam ionization, acceleration and detection.

teristic of the cluster accelerator has recently been published.[10] Atom currents in excess of 9 A_0 at more than 10^4 atoms per charge have been produced, corresponding to energies of less than 100 eV/atom. The data were derived from measuring energy and momentum flux of the beam with a calorimetric pendulum. The beam cross section at the position of the pendulum (see Fig. 1) was 7.5 cm in diameter. Based on these data and considering further improvements in the performance due to modifications of the apparatus[10] the accelerator is expected to meet the specifications of the negative ion source.

III. Cesium Jet Target

General requirements

The cesium charge exchange target has to meet the following conditions:

a) Formation of negative ions requires a target thickness (design value) of:

$$\pi_t = n_t \cdot D_t = 2 \cdot 10^{15} \text{ at./cm}^2 \qquad (1)$$

where n_t = number density and D_t = width of target in the direction of the hydrogen beam (see Fig. 3).

b) The target must accommodate multi-ampere hydrogen beams. Beam aperture areas as high as 20 x 50 cm^2 have been used.[3,4] The present design is for a circular beam with 5 cm diameter.

c) Cesium leakage in the direction of the hydrogen beam should be as small as possible.

These conditions together require to use a curtain-shaped gas jet flowing perpendicular to the hydrogen beam and originating from a twodimensional gas source, typically in the form of a slit nozzle as shown in Fig. 3.

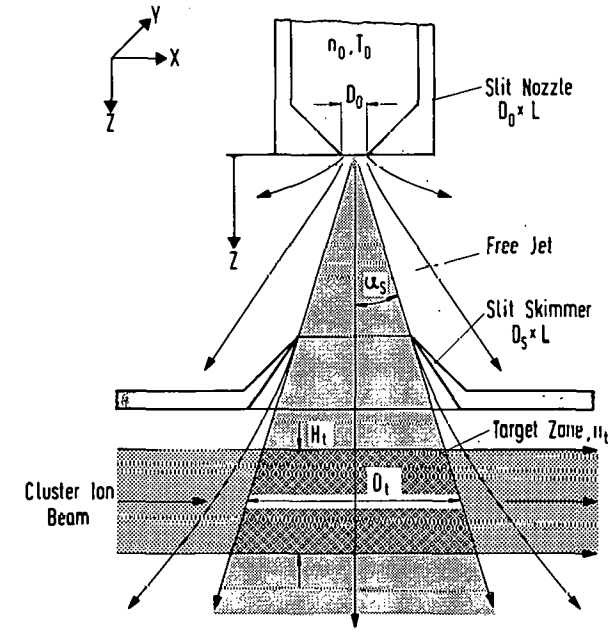

Fig. 3. Formation of gas jet target from the flowfield of a slit nozzle (plane jet).

Design criteria for jet target

The rarefied nature of the jet target may be characterized by the target Knudsennumber defined

as the mean free path, based on target density n_t, divided by the width of the jet target, D_t:

$$Kn_t \equiv \lambda_t/D_t = (n_t \cdot \lambda_t)/(n_t D_t) \qquad (2)$$

For Cs, we use

$$\lambda(n) \cdot n = \lambda_t \cdot n_t = 5.3 \cdot 10^{13} \text{ at./cm}^2 \qquad (3)$$

and obtain from Eqs. (1)-(3) for the Knudsennumber:

$$Kn_t = 0.026 \qquad (4)$$

This low Knudsennumber characterizes the jet target as transition flow, between collision dominated continuum flow and collisionless molecular flow. Note that this result does not depend on how the jet is produced. To minimize the collision-induced widening of the jet all cesium atoms in the jet should have nearly the same velocity, i. e. the jet source should produce a flow with a high Machnumber in the target zone, $M_t \gg 1$. The widening will be relatively more pronounced for jet targets with a great beam aperture width H_t.

For long slit nozzles, i. e. $L \gg z_t$, the skimmer Knudsennumber $Kn_s = \lambda_s/D_s$ is equal to the target Knudsennumber. Some secondary expansion of the flow entering the skimmer will take place, and possible skimmer-induced distortions of the flow must be avoided by e. g. cooled skimmer walls which condense all incident atoms. For cesium, temperatures of about 310 K are sufficient. Skimmer opening width D_s and nozzle-skimmer distance z_s define the flow divergence angle α and the target width D_t. Gas economy asks for large D_s, while uniform target conditions require small D_s.

The flow-producing nozzle requires special attention. Of the various geometries that have been used we discuss first the simple slit nozzle as shown in Fig. 3. The flowfield of the free jet expansion produced by such a nozzle has been studied both experimentally and theoretically. From measurements of the density[11] and from method of characteristic calculation[12] the hypersonic part of the jet can be described by the following equations for the centerline flow properties, valid for the collision-dominated part of the jet and for $z < L$:

$$n(z)/n_0 = 0.2(D_0/z) \qquad (5)$$

$$T(z)/T_0 = 0.34(D_0/z)^{2/3} \qquad (6)$$

$$M(z) = 3(z/D_0)^{1/3} \qquad (7)$$

The total particle flux out of the nozzle J_0 and the limiting flow velocity w_∞ are given by

$$J_0 = 0.324 \cdot n_0 \cdot w_\infty \cdot D_0 \cdot L \qquad (8)$$

$$w_\infty = (5kT_0/m)^{0.5} \qquad (9)$$

$$w_\infty = 17.61\ (T_0/K)^{0.5} \text{ m/s (cesium)} \qquad (9a)$$

Equations (5) - (9) are for a monatomic gas, $\gamma = 5/3$. The fraction θ of the total flux J_0 which constitutes the flux J_s into the skimmer is obtained for small angles $\alpha_s \lesssim 15^0$ from Eqs. (5), (8) and (9):

$$\theta = J_s/J_0 = 1.23 \cdot \text{tg}\alpha_s \qquad (10)$$

Finally, the source parameters n_0 and D_0 are related to the target thickness π_t and the cut θ:

$$n_0 D_0 = 3.08 \cdot n_t \cdot D_t/\theta \qquad (11)$$

This yields for the source Knudsennumber

$$Kn_0 \equiv \lambda_0/D_0 = Kn_t \cdot (n_t D_t)/(n_0 D_0) = 0.324 \cdot Kn_t \cdot \theta \qquad (12)$$

For e. g. $\theta = 1/3$ and $Kn_t = 0.026$ (Eq. (4)) one gets $Kn_0 = 0.0028$. For axisymmetric nozzles this would be low enough to give a Machnumber of about 11 before the jet is so rarefied that no further decrease of T and increase of M occurs. For slit nozzles, the smaller flow gradients should yield higher terminal Machnumbers. Rarefaction effects in plane jets are calculated e. g. in Ref. 13 and 14.

While so far only the product $n_0 D_0$ is fixed we choose $D_0 = 2$ mm. This choice was dictated by not wanting to expose the source materials to Cs at temperatures T_0 exceeding 750 K. Smaller nozzles, requiring higher temperatures, would give a more compact nozzle-skimmer geometry. But they would increase the heat load of the skimmer and the Cs flux J_0, too.

Compared to the sonic slit nozzle[15,16] one may try other nozzle geometries to improve the jet target Machnumber and/or to utilize a higher fraction θ of the nozzle flux J_0 for constant jet divergence α_s. A converging-diverging nozzle was used in Ref. 4, and an external expansion nozzle which consists of two slits on either side of a curved, wedge shaped centerbody in Ref. 3. Data to judge the actual performance of these nozzles are not available. Based on past experience with axisymmetric hypersonic nozzles for cluster beam production we will compare the performance of the sonic nozzle with that from two straight converging-diverging nozzles. Both have a throat width $D_0 = 2$ mm and a divergence angle of $2\alpha = 20.5^0$, the length of the diverging section is 50 and 25 mm, respectively. Assuming that these nozzles would allow to work with $\theta = 50$ %, the nozzle Knudsennumber Kn_e based on density and width of the exit plane is $0.5 \cdot Kn_t = 0.013$ for the design conditions of the jet target. This number is indicative of severe boundary layer growth, and the

experiments will have to show whether or not some improvement of the jet remains.

Construction of the Cesium Jet Target

Fig. 4 gives an overall view of the experimental setup. The main vacuum chamber is a rectangular box, 1 m wide, 0.9 m high and 1.2 m long. The entire Cs circuit is mounted on a flange 0.35 m i. d. in the first half of the chamber, the jet axis being ≈ 2 m away from the earth electrode of the accelerator, see. Fig. 2. The second half of the chamber will accommodate the extraction and analysing systems for the negative current. The experiments will first use a power supply for 100 kV, 1 A for beam pulses up to 10 s with 10 % duty cycle.

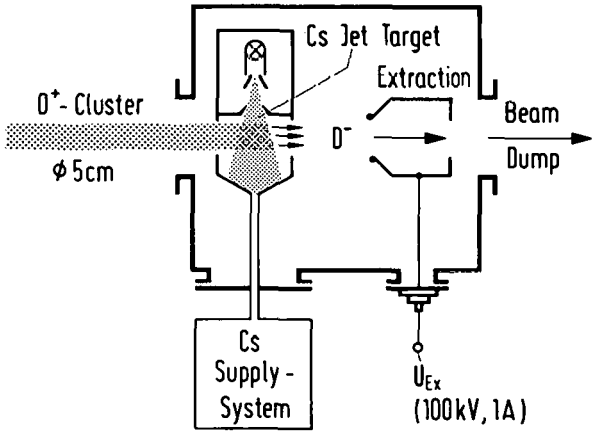

Fig. 4. Vacuum chamber with cesium jet target.

Fig. 5 shows in some more detail the components of the Cs jet target system. In contrast to the design of Refs. 3, 4, 15 and 16 the jet target with nozzle skimmer and collector is within a vacuum chamber, while the cesium oven and the condensate return are outside the vacuum. The vapor line and the condensate return line can be sealed off by all-metal valves.

Special attention has been given to the design of the heating systems. To avoid condensation of Cs within the vapor line from boiler to nozzle, this section is being kept 50 K hotter compared to the temperature of the cesium source in the boiler. Temperature uniformity is achieved by regulated heating circuits, properly positioned temperature sensors and extensive isolation in order to reduce heating power and thus reduce thermal gradients in the heated parts. Up to 16 heating circuits and over 20 thermocouples are used which are controlled and eventually pre-programmed with a Autodata Ten/10 calculating datalogger. All parts of the cesium circuit have been constructed and installed in such a way that all condensed cesium can flow back into the boiler.

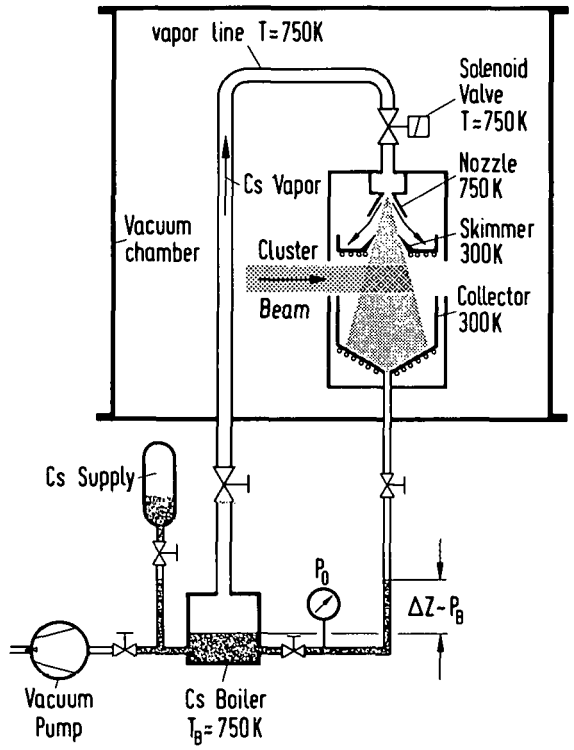

Fig. 5. Cesium jet target system, schematic.

Measurements will be made in a pulsed or steadystate mode. Jet pulses are produced by operating the solenoid valve, good for up to 750 K, mounted above the nozzle. Its open cross section is about 15 times the nozzle throat area of 2·6 cm^2. The jet is condensed, either as liquid or solid, on the skimmer plate and the collector cup, both with separate thermostated cooling circuits. The cut θ can be measured e. g. by collecting the cesium over a given time and subsequently measuring the collected amount in liquid form by a volumetric method, using the hydrostatic pressure in the condensate return line, separated from the boiler. Alternatively, it can be obtained from measuring the heat of condensation given to the cooling fluid. Spatial distribution of the jet target will be monitored with a hot-wire probe.

IV. Vacuum System

Assuming the total 5 A_0 cluster beam is dissipated within the vacuum chamber corresponds to a gas load of 0.5 Torr-l/s (= 0.065 $Pa \cdot m^3 s^{-1}$). In order to minimize the gas pressure as much as possible and thus reduce negative ion losses due to stripping by background collisions the two side walls of the vacuum chamber are lined with cryopumps, giving a combined pumping speed of 100 m^3/s. With full gas load the respective pressure would be $5 \cdot 10^{-6}$ Torr (= $6.7 \cdot 10^{-4}$ Pa) which is well below the limit of $3 \cdot 10^{-5}$ Torr given in Ref. 3.

The major design and fabrication problem with large-area cryopumps are the chevron baffles in front of the cryosurface, usually made out of copper brazed to liquid nitrogen cooled structural elements like e. g. tubes. If the copper becomes soft during this process the geometric accuracy of the chevrons may be lost which results in excessive heat flux to the cryosurface. To avoid these problems we designed together with industry two different types of cryopumps shown in Figs. 6-8.

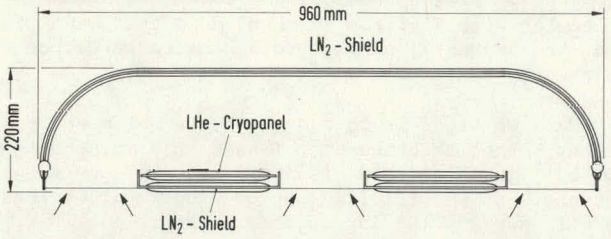

Cryopump Type I

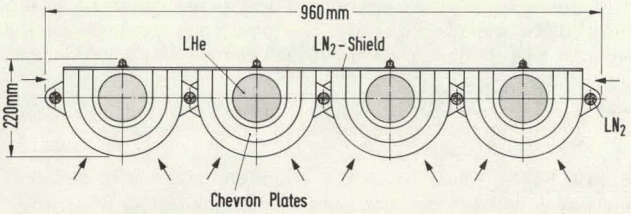

Cryopump Type II

Fig. 6. Pumping geometry of cryopump I and II

Type I is an arrangement of directly cooled LN_2 shield plates surrounding the two cryopanels cooled with LHe. LHe is supplied from a cylindrical reservoir in the upper part of the pump. Preliminary tests have confirmed the design pumping speed of 50 m^3/s per pump. The LHe consumption was 0.5 dm^3/h. As evident from the pump geometry the pumped particles will have typically only one collision with a shield surface before hitting the cryosurface. This may pose problems for steady state pumping of energetic particles. One may solve it by using a microscopically rough surface structure of the shield where it faces the cryopanels so that an incident gas atom or molecule makes multiple reflection - and thus accommodates to the shield temperature - before leaving the surface.

The other pump Type II takes the conventional approach of using chevron baffles, but employs a novel geometrical arrangement. The individual halfcircular chevrons are cold-formed with high dimensional accuracy. They have two extensions at the sides with holes for the LN_2 tubes and are sandwiched between two spacer rings for the braze process. The pump ist about 50 % more expensive than Type I, but it will be more efficient in thermalizing the gas due to the multiple collisions within the baffle structure. If necessary the design of both pumps is readily extended to pump geometries with larger aperture areas.

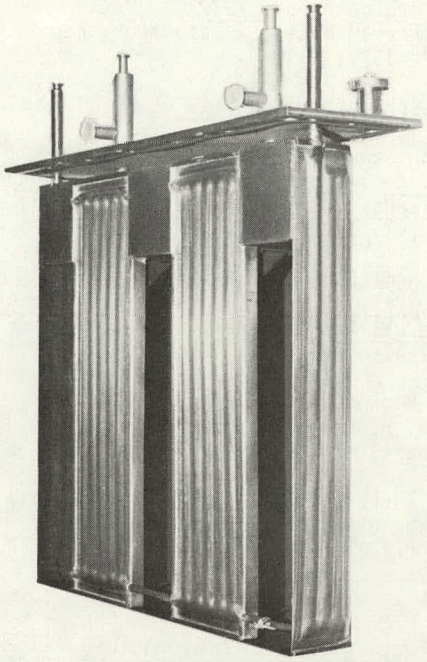

Fig. 7. Cryopump Type I. Manufacturer: NTG Nukleartechnik GmbH, D-6460 Gelnhausen.

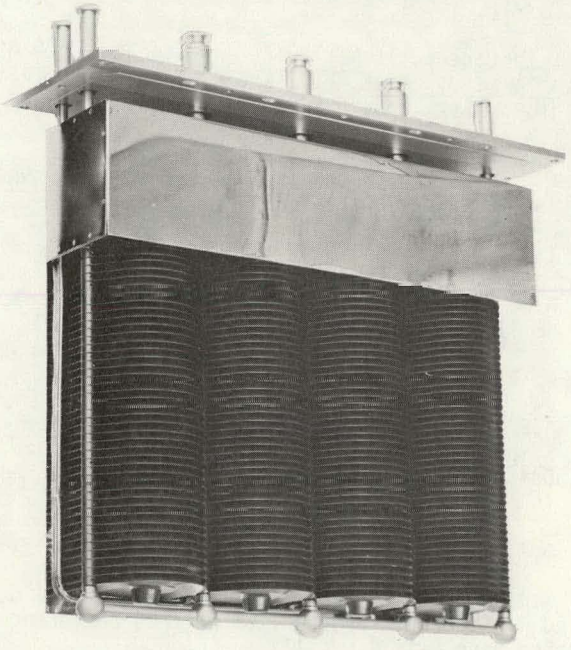

Fig. 8. Cryopump Type II. Manufacturer: Metalldrückerei Schmitt, D-5030 Hürth.

References

1. A summary of previous work on negative ions is given in Proc. Symp. on the Production and Neutralization of Negative Hydrogen Ions and Beams, Brookhaven, 1977, K. Prelec, Editor (Brookhaven National Laboratory Report BNL 50727, 1977).

2. A.S. Schlachter, in Ref. 1, p. 11

3. P. Poulsen and E.B. Hooper, Jr., Proc. 8th Symp. Eng. Problems. of Fusion Research, San Francisco, 1979, IEE Pub. No. 79CH1441-5-NPS, Vol. II, p. 676.

4. N.N. Semashko, V.V. Kuznetsov, and A.I. Krylov, Proc. 8th Symp. Eng. Problems. of Fusion Research, San Francisco, 1979, IEE Pub. No. 79CH1441-5-NPS, Vol. II, p. 853.

5. E.W. Becker, H.D. Falter, O.F. Hagena, P.R.W. Henkes, R. Klingelhöfer, H. O. Moser, W. Obert, and I. Poth, in Ref. 1, p. 322.

6. E.W. Becker, H.D. Falter, O.F. Hagena, P.R.W. Henkes, R. Klingelhöfer, H. O. Moser, W. Obert, and I. Poth, Nucl. Fusion 17, 617 (1977).

7. O.F. Hagena and U. Pfeiffer, Fusion Technology, Proc. of the 10th Symposium, Padova 1978, (Pergamon Press, Oxford, 1979), p. 295.

8. E.W. Becker, H.D. Falter, O.F. Hagena, P.R.W. Henkes, H.O. Moser, W. Obert, and I. Poth, Fusion Technology, Proc. of the 10th Symposium, Padova 1978, (Pergamon Press, Oxford, 1979), p. 331.

9. O.F. Hagena, in Molecular Beams and Low Density Gasdynamics, P.P. Wegener, Editor, (M. Dekker, New York, 1974), p. 93.

10. H.O. Moser, H.D. Falter, O.F. Hagena, P.R.W. Henkes, and R. Klingelhöfer, Proc. 2nd Int. Meeting on the Small Particles and Inorganic Clusters, Lausanne 1980, to be published as special issue of Surface Science.

11. A.E. Beylich, Z. Flugwiss. Weltraumforsch. 3, 48 (1979).

12. F. Ziqan, Z. Naturforsch. 17a, 772 (1962).

13. A.E. Beylich, Proc. 12th Rarefied Gas Dynamics Symposium, Charlottesville 1980, S.S. Fisher, Editor, to be published in the series Progress in Astronautics and Aeronautics.

14. G.A. Bird, AIAA Journal 8, 1998 (1970).

15. H.J. Doucet, M. Bacal, G. Labaune, H. Lamain, J.P. Stephan, Paper No. 39 of this conference. See also Ref. 1, p. 173.

16. E.B. Hooper, Jr., O.A. Anderson, T.J. Orzechowski, and P. Poulsen, in Ref. 1, p. 163.

Acknowledgments

The cooperation with S. Müller, Institut für Reaktorbauelemente, Kernforschungszentrum Karlsruhe, during the initial design and construction of the cesium circuit is gratefully acknowledged.

DISCUSSION

SCHLACHTER I would like to ask you a question about the choice of target thickness of 2×10^{15} atoms/cm^2. If I understood you correctly, these molecules with a proton on them, does that mean that you convert just the proton that is attached to the cluster?

HAGENA We are able to run the system at much higher target thicknesses. I used this value of 2×10^{15} just for comparison and to have some reference. So we will find out by experiment whether we will use 2×10^{15} or whether we go to 1×10^{16}. The point I want to make is that this jet design should be of value not only for our type of experiment but to investigate, in general, the properties of these jets and to compare them with other jet designs, for example the effusive type as discussed in a paper during the previous symposium by LAM which has a collisionality of only 1/38. For this comparison I intended to use this very low target thickness as it will be used by people who make charge exchange with positive ions.

SCHLACHTER But in order to dissociate the molecules, I would imagine you need something like 10^{16}. You have designed that capability?

HAGENA Yes, we have designed that. We can go at least to 5×10^{16}.

EHLERS What are these atoms or molecules bound together with? Is that Vanderwalls forces?

HAGENA Yes.

EHLERS It looks almost like a shotgun shell coming through. Is there any chance of burn-out with all those particles...

HAGENA The first collisions of these clusters with the first cesium atoms will make a shotgun, so it will be an assembly of molecules but the target thickness in the jet is still sufficient. First we had a design where we thought we could utilize even higher incident particle flux densities but then you have the problem that you might burn a hole into your cesium. If you have for example 5 A particle current of hydrogen then the particle current of cesium should not be ½ A but it should be at least 50 A. This puts a limit on the flux density and because we know that each hydrogen will not just make one collision to reach equilibrium but it will make a couple of collisions, one has to be concerned about burning a hole and that has been taken care of.

BACAL What is the amount of cesium in the system and is there any recycling? Do you consider hot water as a good measure of safety?

HAGENA We do not use hot water for the obvious reasons of safety. I just indicated this as a temperature level for having a cryopump for cesium. A cryopump for cesium can run on waste heat if you want to. You do not need refrigerators. That was the only point I tried to make in this connection. Now your question concerning the recycling. In designing the nozzle you have the freedom of choice in the pressure and the width of the nozzle, then it is only the product of density x diameter which is fixed by your experimental requirement. Initially we decided that we would like to operate at not too high a temperature and therefore we will have fairly low pressure but a wide nozzle, namely a slit width of 2 mm. In contrast to the experiment in Grenoble, where the initial design called for 1 to 2% use of the entire jet, we will use about 20 to 30% of the jet so that gives another reduction in the amount of cesium being circulated. In the boiler we will operate at pressures of 10-20 torr at most and this can be handled just by the hydrostatic pressure; we do not need electromagnetic pumping. The cesium can be frozen for sometime and we can interrupt it with a solenoid valve which utilizes an electro-magnet within the vacuum and which can stand very high temperatures. If that does not operate properly we do have another electro-magnetic valve outside the vacuum and even a third one, hand operated, in order to have triple safety to shut off the cesium flow. So by warming up these collectors and let the cesium drain we can recirculate the cesium.

BACAL How much cesium will the system contain?

HAGENA As little as possible, but we will start with ½ kilo or something like that.

DOUCET Did you compute the temperature of the lips of the skimmer in contact with the cesium jet?

HAGENA We made a rough estimate. We know the power density of the incident gas, assuming that the gas expands as it is supposed to do according to the gas dynamic theory, then you know what the power loading is in watts/cm^2. Since the skimmer is made out of copper you know the heat conductivity and you know the heat sink which is this pipe underneath. We estimate that the temperature drop is at most 3 to 5^o, so that the lips will stay cold.

CESIUM SUPERSONIC JET FOR D^- PRODUCTION BY DOUBLE ELECTRON CAPTURE

M. Bacal, J.M. Buzzi, H.J. Doucet, G. Labaune*, H. Lamain, J.P. Stephan
Laboratoire de Physique des Milieux Ionisés, GR29 du C.N.R.S.
Ecole Polytechnique, 91128 Palaiseau Cedex, France

M. Delaunay, C. Jacquot, P. Ludwig
Centre d'Etudes Nucléaires de Grenoble, Grenoble, France

S. Verney
Centre Technique des Industries Mécaniques, Senlis, France

Abstract

A supersonic jet of cesium vapor have been built for D^- production by double electron capture. The produced target thickness $n\ell$ is $3.5\ 10^{15}$ atomes.cm^{-2} for an oven temperature of 600°C. The average cesium jet geometrical thickness is only 2.2 cm when a condensing skimmer is used. The jet flux is determined from calorimetric measurements and is found to be in good agreement with simple slit type jet calculations. The jet profile is measured with a thin thermocouple moving accross the cesium jet.

I. Introduction

The need for sources of intense D^- ion beams for neutral injection into magnetically-confined controlled fusion devices has lead to some new developments of charge exchange cells using alkali metal vapor. The D^- ion beam production by double electron capture relies on the conversion of positive deuterium ions into negative ions in an alkali metal vapor target. Among the alkali metals Cesium provides the highest conversion efficiency[1,2] for low ion energy (< 1 keV) and a target thickness $n\ell \simeq 10^{15} cm^{-2}$. The high conversion efficiency and low ion energy leads to requirements for power and gas pumping much lower than those in alternative vapors such as sodium. Therefore the use of double electron capture systems using Cesium charge exchange targets has been proposed for the production of intense D^- ion beams[3]. There is also some interest for producing intense He^- beams for the diagnosis of tokomak plasma[4].

The need for transporting an intense positive ion beam (100-500 mA/cm^2) of low energy in the double electron capture system using a Cs target results in a very severe limitation of the distances between the positive ion source, the Cesium target and the negative ion accelerator, and also of the admissible Cesium loss through the cell ports. The Cesium target area required to obtain a given total D^- beam current from a single positive ion beam is determined by the density of this positive ion beam and the positive ion-negative ion conversion efficiency. A fusion reactor design study[5] considers a Cesium target area of 0.2 m^2. These requirements limit the possibility of using a heat-pipe Cesium charge exchange cell[6,7] which confines the metal vapor effectively only when the cell radius is much less than the distance between the cell port and the vapor target.

Supersonic flow of Cesium[8] and other alkali metal vapors[9-11] through a slit-type nozzle has already been used to produce the charge exchange target in several double electron capture systems. These flows were pulsed[8] or steady-state[9-11]. A more complex nozzle has been used by Poulsen and Hooper[12] for producing a 25 cm thick target of Na vapor. In this way, geometrically thick (tens of cm) metal vapor targets could be obtained. After crossing the positive ion beam, the alkali metal is either frozen on a surface cooled by liquid nitrogen[8], or condensed as a liquid and recycled[9-11].

The ion optics of the double electron capture system under study at Centre d'Etudes Nucleaires de Grenoble[13] and based on an ECR ion source, requires a geometrically thin cesium target (a few cm only) with a useful area of 25 cm^2. A very thin (0.7 mm) target of sodium has already been produced for a different application by Zankel and Vosicki[14], where a lower $n\ell$ (about 10^{11} cm^{-2}) was required ; this was achieved by strongly collimating the flow from a slit-type nozzle. But the joint requirements of a geometrically thin target of a few cm, and a $n\ell$ product of 10^{15} atomes-cm^{-2} lead to a strongly collisionnal cesium flow which cannot be kept thin except by a supersonic jet.

Most of the supersonic beam systems for non-condensible gases are based on the Kantrowitz-Grey design[15] ; its advantage

*presently at Office National d'Etudes et Recherches Aérospatiales, Châtillon.

is a narrow velocity distribution, resulting from the cooling of the gas during the expansion through the nozzle, corraborated with a collisionless flow at the kimmer. Since our beam is necessarily collisional, we designed it with the idea that the effect of collisions upon the beam widening can be controlled by the use of highly supersonic flow at the skimmer.

The skimming of a beam of condensable metal vapor has several particularities compared to the case of non-condensable gases : the sticking probability for the metal vapor molecules impinging on a surface can be close to 100% when their energy can be absorbed by the surface and when the interface is suitable[14]. Thus the collimation of the central, useful, part of the supersonic beam and the pumping of the unused metal vapor can be ensured by a suitably designed condenser.

II. Supersonic flow through a slit

The isentropic relations for a perfect gas, giving the gas properties as a function of Mach number and stagnation (reservoir) conditons were used in order to find the following analytical relations for the variation of Mach number (M), the density (n) and the temperature (T) with the distance from the slit (R) :

$$M = 3.18\ k^{-1/3}(R/d)^{1/3} \qquad (1)$$

$$n/n_o = 0.16\ k\ (R/d)^{-1} \qquad (2)$$

$$T/T_o = 0.3\ k^{-2/3}(R/d)^{-2/3} \qquad (3)$$

Here d is the width of the slit ; the subscript 'o' indicates stagnation conditions. k is a constant independent of the distance R. The following angular distribution is assumed :

$$n(R, \theta) = n(R, 0) \cos k\theta \qquad (4)$$

It is admitted that at the throat M = 1 and the flow rate (F_N) is given by[14] :

$$F_N = L\ d\ a_o n_o \left(\frac{\gamma+1}{2}\right)^{-\frac{(\gamma+1)}{2(\gamma-1)}} = 0.562\ L\ d\ a_o n_o \qquad (5)$$

Here L is the length of the slit and a_o the sonic velocity :

$$a_o = \left(\gamma \frac{KT_o}{m}\right)^{1/2} = 1.02 \times 10^3\ T_o^{1/2} \qquad (6)$$

Taking into account Eq. (6), we find for F_N :

$$F_N = 573.2\ T_o^{1/2}\ n_o\ dL \qquad (7)$$

With the above angular distribution (Eq.4) the fraction $F(\theta^*)$ of the total flow F_N passing through an angle θ^* can be expressed as :

$$F(\theta^*) = F_N \sin(k\theta^*) \qquad (8)$$

The best fit of Eqs. 1 and 2 to the results of numerical calculations[16] is obtained for the value k = 1.125 (Figures 1 and 2). With this value of k the Mach number, density and temperature of the cesium jet are given by the following expressions, which were used in the design of the cesium jet :

$$M = 3.06\ (R/d)^{1/3} \qquad (9)$$

$$n/n_o = 0.18\ (R/d)^{-1} \qquad (10)$$

$$T/T_o = 0.277\ (R/d)^{-2/3} \qquad (11)$$

Figure 3 illustrates the variation with R/d of Mach number, density and temperature on the axis as given by Eqs. 9-11. We used these equations to calculate the main parameters of the supersonic beam generator. Though the validity of the isentropic relations is questionable, our further experiments showed that Eqs. 9-11 are a fairly good approximation.

The experimental study in a wind-tunnel, using the electron beam technique, of a jet issuing from a slit[17], confirmed the functional dependence of n upon R, given by Eq. 10.

However, Eq. 5 has to be corrected for the non-unidimensional character of the flow, the non-negligible gas viscosity and heat transfer. A good description can be obtained by introducing into Eq. 5 an additional factor C_D, called discharge coefficient[15] :

$$F_N = C_D \times 0.562\ d\ a_o n_o = C_D \times 573.2\ T_o^{1/2} n_o\ d\ L \qquad (12)$$

For the case of a highly collisional flow, $C_D \sim 1.5$.

This correction is equivalent to the assumption of a lower width slit. Therefore, when using Eqs. 7-11 we will consider a slit width

$$d^* = \frac{d}{1.5} \qquad (13)$$

In this generator, the actual slit width was d = 0.06 cm, but we consider in the calculation using Eqs.7-11 an effective slit width d* = 0.04 cm.

The flux F_N can be expressed as a function of the reservoir pressure P_o using the following relationship[18] :

$$n_o = 9.656 \times 10^{18} \frac{P_o}{T_o} \qquad (14)$$

where P_o is in Torr, and n_o is in cm^{-3}. Thus

$$F_N = 5.5 \times 10^{21} \frac{P_o d^* L}{T_o^{1/2}} \qquad (15)$$

A few other factors limit the validity of the theory based on isentropic expansion :

1. The Mach number reaches a limiting value M_L, defined by the Knudsen number at the nozzle $(Kn_N)^{15}$:

$$M_L^{3/2} = \frac{3\sqrt{3}}{4} \frac{1}{Kn_N} \qquad (16)$$

2. The jet through a slit can be limited downstream by a shock 'Mach cylinder' ; its position depends on the pressure ratio[17] :

$$R_c = 5.93\ d\ \left(\frac{P_o}{P_\infty}\right)^{0.617} \qquad (17)$$

This limitation is not severe for cesium as P_o is in the range of a few 100 torrs and P_∞, the cesium pressure in the condensers is given by the surface temperature of the condenser. R_c is easily larger than 1 meter.

3. Condensation in the flow, leading to cluster formation, violates the isentropic character of the flow.

III. Determination of the supersonic cesium jet generator parameters

Figure 4 indicates the main elements of the generator and the used notations. The choice of the various parameters is based upon the following three requirements :

1. The optical thickness($n\ell$) of the Cesium target in the interaction region should be, for optimum D^+/D^- conversion:

$$n\ell \approx 10^{15}\ cm^{-2} \qquad (18)$$

2. The maximum geometrical thickness, ℓ_m, in the interaction region should be of the order of 1 cm ; thus :

$$n(R_m) \times \ell_m \approx 10^{15}\ cm^{-2} \qquad (19)$$

3. The useful area of the cesium target, related to the size of the D^+ beam, is a square of 6 x 6 cm. The central part of the used cesium beam is located at a distance R_m from the nozzle.

Taking into account the requirement given by Eq. 19 in Eq. 9, we define the product $n_o d$ as :

$$n_o d^* = 5.55 \times 10^{15} \left(\frac{R_m}{\ell_m}\right) \qquad (20)$$

The choice of the slit width, defines the necessary density n_o in the cesium oven, and thus the necessary oven temperature T_o and pressure P_o. With R_m = 17 cm and ℓ_m = 1 cm, d^* = 0.84 cm we find :

$$n_o = 2.8\ 10^{18} cm^{-3}$$
$$P_o = 190\ Torr$$
$$T_o = 820°K$$

The cesium flux per unit slit length will be obtained by substituting $n_o d$ from Eq. 20 into Eq. 7 :

$$F_N/L = 3.18 \times 10^{18} (R_m/\ell_m) T_o^{\frac{1}{2}} \qquad (22)$$

With R_m/ℓ_m = 17 and T_o = 820°K, we find :

$$F_N/L = 1.54 \times 10^{21}\ cm^{-1}\ s^{-1}$$

The length of the slit L has to be chosen to ensure a sufficiently homogeneous flux on the required target length λ_2. Obviously :

$$L > \lambda_2 \qquad (23)$$

As mentionned above, the widening of the beam due to the effect of collisions is expected to be controlled by ensuring a high value of the Mach number at the skimmer. Eq.8 gives the ratio R_s/d as a function of the required Mach number at the skimmer. The choice of R_s/d was made to provide $M_S \sim 20$.

The ratio R_s/D (R_s = distance between the slit type nozzle and the skimmer, D = width of the skimmer aperture) is correlated with R_m and ℓ_m by the geometrical condition :

$$\frac{R_s}{D} = \frac{R_m}{\ell_m} \qquad (24)$$

Obviously : $R_m - R_s > \lambda_1$ (25)

where λ_1 is the target size in the direction perpendicular to the slit.

Let us denote F_S the total flux through the skimmer. According to Eq. 8 the ratio D/R_s defines the fraction F_S/F_N :

$$\frac{F_S}{F_N} = \sin\left[k\ \mathrm{arctg}\ \frac{D}{2R_S}\right] \qquad (26)$$

with $D/R_s \sim 20$, we find $F_S/F_N \sim 0.03$.

In a first version of the generator, we used a classical skimmer for which R_s/D = 20 was chosen, according to Eq. 24, while R_s and D were 10 cm and 0.5 cm, respectively. In the second version, a non-classical, condensing skimmer was used, represented by two tubes of the condenser. In this case, R_s = 9.2 cm and D = 1.2 cm, which, according to Eq. 24, gives R_m/ℓ_m = 7.67 and ℓ_m = 2.2 cm.

Table I presents the parameters of the generator, given by this calculation scheme for the two versions of the generator.

IV. Description of the generator

The main components of the generator, shown on Figure 5, are as follows :

. The cesium vapor production and transport circuit

2. The expansion and collimation system (slit-type nozzle and skimmer)

3. The vapor condensation system : a first large condenser is situated in the expansion chamber ; a second and smaller one, is situated immediately behind the interaction region.

4. A liquid cesium recycling system, which ensures the steady state operation of the generator with a minimum quantity of cesium.

IV.1 Cesium vapor production and transport.

The heating and evaporation of the liquid cesium requires a power of about 3 kW. In order to avoid film boiling, the thermal flux through the unit wall surface should not exceed a certain value, which, for sodium, is about 10-15 W/cm^2, but is unknown to us for the case of cesium. We assumed that the mentioned value also applies to cesium. This leads us to design an oven with a diameter of 20 cm and in which the heat is transferred through an area of about 300 cm^2. The oven was built in inconnel 600 ; this material is highly resistant to corrosion by alkali metals, it can be easily welded and does not fragilize in the temperature range between 500-800°C. Since the stress-accelerated corrosion of inconel 600 with cesium has not been extensively studied, we avoided any contact of the welded joints with hot liquid cesium. Argon arc welding was used and the welded joints were submitted to X-ray tests.

Due to the high specific power (10W/cm^2) and to the high working temperature (600-700°C) we chose an electric heating by radiation. The heating is provided by radiation using a Kanthal A_1 resistor situated in the grooves of a plate made of a refractory ceramics. With respect to the heating using a thermocoax, this choice has also the very important advantage of allowing the replacement of the heating element without having to touch to the evaporator.

The temperature is controlled by an integro-differential proportional system. The temperature measurement is provided by a chromel-alumel thermocouple situated on the external face of the evaporator.

Both the evaporator and the vapor duct are covered by thermocoaxial heating elements imbedded in stainless steel to the walls. They are thermally insulated by a 3 cm thick layer of kerlane.

The slit-type nozzle is mounted on the end of the vapor duct, which is also connected to the large condensor situated in the expansion chamber. Suitable thermal gradient and elasticity are achieved by using the geometry presented on Fig. 6.

IV.2 Expansion and collimation system (nozzle and skimmer).

A sonic nozzle has been used, giving a free jet. The slit has been obtained by electro-erosion in inconnel 600. The nozzle is screwed to the end of the vapor duct with inconnel screws covered by a film of boron nitride, which allows demounting after work at high temperature (Figure 6). A coaxial heating element has been brazed with copper on the front (expansion chamber) side of the nozzle. The presence of this element was found unessential after its accidental destruction.

The first version of the generator contained a classical skimmer, made of stainless steel XN26TW, which is resistent to corrosion and can be very well sharpened. This skimmer was cooled by conduction.

Since the experiments indicated cesium re-emission from the hot skimmer surface (200°C) oriented to the interaction chamber, we eliminated this classical skimmer in the further experiments. The beam collimation was then provided by two central tubes of the first condensor, cooled by circulating oil. This collimation method was satisfactory ; it is more appropriate for a condensable vapor jet, where cryogenic pumping of the vapor by suitably cooled surfaces is very effective.

IV.3 Condensation system.

The metal vapor is pumped by condensation on cold surfaces. The residual vapor pressure should be as low as possible in order to limit the interaction between the incident beam and the residual gas. This implies that the sticking coefficient of the incident atoms should be close to 1. One should use a very clean condensing surface, in order to obtain a film condensation on the whole surface. The temperature should be maintained above the melting point, in order to allow the flow of liquid cesium by gravity. We allowed for a thermal flux at condensation of 6 W/cm^2.

The condensation system of the expansion chamber has to eliminate ~ 97% of the energy. The calculation of the flux distribution led us to the geometry presented on Figure 6. Temperature controlled oil

(Transcal 40) circulates through the tubes the oil temperature is controlled by an integro-differential proportional system.

IV.4 Recycling system for liquid cesium.

This system is schematically shown on Fig. 7. The liquid cesium flows along the tubes of the condensor and passes through a filter made of sinthered stainless steel. An electromagnetic pump (capable to convey 10 kg/hour against 1 bar pressure) sends the cesium in the evaporator, through a flowmeter using the Hall effect. A pressure gauge gives the static pressure after the electromagnetic pump and the absolute pressure of the vapor in the evaporator. The pipes as well as the bellow valves are made of stainless steel, respectively NSMC and NS22S.

An automatic control maintains a constant level of cesium in the evaporator. A γ source irradiates a group of Geiger-Mueller counters through the cesium contained in the evaporator. A suitable treatment of the signal gives the cesium level with a precision of 0.1 mm. This signal is compared to a previously established value and a proportional integro-differential system controls the power supply of the electromagnetic pump ($\sim$ 250 A). The whole recycling system is maintained at 60°C.

V. Diagnostics and results

Two types of diagnostics were used :

1. Calorimetry : the power absorbed in each of the two condensors was used to calculate the total cesium flux condensed on the respective condenser (F_C). The product $n \times \ell$ is then obtained from the equation :

$$n \times \ell = F_C / Lv = F_C / L \left(\frac{3\gamma K T_o}{m_{c_s}} \right)^{\frac{1}{2}} \qquad (27)$$

where $v = \sqrt{3}\, a_o$ = velocity of Cesium atoms impinging on the condensor.

The cesium flux measured by calorimetry in the first version of the generator (classical skimmer) is plotted on Fig. 8 as a function of T_o ; this value was inferred from the pressure in the oven measured by the pressure gauge of the recycling system. We also plotted on Fig. 8 the flux of cesium vapor to the two condensors, calculated according to Eqs. 15 and 26. Note the good agreement between experiment and calculation which indicates that there is no strong shock on the skimmer and no jet destruction. $n \ell$ values up to $2.5\ 10^{15}$ atomes.cm^{-2} have been obtained with a classical skimmer for $T_o \simeq$ 600°C. The flux ratio of the cesium flux on the small condenser after the skimmer over the cesium flux on the large condenser located between the nozzle and the skimmer, was found to be around 3% in good agreement with predictions of the above simple two dimensionnal jet theory. But this calorimetric measurements give no indication on the beam profile.

In the second version of the device, the classical skimmer was removed and the two last cooled tubes of the large condenser, distant of 13.4 mm were acting as a condensing skimmer. Figure 9 presents the variations of the measured flux of cesium on the small condenser versus the oven temperature. Figure 10 presents the same variations in the large condenser. Figure 11 presents the ratio of the cesium flux in the two condensers and Figure 12 gives the corresponding values of calculated $n \ell$. Around $T_o \simeq$ 600°C the $n \ell$ reaches $3.5\ 10^{15}$ atomes.cm^{-2} with the condensing skimmer, which is slightly better than the value obtained using a classical skimmer.

2. Measurement of the cesium jet profile by a "thermal probe".

A thermocouple mounted in a thin stainless tube, moving across the cesium jet, has been used as a "thermal probe" : the temperature variations of the probe end containing the thermocouple is a function of the local cesium flux condensing on the probe, of the cesium evaporation and thermal losses due to radiation and conduction.

If we call :

- $V = \pi r^2 d\ell$ the probe volume of length $d\ell$
- r the probe radius including a thickness e of cesium
- r_o the radius of the dry probe
- T^o the temperature of the element $d\ell$ of the probe
- P_C the power deposited on this probe element by cesium condensation
- P_E the power lost by this probe element due to cesium evaporation which is a known function of the local temperature T
- P_R the power lost by radiation
- P_{cc} the power lost by this element by thermal conduction
- $Q(r,T)$ the heat capacity of the element $d\ell$ of the probe
- d_{c_s} the specific weight of the cesium
- m_{c_s} the mass of cesium atoms
- ϕ_C the flux of incoming cesium atoms, condensing on the element $d\ell$ on the probe
- ϕ_E the corresponding cesium flux evaporated,

we have : $V = \pi (r^2 - r_o^2)\, d\ell$

$$\frac{\partial T}{\partial t} = \frac{P_c - P_E - P_R - P_{cc}}{Q}$$

$$\frac{dV}{dt} = \frac{\phi_c - \phi_E}{d_{c_s}} \, m_{c_s}$$

We assume that the probe element dℓ is always a perfect cylinder due to the high cesium capillarity on stainless steel. A sticking coefficient equal to 1 is taken. A complete numerical code should permit to determinate the jet profile from the measurement of the probe temperature variations versus the probe position when the probe is moving with a known velocity.

Several simple approximations can be used : for instance, when the conduction can be neglected, the above equations reduce to a simple differential equation and with a small cesium flux far from the center we can write :

$$\phi(x) \simeq \frac{Q_o}{L+K} \frac{1}{2r_o} v \frac{dT/dx}{\sqrt{1+2\alpha\Delta T}}$$

where Q_o is the heat capacity of the dry probe element dℓ, L+K is the total energie deposited by condensing atome, v is the probe velocity, ΔT is the temperature variation of the probe and α is :

$$\alpha = \frac{Q_o}{d_{c_s}} \frac{m_{c_s}}{L+K} \frac{1}{2\pi r_o^2}$$

the above assumptions give $\alpha\Delta T \ll 1$.

In the center of the jet the cesium flux is too large and the above approximation is no longer valid. Moreover with large temperature variations the losses by thermal conduction along the probe are no longer negligeable and a more complicated model is required. Another simple approximation can be made using the measured temperature variations $v.\partial T/\partial t$ as an approximation of the spatial variations $\partial T/\partial x$ in the estimation of the thermal conduction losses power for the probe element dℓ :

$$P_{cc} = \Lambda \frac{\partial T}{\partial x}$$

For our probe $\Lambda \simeq 1.8\ 10^{-3}$ watts.cm $^oK^{-1}$.

The importance of the conduction losses can be seen from the examination of the temperature variations of the probe for two opposite directions of the probe motion : the conduction losses change of sign giving an overestimate and an underestimate of the cesium flux value . An exemple of these two estimates is shown in Figure 13. corresponding to a jet using only a condensing skimmer. The cesium jet can be caracterized by the thickness at half of the maximum.: this measured thickness is here 2.2 cm equal to the geometrical thickness, corresponding to the straight line trajectories between the nozzle and the condensing skimmer. This shows that there is no evidence of any anomalous widening of the supersonic cesium jet using a condensing skimmer. Figure 14 presents a typical exemple of the jet profile using a classical skimmer. The measured thickness is larger and of the order of 3 cm when the geometrical thickness is only 9 mm. This indicates an important widening of the jet after the skimmer. The jet profile have also large wings which seems to correspond to cesium evaporation coming from the rear part of the skimmer lips heated by condensation. A thermocouple located in the skimmer support, close to the lips, indicated a temperature of 200°C.

Figure 15 gives the measured jet profile parallel to the slit, when a classical skimmer of 8 cm is used.

VI. Conclusions

A device producing a supersonic jet of cesium have been built and tested. The obtained n ℓ is $3.5\ 10^{15}$ atomes.cm^{-2} when the oven temperature is 600°C in steady state operation. The average jet thickness is only 2.2 cm when a condensing skimmer made of two cooled stainless steel tubes is used. The useful size of the cesium target is a square of 6 x 6 cm. This result demonstrates that supersonic, and dense cesium jet can be built, providing a useful vapor target of small thickness and used for double electron capture in the production of intense D^- beam.

Acknoleqdments

It is a pleasure to thank Dr. Blanc from Centre d'Etudes Nucléaires de Cadarache for providing a large part of the recycling device and for help in alkali metal technology. We also thank Pr. O.F. Hagena from Kernforschungszentrum, Karlsruhe, Dr. K. Zankel from Centre Europeen de Recherches Nucleaires, Geneve, Mr. Galley from Centre d'Etudes Nucleaires de Saclay, Dr. Delery from Office National d'Etudes et Recherches Aérospatiales Chatillon, for useful and illuminating discussions.

References

1. A.S. Schlachter, in Ref. 2, pg. 11.
2. Proc. Symp. on the Production and Neutralization of Negative Hydrogen Ions and Beams, Brookhaven, Sept. 26-30 ,1977, BNL 50727.
3. J.E. Osher, Lawrence Livermore Laboratory Report UCID-15893 (1971).
4. L.R. Grisham, D.E. Post, J.C. Weisheit, H.P. Eubank, D.R. Mikkelsen and L.D. Stewart Report PPPL-1661 (May 1980).
5. J.H. Fink, W.L. Barr and G.W. Hamilton IEEE Trans. on Plasma Science, PS-7, 21 (1979).
6. M. Bacal and W. Reichelt, Rev. Sci. Instrum., 45, 769 (1974).
7. M. Bacal, A. Truc, H.J. Doucet, H. Lamain and M. Chretien, Nucl. Instrum. Methods, 114, 407 (1974).

8. E.B. Hooper, O.A. Anderson, T.J. Orzechowski and P. Poulsen, pg. 163 in Ref. 2.

9. B.A. D'yachkov, V.M. Nesterenko and V. Yu. Petrusha, Instrum. and Exper. Techn., 2, 35 (1974) (in Russian).

10. N.N. Semashko, V.V. Kuznetsov and A.I. Krylov, pg. 170 in Ref. 2.

11. H.R. Hiddleston, IEEE Trans. Nucl. Sci., NS-24 1600 (1977).

12. P. Poulsen and E.B. Hooper Jr., 8th Symp. on Engineering Problems of Fusion Research, San Francisco, California, Nov. 13-16 (1979), LBL Reprints 6-6782.

13. R. Geller, C. Jacquot and P. Sermat, pg. 173 in Ref. 2.

14. K. Zankel and B. Vosicki, J. Phys. E, Sci. Instrum., 8, (1975).

15. Molecular Beams and Low Density Gasdynamics, (P.P. Wegener).

16. G. Labaune "Cible mince de vapeur de cesium supersonique pour la production de faisceaux d'ions D^-". Thèse de Docteur-Ingenieur présentée à l'Université de Paris-Sud, Centre d'Orsay, le 9 Juin 1978.

17. G. Dupeyrat, Twelfth Intern. Symp. on Rarefied Gas Dynamics, July 7-11, 1980 (University of Virginia, USA).

18. S. Dushman and J.M. Lafferty, Scientific Foundations of Vacuum Technique, (John Wiley & Sons, 1966) p. 7.

TABLE I

	L	d^*	D	R_S	R_M	ℓ_M	n_0	T_0	P_0	M_S	F_N	F_S/F_N
	CM	CM	CM	CM	CM	CM	CM^{-3}	K	TORR		AT S^{-1}	
I CLASSICAL SKIMMER	8.0	0.04	0.5	10.0	17.0	0.85	2.8×10^{18}	840	247	19.3	1.5×10^{22}	0.03
II CONDENSING SKIMMER	8.0	0.04	1.2	9.2	17.0	2.2	1.1×10^{18}	760	87	18.7	5.6×10^{21}	0.03

THE OVEN PARAMETERS n_0, T_0, P_0 CORRESPOND TO USED VALUES PRODUCING A MAXIMUM DENSITY OF 10^{15} CM^{-3} ON THE AXIS IN THE MIDDLE OF THE USED JET, 17 CM FROM THE NOZZLE.

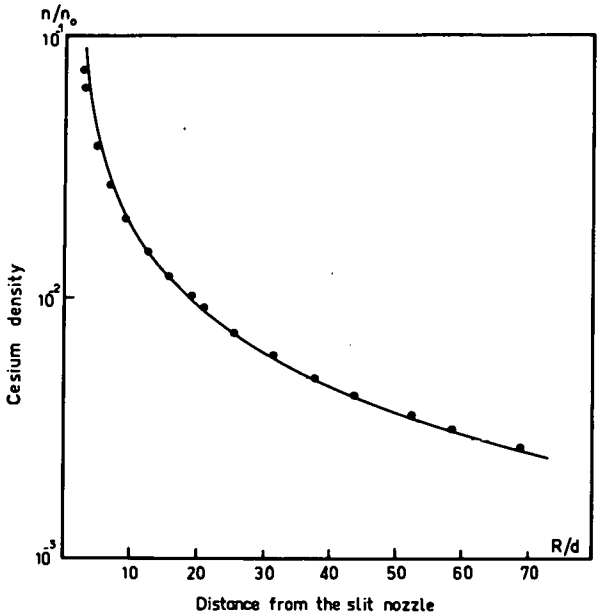

FIG. 1 DENSITY EVOLUTION ON THE AXIS OF A SLIT-TYPE SUPERSONIC JET. THE SOLID LINE REPRESENTS THE DENSITY VARIATIONS GIVEN BY EQ. 2 WITH γ = 1.125. THE DOT (.) REPRESENT RESULTS OF NUMERICAL CALCULATION BY THE METHOD OF CHARACTERISTIC.

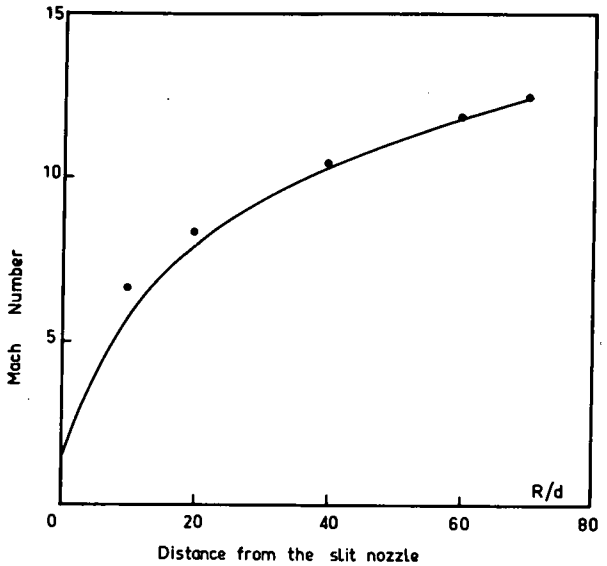

FIG. 2 MACH NUMBER EVOLUTION ON THE AXIS OF A SLIT-TYPE SUPERSONIC JET. THE SOLID LINE REPRESENTS THE MACH NUMBER VARIATIONS GIVEN BY EQ. 1, WITH γ = 1.125. THE DOTS (.) REPRESENT RESULTS OF NUMERICAL CALCULATION BY THE METHOD OF CHARACTERISTIC.

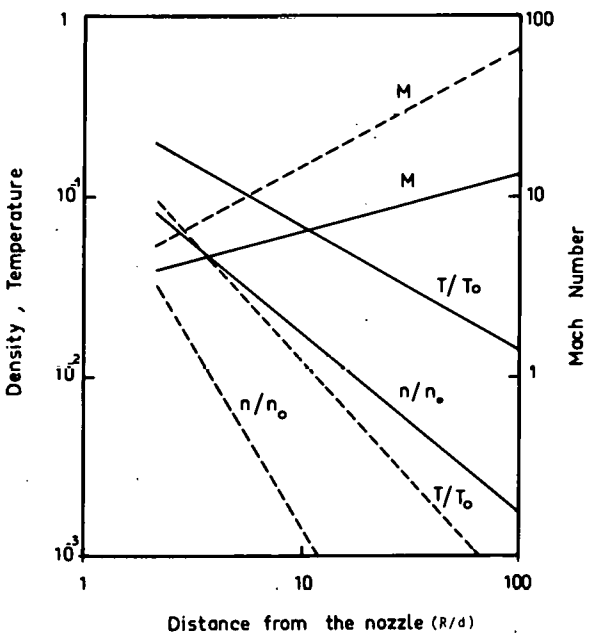

FIG. 3 COMPARAISON BETWEEN SLIT-TYPE AND AXISYMMETRIC JETS OF CESIUM. THE SOLID LINES REPRESENTS THE VARIATIONS OF DENSITY, TEMPERATURE AND MACH NUMBER OF SLIT-TYPE JET AS A FUNCTION OF THE DISTANCE FROM THE NOZZLE. THE DOTTED LINES CORRESPOND TO THE AXISYMMETRIC JET.

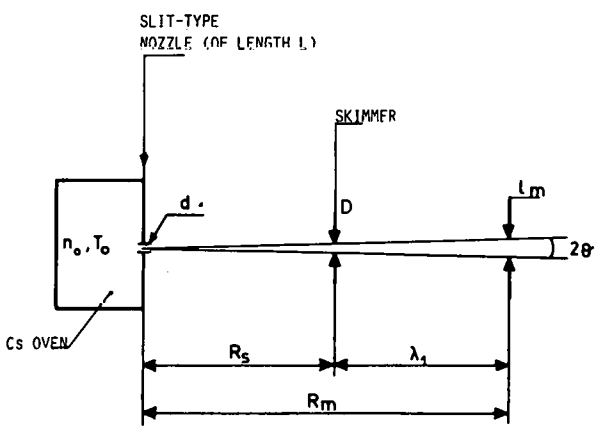

FIG. 4 GEOMETRICAL ARRANGEMENT OF THE CESIUM JET.

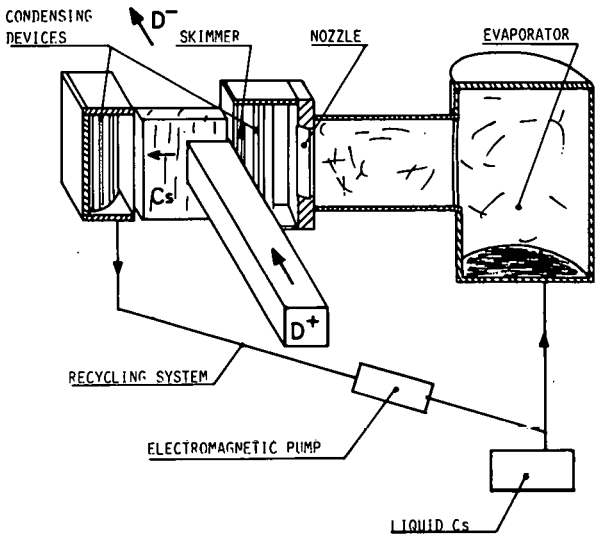

FIG. 5 SCHEMATIC VIEW OF THE CELL.

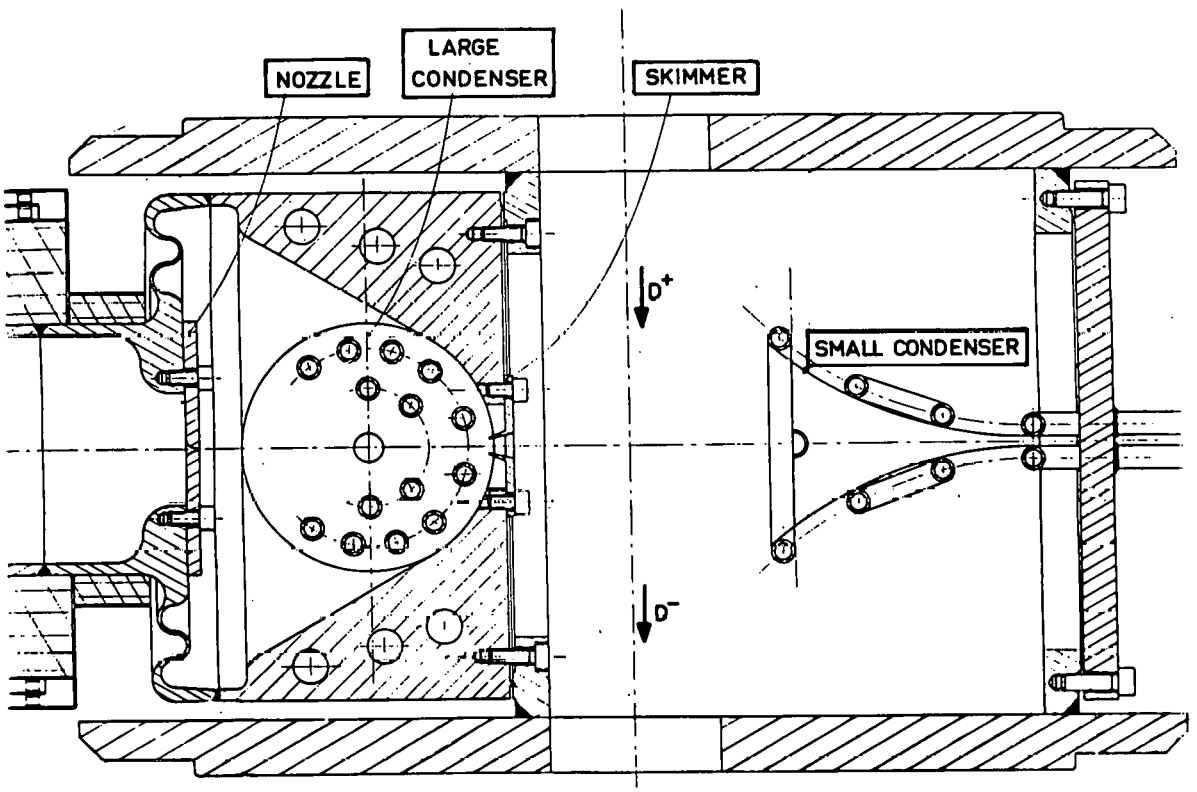

FIG. 6 TOP VIEW OF THE SLIT-TYPE CESIUM JET DEVICE.

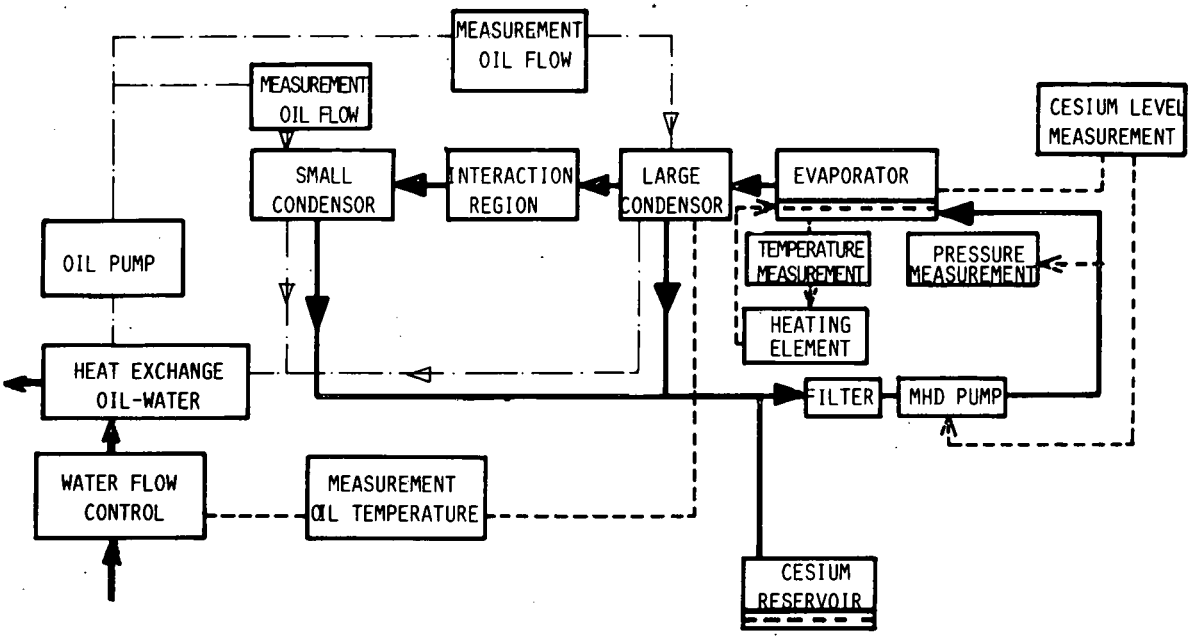

FIGURE 7.

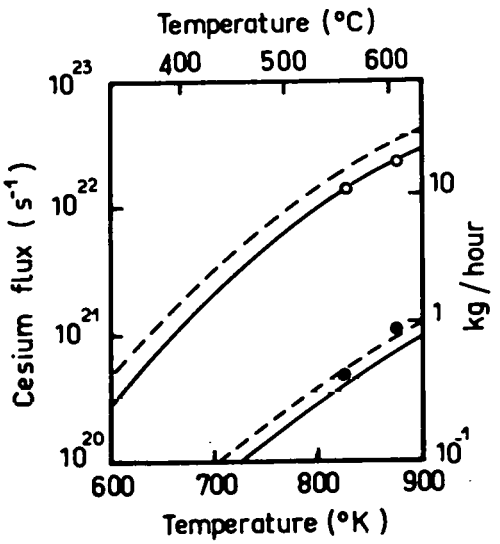

FIG. 8 CESIUM FLUX VERSUS OVEN TEMPERATURE WITH A CLASSICAL SKIMMER.

o ARE EXPERIMENTAL VALUES IN THE LARGE CONDENSER AND • IN THE SMALL CONDENSER - THE DOTTED AND SOLID LINES ARE THEORETICAL CURVES CORRESPONDING TO C_D = 1 AND 1.5 RESPECTIVELY IN EQ. 12

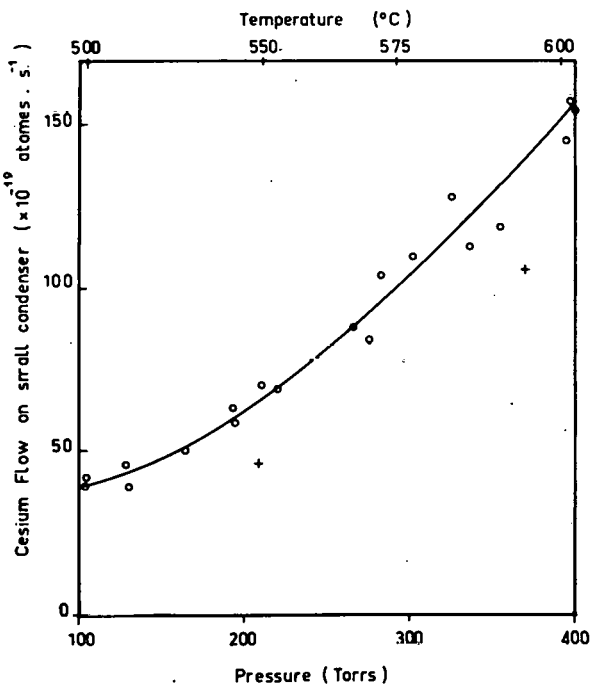

FIG. 9 VARIATIONS OF CESIUM FLOW ON THE SMALL CONDENSER AS A FUNCTION OF OVEN PRESSURE AND TEMPERATURE - O WITH CONDENSING SKIMMER - + WITH CLASSICAL SKIMMER.

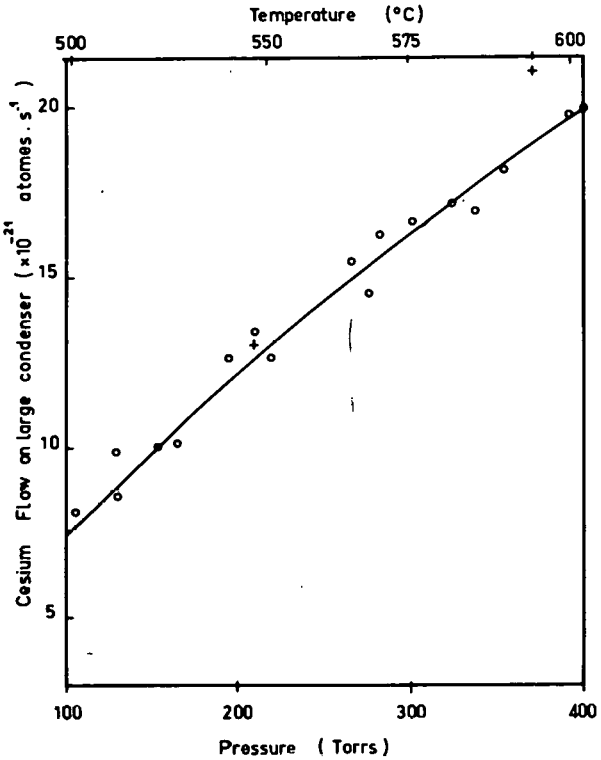

FIG. 10 VARIATIONS OF CESIUM FLOW ON THE LARGE CONDENSER AS A FUNCTION OF OVEN PRESSURE AND TEMPERATURE - O WITH CONDENSING SKIMMER - + WITH CLASSICAL SKIMMER.

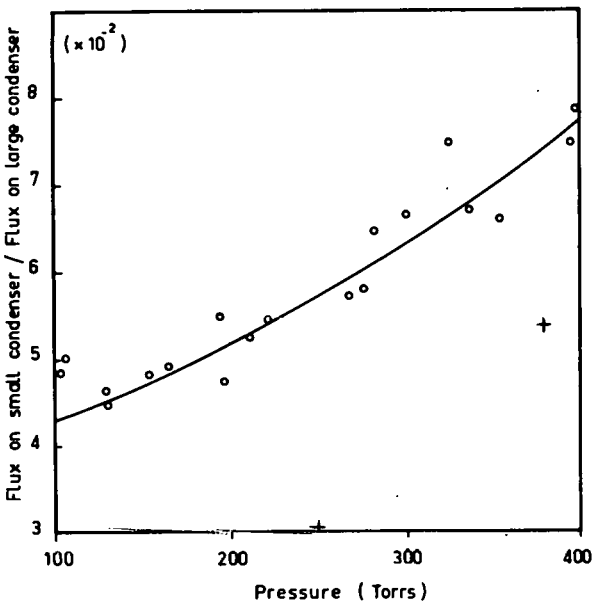

FIG. 11 VARIATIONS OF THE RATIO OF THE CESIUM FLUX IN THE TWO CONDENSERS VERSUS PRESSURE. O WITH CONDENSING SKIMMER + WITH CLASSICAL SKIMMER.

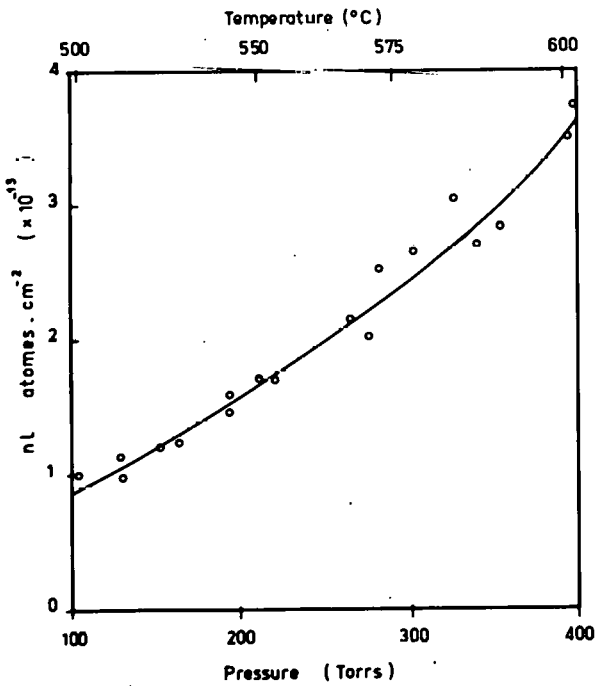

FIG. 12 $n\ell$ VARIATIONS VERSUS OVEN PRESSURE AND TEMPERATURE. O WITH CONDENSING SKIMMER.

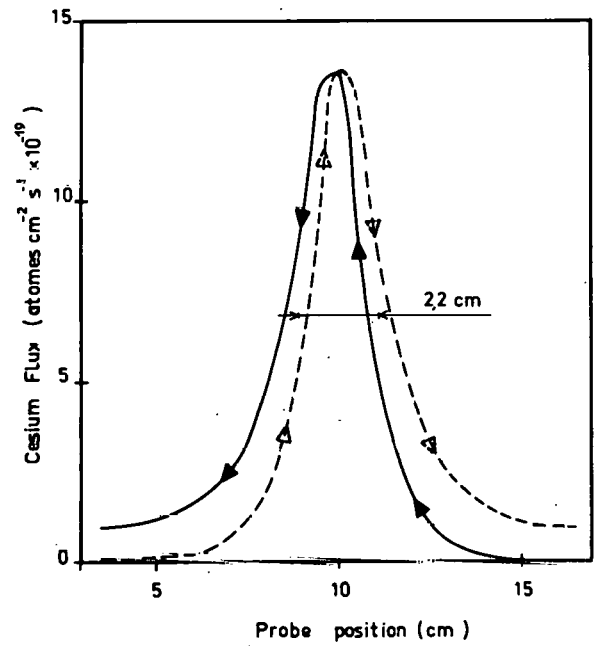

FIG. 13 CESIUM JET PROFILE APPROXIMATION WITH A CONDENSING SKIMMER : THE DIFFERENCE BETWEEN THE TWO CURVES OBTAINED FOR TWO OPPOSITE MOTION DIRECTION GIVES AN IDEA OF THE IMPORTANCE OF CONDUCTION ON THERMAL LOSSES.

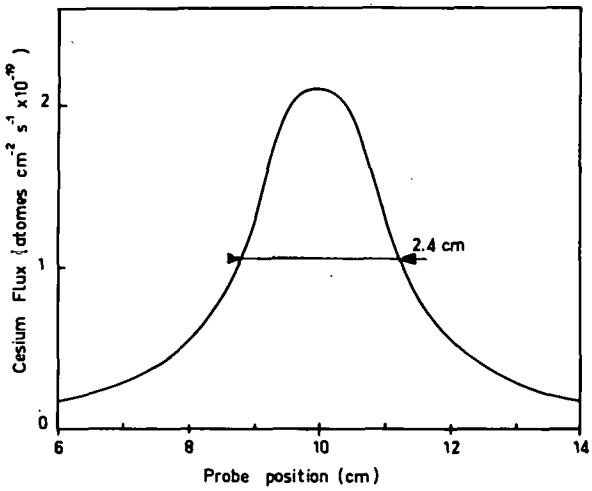

FIG. 14 CESIUM JET PROFILE WITH A CLASSICAL SKIMMER.

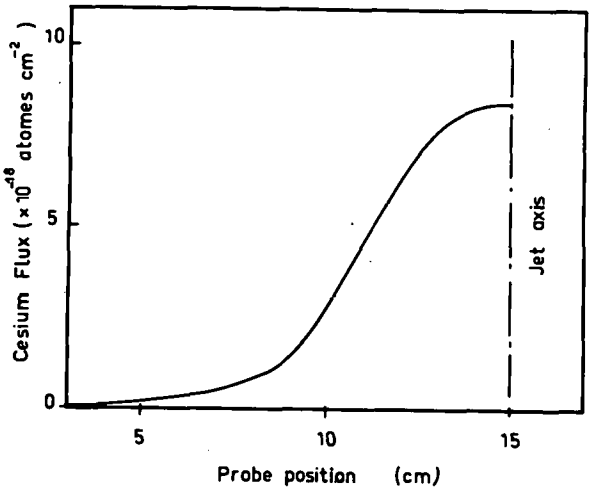

FIG. 15 CESIUM PROFILE PARALLEL TO THE SLIT WITH A CLASSICAL SKIMMER.

DISCUSSION

HAGENA These are very nice results. I am glad that the condensing skimmer works because it is not as trivial as some of you might think because after all we have very high velocity cesium atoms incident on a surface. What I wanted to ask is the theoretical beam performance after the skimmer? You showed after the skimmer a beam profile of 2.2 cm wide, which would be theoretically determined by the actual Mach number of the flow at the skimmer.

DOUCET We just can say that because we see no expansion of the beam, the Mach number is of the order of what is expected, namely around 20, but I can not say it is 18 or 22.

HOOPER The ultimate performance of any of these jets is going to come from re-evaporization of the material that condenses on a surface, then evaporates and perhaps in collisions with the edge of the jet or with other surfaces works its way down the system. Have you estimated the ultimate flux from a condensing skimmer of your type that would work its way down the system?

DOUCET No, I can only say that we have something like 6 W/cm^2 thermal exchange between the cooling tubes and the cesium flow. It can easily go to 10 W/cm^2 and by being careful we can go perhaps a little bit further.

HOOPER Even at the melting point of cesium you have a certain rate of re-evaporation...

DOUCET The rate of evaporation corresponds to the vapor pressure of the cesium at the temperature of the surface. So, as long as you are able to cool the surface enough then the evaporation rate is very low. You have to cool enough, but not too much. If you cool too much the cesium will become solid and then you will close the skimmer with solid cesium. The temperature is chosen to 40°C in order to be sure that the cesium is always liquid everywhere and never solid.

PETERSON What do you estimate is the Cs_2 content in the cesium jet?

GELLER We have a young fellow working on that. The theory is not ready.

Before I close this session I want to thank all the speakers and I have to tell you something highly confidential: we moved away the skimmer of this jet and it works as well.

THIS PAGE

WAS INTENTIONALLY

LEFT BLANK

NEUTRALIZERS

THIS PAGE

WAS INTENTIONALLY

LEFT BLANK

THE STRIPPING OF 30-200 keV H^- IONS

L. W. Anderson, C. J. Anderson, R. J. Girnius, and A. M. Howald
Department of Physics, University of Wisconsin
Madison, Wisconsin 53706

Abstract

Measurements on the stripping of 30-200 keV H^- ions to produce fast H^o atoms are discussed. The maximum neutral fraction is reported for H^- ions incident on a large variety of gas and vapor targets. Efficient neutralization is obtained in Li, Na, Cs, and H_2. We also report measurements of the total charge changing cross sections σ_{-o}, σ_{-+}, σ_{g+}, and σ_{g-} for fast H^- ions and fast ground level H^o atoms incident on a variety of gas and vapor targets.

I. Introduction

A potentially useful method of heating a magnetically confined plasma is by injection of fast neutral deuterium atoms. A beam of fast D^o atoms can be made by accelerating a beam of D^- ions formed at low energy to a high energy and then stripping an electron from some of the fast D^- ions. Using the apparatus shown in Fig. 1,

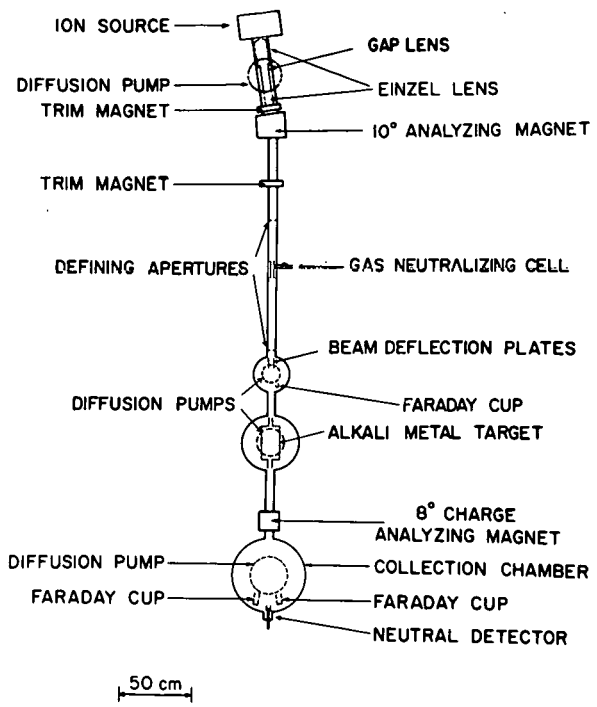

Fig. 1. Schematic diagram of our apparatus.

we have studied the fractional yields and the total charge changing cross sections involved in the production of fast H^o atoms from 30-200 keV H^- ions. At these energies the fractional yields and the total charge changing cross sections are the same for hydrogen or deuterium incident on a target at the same velocity. We have used H_2, He, Ne, Ar, Kr, Xe, Li, Na, K, Rb, and Cs gas and vapor targets for measurements of both fractional yields and cross sections.

II. Measurements of Maximum Neutral Yield

When 30-200 keV H^- ions are incident on a gas or vapor target the neutral fraction increases from zero to a maximum value, F_o^{max}, and then falls to the equilibrium fraction, F_o^{∞}, as the target thickness π (in atoms/cm^2) increases from zero to the thickness necessary for equilibrium. For 100 keV H^- ions incident on a Cs vapor target the positive, neutral, and negative fractions as a function of π are shown in Fig. 2. We have

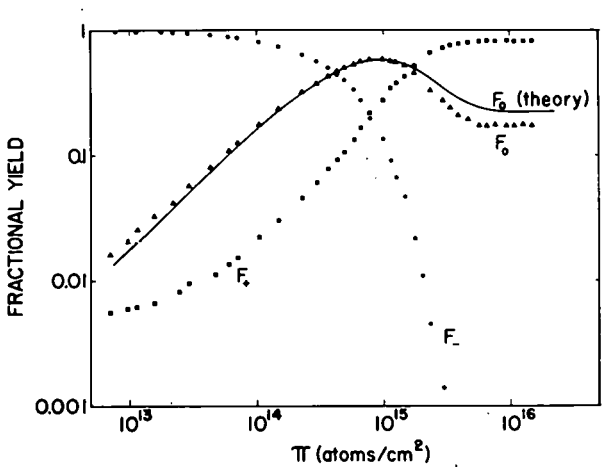

Fig. 2. Fractional yield of H^-, H^o, and H^+ ions when H^- ions are incident on a Cs target with an energy of 100 keV. The solid curve is a theoretical calculation of F_o using a three component theory.

measured the maximum neutral fraction for H^- ion incident on a wide variety of targets including targets other than those previously mentioned. The results of these measurements are shown in Figs. 3 and 4. The value of π at which the neutral fraction is a maximum is shown in Fig. 5.

An interesting aspect to the data shown in Figs. 3 and 4 is the insensitivity of F_o^{max} to energy in the range 100-200 keV. Our measurements together with the measurements of Smythe and Toevs,[1] the measurements of Dimov and Dudnikov,[3] and a calculation of Berkner et al.[3] show that F_o^{max} is constant for H^- incident on H_2

for energies from 100 keV to 14 MeV.

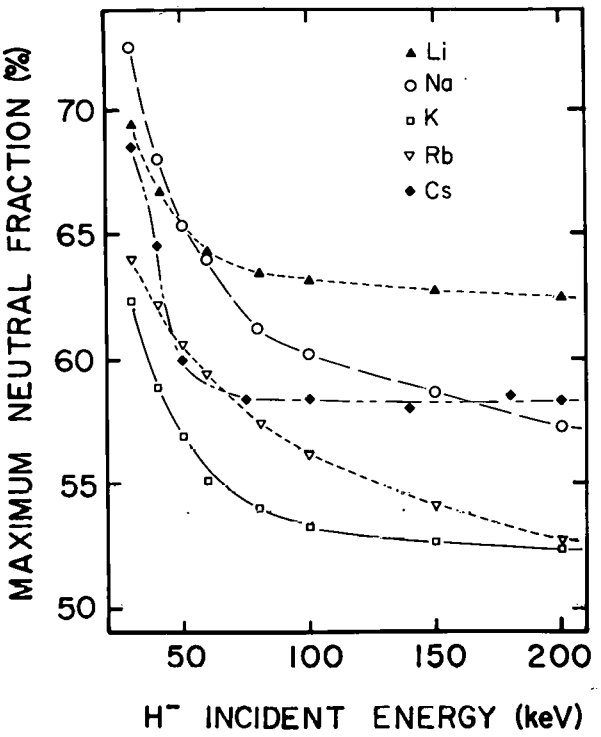

Fig. 3. F_o^{max} as a function of the energy for H^- ions incident on alkali vapor targets.

As can be seen from Figs. 3 and 4 for H^- ions incident in the energy range 100-200 keV Li, Na, Cs, and H_2 are good neutralizers with F_o^{max} = 0.63, 0.60, 0.58 and 0.58 respectively at 100 keV. A higher neutral yield can be obtained with two targets as shown in Fig. 6. For H^- ions incident with energy in the range 100-200 keV the maximum neutral fraction is much larger than the equilibrium neutral fraction. The small value for F_o^∞ for 100-200 keV H^- ions incident is illustrated by our measurements of F_o^∞ for the alkali vapor targets as shown in Fig. 7.

III. Measurements of Charge Changing Cross Sections

We have measured the total charge changing cross sections σ_{-o} and σ_{-+} for 30-200 keV H^- ions incident on a variety of targets. The cross sections σ_{-o} and σ_{-+} are obtained from the variation of the neutral and positive fractions respectively as a function of π for low values of π when H^- ions are incident on the target. Figs. 8-11 show our measurements of σ_{-o} and σ_{-+}. We have also measured σ_{g+} and σ_{g-} for fast (30-200 keV) ground level H^0 atoms incident on the same targets. The cross sections σ_{g+} and σ_{g-} are obtained from the variation of the positive and negative fractions respectively as a function π for low values of π when fast ground level

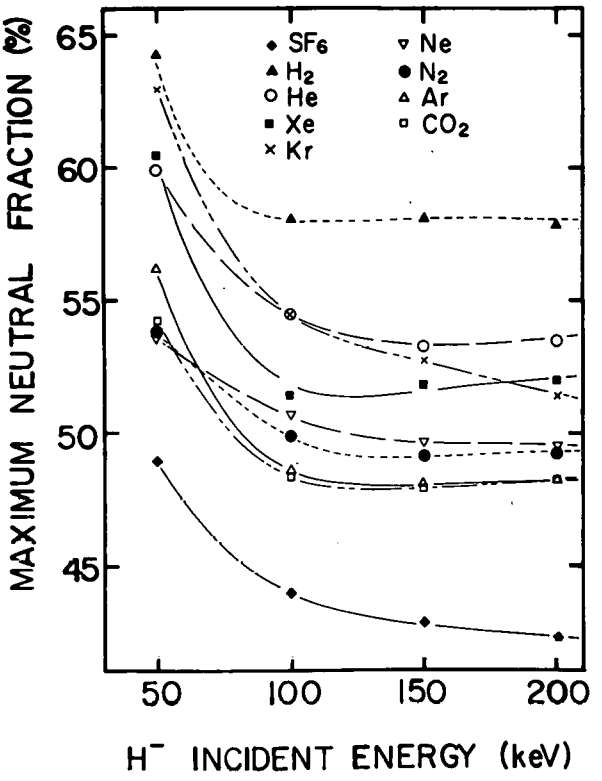

Fig. 4. F_o^{max} as a function of the energy of the H^- ions incident on a variety of gas targets.

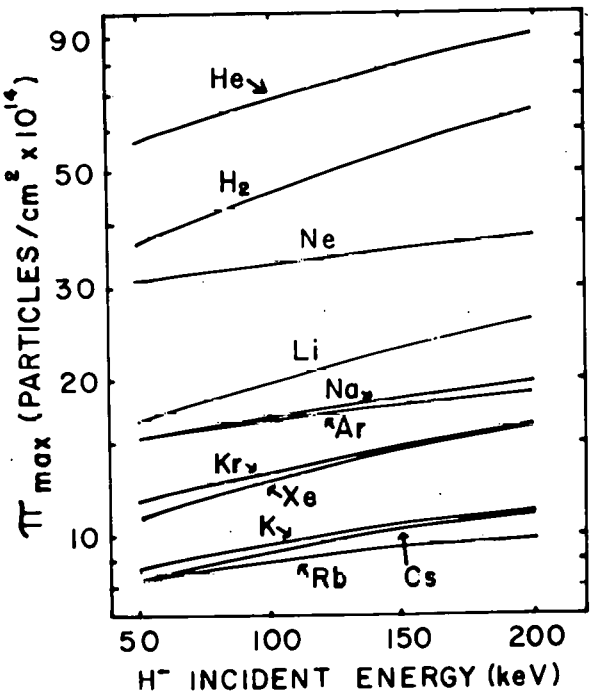

Fig. 5. π_{max} as a function of the energy of the H^- ions incident on a variety of targets.

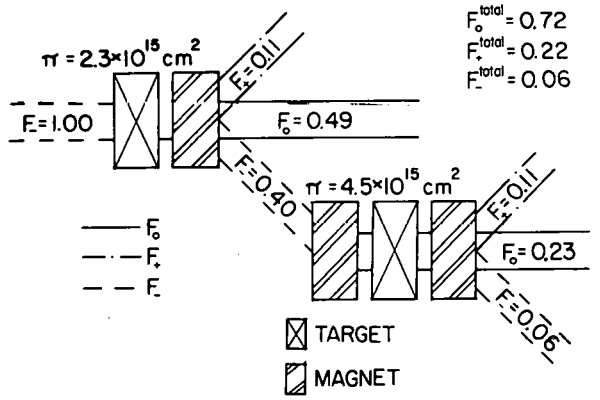

Fig. 6. Two target method for increasing neutral yield.

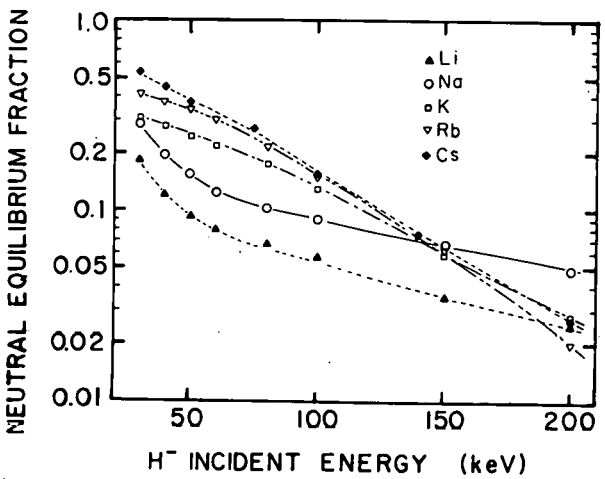

Fig. 7. F_o^{∞} as a function of the energy for H^- ions incident on alkali vapor targets.

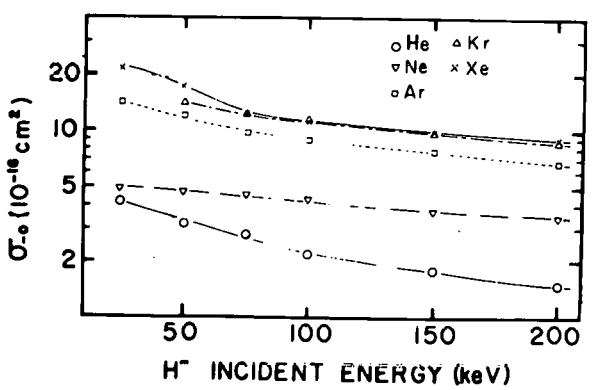

Fig. 8. σ_{-o} as a function of the energy for H^- ions incident on rare gas targets.

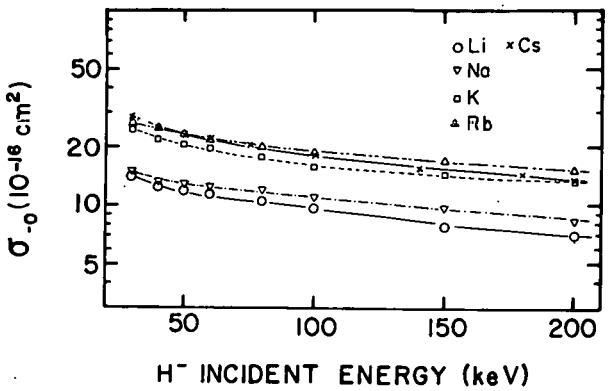

Fig. 9. σ_{-o} as a function of the energy for H^- ions incident on alkali vapor targets.

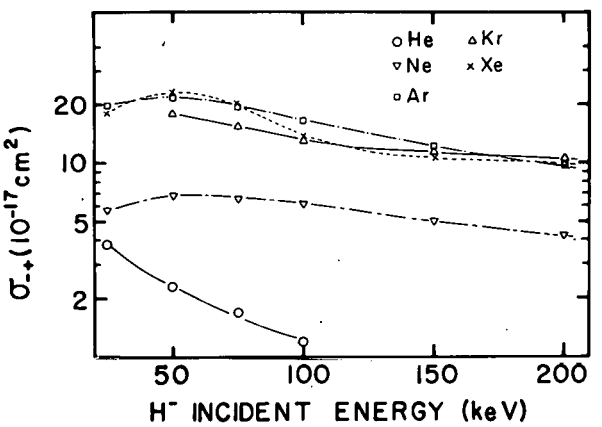

Fig. 10. σ_{-+} as a function of the energy for H^- ions incident on rare gas targets.

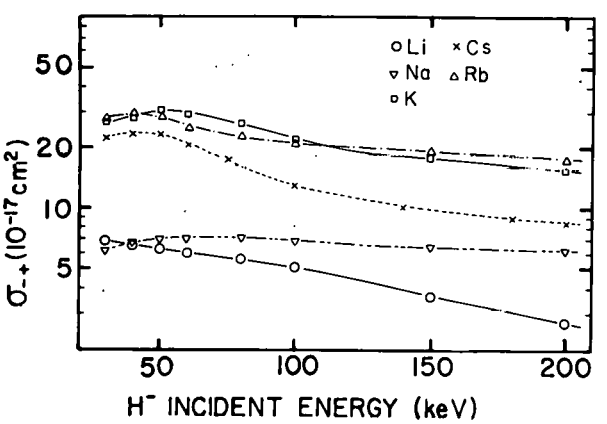

Fig. 11. σ_{-+} as a function of the energy for H^- ions incident on alkali targets.

H^0 atoms are incident on the target. The H^0 atoms are believed to be primarily in the ground level because of the following reasons. The fast H^0 atoms are prepared by stripping H^- ions in Ar. Any H^+ or H^- ions in the beam after the Ar target are deflected by an electric field. The electric field also quenches any H(2s) atoms. The flight time from the Ar target is long compared to the lifetime of an H^0 atom with $n \lesssim 6$. Thus most of the H^0 atoms are in the ground level. Our measurements on σ_{g+} and σ_{o-} are shown in Figs. 12 - 15. Fig. 16 shows measurements with both H^-

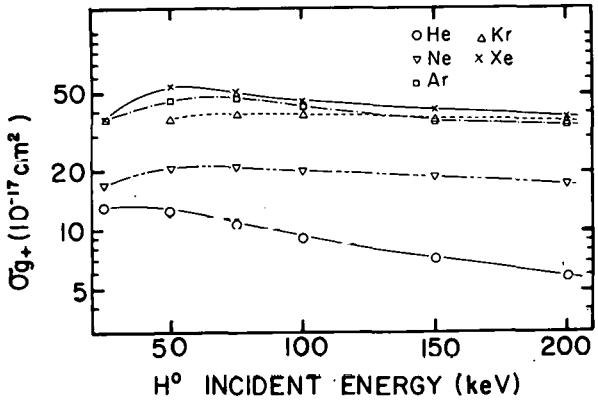

Fig. 12. σ_{g+} as a function of the energy for fast ground level H^0 atoms incident on rare gas targets.

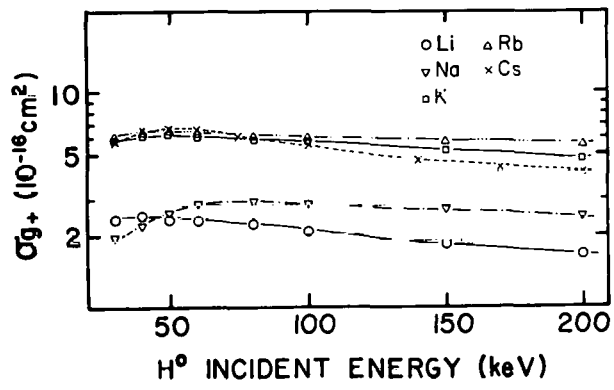

Fig. 13. σ_{g+} as a function of the energy for fast ground level H^0 atoms incident on alkali vapor targets.

and D^- ions (or fast H^0 or D^0 atoms) incident on Xe with the D^- (or D^0) data plotted at half the energy. It is clear from this data that within our errors the cross sections for H^- and D^- incident are identical at the same velocity. Table 1 shows a comparison of our measurements with previous measurements.

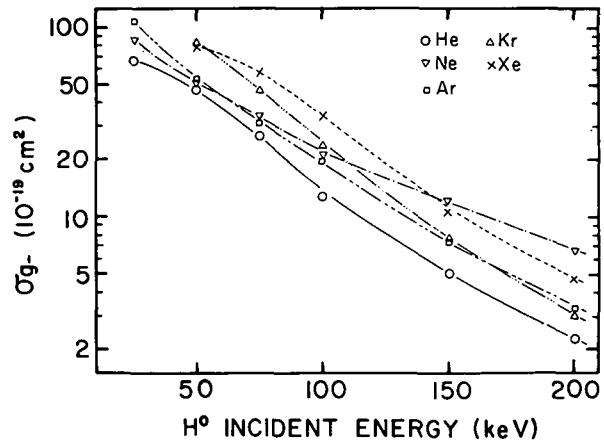

Fig. 14. σ_{g-} as a function of the energy for fast ground level H^0 atoms incident on rare gas targets.

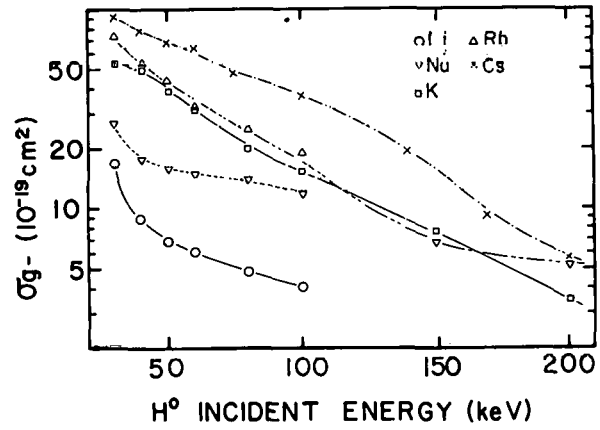

Fig. 15. σ_{g-} as a function of the energy for fast ground level H^0 atoms incident on alkali vapor targets.

IV. Calculation of F_0 as a function of π

We have carried out calculations of the neutralization process using a three component theory and using the experimental cross sections σ_{+0}, σ_{g+}, σ_{-0}, and σ_{-+} (in our analysis σ_{+-}, and σ_{g-} are sufficiently small to be negligible). The results of such an analysis for H^- incident on Co are shown as the solid line in Fig. 2. The calculated neutral fraction agrees well with the experimental values for the range of π up from zero to π_{max} but does not agree well for large values of π. We believe that this is because σ_{g+} is used in the analysis. At low values of π most of the H^- ions that are stripped form ground level H^0 atoms but at high values of π repeated stripping of H^0 atoms to form H^+ ions followed by neutralization by electron capture to form H^0 produces many excited H^0 atoms. The use of σ_{g+} is not appropriate when many of the H^0 atoms are in excited levels.

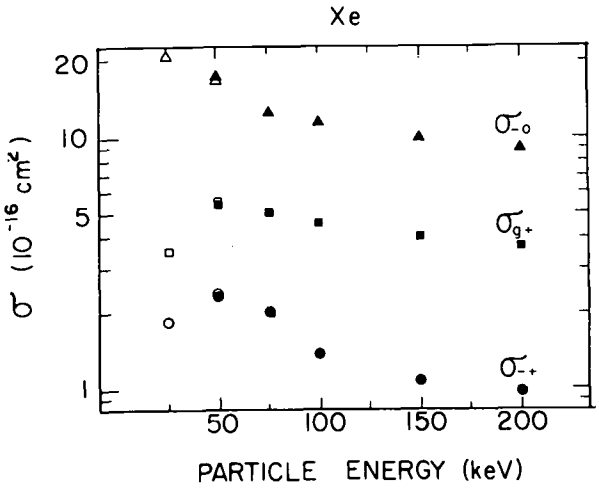

Fig. 16. σ_{-o}, σ_{g+}, and σ_{-+} for H^- (and D^-) and fast ground level H^o (and D^o) incident on Xe. The open symbols are for deuterium incident and plotted at half the energy. As can be seen $\sigma_{-o} > \sigma_{g+} > \sigma_{-+}$ for a Xe target. In fact for all targets we have investigated $\sigma_{-o} > \sigma_{g+} > \sigma_{-+}$.

Bibliography

1. R. Smythe and J. W. Toevs, Phys. Rev. 139, A 15 (1965).
2. G. I. Dimov and V. G. Dudnikov, Sov. Phys. Tech. Phys. 11, 919 (1967).
3. K. H. Berkner, R. V. Pyle, J. W. Stearns, Nucl. Fusion 15, 249 (1975).
4. J. B. H. Stedeford and J. B. Hasted, Proc. Roy. Sec. A227, 466 (1955).
5. J. F. Williams, Phys. Rev. 154, 9 (1967).
6. P. M. Steir and C. F. Barnett, Phys. Rev. 109, 355 (1958).
7. J. Heinemeir, P. Hvelplund, and F. R. Simpson, J. Phys. B9, 2669 (1976).
8. T. J. Morgan, K. H. Berkner, W. G. Graham, R. V. Pyle, and J. W. Stearns, Phys. Rev. 14, 644 (1976).
9. Ia M. Fogel, V. A. Ankudinov, and R. E. Slabospitskii, Sov. Phys. JETP 5, 382 (1957).
10. Ia M. Fogel', V. A. Ankudinov, D. V. Pilipenko, and N. V. Topolia, Soviet Phys. JETP 34, 400 (1958).
11. E. S. Solov'ev, R. N. Ilin, V. A. Oparin and N. V. Fedorenko, Sov. Phys. JETP 15, 459 (1962).
12. J. F. Williams, Phys. Rev. 153, (1967).
13. C. F. Barnett and H. K. Reynolds, Phys. Rev. 109, 355 (1958).
14. L. H. Tobieren, M. Y. Nakai, and R. A. Langley, Phys. Rev. 171, 114 (1968).
15. B. A. D'yachkov, Sov. Atomic Energy 27, 958 (1969).

Table 1.

Comparison of the previous measurements of σ_{-o}, σ_{-+}, σ_{o+}, and σ_{o-} by others with our measurements. For each cross section we show the authors, the reference, and the energy range of the previous measurements and the percentage difference between our measurements and the previous measurements. Thus our measured values for σ_{-o} are less than 10% higher than the previous measurements of Stier and Barnett in the energy range where the measurements overlap.

Ref.		Energy		Ne	Ar	Kr	Xe	Li
σ_{-o}								
Stedeford & Hasted	Ref.4	3-40	keV	+15%	+15%	+110%	+100%	
Williams	Ref.5	2-50	keV	<15%	<15%	+80%	+40%	
Stier & Barnett	Ref.6	3-40	keV	<10%	<10%			
Heinimeier et.al.	Ref.7	50-500	keV		<5%			
Morgan et.al.	Ref.8	1.25-25	keV				<5%	
σ_{-+}								
Fogel' et.al.	Ref.9	5-40	keV	-10%	-20%	-30%	-20%	
Williams	Ref.5	2-50	keV	<5	-20%			
Heinimeier	Ref.7	50-500	keV		-15%			
Morgan et.al.	Ref.8	1.25-25	keV				<5%	
σ_{o+}								
Stier & Barnett	Ref.6	3-200	keV	<10%	<10%			
Fogel' et.al.	Ref.10	5-40	keV	-10%	-30%	-15%	-25%	
Solov'ev et.al.	Ref.11	10-180%		-15%	+10%	+60%		
Williams	Ref.12	2-50	keV	<10%	<10%	+60%	+30%	
Barnett & Reynolds	Ref.13	10-1000	keV		<10%			
Morgan et.al.	Ref.8	1.25-25	keV				<5%	
Toburen et.al.	Ref.14	100-2500	keV		<10%	<10%		
Dryachkov et.al.	Ref.15	10-400	keV					-50%
σ_{o-}								
Williams	Ref.12	2-50	keV	-10%	-30%			
Stier & Barnett	Ref.6	4-30	keV	<5%	<5%			
Morgan	Ref.8						<10%	

DISCUSSION

HOOPER I have heard it suggested more than once that perhaps complex molecules, in particular hydro-carbons, might have very large stripping efficiencies and be easier to handle than either hydrogen or the alkali metals. Do you think there is any reason to be optimistic?

ANDERSON No, I think there is every reason to be pessimistic. Our experience is that the larger the molecule the worse it is for neutral production. SF_6 was very bad, I did not show the data for it, but we have taken data on methane and ethane and ethane was worse than methane and neither was good. In fact they were both down 40% or lower and for that reason I did not show them on the viewgraphs. The problem is that there are two cross sections that come in to that, not just one. I think the cross section to strip the electron from the negative ions is going to be very large. But I think that unfortunately the cross section to σ_{0+} which is the other one that came in, is likely to be even larger; that has been our experience on the gases that we have measured. The more complex the gas the worse the reaction, the lower the neutralization.

STEWART These peaks in the neutral fraction with respect to target thickness, are these going to be broad enough so that with a system one has enough control to keep the neutral fraction at optimum?

ANDERSON I do not know. I can tell you how broad they are. You have to tell me if they are too broad or too narrow, but we can certainly work from something like 5×10^{14} to 2×10^{15} which is a factor of 4.

STEWART When you have a lithium system is it difficult to keep the target density in that kind of a range?

ANDERSON We found it difficult because the only way we have it regulating is through the temperature of the vapor pressure and so if it gets a little too hot the vapor pressure goes up and the target has to cool down before it changes. Now, if you could cool it faster or you have some other way of controlling it, it might be a lot better than our system.

HOOPER Perhaps I could comment on that. With our sodium jet we had no problem at all in maintaining 10-20% line density for at least short periods and this was with very crude feedback systems on temperature.

HAGENA I would agree with that statement. The density of a jet target can be easily controlled. I have another question in regard to the maximum of the target thickness. How does it change with energy? You showed the cross section as a function of energy. The maximum target thickness should also depend somewhat on energy. If we go eventually to 200 keV or 500 keV, one would be interested to know the target thickness.

ANDERSON I think we have a graph of the target thickness at which the maximum is achieved and as I said at the time, for lithium at 150 kV it is approximately 2×10^{15} particles/cm^2. Cesium is appreciably lower, it is about a factor of 2 lower, but on the other hand cesium does have a little more angular scattering, so I am not really sure which one is the better.

HAGENA Sorry I overlooked this graph, as you move to higher energies there are no drastic things to be expected, I guess.

ANDERSON I can not answer your question.

HAGENA Your cross section showed a very gradual behavior.

ANDERSON I would presume that and certainly the calculation of the people at Lawrence Berkeley, Berkner, Sterns and Pyle, indicated that the maximum neutral fraction was insensitive to energy out as far as 14 MeV. So I would anticipate that the η_{max} would show no rapid change either.

MORGAN Have you tried any alkali earths or what would you expect there?

ANDERSON I do not know.

MORGAN You mentioned that using H^- incident beams typically would produce an H_0 beam that was lower in excited states than electron capture. Is there data available on that or is that just kind of speculation?

ANDERSON The only thing we have got on that are some simple-minded calculations. I do not know of any actual measurements.

MORGAN Perhaps not at the high energies.

ANDERSON Measurements are all down around less than 20 kV.

MORGAN Right.

ANDERSON I would worry that 100 kV or 200 kV particle might be more agitated when it came out of a collision, than 10 kV. Like I said, the only thing we have are some very crude calculations and I am not at all sure that they are reliable.

Plasma Neutralizers for H⁻ or D⁻ Beams*

K. H. Berkner, R. V. Pyle, S. E. Savas, and K. R. Stalder

Lawrence Berkeley Laboratory
University of California
Berkeley, California 94720

Abstract

Plasma neutralizers can produce higher conversion efficiencies than are obtainable with gas neutralizers for the production of high-energy neutral beams from negative hydrogen ions. Little attention has been paid to experimental neutralizer studies because of the more critical problems connected with the development of negative-ion sources. With the prospect of accelerating ampere dc beams from extrapolatable ion sources some time next year, we are re-examining plasma neutralizers. Some basic considerations, two introductory experiments, and a next-step experiment are described.

Introduction

The injection of energetic deuterium atoms is a proven technique for heating magnetically confined plasmas in the fusion program. Currently, multi-megawatt hydrogen and deuterium beams with energies up to 50 keV are used, and planned experiments call for about 50 MW of neutral-beam power at energies above 150 keV. At these power levels there is a high premium on maximizing the efficiency for producing neutral beams.

It has been recognized for a long time that the weak electron affinity (0.75eV) of a negative hydrogen or deuterium ion, compared to the binding energy of the electron in a ground-state hydrogen atom (13.6eV), makes efficient conversion of an H^- ion beam to a neutral beam possible even at high energies. In a gas target of optimized thickness the neutralization efficiency can be about 60 percent even for MeV ions.[1]

Riviere and Sweetman[1] showed that the conversion of an H^- or D^- beam to an H^0 or D^0 beam can be considerably more efficient if the target consists of charged particles, i.e., a plasma. A neutralization efficiency, η, of 90% was calculated from cross sections obtained from single-particle interactions in H^--e^- crossed beam experiments. At Novosibirsk, approximately this conversion efficiency was obtained by shooting lithium and magnesium plasmas from conical plasma guns across a 0.5-to 1.0-MeV H^- beam and measuring the growth and decay of the various charge components.[2,3] Values of η=81% for Li and 80% for magnesium were obtained. We are not aware of any other measurements with plasma targets. Some additional information on this topic was given in a paper by Grossman at the first Symposium in 19//.[4]

If they are to be useful, plasma neutralizers must give substantially higher conversion efficiencies than gas cells; also, they must operate dc and have good electrical and gas efficiencies, as well as suitable geometrical configurations. Neutralizer efficiency has not received much attention in the negative-ion system program because the development of negative-ion sources has been, and continues to be, the critical item. As shown in other papers in this symposium, the progress in source development is quite encouraging, and, as ion sources, accelerators, and neutralizers must be compatible, we are re-examining the plasma-neutralizer topic, including a modest experimental effort in the 200-to-300-keV range.

We are investigating two types of plasma neutralizers with a D^- beam from a small research accelerator: One is a high-density, pulsed hydrogen discharge; the other is a low-density cesium plasma produced in a surface-ionization Q-machine. In this paper we present calculations for the neutralization efficiency expected for partially ionized hydrogen and cesium plasmas. The two plasma targets are described, as is a possible next-step experiment. Neutralization results for the two targets are not yet available.

Computations

We have examined several cases of interest for negative-ion-beam plasma neutralizers. The evolution of the beam fractions is given by equations (1) thru (3).

$$\frac{dI^0}{dX} = I^+ \sum_s \sigma^s_{+0} n_s + I^- \sum_s \sigma^s_{-0} n_s - I_0 \sum_s (\sigma^s_{0+} + \sigma^s_{0-}) n_s \quad (1)$$

$$\frac{dI^+}{dX} = -I^+ \sum_s (\sigma^s_{+0} + \sigma^s_{+-}) n_s + I^- \sum_s \sigma^s_{-+} n_s + I^0 \sum_s \sigma^s_{0+} n_s \quad (2)$$

$$\frac{dI^-}{dX} = I^+ \sum_s \sigma^s_{+-} n_s - I^- \sum_s (\sigma^s_{-0} + \sigma^s_{-+}) n_s + I^0 \sum_s \sigma^s_{0-} n_s \quad (3)$$

Where

$$\sum_s \sigma_{ij}^s n_s \equiv \sigma_{ij}^e n_e + \sigma_{ij}^i n_i + \sigma_{ij}^g n_g$$

and $I^- + I^+ + I^0 = 1$

where the subscripts i and j refer to initial and final charge states, respectively, and the superscripts e,i,g refer to electrons, ions, and atoms, respectively. For incident D^-, $I^-(0)=1$.

Not all of the cross sections are known; we present the experimentally known or theoretically estimated cross sections relevant for hydrogen and cesium plasmas in Fig. 1 (Refs. 5-13) and Fig. 2 (Refs. 5-7, 13-16). Excellent review articles covering the cross-section data are in Refs. 17 and 18. At the high energies of interest (E > 200 keV) we assume we can neglect all attachment cross sections.

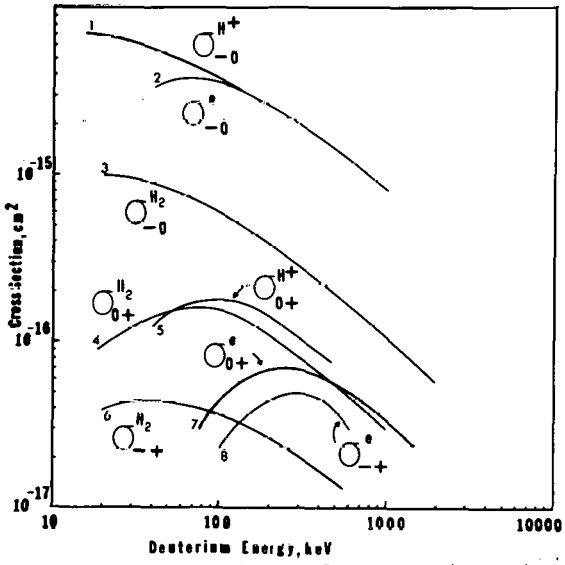

Fig. 1. Cross sections relevant to deuterium plasma neutralizers. Curve 1, Ref. 5; 2, Refs. 6, 7; 3, Ref. 8; 4, Refs. 9, 10; 5, Refs. 11, 12; 6, Ref. 8; 7, Ref. 13; 8, Ref. 14.

We further assume that all target particles are at rest in the laboratory frame. This assumption is valid if the beam velocity is very much greater than electron thermal velocities. For 200 keV D^- this requires that the electron temperature be less than about 5 eV.

For plasma neutralizers we always have $n_e = n_i$. We can then define the degree of ionization as

$$X = \frac{n_i}{n_i + n_g}$$

X equals one for a fully ionized plasma and X equals zero for a neutral gas target.

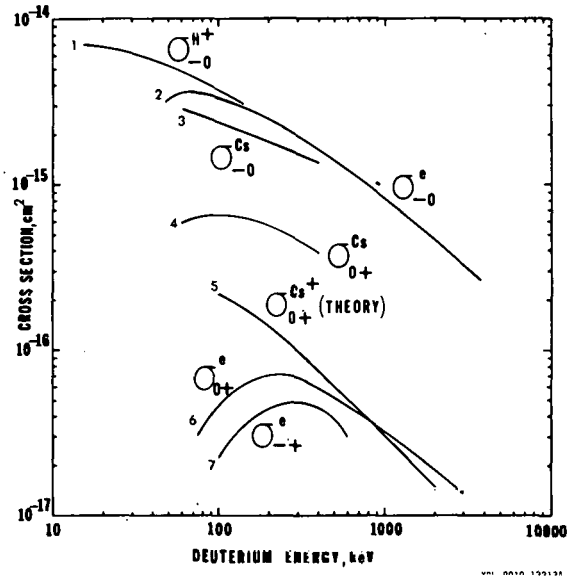

Fig. 2. Cross sections relevant to cesium plasma neutralizers. Curve 1, Ref. 5. ($\sigma_{-0}^{Cs^+}$ is taken to be equal $\sigma_{-0}^{H^+}$ for the purpose of the computations); 2, Refs. 6, 7; 3, Ref. 15; 4, Ref. 15; 5, Ref. 16; 6, Ref. 13; 7, Ref. 14.

Equations (1) - (3) can be integrated analytically. For a homogeneous plasma containing several constituents the maximum neutralization efficiency is

$$\eta_{max} = \frac{\langle\sigma_{-0}\rangle}{\langle\sigma_{-0}\rangle+\langle\sigma_{-+}\rangle}\left(\frac{\langle\sigma_{0+}\rangle}{\langle\sigma_{-0}\rangle+\langle\sigma_{-+}\rangle}\right)^{\frac{\langle\sigma_{0+}\rangle}{\langle\sigma_{-0}\rangle+\langle\sigma_{-+}\rangle-\langle\sigma_{0+}\rangle}} \quad (4)$$

The total integrated line density to achieve the maximum neutralization efficiency is

$$\Pi_{opt} = \frac{1}{\langle\sigma_{-0}\rangle+\langle\sigma_{-+}\rangle-\langle\sigma_{0+}\rangle}\ln\left(\frac{\langle\sigma_{-0}\rangle+\langle\sigma_{-+}\rangle}{\langle\sigma_{0+}\rangle}\right) \quad (5)$$

In equations (4) and (5) we have

$\langle\sigma_{ij}\rangle = \sum_s \sigma_{ij}^s n_s/n_{tot}$ and $n_{tot} = \sum_s n_s$,

and, the total target thickness is

$\pi \equiv \sum_s \int_0^\ell n_s \, dx$.

To illustrate the advantage of a plasma target on the neutralization efficiency for D^- beams, we have solved eqs, 1-3 for plasmas with different degrees of ionization for 300 keV D^-. In Fig. 3 we show the neutralization efficiency η (for negative ion beams, $\eta = I^0$) for a deuterium plasma.

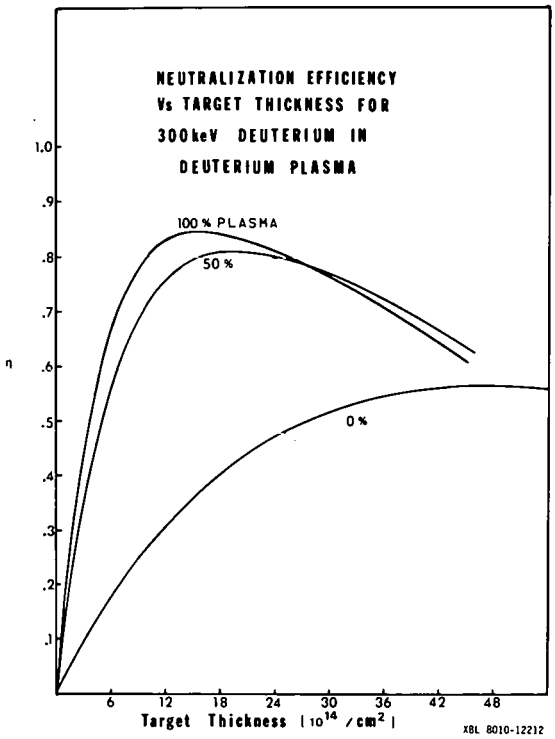

Fig. 3. Neutralization efficiency versus total (electrons and ions and neutrals) target thickness for 300 keV deuterium in a deuerium plasma of various degress of ionization.

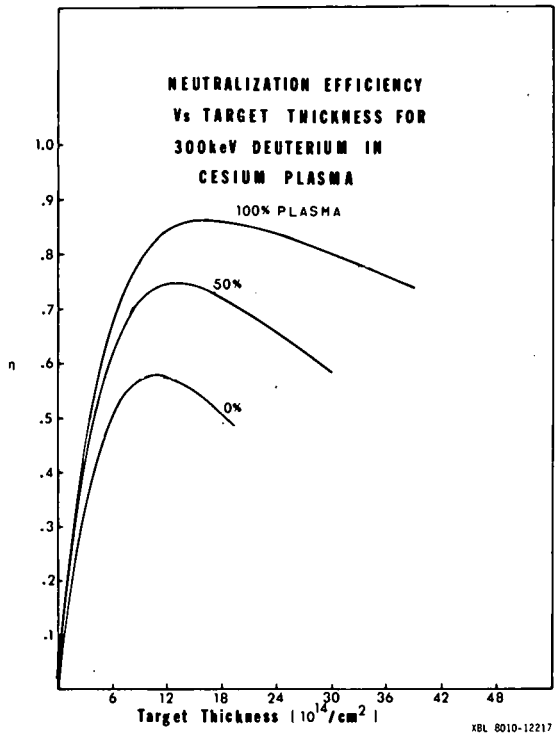

Fig. 4. Neutralization efficiency versus total (electrons and ions and neutrals) target thickness for 300 keV deuterium in a cesium plasma of various degrees of ionization.

We see that the optimum line density (molecules/cm^2) of D_2 gas is about 3 times the optimum line density, $(n_e+n_i)\ell$, of a fully ionized deuterium plasma. In an actual system there will be some neutral gas in the beamline and the maximum conversion efficiency is expected to be between that for pure gas and pure plasma.

The efficiency for D^- in a cesium plasma is shown in figure 4. It is interesting to note that the optimum line density for cesium vapor is about 50 % less than the optimum line density $(n_i+n_e)\ell$ for a fully ionized cesium plasma.

In figure 5 we show the maximum neutralization efficiency as a function of degree of ionization for 300 keV D^- in cesium and deuterium plasmas. We see that the neutralization efficiency for deuterium plasma is fairly high even at low degrees of ionization whereas for cesium plasmas the efficiency rises approximately linearly with the degree of ionization.

Real plasma neutralizers based on deuterium will have a mixture of D^+, D_2^+ and D_3^+. However, we do not have sufficient cross section information to evaluate the effects of molecular ions on neutralizer efficiency.

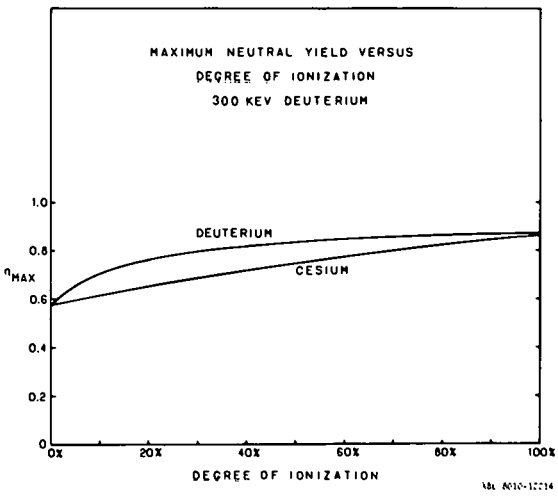

Fig. 5. Maximum neutralization efficiency versus degree of ionization for deuterium and cesium plasmas.

Experimental Program

Hydrogen plasma target

Shown in figure 6 is a plan view of the hydrogen-plasma-target vacuum chamber. D^-

ions from a 300 keV accelerator are steered into the collision chamber and pass through a magnetically confined plasma produced by a hot-cathode (LaB_6) discharge. Gas is pulsed through the anode into the evacuated chamber. The 100 A discharge is pulsed, 1 msec in duration, creating a highly ionized hydrogen plasma, 2 cm X 10 cm in cross section, with a maximum electron line density of 10^{15} cm^{-2} (measured by a movable Langmuir probe and a He-Ne laser interferometer). The measured line density is shown in Fig. 7 as a function of discharge current and magnetic field. The resulting charged and neutral particles then pass between electrostatic analyzing plates and into an analysis chamber. Each charge-state component of the beam is detected and counted separately by an array of diffuse-junction Si detectors and electronic pulse counting equipment. The neutral beam fraction as a function of target thickness is curve fitted to produce an estimate for the maximum neutralization efficiency.

This experiment is operating, but no quotable results have been obtained yet. We also plan to try an atomic-gas, probably argon, target.

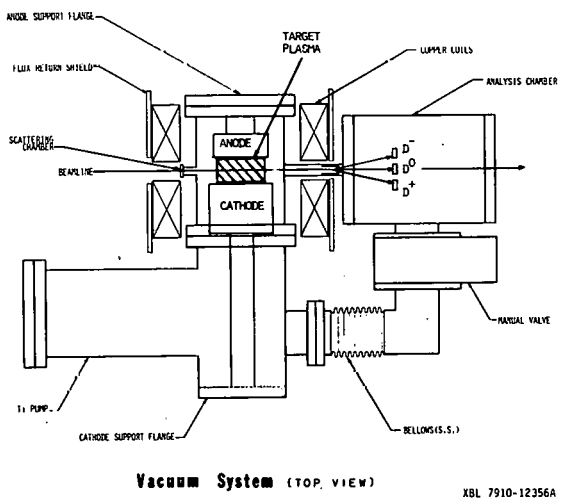

Fig. 6. Experimental arrangement for determination of η_{max} in a hydrogen plasma target.

Cesium plasma target

The cesium plasma target is shown in figure 8. The plasma is a standard Q-Machine plasma originally built for studies of cross sections relevant to heavy-ion fusion. The plasma is formed by spraying cesium vapor on a hot (2700 K) tungsten plate and the contact ionized plasma is confined by an axial magnetic field (B=0.2T). Plasma densities, as measured by Langmuir probes, are variable and are typically 10^{10} cm^{-3}. The diameter of the plasma column is approximately 5 cm. A plasma density profile is shown in Fig. 9. The line density is too small to produce optimum yields and therefore only σ_{-0} and σ_{0+} will be measured. The ambient background pressure is approximately 10^{-6} Torr. Therefore, a plasma chopper is used to separate plasma effects from background gas effects. The vacuum chamber is cooled by liquid nitrogen to keep the cesium atom density below 10^{7} cm^{-3}. The incident D^- beam enters the target region and charged beam particles formed in the plasma are charge-state analyzed in the confining magnetic field. The beams then enter the analysis chamber and will be counted to determine the D^-, D^0 and D^+ fractions. Cross sections are determined from the slope of the D^-, D^0 and D^+ fractions as a function of plasma line density.

This experiment will be performed after the present heavy-ion-fusion-related experiment (C_s^+-C_s^+ cross sections) is completed.

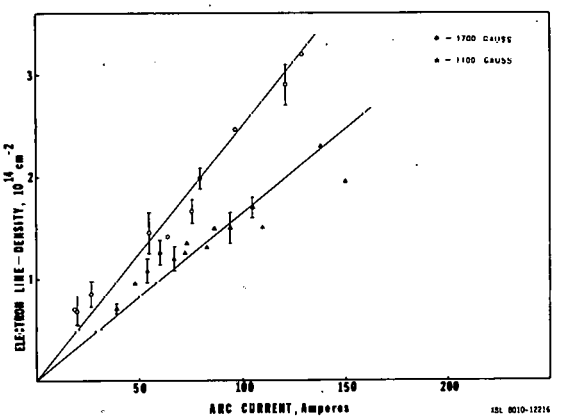

Fig. 7. Electron line density versus arc power for the hydrogen plasma target.

"Practical" plasma target

The experiments described in sections 1 and 2 will yield cross-section information, but the plasma configurations are not suitable for application in practical high-power neutral beam lines. Therefore, our next experimental target will be designed to be compatible with our approach to a multi ampere negative ion accelerator array. We are considering a "magnetic-bucket" arrangement of the general kind described by Ehlers and Leung.[19,20] They have operated a hydrogen discharge in such an arrangement with 10% ionization and ion densities of $2\text{-}3\times10^{12}$ cm^{-3}. Ionization fractions of 0.15-0.20 may be possible.

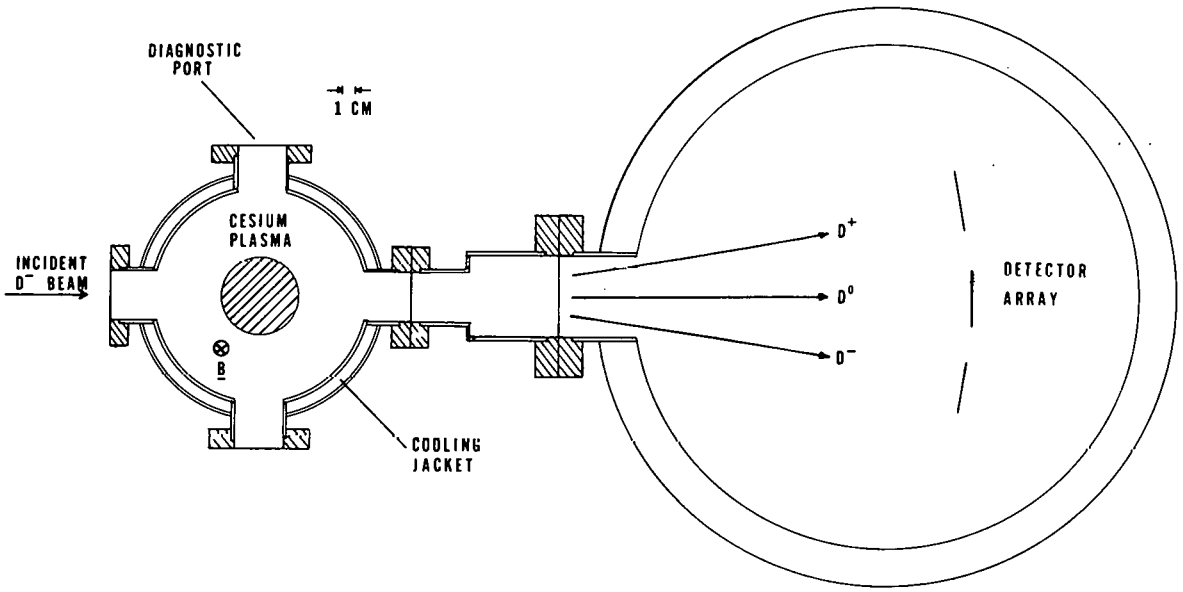

Fig. 8. Experimental arrangment for determination of σ_{-0} and σ_{0+} in a cesium plasma target.

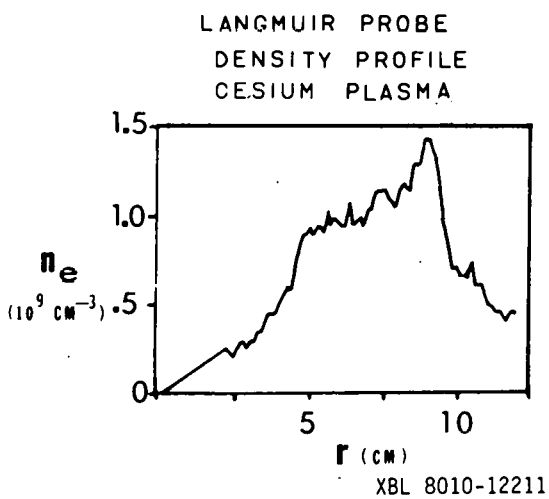

Fig. 9. Electron density (derived from Langmuir probes) vs position in the cesium plasma target.

The magnetic bucket is essentially magnetic field free in the central region. Beam divergence due to the field of the permanent magnets should be small because of the small distance over which the beam crosses the high field regions.

The beam from an accelerator array[21] would pass between the rows of water-cooled permanent magnets and become partially neutralized (Fig. 10). Calculated beam divergences[21] are small enough that the product-beams could emerge from the far side of the array, 50-100 cm downstream.

*This work was supported by the Fusion Energy Division of the U. S. Department of Energy under Contract No. W-7405-ENG-48.

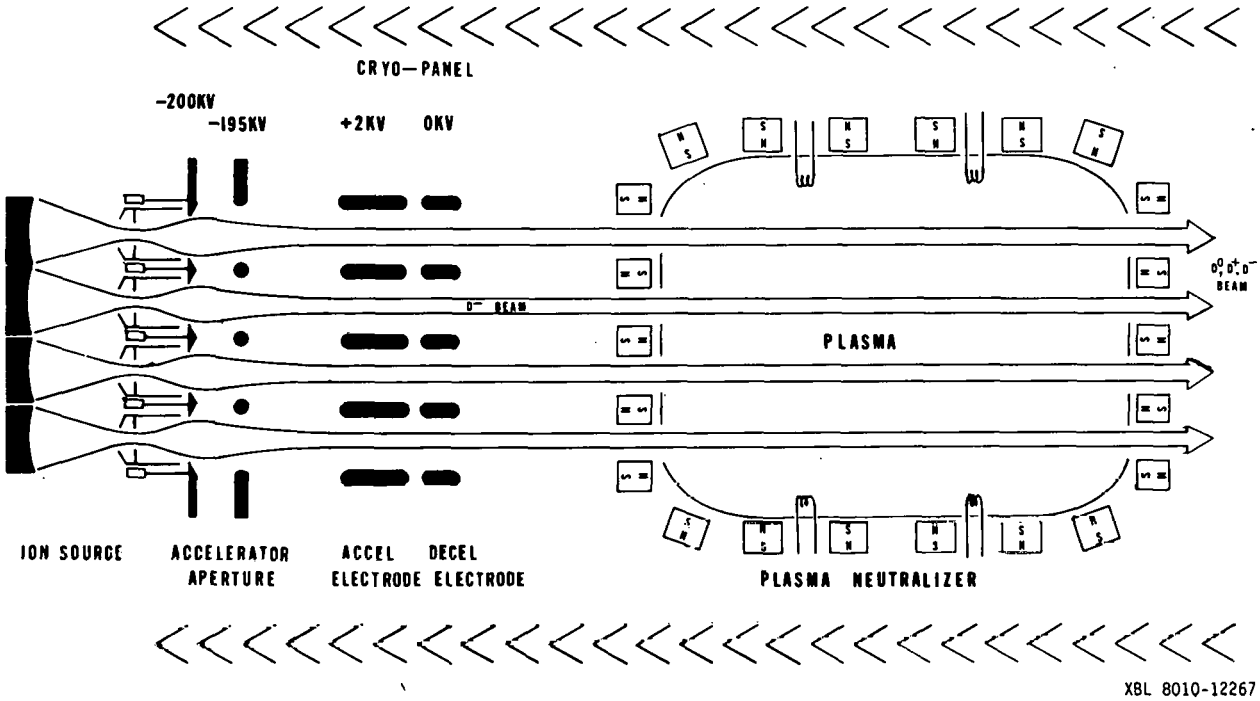

Fig. 10. Schematic diagram of a proposed pratical plasma neutralizer for a 200 keV neutral beam system using a "magnetic bucket" plasma.

References

1. A. C. Riviere and D. R. Sweetman, Bull. of the APS Series II, volume 15, number 11, p.1440 (1970). Also in D. R. Sweetman, et. al., "Fast Neutral Injection for Plasma Heating and Reactor Start-up", Fourth Conference on Plasma Physics and Controlled Nuclear Fusion Reseach, Madison (1971) paper CN-28/K-5.

2. G. I. Dimov and G. V. Roslyakov, Nucl. Fusion 15, 551 (1975).

3. G. I. Dimov, A. A. Ivanov, and G. V. Roslyakov, Sov. Phys. Tech. Phys. 22 , 1091 (1977).

4. M. W. Grossman, Proceedings of the Symposium on the Production and Neutralization of Negative Hydrogen Ions and Beams, September 26-30 (1977), Brookhaven National Laboratory Report BNL 0727.

5. B. Peart, R. Grey and K. T. Dolder, J. Phys. B 9, 3047 (1976).

6. D. F. Dance, M. F. A. Harrison and R. D. Rundel, Proc. Roy. Soc. A 299, 525 (1967).

7. B. Peart , D. S. Waltonard and K. T. Dolder, J. Phys. B. 3, 1346, (1970).

8. J. Geddes, J. Hill, M. B. Shah, T. V. Goffe and H. B. Gilbody, J. Phys. B 13, 319 (1980).

9. M. Stier and C. F. Barnett, Phys. Rev. 103, 896 (1956).

10. L. H. Toburen, M. Y. Nakai and R. A. Langley, J. Phys. Rev. 171, 114 (1968).

11. W. L. Fite R. P. Stebbings, D. G. Hummer and R. T. Brackmann, Phys. Rev. 119, 663 (1960).

12. H. B. Gilbody and J. V. Ireland, Proc. Roy, Soc. A 277, 137 (1964).

13. W. L. Fite and R. T. Brackmann, Phys. Rev. 112, 1141 (1958).

14. B. Peart, D. S. Walton and K. T. Dolder, J. Phys. B, 4, 88 (1971).

15. C. J. Anderson, R. J. Girnius, A. M. Howald and L. W. Anderson, Phys. Rev. A 22, 822 (1980).

16. R. E. Olson, K. H. Berkner, W. G. Graham, R. V. Pyle, A. S. Schlacter and J. W. Stearns, Phys. Rev. Lett. 41, 63 (1978).

17. J. S. Risley, Electronic and Atomic Collisions, N. Oda and K. Takayanagi, ed., 619 (1980).

18. J. W. McGowan, Electronic and Atomic Collisions, N. Oda and K. Takayanagi, ed., 237 (1980).

19. K. W. Ehlers and K. N. Leung, Rev. Sci. Inst 50, 1353 (1979). A magnetic-multipole plasma device is shown in the reference.

20. K. N. Leung, T. K. Samec and A. Lamm Phys. Lett. 51A, 490 (1975).

21. O. A. Anderson, "High Perveance Negative Ion Accelerators", this Symposium.

DISCUSSION

STEWART The neutralizer at the end of your talk, you were estimating a power of 50-100 kW...

PYLE I made it up. I do not know how it scales, I suppose it scales as R^2 or something like that. Then it would take some power like that.

STEWART What was the radius?

PYLE It is going to take something which is of the order of 50 cm.

PETERSON In the case of the experiment, what was the neutral density in the plasma?

PYLE As you can imagine, we do not know. The system is a type that has good vacuum in the beginning of the pulse. Gas is pulsed in and 100 μs or so later the arc is struck. Then the pressure is measured after the pulse is over, which is 1 μs later and it is still low but what the neutral pressure is in the plasma, how many impurities have managed to make it from the wall in a μs, we just do not know.

PETERSON But you think that most of the neutralization is done against ions, is that true?

PYLE Right.

A SIMPLE, EFFICIENT NEUTRALIZER FOR D^- IONS*

J. Fink** and K. Prelec
Brookhaven National Laboratory+
Associated Universities Inc.
Upton, New York 11973

Abstract

A simple deuterium gas cell is described to serve as a neutralizer for negative hydrogen ions in the energy range above 40 keV/nucleon. Neutralization efficiency and cell parameters have been calculated as function of energy, for a single cell as well as for a two-cell scheme. It has been shown that values above 60% are possible in the single cell system and about 75% in the two-cell system.

I. Introduction

Injection of intense beams of neutral hydrogen or deuterium atoms is one of the important methods of heating fusion plasmas. Present neutral beam systems are based on the neutralization of positive ions, a process that becomes less and less efficient as the ion energy increases.[1,2] Another process to produce neutral atoms is by stripping of negative ions. This is more efficient and above 50 keV/nucleon the fraction of negative ions which become neutral does not depend on the energy. Negative ion based systems are considered to be an attractive alternative for sources of neutral atoms in the energy range above 50 keV/nucleon because they offer a higher neutralization efficiency, and therefore a higher power efficiency as well. In addition, a negative ion beam has only the atomic component, resulting in a monoenergetic neutral beam, while in positive ion based systems molecular ion components contribute to fractional energy neutral beam components.[2]

In the range of energies and intensities of interest to fusion devices there are three types of negative ion neutralizers which can be considered in any application: lasers (photo detachment), plasmas or gas (or metal vapors). In the energy range above 50 keV/nucleon, the theoretical limit of the neutralization efficiency is about 60% for gas or vapor systems, about 80% for plasmas and 100% for the photo detachment.[3] However, the complexity, costs of development and fabrication as well as power requirements of the last two systems make them less attractive in the experimental devices of the immediate future compared to simple gas neutralizers. In this paper characteristics of a very simple D_2 neutralizer cell will be described, having an efficiency above 60% at the optimum thickness. By separating the remaining, not neutralized negative ions and letting them pass through a second cell of a similar design the theoretical limit can be made to approach 75%.

A study was conducted on a jet fed cell, in which gas was injected at Mach 10, via a Poulsen type plug nozzle.[4] The concept was abandoned when it was noted that almost half of the stripper thickness was in the beam line outside the jet, when only 1-2% of the gas in the jet was scattered back into the beam line.

It should be noted, that the gas cell described in this paper could be used for positive ion neutralization. However, the gas thickness required for most positive ion beams[2] is much greater, making such an application unlikely.

II. Neutralization Efficiency

Let F^o, F^+ and F^- represent the fractions of the beam which become neutral, positive or remain unchanged after traveling through a thickness π of D_2 gas. The following notations will be used for these processes in D_2 gas:

σ_{-10} - cross section for the electron detachment of a D^- ion;

σ_{-11} - cross section for the double electron loss of a D^- ion;

σ_{01} - cross section for the ionization of D^o;

σ_{10} - cross section for the electron capture of a D^+ ion.

By neglecting other possible, but much less important processes, the rate of change of fractions F^- and F^o is given by equations

$$\frac{dF^-}{d\pi} = -(\sigma_{-10}+\sigma_{-11})F^-$$

$$\frac{dF^o}{d\pi} = \sigma_{-10}F^- - \sigma_{01}F^o + \sigma_{10}F^+$$

$$F^+ = 1 - F^- - F^0 \qquad (1)$$

*Work supported by the U.S. Dept. of Energy.

**On assignment from Westinghouse Electric Corp.

+Operated by Associated Universities, Inc. under contract to the U.S. Department of Energy.

Solution of these equations has the form

$$F^-(\pi) = \exp\left[-\pi(\sigma_{-10} + \sigma_{-11})\right] = \exp(-b\,\pi) \quad (2)$$

$$F^o(\pi) = \frac{\sigma_{10}}{\sigma_{01} + \sigma_{10}}$$

$$+ \frac{\sigma_{-10} - \sigma_{10}}{(\sigma_{01} + \sigma_{10} - \sigma_{-10} - \sigma_{-11})} \exp\left[-\pi(\sigma_{-10} + \sigma_{-11})\right]$$

$$+ \frac{\sigma_{10}\,\sigma_{-11} - \sigma_{-10}\,\sigma_{01}}{(\sigma_{01} + \sigma_{10} - \sigma_{-10} - \sigma_{-11})(\sigma_{01} + \sigma_{10})}$$

$$\cdot \exp\left[-\pi(\sigma_{01} + \sigma_{10})\right] \quad (3)$$

$$F^o(\pi) = A + B \exp(-b\,\pi) + C \exp(-c\,\pi) \quad (3a)$$

In contrast to positive ion neutralizers, where the fraction F^o approaches its equilibrium value, F^o_{eq} for $\pi \to \infty$,[2] neutralizers for negative ions show an optimum, given by

$$\frac{dF^o}{d\pi} = 0$$

which results in the expression

$$\pi_{opt} = \frac{1}{c-b} \ln\left[\frac{-cC}{c-b}\right] \quad (4)$$

The maximum neutralization efficiency is

$$F^o_{max} = F^o(\pi_{opt}) \quad (5)$$

Using cross section values compiled in Table I, fractions F^o, F^- and F^+ have been calculated as a function of cell thickness for a beam energy of 200 keV and plotted in Figure 1. Let us mention that for some combinations of cross-sections in the range of energies below 10 keV/nucleon, the function $F^o(\pi)$ has no maximum, but approaches the ratio $\sigma_{01}/(\sigma_{01} + \sigma_{10})$ for $\pi \to \infty$ (see Figure 2). At low beam energies a practical cell thickness would be one that corresponds to 99% of F^o_{max}. To provide a contrast, the cell thickness for 95% F^o_{max} of a positive ion beam has been calculated and plotted as a function of beam energy in Figure 3, along with cell thicknesses for 100% F^o_{max} and 99% F^o_{max} of negative ion beams.

Even with these high values of F^o_{max}, in the range of interest, up to 40% of the beam power is found to remain in the charged components. Because, in principle a substantial part of the latter is recoverable by deceleration, the power efficiency of the system can be further improved.

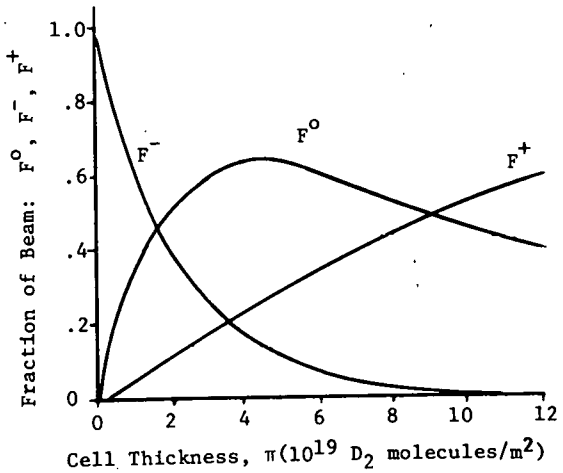

Fig. 1: F^- F^o and F^+ as a function of π for a 200 keV, D^- Beam

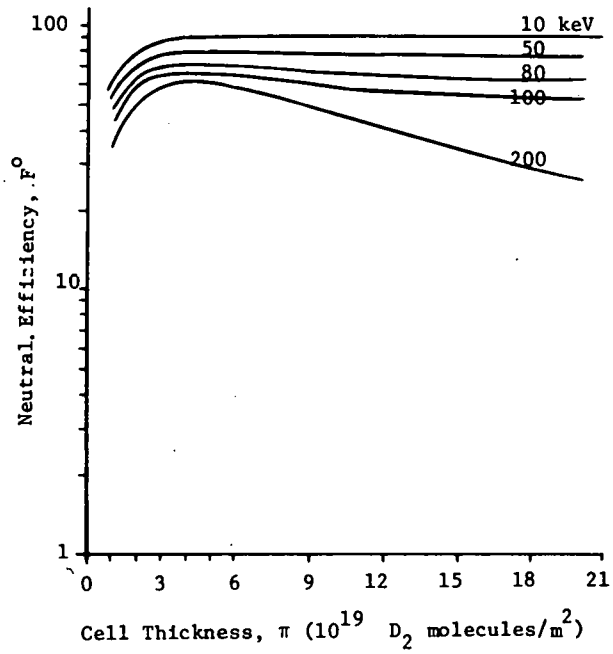

Fig. 2: Neutralization efficiency, F^o as a function of cell thickness

There is another possible way to reduce losses caused by an incomplete neutralization. If the remaining negative ion component, after the neutralizer, is separated from the beam and injected into a second neutralizing cell, the overall neutralization efficiency will be increased. (A

Table I

CROSS-SECTIONS TAKEN FROM REFERENCE 2

(10^{-17} cm^2/D_2 MOLECULE)

Energy keV/deut	D^+		D^0		D^-		D_2^+			D_2^0			D_3^+			
	σ_{10}	σ_{1-1}	σ_{01}	σ_{0-1}	σ_{-10}	σ_{-11}[d]	$\sigma_{D_2^0}$	σ_{D^0}	σ_{D^+}	$\sigma_{D_2^+}$	σ_{D^0}*	σ_{D^+}	$\sigma_{D_2^0}$	$\sigma_{D_2^+}$	σ_{D^0}	σ_{D^+}
10	83	0.13	8.0[b]	1.6	100	4.2	46	74	22	7.7	25	3.3	35	11	72	11
20	80	0.45	9.3[a]	2.5	108	4.5	36	83	22	12	(17)	4.9	41	12.5	91	16
50	47	0.80	13	1.6	85	4.1	16	63	24	19	(9.5)	7.0	30	10.8	83	21
100	17	0.10	14	0.75	65	3.3	4.3	35	24	19	(7.3)	6.9	10	8.2	50	24
200	2.5[a]	0.01	10.8	(0.25)	47	1.9	0.7	13[c]	19	15	5.0	5.8	3.5	5.6	25	22.3
500	0.046[a]	(0)	6.0	(0.06)	25	.74	(0.04)	3.7[c]	10	7.0	3.2	3.8	1.1	3.0	13	15
1000	0.0012	(0)	3.3	(0.02)	15	.36	(0.006)	2.0[c]	5.6	4.2	2.2	2.4	0.63	1.8	6.5	7
Estimated uncertainties	±10%	±30%	±10%	±20%	±15%	±15%	±10%	±10%	±20%	±25%	±25%	±25%	±20%	±15%	±10%	±10%

Estimated uncertainties are as shown under each column except as noted.

[a] ±15%

[b] +10-50%

[c] ±20%

[d] As amended per Reference 5.

() Parentheses indicate extrapolations or interpolations where no uncertainty can be assigned.

a_{ij} (i,j = 1.0,-1) indicates cross section for change charge state i to j.

σ_{D^0}, σ_{D^+}, etc. symbolize cross sections for the production of D^0, D^+, etc.

*Reaction $D_2^0 \rightarrow D^0 + D^+$ only.

similar method was proposed to increase the $D^+ \rightarrow D^-$ conversion efficiency in a C_s cell.[6]) While the second cell should operate at the optimum thickness, the thickness of the first can be optimized for the best overall efficiency. The latter is given by the expression

$$F^o_{tot} = F^o(\pi) + F^-(\pi) F^o_{max} \qquad (6)$$

After substituting for $F^0(\pi)$ (Eq. 3a) and $F^-(\pi)$ (Eq. 2) and putting the first derivative equal to zero, one obtains for the thickness of the first cell

$$\pi'_{opt} = \frac{1}{c-b} \ln \frac{-cC}{b(B+F^o_{max})} < \pi_{opt} \qquad (7)$$

By using this scheme it is possible to reduce losses in the energy range > 100 keV by almost a third. A substantially reduced thickness of the first cell is another advantage of the scheme. It is, however, outside the scope of this paper to deal with possible systems for D^- separation and injection into the second cell.

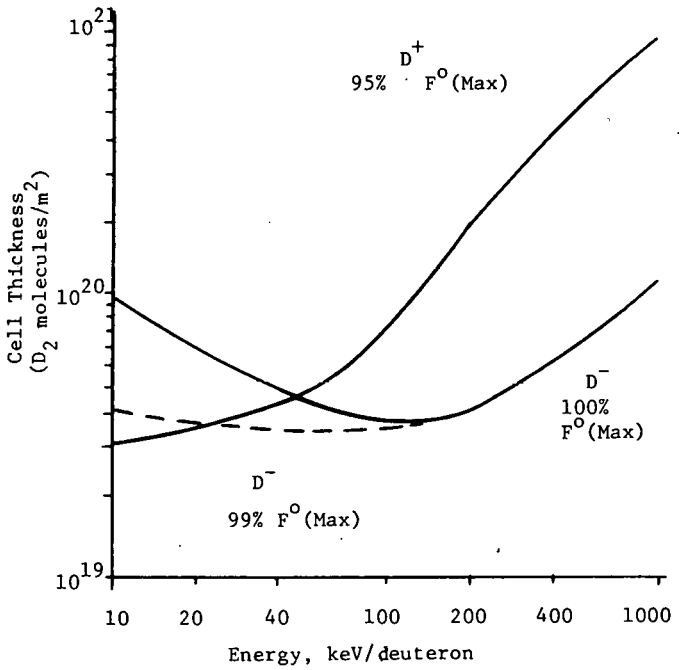

Fig. 3: Comparison of practical positive ion neutralizer cell thickness with practical negative ion stripping cell thickness.

III. Design of the Stripping Cell

Although other types of stripping cells may serve as more advantageous beam line components, a continuously pumped unit, as shown on Fig. 4, is the simplest, requiring the least cost and development effort.

Deuterium gas, at liquid nitrogen temperature, is fed into the central section via external gas plenums. The central chamber is maintained at a pressure p_c (corresponding to a density n_c), while the gas flows through the beam input and output chambers. If the beam line cross section is H x W, the gas flow into the central chamber, required to maintain the density n_c, is found to be

$$\Gamma_G = \frac{1}{4} n_c v_{LN} 2 HW \quad \left[\text{molecules } s^{-1}\right]$$

or, at the liquid nitrogen temperature,

$$Q_T = 8.0 \times 10^{-21} \Gamma_G \quad \left[\text{torr } \ell\ s^{-1}\right]$$

where n_c is the density in m^{-3} and v_{LN} thermal velocity of deuterium molecules at 77.4°K ($v_{LN} = \left(\frac{8kT}{\pi M}\right)^{\frac{1}{2}} = 6.4 \times 10^2$ m s^{-1}).

As the gas flows through the input and output chambers (Fig. 4), it is pumped away by cryopanels mounted on the walls of the cell. If the transparency of the liquid nitrogen cooled baffles is T, the change in the flow $\Gamma(x)$ along the path dx will be

$$d\Gamma(x) = -\frac{1}{4} n(x) v_{LN} T 2 W dx$$

On the other hand, as the density n(x) changes along the beam direction, so will the flow

$$d\Gamma(x) = \frac{1}{4} dn v_{LN} HW$$

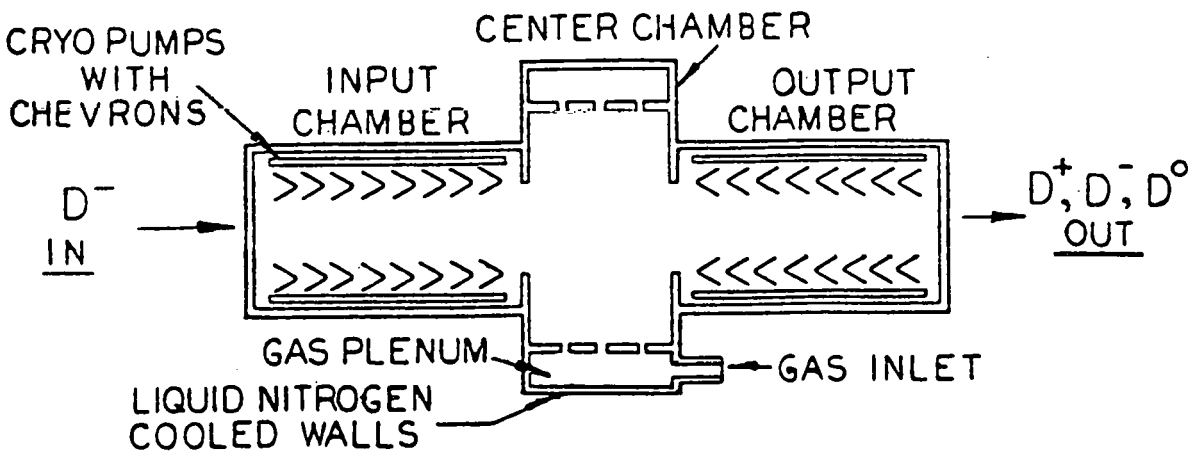

Fig. 4: Gas stripping cell.

Therefore,

$$\frac{dn}{n} = -\frac{2T}{H}\,dx$$

and

$$n = n_c \exp\left(-\frac{2T}{H}x\right) \qquad (8)$$

Thus, the stripping cell can be designed to provide the required thickness π

$$= n_c\, d + \int_0^{\ell_{in}} n\,dx + \int_0^{\ell_{out}} n\,dx \qquad (9)$$

with an overall length

$$L = d + \ell_{in} + \ell_{out}$$

Lengths of the input and output chambers can be chosen to provide desired pressures at the stripper input and exit, respectively.

From Eq. 8 it follows

$$\ell_{in} = \frac{H}{2T}\ln\frac{n_c}{n_{in}} = \frac{H}{2T}\ln\frac{p_c}{p_{in}} \qquad (10)$$

$$\ell_{out} = \frac{H}{2T}\ln\frac{n_c}{n_{out}} = \frac{H}{2T}\ln\frac{p_c}{p_{out}} \qquad (11)$$

After integrating Eq. (9) and substituting for ℓ_{in} and ℓ_{out} one obtains the expression for the density in the central chamber

$$n_c = \frac{\pi + \frac{H}{2T}(n_{in} + n_{out})}{d + \frac{H}{T}} \qquad (12)$$

The relationship between n (in m^{-3}) and p (in torr) is

$$p = 0.987 \times 10^{-5} \times 760\ kT\ n$$

At T = 77.4°K

$$p = 8.0 \times 10^{-24}\ n \qquad (13)$$

The pressure in torr in the central chamber is (at 77.4°K and with π in m^{-2})

$$p_c = \frac{8.0 \times 10^{-24}\pi + \frac{H}{2T}(p_{in} + p_{out})}{d + \frac{H}{T}} \qquad (14)$$

An example has been worked out for the stripping cell design, for beam energies of 80 keV and 200 keV, and results are shown in Table II. It has been assumed that the 10 A D^- beam has the cross section H x W of 0.14 x 1 m^2, that the chevron transparency T is 0.3 and that the required pressures at the input and the exit of the cell are 10^{-4} torr and 10^{-5} torr, respectively. For the design reasons, the length of the central chamber has been chosen d = 0.10 m.

Parameters of this simple deuterium gas stripping cell make the design very attractive. The cell is relatively short (about 1.5 m long) and it can be used in a wide range of energies (80 - 200 keV) with the same gas parameters, because in this interval the optimum thickness and neutralization efficiency are not very sensitive functions of energy (Fig. 2). The required cryopump power is small, about 0.5 J/torr ℓ, and the gas flow out of the cell is only about 5 torr ℓs^{-1}. Should this gas flow be too high, it can be reduced by changing the length of the cell (Eqs. 10, 11).

Table II

Single Cell Design

Beam energy	keV	80	200
Beam height, H	m	0.14	
Beam width, W	m	1	
Input pressure, p_{in}	torr	1×10^{-4}	
Output pressure, p_{out}	torr	1×10^{-5}	
Max. neutralization efficiency, F^0_{max}		72%	63%
Stripper thickness, π_{opt}	m^{-2}	4×10^{19}	4×10^{19}
Central chamber pressure, p_c	torr	6.1×10^{-4}	
Input chamber length, ℓ_{in}	m	0.42	
Output chamber length, ℓ_{out}	m	0.96	
Total cell length, L	m	1.48	
Total gas flow into cell, Q_T	torr ℓs^{-1}	27.3	
Gas flow out of the cell	torr ℓs^{-1}	5	

Table III shows that by using the two-cell design it is feasible to increase the overall efficiency into the range between 70-80%, depending on the energy. The first cell, operating in the underdense regime, is of course somewhat shorter.

Table III

Two Cell Design, First Cell Parameters

Beam energy	keV	80	200
Overall neutralization efficiency, F^0_{tot}		81%	77%
Stripper thickness, π_{opt}	m^{-2}	1.5×10^{19}	2.1×10^{19}
Central chamber pressure, p_c	torr	2.6×10^{-4}	3.3×10^{-4}
Input chamber length, ℓ_{in}	m	0.22	0.28
Output chamber length, ℓ_{out}	m	0.76	0.82
Total cell length, L	m	1.08	1.2
Total gas flow into the cell, Q_T	torr ℓs^{-1}	11.6	14.8
Gas flow out of the cell	torr ℓs^{-1}	5	5

References

1. Riviere, A.C., Neutralization Efficiency, in Neutral Injection Heating of Toroidal Reactors, UKAEA Research Group, Culham Laboratory Report CLM-R 112 (1971).

2. Berkner, K.H., Pyle, R.V., Stearns, J.W., Nucl. Fusion 15, (1975) 249.

3. Proceedings of the Symp. on the Production and Neutralization of Neg. Hydrogen Ions and Beams, K. Prelec, ed., Brookhaven National Laboratory Rep. 50727 (1977).

4. Hooper, E.B., Jr., Poulsen, P.P., Pinkosy, P.A., Anderson, O.A., Duffy, T.J., High Current D^- Production by Charge Exchange in Na: Neutral Beam Application, Lawrence Berkeley Laboratory Rep. LBL-10454, (1980).

5. Stearns, J.W. Private communication, (1980).

6. Osher, J.E., Formation of a D^- Beam for Efficient Production of D^0 at High Energies, Lawrence Radiation Laboratory Rep. UCID-15893, (August 1971).

DISCUSSION

HAGENA You mentioned the transparency of the chevrons of 0.3 and that it is usually 75%. I thought that a chevron transmits only 25% of the incident particles. How come that you use such a high value?

FINK Why we used 0.3? As I recall, relative to the cryopanels in Livermore it is 70%.

HAGENA 70% of the incident flux goes through...

HOOPER You might want to check that again. I believe 30% if you are very optimistic.

HAGENA If I look at your first picture with an array of cryopanels opposing each other, one can of course cut down on the required conductance of the chevrons because thermal radiation at 300 K comes only from the end plates and so you can make a much more transparent chevron if you want to and that may give you back the 30% transparency.

FINK One of the things that is not clear, that influenced this thinking, is the possibility of wanting to pump around a photodetachment cell, so that I am not quite sure what is on the edges. The more conservative number you are calling for may be necessary.

LASER NEUTRALIZATION OF NEGATIVE ION BEAMS FOR FUSION

M. W. McGeoch
Avco Everett Research Laboratory, Inc.
2385 Revere Beach Parkway
Everett, Massachusetts 02149

Abstract

An expression is derived for the efficiency of a D° beam neutralized by laser photodetachment of D^- ions. The effects of ion beam space charge are included. The D° beam efficiency is shown to depend almost equally upon the ion beam emittance, the laser efficiency, the reflectivity of the laser mirrors and the neutral beam power. Beam line efficiency can approach 100% in conditions of interest to current reactor designs.

I. Introduction

Magnetic fusion reactor concepts, with few exceptions, require high power beams of neutral deuterium or tritium for plasma heating.[1] The particle energy requirements range from 120keV (HFCTR) to 1.2MeV (TMR) and the total neutral beam powers range from 40MW (HFITR) to 580MW (TMR). The efficiency of neutral beam generation is important to the overall reactor efficiency, particularly where a high circulating power is required, as in the TMR. The impact of neutral beam efficiency is discussed by Hovingh and Moir[2] where the necessity of using negative ions above about 100kV is discussed. Both the gas and plasma methods of stripping D^- ions to neutral D° atoms have theoretical efficiency maxima, of ~ 0.65 and 0.85 respectively.[2] In addition, these methods add a gas load to the neutral beamline which leads to high pumping requirements and, for metallic stripping cells, can lead to the migration of high Z material into the reactor plasma. Another method of neutralizing D^- ions, using photodetachment, has been under consideration for many years.[3,4] Neutralization by photodetachment can be highly efficient[4] and is completely free from gas load and high Z problems. The object of the present work has been to determine the optimum configuration for laser photodetachment as a function of neutral beam power and particle energy. It is found that the neutral beam production efficiency may approach 100%, considering only the neutralizer losses but excluding D^- production and acceleration losses.

Two different interaction geometries are discussed, in which the laser is either collinear with the ion beam or perpendicular to it. Each geometry is subject to different constraints and has a different relationship to reactor conditions. The ion beam space charge and emittance are shown to strongly affect the optimum beamline efficiency.

II. Interaction Geometries

The collinear and transverse geometries are illustrated in Fig. 1. In the collinear case we consider circular and rectangular beam cross-sections and a constraint angle α which is necessary on two counts: (a) multiple-passes of the laser beam introduce an acceptance angle defined by the entrance and exit ports of the reactor vessel and (b) the paraxial approximation is used in our treatment of ion beam space charge and emittance, so that an explicit upper bound on angle ensures adequate accuracy. For beams of circular cross-section the angular constraint defines a cone of half angle α. For the rectangular, or ribbon beams it is assumed that beam focussing is always into a line in the ribbon plane, and that α refers to an angle perpendicular to the ribbon plane.

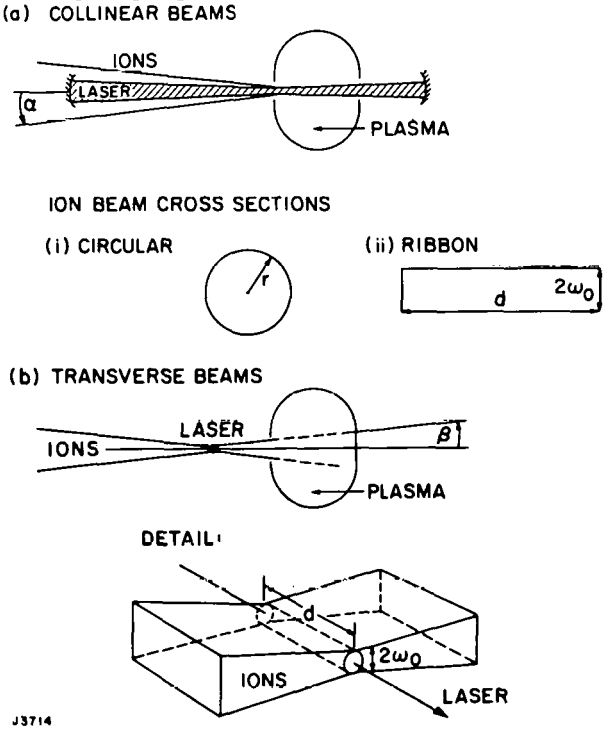

Fig. 1. Schematic interaction geometries: (a) laser beam collinear with ion beam; (b) laser beam transverse to ion beam.

In the transverse case we consider only ribbon beams, of variable aspect ratio. In this case the photodetachment has to occur at a distance from the plasma egion because the multiple-pass optics annot be accommodated inside the reactor blanket structure. This gives rise to an angular constraint β determined by the reactor entrance port. An angle constraint is also necessary to ensure the accuracy of the paraxial approximation.

III. Space Charge Limits

We are considering non-relativistic ion beams. Although in principle a degree of space charge neutralization is possible[5] in the presence of a low background gas pressure, propagation in these conditions may suffer from instabilities. Furthermore a background gas density could degrade the optical perfection of a multiple pass photodetachment cell. Instead, we assume that space charge neutralization is not available, but estimate the space charge 'blow up' length L_s which limits the laser-ion interaction length.

For beams of circular cross-section a simple estimate of L_s is obtained by considering the electric field at the beam surface

$$E = \frac{\rho}{2\pi r\varepsilon_o} \qquad (1)$$

where ρ is the charge density of a beam radius r. The time required for an ion of charge e and mass m_i to accelerate a distance r in this field is

$$\tau = \left(\frac{4\pi r^2 m_i \varepsilon_o}{e\rho}\right)^{1/2} \qquad (2)$$

during which time the ion moves a distance

$$L_s = \tau v = \left(\frac{8\pi\varepsilon_o}{e}\right)^{1/2} \left(\frac{2}{m_i}\right)^{1/4} \frac{\varepsilon_i^{3/4}\, r}{I^{1/2}} \qquad (3)$$

along the beam, where $\varepsilon_i = \frac{1}{2} m_i v^2$ is the ion energy and I is the beam current.

For a ribbon beam we approximate by a plane sheet of charge Q/unit area to obtain the surface field

$$E = \frac{Q}{2\varepsilon_o} \qquad (4)$$

and the interaction length for expansion by distance ω_o is

$$L_s = \left(\frac{8\varepsilon_o\omega_o d}{e}\right)^{1/2} \left(\frac{2}{m_i}\right)^{1/4} \frac{\varepsilon_i^{3/4}}{I^{1/2}} \qquad (5)$$

where $2\omega_o$ is the ribbon thickness and d is its width.

Expressions (3) and (5) differ from more accurate non-analytical expressions by a numerical factor of approximately unity. We simplify these expressions by introducing

$$C_s = \left(\frac{8\varepsilon_o}{e}\right)^{1/2} \left(\frac{2}{m_i}\right)^{1/4} \qquad (6)$$

to give

$$L_s = \frac{\pi^{1/2} C_s \varepsilon_i^{3/4}\, r}{I^{1/2}} \quad \text{(circular beams)} \qquad (7)$$

and

$$L_s = \frac{C_s \varepsilon_i^{3/4} (\omega_o d)^{1/2}}{I^{1/2}} \quad \text{(ribbon beams)} \qquad (8)$$

IV. Photodetachment Power

The cross-section for H^- (or D^-) photodetachment is well known.[6] We present a related quantity $(\frac{\sigma}{h\nu})$ in Fig. 2 which is shown below to represent a 'figure of merit' for different possible photodetachment wavelengths.

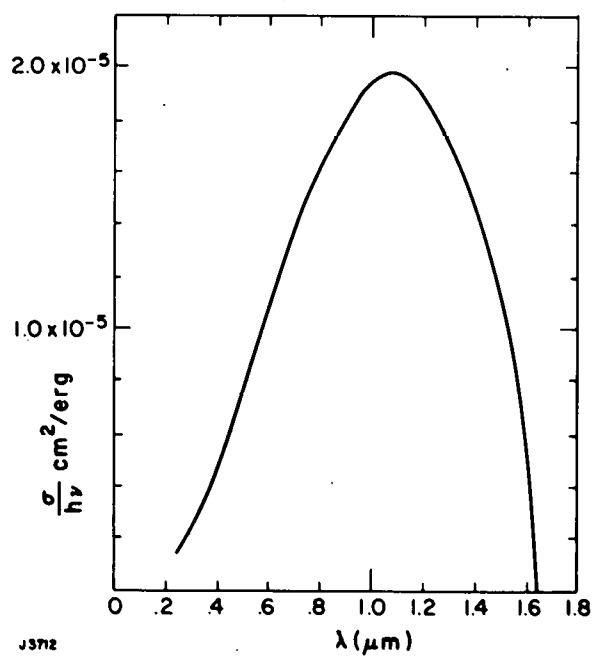

Fig. 2. Optimum wavelength for laser photodetachment derived from the data in Ref. 6.

The threshold is at 1.64μm and the optimum wavelength is 1.1μm. In a laser flux ϕ (power per unit area) the rate of photodetachment is

$$R_p = \frac{\sigma\phi}{h\nu}$$

The time an ion spends in the interaction region is $\tau = L_s/v$, so that the fraction of ions stripped is

$$\eta_s = (1-e^{-\alpha_s}) \text{ with } \alpha_s = \frac{\sigma\phi L_s}{h\nu v}$$

We consider first the collinear geometry: the laser power is

$$P = \pi r^2\phi = \frac{\pi\alpha_s h\nu v r^2}{\sigma L_s} \text{ (circular beams)} \quad (9)$$

$$P = 2\omega_o d\phi = \frac{2\alpha_s h\nu v\omega_o d}{\sigma L_s} \text{ (ribbon beams)} \quad (10)$$

For the transverse geometry the laser power is

$$P = 2\omega_o L_s\phi = \frac{2\alpha_s h\nu v\omega_o}{\sigma} \quad (11)$$

in which we note that the interaction length L_s has cancelled. It is seen from (9), (10), (11) together with (7) and (8) that P is minimized by decreasing the transverse dimensions of the ion beam. However, the degree to which we may focus the negative ion beam is determined by the beam emittance together with the angle constraints that were introduced in II above.

V. Emittance

We are concerned with particle motion transverse to the ion beam and employ an invariant emittance[7] for non-relativistic particles

$$\varepsilon_n = \frac{v}{\pi}\Delta\chi\Delta\chi' \quad (12)$$

where $\Delta\chi$ is the transverse spread of the ion beam, and $\Delta\chi'$ is the full angular spread of the beam particles (which have longitudinal velocity v).

For the collinear case the angle constraint $\Delta\chi' \leq 2\alpha$ leads to

$$r \geq \frac{\pi\varepsilon_n}{4\alpha v} \text{ (circular beams)} \quad (13)$$

$$\omega_o \geq \frac{\pi\varepsilon_n}{4\alpha v} \text{ (ribbon beams)} \quad (14)$$

For the transverse case the angle constraint $\Delta\chi' \leq 2\beta$ leads to

$$\omega_o \geq \frac{\pi\varepsilon_n}{4\beta v} \quad (15)$$

We may now express the photodetachment power P in terms of the ion beam parameters, but not involving the actual dimensions of the interaction region. From (9), (7) and (13) we have

$$P \geq \frac{\pi^{3/2}\alpha_s h\nu\varepsilon_n}{4\alpha\sigma}\left(\frac{I^{1/2}}{C_s\varepsilon_i^{3/4}}\right) \text{(circular beams)} \quad (16)$$

From (10), (8) and (14) we have

$$P \geq \frac{\pi\alpha_s h\nu\varepsilon_n}{2^{1/2}\alpha\sigma}\left(\frac{I^{1/2}}{C_s\varepsilon_i^{3/4}}\right) R_a^{1/2} \text{ (ribbon beams)} \quad (17)$$

where $R_a = d/2\omega_o$ is the ribbon beam aspect ratio. For transverse beams, from (11) and (15) we have

$$P \geq \frac{\pi}{2}\frac{\alpha_s h\nu\varepsilon_n}{\beta\sigma} \quad (18)$$

We note from a comparison of (17) and (16) that in the collinear geometry circular beams require less laser power than ribbon beams for the same ion beam power and transverse emittance. However, the transverse emittance is defined in the direction perpendicular to the ribbon plane and decreases as $R_a^{1/2}$ at constant source area and ion transverse temperature. A more useful generalization is that at constant transverse temperature of the ion source there is no change in the collinear stripping power requirement as the source aspect ratio is varied. Consequently, we employ (16) as representative of the laser power requirement in all collinear geometries. Setting

$$C_2 \text{ (dimensionless)} = \left(\frac{I^{1/2}}{C_s\varepsilon_i^{3/4}}\right), \quad (19)$$

we summarize the power requirements in both the collinear and transverse cases as

$$P \geq \frac{\alpha_s h\nu\varepsilon_n}{\beta_o\sigma} \qquad \beta_o = \begin{cases} \dfrac{4\alpha}{\pi^{3/2}C_2} & \text{(collinear)} \\ \dfrac{2\beta}{\pi} & \text{(transverse)} \end{cases} \quad (20)$$

VI. Multiple Pass Illumination

For both collinear and transverse illumination the optimum laser beam configuration is a folded resonator in which the beam is repeatedly focussed through the interaction region (Fig. 3).

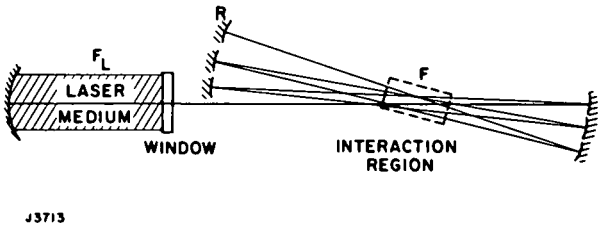

Fig. 3. Geometry for multiple pass illumination in a folded resonator illustrated for N = 6.

For N mirrors external to the laser medium there are 2N transits through the interaction region. The circulating laser power is $P_C = P/2N$. Let the fractional loss per double transit of the laser medium be F_L and the fractional absorption in a single transit of the ion beam be F. For a mirror reflectivity R, the circulating beam experiences a rate of power loss

$$P_{Loss} = \frac{P}{2N}\{2N(1-R) + 2NF + F_L\}$$

For a laser efficiency η_L and electric input power W_L

$$W_L = P_{Loss}/\eta_L = \frac{P}{\eta_L}\{(1-R) + F + \frac{F_L}{2N}\} \quad (21)$$

The loss power is compensated by an equal gain power determined by the rate of pumping in the laser medium. In most laser media there are unavoidable losses due to scattering, turbulence induced refractive index gradients and absorbing molecules. Further, a finite rate of losses will exist due to diffraction out of the aperture defining the gain region. It seems probable that the combination of these effects could lead to $F_L \sim 0.01$ in laser systems of interest for photodetachment. The effect of increasing N is to make these losses negligible relative to mirror losses, i.e.

$$\frac{F_L}{2N} << (1-R) + F \quad (22)$$

It is believed that the satisfaction of (22) will be the principal determinant of N for practical systems. A further advantage of increasing N is that smaller mirrors may be used to handle the reduced circulating power for a given optical damage threshold.

We may express F in terms of the ion beam parameters. For the collinear case $F = n_B\sigma L_s$, where n_B is the number density of ions in the beam. Using $W_B = n_B\varepsilon_i v\pi r^2$ and (7), (13) and (19) we find

$$F = \frac{4}{\pi^{3/2}}\frac{W_B\sigma\alpha}{\varepsilon_n\varepsilon_i C_2} \quad (23)$$

where we have taken the equality in (13), assuming that the ion beam angle has been increased up to the constraint angle 2α

For the transverse case, $F = \sigma n_B d$, which, together with $W_B = n_B\varepsilon_i 2\omega_o d$ and (14) gives

$$F = \frac{2\beta W_B\sigma}{\pi\varepsilon_n\varepsilon_i} \quad (24)$$

again assuming the maximum ion beam angle 2β. We may summarize (23) and (24) by

$$F = \frac{\beta_o W_B\sigma}{\varepsilon_n\varepsilon_i} \text{ where } \beta_o = \begin{cases} \frac{4}{\pi^{3/2}C_2} & \text{(collinear)} \\ \frac{2\beta}{\pi} & \text{(transverse)} \end{cases} \quad (25)$$

VII. Optimization of Neutral Beam Efficiency

We are now able to write down the neutral beam efficiency, including the photodetachment laser in the system. The delivered neutral beam power is $W_B' = \eta_s W_B$, where η_s is the fraction neutralized and W_B is the power of the accelerated ion beam (assuming 100% efficiency of acceleration for the present discussion). The total electric input power = $(W_B + W_L)$, so that the efficiency of the neutral beam is

$$\eta_B = \frac{\eta_s W_B}{(W_B + W_L)} \quad (26)$$

Substituting for η_s and $W_L = P/\eta_L\{(1-R)+F\}$ in the limit of large N, we have

$$\eta_B = \frac{(1-e^{-\alpha_s})}{(1+C_1\alpha_s)} \qquad (27)$$

where

$$C_1 = \frac{h\nu\varepsilon_n}{\beta_o\eta_L\sigma W_B}\left\{(1-R) + \frac{\beta_o\sigma W_B}{\varepsilon_n\varepsilon_i}\right\} \qquad (28)$$

and the equality has been taken in (20) for ion beams at the constraint angles.

We may vary α_s to optimize η_B, which is equivalent to adjusting the laser flux ϕ. At the optimum,

$$\eta_B(OPT) = \frac{e^{-\alpha_s'}}{C_1} \qquad (29)$$

with

$$\alpha_s' = (1 + \frac{1}{C_1}) + e^{\alpha_s'} \qquad (30)$$

(30) is solved graphically and plots of $\eta_B(OPT)$ and α_s' vs. C_1 are shown in Fig. 4 and Fig. 5 respectively.

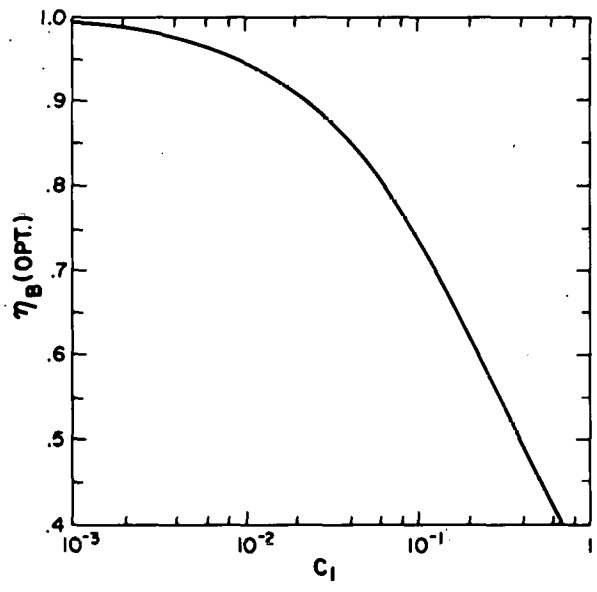

Fig. 4. Plot of Optimized beamline efficiency against the dimensionless parameter C_1.

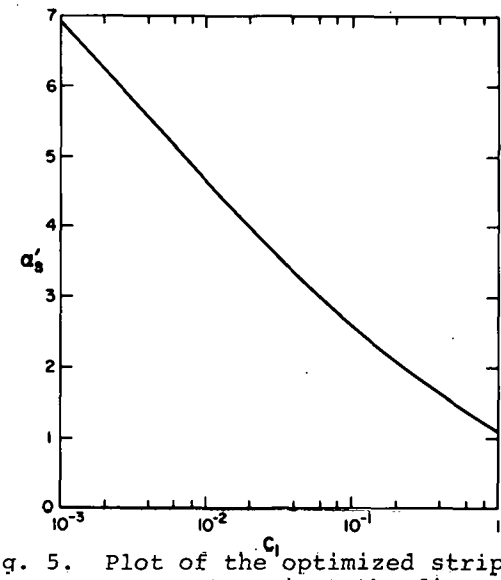

Fig. 5. Plot of the optimized stripping exponent against the dimensionless parameter C_1.

As an aid to calculations we express C_2 in terms of W_B and ε_i using (19), (6) and $W_B = (I\varepsilon_i/e)$:

$$C_2 = \left\{\frac{em_i^{1/4}}{2^{7/4}\varepsilon_o^{1/2}}\right\}\frac{W_B^{1/2}}{\varepsilon_i^{5/4}} \qquad (31)$$

C_2 may be read from Fig. 6 which applies to the case of D^- beams.

VIII. Discussion

For collinear beams the parameter C_2 represents the effect of space charge. For transverse illumination the space charge constraint is still present implicitly in that the ribbon aspect ratio must exceed a certain value. To find this value we make the space charge expansion angle ω_o/L_s for ribbon beams less than the constraint angle β. Using (8) and (19) with $R_a = d/2\omega_o$ we obtain

$$R_a \geq \frac{C_2^2}{2\beta^2} \qquad (32)$$

There is also an upper limit on R_a which is set by diffraction of the laser beam: $R_a \leq \omega_o/\lambda$, where λ is the laser wavelength. This does not impose a severe constraint in cases of practical interest, such as the example discussed below.

The use of our results is demonstrated through an example based on current or very near term technology. We consider the system

$$W_B = 10MW,\ \varepsilon_i = 400kV,\ I = 25\ amps$$

D^- source: 25mA/cm^2, 10cm × 100cm, transverse temperature = 3eV
Laser: η_L = 0.01 at 1.1μm
Mirrors: R = 0.998
Angle constraints: α = 0.1 rad (collinear beam)
β = 0.1 rad (transverse case)

From (12) we calculate $\varepsilon_n = 1.1 \times 10^7$cm^2 rad/sec and from (28) we find C_1 (collinear) $= 6.0 \times 10^{-3}$ and C_1 (transverse) = 1.8×10^{-2}. This gives η_B(OPT) = 96% (collinear) and η_B(OPT) = 91% (transverse). We also note that in the transverse case the ribbon aspect ratio must exceed 6.8. It is clear that very high neutralizer efficiencies may be achieved. The fraction of D^- ions neutralized is very high: η_s = 99.3% (collinear) and η_s = 98% (transverse). The free electrons which are produced may be removed in a low electric or magnetic field. They have a translational energy in the beam direction of 109eV in this example.

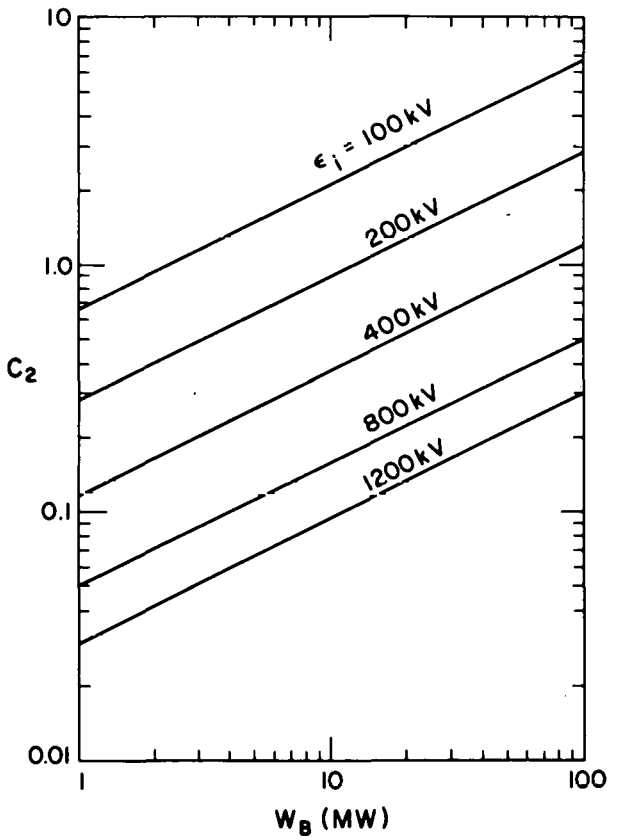

Fig. 6. Chart for C_2 (D^- beams) as a function of ion energy and beamline power.

We note in this example that the second term in (28) was less than 4% of the first term for both geometries. This shows that the losses to the laser beam due to photodetachment absorption may be very small compared to mirror losses. As long as this is true, the optimum beamline efficiency η_B(OPT) increases with increasing beam power W_B, so that the laser photodetachment process becomes relatively more competitive to gas or plasma neutralizers as the beamline power is scaled to reactor levels.

In the example the collinear geometry was more efficient than the transverse geometry by a factor of 3 in C_1. For a given beamline power this tendency is reinforced with increasing ion energy ε_i, which may be seen from the dependence $C_1 \sim \varepsilon_i^{-5/4}$ which applies when the second term in (28) may be neglected. However, the use of a collinear geometry necessitates exposure of the mirrors to reactor particle flux and radiation levels which would make high reflectivity and optical perfection difficult to maintain. For this reason the less efficient transverse geometry may be preferable. Certainly the mirrors would then be well shielded in tubes which ran perpendicular to the beamline particle flux.

The choice of laser is determined not only by wavelength and efficiency, but by the paramount requirement that losses in the laser medium should be very small. Medium homogeneity and freedom from thermal refractive index changes are reasons for choosing a gas as the active laser medium, rather than a solid. For the above example, the circulating power requirement is P_c = 89kW if we assume N = 20. There are no in-principle reasons why such high circulating power levels should not be attainable, although to date there appears to have been very little effort in this direction.

The mirror reflectivity 0.998 assumed in the example is routinely achieved at 1.1μm. It is reasonable to expect an improvement to 0.999 in the near future. The power damage threshold of 1.1μm mirrors is at least 20kW/cm^2 and may probably increase to 100kW/cm^2 with further development. The mirror diameter is determined by the damage threshold, so that a mirror array may be made more compact as the damage threshold increases. Even with existing mirrors it is easy to design a folded laser resonator to give a good overlap between the laser and ion beam.

In conclusion, expressions have been derived which allow an assessment of the efficiency of laser neutralization of

negative ion beams for arbitrary beam power, particle energy and ion source emittance. The efficiency scaling is such that laser neutralization should be considered seriously for reactor scale beamlines. The laser neutralizer has the additional advantages of cleanliness and high conversion efficiency of D^- into D^0.

References

1. "Fusion Reactor Design Concepts," Proc. IAEA Madison Meeting, 1977, (IAEA, Vienna, 1978).

2. J. Hovingh and R.W. Moir, Nuclear Fusion 14, 629 (1974).

3. A.Y. Wong, J.M. Dawson, W. Gekelman and Z. Lucky, Appl. Phys. Lett. 25, 579 (1974).

4. J.M. Fink, W.L. Barr and G.W. Hamilton, IE^3 Trans. Plas. Sci. PS-7, 21 (1979).

5. R.J. Turnbull and E.D. Hooper, Jr., Proc. of the Symposium on Production and Neutralization of Negative Ions and Beams, Brookhaven National Lab., 20-30 Sept. 1977, K. Prelec, Editor BNL Report No. 50727 (unpublished).

6. M.A. Nasciemento and W.A. Goddard III, Phys. Rev. A 16, 1559 (1977).

7. J.D. Lawson, P.M. Lapostolle and R.L. Gluckstern, Particle Accelerators 5, 61 (1973).

DISCUSSION

HOOPER You put in a space charge requirement which I think caught me by surprise because I have always assumed the beams were space charge neutralized due to background plasma affects. Is there any reason why it can not be and what would be the implications if it were?

McGEOCH I made the calculation as if there was no background density whatsoever as the worse case and anything you could do to neutralize it is better. Incidently, as the neutralization occurs the beam becomes neutral and I took a space charge assumption that I went straight through with the same ion beam to limit my length but in fact that was probably wrong by at least a factor of 2. So that would make it more favorable as well.

FORRESTER You might have mentioned it but I did not hear. What would the laser power be to neutralize a 10 MW beam?

McGEOCH I did not mention it but the laser drive power, if you got 90% efficiency, is 10% of 10 MW which is 1 MW and with the laser efficiency being 1% the stimulated emission power is 10 kW. Now this is a bad laser of 1% efficiency but it is a 1 MW drive power and it is a 10 kW stimulated emission power, that keeps the flux up to compensate the optical losses.

PETERSON What do you use for the window losses?

McGEOCH Say ½%. You only encounter the window once every two transits in the photodetachment region.

PETERSON So this all takes place within the vacuum, the mirrors etc.?

McGEOCH Yes, the laser medium is isolated from the beam line by a window.

BACAL I do not understand the relation of laser power to the ion beam power. In our photodetachment experiment we understand that the energy defines the probability of photodetachment independantly, whether you have one ion or ten ions or any power of ions in a certain volume. Is it the scaling related to a bigger volume which you illuminate or how does it enter?

McGEOCH I think in your case with very much more intense lasers, you are going through saturation. As we travel through we saturate the photodetachment but in big beams there is a finite absorption from the ions themselves which must be certainly considered as a loss to the optical power and it turns out that in this case it is very small. In fact, in this example, it contributed less than 1% of the total loss power but you have to include that.

MOBLEY How much is the laser wall power to neutralize a 10 MW beam?

McGEOCH It is a 1% efficient laser.

JACQUOT You use a Fabry-Pérot resonator. You have some problems on the position of the mirror?

McGEOCH Well, several constraints come in. First of all you start with a geometry that fits with the ion beams you have available. In principle you have to have a slight curvature in at least one mirror to keep defraction losses down. In fact, defraction losses I have calculated are small. Then you have a large number of mirrors so you have to have a certain accuracy alignment that is perfectly achievable. Then there is mirror perfection; although you have a large number of mirrors, again, you have to have a constraint in the flatness. Again that is within tolerances, for instance one micron is not a bad wavelength to meet these tolerances. There is one constraint which is quite important and that is the mirror power damage handling ability. One can get manufacturers to quote you 20 kW/cm^2 CW with the prospect of improvement in the future. I would say if I did an experiment I would plan for 10 kW/cm^2.

HAGENA What kind of a laser do you envision for

this wavelength and for this power level and I assume that it should be steady state?

McGEOCH The sort of laser one wants is a low pressure gas laser so there is very little disturbance to the optical beam with little refraction. One candidate which is not ideal but which is a starting point, is the atomic Iodine system in various different realizations. If I had to get an experiment off the ground quickly I would use the chemical atomic I system.

HAGENA The thermal load on the mirrors and so on, that is all very far below the values which one tries to handle in the laser fusion business. Compared to those requirements this is a very modest laser?

McGEOCH It is a different sort of thing. In laser fusion there is a short pulse and you have energy per cm^2. Here there is much heat conduction and lack of thermal distortion from mirrors.

DOLIQUE What do you mean with the space charge taken into account?

McGEOCH Simply, that if I want to get a very good efficiency I have to make a beam with small angles into a thin ribbon because when it is neutralized you can not influence the particle motion any more. This is not possible without space charge repulsion. So what you do is, you decrease the current density in your sheet to a certain value where the particles are not repelled out of the beam before they have gone through a suitable interaction length. But as you said it might not be as bad in practice if you have space charge neutralization.

HOPMAN I come back to the laser efficiency. You quoted 1% for your efficiency of your I laser but gas laser efficiencies of 10% are possible.

McGEOCH Yes, in the infrareds, that is 5 microns, you can do more than 10% but I am afraid, I do not know of anything less than 1.6 microns which does more than 1%. I think there are possibilities for development but there is no demand at the moment for very efficient lasers, CW lasers with small gain cross sections and low operating densities. Everyone is quite happy to work at a high density because it means you can carry away a lot of waste heat. So people tend to work with atmospheric lasers but it is almost an area which has not been approached before because it is not of much interest, as it is here.

PETERSON The mirror can handle this power level inside the vacuum, is that correct?

McGEOCH Yes.

THIS PAGE

WAS INTENTIONALLY

LEFT BLANK

NEUTRAL BEAM SYSTEMS

THIS PAGE

WAS INTENTIONALLY

LEFT BLANK

U.S. NEGATIVE ION NEUTRAL BEAM DEVELOPMENT PROGRAM

H. Stanley Staten
Gregory M. Haas
Franklin E. Coffman
U.S. Department of Energy
Washington, D.C.

ABSTRACT

The needs for neutral beams are reviewed. A simple analysis indicating when 10 ampere negative ion systems are competitive with positive ion systems is presented. The U.S. Negative Ion Development Program Plan is reviewed. Three U.S. laboratories are each developing source concepts through the 1 ampere level. It is expected that sufficient work will be done by the summer of 1981, such that a choice can be made of the source concept most likely to be successful. Effort will then be concentrated on a 10 ampere version.

I. Introduction

The most advanced method of heating modern state-of-the-art magnetically confined plasmas to reactor-like conditions is by intense injection of high energy neutral beams. The recent record plasma temperatures of 7KeV attained in PLT and the 13KeV in 2XIIB are graphic demonstrations of the success of high power neutral beam injection heating. The PLT neutral beam heating experiment is only the first of a succession of planned plasma physics and engineering experiments which are expected to lead to demonstration of economical fusion power as a viable option in the energy future of the world.

Figure 1 shows some of the past and the near term future (∿10 years) expected heating energy needs. Note that while PLT produced significant results, the total energy delivered to the plasma was small (<1/2 Mega Joule) compared to the very near term PDX (∿3 Mega Joule), Doublet-III (∿10 Mega Joule), ISX-C (90 Mega Joule), MFTF-B (∿460 Mega Joule), and the TFTR-TFM (∿50 Mega Joule). The projected need for the Tokamak Engineering Test Facility (ETF) is 250 Mega Joule. Even with the success that has been attained with neutral beam injection, the future needs require very aggressive development.

II. Neutral Beam Systems Requirements

A. Current Projects

The neutral beam systems for current plasma experiments are listed in Table 1. This table lists the basic system requirements. There are significant upgrades under discussion or active consideration that will be discussed in the next section.

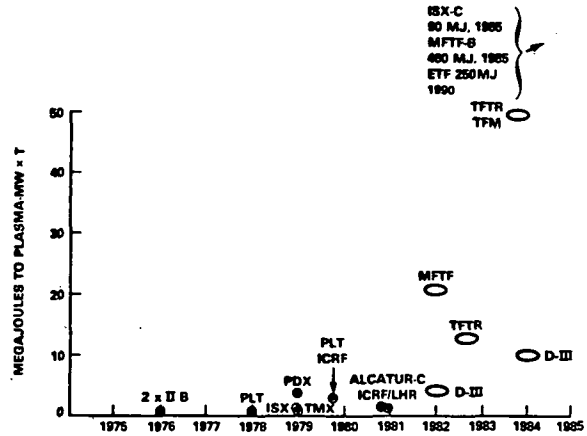

Figure 1. Plasma Heating Requirements

Table 1. Requirements for Current Projects

	Energy (KeV)	Current Per Source (Amperes)	Pulse Length (Milli Secs)	Species (% Full Energy)	Operating Gas
PLT	40	60	300	85%	H,D
ISX-B	40	100	100	85%	H,D
TMX	40	40	25	65%	D
	20	50	25	65%	D,H,He
PDX	50	100	500	85%	H,D
TFTR	120	65	500	85%	H,D
Doublet-III	80	80	500	60%	H only
MFTF	80	80	500	65%	D
	20	100	100	65%	D

B. Upgrades of Current Projects

Both theory and experiment show that improved plasma performance can be achieved by increasing some or all of the injector parameters, including injected particle energy (operating voltage), current, pulse length, and full-energy-fraction. Upgrades currently in progress or in the planning phases are listed in Table 2. The parameters listed in Table 2 are the current estimate of the requirements. They are subject to change as the specific applications are firmed up.

Table 2. Neutral Beam Requirements for Facility Upgrades and Future Projects

Project	Energy (KeV)	Current (Amperes)	Pulse Length (Seconds)	Operating Gas	Need Date Experiment
TFTR/TFM	120	65	1 1/2	D	1983
ISX-C	50	100	30	H	1984
MFTF-B	80	50	30	D	1985
Doublet-III	80	80	≤5-10	H	1986

C. Future Projects

1. Tokamaks

The major problem anticipated with neutral beam heating of large tokamaks is the need for long pulse lengths and the lack of beam penetration. The first response to the penetration problem has been to raise the injection energy, but this entails severe penalties in injection efficiency. As the accelerated positive deuterium ion energy is increased beyond about 200KeV, the efficiency of neutralizing the fast positively charged ions decreases to below 20 percent. (See Figure 2). This low efficiency would necessitate a very large investment in sources, power supplies, pumps, and other hardware. Above ∿75KeV/nucleon*, negative ion injector systems, which have a much higher neutralization efficiency, appear attractive; however, such an injector has yet to be developed.

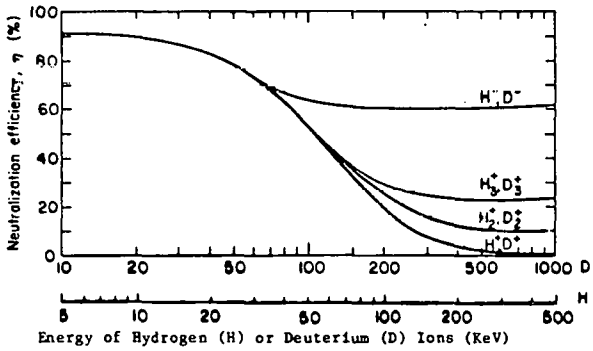

Figure 2. Neutralization Efficiency Versus Energy

As plasma physics understanding has increased and the size of the various tokamak reactor designs decreased, the neutral beam energy requirements also decreased. From this work has emerged the conclusion that positive ion neutral beam injectors of ∿150KeV should be adequate for ETF/FED size devices. The power required to heat plasmas to ignition is not known defintively. Analysis shows that for ETF/FED and INTOR type devices, injected beam power requirements are in the range of 40 to 75 MW. Depending on transport scaling and on the heating scenario adopted, a heating pulse length of 3 to 8s is required to heat ETF/FED and INTOR type devices to ignition. However, various driven plasma scenarios are also under consideration. It may be desirable to use neutral beams for profile control or current drive in which cases, steady state operation of the neutral beam systems may be necessary.

In summary, the Neutral Beam requirements for ETF/FED and INTOR devices are:

POWER	40 - 75MWW
ENERGY	120 - 200KeV (150KeV nominal)
PULSE LENGTH	10 sec to the device pulse length

These neutral beam parameters also appear to be typical of the requirements of a Tokamak Demonstration Reactor.

2. Mirror Systems

Neutral beam injection is the only demonstrated method for maintaining a magnetic mirror plasma. The mirror program is aggressively pursuing the tandem mirror approach where magnetic mirror cells are used to plug the ends of a central solenoid. The neutral beam energy required to drive a simple tandem mirror reactor ranges from 150KeV to 400KeV.

The basic ideas of the tandem mirror have been tested on TMX. The results are very encouraging and in agreement with predictions. The next major proposed step after TMX is MFTF-B. Neutral beams of 80KeV, (30 second), will be used to heat the central cell and end plugs. Use of 80KeV negative ion neutral beams are being considered for pump beam application on MFTF-B because negative ion systems do not produce half and third energy components. Subsequent mirror machines, as presently envisioned, specify negative ion based neutral beams.

III. Negative Ion Applications

The U.S. tokamak community seems satisfied to rely upon positive ion technology for the indefinite future. It is the mirror program needs that provide the incentive for development of negative ion systems. It is instructive to ask what negative ion source would be competitive, i.e., could replace a positive ion source. A simple comparison of the 50 ampere positive ion source now under development for MFTF-B with the 10 ampere negative ion source yields results as shown in Figures 3 and 4.

---

*Energy per nucleon is the key parameter. For 150KeV deuterium, the energy per neucleon is 75KeV. Neutralization efficiency is a function of velocity or energy per neucleon rather than total energy.

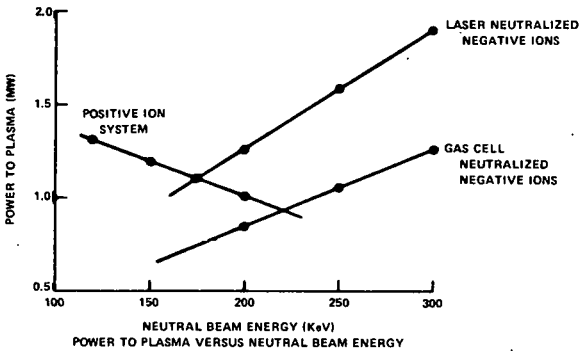

POWER TO PLASMA VERSUS NEUTRAL BEAM ENERGY

Figure 3

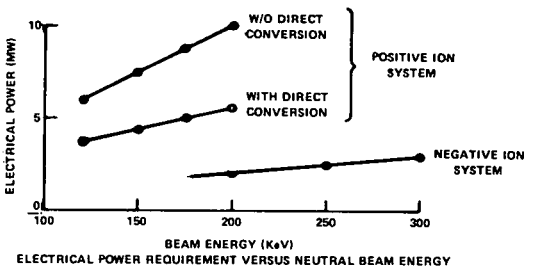

ELECTRICAL POWER REQUIREMENT VERSUS NEUTRAL BEAM ENERGY

Figure 4

Note that even though the negative ion based system is a lower current system, it is still very competative at ETF/FED parameters. If the assumption is made that system costs are proportional to electrical power, the negative ion based system appears even more attractive (Figure 4).

IV. Negative Ion Systems Development

Negative ion sources have not received the same attention that has been directed toward positive ion sources. The feature that makes negative ion systems attractive, namely the ease with which the excess electron is removed, also complicates source development. Adding this excess electron efficiently in a manner where the ion can be efficiently accelerated has proven difficult in the environment of high power neutral beam systems. An additional complicating factor is that the negative ion has the same electrical charge as an electron, but is less mobile. Therefore, an effective means of accelerating negative ions to the desired high energies must be developed which does not also waste energy due to the undesirable acceleration of electrons.

The negative ion sources being studied in the U.S. are basically of two types: surface sources and double charge exchange sources. Surface sources are being studied at BNL, ORNL, and LBL. The double charge exchange source has been studied at LLL and LBL. The technical details of the work by these laboratories is being discussed in considerable detail at this symposium; as such it will not be discussed further here.

V. Negative Ion Systems Program Plan

The negative ion neutral beam development program has proceeded at a modest pace. The program has suffered from low priority and lack of specific user requirements. The proof of principle goal of Table 3 was established about 1 1/2 years ago to provide focus for the work. The program has been working toward this goal. During a program review on April 2 and 3, 1980, the review panel concluded that no source concept is yet capable of 10 ampere operation and as such, none satisfies the proof of principle goal at the present time. The panel also concluded that it is not clear which source is most likely to meet the proof of principle goal. Each laboratory is presently working with sources that produce or are expected to produce about 1 ampere of negative ions. From the results to date, it is not clear which source is most likely to meet the proof of principle goal.

Table 3. Negative Ion Source Proof of Principle Goals

Energy	Low (10-40KeV extaction potential only)
Current	10 A ions (5 A neutrals)
Pulse Length	5 sec to steady state
Gas Efficiency and Optics	As determined by system requirements

The panel recommended that BNL, LBL, and ORNL proceed with their 1 ampere source development through the remainder of FY80 and FY81. The emphasis would be placed not only on parametric performance of the source, but also in obtaining a better understanding of how the source operates. The goal for this period of time is:

Energy:	$\leq$ 40KeV (extraction potential only)
Current:	> 1A
Pulse Length:	5 seconds to steady state

The panel also recommended that in parallel with the 1A demonstration, each laboratory undertake a neutral beam system study illustrating how their particular source concept would be applied to a 10A D^- (H^-), 200KeV neutral injector system. The system study would be used to help guide the experimental program by pointing out areas where the source concept needs improvement and areas where better measurements are needed. The completed system study should be consistent with either achieved source parameters or experimentally-based extrapolation of achieved source parameters, particularly in the critical system areas of gas efficiency, optics/emittance, stacking, power efficiency/cooling, current density, and accelerated electrons. The completed study will aid in evaluation of the source concept by illustrating system design trade-offs required to compensate for source concept weaknesses, and conversely, by illustrating system advantages due to source concept strengths.

Table 4. Negative Ion Neutral Beam Development Budget

FY 1981	$1600K
FY 1982	$2500K (estimated)

The final product of this system study will be a conceptual design of a 10 ampere, 200KeV system and a proposal to proceed with the 10 ampere proof of principle demonstration, followed by building the entire system if warranted by the results.

By following the above course of action, namely, completion of 1 ampere development work and a conceptual design of a 10 ampere, 200KeV system, a foundation will be available upon which to select the concept to be carried through 10 ampere proof of principle and application to a 200KeV system. A review will be scheduled to make this selection in approximately late FY81, so that the 10 ampere work can proceed in FY82.

This scenario is shown in Figure 5.

VI. Budgets

A major consideration in preparing a plan is the projected budget levels. This plan paces the development to fit within the projected budget levels. The budgets shown in Table 4 is for the generic technology development and does not include funds for developing the specific sources for projects.

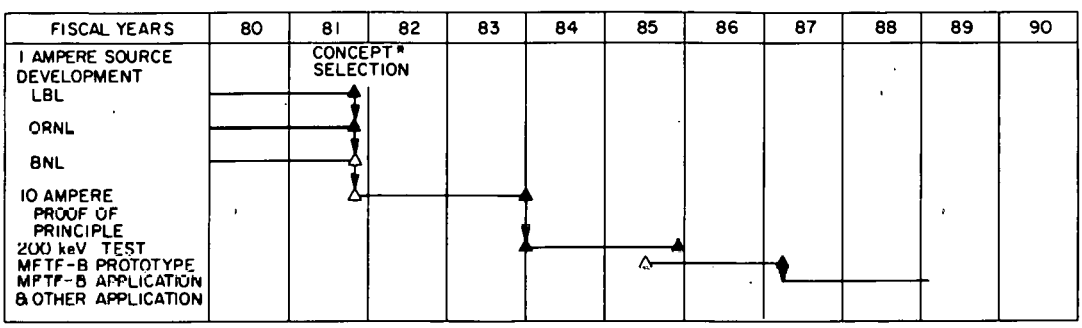

Figure 5. Negative Ion Neutral Beam Program Outline

DISCUSSION

EHLERS What was the negative ion budget for FY'80?

STATEN The 1980 Oak Ridge program was bootlegged in that we authorized them to spend up to a certain percentage of their positive ion budget, which was around 200K. Your budget was 500K and Brookhaven's was 1 M$, so the total budget was a little more than 1.7 M$.

HAGENA Is this for all the expenses of the program or only investment? Does it cover the salaries too?

STATEN This is the total budget including salaries, pencils, paper, solder, travel.

STEWART Could you tell us for FY 81-82 what the split is between positive ions, negative ions and RF in development?

STATEN Let us see if I can remember the numbers. The total neutral beam budget is almost 9 M$. So the difference is what is in the positive ions.

STEWART What about RF?

STATEN It is about 4 M$ in development of the gyrotron.

STEWART For what year is that?

STATEN 1981. The numbers that I give you do not include any of the budgets used directly to support experiments. In the United States when we define an application the development program works jointly with the user and they define, what we call, an MDF or Major Device Fabrication Project and that is funded separately. So presumably an MFTF-B application would be such a joint endeavor of the funding. Hopefully, it will be incremental to a development budget.

STEWART What I am really after is what is the trend?

STATEN The gyrotron budget has tripled in the last two to three years. There has been no money on technology development for other than millimeter waves until this year, and there is $100,000 in '81 and with the expectations that that will go up as soon as money becomes available.

SCHMIDT I think it should be important to point out two things that were strongly recommended during the negative ion review last March. The first one is that there needs to be a proof of principle design goal and I am a little surprised that I have not seen some papers here at the conference, discussing how a source fits in the total concept of a negative ion injector, the accelerator and the neutralizer. It makes little sense to develop these sources if they can not fit into a total system. Secondly, it was also the feeling that groups need to get together and decide on units so that you can make a reasonable judgement about the quality of the different sources in the same type of units.

STATEN I agree with you. One reason why they were not particularly visible is that in the 1980 budget there was not enough money. The money is all obligated to the experimental activities. The systems analysis activities really are just getting under way. In connection with that I might comment that Joel Fink, stationed last year at Brookhaven and now back at Livermore, will coordinate those activities between the laboratories. We felt there was a need for a dedicated person to do that, somebody from the user laboratory, so he could represent the feelings of the people who would end up using it. The one thing that bothered the double charge exchange is, that when they were proposing MFTF-B, they had to decide either to put this device on or not. And the more the user looked the more they concluded they did not want to put it on there. I would just avoid developing something that we are not going to use. I want it readily accepted by a user.

SCHLACHTER The time schedule for applications and limited budgets leads to a situation that worries me quite a bit. Namely, that you are forced to make big decisions soon and I am afraid that that will funnel the money into one approach, which is obviously the objective, at a time when in terms of physics, I think, we are still making big progress and it would be nice if there was a way to keep at least some level of support and not close out all the other options.

STATEN I agree with you but with the budgets that are made available to us to manage this part of the program, I am not sure what else we can do. It seemed to me that it was vitally important to get some concept to the point that it was usable on a physics device. The first criteria is that it is available and works and once that occurs I would hope that the support for improving that, or bringing the other concepts along from a marginal level to a healthy level would follow.

SCHLACHTER I certainly agree with that and I think it is good for all of us if negative ions are going to be used. It is only that the money, given the budgetary levels, gets funnelled to that, to the exclusion of everything else. That is my only concern.

STATEN Well, there are very tight constraints put on the budget. If you look at the U.S. Fusion Energy Budget, Magnetic Fusion Energy for FY '81 and you compare that with the Fiscal '79 budget plus inflation you find a deficit of around $40,000,000. You also find us finishing TFTR, trying to proceed with MFTF-B and trying to initiate EBTP and these are all big money items. You can imagine the budget is very, very tight.

PETERSON You talked about making a decision sometime next summer about the best approach. You are here really talking entirely about direct extraction sources for this particular application, I

gather.

STATEN That is right.

PETERSON What we have seen here is that there are a number of sort of parallel approaches to direct extraction and I suppose what you mean is that you are going to choose from one of those; is that it?

STATEN We are going to choose between the Brookhaven approach, the Berkeley approach and the Oak Ridge approach. One or maybe two of those laboratories will receive increased funding in Fiscal '82.

PETERSON And the other areas will be dropped.

STATEN Depending, maybe dropped, maybe maintained at the same or lower level. It depends a lot on how much we know then, our confidence and recommendations of a review panel as well as the budget. And, realize that the budget for FY '82 is far from being settled.

PETERSON But it seems that there are actually a number of quite parallel approaches.

STATEN That is right.

PETERSON So it is important to choose between which one looks the best.

STATEN I have some confidence that that is not too bad of a thing to do because I see other concepts being pursued elsewhere and if you reduce duplication in the United States, that does not mean that you are taking a promising concept and stopped it completely. I see some of the work being done in Europe providing diversity to what we are doing in the United States. In fact, with a limited budget I would not propose that we duplicate any of it.

MERITS OF D^--BASED NEUTRAL BEAM INJECTORS FOR TOKAMAKS*

L.D. Stewart†, A. H. Boozer, H. P. Eubank, R. J. Goldston
D. L. Jassby, D. R. Mikkelsen, D. E. Post, B. Prichard
J. A. Schmidt, C. E. Singer

Plasma Physics Laboratory, Princeton University
Princeton, New Jersey 08544

Abstract

Model-based efficiencies and costs of D^+ and D^- neutral beam systems are presented and compared. The results of modeling of the heating and the current driving by D^- generated neutral beams are presented. PLT experimental data on heating as a function of beam penetration is presented and discussed. Efficiencies, costs, heating, and current driving are combined to derive the merits of D^--based neutral beam injectors for tokamaks.

I. Introduction

The Engineering Test Facility (ETF) tokamak design work has led to a reassessment of the post-TFTR fusion program. A Fusion Engineering Device (FED) is now being conceptualized to avoid some of the potential problem areas of the ETF. Included in the problem areas perceived for the ETF are the complexity and limited flexibility of the 150 keV, 5-10 sec, D^+ generated neutral beam heating system, the pulsed nature of the device arising from the transformer-driven ohmic current, and the overall cost.

This paper explores the potential of D^- based neutral beam systems for applications to tokamaks. In particular, comparisons are made between D^-neutral beam systems and the ETF-style D^+ neutral beam systems. Results of calculations of D^- neutral beam heating and current driving are presented. PLT experimental data on heating as a function of beam penetration is presented. It is shown that a step from ETF to FED might be done hand-in-hand with a step from D^+ based to D^- based neutral beam systems.

Section II of this paper establishes efficiency and cost bases for quantifying energy-dependent advantages of negative ion systems. Section III and Section IV discuss the advantages of highly penetrating neutral beams for tokamak heating as derived from transport simulation calculations, and as derived from PLT experimental data, respectively. Beam-driven current is discussed in Section V, and conclusions are presented in Section VI.

*This work was supported by US DoE Contract No. DE-AC02-76-CH03073.
†On assignment from Exxon Nuclear Co., Inc.

II. Neutral Beam System

A. Neutral Beam System Efficiencies

Reactor size neutral beam systems based on positive ions and negative ions were modeled in order to establish efficiency and cost bases for quantifying energy-dependent advantages of negative ion systems. The model[1,2] includes losses due to secondary electrons in grid gaps, ionization in grid gaps, premature D^+ charge exchange or premature D^- stripping, less-than-optimum neutralization, fractional energy components and beam divergence. Extraction/acceleration is assumed to be two-stage electrostatic with mechanical characteristics scaled from preliminary results of the LBL TFTR source development program.

One positive ion and three negative ion systems were defined for efficiency and cost comparisons. Table I shows principal parameters of the systems. The positive ion system is based on preliminary ETF and INTOR concepts.[2] Three negative ion systems are presented because of the uncertainty in what a real negative ion based neutral beam system will be like. A system with 5% gas efficiency and a Cs vapor neutralizer was chosen to illustrate relatively low negative ion system power efficiencies, and a system with 10% gas efficiency and a laser neutralizer was chosen to represent relatively high system power efficiencies. A system with 10% gas efficiency and a Cs vapor neutralizer was chosen to generate neutral beam system efficiencies between the extremes. The power efficiencies of this last system are designated to be representative and are used for calculating overall plasma heating efficiencies in Section III.

Calculated efficiencies for the four systems are shown in Fig. 1 as a function of the deuterium beam energy. The efficiencies plotted for the D^+ system are for the full energy power only. It can be seen that even with some pessimism in achievable D^- system efficiencies, the D^- system is as efficient as the D^+ system at the ETF energy of 150 keV.

The rapid fall in efficiency for positive ion systems is crippling and basic. It stems

directly from the rapid fall in neutralization efficiency. The much slower decline in D^- system efficiencies with increasing energy is not as basic. It arises from stripping losses during acceleration. In the model, gap lengths and gap pressures are extrapolated directly from TFTR source data, and imply large stripping losses at high energy. For example, the gap lengths at 100 keV and 500 keV are taken to be 1 cm and 5 cm, respectively, and the stripping losses for the representative D^- system are 15% and 32%, respectively. These losses can in principle be reduced. The larger gaps and/or the Cs vapor neutralizer may allow better pumping than predicted by the model. Also, increasing the gas efficiency directly reduces these losses as can be seen by comparing the two Cs vapor neutralized D^- systems in Fig. 1.

B. Neutral Beam System Costs

Costing is done by assigning projected TFTR costs to 19 beamline components, i.e. arc chamber, plasma grid, extraction grid, high voltage power supply, modulator, etc., then scaling these costs in power, power loading, current, or gas loading, as appropriate.[1] Engineering and prototyping costs are not included in the cost modeling.

Small errors in the projected costs can be expected to arise because the TFTR beam components are not yet all purchased, therefore some component costs will change. More serious errors can be expected because neither long pulse considerations nor reactor level remote handling considerations are represented by the TFTR beams. In order to avoid this more serious problem and yet allow the potential cost advantages of D^- based systems to be illustrated, ratios of the costs per unit of full energy power for the D^- systems and the costs per unit of full energy power for the EFT/INTOR D^+ system at the same energy are presented. The assumption then is that long pulse and remote handling affect the cost of D^- and D^+ systems in the same way, and these effects thus cancel.

Figure 2 shows the cost ratios as a function of deuterium beam energy. The three D^- systems shown and the base D^+ system are those of Table I and Fig. 1. A cost ratio of 1.0 in Fig. 2 means that the cost of the D^- system at that energy is equal to the cost of the ETF/INTOR D^+ system at the same energy. Comparing Fig. 2 with Fig. 1, it can be seen that cost equivalence, between negative and positive ion approaches, comes at higher energies than efficiency equivalence. The reason for this is mostly the poorer gas efficiency of the negative ion systems. One must pay for poor gas efficiency either with large pumps and pumping costs to reduce stripping and reionization losses, or with large sources and power supplies and their costs to make up for all of the lost beam. Again, increased gas efficiency is seen to be a critical item in D^- development.

III. Advantages of D^- Beams for Tokamak Heating

The effectiveness of D^- beams for tokamak heating was explored using a one-dimensional tokamak transport code, BALDUR.[3] The target plasma was one of our versions of the recently proposed FED (Table II). The calculations explored two advantages D^- beams have compared to D^+ beams; better penetration due to their high energy, and their lack of poorly penetrating one-half and one-third energy components.

The tokamak transport code computes the density and temperature evolution of a tokamak. It includes a realistic description of neutral beam injection and heating, alpha particle heating, plasma transport, and plasma fueling and recycling due to neutral gas.

A reference D^+ case was run with 50 MW of heating using a 150 keV, tangential D^+ beam: 38.8 MW @ 150 keV, 7.76 MW @ 75 keV, and 3.45 MW @ 50 keV. D^- cases were run for 40 MW of heating with 150 keV to 600 keV, tangential D^- beams. As would be expected, the higher energy D^- beams provide greater heating at the plasma center, where the energy confinement is best, due to their better penetration. The beam deposition profiles are given in Fig. 3. H(r) is the local source rate (watts/cm^3) at radius r divided by the average source rate, P_b/V, where P_b is the total injected power and V is the total plasma volume. As the D^- energy increases, the deposition profiles are peaked more and more toward the center. The 150 keV D^+ has poorer penetration than the 150 keV D^- beam because of the 75 keV and 50 keV components.

Table III compares the calculated plasma parameters for the D^+ (50 MW) and D^- (40 MW) 150 keV beams. The electron and ion temperatures and the beta's, particularly the central values, are quite close, in spite of the 25% extra power in the D^+ beam. The steady state fusion energy multiplication of the beams, Q_{tech}, is calculated as

$$Q_{tech} = \frac{5\,P_\alpha}{P_b\left(1 - \frac{dE_T/dt}{P_{heat}}\right)},$$

where P_α is the α-power produced, P_{heat} is net beam heating power (beam power minus the charge exchange loss of fast ions), and E_T is the

thermal energy of the plasma. Q_{tech} is lower for the D^+ beam due to the higher total power of the D^+ beam. The lower energy components of the D^+ beam represent an efficiency disadvantage of D^+ beams compared to D^-, since the power of the full energy component is essentially all that matters in a device of this size or larger. In addition, the half and third energy components of the D^+ beam deposit fast ions near the plasma edge. Ions near the edge can strike the wall and limiters since they can either charge exchange with the neutral gas at the edge or leave the plasma on poorly confined orbits. Fast ions striking the wall or limiter might give rise to a significant impurity influx to the plasma, thereby degrading the energy confinement.

The advantages of better beam penetration were explored for D^- beams from energies of 150 keV to 600 keV. The ion and electron temperatures after 5 seconds of 40 MW of injection show a maximum at an injection energy of ~ 400 keV (Fig. 4). The central ion temperature rises rapidly as the beam energy increases from 150 keV showing clearly the advantages of better penetration. $T_i(0)$ falls off slowly for beam energies above 400 keV due to less direct ion heating by the beam ions, because at higher energies the beam begins to heat the electrons directly for the relatively low plasma density used here.

The central β peaks and the average β saturates at ~ 400 keV (Fig. 5). However, Q_{tech} peaks below 400 keV because as the beam energy rises, there is progressively less direct heating of the ions by the beam, and since $\langle\sigma v\rangle_{DT}$ depends on T_i, and Q_{tech} is mostly due to thermal fusion reactions for $Q_{tech} > 1$, Q_{tech} decreases with less ion heating.

Another figure of merit for an auxiliary heating scheme is the amount of injected and primary energy required to reach a specified plasma condition, for example, $\langle\beta\rangle = 4\%$. Figure 6 shows Q_{tech}, the primary energy and injection pulse length required to reach a $\langle\beta\rangle$ of 4%. For energies greater than 300 keV, the energy and injection time are almost independent of beam energy. Q_{tech} at $\langle\beta\rangle = 4\%$ peaks for an injection energy of ~ 250 keV, reflecting the trade off between the decreasing DT fusion cross section, less direct ion heating and better beam penetration as the beam energy increases.

Thus for an FED sized tokamak, D^- beam energies in the range of 300-600 keV produce the highest plasma temperatures and pressures. Beam energies of 250-350 keV produce the highest Q's. All of these parameters are considerably improved over D^+ beams, since the D^+ beams are limited by efficiency considerations to < 200 keV in energy and have significant amounts of one-half and one-third energy components. As illustrated in Fig. 6, the best D^- beam (~ 400 keV) is about twice as efficient as the 150 keV D^- (or D^+ beam) in terms of the required total injected energy to reach $\langle\beta\rangle = 4\%$.

Tangential injection was chosen to explore the current drive potential of D^- beams, which is of particular interest in machines at modest Q and relatively low density, such as the FED of Table II. At higher density or in larger machines, perpendicular injection could be used. These results can be roughly extrapolated to larger values of $\bar{n}_e a$ than used in these FED simulations. Larger minor cross sections would require larger beam energies to achieve good plasma penetration. However, at higher beam energies, the ion heating will not be quite as good as could be expected from the FED cases, since higher energy beams will give progressively more of their heat directly to the electrons. Q_{tech} will increase a little more slowly with beam energy for the same reasons that it peaks at 250-350 keV for FED instead of 400 keV.

Larger target plasmas also offer the possibility of using more modest current ion sources. If a plasma is large enough (a ~ 200 cm) to stop a 1-2 MeV D^o beam, then a given amount of heating power can be supplied by significantly less current. Of course, this reduction in the demand on ion source performance is made at the expense of an increase in demand on accelerator performance.

IV. PLT Experimental Data

Experimental data on the importance of beam penetration to plasma heating is difficult to obtain. Most neutral beam heated tokamaks are operated at plasma densities and beam energies where penetration is not a problem. Since $\lambda_{mfp} \propto E/A$ (= beam voltage/atomic mass), a reasonable parameter describing beam "penetrability" is $E/(A\bar{a}\bar{n}_e)$, where a is the plasma minor radius and $\bar{n}_e$ the line average electron density. Typical neutral beam heated tokamak reactor designs using positive ion based technology envision operation at $E/(A\bar{a}\bar{n}_e) = 3\text{-}6 \times 10^{15}$ keV • cm^2, while current experiments generally fall in the range of $1\text{-}3 \times 10^{14}$ keV • cm^2. Thus, in order to investigate specifically the importance of beam penetration, PLT has recently been operated with D^o injection over a relatively wide range densities reaching $E/(A\bar{a}\bar{n}_e) = 6 \times 10^{-15}$ keV • cm^2. (In evaluating the penetrability, for PLT, we have used an "effective" minor radius of 1.67a in order to take into account the tangential aiming of the

PLT beams.) We have also compared the heating obtained with D^o beams in PLT to that achieved with more penetrating H^o beams at similar densities.

Figure 7 shows the electron heating results obtained in the D^o injection density scan experiments. Surprisingly, the electron heating efficiency did not fall dramatically as the density was increased. In part, this is due to the generally observed improvement of electron energy confinement with increasing plasma density. However the penetrability of the neutral beams varies dramatically over this density range. Fig. 8 shows a simple calculation of H(0) as a function of line average density in PLT. Since the density profiles were not measured in these experiments, $n_e(r)$ was assumed to be parabolic in the calculation. In spite of the uncertainty introduced by this assumption, it is clear that at $\bar{n}_e = 4\text{-}5 \times 10^{13}$ cm^{-3} D^o beam deposition on axis has fallen substantially; indeed, examination of H(r) in this case shows that the heating has become peaked well off axis. Even at the highest densities with D^o injection, however, the electron temperature profile shape changes very little, if at all, during neutral beam heating; thus, the change in the central electron temperature reflects accurately the overall heating efficiency.

Figure 9 serves to explain, in part, the lack of more dramatic electron heating at low density. Tokamak plasmas in general are more susceptible to energy loss through impurity line radiation at lower densities. With high power beam injection at low density in these PLT experiments, a substantial fraction of the central power delivered to the electrons was radiated by metallic impurities, even through carbon limiters were employed. In addition, at low initial plasma densities in PLT, $\bar{n}_e$ cannot be kept constant during injection even by closing the gas feed valve, with the result that the beam heating has to support a substantial dn_e/dt. These factors somewhat confuse the interpretation of the heating results, but if we use only the two beam heating data that is less severely affected by the radiation and density increase, we find that electron heating effectiveness scales, very approximately, as $(1/\bar{n}_e)^{1/2}$.

Figure 10 shows electron heating data from $H^o \rightarrow D^+$ injection at moderate density. Somewhat different plasma conditions on this day are reflected in the higher initial electron temperature. Also beam coupling directly to electrons is more effective with H^o than with D^o beams, so a direct comparison of the two scenarios is not strictly valid. However, at these densities most of the beam power delivered to the ions is coupled locally back into the electrons, so an overall heating effectiveness given by $\Delta T_e/P_b$ is a rough indicator of the effect of beam penetration. Comparing D^o and H^o heating effectiveness, then, we get a scaling in this range of penetrability of approximately $(1/A)^{1/2}$.

We thus estimate from these two PLT experiments that the effectiveness of neutral beam electron heating scales very roughly as the square root of penetrability; i.e., $(\Delta T_e/P_b) \propto [E/(A\bar{a}n_e)]^{\alpha}$, with $1/4 \leq \alpha \leq 3/4$, in the range of penetrability investigated. We conclude that within the experimental uncertainties, and considering the different plasma conditions studied, this scaling is in reasonable agreement with the calculated results for reactor heating by 150 vs. 300 keV D^o beams shown in Fig. 4.

V. Current Drive

The magnitude of the plasma current driven by neutral beams in a large tokamak, such as FED, is dependent on the energy of the injected ions. At beam energies much lower than the critical energy E_c, where the beam energy transfer to the plasma electrons and ions is equal, the current driving efficiency (I_D/P_b, where I_D is the driven current) increases linearly with beam energy. The current driving efficiency of the beam peaks at beam energies of a few times the critical energy and decreases slowly for higher energies. It should be noted that the critical energy for a real discharge with a temperature profile is not well defined; however, the critical energy evaluated for electron temperature near the center of the discharge, where the current is peaked, will give a good measure of optimum injection energy for current drive.

We have studied the capability of neutral injection for driving current in a tokamak with FED-like parameters (Table II, Figs. 3-6) as a function of beam energy. This computation was done by following orbits of a large number of beam particles, using plasma profiles from the BALDUR computations, and applying a correction[4] due to the collisional electron return current. Figure 11 summarizes the results of this study. At low energies, the beam driven current increases linearly with increased beam energy as expected. The improvement in current drive efficiency with increased energy decreases above the critical energy ($\sim$ 600 keV) and the efficiency peaks near several times the critical energy in the central region of the plasma.

Driven current with ECRF and ICRF is similar conceptually to neutral injection if the

beam energy is interpreted as energy of the component of the particle distribution heated by the RF. Although ICRF will have a peak current drive efficiency near the critical energy, ECRF will continue to improve linearly with increasing energy until relativistic effects are encountered. A schematic ECRF efficiency curve is shown in Fig. 11 to illustrate these effects. At low energy the ECRF current drive efficiency may differ from the neutral injection efficiency by factors of 2 or less, depending on Z_{eff} and geometry. At energies approaching 1 MeV, relativistic effects begin to reduce the effectiveness of ECRF and the current drive efficiency will saturate.

It is apparent from these studies that beam energies in the 1 MeV range are optimal from the point of view of driving plasma current with neutral injection. The current drive efficiency of neutral beams with these energies should be comparable to the efficiencies estimated for ECRF and attractive for maintaining a steady state current.

VI. Conclusions

When viewed from the perspective of "improving the ETF," negative ion based beam systems provide important advantages. A D^- based system can have a well defined and optimal beam energy. Positive ion systems have lower energy components which at best waste energy and at worst cause that energy to interact with walls, and thereby lead to impurity buildup. Positive ion systems are limited to ~ 150 keV by efficiency and cost considerations. Negative ion systems in principle remove this constraint with several important consequences. An optimal heating energy can be used: ~ 250 keV for FED or higher for larger devices. Plasma startup can be done without the constraints on radius and/or density arising from a 150 keV beam energy limit. The higher beam energies and efficiencies make driven steady-state tokamak current appear feasible and energetically competitive with the best speculated alternative, ECRH. Finally, the higher energies available from D^- systems will allow heating and driving of subsequent larger tokamaks. So in contrast to D^+, D^- systems can be considered prototypical of reactor systems.

VII. References

1. L. D. Stewart, Conference Record - 1979 IEEE Int. Conf. on Plasma Science (IEEE, New York), paper IE5.
2. L. D. Stewart, Princeton Plasma Physics Laboratory PPPL-TM-329 (1979).
3. D. E. Post, et al., IAEA-CN-37/F-3, Plasma Physics and Controlled Nuclear Fusion Research 1978, Vol. I, IAEA, Vienna, 1979.
4. C. E. Singer, Princeton Plasma Physics Laboratory Report PPPL-TM-313 (1979).

TABLE I

Neutral Beam Systems Compared

Ion	D^+	D^-	D^-	D^-
Neutralizer	D_2	Cs	Cs	Laser
Source Gas Eff.(%)	50	5	10	10
Source Power Eff.(kW/A)	1	10	10	10
Optics Loss(%)	10	10	10	10
Reionization Loss(%)	5	5	5	5
Full-E Ion Current(%)	90	100	100	100
Recovery Eff.(%)	60	0	0	0

TABLE II

FED Parameters

Major Radius: 5.0 m
Plasma Half-width: 1.0 m
Plasma Half-height: 1.5 m
Beam Tangency Radius: 3.4 m
Toroidal Field: 5T
Z_{eff}: 1.5
Plasma Current: 2 MA (80% of α's confined)
Average Density: 9×10^{13} cm^{-3}
(maintained with pellets)

TABLE III

150 keV D^+ and D^- Heating Comparison

	D^+	D^-
Neutral Power	50 MW	40 MW
150 keV	38.8 MW	40 MW
75 keV	7.76 MW	0
50 keV	3.45 MW	0

Plasma Parameters After 5 Seconds of Injection

Central T_i	35.9 keV	36.5 keV
Central T_e	21.2 keV	20.9 keV
Average T_i	15.5 keV	14.8 keV
$\langle\beta_T\rangle$	3.9%	3.6%
Central β_T	8.1%	7.95%
Q_{tech}	4.7	5.6

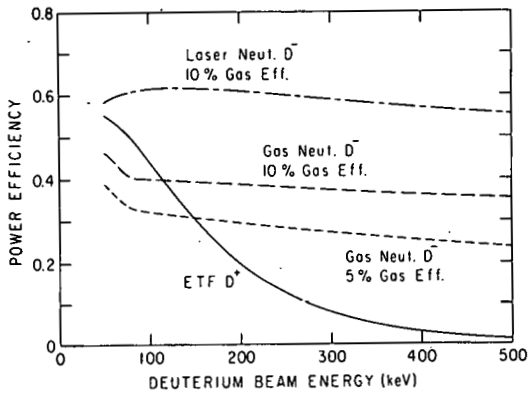

Fig. 1. Neutral beam system power efficiency as function of beam energy.

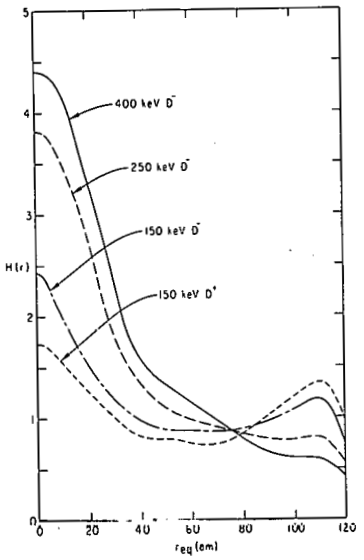

Fig. 3. Neutral beam deposition profiles for 150, 250 and 400 keV D^- beams and for 150 keV D^+ beam.

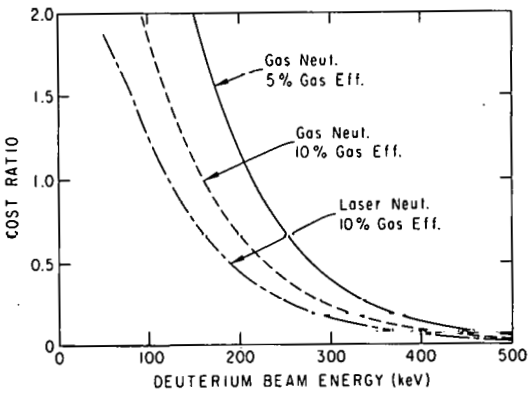

Fig. 2. Ratio of D^- beam system cost to ETF D^+ beam system cost as a function of beam energy.

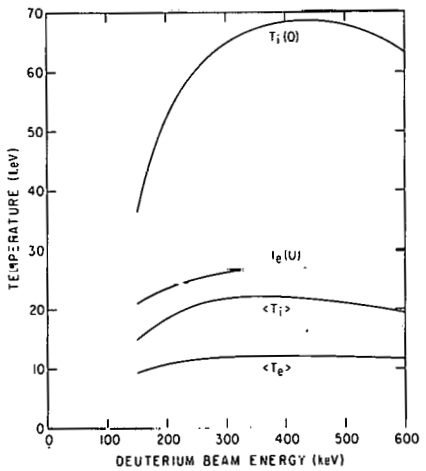

Fig. 4. Central and density-weighted-average ion and electron temperatures after 5 sec of 40 MW neutral injection, as a function of beam energy.

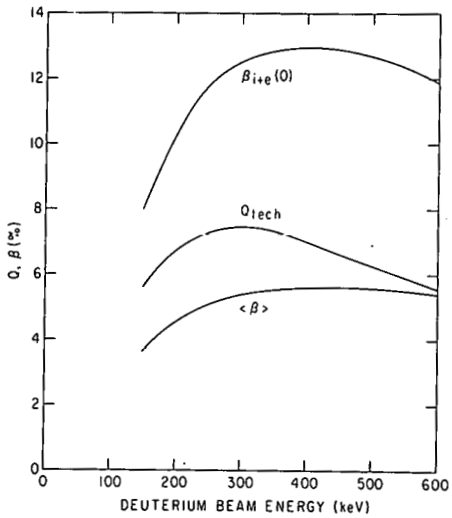

Fig. 5. Central toroidal β of the plasma ions, volume-averaged toroidal β and Q_{tech}, after 5 sec of 40 MW neutral injection, as a function of beam energy.

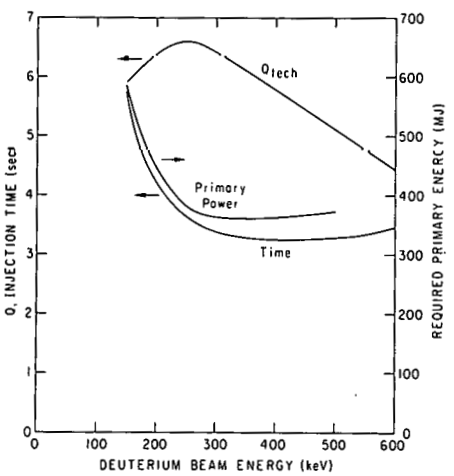

Fig. 6. Required primary beam energy and required injection time to reach an average plasma toroidal β of 4%, and the Q_{tech} at $<\beta>$ = 4%, as a function of beam energy.

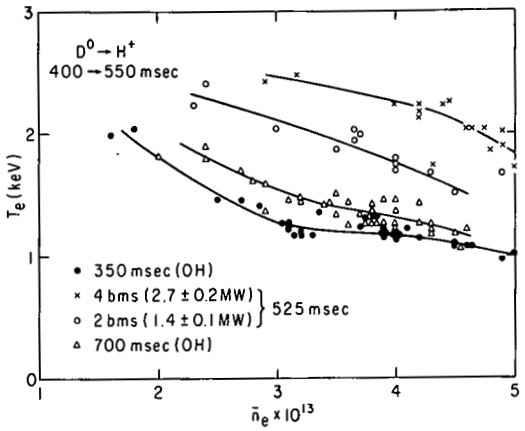

Fig.7. T_e before, during and after injection of a D^0 beam as a function of plasma density.

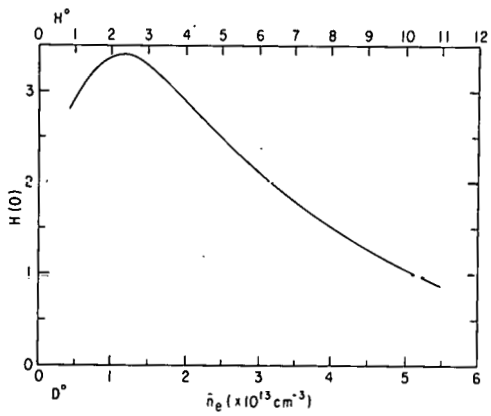

Fig. 8. Approximate H(0) vs. $\bar{n}_e$ for parabolic $n_e(0)$ in PLT.

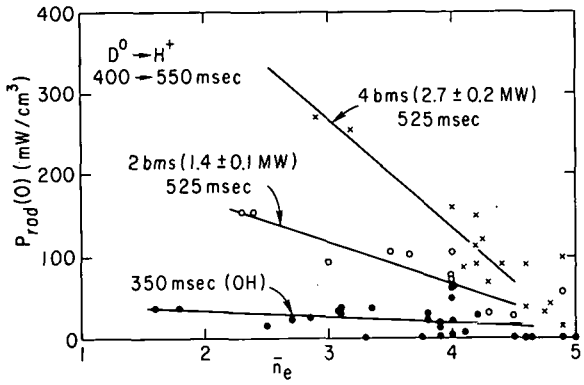

Fig. 9. Bolometrically measured average radiated power, in central 11.5 cm of PLT radius, during D^0 Beam injection, as a function of plasma density.

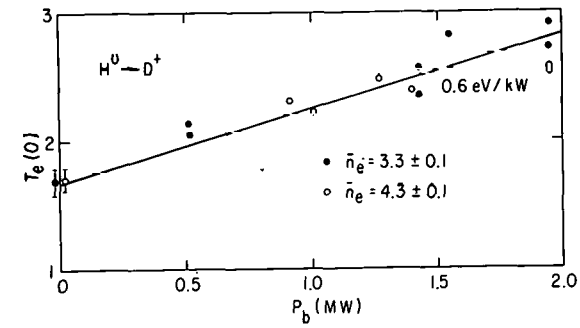

Fig. 10. Electron heating in PLT, using 40 keV H^0 beams, as a function of beam power.

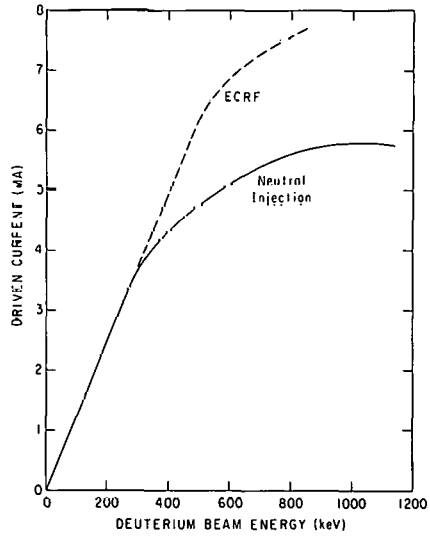

Fig. 11. Plasma current driven by 40 MW of neutral beam as a function of beam energy.

DISCUSSION

SCHLACHTER I have a question about the beam energy deposition profile curves that you showed. For a 150 KeV D^+ and D^- they were not monotonic. They showed a little second peak out near the edge of the plasma. I wondered if you knew what physical effect was making that happen?

STEWART Yes, I think I do, not very specifically because we saw it and looked at it. I think it is because of geometrical effects coupled with the plasma profiles that were assumed. The geometrical effect is, that with the tangential injection the density is going fast and at the same time you are beginning to cross less and less area. If you couple those things together they give little bumps on the outside.

SCHLACHTER They go away at higher energy in that model, apparently.

STEWART Yes, because the outside becomes less and less important with the power getting into the middle, where that effect will disappear. The density profiles are flat in the middle.

HAGENA Your definition of power efficiency and of gas efficiency, is that a universally accepted definition?

STEWART The gas efficiency is the atomic gas efficiency, it is the gas you have to put into the source compared with the ions which come out. The power efficiency is the neutral power that gets to the plasma divided by all the power inputs that I could think of, including pumps, ion sources etc.

HAGENA That is a remarkable high value for 200 keV positive ions: 20%.

STEWART No, was it that high? By the way this has a 60% direct recovery system.

HAGENA That explains it.

HOOPER What are the current driving mechanisms for your beams in ECRH? Are they the same or are they different?

STEWART No, I think I can not answer that detail either. The beams stack up...

HOOPER Momentum transfer in the case of the beams?

STEWART There is momentum transfer but there are also circulating beams because this is tangential injection so you integrate all that together and look at how much net current you have. In ECRH there are several different mechanisms. I do not understand all of them; some of them are coupled to the particular population that happens to be going in one direction and there is also momentum transfer.

HERSHCOVITCH I have been involved in some rf heating experiments. In one of the latest issues of Nuclear Fusion where an analysis was done of experiments in neutral beam heating and where they showed that there is agreement between theory and experiments on the portion of the current that is driven by the neutral beams. On the other hand, when it comes to rf, their experiments are contradictory. One of them is a Japanese experiment and the other one is on Versator II. The Japanese experiment shows that lower hybrid current driven works, while with Versator they showed in a pretty convincing way that there is no evidence.

HOOPER So you are arguing that any current driven mechanism, at this point, is highly speculative.

TSAI You assumed that the negative ion source can be developed as good as a positive ion source with as good a beam quality. Did you take into account the high probability of stripping in the accelerating column with a gas efficiency of only 10%.

STEWART Yes, that is in the model.

HASELTON Jim is also saying that there is charge exchange which gives rise to lower energy tails.

STEWART Without a detailed accelerator design I do not know what is going to happen to those reduced energy neutrals. I would assume that they are not going to have as good optics as the rest of the beam

NEGATIVE DEUTERIUM IONS FOR TANDEM MIRROR NEXT STEP AND TANDEM MIRROR REACTORS*

Gordon Hamilton

Lawrence Livermore National Laboratory, University of California
Livermore, California, USA 94550

Abstract

Recent designs for mirror fusion reactors with good power balance include ambipolar potential plugs to reduce end losses and thermal barriers to maintain a difference in electron temperature between the large-volume central cell plasma and the confining end plugs. These designs led to several new requirements for D^0 neutral beams derived from negative ions at energies of 150 to 200 keV and possibly higher. Such beams are required for injection of fast ions into the plugs and the barrier and for charge-exchange pumping of thermal ions diffusing into the barrier. Negative ions are preferred for these purposes because of their relatively high efficiency of neutralization and their high purity of single-energy D^-. Examples of injector designs for Tandem Mirror Next Step (TMNS) and Tandem Mirror Reactors (TMR) are presented.

I. Introduction

It has long been recognized that negative hydrogen ions will almost certainly be essential for neutral beam injection into mirror fusion reactors and large mirror experiments. This fact has not changed. However, our requirements for negative ions have greatly changed during the past few years because of improvements in our reactor designs. We now need negative ions for several types of injectors for specific purposes. Required beam currents have been reduced and are therefore close to the realm of practicality. Our requirements are sufficiently definite to be useful for guidance in ion-source development.

Historically, the earliest negative-ion requirement for mirror reactors was based upon the fact that the rate of scattering into the loss cone of a magnetic mirror is a strong function of ion energy. A scaling law based upon Fokker-Planck computations relates the ion density, n_i, ion temperature T_i, and scattering lifetime, τ_i:

$$n_i \tau_i \propto T_i^{3/2} \quad . \qquad (1)$$

Consequently, the ion temperature of a magnetically-confined mirror fusion plasma must be high merely to satisfy the Lawson criterion. The most straightforward way to meet this requirement was by high energy injection of neutral atoms (D^0 and/or T^0) derived from D^- and/or T^-. This requirement still exists in our new designs, but is no longer the only motive for negative ions.

A few years ago we were faced with a requirement for improving the Q of a mirror fusion reactor (Q is the ratio of the fusion power produced to the power injected into the plasma). Our single-cell reactor designs of a few years ago were based upon Q's of only 1 to 1.5. They required very high currents of injected beams with efficient recirculation of power and, consequently, high engineering technology and high capital costs.[1] We were required to find ways of raising Q to values of 10 to 30 and thereby to reduce the technology requirements and the capital cost of our designs.

The purpose of this paper is to explain the impact of recent improvements in mirror reactor design upon our requirements for negative ions. We now have several motives for using negative ions, whereas a few years ago we had only one. Our new motives are associated with beam energy requirements and also with beam purity requirements, both of which may be satisfied with negative ions better than with positive ions.

It is necessary first to explain the recent improvements in mirror reactor design and then to explain how these improvements have generated new requirements for negative hydrogen ions. Two inventions, tandem mirrors and thermal barriers were the major impetuses for these new requirements.

II. Tandem Mirrors

The invention of tandem mirrors with ambipolar potential plugs to reduce end losses occurred independently in the USA[2] and in the USSR[3] in 1976. This invention consists of two plugs with high plasma potential at the ends of a large-volume central cell containing the reacting plasma. The ions in the plug are magnetically confined and therefore will operate at $Q < 1$. The ions in the central cell are electrostatically confined with respect to end losses and operate at $Q \gg 1$. Since the central cell is much larger in volume than the two end plugs, the overall $Q > 1$, which results in a positive power balance.

Figure 1 shows the profiles of density and potential for a tandem mirror without thermal barriers. The central-cell ions will be confined for many scattering times and therefore will have a distribution almost Maxwellian. The ion-containment time with respect to scattering over the confining potential, ϕ_c, will be approximately

$$\frac{\text{ion containment time}}{\text{ion-ion collision time}} = \exp(\phi_c/T_i) \quad . \qquad (2)$$

*Work performed under the auspices of the U. S. Department of Energy by the Lawrence Livermore National Laboratory under contract number W-7405-ENG-48.

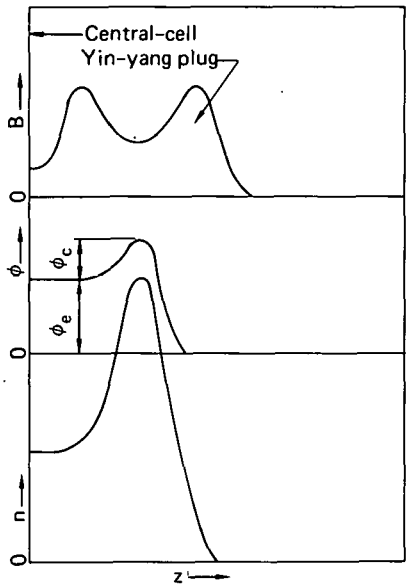

Fig. 1. Axial profiles of magnetic field, B(z), potential, (z), and density, n(z) for a tandem mirror without thermal barriers. The potential of the central cell is ϕ_e and the confining potential is ϕ_c.

Comparing this containment time to that of Eq. (1) we see an improvement by the factor $\exp(\phi_c/T_i)$. As an order of magnitude we must design for T_i of about 30 keV and therefore ϕ_c of about 100 keV. The Q can be increased as high as desired, the only limitations being the economics of the length of the central cell and of the central-cell-plasma density.

The reduction of end losses from a tandem mirror has been experimentally verified in the Livermore Tandem Mirror Experiment (TMX).[4] Other tandem mirror experiments in which these principles are under study are in operation or under construction in Japan, the USSR, and the USA. The success of tandem mirrors during the past few years has caused this to become the main effort of mirror fusion research.

The creation of the high plasma potential in the end plugs is not trivial. The electron distribution is normally Maxwellian because of the high collision frequency of electrostatically contained thermal electrons. Therefore, the plasma potential profile $\phi(z)$ is related to the electron density profile $n_e(z)$ as follows:

$$n_e(z) = n_{max} \exp([\phi(z) - \phi_{max}]/T_e) \quad (3)$$

Consequently, if the electron temperature, T_e, is spatially uniform it is necessary to increase $n_e(z)$ at the plugs enough to produce the required potential of 100 keV or more. The required plug potential must be $\phi_c + \phi_e$, where ϕ_e is the potential of the central-cell plasma and ϕ_c is the confining potential. Our earlier designs[5] based upon this model turned out to have a very high beam energy requirement (1.2 MeV) and also other requirements of advanced technology.

III. Thermal Barriers

More recently[6] it was realized that it is possible to isolate the plug electrons from the central-cell electrons and thereby to heat them unequally. The plug electrons should be hotter than the central cell electrons to maintain the potential difference, ϕ_c. This makes it possible to reduce the plug-plasma density, thus greatly reducing the plug injection requirements. These facts are illustrated by two of our TMR designs, with and without thermal barriers, for which the relevant parameters are displayed by Table I. It is clear that the thermal barriers greatly reduce the plug injection requirements because of the lower density.

Obviously in either case the plug neutral beams must be derived from negative ions because the energy requirement is several hundred keV. However the neutral-beam current requirement has become modest and does not require large extrapolations from D^- sources now under development. The comparison shown in Table I illustrates the motive for thermal barriers.

The thermal barrier must have a sufficiently low plasma potential to prevent the hot plug electrons (~200 keV) from flowing into the cooler central cell (~30 keV). Such a potential profile is shown by Fig. 2. Reduction of the plasma potential in the barrier requires the reduction of the density of electrostatically trapped electrons. The methods of achieving this can be surmised from the equation of quasineutrality in the barrier, in which we must consider three ion populations and two electron populations:

$$n_i(\text{total}) \approx n_e(\text{total}) \quad , \quad (4)$$

where $n_i(\text{total}) = n_{pass} + n_{trapped} + n_{slosh}$, and $n_e(\text{total}) = n_e(\text{thermal}) + n_e(\text{hot})$.

Obviously, in order to reduce the density of electrostatically-trapped electrons, $n_e(\text{thermal})$, it is necessary to reduce $n_i(\text{total})$ and to increase $n_e(\text{hot})$. These populations of ions and electrons will now be defined.

Ions from the central cell pass through the barrier and are reflected by the plug potential back into the central cell. The density of passing ions, n_{pass}, can be reduced first by increasing the area of the tube of flux by a reduced magnetic field in the barrier. Furthermore, the density of passing ions is reduced as the ions are accelerated in the potential well.

Some ions, of density $n_{trapped}$, are trapped either magnetically or electrostatically within the thermal barrier. These ions are trapped at a fixed rate by collisional diffusion of passing ions in velocity space as they flow

TABLE I. Examples of Plug Requirements for Two TMR Designs

Requirement	TMR without thermal barriers,[5] 1977	TMR with thermal barriers,[7] 1979
Required plug potential $\phi_c + \phi_e$	260 keV	210 keV
Plug electron temperature	42 keV	200 keV
Plug plasma density, cm^{-3}	8.6×10^{14}	2.6×10^{13}
Injection energy	1200 keV	400 keV
Neutral Beam Current	220 A	3.2 A

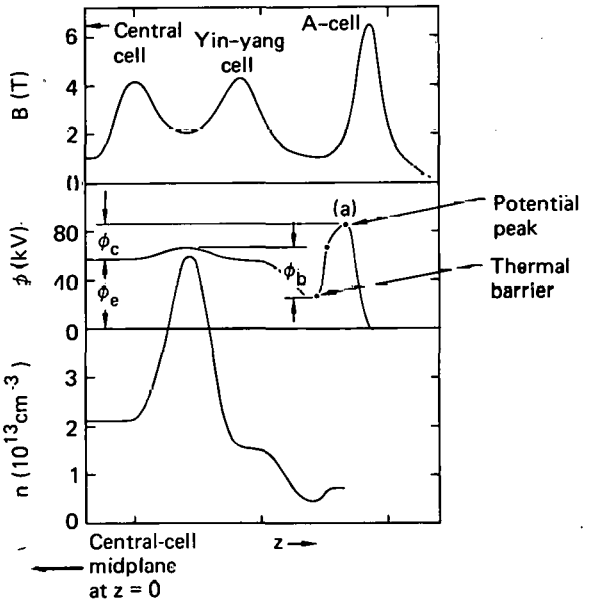

Fig. 2. Axial profiles of magnetic field, B(z), potential, $\phi(z)$, and density, n(z), for a tandem mirror with thermal barriers of the A-cell type. The depth of the barrier potential well is ϕ_b.

through the barrier. They must be removed by some pumping technique such as charge-exchange pumping (to be discussed). We will soon find that charge-exchange pumping generates a second requirement for negative ions.

In order to reduce $n_i(total)$ at the center of the barrier, it is possible to take advantage of a region of velocity space in which trapped ions spend almost all of their time at their turning points at the ends of the barrier and very little time at the center of the barrier, where they have been accelerated by the potential well. The sloshing ions, of density n_{slosh}, must be injected with sufficiently high energy (about 200 keV) so they will not rapidly diffuse in velocity space. Therefore the sloshing ions comprise a third requirement for negative ions for neutral injection.

Finally, it is possible to heat some of the barrier electrons by electron cyclotron resonant heating (ECRH) to sufficiently high temperatures so that they become collisionless and therefore magnetically confined. If the density $n_e(hot)$ of the magnetically confined electrons is a finite fraction of the total density, the potential well will be further deepened.

To illustrate these points, Fig. 3 shows those regions of velocity space where the ions either are passing through the thermal barrier or are trapped within the barrier. The equation of the hyperbola separating the trapped region from the passing region is the following:

$$v_\parallel^2 - (R - 1)\, v_\perp^2 = \phi_b(2q/m) \quad , \qquad (5)$$

and the loss-cone angle, θ_{LC}, defined by the asymptotes of the hyperbola is $\theta_{LC} = \sin^{-1}(R^{-1/2})$.

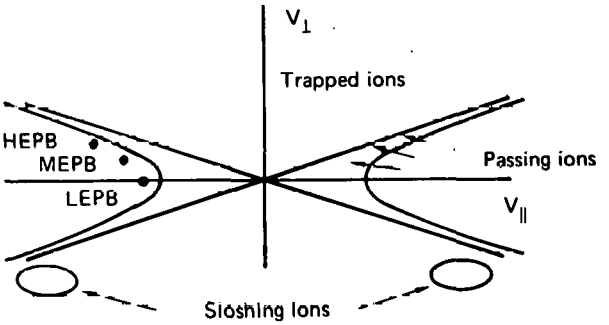

Fig. 3. Regions of velocity space at the center of the thermal barrier in which the ions are either passing through the well or trapped within the well. Arrows indicate the diffusion of trapped and passing ions in velocity space filling up the barrier; ions injected as sloshing ions and by the three pump beams, LEPB, MEPB, and HEPB are indicated in velocity space after acceleration by the potential well.

Here the depth of the barrier potential well is ϕ_b, and the barrier magnetic mirror ratio is R. Also shown in Fig. 3 is the diffusion of passing ions into trapped velocity space and the region occupied by the high energy sloshing ions.

A promising way to remove the trapped ions from the barrier is charge exchange pumping. By this technique a neutral beam is injected almost parallel to the magnetic field. When a trapped ion exchanges charge with the neutral beam, the resulting atom goes to the wall and is thus pumped from the barrier. However, it is essential to arrange conditions such that the injected ion produced by charge exchange becomes a passing ion and does not become trapped in the barrier. For this reason, Fig. 3 shows the pump beams HEPB, MEPB, and LEPB must be injected into a portion of velocity space occupied by passing ions, not by trapped ions. The requirement for this is

$$E_B \geq \Delta\phi/(1 - R \sin^2\theta) \quad , \qquad (6)$$

where E_B is the pump beam energy and θ is the angle between the velocity vector and the B vector at the point the charge exchange or ionization occurs. The neutral-beam current must be sufficient to compensate for the fact that only a fraction of the beam will exchange chargee with trapped ions. Part of the beam will be ionized or will interact with passing ions and will not be effective for charge-exchange pumping.

A large economy in pump power is possible if two or three charge exchange beams are injected into the barrier at different potentials. Most of the trapped ions can be pumped from the upper part of the potential well, where $\Delta\phi$ is small or even less than zero. For this reason our designs include two or three pump beams of different energies, which we denote as the high energy pump beam (HEPB), medium energy pump beam (MEPB), and low energy pump beam (LEPB). The energy E_B and injection angle θ must be chosen such that Eq. (6) is satisfied at all points along the beam path.

Negative ions are preferred for charge-exchange pumping for two important reasons. First of all, Eq. (6) shows that the energy E_B of the HEPB must be at least equal to $\Delta\phi = \phi_b$, which will be at least 100 keV. Negative ions are needed for the usual reason of neutralization efficiency. A second requirement results from problems of positive molecular ions, which contaminate neutral beams by producing atoms with one-half or one-third of the primary beam energy. The fractional-energy components are undesirable in any neutral beam; they are intolerable in a charge-exchange beam if they fail to fulfill Eq. (6) and therefore are trapped within the barrier potential well.

We know of only four ways of preventing fractional-energy beam components being trapped within the barrier:

a. Negative ions provide the most satisfactory solution, since there are no molecular negative ions in the primary beam. Therefore we prefer negative ions even for the MEPB, designed for 60 to 100 keV.

b. The D_3^+ may be separated from positive molecular ions before neutralization either by magnetic deflection or rf acceleration. In either case this involves power losses because of dumping of molecular ions, premature charge exchange in the deflection magnet, and/or rf losses.

c. Trapping within the barrier may be avoided if the primary beam energy is increased to three times the requirement of Eq. (6). This is very inefficient, but may be suitable for smaller experiments, such as MFTF-B.

d. Development of a pure D_3^+ ion source may be possible, but it is impossible to predict whether the purity can be raised above 90%. This is not sufficient for the HEPB.

In our designs, the largest beam current requirement is for the medium energy pump beam (MEPB), for which E_B may be in the range 60 to 100 keV. We would prefer using negative ions to produce the MEPB because of the beam purity requirement. However, we will probably be forced to use positive ions for the MEPB in the near future because positive ions have a large advantage in beam-current density . Table II shows a comparison of beam densities upon which our designs are based. The densities of negative-ion beams assumed to be available in 1990 are based upon goals of existing programs. The beam densities assumed to be available for reactors farther in the future will require upgraded goals.

An interesting possibility for certain geometries of thermal barriers is charge exchange pumping of thermalized alpha particles. In the

TABLE II. Beam Densities for MFE Injection

Assumed availability date	Positive ions 1980	Negative ions 1990	2010
Accelerated ion beam density, mA/cm^2	250	20	100
Grid transparency	0.6	0.25	0.5
Overall density, mA/cm^2	150	5	50

case of a full-sized reactor this would limit the accumulation of alpha particles to about 10^{13} cm^{-3} and thereby make possible steady-state reactor operation. One of the advantages of charge-exchange pumping of alpha particles is that the 3.5-MeV alpha particles would not be pumped from the TMR until they give up at least 90% of their energy to the reactor plasma.

Charge exchange pumping of a He^{++} will occur if the He^{++} captures an electron from an injected D^0 after the He^{++} is accelerated axially by a potential difference $\Delta\phi$ in the thermal barrier. The He^{++} increases its kinetic energy by $2\Delta\phi$ before the charge exchange and then will lose only $\Delta\phi$ kinetic energy as it emerges from the potential well as He^{+}. If conditions are correct the He^{+} will have enough energy to escape over the potential hill of the plug. The high current MEPB will provide enough electron capture targets to pump out the thermalized He^{++} as well as the D^{+} trapped in the barrier.

IV. Tandem Mirror Next Step (TMNS)

During the next few years the tandem mirror experiments active at Livermore will be the Tandem Mirror Experiment (TMX) and the Mirror Fusion Test Facility (MFTF-B). We do not expect that high-current, negative-ion beams will be available early enough to be used in either of these experiments. However, the logical next step in the development of a mirror fusion reactor would be a steady-state, D-T-burning, tandem device designated as TMNS. Parametric studies lead us to a machine with a central-cell length of 50 m, 227 MW of fusion power and an injected neutral-beam power of 50 MW.

Table III is a breakdown of the TMNS neutral-beam specifications. The three high-energy beams will be derived from negative ions and yield an injected power of 26 MW. In this design we must use positive ions for the 66-keV MEPB in spite of the relatively low efficiency, because we need the higher current density for this high-current beam.

Figure 4(a) and (b) show injector modules for TMNS based upon positive ions and upon negative ions. The positive ion module for the MEPB is based upon a 66-keV, 80-A ion source with a bending magnet before the neutralizer for separating the D_1 from the molecular ions. The negative ion module is based upon a 150-keV, 12-A D^- source compatible with sources under development at several of our negative-ion laboratories.

In both cases a three-stage gas pumping system is required to maintain pressures of 10^{-4} Torr before and after the neutralizer; 10^{-5} Torr in the vicinity of the charged beam stop; and 10^{-6} Torr in the injection path from the injector to the TMNS plasma. These pressures are required to avoid large beam losses by collisions with the background gas. In both cases the neutralizer consists of a rectangular duct 1 to 2 m long with gas added to the midplane so that the maximum pressure is 10^{-3} Torr and so that the neutralizer gas thickness is 3×10^{15} molecules/cm^2 for the 150-keV D^- and 7×10^{15} molecules/cm^2 for the 66 keV D^+. In contrast with conventional positive-ion systems, both modules require extra cryopanels between the ion source and the neutralizer to reduce the gas pressure to 1×10^{-4} Torr in this region. The cryopanel design includes a provision for pumping away the condensed gas periodically without shutting down the injection system.

Both systems include beam stops for disposal of the residual charged beam emerging from the

TABLE III. TMNS Neutral Beam Specifications, 1980

	Plug	A-cell	HEPB	MEPB	LEPB	TOTALS
Power absorbed, MW	14	4.1	7.8	12.2	0.25	
E_B, keV	150	200	150	66	2	
I absorbed = P/E_B, A	93	20.5	52	185	125	
I (pump), A	---	---	7.5	67.5	75	
F_1 (ionization)	---	---	0.40	0.36	0.6	
F_2 (attenuation)	1.0	0.9	0.36	0.53	0.9	
$I^0 = I/F_1F_2$, A	93	22.8	52	350	139	
I^0 E_B, MW	13.95	4.56	7.8	23.1	0.278	49.7
Beam species	D^-	D^-	D^-	D^+	D^+	
Neutralization efficiency	0.6	0.6	0.6	0.71	0.9	
Purification efficiency	---	---	---	0.7	---	
Accelerator efficiency	0.9	0.9	0.9	0.9	0.9	
I^+ or $I^- = I^0/\Pi n_j$	172	42	96	782	172	
P^+ or P^-, MW	26	8.4	14.4	52	0.34	
Power supply efficiency	0.95	0.95	0.95	0.95	0.95	
Ion source power (MW) (2 KW/A D^+; 10 KW/A, D^-)	1.7	0.4	1.0	1.6	0.34	
Total power, MW	29	9.3	16	56	0.72	111.0

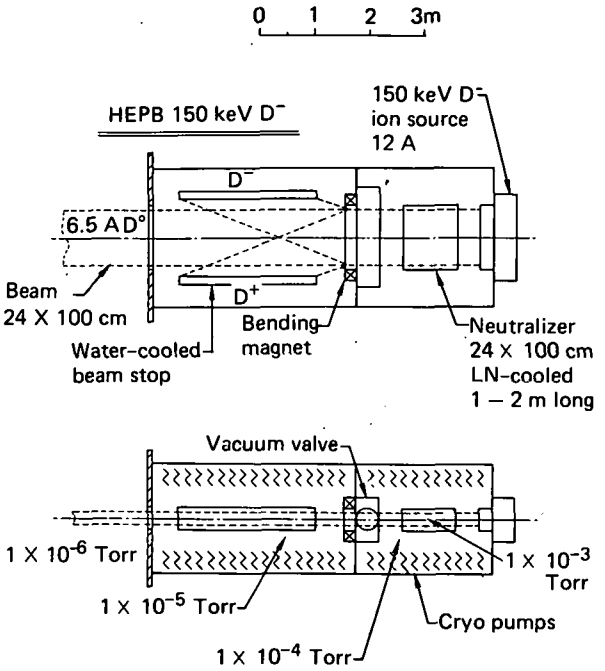

Fig. 4(a). An injector module suitable for the 150-keV HEPB of TMNS. The ion source, emitting 12 A of D^- in an area of 24 × 100 cm is compatible with the development goals of existing programs at negative-ion laboratories. The neutralizer, bending magnet, beam stops, and gas pumping system are shown to scale.

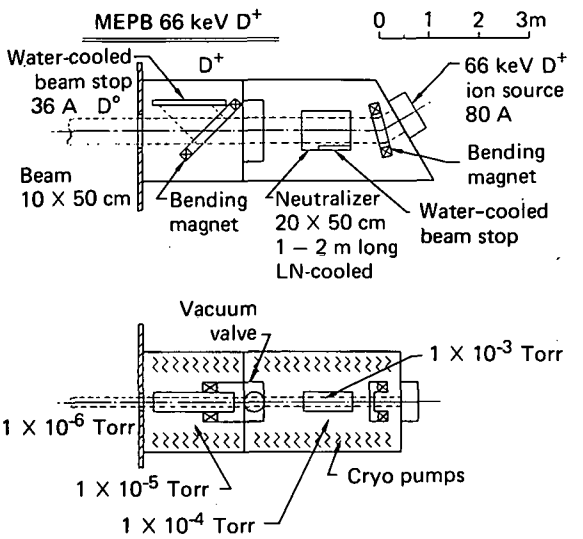

Fig. 4(b). An injection module suitable for the purified 66-keV MEPB of TMNS. The primary beam must be D^+ rather than D^- because of the relatively high beam density required and because of the 10-year construction schedule which does not allow major new developments. Therefore, a purification magnet is required between the ion source and the neutralizer.

neutralizer. Bending magnets may be required for this purpose; the fringing field of TMNS will be sufficient for charged-beam disposal in certain locations. Vacuum valves are required to isolate each injector for maintenance. Superconducting magnetic shielding will be required to exclude the fringing field of 0.1 to 0.2 Tesla and may be mechanically combined with the cryopanels.

Figure 5 shows how arrays of such modules may be installed at each end of TMNS to provide the currents shown by Table III. Here we have allowed for at least one spare module in each array. The assumed gas efficiencies are 35% for positive ions and 10% for negative ions. Beam densities and gas efficiencies are consistent with our expectations for 1990 or before. Because of this 10-year time schedule for TMNS we are trying to avoid advanced concepts such as photo-detachment, high-density D^- beams, rf acceleration or beam energy recovery.

The design of TMNS is still evolving as we optimize the power recovery balance, the plasma stability, and the capital cost. Several versions of magnet designs are under consideration; all of which have similar requirements for neutral beams.

V. Tandem Mirror Reactors (TMR)

Negative ion requirements for full-sized Tandem Mirror Reactors are similar to the requirements for TMNS except for the requirements for larger beam currents and higher efficiencies. Because of the longer time available (~20 years) for development of reactor systems we can use advanced concepts to improve the efficiency of our designs. Neutral-beam energies may be in the same range as the energies of TMNS (150 - 200 keV) or may be somewhat higher. Beam energies much above 500 keV are not expected because the penetration through the plasma would not be suitable for the moderate dimensions and densities of the plasmas of our designs.

For a TMR producing 3,500 MW of fusion power the estimated requirements for neutral beam currents and power are six to eight times larger than the TMNS requirements shown by Table III. However, because of improvements in efficiency during the next 20 years the charged-beam requirements for TMR will be only three to four times larger than the TMNS charged-beam requirements. The improvements we expect are the following:

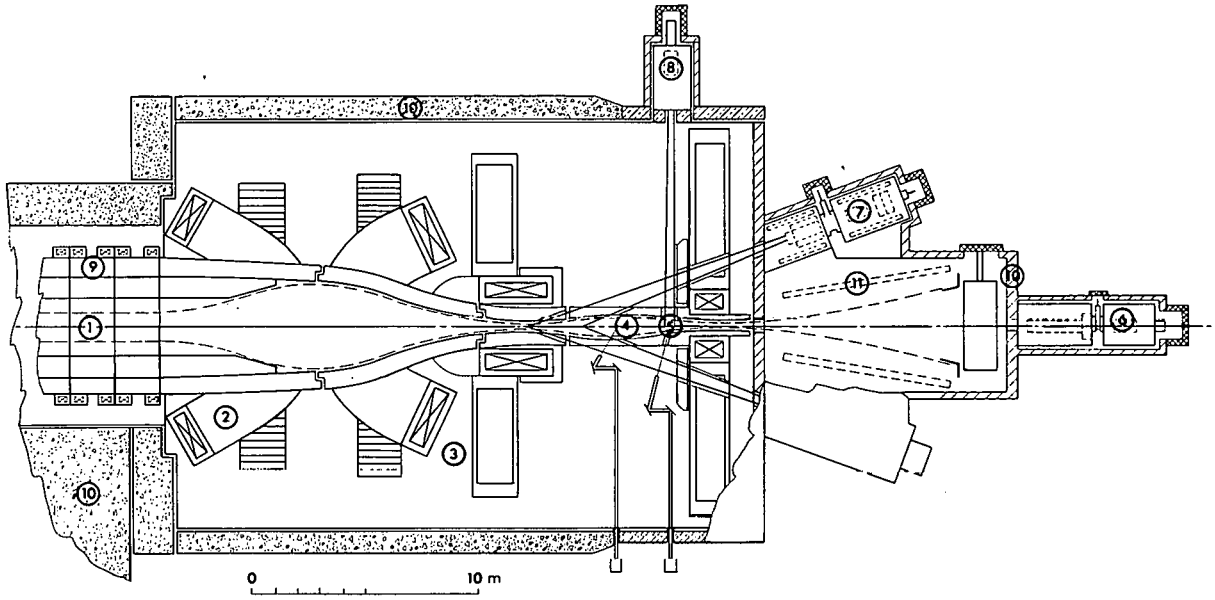

Fig. 5. An overall elevation of one end of TMNS showing the following components: (1) central cell; (2) transition coil and structure; (3) yin-yang coil and structure; (4) thermal barrier; (5) A-cell plug with coil and structure; (6) HEPB, D^-, 6 modules at each end; (7) MEPB, 4 modules at each end, top and bottom; and (8) LEPB, D^+, 3 modules at each end. Also shown are (9) the neutron blanket, (10) radiation shields, and (11) plasma direct converter.

a. High density D^- beams will make it possible to change the MEPB from D^+ to D^-. Consequently the 30% loss in the purification magnet will be avoided. Also, the high D^- beam density will improve the feasibility of photodetachment.

b. Development of advanced neutralizers (photodetachment or plasma cells) will raise the neutralization efficiency from 60% to 80% or more.

c. Beam energy recovery will become economical.

d. Perhaps more efficient techniques will be developed for pumping of thermal barriers.

The concepts of tandem mirrors and thermal barriers permit many variations of magnetic field geometries. Figure 6 shows two of our current designs, which we are now studying for stability, economics, and feasibility. Figure 6(a) shows an A-cell barrier TMR similar to TMNS, while Fig. 6(b) shows an axisymmetric barrier TMR. The axisymmetric design includes a magnetic cusp which avoids the need of a quadrupole magnetic field for plasma stability. Figure 7 shows the geometry of beam injection into the axisymmetric TMR. The beam path of the high-current MEPB is compatible with charge-exchange pumping of thermalized alpha particles. As these designs evolve the requirements for negative-ion beams are changing in magnitude. We find that we can reduce the requirements by shaping the magnetic field and by improving the efficiencies. We are exercising our Fokker-Planck codes and reactor design codes to optimize the geometries and the parameters.

Figure 8 is an overall isometric view of one of our TMR designs,[7] showing the essential components and their relation to each other. The magnetic field geometry is different from those of Figs. 6 and 7 in that the barrier is located between the yin-yang coil and the central cell. The central solenoid, only 56 m long, produces 1770 MW of total fusion power, of which the net power output is 500 MWe. The simplicity and linearity of the central cell is an important asset for maintainability of the fusion blanket.

Acknowledgments

Many people working in the TMNS and TMR groups at LLNL have made contributions to the designs which generate our requirements for negative ions. The individuals in charge of these projects are G. A. Carlson, C. C. Damm, B. G. Logan, and R. W. Moir. Significant contributions relevant to our negative-ion requirements were made by B. M. Boghosian and C. L. Hanson.

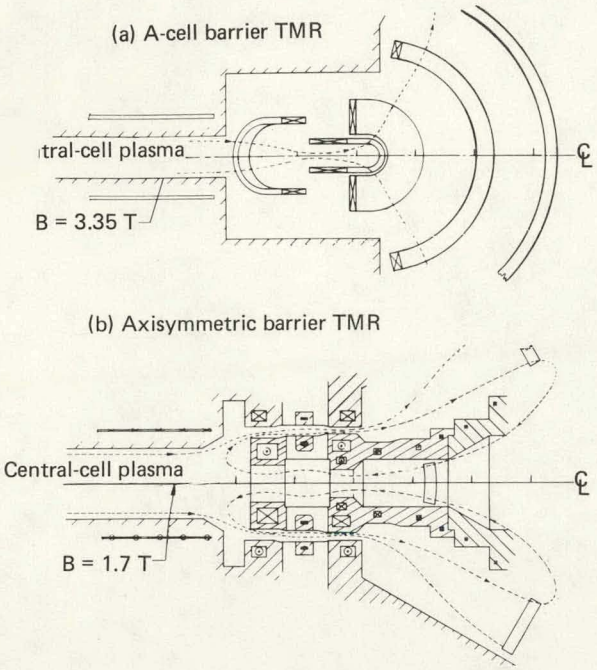

Fig. 6. Two design versions of TMR's with thermal barriers: (a) a TMR with an A-cell barrier similar to that of TMNS; and (b) an axisymmetric TMR stabilized by magnetic cusps.

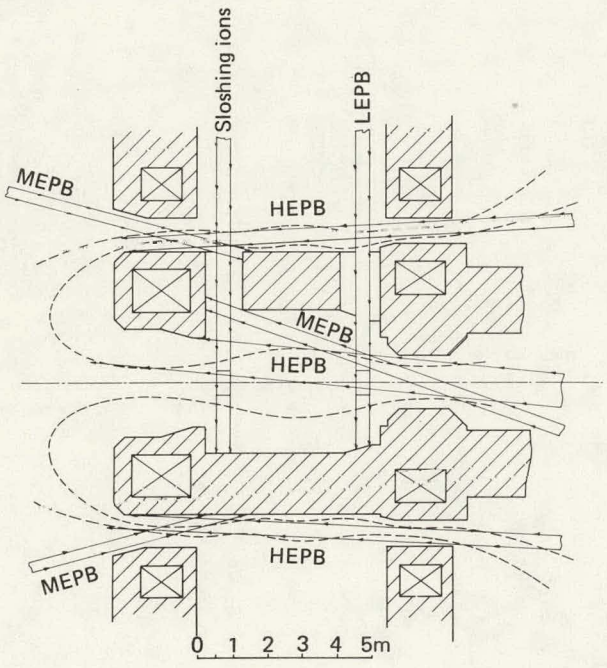

Fig. 7. Beam injection paths for the axisymmetric TMR. Charge-exchange in pumping and sloshing ions is required both for the thermal barrier on the z-axis and the thermal barrier in the outer annulus.

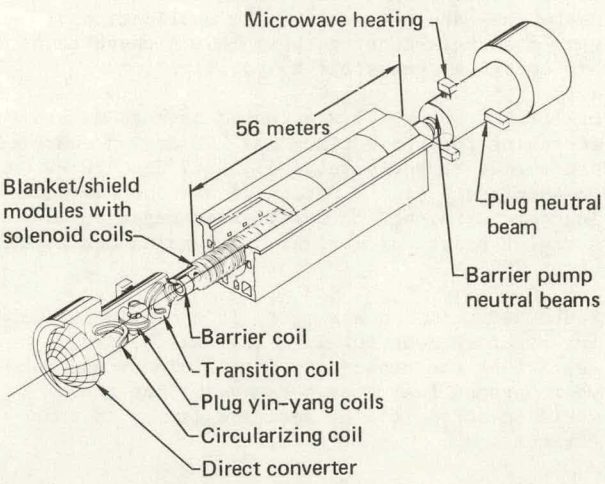

Fig. 8. An overall isometric view of a TMR, showing the relationship and scale size of the major components.

References

1. For example, J. H. Fink, W. L. Barr, and G. W. Hamilton, "Efficient High-Power High-Energy Neutral Beams of the Reference Mirror Reactor," IEEE Transactions on Plasma Science, PS-7 (1979).

2. T. K. Fowler and B. G. Logan, Comments Plasma Phys. 2, 167 (1977).

3. G. I. Dimov, V. V. Zakaidakov, and M. E. Kishinevsky, Fiz. Plasmy 2, 597 (1976).

4. T. C. Simonen, et al., "Plasma Confinement Experiments in the TMX Tandem Mirror," 8th International Conference on Plasma Physics and Controlled Nuclear Fusion Research, Brussels, Belgium (1980).

5. R. W. Moir, W. L. Barr, G. A. Carlson, W. L. Dexter, J. N. Doggett, J. H. Fink, G. W. Hamilton, J. E. Lee, B. G. Logan, W. S. Neef, Jr., M. A. Peterson, and M. E. Rensink, "Preliminary Design Study of the Tandem Mirror Reactor," Lawrence Livermore National Laboratory, Livermore, CA, UCRL-52302 (1977).

6. D. E. Baldwin, B. G. Logan, and T. K. Fowler, "An Improved Tandem Mirror Fusion Reactor," Lawrence Livermore National Laboratory, CA, UCID-18156 (1979).

7. G. A. Carlson, et al., "Tandem Mirror Reactor with Thermal Barriers," Lawrence Livermore National Laboratory, Livermore, CA, UCRL- 52836 (1979).

DISCUSSION

SCHLACHTER When you talked about 150-200 kV neutral beams, were those energies chosen because they are optimum for the application or were designers hedging their best because those are energies accessible by positive ions?

HAMILTON No, these are chosen because we are searching for the optimum and our design energies are varied recently between 150 kV and 400 kV. In this state of the design we are not restricting our preference to positive or negative ions. Our most practical designs are turning out to be about 200 kV.

SCHLACHTER I can see there is a convincing case for negative ions but from the talk before I heard that the cross-over in efficiency was somewhere around that energy range so that these would be accessible by positive ions. Is that correct?

HAMILTON It is accessible by positive ions but not optimum for positive ions but that is not the reason we chose the voltage. The voltage has not been chosen, we are searching for the best voltage.

GRAHAM I get a bit depressed at these things because as I understand it, for one of these reactors you are talking about, you take the output of a medium size present day power station of 500 MW and put that into the neutral beam injection, is that correct?

HAMILTON According to our current designs that is right. We are hoping we can reduce that but at the moment we can not promise anything less than that. We are talking about a reactor that is producing 3500 MW of fusion power and the net electrical output will be 1000 MW. So it is not completely out of sight. I have a report here that has more details than I have time to talk about.

NEGATIVE IONS AS A SOURCE OF LOW ENERGY NEUTRAL BEAMS+

Joel H. Fink*
Brookhaven National Laboratory
Upton, New York 11973

Abstract

Little consideration has been given to the impact of recent developments in negative ion source technology on the design of low energy neutral beam injectors. However, negative ion sources of improved operating efficiency, higher gas efficiency, and smaller beam divergence will lead to neutral deuterium injectors, operating at less than 100 keV, with better operating efficiencies and more compact layouts than can be obtained from positive ion systems.

I. Introduction

In the past it was generally acknowledged that all neutral beam injectors, operating at energies below 150 keV, would be made from positive ions. This was because positive ion beams were available that worked well at lower beam energies. At higher energies, however, their neutralization efficiencies are so poor that even with direct recovery of the energy in the unneutralized fraction of the beam they could not be made into useful beam lines.

Thus the impetus for negative ion development was to provide high energy neutral beams. Electrons can be stripped from negative ions to form neutrals at high efficiencies that are relatively independent of beam energy.

As negative ion technology improves, it becomes more attractive as a basis of low energy injector design. So much so, that if low energy beams are needed in future operating reactors, say 25 years from now, they will most likely be formed from negative ions, stripped by photodetachment.

Positive ions are preferred in today's injectors because there is no immediate need for high energy beams and large negative ion systems have yet to be demonstrated. In addition, they form beam lines which have several important advantages over our earlier concepts of negative ion performance. To be specific, it is believed that positive ion systems have:

a) Ion sources which operate more efficiently.

b) Lower ion losses.

c) Ion sources with higher gas efficiencies.

d) Good operating efficiencies at beam energies below 150 keV, particularly when used with direct energy recovery.

e) Beams of smaller divergence.

f) A larger output of neutrals from an injector of given size.

In the following, I discuss the six items listed above and show the impact of recent negative ion development upon them.

II. Ion Source Efficiency

A measure of ion source efficiency is the power required by the source per ampere of extracted ion current. Evaluated in units of input watts per output amperes, it represents a critical factor in the overall operating efficiency of a low energy neutral beam injector. Divided by the beam energy, it presents the fraction of the power in the accelerated beam which is equal to the power needed to operate the ion source. At very high beam energies, it is not very significant.

Large positive ion sources operate at about 2.5 kW per ampere. Used in a 75 keV beam line, the power going into the ion source is roughly 3.3% of the power in the accelerated ion beam. If such a source were used in conjection with a cesium vapor cell to form negative ions, approximately 20% of the positives would be converted to negative ions and the combination of positive ion source with Cs cell would operate as a negative ion source with an efficiency of 12.5 kW per ampere of negative ions. The power required to operate this source would be about 16.5% of the power in a 75 keV negative ion beam derived from it. At 200 keV, the source would require only 6.3% of the power in the ion beam.

Three years ago, at the previous Brookhaven conference on negative ions, data was presented on the performance of several different types of negative ion sources under investigation at that time.[1] These included a hollow discharge duoplasmatron, as well as several Penning and magnetron sources. The source performance ranged from 18 to 263 kW per ampere, corresponding to 24 to 350% of the energy in a 75 keV beam.

Today, negative ion sources have been reported[2] to work at 5 kW/A, with better performance anticipated in the future. In a 75 keV beam, 5 kW/A represents 6.7% of the beam energy. Whereas three years ago, low energy neutral beams based upon negative ions were out of the question, they now present a viable alternative.

---

*On assignment from Westinghouse Electric Corporation, Pittsburgh, Pennsylvania.

+Worked on under the auspices of the U.S. Dept. of Energy.

III. Ion Losses

During the initial stages of beam formation, some ions become neutralized prematurely, either by charge exchange of positive ions with the background gas, or by electron stripping of negative ions upon impact with the background gas. In either case this constitutes a loss of ions to the beam, provided the newly formed neutrals have not achieved their ultimate energy or assumed their final trajectories.

The loss of negative ions will always be greater than the loss of positive ions to beams of the same energy passing through a background gas of the same density. But as can be seen by the ratio of the two cross-sections, σ_{-10}/σ_{10}, shown as a function of beam energy in Fig. 1, the comparative loss of negative to positive ions is not as serious at low energies as it is at high.

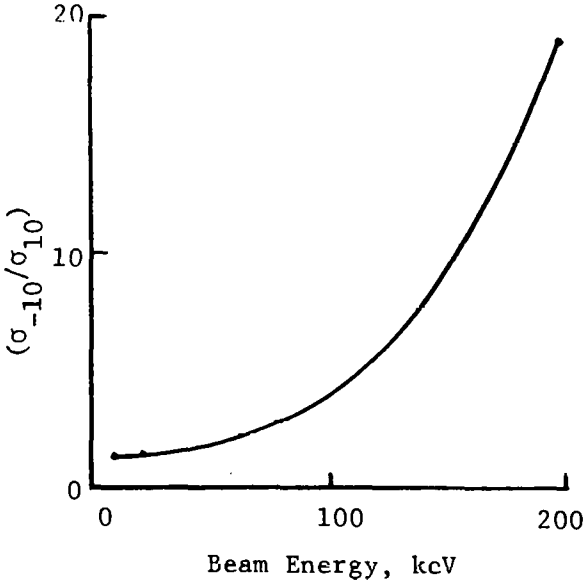

Fig. 1: Ratio of negative ion stripping cross-section, σ_{-10} to the positive ion charge-exchange cross-section, σ_{10}.

To minimize the loss, it is conceivable that the background gas density could be reduced, but only so far. Positive ion beams depend upon electrons, generated by impact ionization of the background gas to provide space-charge neutralization and prevent space-charge blow up. Similarly negative ion beams depend upon positive ions, generated by impact ionization, to provide space-charge neutralization. Because electrons are so much more mobile than ions, the background gas density required to space-charge neutralize a positive ion beam is almost an order of magnitude greater than that required for a negative ion beam. As a consequence, negative ion beams with energies up to 160 keV (where $(\sigma_{-10}/\sigma_{10})$ becomes equal to 10) could theoretically be made to operate with less losses than positive ions - provided the background density can be suitably controlled. Indeed, pumping in the vicinity of the ion sources is critical for satisfactory negative ion beam line performance. This is discussed in the next section on gas efficiency.

Positive ion sources, as used in today's neutral beam injectors, operate at a disadvantage with respect to ion losses. Because the neutral gas flowing out of the source is used to feed the neutralizer cell, the background gas density is considerably higher in the vicinity of the accel grids than is desirable or need be. Redesign of the gas neutralizer cell could make a significant improvement.

In the following section a positive ion beam line is considered in which a deflection magnet is used to separate the D_2^+ and D_3^+ ion components from the desired D^+ ion beam. The neutralization of full energy D^+ ions in the vicinity of the magnet, before they achieved their final trajectory, constitutes a serious loss to the operating efficiency, particularly at low beam energies where σ_{10} is large. Obviously, this is not a good practice. To provide a comparison, another beam line is considered which uses no deflection magnet. The improvement is impressive.

IV. Gas Efficiency

Gas efficiency is another ion source parameter which has improved significantly over the past three years. At the 1977 conference, direct extraction sources were discussed[1] that operated at 1-2% gas efficiency. Recently a magnetron source was described[3] which works at over 6%, while in Russia efficiencies of 10-20% have been reported.[4]

As used in this discussion, gas efficiency is defined as the ratio of ion flow out of the source, in atoms per second, to the flow of room temperature gas into the source, in the same units. It is an important factor in neutral beam injector design because it establishes the quantity of gas which must be pumped away from the vicinity of the source. This can be evaluated from the flow of room temperature gas, Q_B equivalent to that going into the extracted ion beam. The total flow of gas into a source of efficiency, ζ_G is:

$$Q_{iN} = Q_B/\zeta_G, \qquad (1)$$

while the gas which must be pumped away is:

$$Q_P = Q_{iN} - Q_B \qquad (2)$$

and

$$Q_P = (1/\zeta_G - 1)\, Q_B \qquad (3)$$

The gas flow equivalent to a positive ion beam of predominantly atomic D^+ ions extracted at a current density, J_E^+ through a grid of area, A_G and transparency T_G^+ is:

$$Q_B^+ = .1\, J_E^+\, T_G^+\, A_G \quad T\ell s^{-1} \qquad (4)$$

while the gas flow equivalent to a negative ion beam of atomic D^- ions is:

$$Q_B^- = .1\ J_E^-\ T_G^-\ A_G \qquad T\ell s^{-1} \qquad (5)$$

Thus the quantity of gas (evaluated at room temperature) per unit area which must be pumped away from a positive ion source becomes:

$$Q_P^+/A_G = .1\ (1/\zeta_G^+ - 1)\ J_E^+\ T_G^+ \qquad T\ell s^-CM^{-2} \qquad (6)$$

and the corresponding value for a negative ion source is

$$Q_P^-/A_G = .1\ (1/\zeta_G^- - 1)\ J_E^-\ T_G^- \qquad T\ell s^{-1}CM^{-2} \qquad (7)$$

According to the above, a positive ion source, operating at a gas efficiency of 30%, delivering D^+ ions at a current density of $.25ACM^{-2}$, via grids of 40% transparency requires pumps which can remove .023 $T\ell s^{-1}$ of gas per CM^2 of emitting area. A negative ion source, meanwhile operating at a 10% gas efficiency, delivering D^- ions at a current density of $.5ACM^{-2}$ with extraction grids of 10 transparency entails .045 $T\ell s^{-1}$ of gas per CM^2 of source. Thus the pumping load of today's negative ion sources is about twice that of positive ion sources.

A key problem in the vicinity of the ion sources is to remove the gas in such a way that minimizes the ion losses. For the highest pumping speed over the shortest length along the beam line, higher background pressures are required. For the lowest ion losses, a short beam path through lower pressures is preferred. When consideration is given to the way the gas streams out of the ion sources, it is no surprise that after the ion source, the extraction region is the most difficult section of a neutral beam line to design. In the following analysis of a negative ion beam line, it is assumed that over 20% of the extracted ions become lost to the beam in this region.

V. Injector Operating Efficiency

By definition, the operating efficiency of a neutral beam injector is the ratio of the neutral beam power output to the total power input. This is equal to the reciprocal of the sum of the power needed to operate each beam line component per watt of neutral beam output. Thus:

$$\rho = \left[\sum_i (P_i/P_o) \right]^{-1} \qquad (8)$$

In the following, to simplify the analysis, the power required for pumping, refrigeration, and other services are neglected. Hence:

$$\sum_i (P_i/P_o) = P_s/P_o + P_A/P_o + P_p/P_o + (-P_R/P_o) \qquad (9)$$

where P_s/P_o is the power need per output neutral watt of the ion source; P_A/P_o the power need of the ion extractor and accelerator, P_p/P_o the power need of the photo detachment cell and P_R/P_o is the power recovery obtained by dirct conversion of the energy in the unneutralized fraction of the high energy beam.

Three injectors are considered. The first, as shown in Fig. 2 uses an ion source that delivers an ion current density, $J_E = .25\ A/cm^2$ to an accel grid of transparency, $T_G + .4$. The atomic component of the ion beam is $n_1 = 90\%$.

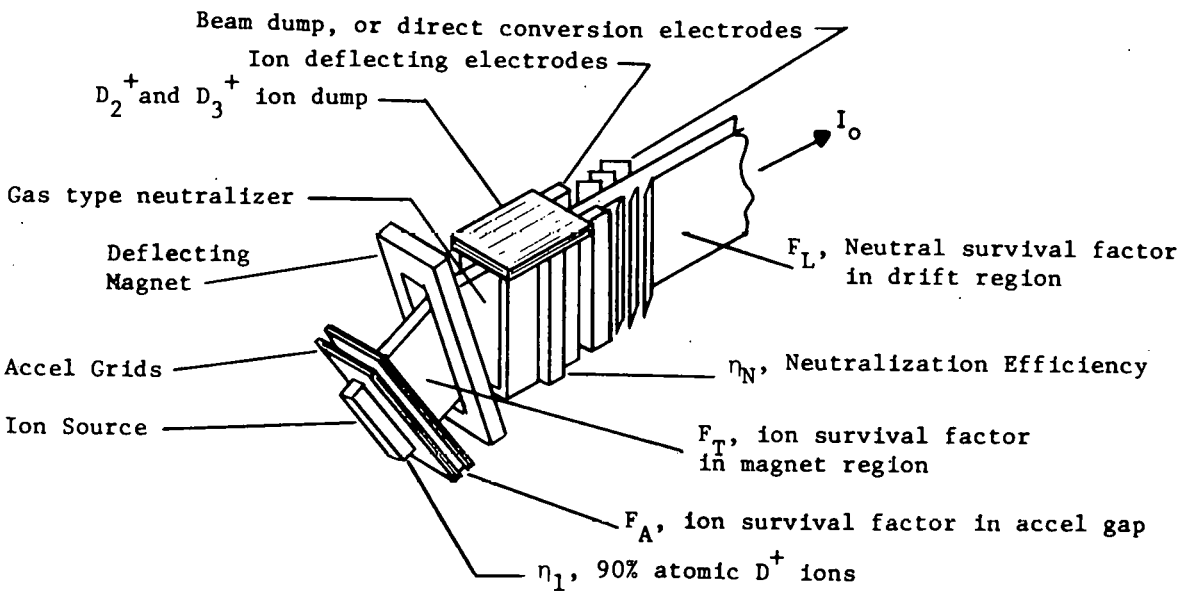

Fig. 2: Neutral beam line based upon positive ions with a deflecting magnet to remove the D_2^+ and D_3^+ molecular ions.

The D_2^+ and D_3^+ components are subsequently removed by a deflecting magnet, which permits a pure D^+ beam to enter the neutralized cell. After neutralization, those ions that remain with the beam are removed by electrostatic deflection, to be collected on a water-cooled beam dump or on biased electrodes for direct energy conversion.

The fraction of extracted ions which make it through the accel grids without suffering charge exchange is:

$$F_A = \left[1 - \int n_A \, \sigma_{10} \, dZ\right] , \qquad (10)$$

While the fraction of atomic ions that remain with the beam after passage through the deflecting magnet is:

$$F_T = \left[1 - n_T \, \sigma_{10} \, Z_T\right] \qquad (11)$$

and, the fraction of high energy neutrals which are not ionized while in transit from the neutralizer cell to the reactor is:

$$F_L = \left[1 - \sigma_{01} \int n_L \, dZ\right] . \qquad (12)$$

These factors are given in Table 1 as evalutated in Reference 5.

TABLE 1

Positive Ion Source with Deflecting Magnet Removing Molecular Ions, Fig. 2

V_o	50 kV	75 kV	100 kV	150 kV	200 kV	Reference
η_L	.90	.90	.90	.90	.90	Assumption
F_A	.94	.93	.92	.91	.91	Ref. 6
F_T	.53	.73	.83	.94	.98	Ref. 6
η_N	.74	.62	.48	.29	.21	Ref. 6
F_L	.95	.95	.95	.95	.95	Ref. 6
η_R	0	0	0	0	0	Assumption
ζ without recovery	.30	.34	.30	.20	.15	Eq. 18
η_R	.75	.75	.75	.75	.75	Assumption
ζ without recovery	.33	.41	.41	.34	.29	Eq. 18

Assumptions:
K_s = 2.5 kW/A: ion source efficiency
ζ_s = 90%, ion source power supply efficiency
ζ_A = 95%, accel power supply efficiency

Using an ion source whose efficiency is K_s = 2.5 kW per ampere, and an ion source power supply with an efficiency, ζ_s = 90%, the power need of the source is:

$$P_s/P_o = \frac{K_s}{\zeta_s V_o} \left(I_E/I_O\right) \qquad (13)$$

in which the ratio of extracted ion current to output neutral current is:

$$I_E/I_O = \left(\eta_1 \, F_A \, F_T \, \eta_N \, F_L\right)^{-1} , \qquad (14)$$

and the neutralization efficiency, η_N equals 95% of the maximum value, i.e.:

$$\eta_N = .95 \left(\frac{\sigma_{10}}{\sigma_{10} + \sigma_{01}}\right) \qquad (15)$$

In the above, σ_{10} and σ_{01} are the neutralizing and ionizing cross-sections of D^+ in D_2 at the beam energy, V_o.

With an accel power supply efficiency, ζ_A = 95%, the power need of acceleration is:

$$P_A/P_O = \frac{1}{\zeta_A} \left(I_E/I_O\right) \qquad (16)$$

With a direct conversion efficiency of η_R = 75%, the energy recovery term is:

$$P_R/P_O = \eta_R \left(\frac{1 - \eta_N}{\eta_N}\right) . \qquad (17)$$

Combining Equations 13 thru 17, the injector efficiency is found to be:

$$\zeta = \frac{\eta_1 \, F_A \, F_T \, \eta_N \, F_L}{K_s/(\zeta_s V_o) + \left[1 - (1-\eta_N) \, \eta_R \, \eta_1 \, F_A \, F_T\right]/\zeta_A} \qquad (18)$$

Values of the various factors are listed as functions of beam energy in Table I.

The second injector shown in Fig. 3 uses the same positive ion source with no deflecting magnet. Thus, $F_T = 1$. Other than that, the efficiency is as given in Equation 18.

$$\zeta = \frac{\eta_1 F_A \eta_N F_L}{K_s/(\zeta_s V_o) + \left[1-(1-\eta_N)\eta_R \eta_1 F_A\right]/\zeta_A} \qquad (19)$$

These values are listed in Table 2.

The third beam line per Fig. 4 uses negative ions, stripped in a photo detachment cell, to form the neutral beam. The negative ions are extracted from the source at some voltage, V_E, to be separated from whatever electrons that may have also been drawn out of the source, and to be transported to the high voltage grid system by sector magnets. After acceleration, the negative ion beam is stripped of electrons in the photo detachment cell. Subsequently, those ions remaining with the neutral beam are electrostatically deflected out of the beam, to be collected on water-cooled beam dumps.

The fraction of the negative ions that are not stripped during extraction is:

$$F_E = \left[1 - \int \eta_E \sigma_{-10}\, dZ\right], \qquad (20)$$

while the fraction that survives transport through the sector magnets is:

$$F_T = \left[1 - \eta_T \sigma_{-10} Z_T\right], \qquad (21)$$

and the surviving fraction that get past the accelerator is:

$$F_A = \left[1 - \int \eta_A \sigma_{-10}\, d\right]. \qquad (22)$$

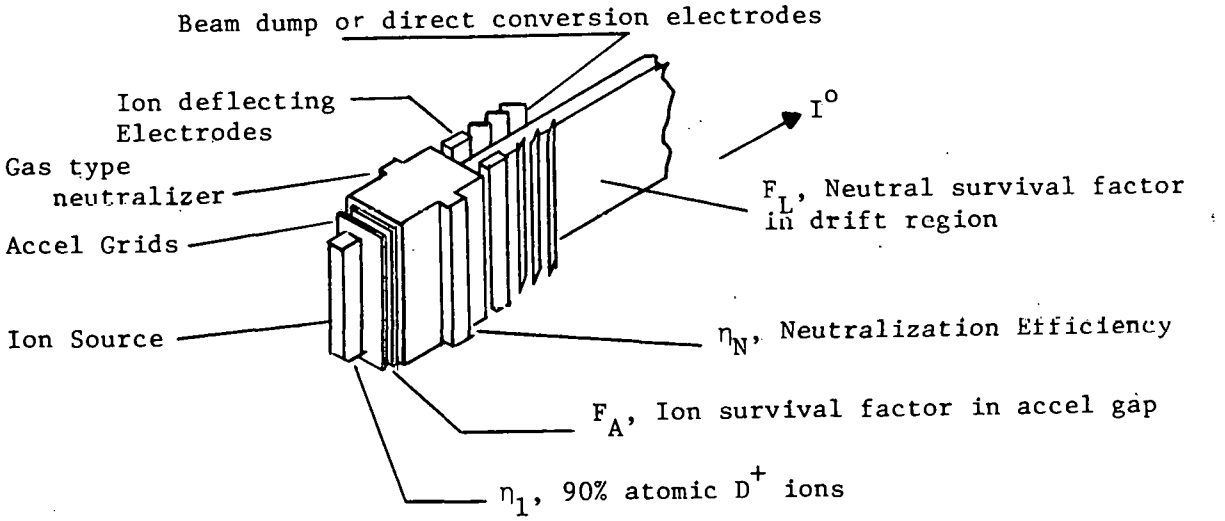

Fig. 3: Neutral beam line based upon positive ions.

TABLE 2

Positive Ion Source, Fig. 3

V_0	50 kV	75 kV	100 kV	150 kV	200 kV	Reference
η_1	.90	.90	.90	.90	.90	Assumption
F_A	.94	.93	.92	.91	.91	Ref. 6
η_N	.74	.62	.48	.29	.21	Ref. 6
F_L	.95	.95	.95	.95	.95	Ref. 6
η_R	0	0	0	0	0	Assumption
ζ without recovery	.56	.47	.36	.21	.16	Eq. 19
η_R	.75	.75	.75	.75	.75	Assumption
ζ without recovery	.68	.62	.53	.38	.30	Eq. 19

Assumptions:
K_s = 2.5 kW/A ion source efficiency
ζ_s = 90%, ion source power supply efficiency
ζ_A = 95%, accel power supply efficiency

Finally, the fraction of neutrals that make it to the reactor is F_L, as in Equation 12.

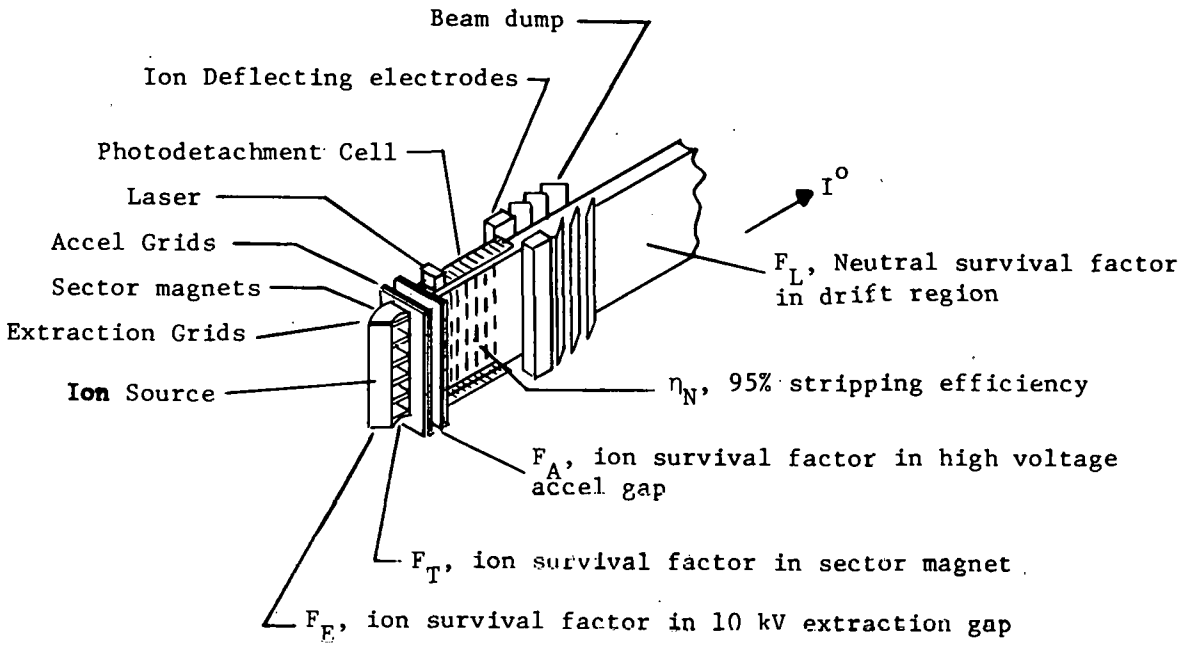

Fig. 4: Neutral beam line based upon negative ions, stripped by photo detachment.

TABLE 3

Negative Ion Source with Photo Detachment, Fig. 4

V_0	50 kV	75 kV	100 kV	150 kV	200 kV	Reference
F_E	.93	.93	.93	.93	.93	Ref. 6
F_T	.77	.77	.77	.77	.77	Ref. 6
F_A	.99	.99	.99	.98	.98	Ref. 6
η_N	.95	.95	.95	.95	.95	Assumption
F_L	.95	.95	.95	.95	.95	Ref. 6
P_p/P_o	.49	.40	.35	.28	.24	Eq. 25
ζ	.48	54	.58	.62	.63	Eq. 26

Assumptions:
K_s = 5 kW/A: ion source efficiency
ζ_s = 90%, ion source power supply efficiency
$\zeta_A \zeta_E$ = 95%, extractor and accel power supply efficiency
V_E = 10 kV, extraction voltage
α = .5, ratio extracted electron to negative ion current.

The power need of the source is as shown in Equation 13. For the negative ion source let K_S = 5 KW/A and:

$$I_E/I_O = \left(F_E\, F_T\, F_A\, \eta_N\, F_L\right)^{-1} \qquad (23)$$

Using photo detachment let the stripping efficiency, η_N = 95%.

The power need of extraction and acceleration is:

$$P_A/P_O = \frac{1}{\zeta_A V_O}\left[V_E\left(1+\alpha\right) + \left(V_O - V_E\right) F_E F_T\right], \qquad (24)$$

in which the efficiency of the extraction power supply is taken to be the same as that of the high voltage power supply, i.e. ζ_A = .95.

In the above the current of electrons that is extracted along with the negative ions is equal to a fraction, α of the extracted ion current, I_E. In the following α is taken to be .5.

Finally, the power need of the photo detachment cell[6,7] is:

$$P_p/P_O = \frac{6.5 \times 10^3 (1-R)}{J_A\, T_G\, S\, V_O^{\frac{1}{2}}\, \eta_N\, \zeta_L}\, \ell_n \left[\frac{1}{1-\eta_N}\right] \qquad (25)$$

In the above, the laser which excites the photo detachment cell is assumed to work at an efficiency, ζ_L = 1.5%, the mirrors along the edges of the cell have a reflectivity, R = 99.9%, and the separation between mirrors is S = 250 cm. The negative ion current density entering the cell is J_A = 0.1 A/cm^2, through a grid of transparency, T_G = 50%.

The injector efficiency is:

$$\epsilon = \frac{F_E F_T F_A \eta_N F_L}{K_S/(\zeta_S V_O) + 1/(\zeta_A V_O)\left[V_E(1+\alpha) + (V_O - V_E) F_E F_T\right] + (P_p/P_O) F_E F_T F_A \eta_N F_L} \qquad (26)$$

The results are shown in Table 3 and plotted in Fig. 5.

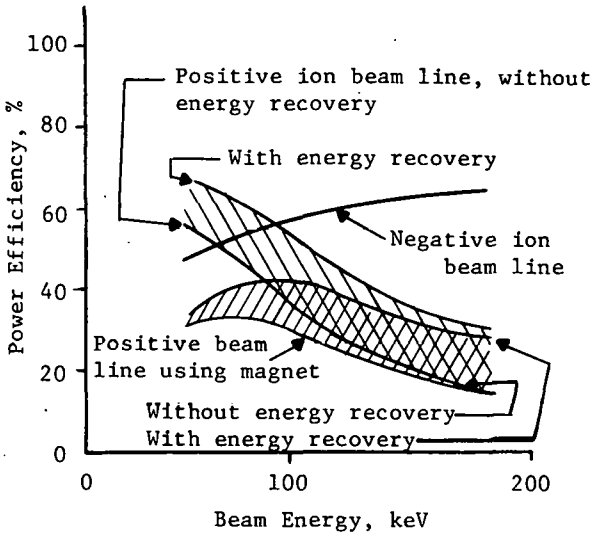

Fig. 5: Beamline power efficiencies.

VI. Beam Divergence

The ions originate from a slotted grid structure, which is curved to form a focus at point 0 in the focal plane, as shown in Fig. 6.

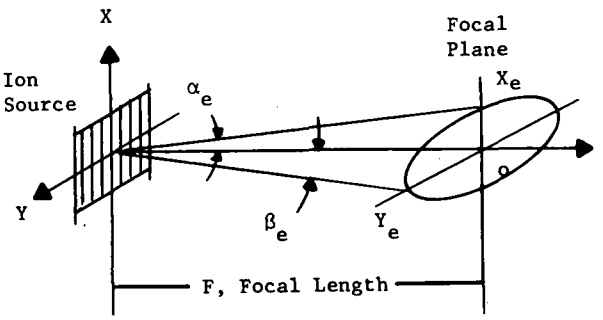

Fig. 6: Beam optics.

In the focal plane the beam is assumed to have a gaussian current distribution over all radii. Thus, if X_e is the radius in the focal plane, parallel to the grid slots, that corresponds to a beam current density which is 1/e times the peak axial value at point 0, and Y_e is the corresponding radius, normal to the grid slots, the focus of points at which the current density is 1/e times the peak value is:

$$(X/X_e)^2 + (Y/Y_e)^2 = 1, \qquad (27)$$

and the beam current density throughout the focal plane is:

$$J = \hat{J}_0 \exp \left\{ \left(X/X_e\right)^2 + \left(Y/Y_e\right)^2 \right\} \qquad (28)$$

The peak current density, $\hat{J}_0$ is found by integrating the above over the entire focal plane, thus:

$$\hat{J}_0 = \frac{I_0}{\pi_F^2 \alpha_e \beta_e} \qquad A\ cm^{-2} \qquad (29)$$

in which F is the focal length, and the beam angles are

$$\alpha_e = X_e/F \qquad (30)$$

$$\beta_e = Y_e/F \qquad (31)$$

Data from the analysis of neutral beams formed from positive ions extracted via slotted grids show the beam angles to be relatively constant over an energy range from 20 to 120 keV. α_e and β_e are approximately .5° and 1.5°, respectively.

Theoretically, these angles should be a function of the ion temperature in the source, and they should vary inversely with the square root of the beam energy. That the angles do not behave this way, is indicative of some other factor, (such as the grid design or the interaction of the beam with the background plasma in the neutralizer) taking a dominant role in control of the beam divergence. Unfortunately, we do not know what causes the descrepancy, and we have no comparative data for negative ion beam lines.

Early measurements of the emittances of negative ion beams indicated that they were considerably larger than those of positive ion beams. More recent measurements however, indicate that they are not much more than two times larger.[3] Obviously, considerable work must be done in this field, not only to improve the emittance of negative ion beams, but to understand the process and to improve the positive ion beam angles, as well.

There is no basic reason why the emittance of a neutral beam formed from negative ions should be worse than one originating as a positive ion beam, in fact negative ions might form more favorable neutral beams, because the beam-plasma interaction in a photodetachment cell

should be considerably less than that in a gas neutralizer.

VII. Beam Packaging

A well-designed neutral beam injector will provide a maximum neutral current from the smallest possible assembly. To form a compact, high current unit, the component beam lines must be mounted closely together. But the packaging is limited by the need to keep each beam line electrically isolated from its neighbors. In the event of a beam line failure, the voltage in each beamline may have to be turned off and allowance made to permit the remaining beam lines to continue operation.

Geometric considerations make it desirable to operate the ion sources at high voltage. This makes the water and electrical connections more complicated as they must be designed for remote operation. However it eliminates the extra space needed between beamlines to insulate the adjacent neutralizer cells, which are at high voltage, if the ion sources are at ground.

In this study, the ion sources are assumed to be at high voltage, mounted in grounded enclosures as shown in Fig. 7, with the neutralizer at ground.

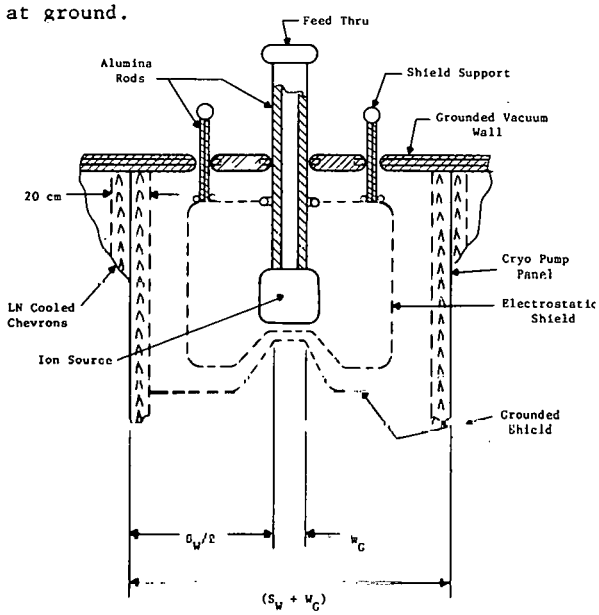

Fig. 7: Ion source housing.

A configuration of stacked ion sources is shown in Fig. 8. W_G and H_G represent the active width and height of each grid, while S_W and S_H are the corresponding grid to grid spacings. From the figure it can be seen that the neutral current output per unit area of stacked ion sources is:

$$J^o_{AV} = \frac{J_E \, T_G \, W_G \, H_G \, (I_O/I_E)}{(W_G + S_W)\,(H_G + S_H)} \qquad (32)$$

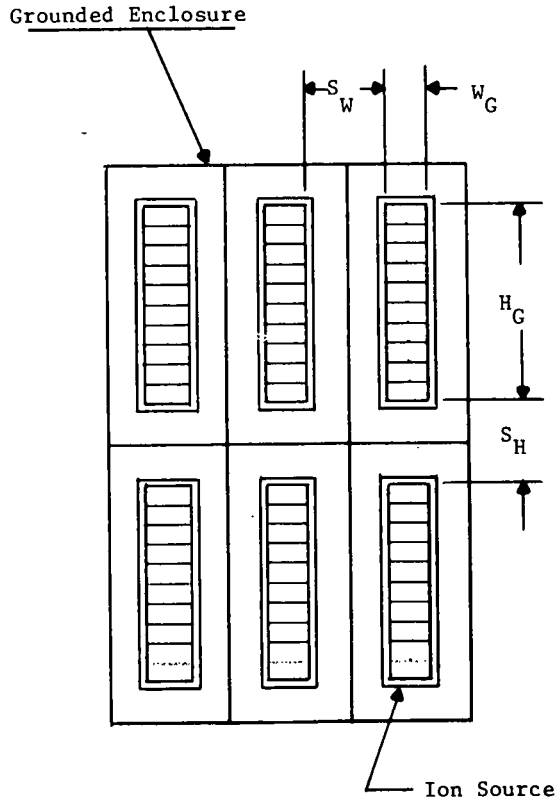

Fig. 8: Stacked ion sources.

Obviously, the most advantageous packaging results from the ion source with the largest emitting area. But the ion source dimensions are restricted by practical considerations. With a slotted grid, the grid width is limited by the ability of each grid rail to remove heat. Consistent with positive ion source design, it is assumed that the grid width, W_G is 12 cm.

The maximum tolerable source length, assuming the grids are built up out of smaller sections, depends upon what can be handled remotely, provided the energy stored in the high voltage electrodes is not excessive. I assume that a source 250 cm in length will be acceptable.

Calculated estimates[5] of the energy stored in the shield and grid structure of sources delivering current densities equal to .25 and .1 A cm^{-2} are plotted in Fig. 9. They appear to be acceptable.

The spacing between sources is determined either by consideration of pumping, high voltage insulation or beam line geometry. The gas load is assumed to be taken care of by placing cryopumps along the grounded walls of the source enclosure. With 4 cm on each side of the grid to the edge of the ion source, 20 cm for the double sided cryopanel shown in Fig. 7, the minimum allowable grid to grid spacing, as determined by voltage insulation is:

$$S_E = (28 + 2\ Vo/E_F) \qquad (33)$$

in which the average field between electrodes, E_F = 20 kV/cm.

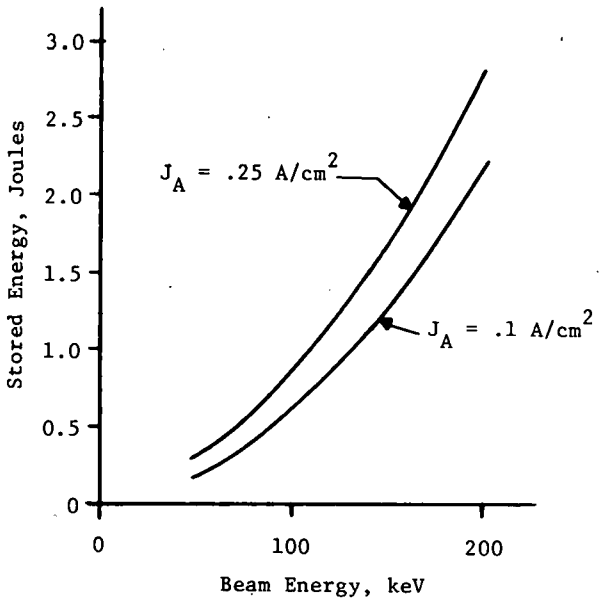

Fig. 9: Estimates of energy stored between grids and shields.

The geometric constraints of spacing are shown in Fig. 10. With a focal length, F and a clearance length, L_W between beam lines, the spacing between sources in a direction parallel to the grid slots is:

$$S_W = \left(\frac{5FL_W}{F-L_W}\right) \alpha_e \ , \qquad (34)$$

while the spacing in the direction perpendicular to the slots is:

$$S_H = \left(\frac{5FL_H}{F-L_H}\right) \beta_e \ . \qquad (35)$$

Values of spacings, S_E, S_W, and S_H are shown plotted in Fig. 11 for F = 1000 cm, L_W = 400 cm and L_H = 200 cm; for α_e and β_e equal to .5 and 1.5° over the full range of energy, and for the theoretical case where they vary inversely with the square root of the beam energy. It is evident that the separation between grids must satisfy, S_E per Equation 33 in all cases.

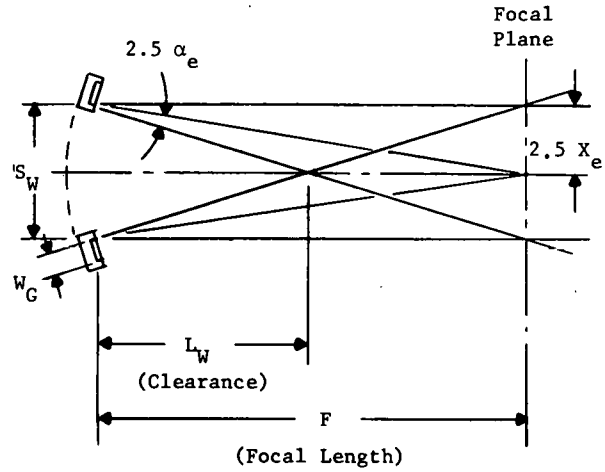

Fig. 10: Beam line geometry.

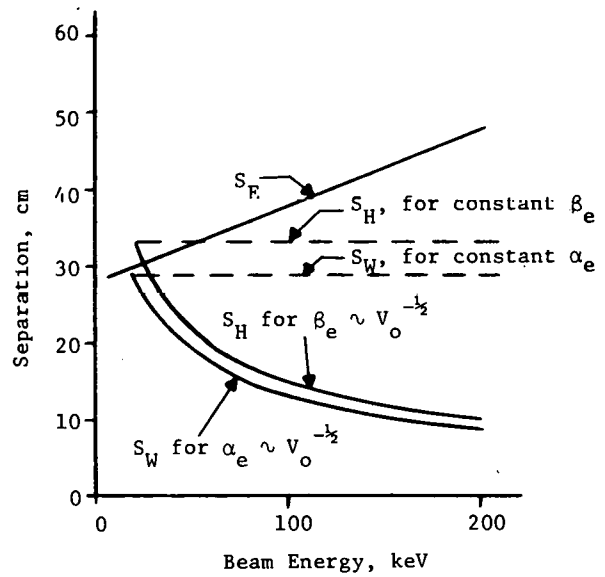

Fig. 11: Separation between grids.

Values of the neutral current output unit area of stacked ion sources are shown in Fig. 12. For the positive ion sources, J_A = .25 A/cm^2 and T_G = .4, while for the negative ion source, J_A = .1 A/cm^2 and T_G = .5. The ratio I_O/I_E was taken from Equations 14 and 23.

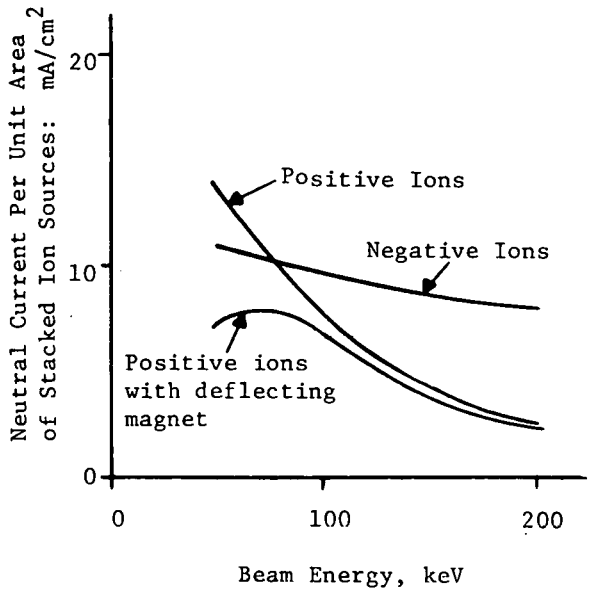

Fig. 12: Neutral current per unit area of stacked ion sources

VIII. Conclusion

The direct extraction sources of negative ions[8] have started a trend of development that will lead to neutral beam injectors of higher efficiency and smaller size than was previously envisioned. In regards to the six advantages that positive ions had over low energy negative systems, it now appears that:

a) The efficiency of negative ion sources has improved to the point where they can be effectively used in low energy beam lines.

b) With good pumping designs, negative ion losses need not be worse than the positive ion losses in today's systems.

c) Negative ion sources can now be designed with gas efficiencies that are as much as one-third to one half that of positive ions.

d) Taking advantage of the anticipated development of photo detachment, negative ion systems will have better operating efficiencies than those of positive ions - over a broad range of beam energies.

e) Neutral beams formed from negative ions will have divergences that at least will be of the same order of magnetude of those obtained from positive ions.

f) The output of neutrals from an injector based upon negative ions will be competative with one of equal size based upon positive ions over a broad range of beam energies.

References

1. K. Prelec, "Development of H^- Sources at Brookhaven National Laboratory," Proc. of the Sym. on the Production and Neutralization of Negative Hydrogen Ions and Beams, Page III, Brookhaven National Laboratory, Sept. 26-30, 1977.

2. Yu. I. Bel'chenko, V.G. Dudnikov, "Negative Ion Production in Surface Plasma Sources with Unclosed Electron Drift Discharges," Journal De Physique, p. C7-501, July 1979.

3. J.G. Alessi, Th. Sluyters, "Regular and A Symmetric Netative Ion Magnetron Sources with Grooved Cathodes," Brookhaven National Laboratory Report, BNL 27942-1980, Submitted to Review of Scientific Instruments.

4. K. Prelec, "Efficiency of H^- Sources with Cathode Grooves", Brookhaven National Laboratory, AGS Division H^- Technical Note 52, February, 1980.

5. J.H. Fink, "Neutral Beam Injectors for 1990 and 2005, Lawrence Livermore Laboratory Report, 1980.

6. J.H. Fink, G.W. Hamilton, "Another Look at Photo Detachment of Negative Deuterium Ions in Neutral Beam Injectors", Lawrence Livermore Laboratory Report, 1980.

7. M. McGeoch, Avco Everett Research Laboratory, private communication, 1980.

8. Yu. I. Bel'chenko, G.I. Dimov, V.G. Dudnikov, "Physical Principles of the Surface Plasma Method for Producing Beams of Negative Ions", Proc. of the Sym. on the Production and Neutralization of Negative Hydrogen Ions and Beams, p. 79, Brookhaven National Laboratory. Sept. 26-30, 1977.

DISCUSSION

McGEOCH What was the laser efficiency you assumed in your comparison of positive and negative ion based neutral beam systems with photodetachment?

FINK The photodetachment I assumed was 95% and the positive ion efficiency came from the neutralization data relative to the energy.

McGEOCH No, I asked the laser efficiency.

FINK I used 1½% efficient lasers in the calculation, I assumed 99.9% reflectivity and I defined it as 2½ meters high by 12 cm. The significance of using photodetachment is that it made the efficiency so good at low energy. The fact

is that you have to save enough energy or power in order to be able to power the optical system. If you do not make a net savings you do not have an efficient system. Where the savings come from is the difference between the neutralization and the amount of power you put inside the cell. Since very little loss of light goes into interaction with the beam, the bigger you make the optical system the bigger the savings. So a measure of the effectiveness of the photodetachment is the number of amperes needed to make it break even. So the number of amperes is the vital factor.

GELLER I just want to make a comment. It is remarkable that whatever the scenario is, you always come back to a current density of 10-20 mA/cm^2 and to stacking of sources. It is good for you, it is good for the Tokamaks, so I think we are near the reality.

FINK May I comment on that. Again I am wearing my Brookhaven hat. One of the things which you can not measure, to some extent, is what establishes that limit. When you go down, can you do more and get a higher current density? Look at the Brookhaven source, for instance, where the density of ½ A/cm^2 is coming out of the ion source. I guess a reasonable man would sweat a little and say: is that going to be a CW condition? On the other hand if the ½ A is reasonable then going from the ½ A down to 20 or 25 mA/cm^2 is a question of how you handle the beam from there on. And, this is a skill that I do not think you or I really have concentrated on enough to know whether 25 is a limit due to fear or a limit due to judgement. If you look at the other sources it is an interaction of the density in the way they operate the source. That is also slightly negotiable. I do not know whether it is a fundamental limit or merely a limit that we are assuming now. Is that a fair statement.

GELLER I agree with you, but for instance when we say we can only have 3 kW/cm^2 at the port of the Tokamak, we know what we are talking about. But you for instance, why do you have the same kind of energy per cm^2?

HAMILTON When I said 5 mA/cm^2 that number is determined by what we think that the development laboratories can do. We do not want to ask for more. In the future, I am asking for more, for 50 mA/cm^2 but not immediately.

MOBLEY This is a comment to your remark about why you end up in the same region. I think, as an accelerator physicist who had several years of exposure to the plasma community at Berkeley, I think we come back to the same place because there are assumptions made within this group that do not vary very widely about how you would proceed. You use the word beam optics for the quality of an ion source. For high energy physics, Livingston, Courant and Schneider-beam-optics are quite different. I consider the other ion source beam lines have no optics at all. The optics is in back of the extractor grid and you let it go from there. If you further assume that 200 kV or 150 kV is the operating energy then you can speak of mA/cm^2. John Dawson suggests acceleration of neon and heats plasma with neon. When you really want to talk about power per cm^2 you use 10 MeV neon. So you can change these parameters with one assumption about the system and if the accelerator is different a lot of those assumptions could change.

FINK If I can dream you can dream.

A D⁻ ION ACCELERATOR IMMERSED IN A MAGNETIC FIELD

[::] J.L. Foucher, R. Geller, C. Jacquot, J.C. Rocco, P. Sermet
[::::] J.B. Bergström, H.G. Gustavson, Hellblöm, R. Pauli
[::] Association EURATOM-CEA

Département de Recherche sur la Fusion Contrôlée
Service IGn - Centre d'Etudes Nucléaires
85 X - 38041 GRENOBLE CEDEX (France)

[::::] Association EURATOM-NE (SWEDEN)

Studsvik-Energi Teknik AB, S-100
Nykoping (Sweden)

Abstract

An analysis of the physical condition of a D^- accelerator immersed in a high magnetic field is being considered. At the entrance the D^- current density is 10-15 mA/cm^2 and the final energy is 300 keV. A compressed beam could be achieved and consequently a final current density of 20-50 mA/cm^2 is obtained.
An electrostatic reflector for electrons with a high transparency is defined. A maximum of 10^{11} e/cm^3 electron density can be reflected. The steady state electric field in the accelerator is of the order of 22 kV/cm.

Introduction

In the previous paper [1] we obtained a D^- ion source using the double charge exchange of D^+ ions on a supersonic cesium jet. The main parameters in d.c. operation were an average current density of 10-12 mA/cm^2 at 1 keV kinetic energy. The background pressure was roughly 10^{-5} Torr, and the cesium plasma density was of the order of 10^{11} e/cm^3.

The parasite cesium flux was lower than 10^{14} at/cm^2/s and a steady state electric field in the positive ion source of 30-40 kV/cm was maintained (without breakdowns). For a better transportation of charged particles (D^+, D^-) at low energies, a more or less uniform magnetic field is applied so that the beams are totally immersed in the solenoidal field.

With this type of D^- source, one has to design a system which accelerates a current of 50-75 mA (average current density 10-15 mA/cm^2) at full energy (300 keV) in steady state operation.

In the D^- acceleration it is absolutely necessary to avoid the acceleration of the plasma electrons. One has to obtain the best beam quality in order to solve the critical problems of D_0 transportation in the torus.

The extrapolation of such an accelerator is made by using a slit geometry, and the reasons behind these are :
- an extrapolation of the D^+ source based on the principle of the electron cyclotron resonance and the supersonic cesium jet is more practical in constructing a slit.
- a large perveance with a low electric field and the minimum divergence angle is more easily obtained.
- finally the problems associated with the neutralizer could not be so critical.

A schematic view of a neutral injector based on the acceleration of 3A D^- ions is shown in fig. 1.

Preliminary considerations of the D^- accelerator

Supposing one can find an electrostatic configuration of a magnetized accelerator with a minimum of aberrations, the final beam qualities are totally determined by the initial qualities of the low energy D^- beam, if these two conditions are fullfilled :

1) Minimum final azimutal velocity

The D^- ion source is immersed in a high magnetic field (0.4 T). Because the space charge effects of the D^- beam is practically cancelled, the low energy D^- trajectories are more or less "frozen" along the magnetic field lines.

The ripples around these magnetic field lines are of the order of the larmor radius :

$$\langle \rho_l \rangle = \frac{m\langle v_\perp \rangle}{eB} \simeq \frac{r_b}{10} \qquad \text{where}$$

$\langle v_\perp \rangle$ is the average perpendicular velocity of the D^-
m is the D^- mass
e is the electronic charge
B is the magnitude of the magnetic field
r_b is the outer beam radius.

Consequently the D^- accelerator should be immersed in the magnetic field. If the magnetic field is cancelled before the conversion of D^- into D_0, the D^- beam will be rotating with an azimutal velocity θ_f determined by the Busch's relationship, and it will contribute an increase in the final transverse velocity

$$\dot{\theta}_f = \frac{1}{2\pi r_f^2} \frac{e}{m} \left[\psi_f - \psi_i\right] + \left(\frac{r_i}{r_f}\right)^2 \dot{\theta}_i$$

where r_i, r_f are the initial and the final radius of the outer particles, ψ_i and ψ_f are the magnetic flux at the entrance and the exit of the accelera-

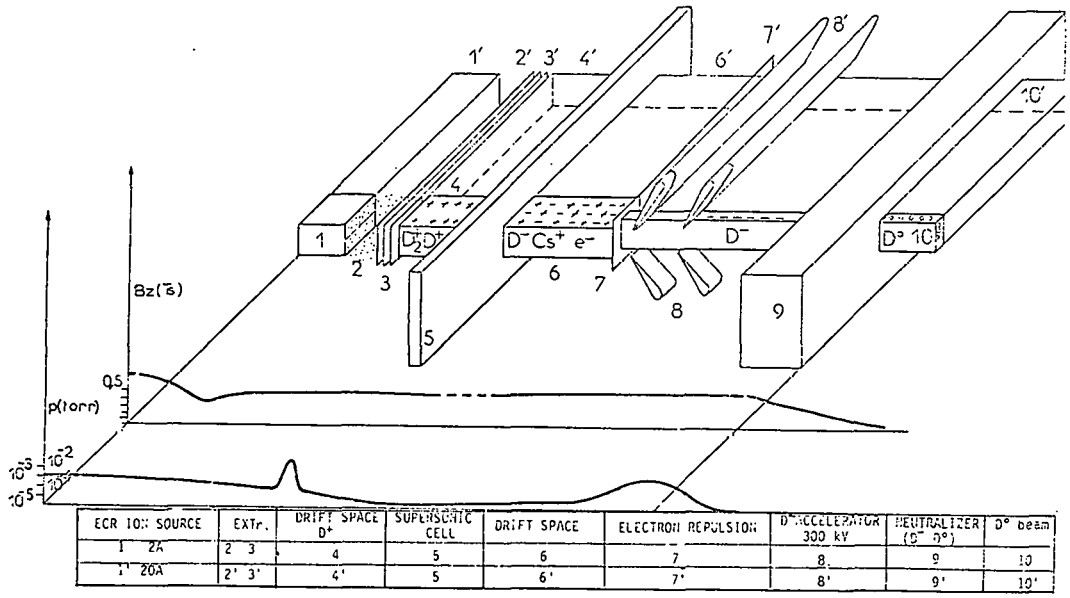

ECR ION SOURCE	EXTr.	DRIFT SPACE D^+	SUPERSONIC CELL	DRIFT SPACE	ELECTRON REPULSION	D^- ACCELERATOR 300 kV	NEUTRALIZER (D^- D^0)	D^0 beam
1 2A	2 3	4	5	6	7	8	9	10
1' 20A	2' 3'	4'	5	6'	7'	8'	9'	10'

Fig. 1- Schematic view of the French-Swedish extrapolated accelerator

tor and θ_i and θ_f the initial and final angular velocity.

In our case $\theta_i = 0$ and

$$\dot{\theta}_f = \omega_{Li}\left[\frac{B_f}{B_i} - \frac{r_i^2}{r_f^2}\right]$$

where $$\omega_{Li} = \frac{eB_i}{2m}$$

According to the laminar model the final angular velocity is zero if the magnetic flux for the outer particles is conserved. When the beam size is changing with the effect of the external and space charge electric fields the magnitude of the magnetic field will change in such a way that the trajectories of the ions follow the magnetic field lines.

2) Minimum final radial velocity

The electrostatic electrodes should be determined in such a way that the final radial velocity is minimum. This condition is similar to the condition of the classical neutral injector. For example a classical Pierce geometry with a constant beam radius is not convenient for this purpose.

Indeed, this type of accelerator gives a diverging beam due to the lens effect of the exit hole (or slit).
The exit angle is defined by the relationship :

$$\text{Arc tg}\alpha = \frac{r_b}{f} = \frac{r_b(E_2-E_1)}{nV}$$

where E_1, E_2 are the electric field on each side of the hole
V is the total voltage applied on the lens
n = 2 for a slit
n = 4 for a hole

In our case with accel-decel final electrodes where $E_2 \simeq -E_1$ and with the slit configuration we obtain :

$$\text{Arc tg}\alpha = \frac{4}{3}\frac{r_b}{d}$$

where d is the distance determined by the classical Child-Langmuir law. Because the initial kinetic energy (1 keV) is a small fraction of thc final energy, no correction is necessary.

As a numerical example for V = 330 kV and r_b = 1.25 cm the exit angle is too large ($\simeq 3°$) and hence,the inconveniency of the neutral injector application is evident.

Other solution proposed in fig. 2 and 3 are analyzed :
In fig. 2, a converging Pierce injector is followed by a constant electric field accelerator.
In fig. 3, a diverging Pierce injector is followed by a constant electric field accelerator.

In order to conserve the constant magnetic flux in the above two cases, it is necessary to increase the magnetic field. But in the secondcase the electric field near the entrance is very low, which minimizes the unwanted effects of the cesium parasite flux. The first solution could be of interest in a case where the exit aperture size is minimized (the case of a reactor with a high neutrons flux).

Furthermore a small radius is probably necessary to simplify the neutralizer problems (the prohibitive energy losses due to the electrons).

By using a computer code derived from the S.L.A.C. code [2] one presents a simulation of the laminar trajectories with a diverging Pierce injector which is totally immersed in a magnetic field [fig. 4].

The initial current density is 16 mA/cm^2 and the final current density is 27 mA/cm^2. The final magnetic field is 6700 Gauss.

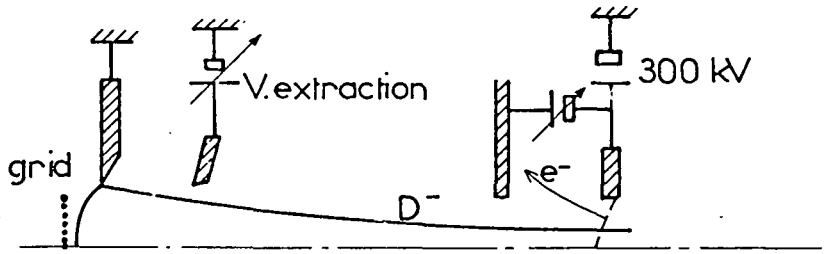

Fig. 2- Converging Pierce injector

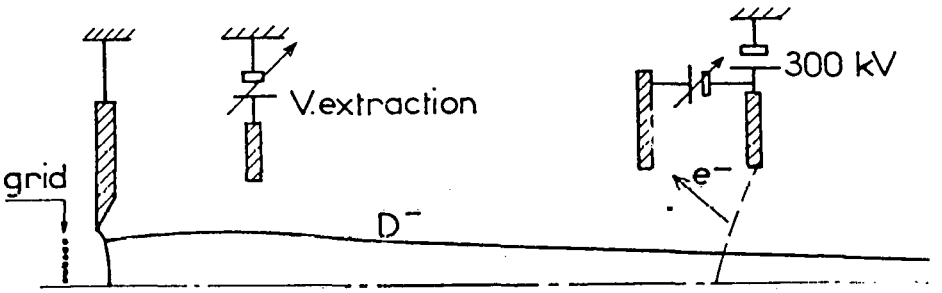

Fig. 3- Diverging Pierce injector

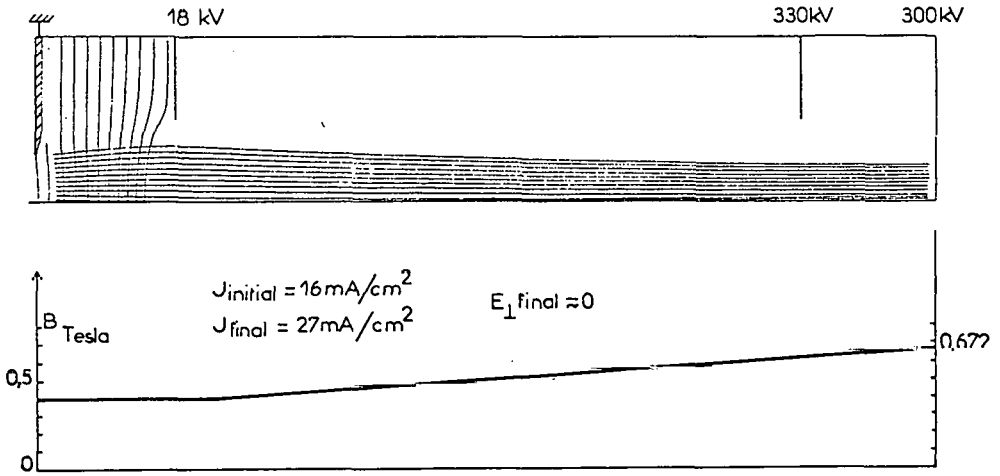

Fig. 4- Optimum configuration of a diverging Pierce injector obtained by computer code simulation

Electrons elimination

With a D^- accelerator immersed in a high magnetic field the cesium plasma density is not negligible ($n_e \simeq 10^{11}$ e/cm^3), and an efficient system has to be built in order to avoid the acceleration of the electrons at full energy.

Different technics could be employed (modulation of the magnetic field or deceleration electrodes). All these technics should be efficient and should not disturb the D^- beam qualities at low energy.

The description of an electrostatic technic using grids with high transparency is as follows [fig. 5].

This grid located at the entrance of the accelerator, is composed of molybdenum wires of diameter 50 µm, and the distance between two wires is 500 µm (the transparency is 90 %).

The grid is biased at a voltage of -100 V with respect to the plasma potential which is grounded. One can expect a D^- beam with an initial energy of 1 keV to be slightly affected by the presence of such a low negative potential.

These wires are heated by all the Cs^+ current, and by 10 % of D^- and diverging D_0 atoms at low energy :

The equilibrium temperature of the grid is not sufficient to produce thermoelectronic emission.

For conserving the optical qualities, each wire can extand along its axis under the heating effect.

When a negative potential is applied to a grid totally immersed in a plasma, an emissive sheath is created around the wire [fig. 5] and the plasma diffuses between the sheaths. If the sheath

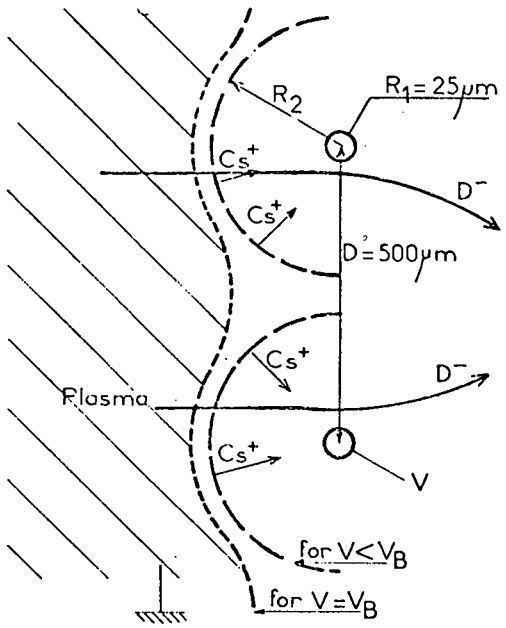

Fig. 5- Electrostatic electron suppressor principle (wires configuration).

thickness is equal to the half distance between the wires, the diffusion is stopped. All the Cs^+ ions are collected on the grid (they are reflected by the electric field of the accelerator). The cesium ion current density is given roughly by the Bohm relationship :

$$J_{Cs} \sim 0.4\, n_{iCs}\, q_e \left[\frac{2KTe}{M_i}\right]^{1/2}$$

where n_{iCs} is the cesium ionic density
q_e the electronic charge
Te the plasma electronic temperature
K the Boltzman's constant
M_i the cesium mass

If the plasma boundary is such that the saturated current density J_{Cs} is equal to the current density J_{CL} given by the Child-Langmuir law in the cylindrical diode configuration, then

$$J_{Cs^+} = J_{CL} = \frac{4}{9}\frac{2}{R_2}\frac{\varepsilon_0}{H^2\left(\frac{R_2}{R_1}\right)}\left(\frac{q_e}{M_i}\right)^{1/2}\frac{V^{3/2}}{R_1}$$

where R_1 is the wire radius
R_2 the sheath radius
ε_0 the vacuum permittivity
$H^2\left(\frac{R_2}{R_1}\right)$ is a function tabulated in [3]
V is the potential difference between the grid and the plasma.

By combining the two relations one can write

$$V_b = \left[\frac{0.9\, n_{iCs} H^2}{\varepsilon_0 (1-T)}\right]^{2/3} (q_e KTe)^{1/2} R_1^{4/3}$$

where T is the grid transparency
V_b is stoppering voltage

$$R_2 = \frac{D}{2}$$

The figure 6 shows the evolution of the voltage module versus the plasma density for an electronic temperature of 1 eV, a constant transparency of 90 % and for two values of the wires diameter.

In the case of a symmetrical geometry with a uniform magnetic field of 0.4 Tesla, the magnetic field does not affect the theoretical value of the V_b potential [4] (fig. 6).

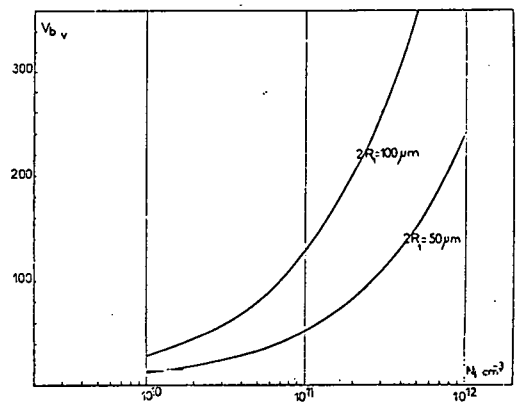

Fig. 6- Suppressor voltage versus cesium plasma density.

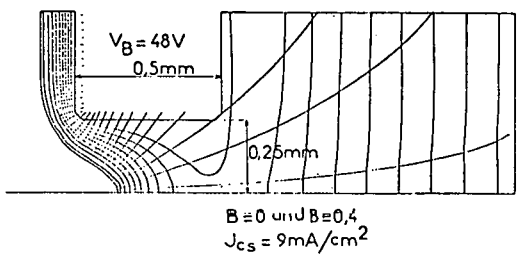

Fig. 7- Axisymmetric electrons suppressor simulation with and without magnetic field.

Conclusion

A converging or diverging Pierce preaccelerator followed by a constant electric field accelerator could be built with a current density of 12 mA/cm^2, a total current of 50 mA, and a final energy of 300 keV. The steady state electric field is low (22 kV/cm) and the magnetic field is determined in such a way that the beam quality is not affected by the presence of the B field . A compression factor could be obtained and consequently the

current density is increased (25 to 50 mA/cm^2). Then a plasma neutralizer is used in a high magnetic field.

The extrapolation of this preliminary accelerator to a full current accelerator of 3-4 A will be envisaged with some precautions about the shape of the magnetic field, and a new computer code taking into account a slit geometry system immersed in a magnetic field will be developped.

In order to avoid the electron acceleration, an electrostatic system has been determined and will be tested.

References

1. M. Delaunay, and al., Proc. 2nd Int. Symp. on the Production and Neutralization of Negative Hydrogen Ions and Beams, Brookhaven 1980.

2. W.B. Herrmannsfeldt, "Electron Trajectory Program", Standford linear accelerator center, Report S.L.A.C.-166 (1973).

3. G.A. Nagy, M. Szilagyi, Introduction to the Theory of Space-Charge Optics, (Mac Millan, London, 1974).

4. J.L. Foucher, Thesis, Grenoble (1980).

DISCUSSION

HOOPER I am not sure if I followed fully the consequences of having a grid in the beam. Certainly if there were no magnetic field present there would be a scattering of the beam by the electric fields around the grid. Is that still true when there is a strong magnetic field applied?

JACQUOT We see the same problem for the positive ion source because you have a plasma which goes in the direction of the positive ion source and we stop the electrons on the grids of the positive ion source. When we create a plasma in the cesium jet, the cesium plasma diffuses on each side of the jet; it diffuses towards the accelerator and towards the positive ion source and we stop effectively the plasma in the positive ion source. The magnetic force is less important than the electric force.

HOOPER It seems to me though, there is a very important difference between the stopping of the plasma at your positive ion source and the stopping of the plasma at the entrance to your high voltage accelerator. In order to stop the plasma at the entrance to the high voltage accelerator you have a grid with a very fine mesh compared to the entrance aperture of the high voltage accelerator, so that any scattering or angular effects, introduced into the beam by that grid, cannot be corrected in the accelerator because they are effectively a temperature. Whereas when you look at the positive ion accelerator, you are blocking the plasma that is flowing back down a gap that has the same size as the acceleration gap of your accelerator. It is a very different effect, I would think.

JACQUOT You mean that you have some extra temperature for D^- on the grids?

HOOPER Yes.

JACQUOT Yes we have that but it is of the order of maximum 100 V. If we are very pessimistic the perpendicular energy is of the order of 100 V and we have to compare 100 V to the final acceleration of 300 kV. In the positive ion source we have already this temperature and we have to accelerate the beam to very high energy so that the final angle should be less than 1^o. The final beam qualities are given by the initial beam quality of the accelerator.

HOOPER I see.

HAMILTON I think Bick is thinking about the aberrations caused by the fringing fields of the grids that suppress the electrons but there are ways of avoiding these aberrations by using two grids at the same potential with a space between them.

LARGE-APERTURE D^- ACCELERATORS*

O. A. Anderson+

Lawrence Berkeley Laboratory
University of California
Berkeley, California 94720

Abstract

Accelerator designs are described for D^- produced by double charge exchange, by the ion magnetron, and by the LBL bucket source; in all three cases the accelerators employ a single slot per module. High and low energy designs are discussed; in the latter cases the perveances are much larger than in typical D^+ accelerators.

1. Introduction

Magnetic fusion applications may require large currents of D^- in the next few years. Since D^- is not as easy to produce as D^+, a different approach to accelerator designs is indicated for the two cases. In multi-grid D^+ accelerators, 50-60% of the ion current flowing toward the grids is transmitted on through the accelerator; the grids intercept the rest. In the case of D^-, with less copious production, it is desirable to avoid this interception. Therefore, in the D^- accelerators described here, multiple grids are not used; each module has one large entrance aperture which transmits essentially 100% of the D^- ions produced by the source. Accelerators for three types of sources are discussed: *double charge exchange*,[1-3] *ion magnetron*,[4-5] and the LBL D^- source.[6-8] A convenient module in each case has an entrance aperture 5 cm by 50 cm (or perhaps 10 cm by 100 cm).

These large slot dimensions give additional benefits: electrodes are rugged, voltage gradients are low, and stripping cells are conveniently accommodated.

Certain problems or unusual situations may occur in these designs. For example, in early stages of testing one may wish to accelerate large currents to relatively low energies (40 - 100 keV). This leads to accel gaps which may be shorter than the size of the entrance aperture. The associated problems are discussed in Sections 3 and 5. In these lower energy designs the incoming D^- beam may already have a significant fraction of its final energy, with the effect discussed in Section 3.

Sections 4 and 5 illustrate cases in which the incoming D^- beam has a large systematic divergence which must be eliminated by the accelerator. A more difficult problem arises from non-uniform current density over the entrance aperture; this is discussed in Section 5.

2. Computational model

The results presented here were obtained with the WOLF code[9]. This code can adjust electrode shapes, positions and voltages to minimize the beam divergence. It also finds the correct emitter shape, where the "emitter" in WOLF terminology stands for an equipotential sheath edge. In positive ion applications the E-field on the plasma side of the emitter (the left side in Fig. 1a) is first found by solving the Tonks-Langmuir equation. Then, on the right side of the emitter, an iteration is done: WOLF computes ion trajectories and solves Poisson's equation (including electrons) with the equipotential boundary condition. The shape of the emitter is adjusted until the computed field equals the Tonks-Langmuir field.

With negative ion sources, the neutralizing plasma on the left of the emitter contains both positive ions and (at least a few) electrons. In some cases the presence of three species could make the computational work more difficult. But in the present applications the WOLF computational model is actually simplified: there is a pure D^- beam being accelerated to the right of the emitter (Fig. 1a); positive ion and electron space charges are neglected. And the electric field E_{em} at the plasma edge (the emitter) is so small that it may be set equal to zero. The analysis which leads to this model is given in Ref. 10.

In physical terms, the electrode system accelerates the D^- beam (and any electron current) but turns back the neutralizing positive ions from the plasma on the left. These neutralizing ions are too cold (characteristic energy certainly less than 1 eV) to penetrate appreciably into the acceleration region; this is a basic simplification. Ref. 10 shows that one can choose an equipotential emitter surface on which $n_+ \ll n_{beam}$ and also $E_{em} < 50$ V/cm; the initial D^- energy is assumed (consistent with the following examples) to be in the range 200 to 15000 eV. Furthermore, plasma electrons may also be ignored in these examples. In a practical

accelerator, an electron current as large as 10% of the D^- current would probably be unacceptable, and would need to be suppressed (eg. by magnetic fields[5,8] or by a flow pattern[11]) before the D^- beam reaches the accelerator aperture. The calculation for the worst case gives $n_e/n_{beam} \sim 0.1$ at the emitter surface.[10] But this ratio falls very rapidly to the right because of the small electron mass, and the effect of electron space charge can be represented by a very slight shift in the emitter position, without noticeable effect on the beam optics.

3. Double charge exchange D^- accelerator

The first case studied was a low energy (100 keV) test accelerator for a 10 keV D^- beam obtained from a sodium cell.[2,3] The entrance aperture width w was 5 cm, with J = 20 mA/cm^2. The perveance per square $P_\square = w^2J/V^{3/2}$ was therefore 1.6×10^{-8} pervs, which is rather large for deuterium. (Compare 2.2×10^{-9} for TFTR). The accel electrode is therefore quite close to the entrance aperture, as seen in Fig. 1a; in fact the ratio of accel length to aperture size is only 1.40. To reduce aberrations the electrodes were given the special shapes shown in the figure. A trim electrode curves the equipotential lines near the emitter as shown. It has nearly the same potential as the entrance electrode, and could be formed as an extension of it. But as a separate piece, with adjustable potential, it provides convenient experimental control over the optics.

The emittance diagram (Fig. 1b) shows exit angle vs position for each accelerated beamlet. The random transverse D^- energy at the entrance aperture (emitter) was taken to be 9 eV, based on 1 eV at the D^+ source, and a compression factor of 3 in the D^+ accelerator. The resulting emittance diagram at the exit is seen to be dominated by random energy rather than aberrations; θ_{rms} is 18.7 mrad giving $\sqrt{2}\,\theta_{rms} = 1.52°$.*

Acceleration from 5 keV entrance energy was studied, using the same configuration and potentials as for 10 keV.[2] As might be expected, the plasma surface is shifted for this case. The shift is in the downstream direction, as predicted by a simple analysis.[12] A consequence of this shift is that in mixed beams resulting from the presence of molecular ions in the original source (eg. mixed 5 and 10 keV D^- beams) the emitter position lies between the two extremes. At the minimum rms divergence, one component is underfocussed and the other overfocussed.[2]

---

* $\sqrt{2}\,\theta_{rms}$ would be the 1/e halfwidth for the case of a Gaussian transverse energy distribution.

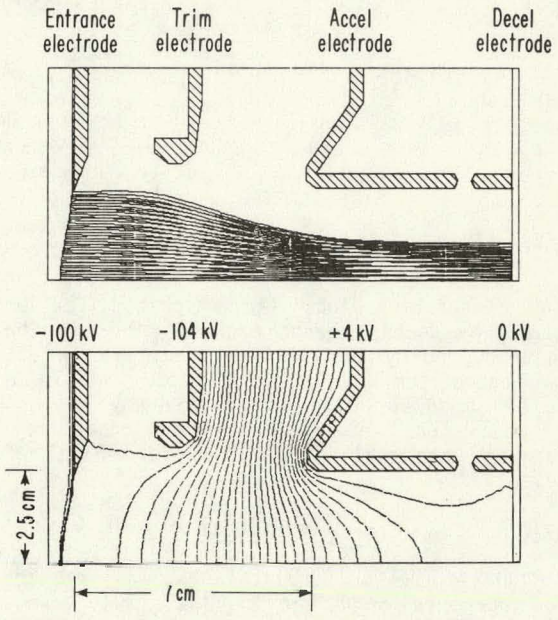

XBL 8010-2189

Fig. 1a: Test accelerator for D^- from double charge exchange in sodium: 5A entering 5 cm x 50 cm slot. Ion trajectories (above) and equipotentials (below) are shown.

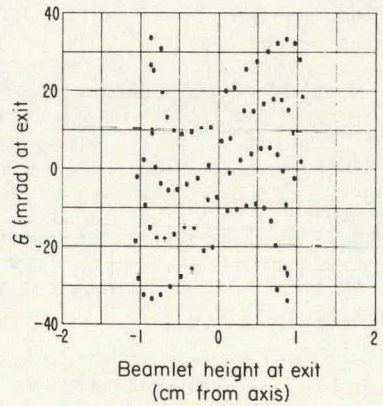

Fig. 1b: Emittance diagram.

Figure 1a can be scaled to represent a 200 keV D^- accelerator with 14 mA/cm^2 entering at 20 keV over a 10 cm aperture width. If the slot were 140 cm long, then 20 A of D^- would be accelerated. The effective beam divergence would be reduced to about 1°.

Although in Fig. 1 the current density is assumed uniform over the aperture, a variation is expected in practice, with the results shown in Ref. 2. A similar problem is discussed for a different type of source in section 5 of the present report.

4. Ion magnetron sources

The steady-state sources being developed at BNL are expected to produce 0.5 to 1.0 A of beam per unit.[4,5] The current density at the cathode is quite large, but the extracted beam (around 15 keV) has a half angle of 200 mrad and quickly expands to sizes and current densities of the sort discussed in Sections 3 and 5. In fact, it is easy to arrange an array of BNL sources which would fill one of these entrance slots fairly uniformly. The problem is the large transverse energy (600 eV using the above numbers). However, Fig. 2 shows that these diverging beams can be successfully straightened. This example has electrodes and parameters similar to those in Fig. 4a, Section 5. A higher current example would look like Fig. 1a.

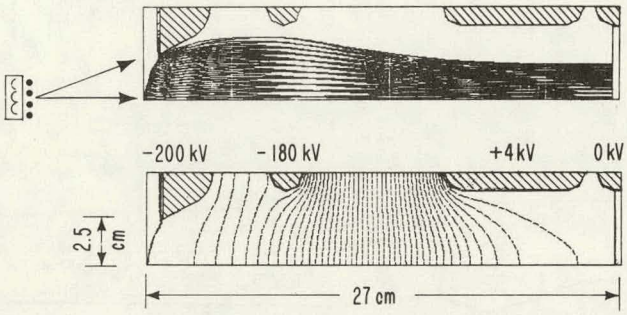

Fig. 2a: Acceleration of 15 keV diverging beam from ion magnetron source.

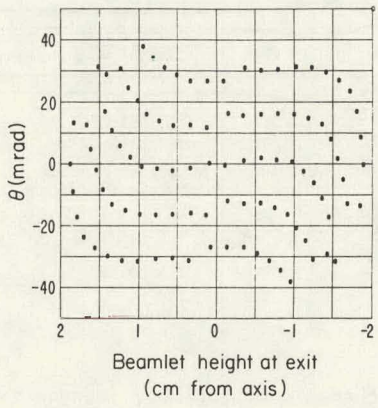

Fig. 2b: Emittance diagram.

5. LBL source

The D^- source being developed at LBL[6-8] uses a converter plate similar in shape to the BNL cathode but scaled to much larger size with appropriately lower current density, so that it is naturally compatible with large-aperture acceleration. The separate extractor (~15 keV) used at BNL is not needed. The accelerators shown in Figs. 3 to 6 work directly with the D^- or H^- beam which is produced at the converter plate and accelerated through the sheath. The entrance energy is therefore around 200 eV; there may be an additional cold component from volume production, which tends to be small at low gas pressures and is neglected in the present computations. Two cases have been studied: a 40 keV test accelerator with a single module, and a 200 keV multiple module version. The first configuration, shown in Fig. 3a, is similar to the one in Section 3 except that the aspect ratio is even more unfavorable (the accel spacing is actually smaller than the entrance size). The perveance per square is 2.5×10^{-8}. The emittance diagram (Fig. 3b) shows strong aberrations. Although these could be reduced with further design effort, the design may be adequate for initial tests. Fig. 3 does at least demonstrate once again that a diverging entrance beam is readily straightened and focussed.

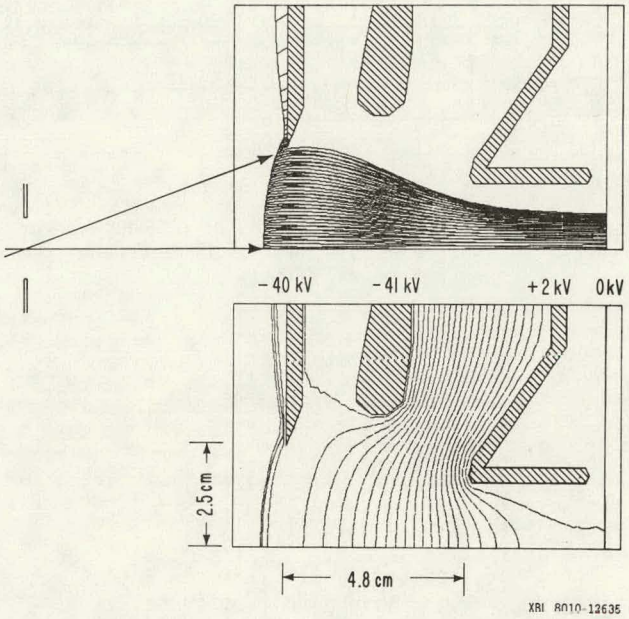

Fig. 3a: Low energy accelerator for LBL bucket source: 1.4 A of H^- entering 5 cm x 25 cm slot.

The 200 keV design (Fig. 4a) allows nearly complete control of aberrations as shown in the emittance diagram (Fig. 4b). The favorable aspect ratio here allows slender electrodes with high transparency for gas pumping. The exit beam divergence (0.48°) is near the theoretical limit for the input conditions. This design is intended for modular stacking as shown in Fig. 5. The open electrode arrangement gives fast enough pumping to eliminate nearly all D^- stripping up to and through the accelerator.

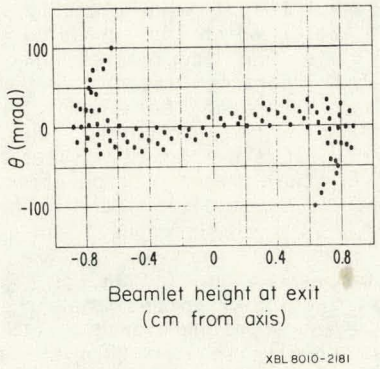

Fig. 3b: Emittance diagram.

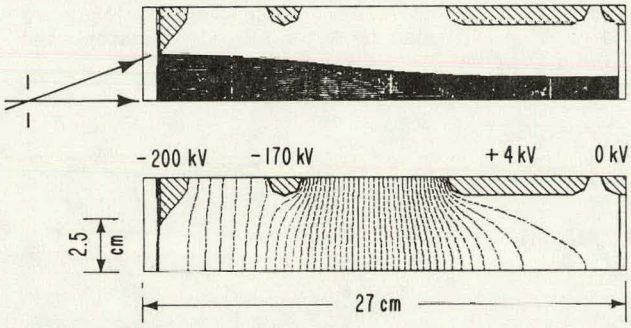

Fig. 4a: 200 keV accelerator for LBL bucket source module: 4 A of D^- entering each 5 cm x 100 cm slot.

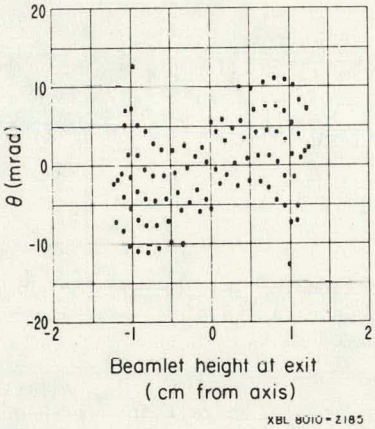

Fig. 4b: Emittance diagram.

In the computations for Figs. 3 and 4, the current density was taken to be uniform over the entrance aperture (except for a small cosine effect). This corresponds to a system without vignetting, as illustrated in Fig. 6: the converter plate is large enough (relative to the entrance aperture) to allow for the finite width of the collimating slit. In such an arrangement, though, a good part of the D^- current passing through the collimating slit fails to enter the entrance aperture and is wasted.

Thus in the practical system shown in Fig. 5 a compromise is effected: the converter plates would just map onto the entrance apertures if the collimating slits were infinitely thin. Then, when the slits are opened to practical sizes (eg. 2 cm), most of the D^- is accelerated, but vignetting occurs as seen in the current profile in Fig. 7a. This leads to a difficulty, because the beam can not be accelerated by the Pierce gun principle, which is used in Figs. 1-4 (and in the LBL positive ion accelerators). In the Pierce gun a suitably angled entrance electrode is in contact with the edge of a uniform beam. Pierce's solution does not apply to a vignetted beam.

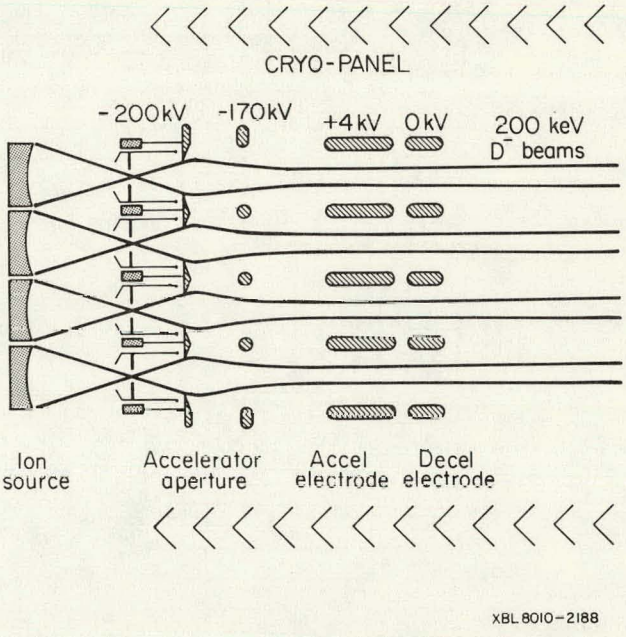

Fig. 5: Schematic of LBL multi-module sytem: D^- current density 50 A/m^2.

Fig. 7b shows the actual results of running the vignetted beam (Fig. 7a) through the electrode system of Fig. 4. The emittance diagram (Fig. 7b) shows extreme overfocussing of the edge beamlets, which cross over before reaching the exit. For comparison, the unvignetted emittance outline (Fig. 4b) is roughly represented by the dashed line seen superimposed on Fig. 7b.

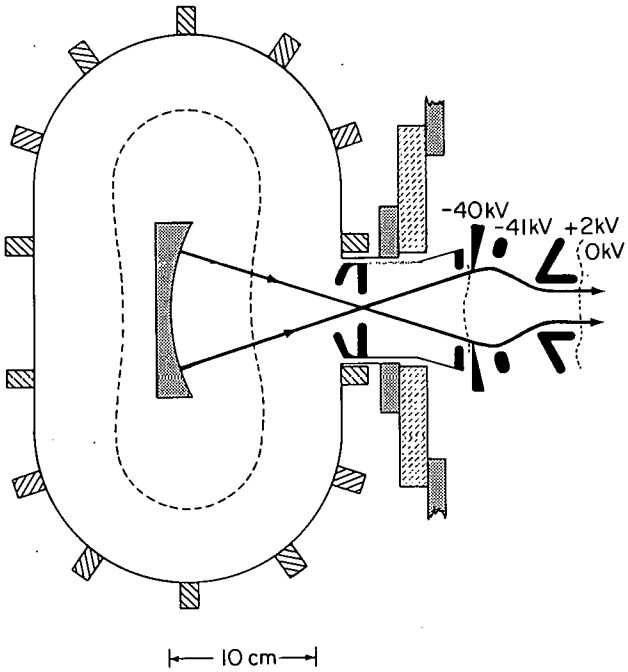

Fig. 6: Configuration assumed for Fig. 3; note converter plate extensions.

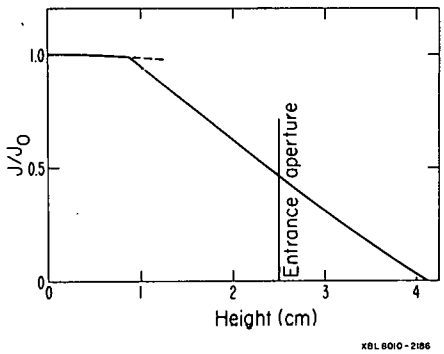

Fig. 7a: Vignetted current profile at accelerator entrance aperture (unextended converter plate; 2 cm collimating slit).

There are obvious ways to circumvent this problem without wasting D^- ions: one could perforate (or otherwise modify) the central region of the converter plates to reduce D^- production relative to the edges, or one could look for a different entrance electrode arrangement not based on the Pierce gun principle. The latter approach is under investigation, with encouraging results.

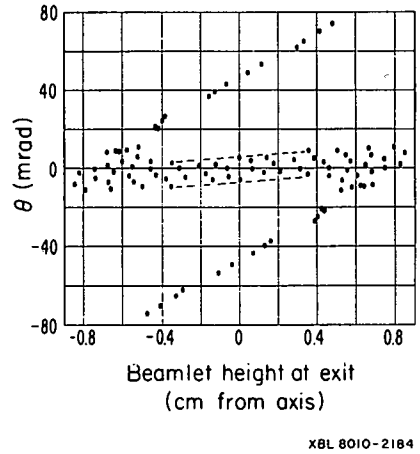

Fig. 7b. Emittance diagram for vignetted beam (Fig. 7a). See text.

Acknowledgements

The author is grateful to W. S. Cooper for many helpful discussions and to C. F. Chan and L. Soroka for destroying several WOLF bugs.

References

*This work is supported by Fusion Energy Division, U. S. Department of Energy, under contract W-7405-ENG-48.

1. E. B. Hooper, Jr., O. A. Anderson, T. J. Orzechowski, and P. Poulsen, "60 keV D^- Beams Using Double Charge-Exchange System," Proc. Symp. Prod. and Neut. Negative Hydrogen Ions and Beams, Brookhaven, 1977, K. Prelec, Editor, p. 163.

2. E. B. Hooper, Jr., P. Poulsen, P. A. Pincosy, O. A. Anderson, T. J. Duffy, "High Current D^- Production by Charge-Exchange in Na: Neutral Beam Application," LBL-10454, unpublished (1980).

3. E. B. Hooper, Jr., P. Poulsen, O. A. Anderson, "Optimized System for D^- Production from Charge Exchange in Alkali Metals," LBL-10917, submitted to Nuclear Fusion.

E. B. Hooper, Jr. and P. Poulsen, "Prospects for negative ion systems based on charge exchange," submitted to 2nd Int. Symp. on Prod. and Neut. of Negative Hydrogen Ions and Beams, Brookhaven, 1980.

4. K. Prelec, "Progress in the Development of High Current, Steady State H^-/D^- Sources at BNL," Submitted to 2nd Int. Symp. on Prod. and Neut. of Negative Hydrogen Ions and Beams, Brookhaven, 1980.

J. Alessi and Th. Sluyters, "Regular and Asymmetric Negative Ion Magnetron Sources With Grooved Cathodes," Submitted to 2nd Int. Symp. on Prod. and Neut. of Negative Hydrogen Ion and Beams, Brookhaven, 1980.

5. Th. Sluyters and J. Alessi, "Extraction and Transport of H^-, D^- Beams from Magnetron sources," Submitted to 2nd Int. Symp. on Prod. and Neut. of Negative Hydrogen Ions and Beams, Brookhaven, 1980.

6. K. W. Ehlers and K. N. Leung, "Multicusp Negative Ion Source," Rev. Sci. Instrum. 51, 721 (1980).

7. K. W. Ehlers and K. N. Leung, "Characteristics of Self-Extraction Negative Ion Source," Submitted to 2nd Int. Symp. on Prod. and Neut. of Negative Hydrogen Ions and Beams, Brookhaven, 1980.

8. K. W. Ehlers and K. N. Leung, "Electron Suppression in a Multi-cusp Negative Ion Source," Submitted to J. Appl. Phys. Lett.

9. W. S. Cooper, K. Halbach, and S. B. Magyary, "Computer-Aided Extractor Design", Proc. 2nd Symp. on Ion Sources and Formation of Ion Beams; Berkeley, CA. Rept. LBL-3399, pp. II-1-6 to II-1-10 (1974).

10. O. A. Anderson, "Computational Model for Negative Ion Plasma Boundary," unpublished.

11. O. A. Anderson and E. B. Hooper, Jr., "Plasma Production and Flow in Negative Ion Beams," Symp. on Prod. and Neut. of Negative Hydrogen Ions and Beams, Brookhaven, 1977.

E. B. Hooper, Jr., O. A. Anderson, and P. A. Willmann, "Production and Flow of Plasma in Ion Beams" Phys. Fluids 22, 2334 (1979).

12. O. A. Anderson, "Modification of Childs' Law in Ion Beam Systems," LBL-10642, unpublished (March 1980).

DISCUSSION

SHERMAN What was the nature of the non-uniformity in the distribution, that you put in there, where you saw the largest divergencies?

ANDERSON It was exactly as shown on the slide. It falls to 50% at the edge.

SLUYTERS In your calculations you started with an ideal situation at the entrance of the accelerator. In practice you have the transport channel as Leung has described, so that your initial conditions are completely different. How can you calculate these trajectories without taking into account the transport of the H^- beam between the source and the accelerator?

ANDERSON We do take that into account. The model is that the whole system is sufficiently close coupled that positive ions are available from the source, whatever the source may be, and those positive ions then neutralize the negative beam up to the plasma edge that I showed in these pictures. The ions are coming along following field free trajectories. There is no electric field in this region because of the positive ions there. That is the model, once they reach this point the positive ions are all turned back. There is a transition that occurs over a very narrow range of potential, less than ½ V or so, because the positive ions are so cold. So, this is a very thin region where you go from field free conditions to a condition where your negative ions see the accelerating field. And, what we do with the Wolf program is solve the Poisson equation etc.

SLUYTERS Your calculations were apparently done without the beam transport.

HOLMES What determines the shape of the boundary? It looks very nice and spherical.

ANDERSON We choose some equipotential line that we call the plasma edge. Now before we start iterating the problem, we solve Poisson equations and find some electric field distribution along that boundary. This in general will not be the correct electric field which is 0. What the Wolf program does is calculate by a matrix inversion how far you move this over to reduce the field to 0. It does that, finds out whether it did it correctly and keeps iterating until it is in fact 0 field all along that boundary.

JACQUOT In your double charge exchange system you take into account the modification of the Child-Langmuir law at the boundary because you have a kinetic energy which is not a small fraction of the final energy?

ANDERSON Definitely I took it into account. It makes a substantial difference. For example if the energy is 5 kV instead or 10 kV, this boundary moves back. I just want to comment that if you have a mixture of a 5 and 10 kV beam

then it would have to find some compromise. It could not be correct for both of them. What this means is that you would have over-focussing for one component and under-focussing for the other.

ACQUOT I have a second question about your bucket fence extraction. Do you have an idea of the temperature of the D^- ion beam at the entrance of this area?

ANDERSON Yes. What we did in the calculation was to take the worse case and assume that the beams were coming isotropically off of the converter plate so the temperature was determined by the width of the aperture and it comes out to be about 5 eV.

THIS PAGE

WAS INTENTIONALLY

LEFT BLANK

PANEL SESSIONS

THIS PAGE

WAS INTENTIONALLY

LEFT BLANK

PANEL SESSION: FUNDAMENTAL PROCESSES IN SOURCES

Panel Members: A.S. Schlachter (Moderator), M. Bacal,
J.N. Bardsley, D.H. Crandall, J. Hiskes, J. Los

SCHLACHTER I think it has been evident during the conference so far, that there have been impressive advances not only in negative ion sources but in the atomic physics related to negative ion sources as well. Part of this, no doubt, is due to the effective interaction that has taken place between those of us who concentrate on atomic physics and those who concentrate on the negative ion sources. It has also been very rewarding, I think, that the interaction has gone both ways; that is, some of the progress in ion sources has certainly come about as a result of advances that have been made in atomic physics, but also advances in ion sources have prompted new investigations of atomic physics as well as the ion sources. It is of course desireable to continue this interaction, and part of that consists of getting feedback from those who actually build and use negative ion sources to those who are concerned primarily with the atomic physics. Our panel this morning will be on basic processes in ion sources. There will be another panel discussion this afternoon on the ion sources themselves. I would like to ask your cooperation in trying to limit the topics discussed to fundamental processes. We begin with a brief statement from each member of the panel as to what he/she sees as the future direction of atomic physics as related to negative ion sources. After that the discussion will be open and anyone who has either a comment or a question will be welcome to participate.

I will start with Dr. Hiskes for a statement. I would like you to hold any questions or comments until after all the members of the panel have made their brief statement.

HISKES Let us divide the program into the three areas: the double charge exchange, the surface, and the volume processes. In the double charge exchange area the most exciting possibility is the prospect of a very high equilibrium yield using the strontium and calcium vapors. There is a suggestion from experiment and from theory of Olson that this yield might be larger than the 35% yield which has so far been observed with cesium. In the surface arena there is still reason to believe that we have yet to find the optimum surface alkali-transition metal. A list of substrate candidates based upon certain criteria were presented in the paper by P. Schneider and myself. Ken Ehlers considered somewhat different criteria and developed a different list, but there were some regions of overlap, and this may be the first place to look. In volume processes the one parameter that is still the most elusive is the number of bounces that a molecule experiences with the wall and still retains its vibrational excitation. There is a chance of deducing that number from the CARS experiment using the Bardsley-Wodehra cross sections, and there is also the prospect of understanding that number from the calculations which Arnold Karo has initiated and which he described at this symposium.

LOS Everyone interpreted this panel in his own way. You asked me what the future plans were in: not atomic physics but surface physics. I hope you still have in mind, more or less, the results which were obtained by double charge transfer of protons or deuterons on cesium-coated surfaces. We measured some efficiencies of 35 to 40% at a perpendicular velocity of 2×10^6cm/sec. Now there are two short questions. One is, what would happen when you start not with an H^+ but with an H^0? I think you will attain larger efficiencies. The second question is more important for practical applications in sources: what will hydrogen contamination of the surface do? These questions will certainly be investigated in the near future. More interesting from the fundamental point of view is what will H_2^+ and H_3^+ do when colliding with the surface? When you have an H_2^+ it should neutralize when it meets the surface. If it neutralizes in an dissociative state (which I think is very likely) then the neutralization takes place in front of the surface, at distances of the order of 10 a_o and you would get on the surface two hydrogen atoms. Or, if the H_2^+ survive and come closer to the surface, then I would think it would be most probable that it will neutralize according to an Auger mechanism and go to a bound state. How it dissociates then, I do not know. I think it is also of fundamental interest to know, if the surface is of importance for vibrational excitation of a hydrogen molecule.

BACAL I want to comment on the two ways we followed in the last years in the understanding of negative-ion formation in plasmas. I think we have to continue to work on these two ways. One of the problems is atomic data. We got a lot of information in recent years about new processes, but we still need more, especially if we want to analyze the high density regime. We will certainly like to know a lot about the branching ratios in many reactions, branching relevant to vibrationally excited levels. So we would like to know what doubt there is associated with dissociative recombination of H_3^+ in terms of producing vibrationally excited hydrogen. The same question is relevant for H^- and H_2^+ in combination. We would like to know more about a new process which has been suggested today by Dr. Los, which is formation of H_2 vibrationally excited by the combination on the wall by two atoms of hydrogen. We did not consider this process; maybe it is a very important one. Of course, we have to know more about these bounces and about the loss of vibrational excitation on the wall. We need to know that for each of the vibrational levels: what is important in collisions with the wall but especially for the highest vibrational levels. We would like to go back maybe to the dissociative attachment. We think, we know everything about

dissociative attachment in vibrationally excited hydrogen. Of course theory has done a lot for us but maybe somehow we can try to measure cross sections for the highest vibrationally excited molecules. We deal with theoretical cross sections. Do we have enough confidence in them? Maybe it is a difficult experiment, but maybe it can be done. Well, I go back to a reaction which we know a lot about and still do not know enough. It is the formation of H_3^+ in the ion-molecule reaction $H_2^+ + H_2$. We have had a lot of data on that, and in fact when you look at these data, you see a discrepancy of a factor of 5. This is a reaction which is very important not only in positive ion sources but also in negative ion sources. It is a puzzling situation, because in certain types of positive ion sources one uses a certain value, while in a different type source with a different density range, one implies another value for this reaction rate. So, I think the problem is that the reaction depends, in fact, on vibrational excitation. Maybe it is time to consider experiments in which we control these processes and measure the reaction rate for that.

Let us now talk about measurements. This brings us to the question of diagnostics. I would say that the progress we made in recent years was related to the use of new diagnostics. We would not have understood volume production if we would not have had probe measurements in the beginning, and more recently photodetachment. I wonder whether it is not a step to take by all people who use negative ion sources and have them involved somehow to try to use this diagnostic and give to the computer people and theorists more valuable data about the plasma conditions. We have such excellent computer facilities. We know people who can compute for you a lot and give you a lot of indications of how it should behave, but you have to give them some information about temperature, densities, etc. So I think an important trend in our future work should be use of diagnostics, not only one kind of diagnostic but trying to know about more things which happen in our plasma and ion sources. In our particular case we will certainly use photodetachment and improve it by use of new wavelengths and other things. We would also like to develop techniques to measure vibrational excitation in plasmas and improve and continue work on that. Developing these diagnostics may also be useful for the atomic physicists, who want to make experiments on vibrationally excited molecules and measuring cross sections, which are useful not only for studying plasma but also for studying cross sections.

CRANDALL This is something to help me out, I hope it does not confuse everybody else. One of the very important issues, I think, we are dealing with right here, is how we communicate between basic-physics people and ion-source people. We need some more activity, I think, in what I call translation between the two groups. So these guys were translators and there were probably some others. That is very helpful from my prospective that modeling has been done to try and understand how the atomic physics interfaces with the production and destruction, both in the ion source and transport jets and what have you. So, I think we need more of that to help this beneficial communication, that Schlachter talked about, between the atomic-physics people and the ion-source people. Here are some questions which other people have already talked about. I will not say anything more about it for the moment, I am sure, they will be discussed in greater detail. For volume processes, I want to point out that a meeting in Paris in May, that was called by the IAEA, there was a small group of people to discuss the atomic data needs of fusion. This table is one page of a fairly lengthy report which will appear in Physica Scripta soon and has some of the same issues addressed in terms of ion sourcery. These other things have to do with plasma diagnostics and diagnostics on the beams themselves, which we have not talked about, but certainly those things were there. There is some discussion of those needs in that report, so it might be interesting reading. But I do not think it says anything very different from what we have talked about.

In contrast to what somebody else said, I think that the double capture concept is much clearer to atomic physicists than are ion sources, and I think we are in a much better position to model that and to interpret what has been done and to understand exactly how much you can get out of it. Other people have mentioned that the most exciting additional atomic physics possibility is calcium and strontium at very low energies. It seems to me, from what was presented this morning, that the Europeans have a vested interest in this, more than we do in the U.S., because I do not think we have any real specific plans to use that, whereas you have several systems working at very low energies with magnets to confine the beams. If you got higher efficiency with calcium that might be very important to you. So that might represent a logistics problem, if the U.S. scientists measured for the European community.

Then, what I think is the most difficult and biggest feature is just trying to understand what is going on in ion sources. What we need here, in addition to the translators I already mentioned, is some better language which could come from the diagnostics. Martha Bacal's work and the others from Ecole Polytechnique pretty well diagnosed their sources but it is a lot different than the kind of ion sources that people are really working with. We need to know, if we are going to try to optimize those ultimate ion sources, a lot of things we are not yet finding out. We need these translators and this language to tell us a lot more things about the discharge. For instance, where is the cesium in this discharge? Is it on surfaces? Is it in the plasma and to what extent? What are the parameters of the discharge, sometimes that might be valuable information. But beyond the parameters like temperature and density, I think we like to know what the constituents are and what the states of those constituents are. I think the possibility exists for some gimmicks that have not been tried yet, to help increase the

the negative ion production. So far we do not know anything wrong with vibrational excitation. We do not know much or anything at all on how that would affect surface production. We think it would be beneficial to volume production, but the question arises: how can you have 1 eV temperature plasma with 3 eV of vibrational temperature in the molecules? Can you sustain that thing or can you somehow jack it up artificially. I think those are questions that are worth addressing, but we really need better diagnostics.

One of the questions that I have and I hope we can come back to: what is the relative language here about charge exchange versus volume production in real ion sources. Some people always say that charge exchange is what causes this peak that does not move, when you put the plasma on the surface and other people think that that is volume. I think we do not have a clear understanding of what the relevant atomic physics processes really are. There is one other thing. I mentioned molecular negative ions in my talk. There is a question about whether these exist, and Bardsley can say immediately and simply that he does not believe that these negative ions exist. There has been some experiments that looked at H^{--}, which I think everybody agrees probably are not correct. Then there are these experiments on molecular ions which, as far as I know, are still dependable according to the authors. The important thing about this is that those are 8 orders of magnitude less intense that the H^- or D^- coming out of an ion source, so for the purpose of this group it may not be a very interesting question. It might be interesting from a basic science point of view, but I do not think it has very much influence on your production process. I think we should have that kind of realism about that.

BARDSLEY I was going to resist the impulse to say anything about H_2 but since Dave brought it up... There are three controversial negative ions, which have been seen by experimentalists. I think on H^{--} we have very strong theoretical arguments to say that it does not exist. On H_2^-, I have done some calculations in an attempt to find a stable state. We know that the lowest states are very unstable and that they have lifetimes of order 10^{-15} seconds, but this beats the $^4\Sigma^-$ state might possibly be stable if it lies below all the higher parent triplet states. However, we have tried for a couple of years to calculate this stable negative ion but so far have not succeeded. I am not convinced therefore that it does exist, and I will be very surprised if it does. Finally, the doublet state of He^- was reported to have been produced in Belfast by capture of two electrons in a single collision from H_2. You would not expect to form the quartet state in this type of collision, as you well know. The Belfast group argues in their paper that there is evidence for this doublet state of He^-, one of the components of a single collision process. Again this is something which theorists do not believe in. But as Crandall has said, these are probably not of any great importance for this program, but are the kind of interesting little academic questions that I will be glad to discuss with anyone. As for the need for cross section data, let me just mention the problem of molecular neutrals and ions. We see in many different applied areas, wherever molecules are involved, not only a need for the overall rates but very detailed information that you need to know. For example, what are the branching ratios for producing various different final states, or how does the cross section depend on the initial vibrational, electronic or rotational state in the molecule? These are very very difficult questions. They are hard theoretically; they are even more difficult experimentally. It is very difficult to study these effects. I would really like to know whether there are important problems involving molecules for which you need detailed information. If you want experimental information it is going to involve the development of new techniques, it is going to be expensive, proposals are going to have to be written to the NSF and to various other agencies. If this really is not important, please tell us so. If you think it is important tell us what is needed and we will send off proposals and work towards it. I would also like to know from users whether they need more calculations of detachment, etc. On behalf of the panel, I am looking forward to hearing from you about what your future needs are.

SCHLACHTER I think that from all of the talks I have heard so far during this meeting that it is too early to limit ourselves to one choice of negative ion source, and it is too early to say we know enough atomic physics, that we can go ahead and design and build a source, although one might be needed. There are three types of sources that have been discussed. In the case of surface sources, I think the progress in basic physics has been quite dramatic in terms of seeing mechanisms for negative ion formation on surfaces. In addition to those, as Dr. Los has said, there is very definitely a need to know how these surfaces will behave in real ion sources, when you have contamination present, when you have fluxes of the molecules present, how these surfaces will behave under sputtering. In other words, we need to know how useful they will be, although we do have evidence that negative ions are made on surfaces in actual sources, which is very encouraging.

For volume production, I think the progress, especially in physics understanding, has been dramatic; yet I think there is a lot of atomic physics we need to know in order to scale these up to densities that are useful for making intense negative-ion beams.

In the case of double charge transfer, here again, I think we have acquired a considerable data base, which is certainly in much better shape than three years ago. There are however a few gaps and discrepancies, particularly at low energy. There is also a lot of information that is missing, namely, what happens when you send an intense beam through the metal vapor target. We need to know about ionization of the target. We need to know

how the D^- that are formed in the target will interact with the plasma that results from the passage of the fast beam through the target. In addition, we have to know enough about scattering and angular phenomena so that we can predict and model not only the F^∞ but also the conversion efficiency. I was particularly impressed this morning by the agreement of Dr. Hooper results with model calculations. Wilmer Anderson commented that Hooper's results agree better with theory than the experiments agree with themselves! I am pleased now to open this panel to comments or questions that you would like to address to anyone on the panel.

ANDERSON I want to comment on Dr. Hiskes' comment that double charge transfer in alkaline earthes is important. That seems right, and Tom Morgan or Fred Schlachter no doubt will measure the cross sections and the equilibrium yield. One thing I had not really appreciated this morning which I heard in Dr. Hooper's talk, is that if you have two dimensional focusing, you really need to work at quite higher energy than if you have one dimensional focusing. I would like to address this question to Dr. Hooper or Dr. Hiskes: what will happen if you have a target that gives an equilibrium yield of 50% at 200 eV, can you get in a one dimensional focus a beam that has a current density comparable to what you can get out of sodium, cesium or rubidium which also has the same current densities or better?

HOOPER I think you have to work with a very different system than anyone has tried now. It is going to be very limited by what you can do in the positive ion source, because in the conventional positive ion source these energies do not work very well. Perhaps something along the lines of the work that Dr. Forrester has done could give a high enough primary current that would permit the total current to be obtained. The estimates I have made indicate that the current density you will end up with, if you can in fact obtain a high primary current, will be comparable to the sort of current densities that we have seen elsewhere, but your efficiencies, your gas and power efficiency and all that, could be appreciably greater. I think the accelerator is probably going to be a multi-aperture type of accelerator, rather than a single aperture such as I was modeling this morning. This is because the dimensions and total currents you will be dealing with will be such that the accelerator will not be able to handle them in a single aperture. I think they will require a considerable amount of ingenuity and rethinking of assumptions to apply a source working down to a couple of hundred eV, with calcium or something like that, but I think it is also a wide open field for somebody to come in and do some good work.

ANDERSON You said this morning, that for two dimensional focusing of the 200 eV beam, even if it has a 50-60% equilibrium yield, will not be as useful, for example, for injection into a Tandem or another accelerator.

HOOPER That is correct. On the other hand the total current that you produce of course would be much greater. So that I think you will have to break away from the assumptions that I made for two dimensional focusing. For example, the focusing from your primary source will be much less important at those lower energies.

EHLERS I want to comment on two things, one volume and one surface. It seems to me that what you folks need from us is some real practical laboratory answers as to I (H^-) versus I (H^+) in a plasma volume. It seems to me we can provide these for you; it does border a bit on physics and the sorts of things we do not have time or budgets to do. But I have a feeling that before the next meeting a lot of those numbers will be available to you. That does not mean volume production will be a good candidate to answer our problems but it sure would answer some of these others. Then it seems to me too, that in terms of volume that you postulate a rather difficult vibrational process as an explanation. I am wondering if we are getting too technical, is it possible that there is something going on that theorists normally do not consider, maybe some chemical activity, or the sort of things that happen in the real world but that do not appear on paper. I think you should look at those as well. In terms of surface work, I do not know what is going on. I certainly wish I did in terms of what the production mechanism is. I am very interested in Dr. Los' work but I am really confused about this 200 volts which we both find and certainly have different explanations for. In other words it would be real nice to know what the answer is, and I do not know what kind of information we could contribute to you that would be useful in telling us just what goes on on those surfaces.

LOS Indeed, both of us have used the number two hundred electron volts, and then you think you are talking about something which is the same. However, I cannot imagine that 200 electron volts would be the appropriate energy with which you leave the target and which is optimum. There are two explanations. In the first place, as you are directing the incoming particles more or less normal to the surface, I suppose there is a lot of penetration and backscattering from deeper lying surfaces. After a number of hard collisions they will evaporate again from the surface. That you could see, when you could energy analyze carefully the beam, because then it should come out. What is the initial translational energy when it leaves the surface? When that is close to 0, then I would say you penetrate the surface and look to backscattered particles from deeper-lying layers. The other possibility is that as you still have to go through a sheet of plasma, there might be all types of destruction cross sections which are very high at low energies, and then I think dominantly of resonant processes, which are sloping down at higher energies. Of course when your creation is sloping up and your destruction is sloping down you get something like a maximum, which might easily lie at something of the order of 100

electron volts. These are the two explanations I could offer.

EHLERS We surface people should put some stronium or calcium in our systems and see if our ources work better than they ever did before.

CRANDALL Has anybody done something like that?

EHLERS Not that I know of. We will get to that, do not worry.

CRANDALL If it is just a work function effect, you probably will not gain much, right?

EHLERS Yes.

SCHLACHTER It was my understanding from the discussion of the other day, that it was much more complicated than work function.

HISKES One does not expect as low a minimum work function with the alkaline earths as with the alkali absorbates, and this has been something of a deterrent against promoting the alkaline earths.

BARDSLEY I make a comment on your earlier point. That is the amount of detail we developed on vibrational excitation, as inspired Martha's experiment. It was intended as just an attempt to rationalize the experiment. The basic theory was done fifteen years ago (maybe twenty years ago). It was abandoned at that time because people thought it was irrelevant, that nobody would be concerned with such details. Let me reinforce Martha's request: if you believe there may be other processes going on, then please add some diagnostics to tell us just what other junk you have that may be causing these additional processes; it would be a shame if we were building castles on poor foundations and that there really were no need for us to go into these detailed investigations.

HOOPER Along the lines of other diagnostics: is there any substance you could put into the discharge in small quantities which would destroy vibrationally excited molecules without having other significant effects and hence to be the test for the importance of those molecules?

BACAL I want to make a different comment. I want to make the comment: maybe we can put something into the plasma which would enhance the vibrationally excited molecules! I would draw your attention to the talk of Mr. Bailey who suggested a way of just not putting the hydrogen from a bottle but putting the hydrogen from something like a microwave discharge. This would enhance vibrational excitation. But maybe your suggestion is fine too.

CRANDALL I think this is a good question: does anybody know of a process that would really do that?

BACAL Well, I think we know about this process: atomic hydrogen and water vapor. At least two, but maybe there are other ones. Mr. Bailey, maybe you know?

BAILEY I think atomic hydrogen is a real culprit. That is why further cross sections are required. I would be very interested in knowing the scaling of the dissociation cross section with vibrational state. We can look at how nice dissociative attachment scales, but we do not want to dismiss a reaction which may be detrimental to the state of vibrational excitation. So I think some attention may be warranted in that area.

GRAHAM I think it might be interesting to look at the work of people who work with drift tubes. I notice they enhance or change the internal energy of the types of things they are interested in. I think it might apply for hydrogen as well. They put in trace elements of the inert gases etc., and they find that that changes for some reason the internal energy distribution in the molecule they are studying. That might be something we could consider.

LEUNG I would suggest, that we should look into the H^- in sources like Geller's ECR. He is using a different kind of production mechanism so there may be a lot of excited vibrational states.

BACAL Sure, There is no reason why we are now confined to a source in which we have a hot filament and so on. We should maybe look to a source which allows getting higher densities. However, we keep the old source, because we do not fully control all the things which are important, and we are afraid that making a big change would lead us to lose all the negative ions. So we are trying to make small changes, controlled ones, in which we try to get a contact between the old device and the new one, and find their characteristics. Maybe it is time to go also to other types of discharges and look how many negative ions they have, we may have some surprises.

ALLISON I would like to answer the request for a shopping list of cross sections, that Bardsley brought up. If nobody else wants any, I have some that I would like to see. For surface plasma sources the only measurements we really have are secondary emission for electrons and H^- ions given by Dimov. They are rather difficult measurements in a source with quite a bit of uncertainty in them. So it seems to me that it would be interesting to know what happens when protons or H_2^+ with energies that are used in the typical surface sources, hit one of these cathodes or emitters and measure that as a function of the coverage. Also of interest would be looking at what the sputtering of the cesium is for $\theta = 0.6$ which is the typical value people think they have.

EHLERS Could I add to that. I have always been surprised that the last time I looked (which is 15 years ago) the cross section for electrons onto the molecule was not known above maybe 30 electron volts and it was rising strongly there. I was wondering if there is any plan to do that

one or has it been done, above that energy?

CRANDALL What is the process?

EHLERS Electrons in H_2 going into $H^+ + H^- +$ electron. Schultz did some work, and there is some work by the Russians, that went to maybe 30-35 eV, but it is not known above that. At that point it was rising rather steeply, it was in the 10^{-19} cm^2 ballpark.

BACAL We do not know that cross section. It is a very good question. I mean we do not know anything about producing negative ions by high energy electrons.

HAGENA Coming back to that question about electrons hitting hydrogen molecules, I was glad that two panel members brought up the problem of hydrogen molecules. Of course from the cluster-beam point of view we are most interested in having more information on how the energetic hydrogen molecules will behave not only when colliding with strontium or calcium (setting aside the problems of making a strontium or calcium target, which is apparently not quite obvious to make) but also from the point of view of having molecular beams hitting a cesiated surface. Looking for example at the ion-source model presented by Hopman from the group of Amsterdam, I could imagine a cluster beam onto such a surface and find out what happens. Almost all cross sections are not known and of course we would like to make these experiments, but it is certainly better to have a priori some data.

SCHLACHTER I would like to comment on the question of the molecular ions. We studied $D_2^+ +$ sodium which goes either to D_2^0 or to $D^+ + D^0$. Both reactions eventually lead to D^- formation. What we found is that both of these channels have similar likelihood. What this means is that the D^- yield for D_2^+ incident on sodium vapor will have a complex dependence on sodium target thickness, depending on the dissociation cross sections. We found that for 8 keV D_2^+ incident on sodium vapor, about half the D_2^+ goes into the $D_2^+ \rightarrow D^+ + D_o$ reaction channel in a thin target, and that the resulting 4 keV D^+ and D^o give the expected D^- equilibrium yield for a target thickness of about 10^{15} atoms/cm^2. The other half of the incident D_2^+ go into the $D_2^+ \rightarrow D_2^o$ reaction channel. The dissociation cross section for D_2^o is apparently very small, so a target thickness in excess of 10^{16} atoms/cm^2 is required to dissociate the D_2^o and to give the expected D^- equilibrium yield.

JACQUOT We have given some thought to the possibility of production of D^- by volume processes in the ECR source. We have not observed D^- ions from the source when we apply rf power. But when we stopped the rf power we observed a small quantity of D^- ions in the after glow of the discharge. If we suppose that the production of vibrationally excited molecules is mainly responsible, for example from collision of H_3^+ with the wall, I think it is not a good idea to build a high density source to produce D^- ions. In general H_3^+ is produced at low discharge power or low power in the ECR source and high pressure. If you have high pressure and low power, it is difficult to obtain high current density of D^- and good gas efficiency. We have to find another mechanism to produce vibrationally excited H_2 molecules from H_3^+ collisions. This is my impression.

BACAL I would like to repeat something I spoke about in my talk. We do not think now, contrary to what we were saying 6 months or 1 year ago, that H_3^+ is really responsible for the vibrational excitation in the volume production. Due to the idea of Wulf Kunkel which was suggested to us 6 months ago, and which John Hiskes has developed since, we think that only the fast electrons are very important in producing vibrational excitation, and H_3^+ may help by something like 30-50%, but we do not really need H_3^+ for producing vibrational excitation in the plasma. The only thing we think we need are fast electrons. However at high densities this may change. So, please do not only think about volume production in terms of needing H_3^+. We think we do not really need H_3^+ under all circumstances. However, I would like to consider also other ion sources, for instance the Berkeley source. Do we know anything about the negative ions in it? From the fact that there are indications of high vibrational excitation states, I would say maybe this Berkeley high density source contains a lot of negative ions.

SCHLACHTER Does anyone have a comment on that?

EHLERS I have a comment. One thing wrong with physics is that people never publish things that do not work. There are certain things that do not work which are very interesting to the theorist. For example, it figures that in the volume O^- should be easy to make. Yet in admitting air in the volume source I was surprised to find that it was much easier to make H^- than O^-. On surfaces, for example, you could make O^- easily and if you make the mistake of putting chlorine in your system, you will have chlorine minus that will not quit. If we could run a reactor on chlorine minus, we would really have it made. But most of these things do not get published and there should be notes made that the theorists could see. Disappointing information may be very interesting, theoretically.

FINK I would like to ask Martha, relative to what I have heard here, whether some of her types of experiments could be conducted with a small background vapor pressure of cesium. There is some hint that cesium enhances everything in the negative ion process and I wonder whether she would like to see something in that realm.

EHLERS We could tell you that it does!

BACAL Well, we can do experiments with cesium. But we have a certain amount of man-power or woman-power and we can not do everything, unless somebody helps us, so please do. In the meantime we also listen to advice, and I even heard advice

two days ago from John Hiskes: do not put cesium into your source before you understand everything. We did many experiments with Leung. I remember that in fact we put cesium in the hydrogen plasma. Cesium is a marvelous getter, you all know that. But do we think enough about that when we discuss effects of cesium? What we say was an increase in H^-. But why? Because all the heavy ions, which we certainly had there, O^- or OH^- and so on, all those ions, their peaks decreased and everything went into H^-. So, one should be very careful when discussing what cesium does. Let us remember the old things we knew about vacuum techniques, about getters. When we put in something which is not perfect, we get a lot of gettering effect and some other reactions. So, again, we need diagnostics, we need mass spectrometers. Does everybody understand what cesium does in surface production? Maybe cesium does a lot because of its gettering effect on water or other matter.

HISKES Another reason for keeping cesium out of the volume is simply that the users are not very enthusiastic about cesium in the beamline. The volume sources may be our best long-term bet for producing a negative ion source free of any alkali contaminants.

CRANDALL I had a comment to something that Ken Ehlers brought up, that I thought I might dispose of. It has to do with the production of H^- from H_2 molecules. That was discussed somewhat more actually 3 years ago, except for the 3.75 eV resonance. He complained that beyond about 25 volts there is not any data and the cross section for H^- production was rising. But, there are several things happening here. What we have talked about most this meeting, is right down here at 3.75 eV, at the low energy, there is a little resonance, it is dinky, it is just considered ground state, but if you put in 5 orders of magnitude with vibrational excitation it gets to be pretty important. I think it is right to think that it is very important to ion sources, and probably without Martha's work we never would have figured it out. We had been excited about that, but we probably may get a little carried away, for the sources that are going to be put on the first Tokamaks or whatever, the surface sources are very important. We do not really understand what is going on in there. You raised the question whether or not this resonance could be important. There are other resonances in here, some of them are bigger, for ground state at least. I do not think there is as much vibrational excitation effect, but out here, this is supposed to be a process referred to as polar dissociation, which Bardsley could probably tell you more about than can I. Basically I do not think it is much different in principle than direct ionization of an atom, which has a threshold. This one has a threshold of about 17 eV, and typically peaks out at 3 times threshold. So it would be extremely unusual, if this rose much higher than 2 or 3 times that number. In that sense I think it is not likely to be a really major contribution to direct production. Maybe somebody else has a different statement.

SCHLACHTER Thanks, Dave. Since we are running a little short on time, I would like to be sure that Dr. Hiskes has a chance to comment about surfaces.

HISKES I want to bring up the experiment that Leung described on Monday. One of the things that they have done for us is to identify at least three different sources of negative ions in the bucket sources. If you look at the energy spectrum of the negative ions, there is first of all a high energy yield. By looking at the negative ions coming from the three different species H^+, H_2^+ and H_3^+, they have provided convincing evidence that this is really a high energy backscattering yield caused by positive ions accelerated through the sheath. By adjusting extraction potentials they have identified a low-energy peak which is clearly volume production. In addition they have found a source of negative ions that apparently originate with energies near the cathode potential. There is some question as to the origin of these negative ions. One clue is the fact that the peak is very narrow, less than about 10 electron volts. There are two prominant suggestions for the source of these ions which have come to be referred to as the low energy peak. One mechanism is the desorption of hydrogen on the cathode by positive cesium ions falling through the sheath potential and striking the cathode with about 100 eV. I have tried to estimate here the negative ion current that one would expect. It is equal to the cesium ion density times the flow velocity (the sound velocity) multiplied by a desorption NISEC. In the experiment of Leung and Ehlers, the positive ion density is about 6×10^{10}. For the upper limit of the cesium density we take this value. However, the cesium ion density has turned out to be a rather elusive parameter at this conference. There have been even suggestions that it could be very low but talking with the people from Los Alamos a reasonable low limit might be 1% of the total positive ion density. The sound velocity of the cesium moving towards the cathode is 10^5 cm/second. The desorption NISEC estimate has considerably uncertainty. Several years ago, Kishinevskii and Bender published an experiment in which the surface had been exposed first to a discharge, loading the surface with hydrogen with at least 5-20 electron volt hydrogen implantation. Then they bombarded this loaded surface with cesium ions in the energy range 1 keV to 5 keV. They found a large desorption NISEC 1.45 I recall the peak was about 1.5. Unfortunately, they did not extend the experiment to lower energies nearer 100 electron volts. At this conference, Seidl reported similar experiments, in which he covered the whole range from about 100 eV to 10 keV using cesium ions incident on LiH. It is not the same experiment, but they are similar in that the target was again loaded with hydrogen. But his number at 100 eV is about 5%. If we take the upper limits for all these factors and multiply them together, we get something like 1.6 mA/cm^2 as the sputtering yield. If we take a pessimistic view and multiply all the lower limits we get a number which is several hundred times smaller, .005 mA/cm^2.

Another contender for explaining the low-energy peak would be fast atoms coming out of the discharge. There are a large number of reactions that generate fast atoms, for example the dissociation of molecules into two hydrogen atoms. These 2-4 eV atoms hit the surface and make negative ions. The estimate for the H^- yield is given by the atomic flux times some appropriate NISEC, together with some geometric factor for which I have taken 1/8 of the isotropic distribution. The equilibrium density of atoms can be calculated rather easily by assuming dissociation with the fast electrons, the density coming into equilibrium depending on the wall collision rate and the number of wall bounces. The neutral molecular gas density is taken to be 4×10^{13} cm^{-3}. The number of fast electrons was suggested to me by Bill Cooper et al., who have studied these ion source discharges with computer models and is taken to be 1/10 of the total electron density for a high power system. We need a NISEC for these fast atoms. The paper by Los reported a large NICEC of 0.35. If we use a number 3 for the wall bounces, we come up with a current density which is about 4 mA/cm^2, a number which is comparable to the sputtering number. However, if we are on the pessimistic side we can allow no more than 1 bounce and if we take Peter Schneider's value for the NISEC on thick cesium, 1 or 2 eV we come up with a smaller number, 10^{-3}, a thousand times smaller. The interesting point is that these numbers are comparable and the spread of uncertainties is comparable. I would like to direct your attention to this problem and request whatever data would be obtained to clarify this question.

ALLISON You do not have on there proton bombardment or did I miss it somewhere?

HISKES We discussed that a year or two ago in various papers and we decided that was about 1% of the high energy backscattering. It could not be much more than about 10% of the high energy backscattering. I presume you are thinking about the 100 eV protons striking the surface, dislodging the hydrogen. This yield is probably larger than both the lower limits I have estimated.

ALLISON Let me then direct the question to the Brookhaven people. What do they derive from their magnetron? How do their results in the magnetron compare with values of K and γ given by Dimov? Are they in that ballpark?

PRELEC I can comment on both of these questions. First, values given for K and γ for the Penning source by Dimov and Dudnikov may not be correct. Because I think those values were obtained by the yield of the charged component of the cathode current only. So, if you take into account the neutral bombardment by fast neutrals moving to and fro between the two cathodes, you may get lower yields, because fast neutral particles will also induce K processes and γ processes. Second question, what are Brookhaven's results? We do not know that, we have not measured it, but what we do know is the ratio of the H^- current density at the slit of the source to the cathode current density. Again, only the charged component. This was between 3% and 8%, 3% for the standard magnetron sources, 8% for the grooved sources and this probably reflects reduced losses by about a factor of 2 in the plasma.

ALLISON If I take Dimov's results for K and γ I calculate 11%.

SCHLACHTER I believe we are running out of time so I think I shall draw this to a close, as you had a chance to ask everything about atomic physics that you wanted to know (but were afraid to ask). I am sure that this is neither the beginning nor the end of the dialogue, since we are all delighted to work on problems for which there is a need for the answers. I would like to thank the panelists and all of you for this discussion.

PANEL SESSION: SOURCES OF NEGATIVE IONS

Panel Members: K. Prelec (Moderator), P. Allison
K.W. Ehlers, A.T. Forrester, R. Geller, W. Stirling

PRELEC I will make an opening statement and then each panel member will follow with his statement. After that, the discussion will be open and we would invite comments or questions on any topic of interest to the design of negative ion sources. I feel that it should also extend into the area that we mentioned this morning as that covered by interpreters: liaison with the fundamental processes in sources; on the other side we should consider the formation of beams from negative ion sources.

Let me say a few words about the progress this field has made since the last symposium. First we have noticed quite an improvement in existing designs of sources. In the design of magnetron sources, grooves have been rediscovered and the asymmetric discharge chamber applied. We also became aware of the cooling requirements and we have designed sources with cooled electrodes. In the area of Penning type sources, which include calutron sources, there was a great deal of work done on methods for the electron removal from the extraction area and energy recovery from the electron component. There was progress made in the performance of the modified duopigatron and quite impressive progress on volume production, and so on.

There were several new designs that were not described at the last symposium, for example, the LBL self-extracted source or the Amsterdam approach by beam-surface production of negative ions. The semi-planotron from Novosibirsk was described recently showing very impressive results and the last, but not least, are the hollow cathode experiments with plasma injection into an electrode system.

Next, I would like to summarize the state of the art of H^- ion source performance. Currents of up to 1 A have been extracted as a beam but in the pulsed mode of operation (several tens of milliseconds). Steady state negative ion production and self-extraction (without additional energy) have been shown at the level of 0.5 A (I am referring to the LBL source), and at about 100 mA from a semi-planotron type of a source, reported by the Novosibirsk group. The power efficiency that has been reached is about 5 to 10 kW/A at best, and down to 2 kW/A in Novosibirsk, but unfortunately their representatives are not here to give more details. The gas efficiency of BNL sources is about 5%. Ken Ehlers quoted the other day 35% for the LBL self-extracted source, but I am still not fully convinced about that number. The magnetron and semi-planotron sources from Novosibirsk have been quoted as having 10 to 20% gas efficiency. Now, the discrepancy between 5% reported from Brookhaven and other laboratories in this country, and 10 to 20% at Novosibirsk may be due to the method of measurements and may also be due to the fact that their sources operate with much higher current densities, much higher plasma densities and, therefore, possibly higher ionization degrees in the discharge.

Next, I would try to define or describe an ideal source, what it should look like. Concerning the power efficiency, I guess, as long as the energy requirement per H^- ion is small compared to the final beam energy, this parameter is not so important. For example, if the final beam energy is 200 keV and we spend 10 keV to produce an H^- ion, it is not so critical to reduce it much further. What is important, is that the electrodes can be easily cooled and this is related to the power efficiency of the source. Gas efficiency is another important parameter: an ideal source should have 100% efficiency, which would mean that nothing but H^- ions is coming out of the source, but I guess if we settle at 50%, that is pretty close to an ideal source.

The beam current density will be defined basically by the beam line requirements, by people who are going to use the source. A more relevant parameter may be the current density per unit of wall area or structure area, and not the density in the extraction slit, because the former will determine the size of the whole system as it is attached to the accelerator and to the rest of the beam line. Further, such an ideal source should have no contaminants coming out of it, it means no cesium, no heavy ions. Also, the beam that will be formed using negative ions produced in such a source should fit the rest of the beam line, and eventually fit the injection port of a fusion device. Because we deal with negative ions, we would like also to have a negligible electron component coming out of the source. This could be a list of topics that have to be discussed

I must admit, while I was making the notes to describe the state of the art and what has been achieved since the last symposium, I became more and more optimistic, but when I started to write down what still would have to be done and how far we are from such an ideal source, my enthusiasm started to go down. First, we have to study efficient gas discharges if we are to use the surface method of production of negative ions. This means that they have to operate with a very high ionization degree and that they have to be stable during very long pulses (even in a d.c. mode); candidates are the hollow cathode discharges, maybe some arcs. This objective may include some contradictory requirements. For example, we would like to have a relatively high plasma density to produce the necessary flux to bombard the conversion electrode. But a high plasma density is bad for the transport of negative ions from the surface to the extraction slit. It follows that such a discharge has to be relatively dense, but on the other hand not too thick. In order to design the electrodes for such a dis-

charge, we have to understand processes in discharges, properties of different species in the discharge, not only ions, but also atoms and molecules, and so on. This would include also the optimization of the shape of electrodes of such a discharge. The second topic would be studies of surface converters, and this would be relevant also for the FOM approach of surface-beam production. What we would like to have ideally is a surface that has a low work function and does not need a continuous diffusion of cesium, a surface that would withstand bombardment by particles of 50, 100 or so electron volts, at power densities of several hundred watts/cm^2, operating steady state and retain the same work function for many hours. Also, it should not release contaminants. However, if such a surface remains a dream only and we do need cesium, then we should know what the best way is to inject cesium, what is happening to that cesium and try to minimize the loss of cesium.

Finally, concerning the beam formation we have to know more about what is happening in the source, where H^- ions and electrons are formed, because we would like to have a very low electron load and a very high H^- yield with very good beam optical properties. We have to make phase space measurements in all six dimensions so that we know how to design a good optical system with low losses and delivering a beam with satisfactory properties. If we can not get rid of electrons by designing the source itself, we should then study methods to remove them before they reach a high energy. I could go on like this for quite a while, but let me invite Dr. Geller to make the statement.

GELLER Let me try to raise the enthusiasm again. In fact, you know the INTOR device has requirements for 10 megawatts of D^o, injected at 400 or 500 keV. That is a fact. So, our duty is to try to fulfill what INTOR asks, let us say, in 8 years or 10 years. When one looks at the INTOR requirements, then it becomes clear that what one needs is something like 10 mA/cm^2 of D^-, not more, not less. We need for ignition something like 3 kW/cm^2 at the port area of the Tokamak, which is a good number for neutral beam heating as well as for R.F. This is not a big current density. The philosophy of the ion sources must be the following: one has to develop a beam system such that when the ignition will be reached, the technology should be the good one and not that we say that the neutron environment will kill the source in one minute as soon as ignition is reached. So, the problems become different. We have to look for 10 mA/cm^2 continuous regime, a big source, let us say, of 5 amperes of steady state, capable of operating inside a neutron environment or to be protected against a neutron environment.

Last year we found it was a tough task. This year, we say, we have the source. It is an overstatement, but one has to make some overstatements. Our source delivers 10 mA/cm^2 steady state. It can be protected and it has a good gas efficiency. So, for us the problems are already further down the line but this is not the topic of this panel meeting. Nevertheless, I want to insist on the importance of beam line pumping. If I can just show you something. On one side you see what people ask for, a positive beam line injector requiring cryopumps of 300,000 ℓ/second per megawatt at 150 kV injection. The main objection is, if we have a neutron environment, what will happen to the condensed tritium on the cryopumps? Who knows! People say it will just be released. So, we think it would be better, if possible, to make use of classical pumps, because if in 10 years we get ignition and all the work is useless, it would be safer to work with classical pumps. We think that in the D^- beam line this becomes perfectly possible because if you increase the energy, you have less current to transport and you need much less pumping. Our calculations show that we need probably a pumping capacity of 50,000 ℓ/sec. per megawatt. Therefore, I think gas efficiency is very important. When people think that they can work with cryopanels it is up to them, but I do not dare.

There is a second problem with neutrons streaming out of the Tokamak. If one sees the positive ion injectors, it is clear that the line is short and that the neutrons, when they come out from the Tokamak, go straight to the source. We think that the only way to protect the source is to lead the beam through a bend. People here at Brookhaven are ashamed to show the bending magnet. I think that is a good thing.

PRELEC Do we have to be proud of it?

GELLER Maybe, but I would say it is the safest way to protect your source. It is clear, one can not close the Tokamak port during ignition as long as one injects the neutrals. The gate must be open and during that time, all the neutrons can kill your ion source. So, I think, we have not yet solved this problem, but we think that the steering of the D^- beam is a very strong argument in favor of D^- injectors. Finally, in order to make a long story short, I show you what we intend to do, and what you have seen this morning. We have an ECR ion source module which gives, let us say 1 A of D^+. This is one module. We think that we can just, through scaling, go up to 20 A and reach what one needs, something like 2 A of D^o at 500 keV entering the INTOR device. That corresponds to 4 A of D^+ can be produced by 20 kW of R.F. power in the ECR source. Now you know nearly as much as I know about our project.

At these meetings there are, fortunately, two philosophies. The old philosophy is Hooper's, which is our double charge exchange; we just think it will work. The other one is maybe also a double charge exchange! I don't know if that will work.

PRELEC I guess we are now convinced that we have to work on negative ions, aren't we?

EHLERS One thing nice about a symposium of this type is that you do get caught up on the developments in ion source development using all three

of the systems. There has been very little work done on volume systems, in terms of an ion source, but certainly we have looked relatively closely t double charge exchange and surface. I personlly, even though I am at present working on surface production, am exceedingly interested in all forms of negative ion production and I will tell you why. Thinking about the whole system, in the quiet of my own room without anyone forcing their biases on me, I conclude that the so-called best negative ion generator may well turn out to be related to the particular accelerator that you use. For example, if one accelerates to half a million volts, I honestly can not say in my own mind that it would be a D.C. accelerator. I can certainly believe that for 200, 300 kV, D.C. will be fine. But, if you take a half a million volt generator at 10 amps you get 5 megawatts sitting there ready to go off and it will, believe me, and that is an awful lot of energy storage. So, somewhere along the line between a 100 and 400, 500, 600 kilovolts (and only time will tell) we are going to have to leave D.C. and consider very seriously some other method of accelerating ions. At the moment, that leaves us really with R.F. where we do not have energy storage to really worry about - things like the Maschke device, for example, where we pay a big penalty in that we lose 25%. We accelerate beams for let us say less than 25% of D.C. time but we certainly make gains. Now, the source of the type I am building, I feel is designed for a D.C. accelerator. I think it would be very difficult, I do not say it can not be done, but I say I think it would be difficult to adapt it to feed the optics required for a Maschke device. If you go to a Maschke device in which you would be saying you want energies of 1 MeV perhaps or more, and Lord knows where the top of the energy requirements will eventually lead us, it very well could be that we would look at the total situation and say that surface production is not the way to go. We may have to reconsider double charge exchange or even volume, if it is available at the time. There is nothing wrong with any of these methods of formation. Each of the methods of formation must be considered when you consider the energy to which you are going, the current to which you have to go and how you are going to get there. Now, in a sense, volume is the only one that we have not really investigated and I can tell you the enemy there. Let us assume, for example, that we have a 200 mA/cm^2 density made up of all ions plus and minus, and we have, let us say, 1% that are negative, that means for 200 mA ion density we would extract 2 mA/cm^2 H^- and that might not be too interesting. So, we should find ways of getting higher than that. But, the problem here is that you will also extract electrons and they are related to the positive ions, which means you will have something like the square root of 1836 times as many positive ions. So, for every 2 mA of negative ions you would extract at a 1% level, they would have 8 A of electrons. Somehow, we have got to find a way to be clever or cut and find ways around this. I will not say it can be done, I will not say it can not. But volume does have to be reinvestigated, particularly as several of us have mentioned here, if cesium turns out to be the deadly enemy of the Tokamak or a fusion device. So, what I am really saying is that I feel we have to be flexible. I know we in Berkeley will borrow from any of you who are successful if we have to make a machine.

FORRESTER I have long made the point that positive ion systems would have to become extraordinarily gas efficient compared to any sources that now exist, because of the reason that Dr. Geller made that the source has to be able to be out of the line of the neutrons sailing back towards the source, otherwise we could not expect sources to hold up very long. It is sort of amazing that it turns out that that goal is much easier to achieve with negative ion sources than with positive ion sources. Well, for that reason and many other reasons, I have reached the conlusion, at this meeting, (and it is surprising to me, because I would not have expected it before) that if I were making bets, I would bet on negative ion systems now, in spite of the moderator's remarks about all the things that have to be done. I have a very encouraging feeling about negative ion systems, not just in the range of 400 kV kind of level. I am not going to speak about all the surface systems that look so encouraging and volume systems, because I am not doing any work in that direction. Neither, as a matter of fact, am I doing anything in respect to generating double charge exchange negative ions at present, but I do have a beam, which I think ought to receive some mention. I did mention it briefly on the floor and got a fair amount of interest. So, let me just detail somewhat what I think is a very encouraging beam of ions for double charge exchange.

We have a plasma source here, the nature of which has been described elsewhere. But the extraction system is what is so simple about it. It is a very fine mesh extraction system and the ions are extracted between the plasma that is inside the source and the grid. We are presently extracting from an 8 cm x 8 cm area a beam of the order of about 24 amperes. If this is about 72% efficient, then the current that would come out is somewhat less than 20 A. We did a measurement on the profile during the week just before I left. At about 1 meter from the source, we had a little calorimeter which scanned the beam. If you take the intensity at the center, it is about 10% of the total current, that would correspond to about $\pm 5^o$ divergence. I am sure that most of the current that comes out is charge exchanged, so we are measuring both the H^o and H^+ with the calorimeter. I am sure that radiation from the cathode would not likely register. So, we are a little bit puzzled about where the rest of it goes, but, nevertheless, even at 1 meter, the density is of the order of about 25 mA/cm^2. I might add, that we expect within this month to have a 10 cm by 40 cm source. We have problems in propagating such a beam in the chamber. You can believe that that is by far the biggest kind of perveance beam that has ever been run. There is an amazing amount of fireworks that go on for phenomena that are not well understood. But, we hope within the next month that we have

a 100 A beam at 400 V and that should go a long way toward adding more encouragement to the great results of Bick Hooper with respect to double charge exchange. I would like to see some analysis done on what the nature of the acceleration in a multi-aperture system would be like. I am not at all convinced that there has to be 50 or 60% interception in a multi-aperture system. The reason that the ordinary extraction systems are 40 or 50% opaque has to do with the power loading and the necessity of cooling that region. The power loading comes from two sources, the plasma bombardment on one side and electron streaming back from electrodes on the other side. Without that electron streaming back to these electrodes it might be possible, to have the equivalent of the plasma electrode simply consisting of some tungsten rods of the order of 0.060" perhaps. If you are talking of 20 mA/cm^2 at 400 V, that is 8 watts, one could stand a lot more than that on tungsten electrodes without any cooling and perhaps have a plasma electrode which is 80% open rather than only 50% open. There is a lot of design work required, but I think I will close my remarks now.

STIRLING I would like to direct my remarks to the surface ionization source. I think one of the most serious problems is that of the converter surface. We do not have as yet the ideal surface our moderator spoke about. So, I would like to take just a moment to talk about the nitty-gritty problem of putting cesium on a converter. I think in the last couple of years, we have seen that sources operating in the A/cm^2 or higher density range are limited in pulse length to the order of a millisecond or so. If we get down to 0.5 A to an ampere, the pulse length may be tens of milliseconds; at a few hundred mA/cm^2 it will get to 100 ms, 50 to 100 mA/cm^2 goes in the seconds range and tens of mA/cm^2 is in the steady state range as Ken Ehlers has reported. Adding one more piece of information: Allison has said he has run at 80 mA/cm^2 steady state. What is the difference that he can do that? Is it a matter of cooling? If so, one can only cool, say for a given plasma density and perhaps at a different plasma density one would have to sweep the beam in order to condition a source system? Would it also operate stably without cesium depletion? So, I guess my comments are a question. What is the governing factor for a reliable, proper cesium covered converter surface? And, how can we maintain it and how sensitive will it be to a variation in the bombardment current on that surface during conditioning? I feel that is a very serious problem for the surface plasma sources.

ALLISON As far as I know, the only people who have operated surface plasma sources in the D.C. mode of any sort are the Novosibirsk people, who I believe, at the Grenoble meeting, reported a 100 mA cw out of a semi-planotron. I think I have seen a report on that. Perhaps one reason that we may be able to operate in the 80 mA/cm^2 continuous mode is that the surface, that has the bombardment, is the cathode. That is a relatively high current density bombardment. Perhaps that pumps the cesium, I do not know. I also do not know what the current level in the semi-planotron from Novosibirsk is, but I have a notion it is in the 20 A/cm^2 range, so this may be the answer to that.

Since I am not in the fusion business, let me list some of the things that occurred to me about H$^-$ sources for accelerator use which is my interest. One thing I think is very attractive is the quiet discharge. For example, in a quiet mode, one can get a much lower emittance and this makes, for example, the Ehlers type source sound very attractive because it is inherently a quiet mode source. So, I think that is a real plus for an accelerator source. Some accelerators that are being built now will have very high power densities. Some that have been built, of course, already have that. The Los Alamos meson factory operates at an average power of 1/2 MW over a small fraction of a cm^2 and successful operation at that level requires very careful tailoring of the emittance. In the accelerator the current densities are sometimes hundreds of mA/cm^2 and the power densities are very high. So one has to pay a lot of attention to the emittance, which perhaps is not so important for fusion devices.

I guess I do not see that for the accelerator use, we worry a lot about electron loading or gas efficiency, although there is certainly a limit to that. The best results on the electron loading seem to be about 50% of the beam reported by the Brookhaven group and the values range up quite a bit higher from there. Perhaps a problem with the Ehlers source is that there may be a lot of electrons extracted from that. So, one has to look at that very carefully.

PRELEC Before we open the discussion, I would like to follow Ehlers comment, that if we are to use MEQALAC, or similar structures, that we may have to consider again volume production. I would disagree with that statement because MEQALAC is basically a low transparency structure. It needs quadrupoles, it needs limiting apertures, but it still has a relatively high acceptance so we may have to go to surface-plasma, high current density sources with low wall transparency, even possibly using shaping of the cathode so as to match the source to the acceptance of the MEQALAC.

EHLERS I agree, you can dream ways out. Nevertheless one has to be practical in the long run and one has to keep an open mind on all systems

PRELEC I agree with that. I would like to ask speakers to state their name, even for the smallest comment, because sometimes an answer, yes or no, may be a very important reference later on.

HOPMAN I just want to add to the remark by Stirling. He said that there seems to be a relation between current density and pulse length, maybe something like the product is a constant. This is, at the moment, an experimental fact observed in the surface plasma sources, where the converted surface is in the plasma. In this case,

the heating of the surface is predominantly by particles that have the sheath voltage as their energy. They strike the surface perpendicular, penetrate in the surface and lose a large fraction of their energy scattering back to the discharge as a negative ion. I think it is one of the advantages of the Amsterdam approach, that makes use of the specular reflection. The loss of energy to the surface is appreciably lower than when the hydrogen penetrates into the surface. This is the reason why we think that we can go to fairly high current densities even at D.C. operation.

LOS I would also come back to Stirling's remarks or maybe the question he asked. I suppose that in a converter, the coverage of the surface will be a dynamic process. Particles are removed and particles are coming to the surface. Now the sticking coefficient of cesium which moves to the surface will be dependent on the energy and when it comes as an ion and has to traverse the plasma sheath, it will depend on what energy it gains whether it will be reflected or whether it will stick to the surface. We did measurements on potasium on tungsten surfaces and there you see that at an incident energy of 10 eV some 50% is sticking to the surface and 50% is reflected from the surface. With cesium, being much heavier, the number will be shifted upward to maybe 40-50 eV. So, I think a very tricky or delicate parameter will be at what energy the coverage with cesium is optimum and that might solve the discrepancy between two types of experiments.

FORRESTER I would like to encourage someone to try to use a porous tungsten matrix with cesium delivery from the rear. It is well developed, if not simple technology, but porous tungsten is a common enough thing. It can be fastened into molybdenum manifolds by electron beam welding. At the kind of temperatures one needs, that is as low as 40°C or lower, the cesium will diffuse (the diffusion length is virtually infinite) you will get cesium covering the front surface. It sounds much better than delivering it from the front.

EHLERS But you will not have a monocrystal if it turns out that that is needed as in the FOM institute.

LOS How uniform is the surface?

FORRESTER It can be made extremely uniform, but it is a porous surface. It can be made with selected spherical powders, for example, which we found important in ion generation. These operate, of course, at temperatures like 1400°K, but you can make it with selected powders with pore sizes of the order of a micron. You can make it to any density you want, then you machine it to whatever shape while it is still with copper or silver, and then drive this out to be left with the porous matrix.

STEWART I want to make a comment concerning the effect of neutrons which two of the panel members talked about. In conjunction with the INTOR and ETF studies, I looked at the effect of neutrons fairly briefly. I think it is difficult to find data. There is a study that I hope is still in progress at Livermore which J.D. Lee is involved in and that is probably the best thing that I have seen, although it is not very conclusive; it is done for mirrors. I tried to take some of that and other data I could find and apply it to ETF and INTOR and bigger devices. I concluded, that with respect to neutrons streaming down a big beam line, a short, big positive beam line like ETF, that there would be heating of the cryopanels, but that one could design around that, in particular, one could go to a bigger refrigeration system and you could handle it. Probably the worst thing that can damage the ion source would happen to insulators and you would start worrying about breakdown. But I concluded that....

FORRESTER How about magnets? Excuse me for interrupting.

STEWART I do not know about the cobalt-samarium cross section, that is a possibility. The insulators, though, maybe need replacement after six months to a year of exposure to the neutrons and that certainly is not a problem, I think. The one thing that sort of remains up in the air, as far as I am concerned, is that there is some data that indicates when you come to breakdown levels from just neutrons but there is nothing that tells you about the combined effects of neutrons, ions, electrons and radiation from the Tokamak and so on. Overall, it looks to me that the shielding might be a myth and that one should challenge the conclusion that you have to get the ion source out of the way. So, maybe you do not have to worry about the bending magnet. You can design around it, perhaps it is not a problem.

FORRESTER I never did locate anything on damage to samarium-cobalt magnets by high energy neutrons. I did find damage to ceramic magnets by thermal neutrons and it looked bad. I forgot the numbers, I have to relate it to the flux and it looks like one could not expect the source to last for a year in the kind of neutron flux we have.

TSAI Regarding this neutron damage on the insulator of the ion accelerator, you have to look at the incident angle from the injection port back to the source. This angle is really small and in the vacuum box, where the source is located, one can shield the insulator very well.

GELLER Yes, but in a Russian paper, I do not have it here, the conclusion was that after a couple of weeks one has to change the ion sources. They assume injection of the neutral beam during 60 seconds, like a reactor. Just if we have to reinject the neutrals, we have to open a gate. With this kind of operation, they say that the insulators would be badly damaged and probably the cryopanels will also be heated up. To what extent, I do not know, and they speak about remote handling if one wants to change the ion source; everything is radioactive.

MOBLEY I work with Al Maschke on the MEQALAC beam. We have a lot of applications in mind, including protection of expensive instrumentation (that is outside the Tokamak) against neutrons. Radiation damage goes as $1/R^2$ and you can shield it if your beam line is rather long and narrow. In this type of accelerator we are talking about, each individual channel is long and narrow and one could have the option of going through holes in a two meter slab of concrete. On the other hand, one could have mere electrostatic transport channels that could exist of little quadrupoles of tungsten with the insulating materials rather far from the direct view of the neutron port. So, if it should turn out that the MEQALAC would be an attractive accelerator scheme, I think those problems are solved just by the nature of the device.

HAGENA Up to the opening session I was a strong believer that energetic particle currents in the low energy range were well produced by the cluster method. Then there came your source (Forrester) which is on the blackboard there, and which is, of course, a nice source if one sees the numbers, except that later on you sort of step back a little bit when you say you do not know where all the current of 20 A was going to. So this, of course, is of much interest for those who want to use it.

FORRESTER I hope shortly to have it diagnosed so we understand everything that is happening.

HAGENA If you monitor the beam profile with the calorimeter and measure the neutrals as well as the charged particles, you find only 10%. How did you measure the 20 A in the first place. Was it just a current drain?

FORRESTER That was the current from the power supply and then we scanned with a calorimeter across the beam.

HAGENA At 1 meter distance?

FORRESTER Yes.

HAGENA That gives a little bit more hope for the cluster beam.

FORRESTER Actually, it is a little bit more than that, because we have the temperature of the grid. We did not measure that, but if you look at it, you see that the grid glow brightly and you know there is more than a hundred watts/cm^2.

HAGENA But still there are beams of 400 eV. The cluster beam works best the lower the energies are and that is certainly an advantage to be exploited. Also, I am glad that apparently this method is not commented upon by anybody on the panel, so we may be still sitting there and working on this method without being disturbed by other people.

SCHMIDT As many of you probably know, I am very interested in the magnetron source. I have some comments that I think I would like to make that is directed more towards the research that should go on in the magnetron. If I may, I would like to use the blackboard for a few minutes. I have made these comments to individuals, but they just do not have the time to get around to it. I think now is the time to sort of press the issue. We know that there is the regular magnetron with a 1 mm gap and it works in a certain way and recently at Brookhaven the new magnetron, the asymmetric one with a 5 mm gap in back, 1 mm in front has shown significant improvement in the gas efficiency and operation of this source. I have questioned really the mechanism for the improvement and most people say well, you have the low pressure discharge occuring in the back and it becomes more dense up in the front region and I strongly question whether this source would not even be better yet if it were 5 mm all the way around.

PRELEC That is the case. We have the expansion chamber in the front as well.

SCHMIDT Well, the expansion chamber does not contribute to the dense plasma region. The dense plasma region stays behind the expansion chamber, so I am saying to make the thing symmetrical again by 5 mm and people keep saying: well, that is going to put more gas in the front, we are going to get more scattering and lose beam again. But, I contend it has not been done or at least has not been done systematically. Yet, at the same time, I think to some extent I may have tried it and have some information on this. That is why I would like to encourage you to try it. I apologize for not having tried it myself, but then we are an accelerator lab, not an ion source lab and we have got something working that satisfies our program now. Several years ago, with a summer student, I was trying to think of a way of reducing the gas flow or improving the gas efficiency of the source. I made a source that had a stainless steel cap, everything made of stainless steel; so, it is a very dirty system. I had a 2 cm anode to cathode gap all the way around. It was completely symmetric and this source operated in very nice plasma conditions. I would have to admit it was done totally in a belljar and I was able to drop the pressure down to 20 microns and still keep the plasma operating. The plasma voltage dropped to something like 200 volts and when I looked at the beam that actually came out of the extraction gap in this source (with no extractor, just the 200 volts cathode-to-anode voltage), I had a very nice plume of ions coming out of that source that I could compare to what I did when I first got the magnetron. It had a very similar amount of ions coming out of that source. Just by visual comparison I would have said that this was putting out as much beam as that one did with a much lower amount of gas in the source; and, so, I question whether the improvement is because of the asymmetry or whether the symmetric case might not even be better yet. It is starting to approach Ken's source in a way, but it is still a magnetron in another way. So, I think it is some direction that you might think about sometime.

PRELEC You may have just misunderstood me when I said that we have 5 mm all around. You know the addition of that chamber in the back actually made the source more symmetric than it was before.

SCHMIDT I realize that.

PRELEC So, now we have about 5 mm in front and 5 mm in the back.

SCHMIDT I have another thing I did not mention here. I have sliced 1 mm off on the front of my cathode on the test bench and improved intensity from it. So, there are just some systematic changes that can be tried to see which direction really to go. I think that would be nice to know.

EHLERS I would like to add a comment to your words, Chuck. I have seen E x B discharges operate real well in pressures of 10^{-7}, if you had half a meter for the radius, so I think what you say is right.

HOLMES I have just noticed, listening to all the papers during this week that if you take all the different types of sources, the magnetron, the calutron, the bucket source and you extract the current density in mA/cm^2 and you divide it by the source operating pressure in mTorr, you always come up with a number lying between 5 and 20. With all the different types of sources, does this suggest that there is some fundamental mechanism there?

PRELEC The gas efficiency is also between 5 and 20%.

JACQUOT I would like an answer to a question about the MEQALAC accelerator. What is the total efficiency in kilowatt beam per R.F. kilowatt power?

MOBLEY I can just repeat the kind of numbers from our R.F. engineers. We think we could make a linac with 90% beam loading. That is to say, of the R.F. power to the accelerated structure, 90% of that is going into the beam without having an unstable resonator. That has not been done in linear accelerator technology. R.F. power conversion efficiency from D.C. plate supply or wall socket can be 40% without really trying very hard. There are other ways to get higher efficiency, but one could then say that 45% x 90% would be something we would shoot for in a larger current device.

JACQUOT My second question about the MEQALAC structure. It seems to me that the background gas pressure at the entrance of the MEQALAC should be lower than in the classical electrostatic system because with the quadrupole aperture there is more material in the accelerator and we have to avoid high flux at the entrance of the MEQALAC.

MOBLEY So far, our thinking is that the critical pressure region is in the first accelerating grid from an ion source, while extracting 0.5 A/cm^2. The voltage gradients required on the quadrupoles tend naturally to be 10 to 15%, that is, the quadrupole voltage is about 15% of the injected energy, and already you are some distance away from the source where gas is streaming out. So, we tend to feel that if we can hold the voltage on the extractor grids we can hold the voltage on the quadrupoles ten times more easily.

DOUCET I would like to make a general comment on the use of cesium in the sources. I think this is relevant to most sources. It seems to me that when we speak about cesium we have to be a little bit more cautious. In fact, we very often say we want no contaminant and cesium is a contaminant, so we would like to avoid cesium. We also say the user of the neutral beam will be very frightened by cesium, so we have to avoid cesium in the devices. Now, when we speak like that, then I think that 20 centuries ago, in the old times, people were worrying that the sky could fall on their heads and the question is: do we go on thinking the same way? I really believe today we have to put numbers in and to look at real things. When we are worrying about cesium in a Tokamak the question is: how much cesium we have and how can you compare these contaminants with what is coming from, for example, the tungsten limiter? I think we have now to ask a question to the people of the Tokamak community: how much cesium can you accept in a Tokamak? It is not a question to say we do not want any cesium, but the question is: how much can you accept? Then, we can look back to a system including the neutralizer and see if the quantity of cesium, that we can expect in a normal operation and during an accident is acceptable. I am pretty sure that we will be able to satisfy most of the requirements. I can just tell you one story of the group. We have designed, as you know, a cesium jet for Grenoble and we are worrying that the cesium could migrate to the source, but you have heard that Jacquot has no problem when the electrodes are 35 mm from the main jet. If you look at the quantity of cesium flowing there, it is tremendous and you can expect a small quantity of cesium to migrate into the Tokamak. You can also worry that some cesium will go into the accelerator, but I am sure a lot of you are worrying that some electrons are going to the accelerator, which could be worse. So, my comment is that before we worry, we have to look at the contamination in a more precise way. I would like to say that there are many ways to stop the cesium. You can have some migration of cesium through the gap but also through the surface. Surface migration is slow, but it is there and you have to take care about that. There is a very important and simple technique to stop this migration or to reduce it very much and that is the use of graphite. Graphite provides some components with cesium which permit it to lower the vapor pressure of cesium by a factor of 10^2 to 10^3 with respect to the vapor pressure of the liquid cesium. So, even if you want to be extremely conservative in your requirement, you can cool the graphite and you will reduce very much the vapor pressure of cesium. Also, the migration along the graphite will be very much reduced. So, in fact, we have

techniques today to reduce that and I really think we can design sources which use cesium.

FORRESTER I think Dr. Doucet has made a very important point. I have used graphite, not as a block, but a little bit of aquadag. For example, aquadag on a glass surface can be seen to go through phase changes depending on the amount of cesium it soaks up. It is blue in one phase and red in another. Therefore, one can see the amount of cesium that one has by the actual color of an aquadag film inside a vacuum tube. There is another very important piece of information which I would like to pass on to you. It has been known to the community of people who make photo-tubes which use cesium. For many, many years, it is practically impossible to hold voltage across an insulator if even a small amount of cesium gets back there. I am surprised that there has not been some complaints about difficulties of holding voltage once you introduce cesium into a system, because even a very small amount of cesium makes a continuous coating over an insulator. It becomes conductive and any small voltage drives off the cesium and causes a discharge. That problem has a very simple cure by either an insulator of lead glass or use of a lead glass glaze on the insulators. It is as easy as any other glaze. I am not sure the phenomena is well understood. I presume that what happens is, that the lead oxide in lead glass reacts with cesium to give cesium oxide in free lead; the free lead is isolated atoms. You can fire lead glass in a hydrogen environment until it is black from the amount of lead released and still not have it conducting, where as with an invisible amount of cesium, you can bake out a tube that has cesium at some high temperature for hours and days and still not get the cesium down to the point where it could hold voltage, unless you have a small length of lead glass involved. It is a very important, well known secret in the right community.

HOPMAN Just a comment or a partial answer to Doucet. For a Tokamak reactor you think of a density of 10^{14}. Calculations have clearly shown that the fraction of heavy metals, like they have done for tungsten, etc. should be less than 10^{-5}. Take now the same fraction for cesium. Then the maximum cesium influx during the complete heating cycle, with neutral beams, should be something like 10^{18} atoms. That is the limit you asked for. It must be less than that.

DOUCET Which is very large.

HOPMAN It is very, very large indeed. Less, I guess, than the numbers I have heard here.

DAGENHART I would like to direct my question to Dr. Ehlers. The 35% gas efficiency you quoted for your self-extraction source, could you comment further on that? And, what is the conductance from your system to your pumps?

EHLERS This, of course, is the whole question. We do not have a hard vacuum at the outside. Now, if you demand a hard vacuum at the outside, you have to undoubtedly, admit a little bit more gas, which would mean in turn that your gas efficiency would go down. I strongly believe, however, that as the source pressures go down, such as in the case of Dr. Geller, your gas efficiency will go up. I think we will all find that. In Geller's case, for example, he can quote numbers like 50%. I have gained a little confidence in talking with him that our 35% or so may not be all that bad, but I do not want to state more. As I mentioned, we can go over 100% by shutting the pumping off completely.

DAGENHART For how long can you maintain the 35%? Is that a several hour number?

LEUNG Well, I would like to talk about H^- production by volume because everybody is talking about surface production. The main concern for extraction of H^- from volume is the flow of electrons. We get electrons out as well as H^-. Recently we have done an experiment to try to reduce the electrons extracted. We start with a simple bucket source and then extract the H^-. We look at it with a mass spectrometer and Faraday cup. We found to our surprise that if you put in the source a magnetic screen consisting of permanent N-S magnets that the amount of H^- is the same whether you have this magnetic screen in it or not. However, the electron current drops by orders of magnitude. The optimum condition comes when the plasma potential of both chambers is almost the same. Martha Bacal was in Berkeley the last couple of weeks and she participated in this experiment. Ken suggested that perhaps we can put multistage screens of magnets, two or three, so that you can reduce the electron current even further. So, this is just some success in eliminating the electrons.

JACQUOT What is the pressure in a D^- injector? I can not envision that the minimum transport line for a D^- beam will be of the order of 5 meters. With 5 meters of transport of D^- at 300 kV and a pressure of 10^{-5} torr how much of H^- gets destroyed? Can someone give an answer to this question?

SLUYTERS Why a beam line of 5 meters?

JACQUOT Because this already exists, for example, in the positive beam lines for TFTR.

HOOPER For a pressure of 10^{-5} and 5 meters, the line density is 1.5×10^{14}. The stripping coefficient or cross section is approximately $2.10^{-15} cm^2$ so if you multiply the two together, you get 0.3. So, if you start with H^-, 30% will be converted to neutrals, approximately.

FINK Why again the 5 meters? I do not understand how you have arrived at that.

JACQUOT Because, it seems difficult to envision a neutralizer (a gas cell or a plasma cell) near the end of the electrostatic accelerator because there are probably many problems. With a low D^- current density (10 mA/cm^2) we have to produce

neutrals close to the Tokamak, because if you produce a neutral at 5 meters or 10 meters from the Tokamak with 10 mA/cm^2 of D^- current density, it is lower than 1 mA/cm^2 at the entrance of the Tokamak. Therefore, it is better to put the neutralizer close to the Tokamak rather then to transport the D^- beam at 300 kV over a long distance.

FINK As I understand it, you could transport the neutrals through many meters if the background pressure is low enough. So, you have to just continue to pump more in the transport region and then your loss would not be anywhere near what you would have with transporting negation ions.

JACQUOT Do you expect a pressure of 10^{-6} torr, for example, in your Tokamak with a beam of 1 MW?

FINK It should be possible if you have enough pumping along the beam line. Yes.

PRELEC We can continue the discussion on the beam line tomorrow.

I have a question to specialists in volume H^- production. If the confinement of negative ions in your volume is very good, is it possible that once you start to extract the H^- ions out of that plasma volume, that the production rate via the excited states and other processes will not be sufficient to maintain that high density of H^- ions?

BACAL We have to consider the loss in the extraction.

PRELEC This is my question: what is the relative importance of the loss through the extraction compared to other losses in the volume?

BACAL Well, I think we have an important loss which is mutual neutralization. It will depend on the ratio of the volume to the surface. Isn't that why you need a big volume to extract a big current so that they have a big production in the volume and a small loss on the surfaces? So confinement should be good everywhere and we should just allow loss from the part of the surface where we extract.

DOUCET I would like to answer that question in another way. Although we have some idea, we have no good proof today, what exactly is the process in the volume production. So, you can make a guess. First guess is really volume production and no effect from the surface. Then you can say that we are working in a D.C. state, so the production has to be equal to the losses. We do not know very well the production processes, but we know the losses. So, we can discuss the losses and we can say that if we work with a plasma density of around 10^{11} cm^{-3}, which is the maximum density we are thinking about, this corresponds to the current density needed for the extraction. Then if you extract the beam you can run in a suitable new operation as long as you provide there the needed power. Now, if you go to the surface production, then you have a change by a factor of roughly 100 in the volume of plasma needed. It is a question of ratio of the volume to the surface. When you use a bucket source, the bucket does not require very large power to increase the volume. You can use a large source and a small extraction current density and the electrical power needed for such a large volume is very close to that what is needed to power a small one. So, in both cases, I would say that we can extract current density of around 1, 10, 20 mA/cm^2 without destroying the plasma.

PRELEC I guess the time is almost up. Before we close, I would like to show you a few slides from the paper that Dr. Dudnikov sent to us, which are related to the energy spectra of negative ions and fast neutrals. (See Dudnikov's paper in this proceedings.)

EHLERS Could I add one comment on the chart you showed with the low energy negative ions? We have been seeing that for some months and we have been arguing with each other as to what its cause might be. We initially thought it might be in our spectrometer, but we decided it could not be as we did not see it on the positive ion spectra. I should add, we see it on all negative ions regardless of how they are produced whether they are produced from surface, whether they are produced from volume and, so, I would say that it must be some effect outside of the extractor region.

PRELEC So this would agree with Dr. Dudnikov.

EHLERS Incidentally, those little perturbations were on all of our slides.

HOOPER Could I ask a question? How do you know you are not accelerating an impurity that contains hydrogen which is then breaking up and leaving you with, say, H^- at a lower energy?

EHLERS Well, I can not answer your question because we have not come up with a model yet as to what it could be. There is a definite ramp there. The width of the energy reduction is limited, we think. We do not know what it is due to.

PETERSON How much does the energy vary from the actual positive potential?

EHLERS We have not really calibrated that yet. Would you guess 40 volts, 50 volts, something like that order? We will look into it further and we will let you know.

TSAI From the second view-graph you just showed, there is the low energy peak. Does that indicate charge exchange loss in the accelerator column?

PRELEC If I may, I will refer you to the original paper.

TSAI The reason why I mention this is because the pressure in the accelerator area is a few microns. It is quite possible that there is a lot of charge exchange. This will effect the beam

optics problem and electrode loading in practically all negative ion sources. Up to now we have seen a lot of progress in negative ion sources. I think the next problem we need to look into very carefully is the beam optics problem, because we are all talking about the injection into the Tokamak and 5, 10 meter beam line. If the beam optics is poor, we can not talk about injection because an important part gets lost along the way. I think that is probably the next most important problem in negative ion research.

PRELEC I would like to thank the panel members and the audience. This session is closed.

CONCLUDING REMARKS

THIS PAGE

WAS INTENTIONALLY

LEFT BLANK

CONCLUDING REMARKS

(K.W. Ehlers)

In a sense one rapidly has to extemporize if you are going to conclude a program that just ended. Bill Graham gave me a small cartoon a moment ago which perhaps can say it better than I: "I am sick of it, I am sick of fusion, I am sick of fission and I am going home." I suppose you could add negative ions to that. I assure you I am not going to talk very long so that you will be impeded from going home.

I am sort of reminded of an old song which I am sure most of you are acquainted with. It came out during WW II which was sort of made famous by the Andrew Sisters and the lyrics went: "You want to accentuate the positive and eliminate the negative, don't mess with Mister-In-Between, whoever that is." I have a feeling the lyricists in our case, in terms of neutral beams, just might be wrong, because I certainly think there is a future for neutral beams if we can work out all the kinks. But, there is something rather negative about the word negative. I know, your neighbors for example, if they found out you were working in negative ions they would not be too happy, they would be much more pleased if you were in the positive ion program. So, we have got that connotation to bare with and some day we will perhaps be able to outlive it.

Negative ion systems do indeed extrapolate to reactors. A situation that positive ion beams may not be able to do. We hope very sincerely that the microwave people are able to heat plasmas because when we are in both the positive and negative ion business, regardless of our job, the ultimate aim is to get fusion to work. And, I do not really care who does it or how it is done so long as the job gets done.

This conference, like the last one, has been extremely enjoyable to me. I listened to and enjoyed every paper, I did not hear what I thought was a bad one and I think I learned something from every one of them. The week went extremely fast and it seems rather surprising to me that this is the last talk.

To summarize this program, however, I suppose we have to kind of compare it with where we were three years ago. We started with theory in the theoretical sessions. We have volume production, double charge exchange and surface production. Three years ago volume production did occupy a good bit of the program and the theorists were a bit shocked to find that conceivably negative ions existed in plasma volumes, normal garden variety plasma volumes, to a degree of I^-/I^o in excess of about 10^{-4}. Today it looks very definitely they might exist to the tune of 10^{-2} and maybe even more. So, they had their work cut out for them and indeed in three years they have done it. They all went out and vibrated their molecules to the tune of about V = 5 or 6. They gained 5 orders of magnitude in three years and now they are able to explain the whole thing. Conceivably they are right, I hope they are, but if we ever find 100%, I think they will have an explanation that will take care of it.

In terms of double charge exchange the situation looks more clear as far as physics is concerned. As Fred Schlachter says, the confusion does not really exist anymore, the confusion of the old data and the new, seems to be one of how the data was taken, namely, there was some scattering going on in the experiments at these very low energies and the explanation sounds sensible to me. It does, however, warn us that if we use these extremely low energies, that scattering will not just disappear and we have got to keep in mind that these beams at low energies are going to be scattered around. We can not ignore that either, particularly in view of the new data indicating that the alkaliners might be very interesting, the strontiums, the bariums and things of that nature. So, we have got some work to do on the experimental side to see just how that particular effect might aid us.

When it comes to surface we still, at least in my mind, do not know what is really going on. John Hiskes is sure that we do. To us, in the lab who talk with John weekly (we do communicate quite well and it is important that we communicate with our theorists) we are still arguing back and forth and I think by the time we have another conference of this type we are going to know a lot of answers. We are going to have some experimental data that will aid the theorists and they are going to be able to tell us what is going on.

So, in the last three years we have found that our theorists and our atomic physicists have been very busy, they are alive and happy and I am sure they are going away from here with a bag of orders to fill which is going to be more than ample to keep them busy for some time. I would like to thank them for being at this conference. We enjoyed their talks, they are doing good work and we need them badly.

In the terms of the experimental devices, things certainly have changed. The ball game, sort of, just begun three years ago. Brookhaven had gotten a hit and they were heading for first base, everything was going along fine but somebody picked up the base and ran. The rules of the game changed. We were no longer interested in very short pulses of high current density. We had to face up to the situation that dc beams would be needed and everybody had to go back and scramble to catch up with this. Since that point in time we have had a few casualties. Three years ago, TRW was here. They were talking about a negative ion laser produced plasma. Our own double charge exchange program phased down largely because of budgets. In the interim we have picked up some programs, largely in Europe and around, so we have got an additional group composed of Oak Ridge, ourselves, Culham, the group in Grenoble, FOM, the

group in Karlsruhe, all with different approaches. We have got to follow exactly what happens in each of these groups. We are all standing at the sidelines waiting for our turn at bat and we are all trying to get to first base too. First base is even a distance away but really it is second base we have got to get to by the end of next fall. At least those of us in the American program. We have got to get there with 1 A at 40 kV and that is no small aim or objective. If we make it, our tongues are going to be hanging out and we are going to be real tired. For example, I am a bit depressed this morning to learn that we at Berkeley are going to lose a young, extremely capable engineer. He is leaving because of the usual reasons, he is over-worked and under-paid and it is problems of this type that face us in the real world. They keep us from reaching our goals and objectives and we have got to have a lot of help and we certainly have to have a lot of dedication. But, particularly the younger people are not in all cases as dedicated as we would like them to be, because you can not eat dedication anymore, you even have to pay taxes on it. If we get to second base on time, which as I say will be a very hard job, at that point we have to regroup a little bit, we have got to learn to accelerate beams to higher energies and then start out for third base. To get to third base we have to neutralize these particles in a sensible way. This conference, over the last, had a number of very fine papers, I thought, on the neutralization situation. At least we are thinking about it. Today we heard papers about acceleration and those did not really appear in the first conference. We are moving along, there has been a lot of change in three years. Neutralizing, for example, looks as if it is not all that nice to use gas cells. But people did come up with more exotic ways of neutralizing or stripping the negative charge from the negative ions and those look like they may have some promise. I was interested in the thought that it might take a megawatt of power to get 10 kW for a laser system and you say, that is terrible, but if you increase the stripping efficiency from 60% to 80% in a 5 MW beam you have got it for nothing in terms of power. So anything that will increase that stripping efficiency by sizeable percentages is going to be worth what it costs in terms of power.

Well, if we get to third base, we still have not won the game. At that point we have got to start putting this whole works in a package to satisfy the groups we heard from today. And, again, we have got to figure out how we do this at the voltages and the currents that they need and if we finally succeed in doing that, we will cross home plate and it will have, perhaps, won the game by the sort of familiar score of 1 to 0.

At this conference, I think in the halls particularly, I heard the same comments I heard three years ago and in that score we did not change, namely, we have got vast aims and goals and we are trying to do that on half vast budgets. Stan Staten agrees with that and I am afraid, really, that we are not going to get vast budgets until we convince the whole world that our ideas are not half vast. So, we have got a big job ahead of us. Whether we win or whether we lose, time will tell, but I think the last three years despite of what some of us may think, have been very productive. So, I am going to close with that as a summary with one addition. I want to add to the fact that Brookhaven has certainly done it again. They have accumulated together in this room the very sizeable percentage of the whole worlds population of scientists and physicists who are interested in negative ion beams, primarily for neutral beams but also our associated colleagues from the accelerator industry. At the talks that those boys gave, we learned that indeed in the accelerator group we have already started to accentuate the negative, as a matter of fact at Fermi Lab they have even eliminated the positive. So, maybe they are leading the way for us. But, putting on a symposium of this type is no small feat and at this time I would like to thank Theo Sluyters. Last meeting Krsto Prelec carried the ball, this time it was Theo's job but his job was not only his, though he certainly carried the lion's share of it. I want to thank the fellows who poked those microphones at us and tried to get some sensibility or legibility out of what we were saying in soft tones. I want to particularly thank the two girls who are standing by the door who have tried to take care of all our problems. They have done a magnificent job and at this point in time I think we should stand up and give them a rousing hand of applause.

So, until we all meet again, hopefully in three years, conceivably less, I wish you all good luck, you are going to need it.

LIST OF ATTENDEES—LIST OF AUTHORS

THIS PAGE

WAS INTENTIONALLY

LEFT BLANK

List of Attendees

J.G. Alessi, 930
Brookhaven National Laboratory
Accelerator Department
Upton, New York 11973

P. Allison
Los Alamos Scientific Laboratory
P.O. Box 1663
Los Alamos, New Mexico 87545

L.W. Anderson
University of Wisconsin
Physics Department
Madison, Wisconsin 53706

O.A. Anderson
Lawrence Livermore Laboratory
P.O. Box 808
Livermore, California 94550

M. Bacal
Ecole Polytechnique
Laboratoire de Physique des Milieux
Palaiseau Cedex, 91128
France

W.F. Bailey
Air Force Institute of Technology
Wright Patterson AFB
Dayton, Ohio 45433

J.N. Bardsley
University of Pittsburgh
Physics Department
Pittsburgh, Pennsylvania 15260

G. Basbas
Physical Review Letters
P.O. Box 1000
Ridge, New York 11961

R.R. Borchers
Lawrence Livermore Laboratory
P.O. Box 808
Livermore, California 94550

M.J. Coggiola
Stanford Research Institute
333 Ravenwood Avenue
Menlo Park, California 94025

D.H. Crandall
Oak Ridge National Laboratory
P.O. Box X
Oak Ridge, Tennessee 37830

W.K. Dagenhart
Oak Ridge National Laboratory
P.O. Box X
Oak Ridge, Tennessee 37830

J.M. Dolique
University of Grenoble
Laboratoire de Physique des Plasmas
Equipe de Recherche Associée AU C.N.R.S.
Grenoble
France

H.J. Doucet
Ecole Polytechnique
Laboratoire de Physique des Milieux
Palaiseau Cedex, 91128
France

K.W. Ehlers
Lawrence Berkeley Laboratory
University of California
Berkeley, California 94720

J.W. Fink, L-434
Lawrence Livermore Laboratory
P.O. Box 808
Livermore, California 94550

A.T. Forrester
University of California
Physics Department
Los Angeles, California 90024

R. Geller
Centre D'Etudes Nucléaires
Dept. de Physique du Plasma
et de la Fusion Controlée
85 X Grenoble Cedex
France

W.G. Graham
New University of Ulster
Physics Department
Coleraine BT 52 1Sa
Northern Ireland

O.F. Hagena
Kernforschungszentrum Karlsruhe
Institut für Kernverfahrenstechnik
75 Karlsruhe 1
Postfach 3640

G.W. Hamilton
Lawrence Livermore Laboratory
P.O. Box 808
Livermore, California 94550

A. Hershcovitch, 911-B
Brookhaven National Laboratory
Accelerator Department
Upton, New York 11973

J.R. Hiskes
Lawrence Livermore Laboratory
P.O. Box 808
Livermore, California 94550

A.J. Holmes
Culham Laboratory
Applied Physics & Technology Div.
Abingdon, Oxfordshire
OX14 3DB
England

E.B. Hooper
Lawrence Livermore Laboratory
P.O. Box 808
Livermore, California 94550

H.J. Hopman
FOM-Inst. for Atom and Molecule Physics
Kruislaan 407
1098 SJ Amsterdam
The Netherlands

F.N. Huffman
Thermo Electron Corp.
101 First Avenue
Waltham, Massachusetts

C. Jacquot
Centre D'Etudes Nucléaires
Dept. de Physique du Plasma
et de la Fusion Controlée
85 X Grenoble Cedex
France

A.M. Karo
Lawrence Livermore Laboratory
P.O. Box 808
Livermore, California 94550

V. Kovarik, 911B
Brookhaven National Laboratory
Accelerator Department
Upton, New York 11973

T. Kuroda, 930
Brookhaven National Laboratory
Accelerator Department
Upton, New York 11973

R.A. Larson, 911B
Brookhaven National Laboratory
Accelerator Department
Upton, New York 11973

K.N. Leung
Lawrence Berkeley Laboratory
University of California
Berkeley, California 94720

J. Los
FOM-Inst. For Atoma and Molecule Physics
Kruislaan 407
1098 SJ Amsterdam
The Netherlands

R. McKenzie-Wilson, 911A
Brookhaven National Laboratory
Accelerator Department
Upton, New York 11973

M.W. McGeoch
AVCO Everett Research Lab., Inc.
2385 Revere Beach Parkway
Everett, Massachusetts 02149

F.W. Meyer
Oak Ridge National Laboratory
P.O. Box X
Oak Ridge, Tennessee 37830

T.J. Morgan
Wesleyan University
Physics Department
Middletown, Connecticut 06457

P.F. Oettinger
Thermo Electron Corp.
101 First Avenue
Waltham, Massachusetts

H. Okamura
Institute of Plasma Physics
Nagoya University
Nagoya 464, Japan

R.E. Olsen
Stanford Research Institute
333 Ravenwood Avenue
Menlo Park, California 94025

R. Pauli
Studsuik Energiteknik AB
S-61182 Nyköping
Sweden

J.R. Peterson
Stanford Research Institute
333 Ravenwood Avenue
Menlo Park, California 94025

K. Prelec, 911B
Brookhaven National Laboratory
Accelerator Department
Upton, New York 11973

R.V. Pyle
Lawrence Berkeley Laboratory
University of California
Berkeley, California 94720

J.C. Rocco
University of Grenoble
Laboratoire de Physique des Plasmas
Equipe de Recherche Associée Au C.N.R.S.
Grenoble
France

A.S. Schlachter
Lawrence Berkeley Laboratory
University of California
Berkeley, California 94720

C.W. Schmidt
Fermi National Accelerator Laboratory
P.O. Box 500
Batavia, Illinois 60510

M. Seidl
Stevens Institute of Technology
Castle Point Station
Hoboken, New Jersey 07030

J.D. Sherman
Los Alamos Scientific Laboratory
P.O. Box 1663
Los Alamos, New Mexico 87545

Sluyters, Th., 911B
Brookhaven National Laboratory
Accelerator Department
Upton, New York 11973

H.V. Smith
Los Alamos Scientific Laboratory
P.O. Box 1663
Los Alamos, New Mexico 87545

H.S. Staten
U.S. Department of Energy
Office of Fusion Energy, MS G-234
Component Development Branch
Washington, DC 20545

L.D. Stewart
Princeton Plasma Physics Laboratory
Princeton University
P.O. Box 451
Princeton, New Jersey 08540

W.L. Stirling
Oak Ridge National Laboratory
P.O. Box X
Oak Ridge, Tennessee 37830

P.M. Stone, Chief
U.S. Department of Energy
Office of Fusion Energy, MS G-234
Experimental Plasma Research Branch
Washington, DC 20545

C.C. Tsai
Oak Ridge National Laboratory
P.O. Box X
Oak Ridge, Tennessee 37830

THIS PAGE

WAS INTENTIONALLY

LEFT BLANK

List of Authors

Bassi, J.G....153,166
Allison, P....171,178,184,373
Alvarez, I....106
Anderson, C.J....285
Anderson, L.W....285
Anderson, O.A....355

Bacal, M....90,95,270,365
Bailey, W.F....33
Bardsley, J.N....10,365
Bergstrom, J.B....350
Berkner, K.H....291
Boozer, A.H....321
Bruneteau, A.M....90,95
Buzzi, J.M....270

Cisneros, C....106
Coffman, F.E....315
Coggiola, M.J....58
Crandall, D.H....1,365

Dagenhart, W.K....217
Deboni, T.M....74
Delaunay, M....255,270
Dolique, J.M....81
Doucet, H.J....90,95,270
Dudnikov, V.G....137

Ehlers, K.W....65,198,207,373,385
Eubank, H.P....321

Feezell, R.R....225
Fink, J.W....298,339
Forrester, A.T....373
Foucher, J.L....255,350

Garscadden, A....33
Geller, R....255,350,373
Girnius, R.J....285
Goldston, R.J....321
Graham, W.G....95,126
Granneman, E.H.A....233
Green, T.S....213
Greer, J....111
Gustavson, H.G....350

Haas, G.M....315
Hagena, O.F....263
Hamilton, G.W....90,95,330
Haselton, H.H....217,225
Hellblom,....350
Henkes, P.R.W....263
Hershcovitch, A....160
Hiskes, J.R....15,74,365
Hodges, R.V....58
Holmes, A.J.T....213
Hooper, E.B....207,247
Hopman, H.J....233
Howald, A.M....285
Huestis, D.L....58
Huffman, F.N....119

Inman, M....213

Jacquot, C....255,270,350
Jassby, D.L....321

Kaneko, O....240
Karo, A.M....74
Kelley, G.G....217
Kim, J....217
Klingelhofer, R....263
Krevet, B....263
Kuroda, T....240

Labaune, G....,270
Lamain, H....270
Leung, K.N....65,198,207
Los, J....365
Ludwig, P....255,270

Massman, P....233
Mayo, M....106
Mazhari, F....255
McGeoch, M.W....304
Meyer, F.W....1
Mikkelsen, D.R....321
Morgan, T.J....106
Moser, H.O....263

Nachman, M....90

Oettinger, P.E....119
Oka, Y....240
Okamura, H....240
Olson, R.E....51
Overbosch, E.A....23

Pargellis, A.N....111
Pauli, R....350
Peterson, J.R....58
Post, D.E....321
Poulsen, P....247
Prelec, K....145,160,298,373
Prichard, B....321
Pyle, R.V....194,291

Ricard, E....255
Rocco, J.C....255,350
Ryan, P.M....225

Savas, S.E....291
Schechter, D.E....225
Schlachter, A.S....42,365
Schmidt, C.W....189
Schmidt, J.A....321
Schneider, P.J....15
Seidl, M....111
Sermet, P....255,350
Sherman, J.D....171,178,184
Singer, C.E....321
Sluyters, Th....153,166
Smith, H.V....171,178,184
Stalder, K.R....291
Staten, H.S....315
Stephan, J.R....270
Stewart, L.D....321
Stirling, W.L....217,225,373
Stone, J....106

Tsai, C.C....217,225

van Bommel, P.J....233
van Wunnik, J....23
Verney, S....270

Whealton, J.H....217,225

Zadworny, F....255

U.S. GOVERNMENT PRINTING OFFICE: 614-090-#37